

Johan Huijsing

# Operational Amplifiers

Theory and Design

*Second Edition*

 Springer

# Operational Amplifiers

2nd Edition



Johan Huijsing

# Operational Amplifiers

Theory and Design

2nd Edition

 Springer

Prof. Johan Huijsing  
Delft University of Technology  
Faculty of Electrical Engineering  
Mathematics and Computer Sciences (EEMCS)  
Mekelweg 4  
2628 CD Delft  
Netherlands  
j.h.huijsing@tudelft.nl

ISBN 978-94-007-0595-1 e-ISBN 978-94-007-0596-8

DOI 10.1007/978-94-007-0596-8

Springer Dordrecht Heidelberg London New York

Library of Congress Control Number: 2011925998

© Springer Science+Business Media B.V. 2011

No part of this work may be reproduced, stored in a retrieval system, or transmitted in any form or by any means, electronic, mechanical, photocopying, microfilming, recording or otherwise, without written permission from the Publisher, with the exception of any material supplied specifically for the purpose of being entered and executed on a computer system, for exclusive use by the purchaser of the work.

*Cover design:* eStudio Calamar S.L.

Printed on acid-free paper

Springer is part of Springer Science+Business Media ([www.springer.com](http://www.springer.com))

*To my dear wife Willeke and children Hans, Adriaan, Mirjam,  
and Reineke, who have given me love and support.*



# Acknowledgements

Simon Middelhoek stimulated me to write this overview book.  
Wim van Nimwegen drew pictures in a very clear way.  
Ovidiu Bajdechi wrote the problems and simulation exercises.  
Anja de Koning and Mary van den Berg typed original manuscript.  
Wendy Sturrock and many students helped to correct this book.  
Maureen Meekel provided computer support.  
Thanks to all.

Above all, thanks to God through Jesus Christ, who is the Lord of my life.





# Contents

<b>1. Definition of Operational Amplifiers</b> .....	1
Nullor Concept .....	1
Classification Based on Number of Floating Ports .....	1
1.1 Operational Inverting Amplifier .....	2
Current-to-Voltage Converter .....	3
1.2 Operational Voltage Amplifier .....	3
Non-Inverting Voltage Amplifier .....	3
Voltage Follower .....	4
1.3 Operational Current Amplifier .....	5
Current Amplifier .....	5
Current Follower .....	6
1.4 Operational Floating Amplifier .....	7
Voltage-to-Current Converter .....	7
Voltage and Current Follower .....	7
1.5 Conclusion .....	8
1.6 References .....	10
<b>2. Macromodels</b> .....	11
2.1 Operational Inverting Amplifier .....	11
Definition of: Offset Voltage and Current, Input and Output Impedance, Transconductance .....	11
2.2 Operational Voltage Amplifier .....	12
Definition of: Input Bias Current, Input Common-Mode Rejection Ratio .....	13
2.3 Operational Current Amplifier .....	14
Definition of: Output Bias Current, Output Common-Mode Current Rejection Ratio .....	14
2.4 Operational Floating Amplifier .....	15
Using All Definitions .....	16

2.5	Macromodels in SPICE .....	16
	Macromodel Mathematical .....	16
	Macromodel Miller-Compensated .....	17
	Macromodel Nested-Miller-Compensated .....	18
	Conclusion .....	18
2.6	Measurement Techniques for Operational Amplifiers .....	19
	Transconductance Measurement of an OTA .....	20
	Voltage Gain Measurement of an OpAmp .....	21
	Voltage Gain and Offset Measurements of an OpAmp .....	22
	General Measurement Setup for an OpAmp .....	22
2.7	Problems and Simulation Exercises .....	24
	Problem 2.1 .....	24
	Solution .....	25
	Simulation Exercise 2.1 .....	27
	Simulation Exercise 2.2 .....	28
2.8	References .....	28
<b>3.</b>	<b>Applications .....</b>	<b>31</b>
3.1	Operational Inverting Amplifier .....	31
	Current-to-Voltage Converter .....	32
	Inverting Voltage Amplifier .....	33
3.2	Operational Voltage Amplifier .....	34
	Non-Inverting Voltage Amplifier .....	34
	Voltage Follower .....	35
	Bridge Instrumentation Amplifier .....	35
3.3	Operational Current Amplifier .....	37
	Current Amplifier .....	37
3.4	Operational Floating Amplifier .....	38
	Voltage-to-Current Converter .....	38
	Inverting Current Amplifier .....	39
	Differential Voltage-to-Current Converter .....	40
	Instrumentation Voltage Amplifier .....	42
	Instrumentation Current Amplifier .....	42
	Gyrator Floating .....	43
	Conclusion .....	44
3.5	Dynamic Range .....	44
	Dynamic Range Over Supply-Power Ratio .....	45
	Voltage-to-Current Converter .....	46
	Inverting Voltage Amplifier .....	47
	Non-Inverting Voltage Amplifier .....	47
	Inverting Voltage Integrator .....	48
	Current Mirror .....	49
	Conclusion Current Mirror .....	50
	Non-Ideal Operational Amplifiers .....	50
	Conclusion .....	52

- 3.6 Problems ..... 52
  - Problem 3.1 ..... 52
  - Solution ..... 53
  - Problem 3.2 ..... 54
  - Solution ..... 54
  - Problem 3.3 ..... 55
  - Solution ..... 55
- 3.7 References ..... 56
  
- 4. Input Stages ..... 59**
  - 4.1 Offset, Bias, and Drift ..... 59
    - Isolation Techniques ..... 60
    - Balancing Techniques ..... 60
    - Offset Trimming ..... 65
    - Biasing for Constant Transconductance  $G_m$  Over Temperature ..... 67
  - 4.2 Noise ..... 70
    - Isolation Techniques ..... 70
    - Balancing Techniques ..... 72
    - Conclusion ..... 73
  - 4.3 Common-Mode Rejection ..... 73
    - Isolation Techniques ..... 74
    - Balancing Techniques ..... 74
    - Combination of Isolation and Balancing ..... 75
    - Common-Mode Cross-Talk Ratios ..... 76
    - Parallel Input Impedance ..... 76
    - Collector or Drain Impedance ..... 78
    - Tail Impedance ..... 78
    - Collector-Base Impedance ..... 79
    - Base Impedance ..... 79
    - Back-Gate Influence ..... 79
    - Total CMCR ..... 80
    - Conclusion ..... 81
  - 4.4 Rail-to-Rail Input Stages ..... 82
    - Constant  $g_m$  by Constant Sum of Tail-Currents ..... 83
    - Constant  $g_m$  by Multiple Input Stages in Strong-Inversion CMOS ..... 86
    - Constant  $g_m$  by Current Spillover Control ..... 87
    - Constant  $g_m$  in CMOS by Saturation Control ..... 91
    - Constant  $g_m$  in Strong-Inversion CMOS by Constant Sum of  $V_{GS}$  ..... 92
    - Rail-to-Rail in CMOS by Back-Gate Driving ..... 95
    - Extension of the Common-Mode Input Range ..... 95
    - Conclusion ..... 96
  - 4.5 Problems and Simulation Exercises ..... 96
    - Problem 4.1 ..... 96
    - Solution ..... 97
    - Problem 4.2 ..... 98

- Solution ..... 98
- Problem 4.3 ..... 99
- Solution ..... 100
- Simulation Exercise 4.1 ..... 100
- Simulation Exercise 4.2 ..... 102
- Simulation Exercise 4.3 ..... 102
- 4.6 References ..... 104
  
- 5. Output Stages ..... 105**
  - 5.1 Power Efficiency of Output Stages ..... 105
  - 5.2 Classification of Output Stages ..... 110
  - 5.3 Feedforward Class-AB Biasing (FFB) ..... 112
    - FFB Voltage Follower Output Stages ..... 112
    - FFB Compound Output Stages ..... 117
    - FFB Rail-to-Rail General-Amplifier Output Stages ..... 119
    - Conclusion ..... 128
  - 5.4 Feedback Class-AB Biasing (FBB) ..... 128
    - FBB Voltage-Follower Output Stages ..... 129
    - FBB Compound Output Stages ..... 130
    - FBB Rail-to-Rail General Amplifier Output Stages ..... 135
    - Conclusion ..... 140
  - 5.5 Saturation Protection and Current Limitation ..... 141
    - Output Saturation Protection Circuits ..... 141
    - Output Current Limitation Circuits ..... 143
  - 5.6 Problems and Simulation Exercises ..... 145
    - Problem 5.1 ..... 145
    - Solution ..... 146
    - Problem 5.2 ..... 146
    - Solution ..... 147
    - Problem 5.3 ..... 148
    - Solution ..... 148
    - Problem 5.4 ..... 149
    - Solution ..... 149
    - Problem 5.5 ..... 150
    - Solution ..... 150
    - Simulation Exercise 5.1 ..... 151
    - Simulation Exercise 5.2 ..... 152
  - 5.7 References ..... 153
  
- 6. Overall Design ..... 155**
  - 6.1 Classification of Overall Topologies ..... 155
    - Nine Overall Topologies ..... 156
    - Voltage and Current Gain Boosting ..... 160

Input Voltage and Current Compensation ..... 160

6.2 Frequency Compensation ..... 162

    One-GA-Stage Frequency Compensation ..... 163

    No Internal Poles Without Cascodes! ..... 165

    Two-GA-Stage Frequency Compensation ..... 166

    Two-GA-Stage Parallel Compensation (PC) ..... 167

    Two-GA-Stage Miller Compensation (MC) ..... 170

    Remark on the Order of Pole Positions ..... 172

    Three-GA-Stage Frequency Compensation ..... 177

    Three-GA-Stage Nested Miller Compensation (NMC) ..... 178

    Three-GA-Stage Multipath Nested Miller Compensation  
    (MNMC) ..... 181

    Four-GA-Stage Frequency Compensation ..... 184

    Four-GA-Stage Hybrid Nested Miller Compensation (HNMC) ..... 184

    Four-GA-Stage Multipath Hybrid Nested Miller Compensation  
    (MHNMC) ..... 187

    Four-GA-Stage Conditionally Stable MHNMC ..... 189

    Multi-GA-Stage Compensations ..... 189

    Compensation for Low Power and High Capacitive Load ..... 189

    Active Miller Compensation ..... 190

    RC or Distributed RC Compensation Network ..... 190

    Damping Compensation Network ..... 192

    Quenching Capacitor Network ..... 193

    Reversed Nested Miller Compensation (RNMC) for Low Power  
    and High Capacitive Load ..... 195

    Conclusion ..... 196

6.3 Slew Rate ..... 198

6.4 Non-Linear Distortion ..... 200

    Conclusion ..... 205

6.5 Problems and Simulation Exercises ..... 205

    Problem 6.1 ..... 205

    Solution ..... 205

    Problem 6.2 ..... 206

    Solution ..... 207

    Problem 6.3 ..... 207

    Solution ..... 207

    Problem 6.4 ..... 208

    Solution ..... 208

    Problem 6.5 ..... 209

    Solution ..... 209

    Simulation Exercise 6.1 ..... 210

    Simulation Exercise 6.2 ..... 211

6.6 References ..... 211

<b>7. Design Examples</b> .....	213
Nine Overall Topologies.....	213
7.1 GA-CF Configuration .....	213
Operational Transconductance Amplifier.....	213
Folded-Cascode Operational Amplifier.....	215
Telescopic-Cascode Operational Amplifier .....	219
Feedforward HF Compensation.....	220
Input Voltage Compensation .....	221
Input Class-AB Boosting .....	223
Voltage-Gain Boosting.....	224
Conclusion .....	225
7.2 GA-GA Configuration.....	226
Basic Bipolar R-R-Out Class-A Operational Amplifier.....	226
Improved Basic Bipolar R-R-Out Class-A Operational Amplifier.....	228
Basic CMOS R-R-Out Class-A Operational Amplifier .....	229
Improved Basic CMOS R-R-Out Class-A Operational Amplifier .....	229
Conclusion .....	231
7.3 GA-CF-VF Configuration .....	231
High-Speed Bipolar Class-AB Operational Amplifier .....	231
High-Slew-Rate Bipolar Class-AB Voltage-Follower Buffer.....	234
Conclusion .....	235
7.4 GA-GA-VF Configuration .....	235
General Bipolar Class-AB Operational Amplifier with Miller Compensation .....	235
$\mu$ A741 Operational Amplifier with Miller Compensation .....	237
Conclusion .....	239
7.5 GA-CF-VF/GA Configuration .....	239
High-Frequency All-NPN Operational Amplifier with Mixed PC and MC.....	239
Conclusion .....	241
7.6 GA-GA-VF/GA Configuration.....	242
LM101 Class-AB All-NPN Operational Amplifier with MC .....	242
NE5534 Class-AB Operational Amplifier with Bypassed NMC.....	244
Precision All-NPN Class-AB Operational Amplifier with NMC .....	245
Precision HF All-NPN Class-AB Operational Amplifier with MNMC.....	246
1 GHz, All-NPN Class-AB Operational Amplifier with MNMC .....	249
2 V Power-Efficient All-NPN Class-AB Operational Amplifier with MDNMC.....	249
Conclusion .....	251
7.7 GA-CF-GA Configuration.....	251
Compact 1.2 V R-R-Out CMOS Class-A OpAmp with MC.....	252
Compact 2 V R-R-Out CMOS Class-AB OpAmp with MC.....	254
Compact 2 V R-R-In/Out CMOS Class-AB OpAmp with MC.....	256

- Compact 1.2 V R-R-Out CMOS Class-AB OpAmp with MC..... 259
- Conclusion ..... 261
- 7.8 GA-GA-GA Configuration..... 261
- 1 V R-R-Out CMOS Class-AB OpAmp with MNMC..... 261
- Compact 1.2 V R-R-Out BiCMOS Class-AB OpAmp  
with MNMC ..... 265
- Bipolar Input and Output Protection ..... 267
- 1.8 V R-R-In/Out Bipolar Class-AB OpAmp (NE5234)  
with NMC..... 267
- Conclusion ..... 271
- 7.9 GA-GA-GA-GA Configuration..... 271
- 1 V R-R-In/Out Bipolar Class-AB OpAmp with MNMC ..... 271
- 1.2 V R-R-Out CMOS Class-AB OpAmp with MHNMC..... 276
- Conclusion ..... 280
- 7.10 Problems and Simulation Exercises ..... 281
- Problem 7.1 ..... 281
- Solution ..... 281
- Problem 7.2 ..... 283
- Solution ..... 283
- Problem 7.3 ..... 284
- Solution ..... 284
- Problem 7.4 ..... 285
- Solution ..... 285
- Simulation Exercise 7.1..... 287
- Simulation Exercise 7.2..... 288
- 7.11 References..... 288
- 8. Fully Differential Operational Amplifiers ..... 291**
- 8.1 Fully Differential GA-CF Configuration..... 291
- Fully Differential CMOS OpAmp with Linear-Mode  
CM-Out Control..... 292
- Fully Differential Telescopic CMOS OpAmp with Linear-Mode  
CM-Out Control..... 294
- Fully Differential CMOS OpAmp with LTP CM-Out Control ..... 294
- Fully Differential GA-CF CMOS OpAmp with Output Voltage  
Gain Boosters ..... 295
- Fully Differential GA-CF CMOS OpAmp with Input-CM  
Feedback CM-Out Control..... 296
- Fully Differential CMOS OpAmp with R-R Buffered Resistive  
CM-Out Control..... 297
- 8.2 Fully Differential GA-CF-GA Configuration..... 299
- Fully Differential CMOS OpAmp with R-R Resistive  
CM-Out Control..... 299
- Conclusion ..... 301



8.3 Fully Differential GA-GA-GA-GA Configuration.....	302
Fully Differential CMOS OpAmp with Switched-Capacitor CM-Out Control.....	302
Conclusion .....	302
8.4 Problems and Simulation Exercises.....	303
Problem 8.1 .....	303
Solution .....	304
Problem 8.2 .....	305
Solution .....	305
Simulation Exercise 8.1.....	306
8.5 References .....	307
<b>9. Instrumentation Amplifiers and Operational Floating Amplifiers ....</b>	<b>309</b>
9.1 Introduction.....	309
9.2 Unipolar Voltage-to-Current Converter.....	311
Unipolar Single-Transistor V-I Converter.....	312
Unipolar OpAmp-Gain-Boosted Accurate V-I Converter.....	312
Unipolar CMOS Accurate V-I Converter .....	313
Unipolar Bipolar Accurate V-I Converter .....	314
Unipolar OpAmp Accurate V-I Converter .....	315
Conclusion .....	316
9.3 Differential Voltage-to-Current Converters.....	316
Differential Simple V-I Converter.....	316
Differential Accurate V-I Converter.....	317
Differential CMOS Accurate V-I Converter .....	318
9.4 Instrumentation Amplifiers.....	319
Instrumentation Amplifier (Semi) with Three OpAmps.....	319
Instrumentation Amplifier with a Differential V-I Converter for Input Sensing .....	320
Instrumentation Amplifier with Differential V-I Converters for Input and Output Sensing .....	322
Instrumentation Amplifier with Simple Differential V-I Converters for Input and Output Sensing.....	323
Instrumentation Amplifier Bipolar with Common-Mode Voltage Range Including Negative Rail Voltage.....	324
Instrumentation Amplifier CMOS with Common-Mode Voltage Range Including Negative Rail Voltage.....	325
Instrumentation Amplifier Simplified Diagram and General Symbol .....	326
Conclusion .....	327
9.5 Universal Class-AB Voltage-to-Current Converter Design	
Using an Instrumentation Amplifier .....	328
Universal V-I Converter Design with Semi-instrumentation Amplifier .....	328
Universal V-I Converter Design with Real Instrumentation Amplifier .....	329

- 9.6 Universal Class-A OFA Design ..... 331
  - Universal Class-A OFA Design with Floating Zener-Diode Supply . 331
  - Universal Class-A OFA Design with Supply Current Followers ..... 332
  - Universal Class-A OFA Design with Long-Tailed-Pairs ..... 333
  - Conclusion ..... 337
- 9.7 Universal Class-AB OFA Realization with Power-Supply
  - Isolation ..... 337
  - Universal Floating Power Supply Design ..... 338
  - Conclusion ..... 338
- 9.8 Universal Class-AB OFA Design..... 338
  - Universal Class-AB OFA Design with Total-Output-Supply-Current Equalization..... 339
  - Universal Class-AB OFA Design with Current Mirrors ..... 341
  - Universal Class-AB OFA Design with Output-Current Equalization..... 343
  - Universal Class-AB Voltage-to-Current Converter with Instrumentation Amplifier..... 344
  - Conclusion ..... 345
- 9.9 Problems ..... 345
  - Problem 9.1 ..... 345
  - Solution ..... 345
  - Problem 9.2 ..... 347
  - Solution ..... 348
  - Problem 9.3 ..... 348
  - Solution ..... 349
- 9.10 References..... 349

**10. Low Noise and Low Offset Operational and Instrumentation**

- Amplifiers** ..... 351
  - 10.1 Introduction ..... 351
  - 10.2 Applications of Instrumentation Amplifiers..... 352
  - 10.3 Three-OpAmp Instrumentation Amplifiers..... 354
  - 10.4 Current-Feedback Instrumentation Amplifiers ..... 355
  - 10.5 Auto-Zero OpAmps and InstAmps..... 358
  - 10.6 Chopper OpAmps and InstAmps ..... 361
  - 10.7 Chopper-Stabilized OpAmps and InstAmps ..... 366
  - 10.8 Chopper-Stabilized and AZ Chopper OpAmps and InstAmps .... 372
  - 10.9 Chopper Amplifiers with Ripple-Reduction Loop ..... 376
  - 10.10 Chopper Amplifiers with Capacitive-Coupled Input..... 382
  - 10.11 Gain Accuracy of Instrumentation Amplifiers ..... 389
  - 10.12 Summary Low Offset..... 396
  - 10.13 References ..... 397

- Biography** ..... 399

- Index** ..... 401



# Summary

This 2nd edition has two main additions: a chapter on low-offset amplifiers and a part on frequency compensation at high capacitive loads. Furthermore many improvements have been made.

A systematic circuit design of operational amplifiers is presented. It is shown that the topology of all operational amplifiers can be divided in nine main overall configurations. These configurations range from one gain stage up to four or more gain stages. Many famous designs are completely evaluated.

High-frequency compensation techniques are presented for all nine configurations even at high capacitive loads. Special focus is on low-power low-voltage architectures with rail-to-rail input and output ranges.

An additional chapter on systematic design of  $\mu\text{V}$ -offset operational amplifiers and precision instrumentation amplifiers by applying chopping, auto-zeroing, and dynamic element-matching techniques has been added.

The design of fully differential operational amplifiers and operational floating amplifiers is being developed. Also, the characterization of operational amplifiers by macromodels and error matrices is presented, together with measurement techniques for their parameters.

Problems and simulation exercises have been supplied for self-evaluation.



# Introduction

The goal of this book is to equip the circuit designer with a proper understanding of the theory and design of operational amplifiers (OpAmps). The core of the book presents the systematic design of operational amplifiers. All operational amplifiers can be classified into a periodic system of nine main overall configurations. This division enables the designer to quickly recognise, understand, and choose optimal configurations.

Chapter 1 defines four basic types of operational amplifiers on the basis of the external ground connections of the input and output ports of generalized linear active network elements. Whether an input or output port needs to be isolated from ground has a big impact on the circuit design of the input and output stages, as will be shown in later chapters.

A complete set of linear parameters, by which each of the above four basic types of operational amplifiers can be quantified, is given in Chapter 2. This provides the reader with a sense of which parameters are most important. Chapter 2 also presents macromodels and measurement techniques for OpAmp parameters.

A systematic treatment of sources of errors in important applications of the above four basic types of operational amplifiers is presented in Chapter 3.

Input stages are evaluated in Chapter 4. Important aspects such as bias, offset, noise, and common-mode rejection are considered. Low-voltage input stages with a rail-to-rail input voltage range are extensively discussed.

A classification of push-pull output stages is presented in Chapter 5. Three possible topologies are explored: voltage follower stages, compound stages, and rail-to-rail general amplifier stages. Designs are presented with feedforward and feedback biasing class-AB techniques. Emphasis is on voltage and current efficiency.

A classification of operational amplifiers into nine main overall configurations is presented in Chapter 6. The classification consists of two two-stage OpAmps, six three-stage OpAmps, and one four- or multi-stage OpAmp. High-frequency compensation techniques are developed for all configurations ranging from one gain stage up to four or more gain stages. Methods are presented for obtaining a maximum

bandwidth over power ratio for certain high capacitive load conditions. Slew-rate and distortion are also considered.

Chapter 7 presents design examples of each of the nine main configurations. Many well-known OpAmps are fully elaborated. Among them are simple CMOS OpAmps, high-frequency bipolar OpAmps, Precision bipolar and BiCMOS OpAmps, low-voltage CMOS and bipolar OpAmps, and OpAmps with a high output drive capability in CMOS as well as in BiCMOS technology.

The design of fully differential operational amplifiers with common-mode feedback is developed in Chapter 8. Special focus is on low-voltage architectures.

When the output port as well as input port are designed such that they are both isolated from ground, the most universal linear active network element is created: the operational floating amplifier. The concept of this OpAmp gives the designer the freedom to work with current signals as well as voltage signals. Realizations of operational floating amplifiers are developed in Chapter 9 also in relation to instrumentation amplifiers.

An additional Chapter 10 has been added on the systematic design of  $\mu\text{V}$ -offset operational amplifiers and precision instrumentation amplifiers by applying chopping, auto-zeroing, and dynamic element-matching techniques.

Problems and simulation exercises have been supplied for most of the chapters to facilitate self-evaluation of the understanding and design skills of the user of this book.

# Notation

<i>OpAmp</i>	operational amplifier
<i>OA</i>	operational amplifier
<i>OIA</i>	operational inverting amplifier
<i>OVA</i>	operational voltage amplifier
<i>OCA</i>	operational current amplifier
<i>OFA</i>	operational floating amplifier
<i>GA</i>	general amplifier stage
<i>VF</i>	voltage follower stage
<i>CF</i>	current follower stage
<i>CM</i>	current mirror stage
<i>IA</i>	instrumentation amplifier
<i>a</i>	temperature coefficient
$A_v$	voltage gain
$A_{vo}$	DC voltage gain
$\beta$	current gain of bipolar transistor
$B_v$	voltage attenuation of feedback network
<i>C</i>	capacitor value
<i>Ch</i>	Chopper
$C_{ox}$	specific capacitance of gate oxide
$C_M$	Miller capacitor value
$C_P$	parallel capacitor value
<i>D</i>	distortion
<i>f</i>	frequency
$f_T$	transit frequency of a transistor
$f_o$	zero-dB frequency
$g_m$	transconductance of a transistor
<i>i</i>	small-signal current
<i>I</i>	current
$I_B$	bias current
$I_C$	collector current



$I_D$	drain current
$I_E$	emitter current
$I_S$	supply current
$I_Q$	quiescent current
$k$	Boltzman's Constant $K = \mu C_{ox} W/L$
$L$	length of gate in MOS transistors
$M$	CMOS transistor
$R$	resistor value
$S$	signal
$S$	switch
$S_r$	slew rate
$T$	generalized transistor
$Q$	bipolar transistor
$v$	small-signal voltage
$V$	voltage
$V_B$	bias voltage
$V_{CC}$	positive supply voltage with bipolar transistors
$V_{DD}$	positive supply voltage with MOS transistors
$V_{EE}$	negative supply voltage with bipolar transistors
$V_G$	generator voltage
$V_{GS}$	gate-source voltage
$V_{GT}$	active gate-source voltage ( $V_{GS} - V_{TH}$ )
$V_S$	total-supply voltage
$V_{SN}$	negative supply voltage
$V_{SP}$	positive supply voltage
$V_{SS}$	negative supply voltage with MOS transistors
$V_T$	thermal voltage $kT/q$
$V_{TH}$	threshold voltage of MOS device
$W$	width of gate in MOS transistors
$\mu$	mobility of charge carriers

## Extrinsic device parameters

$R_L$
$C_L$
$C_M$
$R_D R_C$
$R_G R_B$
$R_S R_E$

**Intrinsic Small-signal transistor parameters** $r_{ds} r_{ce} r_o$  $r_{gs} r_{be}$  $r_s r_e$  $c_{ds} c_{ce}$  $c_{gs} c_{be}$  $g_m g_m$  $\mu_n \mu_p$  $\beta_n \beta_p$



# 1. Definition of Operational Amplifiers

## Nullor Concept

In 1954 Tellegen introduced the concept of a universal active network element under the name of “ideal amplifier” [1.1]. The name “nullor”, generally accepted now, was given to it by Carlin in 1964 [1.2]. The symbol of a nullor is shown in Fig. 1.1.

The nullor is defined as a two-port network element whose ports are called input and output ports and whose input voltage  $V_i$  and input current  $I_i$  are both zero, so:

$$\begin{aligned} V_i &= 0, \\ I_i &= 0 \end{aligned} \tag{1.1}$$

The nullor concept only has significance if a passive network external to the nullor provides for a feedback from the output port into the input port [1.3]. The output voltage  $V_o$  and the output current  $I_o$  will be determined by the passive network elements in such a way that the input requirements  $V_i = 0, I_i = 0$  are satisfied.

An accurate signal transfer requires, firstly, accurate passive components and secondly, a practical nullor realization which approximates  $V_i = 0, I_i = 0$ .

This implies that the nullor realization should have a high gain, a low input noise, and low offset voltage and current (see Sect. 2.1). All linear and non-linear

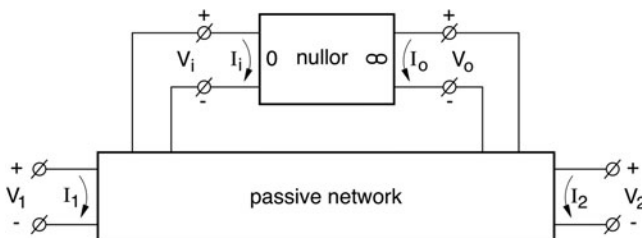


**Fig. 1.1** A two-port network composed of a passive network and a nullor

analog transfer functions can be implemented with nullor realizations and passive components.

## Classification Based on Number of Floating Ports

We will now classify four nullor types on the basis of the number of ports which are floating, beginning with both ports grounded and ending with both ports floating. There are two main reasons for this kind of classification. Firstly, the larger the number of ports which are grounded the simpler the construction of the active device will be. Secondly, the larger the number of grounded ports the lower the number of possible feedback topologies will be allowed.

We will give each of the four nullor types a name which will be explained later. The first one with two grounded ports will be called operational inverting amplifier (OIA). The second one with the input port floating and output port grounded will be called operational voltage amplifier (OVA). The third one with the input port grounded and output port floating will be called operational current amplifier (OCA). Finally, the fourth one with both ports floating will be called operational floating amplifier (OFA). The adjective “operational” was coined by John R. Ragazzini and his colleagues in a paper [1.4] published in 1947. That paper described the basic properties of an OIA used with linear and nonlinear feedback. The adjectives “inverting” (I), “voltage” (V), “current” (C), or “floating” (F), are given by the present author to distinguish the four types of Operational Amplifiers according to their most striking attribute, as we will see in the next sections of this chapter. The most popular one, the OVA will be shortened to OpAmp in most parts of this book, where the distinction between the different types is not needed.

### 1.1 Operational Inverting Amplifier

A practical approximation of a nullor having both ports grounded will be called an “operational inverting amplifier” (OIA). The grounded input port makes the construction of the input stage relatively easy, because it only needs to function at one voltage level [1.4, 1.5]. Similarly, the grounded output port makes it relatively easy to construct an output stage having a high power efficiency, because the current return path can be directly connected to the grounded supply voltages. The negative sign (inverting) of the amplification factor makes it possible to obtain stable negative feedback with passive components connected directly from the output to the input port. The parallel connection of the feedback circuit at the input and output of the amplifier results in a low virtual entrance impedance (see Sect. 3.1), suitable for accurate current sensing at virtual zero input power, and a low exit impedance, suitable for obtaining an accurate output voltage. The simplest realization is a differential transistor pair.

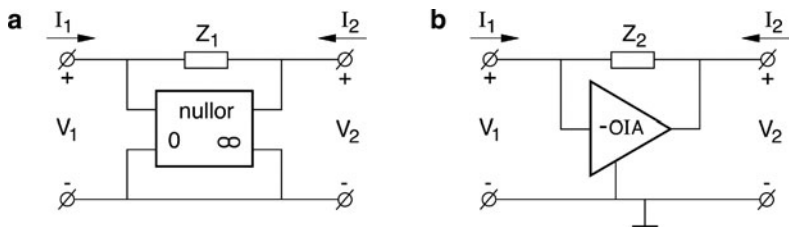


Fig. 1.1.1 Transimpedance amplifier (a) with a nullor symbol and (b) with an OIA symbol

### Current-to-Voltage Converter

The most simple application of an OIA is the transimpedance amplifier or current-to-voltage transactor. This circuit is shown in Fig. 1.1.1a with a symbol of a nullor and in Fig. 1.1.1b with a practical symbol of an OIA.

The current-to-voltage transfer factor

$$Z_t = V_2/I_1 = -Z_1, \quad \text{at } V_1 = 0 \tag{1.1.1}$$

can be accurately determined by  $-Z_1$  if the OIA satisfies two requirements: firstly, a high gain, and secondly, a low input offset voltage and offset current. A high gain also assures low entrance and exit impedances.

## 1.2 Operational Voltage Amplifier

A practical nullor approach having only the output port grounded and the input port floating [1.6, 1.7] will be called “operational voltage amplifier” (OVA) or OpAmp. Currently, it is the most widely applied universal active device. The floating character of the input port imposes special demands on the construction of the input circuit, as will be discussed in Sects. 4.3 and 4.4. The floating input port allows series coupling of negative feedback.

This results in a high entrance impedance suitable for accurate voltage sensing at virtual zero input power. The parallel coupling of the feedback network with the grounded output port assures a low exit impedance.

### Non-Inverting Voltage Amplifier

The most essential application of the OVA is the non-inverting voltage amplifier or voltage-to-voltage transactor. The circuit is drawn in Fig. 1.2.1a with a nullor symbol and in Fig. 1.2.1b with a practical amplifier symbol for an OVA.

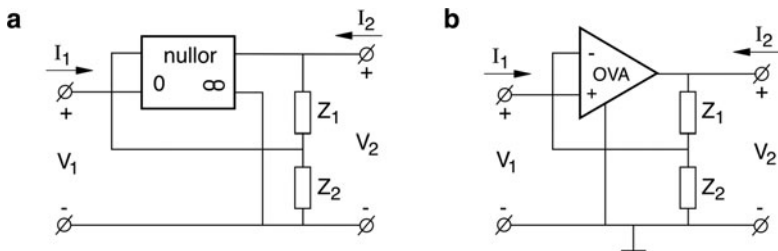


**Fig. 1.2.1** Voltage amplifier (a) with a nullor symbol and (b) with an OVA symbol

The voltage amplification factor

$$A_u = V_2/V_1 = (Z_1 + Z_2)/Z_2, \quad \text{at } I_1 = 0 \quad (1.2.1)$$

can be accurately determined by the impedance ratio  $(Z_1 + Z_2)/Z_2$  if the OVA satisfies the requirements: a high gain, a low input offset voltage and current, independent of the common-mode voltage of the input port, and a low input bias current. A high gain assures a high entrance impedance and a low exit impedance.

### ***Voltage Follower***

A special situation occurs if the OVA has its negative input terminal connected with the output terminal. We will call such a device a “voltage follower” (VF), because the exit voltage follows the entrance voltage. The construction of a universal active device with this connection may be simpler than without this connection, because no voltage shifting is required between the input and output. The VF circuit is given in Fig. 1.2.2b with an OVA symbol.

The voltage follower has the unique property that the voltage amplification factor

$$A_u = V_2/V_1 = 1 \quad \text{at } I_1 = 0 \quad (1.2.2)$$

precisely equals plus unity, independently of any passive components, if the amplifier satisfies the three requirements: high gain, low input offset voltage and current, and a low input bias current. The accuracy of the plus-unity voltage transfer is not limited by the tolerances of any passive components. Note that the accuracy of the minus-unity voltage transfer of a voltage inverter does depend on the tolerance of a ratio of two impedances, as shown in Sect. 3.1, Fig. 3.1.2.

The voltage follower uses the most important attribute of a floating input port, viz. that the potential at one input terminal precisely follows the potential at the other input terminal.

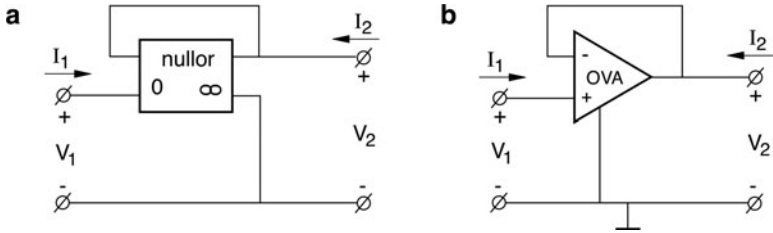


Fig. 1.2.2 Voltage follower (a) with a nullor symbol and (b) with an OVA symbol

### 1.3 Operational Current Amplifier

A nullor approximation which has only the input port grounded and the output port floating [1.8] will be called an “operational current amplifier” (OCA). An output port with a floating character is difficult to construct, as we will see in Chap. 9. However, this labour is rewarded for applications requiring a high output impedance by using feedback in series coupling with the output port. This series feedback results in an exit with a current-source character, while the grounded input port with parallel feedback assures a low entrance impedance.

#### *Current Amplifier*

The most elementary application of the OCA is a current amplifier, whose circuit is shown in Fig. 1.3.1b with an OCA symbol. The amplifier is the current dualogon of the voltage amplifier of Fig. 1.3.1b. The amplification factor

$$A_1 = -I_2/I_1 = -(Y_1 + Y_2)/Y_1, \quad \text{at } V_1 = 0, \quad (1.3.1)$$

is accurately determined by the admittance ratio  $(Y_1 + Y_2)/Y_1$  if the amplifier satisfies: a high gain, a low input offset voltage and current, and an output port

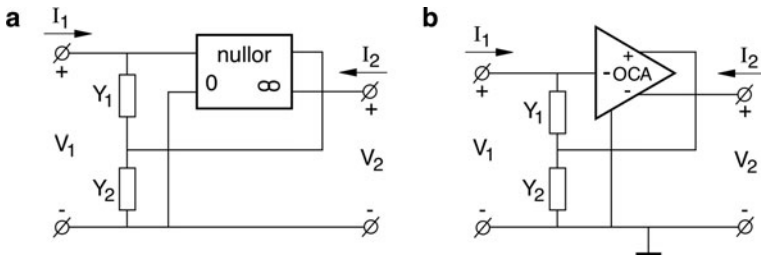


Fig. 1.3.1 Current amplifier (a) with a nullor symbol and (b) with an OCA symbol



with a low output bias current, because this current is directly added to the output. Note, that the minus sign merely results from the choice of the opposite current notations of  $I_1$  and  $I_2$ . The low entrance impedance allows current sensing at a low entrance voltage  $V_1$ .

The current source character at the exit yields an accurate current transfer independently of the load impedance.

### ***Current Follower***

A special situation occurs if the negative input terminal of the OCA is connected with the output terminal. We will call such a configuration a “current follower” (CF), because the exit current follows the entrance current. This circuit is the current dualogon of the voltage follower. The circuit is drawn in Fig. 1.3.2a with a nullor symbol and in Fig. 1.3.2b with an OCA symbol.

The current follower has the unique attribute that the current amplification factor

$$A_i = -I_2/I_1 = 1, \quad \text{at } V_1 = 0, \quad (1.3.2)$$

precisely equals plus unity, independently of any passive component values, if the gain is high, the input offset voltage and current is low, and if the output port has a low bias current. In contrast, the current-amplification factor of a current mirror, which nominally is minus unity, does depend on the matching of two passive elements (see Sect. 3.4).

Note that the minus sign in Eq. 1.3.2 is needed because the output current  $I_2$  is defined in the opposite direction regarding  $I_2$ , when the current is being transferred through the CF.

The current-follower action reveals the most important attribute of a floating output port, namely that the current which flows into one output terminal is precisely followed by the current which flows out of the other output terminal. This attribute is the very dualogon of the voltage-follower action of a floating input port.

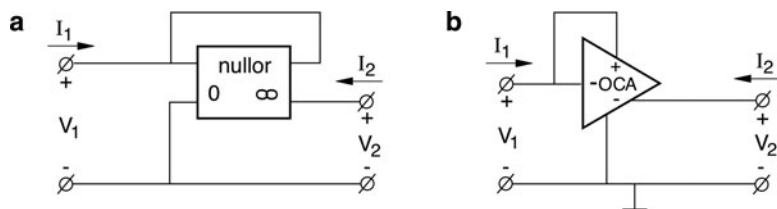


**Fig. 1.3.2** Current follower (a) with a nullor symbol and (b) with an OCA symbol

### 1.4 Operational Floating Amplifier

A nullor approximation which has both the input and the output ports floating [1.9] will be called an “operational floating amplifier” (OFA) [1.8, 1.9]. Earlier it was called a “monolithic nullor” [1.10], or second generation current conveyer [1.11]. The construction of such a universal active device combines the demands of both floating input and output ports.

The OFA provides the maximum freedom for composing feedback configurations. With simple passive components it is possible to apply negative feedback in series with input and output ports, which results in both a high entrance and exit impedance.

#### Voltage-to-Current Converter

A specific application of the OFA is the voltage-to-current converter or transadmittance amplifier. Such a circuit is shown in Fig. 1.4.1a with a nullor symbol and in Fig. 1.4.1b with a practical OFA symbol.

$$Y_t = I_2/V_I = Y_I, \quad \text{at } I_1 = 0 \tag{1.4.1}$$

will be accurately determined by one admittance  $-Y_I$  if the amplifier satisfies four requirements: high gain, low input offset voltage and current, low input bias current, and low output bias current. The negative feedback in series with both ports ensures a high entrance impedance and a high exit impedance, which gives the transactor a voltage-sensing entrance and a current-source exit character.

#### Voltage and Current Follower

In fact, the transadmittance amplifier of Fig. 1.4.1a, b does not apply all potentialities of the OFA. It is applied in the special case in which the lower terminal of the

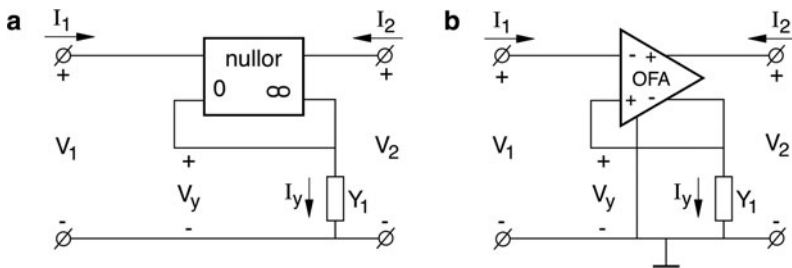


Fig. 1.4.1 Transadmittance amplifier (a) with a nullor symbol and (b) with an OFA symbol

input port is connected with the lower terminal of the output port. This connection may simplify the construction of the OFA, because no voltage level shifter is needed between the input circuit and one output terminal, as we will see in Sect. 9.2. An OFA with this connection can be called a “voltage and current follower” (VCF).

A nullor which has this connection is also called a “three-terminal nullor” or a “unitor” [1.12]. In Fig. 1.4.1b the VCF firstly acts like a voltage follower, accurately transferring the entrance voltage  $V_I$  towards the voltage  $V_y$  on the upper side of the admittance  $Y_I$ , and secondly like a current follower, accurately transferring the current  $I_y$  through the admittance  $Y_I$  towards the current  $I_2$  at the upper exit terminal.

## 1.5 Conclusion

A classification of universal active devices has been given on the basis of the number of ports which are connected to ground or to each other. The more ports not internally connected, the more freedom there is in the choice of the feedback configuration although this creates more complications with the construction of the device. Figure 1.5.1 presents an overview of the four types of active devices with different grounding schemes while Fig. 1.5.2 gives the three types of followers with one interconnection between the ports.

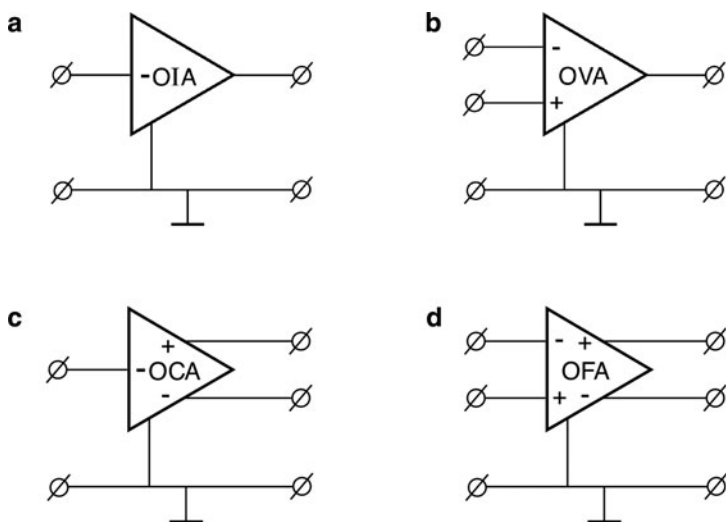


**Fig. 1.5.1** (a) Operational inverting amplifier (OIA), (b) operational voltage amplifier (OVA) or OpAmp, (c) operational current amplifier (OCA) and (d) operational floating amplifier (OFA)

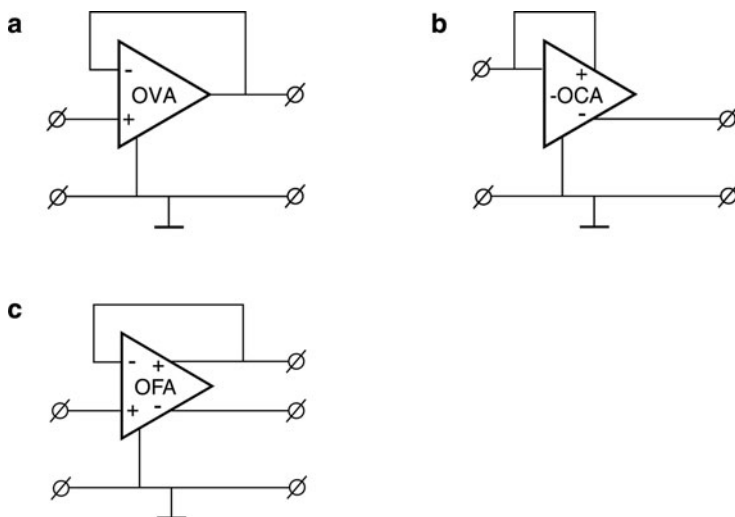


**Fig. 1.5.2** (a) Voltage follower (VF) with an OVA symbol, (b) current follower (CF) with an OCA symbol and. (c) voltage and current follower (VCF) with an OFA symbol

Four transfer functions are particularly suited to accurate signal transfer. They can be implemented with the four basic types of active devices:

- Current-to-voltage converter with an OIA
- Voltage-to-voltage converter with an OVA
- Current-to-current converter with an OCA
- Voltage-to-current converter with an OFA

In the ideal case, their signal transfer is independent of the source and load impedances. Moreover, the signal transfer depends on the theoretical minimum number of passive components.

Three transfer functions have the unique attribute that their accuracy is independent of any passive components. These types are:

- Voltage follower (VF) with an OVA
- Current follower (CF) with an OCA
- Voltage and current follower (VCF) with an OFA

If each of these seven types of functions were realized with nullor approximations which do not have the right ports floating, a larger number of passive components and/or active devices is needed. Such realizations are less accurate and usually more expensive than the realizations with the right kind of active devices.

The requirements to be satisfied by the universal active devices are:

1. high gain, with a stable high-frequency close-loop feedback behavior,
2. low input offset and noise voltage and current,

3. when a floating input port is needed, a low input bias current,
4. when a floating output is needed, a low output bias current.

It is remarkable that the grades of perfection of the four requirements mentioned have no absolute limits. This means that there is a large area of technical exploration present for the design of active electronic building blocks.

## 1.6 References

- [1.1]. B.D.H. Tellegen, La recherche pour une serie complete d'elements de circuit ideaux non-lineaires. Rend. Sem. Mat. Fis. Milano **25**, 134–144 (1954)
- [1.2]. H.J. Carlin, Singular network elements. IEEE Trans. Circ. Theory **CT-11**, 67–72 (1964)
- [1.3]. B.D.H. Tellegen, On nullators and norators. IEEE Trans. Circ. Theory **CT-13**, 466–469 (1966)
- [1.4]. J.R. Ragazzini et al., Analysis of problems in dynamics by electronic circuits. Proc. IRE **35**, 444–452 (1947)
- [1.5]. G.A. Korn, F.M. Korn, *Electronic Analog and Hybrid Computers* (McGraw Hill Book Company, New York, 1964)
- [1.6]. J.G. Graeme et al., *Operational Amplifiers, Design and Applications* (McGraw Hill Book Company, New York, 1971)
- [1.7]. J.G. Graeme, *Applications of Operational Amplifiers, Third Generation Techniques* (McGraw Hill Book Company, New York, 1973)
- [1.8]. J.H. Huijsing, Operational floating amplifier. IEE Proc. **137**(2), 131–136 (1990)
- [1.9]. J.H. Huijsing, Design and applications of the operational floating amplifier (OFA): the most universal operational amplifier. J. AICSP **4**, 115–129 (1993)
- [1.10]. J.H. Huijsing, J. de Korte, Monolithic nullor – a universal active network element. IEEE J. Solid-St. Circ. **SC-12**, 59–64 (1977)
- [1.11]. A.S. Sedra, K.C. Smith, A second generation current conveyer and its applications. IEEE Trans. **CT-17**, 132–134 (1970)
- [1.12]. A.W. Keen, A topological nonreciprocal network element. Proc. IRE **47**, 1148–1150 (1959)

## 2. Macromodels

The qualities of the universal active devices mentioned in Chap. 1 can be specified by their macromodels or equivalent circuits and by transfer matrices. These representations should contain all elements for quantifying the four qualities of gain, offset, and if applicable, the bias current of input and output ports. Macromodels may also include the HF parameters and non-linear effects.

The first four sections of this chapter contain only a linear representation of the macromodels of the four types of OpAmps. The elements may include a complex description to include the HF behavior.

Non-linear behavior will be represented by SPICE macromodels for OpAmps in Sect. 2.5.

Measurement techniques for Operational Amplifiers are discussed in Sect. 2.6.

### 2.1 Operational Inverting Amplifier

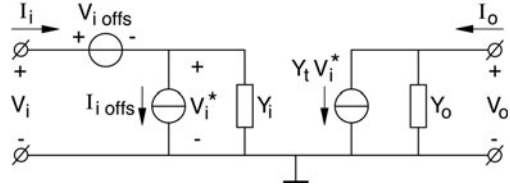
The operational inverting amplifier is a three-terminal network in which one terminal is grounded. The equivalent circuit of Fig. 2.1.1 contains all elements of a uni-lateral driven source. The simplest uni-directional realization is a single transistor.

#### *Definition of: Offset Voltage and Current, Input and Output Impedance, Transconductance*

For the purpose of standardization, all elements are chosen such that the currents at the terminals can be expressed in the voltages at the terminals. Thus, most elements are admittances. The main element is a voltage-controlled current source with a transadmittance  $Y_r$ .

Together with the input admittance  $Y_i$  and output admittance  $Y_o$ , these three admittances form the essential ingredients of an active device. The admittances may be taken as a Laplace transform to represent the high-frequency response.

**Fig. 2.1.1** Equivalent circuit of an operational inverting amplifier (OIA)



No elements are added to represent internal feedback because of the reasonable simplification that a universal active device with more than one internal cascaded amplifier stage is unilateral. And if there is internal feedback, for instance by heat transfer on the chip, this should be considered separately.

An offset voltage source  $V_{i\text{offs}}$  and an offset current source  $I_{i\text{offs}}$  have been added on the input side. They represent all additive DC errors of the device. In addition, they may include all noise quantities. The input voltage after subtraction of the offset voltage has been denoted by  $V_i^*$  (with asterisk).

The errors of an active device application directly follow from the deviations from the input requirements  $V_i = 0$  and  $I_i = 0$ . For that reason, we will choose a mathematical description of the device which directly produces the deviation from the ideal behavior. Such a description for each of the different kinds of devices will be called an error matrix. In the case of an OIA, being a two-port element, the error matrix is equal to the following chain matrix:

$$\begin{vmatrix} V_i \\ I_i \end{vmatrix} = \begin{vmatrix} 1/Y_t & Y_o/Y_t \\ Y_i/Y_t & Y_i Y_o/Y_t \end{vmatrix} \begin{vmatrix} I_o \\ V_o \end{vmatrix} + \begin{vmatrix} V_{i\text{offs}} \\ I_{i\text{offs}} \end{vmatrix} \quad (2.1.1)$$

The error matrix clearly shows the requirements to be met by the OIA.

Firstly, a high transadmittance  $Y_t$  is needed. This also includes a high voltage amplification factor  $A_v = -Y_t/Y_o$  and a high current amplification factor  $A_i = Y_t/Y_i$ . Secondly, the input offset voltage  $V_{i\text{offs}}$  and current  $I_{i\text{offs}}$  should be low, and so should be the spectral input noise voltage  $V_{in}$  and current  $I_{in}$ , which denote the noise components of the offset quantities.

## 2.2 Operational Voltage Amplifier

The operational voltage amplifier is a four-terminal network of which one terminal is grounded. An equivalent circuit is drawn in Fig. 2.2.1. For an adequate description of the floating character of the input port we should distinguish the differential-mode (DM) input voltage  $V_{id} = V_{i1} - V_{i2}$  and current  $I_{id} = (I_{i1} - I_{i2})/2$  from the common-mode (CM) input voltage  $V_{ic} = (V_{i1} + V_{i2})/2$  and current  $I_{ic} = (I_{i1} + I_{i2})/2$ . The simplest realization is a differential transistor pair with a common tail current source.

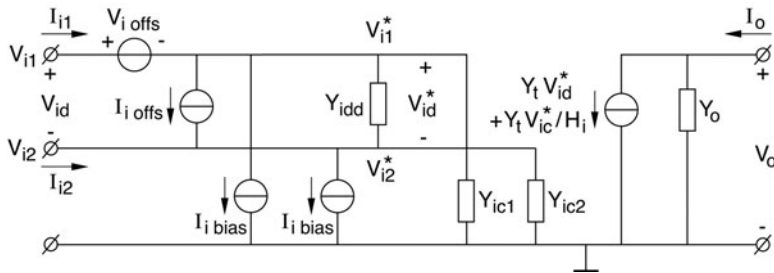


Fig. 2.2.1 Equivalent circuit of an operational voltage amplifier (OVA)

### **Definition of: Input Bias Current, Input Common-Mode Rejection Ratio**

The basic three elements, the admittances  $Y_t$ ,  $Y_{idd}$  and  $Y_o$ , are the normal ones in each active device. They have already been discussed along with the equivalent circuit of the OIA. In addition, there are the common-mode input admittances  $Y_{ic1}$  and  $Y_{ic2}$  and two common-mode input bias-current sources with an equal value  $I_{ibias}$ . Furthermore, the CM input voltage  $V_{ic}^*$  causes an output current  $V_{ic}^* Y_t / H_i$  in addition to the current  $V_{id}^* Y_t$  of the main voltage-controlled current source. This is the result of a crosstalk of the CM input voltage  $V_{ic}^*$  on the DM input voltage  $V_{id}^*$ . The factor  $H_i$  is called the “common-mode rejection ratio” (CMRR)  $H_i = (\delta V_{ic}^* / \delta V_{id}^*)_{I_o, V_o}$ . The reciprocal factor  $1/H_i$  can be called the “common-mode crosstalk ratio” (CMCR). All these additional elements show the non-ideal floating character of the input port.

The main errors of an OVA are quantified by the following error matrix (2.2.1):

$$\begin{vmatrix} V_{id} \\ I_{id} \\ I_{ic} \end{vmatrix} = \begin{vmatrix} 1/Y_t & Y_o/Y_t & 1/H_i \\ Y_{id}/Y_t & Y_{id}Y_o/Y_t & Y_{id}/H_i \\ \cdot & \cdot & Y_{ic} \end{vmatrix} \begin{vmatrix} I_o \\ -V_o \\ V_{ic}^* \end{vmatrix} + \begin{vmatrix} V_{ioffs} \\ I_{ioffs} \\ I_{ibias} \end{vmatrix} \quad (2.2.1)$$

with :  $V_{id} = V_{i1} - V_{i2}$

$$V_{ic} = (V_{i1} + V_{i2})/2$$

$$I_{id} = (I_{i1} - I_{i2})/2$$

$$I_{ic} = (I_{i1} + I_{i2})/2$$

$$Y_{id} \simeq Y_{idd}$$

$$Y_{ic} = (Y_{ic1} - Y_{ic2})/2$$

$$V_{ic}^* = V_{ic} - V_{ioffs}/2 \simeq V_{ic}$$

The four elements in the upper-left part of the matrix represent the basic description of any controlled source, as discussed along with the OIA. The right-hand part



of the matrix contains all errors caused by the non-ideal floating character of the input port. An OVA should have a high value of the CMRR  $H_i$  and a low input admittance  $Y_{ic}$ . The dots in the matrix represent normally negligible effects.

Finally, the input bias current  $I_{ibias}$ , which is also a result of the non-ideal isolating or floating character of the input port should be low and is placed in the separate column of additive error sources.

### 2.3 Operational Current Amplifier

The operational current amplifier is a four-terminal device in which one input terminal is grounded. An equivalent circuit is shown in Fig. 2.3.1. The floating character of the output port can best be emphasized by distinguishing the differential-mode output voltage  $V_{od} = V_{o1} - V_{o2}$  and current  $I_{od} = (I_{o1} - I_{o2})/2$  from the common-mode output voltage  $V_{oc} = (V_{o1} + V_{o2})/2$  and current  $I_{oc} = (I_{o1} + I_{o2})/2$ . The simplest realization is a differential transistor pair with a common tail current source.

#### ***Definition of: Output Bias Current, Output Common-Mode Current Rejection Ratio***

In addition to the elements of an OIA, the equivalent circuit contains the elements which express the parasitic liaisons between the output port and ground. Firstly, there are the common-mode output admittances  $Y_{oc1}$  and  $Y_{oc2}$ . Secondly, we have two output bias sources with an equal value  $I_{obias}$ . Thirdly, these bias currents are modulated as a function of the input voltage  $V_i^*$  with a transconductance  $Y_t/H_o$ .

The quantity  $H_o$  will be defined as the output common-mode current rejection ratio (CMCRR) for the output currents. The reciprocal quantity  $1/H_o$  will be called the output common-mode current crosstalk ratio (CMCCR). It describes the current crosstalk of a DM output current  $I_{od} = V_i^* Y_t$  on the CM output current  $I_{oc} = V_i Y_t/H_o$

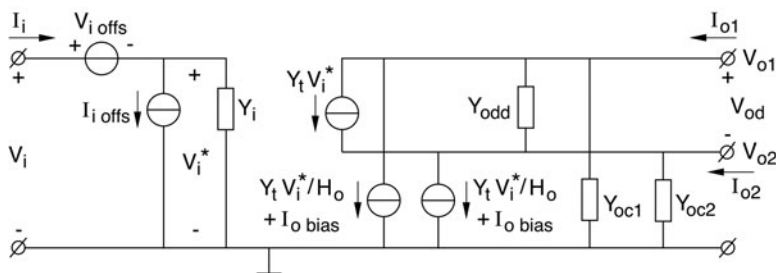


Fig. 2.3.1 Equivalent circuit of an operational current amplifier (OCA)

at  $V_{od} = V_{oc} = 0$ . The CMCRR for output currents is dual in regard to the CMRR for input voltages.

The main errors are quantified in the following error matrix (2.3.1):

$$\begin{vmatrix} V_i \\ I_i \\ I_{oc} \end{vmatrix} = \begin{vmatrix} 1/Y_t & Y_{od}/Y_t & \cdot \\ Y_i/Y_t & Y_i Y_{od}/Y_t & \cdot \\ 1/H & Y_{od}/H_o & Y_{oc} \end{vmatrix} \begin{vmatrix} I_{od} \\ -V_{od} \\ V_{oc} \end{vmatrix} + \begin{vmatrix} V_{ioffs} \\ I_{ioffs} \\ I_{ibias} \end{vmatrix} \quad (2.3.1)$$

with :

$$V_{od} = V_{o1} - V_{o2}$$

$$I_{od} = (I_{o1} - I_{o2})/2$$

$$V_{oc} = (V_{o1} + V_{o2})/2$$

$$I_{oc} = (I_{o1} + I_{o2})/2$$

$$Y_{od} \simeq Y_{odd}$$

$$Y_{oc} = (Y_{oc1} + Y_{oc2})/2$$

Again, the four elements in the upper-left part of the matrix represent the errors of any controlled source, as described along with the OIA. The elements of the lower row represent the non-ideal floating character of the output port. An OCA should have a high CMCRR  $H_o$  and a low CM output admittance  $Y_{oc}$ . Moreover, the output bias current  $I_{obias}$  must be placed in the column of additive error sources. The dots in the matrix stand for negligible effects.

## 2.4 Operational Floating Amplifier

The operational floating amplifier is a five-terminal network in which one terminal is grounded. An equivalent circuit is shown in Fig. 2.4.1. The floating character of the input and output ports can best be expressed by distinguishing DM and CM input and output voltages and currents, as was done with the OVA and OCA.

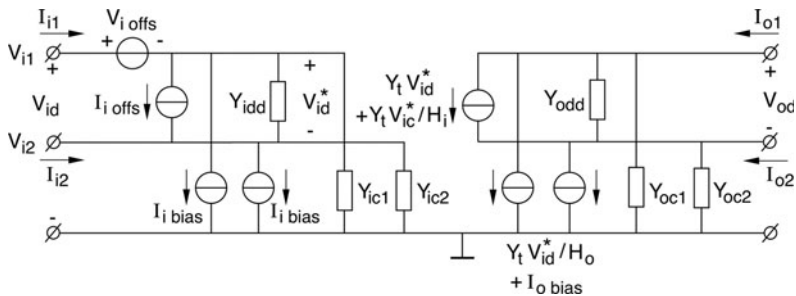


Fig. 2.4.1 Equivalent circuit of an operational floating amplifier (OFA)

## Using All Definitions

The equivalent circuit contains all elements of a driven source:

$Y_t V_{id1}^*$ ,  $Y_{idd}$  and  $Y_{odd}$ , the offset sources  $V_{ioffs}$  and  $I_{ioffs}$ ; all elements which represent the liaisons of the input port with the common ground:  $Y_{ic1}$ ,  $Y_{ic2}$ ,  $I_{ibias}$  ( $2x$ ) and  $V_{ic}^* Y_t / H_i$ ; and all elements which have the same function for the output port:  $Y_{oc1}$ ,  $Y_{oc2}$ ,  $I_{obias}$  ( $2x$ ) and  $V_{id}^* Y_t / H_o$  ( $2x$ ). These elements have been discussed with the OIA, OVA, and OCA. The simplest realization is a differential transistor pair with a common tail current source.

$$\begin{pmatrix} V_{id} \\ I_{id} \\ I_{ic} \\ I_{oc} \end{pmatrix} = \begin{pmatrix} 1/Y_t & Y_{od}/Y_t & 1/H_i & \cdot \\ Y_{id}/Y_t & Y_{id}Y_{od}/Y_t & Y_{id}/H_i & \cdot \\ \cdot & \cdot & Y_{ic} & \cdot \\ 1/H_o & Y_{od}/H_o & \cdot & Y_{oc} \end{pmatrix} \begin{pmatrix} I_{od} \\ -V_{od} \\ V_{ic}^* \\ V_{oc} \end{pmatrix} + \begin{pmatrix} V_{ioffs} \\ I_{ioffs} \\ I_{ibias} \\ I_{obias} \end{pmatrix} \quad (2.4.1)$$

The errors of the OFA are quantified by the error matrix (2.4.1):

The four elements in the upper-left part of the matrix represent the errors of any controlled source as discussed along with the OIA. The elements of the third column represent the non-ideal floating character of the input port, described along with the OVA, while the elements of the fourth row do the same with regard to the output port, described along with the OCA. The elements in the additional row represent all offset and bias sources. The dots in the matrix stand for negligible effects.

## 2.5 Macromodels in SPICE

In Sects. 2.1–2.4 we have presented linear circuit models for the four Operational Amplifier types OIA, OVA, OCA, and OFA. These are theoretically correct but not always practical. The main practical shortcoming is the lack of non-linear behavior description. It is desirable for shortening the simulation time in SPICE simulations of large systems with many Operational Amplifiers, to have relatively simple macromodels, which nevertheless do take into account the non-linear behavior, saturation effects, and slew rate.

### Macromodel Mathematical

In some cases, like the use of OpAmps in switched capacitance circuits, it is often sufficient to have only the non-linear behavior of the input stage modeled. In some SPICE programs this can be entered by a formula description. An example of such a description is given by Lin et al. in [2.1] of a circuit like Fig.6.2.8b and shown in Fig. 2.5.1.

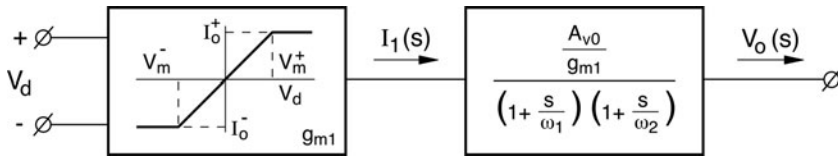


**Fig. 2.5.1** A two-pole model taking into account the slew rate limitation. The maximum available currents of the input stage are given by  $I_0^+$  and  $I_0^-$ . The transfer has the characteristic slope of  $g_{m1}$

The description consists of two blocks. The first block describes in a first-order approximation the non-linear behavior of the input stage. The second block describes the frequency response with two-poles. With this model the slewing and settling behavior can be modeled in first-order approximation. For further details see [2.1].

### Macromodel Miller-Compensated

If we need to take a larger number of non-idealities and non-linearities into account, such as input offset and noise and saturation effects we need to use a more extended macromodel.

As an example the SPICE macromodel of Boyle et al. [2.2] is shown in Fig. 2.5.2. It models the input stage by using the differential pair  $M_1$  and  $M_2$ , diodes  $D_3$  and  $D_4$  to model saturation effects at the output, and a Miller (Chap. 6) compensation with  $C_2$  across the output stage. The parasitic currents of the protection diodes at the input are modeled by means of current sources  $I_{B1}$  and  $I_{B2}$ . The output current is limited by the diodes  $D_1$  and  $D_2$  together with the series resistor  $R_{O1}$  and a reproduction of the output voltage across  $R_C G_C V_{out}$ . The same model can be used with a bipolar input stage for a bipolar amplifier. The input bias current

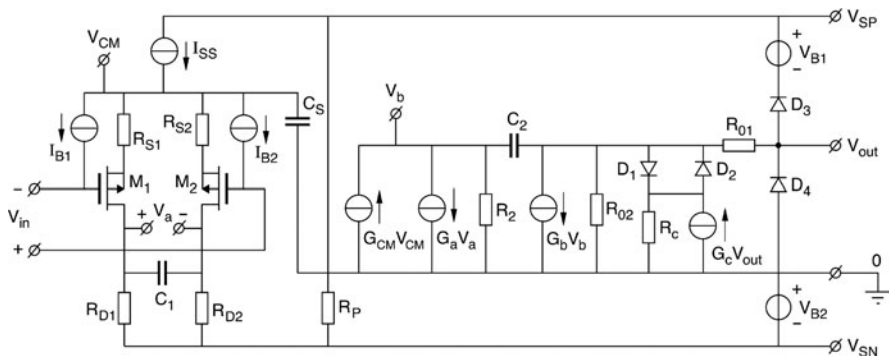


**Fig. 2.5.2** SPICE macromodel of a Miller-compensated two-stage CMOS operational amplifier according to Boyle et al. The input stage is modeled by a differential transistor pair, while the output stage is built up by driven sources and saturation diodes

sources may be left out in that case, because they are already built in the bipolar transistor models.

The macromodel can also be used when a voltage follower is added at the output as a third stage like in the  $\mu\text{A}741$  of Fig. 7.4.2.

More precise macromodels have been presented by Mark Alexander and Derek Bowers [2.3], and others.

### ***Macromodel Nested-Miller-Compensated***

The effects of common-mode-depending bias currents and saturation become even more serious in the application of low-voltage OpAmps with rail-to-rail input and output voltage ranges, such as the bipolar OpAmp NE 5234, as explained with Fig. 7.8.3. A SPICE macro-model should incorporate these effects. An example of such a model is given by Feyes et al. [2.4] using controlled sources and diodes. However, a simpler model is shaped if we just equip the input and output stages with transistors using strongly simplified transistor models, while we use controlled sources for the intermediate stage similar to Boyle's approach. This is shown in Fig. 2.5.3a, b.

The input stage is composed of two complementary transistor pairs and a tail current selector, as explained with Fig. 4.4.4. Two different offset sources can be inserted, one for each pair. The output stage is modeled together with its R-R saturation properties by two complementary bipolar transistors  $Q_{11}$  and  $Q_{12}$ , and a translinear class-AB loop through  $D_{11}$ ,  $D_{12}$ , and a floating supply source replica  $V_{SP} - V_{SN}$ , as explained with Fig. 5.3.13b. The diodes  $D_{13}$  and  $D_{14}$  prevent internal overdriving.

The intermediate stage is linearly modeled by a simplified transistor model. The total macromodel has three poles: one at the output determined by the load capacitance, one at the input of the output stage determined by the diffusion capacitors of the output transistors, and one at the input of the intermediate stage determined by  $R_{22} C_{22}$ . These three poles are handled by nested-Miller-compensation through  $C_{M1}$  and  $C_{M2}$ , as explained with Fig. 6.2.16.

With this model the change in input bias current and offset voltage and saturation effects are properly modeled when the common-mode input voltage passes from below the negative rail up even across the positive rail. The noise is also being properly modeled together with the slew rate and frequency characteristic. At the output a proper saturation behavior near the negative and positive rail voltage is modeled.

### ***Conclusion***

In conclusion, in SPICE simulations of large systems where many OpAmps and other components function together the simulation time can be much shortened by using simplified macromodels for the Operational Amplifiers. These macromodels often

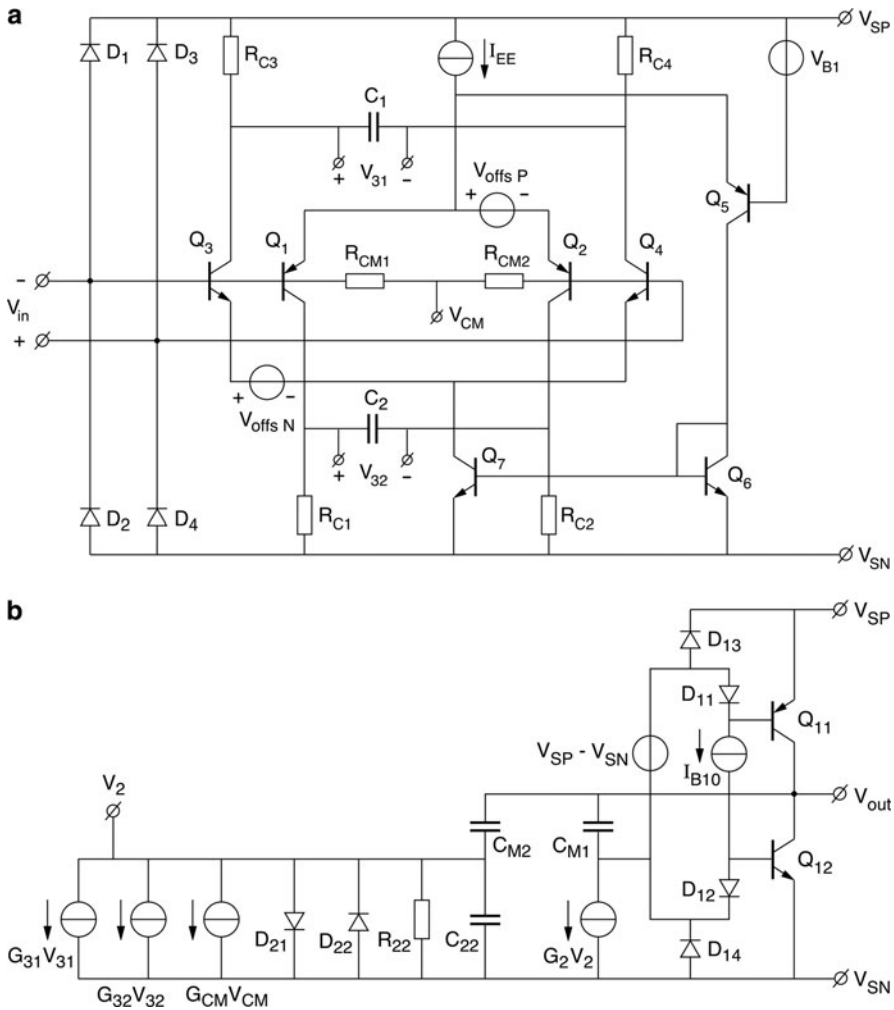


**Fig. 2.5.3** (a) A SPICE macromodel of a low-voltage bipolar R-R input stage for a three-stage bipolar OpAmp. (b) A SPICE macromodel of a low-voltage-nested-Miller-compensated intermediate and output stage of a three stage bipolar OpAmp with R-R output

use transistor models at the input and at the output, where the largest non-linearities occur, while linear controlled current sources are used in the central part of the model.

## 2.6 Measurement Techniques for Operational Amplifiers

The measurement of Operational Amplifier characteristics is not easy because their parameters can seldom be directly found in an open circuit. The gain is so large that any offset and noise will drive the output in complete saturation. Hence the OpAmp

has to be placed in a stable feedback measurement setup and the parameters to be measured have to be indirectly measured.

### ***Transconductance Measurement of an OTA***

Exempt from the mentioned problem is the measuring of the transconductance  $Y_t = G_m$  of an OTA (Sect. 7.1). This value is so low, that it can be easily directly measured. A voltage source  $V_s$  can be directly connected to the input as shown in the first measurement approach of Fig. 2.6.1. The top-top value should not be larger than about 20 mV, in order that the input stage is not being overdriven in its non-linear region. At the output a relatively small resistor, i.e.,  $R_L = 1 \text{ k}\Omega$  can be connected to ground. The  $G_m$  can be found as the ratio of the output voltage and the input voltage divided by the load resistance  $R_L$ . So:

$$Y_t = G_m = V_o / (V_i R_L) \quad (2.6.1)$$

The output load resistor  $R_L$  may not be too large. Otherwise the parasitic open output conductance  $Y_o$  in parallel with  $1/R_L$  will make the measurement inaccurate. This is particularly the case at high frequencies where the parallel output capacitance  $C_L$  will attenuate the output voltage strongly. The situation is drawn in Fig. 2.6.1.

For the measurement of offset and noise of an OTA the same setup can still be used. At a grounded input the output voltage indicates the offset through a calculation by the value of the transconductance and the load resistance according to:

$$V_{offs} = V_o / (G_m R_L) \quad (2.6.2)$$

However, if we want to measure the open voltage gain  $A_V$ , the above setup does not fit anymore. The load resistance  $R_L$  has to be chosen larger than the open output resistance  $R_o = 1/G_o$  and the offset would fully drive the output to one of

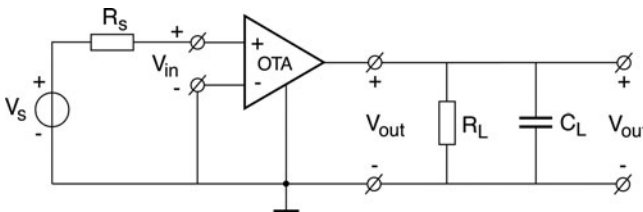


**Fig. 2.6.1** Measurement of the transconductance  $Y_t = G_m$  of an OTA

the supply rails. Fiddling with a DC input bias voltage would help in some cases, but cannot be a standard measurement procedure. This can only be used in SPICE simulations as we may expect perfectly matched transistors and an inherent low offset.

### Voltage Gain Measurement of an OpAmp

The second closest approach is to use feedback for proper biasing in such a way that the negative input terminal is fed back by a resistor  $R_I$  with a value larger than the open output resistance  $R_o$  but capacitively grounded. The situation is depicted in Fig. 2.6.2.

The external loop contains an extra pole at a time constant  $\tau_I = R_I C_I$ . This must be larger than the DC gain  $2 A_V$  multiplied by the dominating time constant  $\tau_d = R_o C_p$  of the open-loop amplifier, to satisfy the stability of the loop. As the dominating pole frequency  $1/2 \pi \tau_d$  may easily be as low as 1.6 kHz at  $R_o = 10 \text{ M}\Omega$  and  $C_p = 10 \text{ pF}$ , the external pole frequency  $\tau_I$  must be lower than 0.008 Hz at a voltage gain  $A_V$  of  $10^5$ . When we choose  $R_I = 100 \text{ M}\Omega$ ,  $C_I$  must have a value larger than 0.2  $\mu\text{F}$ . The voltage gain as a function of the frequency (Bode plot) can now be measured as  $A_V = V_o/V_i$  with a network analyzer with active probes ( $C_{in} < 3 \text{ pF}$ ). If we do not take  $\tau_I$  large enough, the phase margin could become too low and the circuit may multivibrate at a low frequency.

The above solution may work well with most CMOS OTAs. But if the open output resistor  $R_o$  becomes larger, a problem arises as the value of  $R_I$  is limited.

If the input stage has bipolar transistors, the feedback resistor has to supply the input bias current. This requires a much lower value of  $R_I$  and a higher value of  $C_I$ .

A possible solution will then be to insert a single-transistor voltage-follower buffer between the output and the connection to the feedback resistor  $R_I$  in order not to load the open output too much. In SPICE simulations we can easily solve the problem by replacing  $R_I$  by a large inductance  $L_I$ , so that there is no DC loss across this element.

With an OpAmp with two or more gain stages the open output impedance is normally so low that a much lower value of  $R_I$  is allowed.

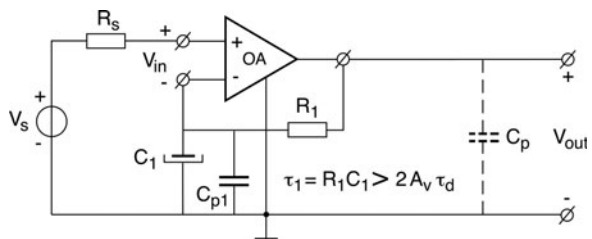


**Fig. 2.6.2** Measuring the open-loop frequency response  $A_V = V_o/V_i$  of an operational amplifier



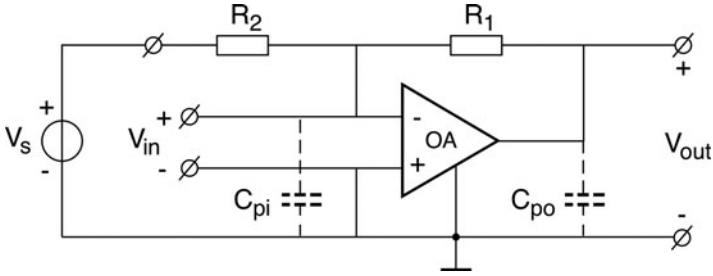


**Fig. 2.6.3** Inverting feedback configuration for measuring the open-loop frequency response  $A_V = V_o/V_i$  of an operational amplifier

### ***Voltage Gain and Offset Measurements of an OpAmp***

A third, simple, and effective solution is to use an inverting amplifier feedback configuration as shown in Fig. 2.6.3.

The idea is to apply the amplifier in an inverting configuration with a minus unity gain at  $R_2 = 10\text{ k}\Omega$ ,  $R_1 = 10\text{ k}\Omega$ , or i.g. with a gain of  $-100$  at  $R_2 = 1\text{ k}\Omega$ ,  $R_1 = 100\text{ k}\Omega$  inverting configuration. The voltage gain can be measured by a network analyzer by simply connecting one active probe to the output and the other active probe to the input of the amplifier.

The only care we must take is that the probe capacitance  $C_{pi}$  at the input does not cause a pole in the loop at a frequency where the loop gain is still larger than unity. This should not be a problem at a strong feedback attenuation  $B_V = R_2/R_1$ . The frequency characteristic can be measured with this third method up to several hundred megahertz.

If the open output impedance  $R_o$  is high, then  $R_1$  must also be chosen sufficiently high to avoid degradation of the measured voltage gain. This inverting-amplifier setup also allows us to simply measure the offset between the input terminals. The input voltage noise can also be measured at the input in a frequency band where the feedback is active, or  $A_V B_V > 1$ .

In conclusion, of these three simple measuring setups, the third measuring circuit is quite powerful.

### ***General Measurement Setup for an OpAmp***

The above methods do not satisfy a general measurement setup in which more parameters can be measured, such as common-mode rejection. The measurement of the CMRR is particularly difficult as we cannot apply feedback for biasing, as the feedback will destroy the CMRR by its ground connection (see Sect. 4.3). Alternatively we can superimpose on the supply voltages and the output reference voltage

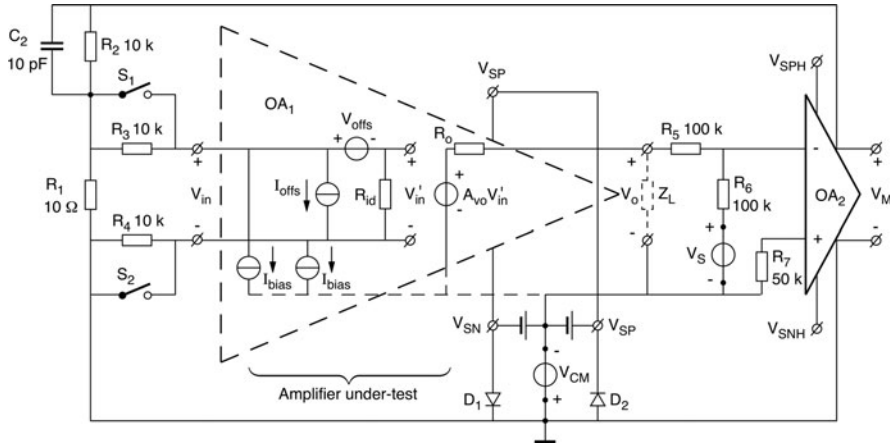


**Fig. 2.6.4** General low-frequency measurement setup for voltage gain  $A_V$ , bias current  $I_{bias}$ , offset voltage  $V_{offs}$ , noise voltage  $V_n$ , and common-mode rejection CMRR of an operational amplifier  $OA_1$  under test aided by a helping operational amplifier  $OA_2$

a common-mode voltage. For that purpose we need to place the device under test in a feedback loop with the aid of a second amplifier. As a fourth example, a more general low-frequency setup is given in Fig. 2.6.4 [2.5].

The amplifier under test,  $OA_1$ , is supplied with positive and negative supply voltages, respectively  $V_{SP}$  and  $V_{SN}$ , while a common-mode voltage source  $V_{CM}$  moves the supply voltages and the output reference voltage in regard to the input voltages. A broadband helping amplifier  $OA_2$  compares the output voltage  $V_o$  of the amplifier under test with a source voltage  $V_s$  and amplifies the difference to the output measurement voltage  $V_M$ . This voltage is being fed back to the input of the amplifier under test by an attenuation network  $B_v = R_1/R_2$  and bias current measurement resistors  $R_3$  and  $R_4$ . The capacitor  $C_2$  provides phase lead to stabilize the long loop through two amplifiers. The low-frequency voltage gain can be measured by dividing  $V_s$  by  $(R_2/R_1) V_M$ , so:

$$A_V = V_s R_1 / R_2 V_M \tag{2.6.3}$$

This can be done, for instance, by a network analyzer. Active probes need not be used, depending on the impedance levels of the source and output of  $OA_2$ . Load conditions can be changed by applying  $Z_L$ . The measurement of the frequency characteristic is correct up to about 1 MHz, which is the pole of the feedback network.

For an offset measurement the switches  $S_1$  and  $S_2$  have to be closed. The output voltage  $V_M$  represents the input offset voltage amplified by the inverse feedback attenuation.

$$V_{offs} = V_M R_1 / R_2 \tag{2.6.4}$$

The spectral input noise can also be read from  $V_M$ .

$$V_{nin} = V_M R_1 / R_2 \quad (2.6.5)$$

The bias current  $I_{bias}$  can be found by opening only  $S_1$ .

$$I_{bias} = V_M R_1 / R_2 R_3 \quad (2.6.6)$$

The offset current  $I_{offs}$  similarly can be found by opening both switches  $S_1$  and  $S_2$  and by using equal resistors  $R_3 = R_4$ .

$$I_{offs} = V_M R_1 / R_2 R_3 \quad (2.6.7)$$

For the measurement of the common-mode rejection ratio a common-mode voltage source  $V_{CM}$  has to be used which is able to drive the supply-voltages  $V_{SP}$  and  $V_{SN}$  of the device under test. The result can be measured as:

$$CMRR = V_{CM} R_2 / (R_1 V_M) \quad (2.6.8)$$

Note that the loop gain of the measurement setup is high ( $A_{01} A_{02} R_2 / R_1$ ). The high frequency behavior of the loop is determined by the two dominating time constants of both amplifiers. The stability of the loop is ensured if the help amplifier  $OA_2$  has a high dominating pole frequency, say 1 MHz, and if the feedforward capacitor  $C_2$  corrects the phase lag of  $OA_2$  above that frequency. The measurement setup may function up to frequencies of 1 MHz.

In conclusion, we have seen that it is not easy to measure OpAmp parameters for we have to take care of proper biasing simultaneously. For SPICE simulations, the second method can be used to measure frequency characteristics. The third method is powerful in practical situations. The measurement of the CMRR is particularly difficult, as we cannot apply feedback to properly bias the OpAmp as this destroys the CMRR. A proper method is to alternatively move the supply with a common-mode voltage. This is done in the fourth general measurement setup.

## 2.7 Problems and Simulation Exercises

### **Problem 2.1**

Figure 2.5.2 shows a Boyle type macromodel developed for CMOS operational amplifiers. Starting from that picture, calculate the parameters of an operational amplifier with a differential gain  $a_{VD} = 100$  dB, common-mode rejection ratio  $CMRR = 90$  dB, unity gain bandwidth  $f_{0dB} = 10$  MHz with a phase margin  $\varphi_m = 76^\circ$ . The slew-rate specifications are  $S_{rp} = 10$  V/ $\mu$ s for rising output voltage and

$S_{rn} = 9 \text{ V}/\mu\text{s}$  for falling output voltage. A short-circuit current  $I_{SC} = 7 \text{ mA}$  should be supplied at the output, with an output DC impedance  $R_{out} = 1 \text{ k}\Omega$ . Supply voltages are  $V_{SP} - V_{SN} = 3 \text{ V}$ , and the macromodel should dissipate  $P_d = 3 \text{ mW}$ . No capacitive or resistive load is present.

### **Solution**

The gain in the first stage is chosen to be equal to unity:

$$R_{S1} = R_{D1} - 1/g_{m1} \quad (2.7.1)$$

As  $R_{D1}$  usually has values around  $2/g_{m1}$  for convenient common mode input range,

$$R_{D1} = 2/g_{m1} \quad (2.7.2)$$

In order to calculate  $g_{m1}$ , weak inversion transistors will be considered for the input stage with an approximate  $g_{m1}$  given by

$$g_{m1} = \frac{I_{SS}}{100 \text{ mV}} \quad (2.7.3)$$

The tail current  $I_{SS}$  results from  $S_{rp}$  value and a convenient Miller capacitor:

$$\begin{aligned} C_2 &= 2 \text{ pF} \\ I_{SS} &= C_2 S_{rp} = 20 \mu\text{A} \end{aligned} \quad (2.7.4)$$

Returning to  $R_{D1}$  and  $R_{S1}$  values:

$$\begin{aligned} R_{D1} &= 2/g_{m1} = 200 \text{ mV}/I_{SS} = 10 \text{ k}\Omega \\ R_{S1} &= R_{D1} - 1/g_{m1} = 1/g_{m1} = 5 \text{ k}\Omega \end{aligned} \quad (2.7.5)$$

Using these values, the unity gain bandwidth results:

$$f_{0dB} = 1/2 \pi R_{D1} C_2 = 8 \text{ MHz} \quad (2.7.6)$$

which is close enough to the desired bandwidth. It can be increased by choosing a lower value for  $R_{D1}$ . The gain in the virtual intermediate stage of the model is larger than unity, given by its components  $G_a$  and  $R_2$ :

$$\begin{aligned} G_a &= 1/R_{D1} = 0.1 \text{ mS} \\ R_2 &= 100 \text{ k}\Omega \end{aligned} \quad (2.7.7)$$

The output impedance will be equal to  $R_{OI}$  for frequencies above:

$$f_c = 1/2 \pi R_{O2} C_2 (1 + R_2 G_b) = 79 \text{ Hz} \quad (2.7.8)$$

Below this corner frequency, the DC output impedance is

$$R_{out} = R_{OI} + R_{O2} \quad (2.7.9)$$

Because the short-circuit current will be given by the ratio of a diode voltage and  $R_{OI}$ ,  $R_{OI}$  should be less than DC output impedance:

$$R_{OI} = 100 \Omega \quad (2.7.10)$$

The rest of the gain up to  $a_{VD} = 100 \text{ dB}$  is given by the third stage:

$$\begin{aligned} R_{O2} &= R_{out} - R_{OI} = 900 \Omega \\ G_b &= a_{VD} R_{DI} / R_2 R_{O2} = 11.1 \text{ S} \end{aligned} \quad (2.7.11)$$

The gain of the  $R_c G_c$  voltage repeater should be equal to unity with an  $R_c$  value much smaller than  $R_{OI}$ , so:

$$\begin{aligned} R_c &= 10 \Omega \\ G_c &= 0/R_c = 0.1 \text{ S} \end{aligned} \quad (2.7.12)$$

This voltage repeater puts the difference between the voltages at the output and at the internal output on  $R_{OI}$ , such as if a difference exists the maximum current supplied is the short-circuit current:

$$I_{SC} = V_D / R_{OI} = 0.6 \text{ V} / 100 \Omega = 6 \text{ mA} \quad (2.7.13)$$

To correct the short circuit current value to the desired 7 mA, the diode threshold voltage can be changed to 0.7 V for simulation purposes. The  $S_{rn}$  value is controlled by  $C_S$ :

$$C_S = (I_{SS} / S_{rn}) - C_2 = 0.22 \text{ pF} \quad (2.7.14)$$

The common-mode rejection ratio is given by  $G_{cm}$ :

$$G_{cm} = 1/R_{DI} \text{ CMRR} = 3 \text{ nS} \quad (2.7.15)$$

For the desired phase margin,  $C_I$  introduces a second pole

$$p2 = 1/2R_{DI} C_I \quad (2.7.16)$$

which produces:

$$C_I = (C_2 \tan \varphi_m) / 2 = 46 \text{ fF} \tag{2.7.17}$$

The power dissipated by the whole macromodel is modeled by  $R_p$  which takes the value:

$$R_p = \frac{V_{SP} + V_{SN}}{P_d - (V_{SP} + V_{SN})I_{SS}} = 1.0 \text{ k}\Omega \tag{2.7.18}$$

### Simulation Exercise 2.1

The Boyle macromodel depicted in Fig. 2.7.1 can be simulated for AC analysis using a simulation setup as shown in Fig. 2.7.2.

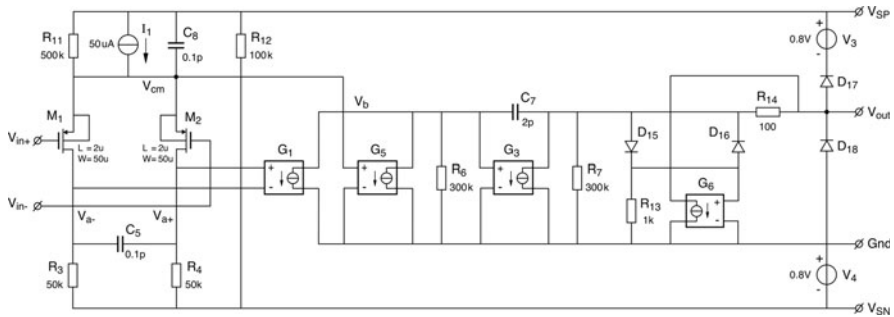


Fig. 2.7.1 Boyle macromodel for a two-stage operational amplifier

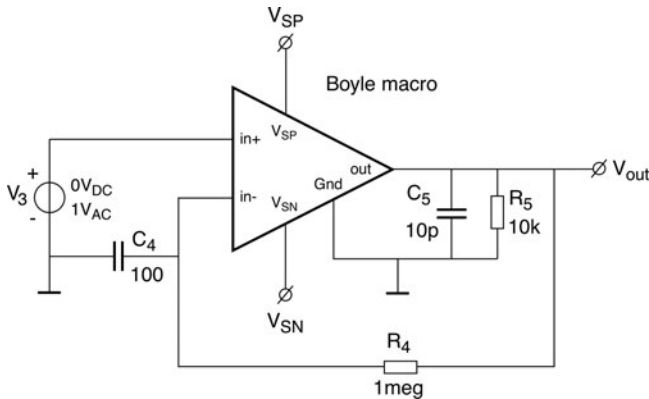


Fig. 2.7.2 Differential gain simulation for an OpAmp macromodel

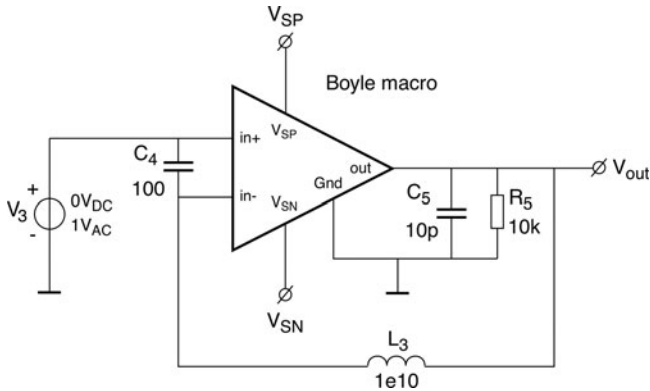


Fig. 2.7.3 Common-mode to differential crosstalk simulation

The use of ideal high-valued capacitors and resistors allow the simulator to solve correctly the biasing point for the transistors inside the operational amplifier. At DC, the amplifier is basically a repeater with the positive input connected to ground. What is the low limit frequency for a DC voltage gain simulation, considering the effect of  $C_4$ ? What can be the additional benefits of replacing  $R_4$  with an inductor?

### Simulation Exercise 2.2

The circuit shown in Fig. 2.7.3 is used to simulate a Boyle macromodel of an operational amplifier for AC solution of common-mode to differential crosstalk.

Using this crosstalk gain and the differential gain, the common-mode rejection ratio can be calculated. At DC, the inductor keeps the operational amplifier in a repeater configuration, while above a limit frequency given by the  $L_3C_4$  time constant, both inputs of the operational amplifier are tied together and the circuit is placed in an open-loop configuration. Simulate this circuit using the Boyle macromodel shown in Fig. 2.7.1 and decrease the common-mode rejection ratio with 20 dB by adjusting the  $G_5$  transconductor. What other circuit elements in Fig. 2.7.1 affect the common-mode to differential crosstalk?

## 2.8 References

- [2.1]. J.C. Lin, J.H. Nevin, A modified time domain model for nonlinear analysis of an operational amplifier. IEEE J. Solid-St. Circ. **SC-21**(3), 478–483 (1986)
- [2.2]. G.R. Boyle, B.M. Cohn, D.O. Pederson, J.E. Solomon, Macromodelling of integrated circuit operational amplifiers. IEEE J. Solid-St. Circ. **SC-9**(6), 353–364 (1974)

- [2.3]. M. Alexander, D.F. Bowers, New Spice compatible OpAmp model boosts AC simulation accuracy. EDN February 15 (1990)
- [2.4]. J.H.A. Feyes, R. Hogervorst, J.H. Huijsing, *Macromodeling Operational Amplifiers*, vol. 5, ISCAS 93 Conference, London, Proceedings pp. 681–684
- [2.5]. J.A. Connelly, *Analog Integrated Circuits* (John Wiley and Sons, New York, 1975)





## 3. Applications

This chapter describes a number of general applications suitable for quantifying the requirements of universal active devices or Operational Amplifiers. The transfer of each example is described by a matrix containing, firstly, one or more nominal values, and secondly, error terms having low values. The nominal values are determined by the circuit configuration and by the gain-setting passive components in the circuit. The error terms are determined by the non-idealities of the active devices as discussed in Chap. 2. Each of the error terms can be relatively easily expressed as a sum of errors caused by:

*firstly*, the non-zero input voltage;  
*secondly*, the non-zero input current;  
*thirdly*, if the input port is floating, the CM input current; and  
*fourthly*, if the output port is floating, the non-zero CM output current.

With the aid of these error terms one can estimate the required specifications of the active devices or Operational Amplifiers.

In the last section particularly the requirements of OpAmps are evaluated based on the desired dynamic range.

It appears that for an optimum ratio of dynamic range and supply power the output of an Operational Amplifier should have a current-efficient class-AB biasing and a voltage-efficient rail-to-rail voltage range. In some cases the input should also have a voltage-efficient rail-to-rail common-mode voltage range.

### 3.1 Operational Inverting Amplifier

The operational inverting amplifier has both the input and output ports grounded which restricts the feedback to parallel connections. This results in applications with a low input and output impedance.

## Current-to-Voltage Converter

As we have already discussed in Sect. 1.1, the transimpedance amplifier or current-to-voltage converter is the most basic application of the OIA. This amplifier configuration is drawn in Fig. 3.1.1 together with the source and load circuits.

For a description of the transfer we choose a kind of matrix which clearly presents the nominal transfer and additionally presents all errors in relation to the input quantities  $V_i$  and  $I_i$ . For a two-port the total matrix is equal to the chain matrix. The matrix of Fig. 3.1.1 is given in Eq. 3.1.1:

$$\begin{vmatrix} I_1 \\ V_1 \end{vmatrix} = \begin{vmatrix} 1/Z_m + 1/Z_{te} & 1/A_{ie} \\ 1/A_{ve} & 1/Y_{te} \end{vmatrix} \begin{vmatrix} V_2 \\ -I_2 \end{vmatrix} + \begin{vmatrix} I_{1offs} \\ V_{1offs} \end{vmatrix}; \quad (3.1.1)$$

with:

$$\begin{aligned} 1/Z_m &= -1/Z_2 \\ 1/Z_{te} &\simeq -Y_2(Y_2 + Y_0)/Y_t - Y_i(Y_2 + Y_0)/Y_t \\ 1/A_{ie} &\simeq -Y_2/Y_t - Y_i/Y_t \\ 1/A_{ve} &\simeq -(Y_2 + Y_0)/Y_t \\ 1/Y_{te} &\simeq -1/Y_t \\ 1_{Ioffs} &\simeq V_{i\ off}/Z_2 + I_{i\ off} \\ V_{1offs} &\simeq V_{i\ off} \end{aligned}$$

and with  $Y_2 = 1/Z_2$

The nominal term  $1/Z_m$  represents the minus reciprocal value of the nominal impedance  $-1/Z_2$ . All other terms are error terms caused by non-idealities as described by the error matrix (2.1.1). Each error term can be written as a sum of partial errors which originate, firstly, from the non-zero OIA input voltage  $V_i$  and secondly, from the non-zero input current  $I_i$ . The first error term  $1/Z_{te}$  represents an entrance error current  $V_2/Z_{te}$  as a function of the exit voltage  $V_2$  at  $-I_2 = 0$ . This error current is composed of two partial error currents:  $V_2 Y_2 (Y_2 + Y_0)/Y_t$

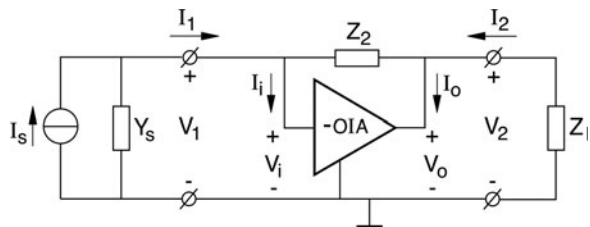


**Fig. 3.1.1** Transimpedance amplifier with source and load circuits

following through  $Y_2$  as a consequence of the non-zero input voltage  $V_i = -V_2(Y_2 + Y_0)/Y_t$  and the non-zero input current  $I_1 = -V_2Y_i(Y_2 + Y_0)/Y_t$ . The second error term  $1/A_{ie}$  represents an entrance error current  $I_2/A_{ie}$  as a function of  $-I_2$  at  $V_2 = 0$ . This error current is composed of two partial error currents:  $I_2Y_2/Y_t$  flowing through  $Y_2$  as a consequence of the input voltage  $V_i = I_2/Y_t$ , and the input currents  $I_i = I_2Y_i/Y_t$ . The other error terms are built up in the same way. The input offset voltage  $V_{ioffs}$  and current  $I_{ioffs}$  give rise to the entrance offset voltage  $V_{1off}$  and current  $I_{1off}$ , as presented. The spectral input noise voltage  $V_{in}$  and current  $I_{in}$  can be thought of as superimposed on the relevant offset quantities [3.1, 3.2]. An extra entrance noise current, caused by the noise current  $I_{Z2n}$  of the impedance  $Z_2$ , is present.

### Inverting Voltage Amplifier

Another important application of the OIA is the inverting voltage amplifier, a configuration widely used in analog computer circuits. The circuit is shown in Fig. 3.1.2. The matrix is given in Eq. 3.1.2:

$$\begin{vmatrix} V_I \\ I_I \end{vmatrix} = \begin{vmatrix} 1/A_{vn} + 1/A_{ve} & 1/Y_{te} \\ & 1/Z_{te} \end{vmatrix} \begin{vmatrix} V_2 \\ -I_2 \end{vmatrix} + \begin{vmatrix} V_{1off} \\ I_{1off} \end{vmatrix}; \tag{3.1.2}$$

with

$$\begin{aligned} 1/A_{vn} &\simeq -Z_1/Z_2 \\ 1/A_{ve} &\simeq -(Z_1 + Z_2)(Y_2 + Y_0)/Y_tZ_2 - Z_1Y_i(Y_2 + Y_0)/Y_t \\ 1/Z_{te} &\simeq -1/Z_2 \end{aligned}$$

An important disadvantage of the inverting voltage amplifier is its large entrance current error  $V_2/Z_{te} \simeq -V_2/Z_2$ . The non-inverting voltage amplifier using an OVA, which will be described in the next section, does not have this disadvantage.

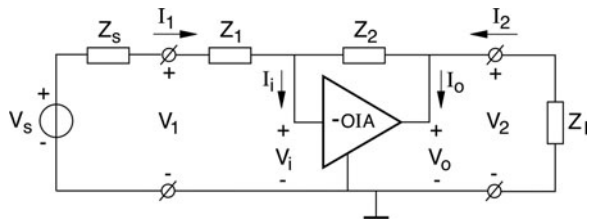


Fig. 3.1.2 Inverting voltage amplifier with source and load circuits

## 3.2 Operational Voltage Amplifier

The operational voltage amplifier (OVA) has a floating input port that provides applications with a high input impedance by a serial feedback through the input port.

### Non-Inverting Voltage Amplifier

The most basic application of the OVA is the non-inverting voltage amplifier (see Sect. 1.1.2) as shown in Fig. 3.2.1

The transfer of the circuit can be described by one nominal value and error terms having low values, as described by matrix (3.2.1):

$$\begin{vmatrix} V_1 \\ I_1 \end{vmatrix} = \begin{vmatrix} 1/A_{vn} + 1/A_{ve} & 1/Y_{te} \\ 1/Z_{te} & 1/A_{ie} \end{vmatrix} \begin{vmatrix} V_2 \\ -I_2 \end{vmatrix} + \begin{vmatrix} V_{Ioffs} \\ I_{Ioffs} \end{vmatrix}; \quad (3.2.1)$$

with:

$$\begin{aligned} 1/Z_{vn} &= Z_1/(Z_1 + Z_2) \\ 1/A_{ve} &\simeq (Y_0 + Y'_s)/Y_t + Y_{id}(Y_0 + Y'_s)/Y_p Y_t + 1/A_{vn} H_i - Y_{ic1}/Y_p A_{vn} \\ 1/Y_{te} &\simeq 1/Y_t + Y_{id}/Y_p Y_t \\ 1/Z_{te} &\simeq Y_{id}(Y_0 + Y'_s)/Y_t + Y_{ic2}/A_{vn} \\ 1/A_{ie} &\simeq Y_{id}/Y_t \\ V_{ioffs} &\simeq V_{ioffs} + I_{ioffs}/Y_p + I_{ibias}/Y_p \\ I_{Ioffs} &\simeq +I_{ibias} \end{aligned}$$

and with  $Y_i = 1/Z_1$ ,  $Y_2 = 1/Z_2$ ,  $Y_p = Y_1 + Y_2$ ,  $Y'_s = 1/(Z_1 + Z_2)$

The reciprocal nominal value of the voltage amplification factor is  $1/A_{vn} = Z_1/(Z_1 + Z_2)$ . All other matrix elements are error terms caused by non-idealities. The first error term  $1/A_{ve}$  represents the entrance error voltage  $V_2/A_{ve}$  as a function

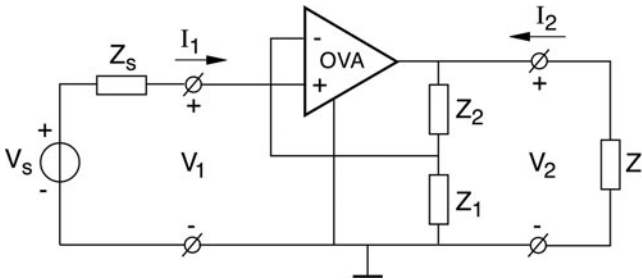


Fig. 3.2.1 Voltage amplifier with source and load circuits

of the exit voltage  $V_2$  at  $-I_2 = 0$ . The error voltage is the sum of four partial error voltages. The first of these partial error voltages  $V_2(Y_0 + Y'_s)/Y_t$  represents the differential input voltage  $V_{id}$  needed to generate the exit voltage  $V_2$ .

The second partial error voltage  $V_2Y_{id}(Y_0 + Y'_s)/Y_pY_t$  is the voltage loss across the parallel admittance  $Y_p = Y_1 + Y_2$  of the feedback network as a result of the differential input current  $I_{id} = V_2Y_{id}(Y_0 + Y_s)/Y_t$ . The third partial error voltage  $V_2/A_{vn}H_i$  is the equivalent differential input voltage  $V_{id}$  evoked by the crosstalk  $1/H_i$  from the CM input voltage  $V_{ic} = V_2/A_{vn}$ . The fourth partial error voltage  $-V_2Y_{ic1}/Y_pA_{vn}$  is the voltage loss across the parallel admittance  $Y_p = Y_1 + Y_2$  of the feedback network as a result of the common-mode input current  $I_{ic} = V_2Y_{ic1}/A_{vn}$ . The other error terms are built up in the same way. In addition to the offset and noise quantities of the OIA (see Sect. 3.1), there are the input bias current  $I_{ibias}$  and the input bias noise current  $I_{ibn}$  and their effects. An extra entrance noise voltage, caused by the noise voltage  $V_{Zpn}$  of the parallel impedance  $Z_p = 1/Y_p$ , is present.

### Voltage Follower

If we choose  $Z_1 = \infty$  and  $Z_2 = 0$ , the voltage amplifier becomes a voltage follower with a nominal voltage amplification factor  $A_{um} = 1$  in that all error contributions with a  $Y_p$  in the denominator disappear.

### Bridge Instrumentation Amplifier

A bridge instrumentation amplifier can be built with an OVA and bridge of four impedances  $Z_{11}$  through  $Z_{22}$  (Fig. 3.2.2). The circuit can be thought to be composed partly from the inverting voltage amplifier (Fig. 3.2.2) and the non-inverting

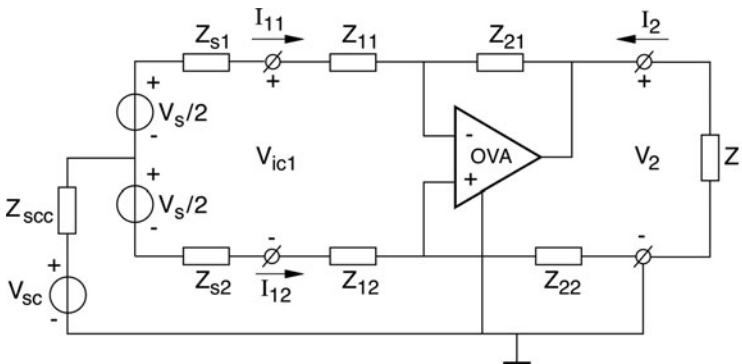


Fig. 3.2.2 Bridge instrumentation amplifier with source and load circuits

voltage amplifier (Fig. 3.2.1). If the bridge is well balanced, which means that  $\Delta Z_b/Z_b = 1 - Z_{21}Z_{12}/Z_{22}Z_{11} \ll 1$ , the circuit only amplifies the differential-mode entrance voltage  $V_{id}$  while the common-mode entrance voltage  $V_{ic}$  is rejected. The circuit of a bridge instrumentation amplifier is given in Fig. 3.2.2 and the matrix with the error terms in Eq. 3.2.2.

$$\begin{vmatrix} V_{Id} \\ I_{Id} \\ I_{Ic} \end{vmatrix} = \begin{vmatrix} 1/A_{vn} + 1/A_{ve} & 1/Y_{te} & 1/H_e \\ & 1/A_{te} & 1/A_{ie} \\ \cdot & \cdot & 1/Z_{Icc} \end{vmatrix} \begin{vmatrix} V_2 \\ -I_2 \\ V_{ic} \end{vmatrix} + \begin{vmatrix} V_{ioffs} \\ I_{ioffs} \\ I_{ibias} \end{vmatrix}; \quad (3.2.2)$$

with:

$$\begin{aligned} 1/A_{vn} &= -Z_{11}/Z_{21} \\ 1/A_{ve} &\simeq -\Delta Z_b/2Z_b(A_{vn} + 1)A_{vn} \\ &\quad - (Z_{11} + Z_{21})(Y_0 + Y_{21})/Y_t Z_{21} - (Z_{11} + Z_{12})Y_{id}(Y_0 + Y_{21})/Y_t \\ &\quad - 1/2H_i A_{vn} - Y_{ic1}/2Y_{11}A_{vn} + Y_{ic2}/2Y_{12}A_{vn} \\ 1/H_e &\simeq -\Delta Z_b/Z_b(A_{vn} + 1) \\ &\quad - 1/Y_t Z_{21} - (Z_{11} + Z_{12})Y_{id}/Y_t(Z_{11} + Z_{21}) \\ &\quad - 1/H_i - Y_{ic}/Y_{11} - Y_{ic}/Y_{12} \\ 1/Z_{Icc} &\simeq 1/(Z_{11} + Z_{21}) \end{aligned}$$

and with:

$$\begin{aligned} \Delta Z_b/Z_b &= 1 - Z_{21}Z_{12}/Z_{22}Z_{11} \ll 1 \\ Y_{11} &= 1/Z_{11}, \quad Y_{12} = 1/Z_{12}, \quad Y_{21} \simeq 1/Z_{21}, \quad Y_{22} = 1/Z_{22} \end{aligned}$$

The main disadvantage of this type of instrumentation amplifier is that the bridge resistors establish a connection between the input port of the OVA and the output and ground. This destroys the CM isolation barrier of the input port of the OVA and thus destroys the CMRR of the application. Therefore, the common-mode crosstalk ratio (CMCR)  $1/H_e$  is directly determined by the imbalance  $\Delta Z_b/Z_b$  of the bridge and a factor  $1/(A_{vn} + 1)$  depending on the nominal amplification factor  $A_{vn}$ . Another disadvantage is the relatively low CM entrance impedance  $1/Z_{Icc} = 1/(Z_{11} + Z_{21})$  which is also caused by the lack of a CM isolation barrier.

The latter disadvantage can be overcome by connecting the input terminals in cascade with either two voltage followers, one for each terminal, or two voltage amplifiers of the type of Fig. 3.2.1, joined in a balanced configuration by connecting the bottom sides of  $Z_i$  to each other, instead of to ground.

A basically better way to build an instrumentation amplifier which does have a CM isolation barrier is to use two OFAs. An example of such an instrumentation will be given in Sect. 3.4.

### 3.3 Operational Current Amplifier

The operational current amplifier has a floating output port, which allows a high output impedance or current output by a serial feedback through the output port.

#### Current Amplifier

The most basic application of the OCA is the current amplifier (Sect. 1.3). This configuration is given in Fig. 3.3.1 together with its source and load circuits.

The nominal amplification factor and error terms with small values can be described by the matrix of Eq. 3.3.1.

$$\begin{vmatrix} I_1 \\ V_1 \end{vmatrix} = \begin{vmatrix} 1/A_{in} + 1/A_{ie} & 1/Z_{te} \\ 1/Y_{te} & 1/A_{ve} \end{vmatrix} \begin{vmatrix} -I_2 \\ V_2 \end{vmatrix} + \begin{vmatrix} -I_{1offs} \\ V_{1offs} \end{vmatrix}; \quad (3.3.1)$$

with:

$$\begin{aligned} 1/A_{in} &= Y_l / (Y_l + Y_2) \\ 1/A_{ie} &\simeq Y'_s / Y_t + Y_i / Y_t + 2H_o / A_{in} - Y_{oc1} / Y_p A_{in} \\ 1/Z_{te} &\simeq Y_{se} Y_{od} / Y_t + Y_i Y_{od} / Y_t + Y_{oc2} / A_{in} \\ 1/Y_{te} &\simeq 1 / Y_t \\ 1/A_{ve} &\simeq Y_{od} Y_t \\ I_{1offs} &\simeq V_{ioffs} Y_t + I_{ioffs} + 2I_{obias} / A_{in} \\ V_{1offs} &\simeq V_{ioffs} \end{aligned}$$

and with:  $Y_p = Y_l + Y_2$ ,  $Y'_s = 1 / (1 / Y_l + 1 / Y_2)$ , neglecting  $Y_{od}$  against  $Y_p$

The reciprocal value of the nominal current amplification factor is  $1/A = Y_l / (Y_l + Y_2)$ . All other terms are error terms caused by non-idealities. The first error term  $1/A_{ie}$  can be written as the sum of four partial error terms.

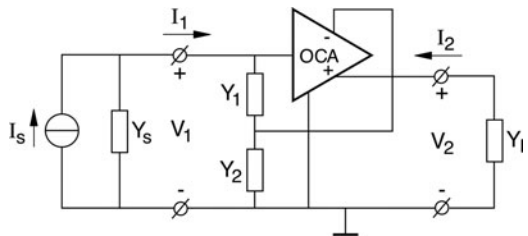


Fig. 3.3.1 Current amplifier with source and load circuits



The first partial error  $Y'_s/Y_t$  represents the entrance error current  $-I_2Y_s/Y_t$ . This results from the current  $V_iY_s$  flowing through the series conductance  $Y'_s = 1/(1/Y_1 + 1/Y_2)$  as a consequence of the input voltage  $V_i = -I_2/Y_t$  needed to deliver the exit current  $-I_2$ . The second partial error  $Y_i/Y_t$  simply represents the input current  $I_i = -I_2Y_i/Y_pY_t$  which is needed to deliver the exit current  $-I_2$ .

The third partial error  $2/H_oA_{in}$  is caused by the crosstalk  $1/H_o$  of the DM output current  $I_{od} = -I_2$  on the CM output current  $I_{oc}$ . Double this value (from both output terminals) must be counted.

The fourth partial error  $-Y_{oc1}/Y_pA_{in}$  is a result of the error current  $I_2Y_{oc1}/Y_p$  which flows into the CM output impedance  $Y_{oc1}$  in parallel with the parallel admittance  $Y_p = Y_1 + Y_2$  as a function of  $-I_2$ . The other error terms are made up in the same way. In addition to the offset quantities mentioned with the OIA, there are the output bias current  $I_{obias}$  and output bias noise current  $I_{obn}$ . There is an extra entrance noise current caused by the noise current  $I_{YSN}$  of the series admittance  $Y'_s = 1/(1/Y_1 + 1/Y_2)$ .

### 3.4 Operational Floating Amplifier

The operational floating amplifier is the most versatile OpAmp. It permits series feedback through the input and output ports. This allows for applications with a high input and output impedance.

#### *Voltage-to-Current Converter*

The most basic application of the OFA is the transadmittance amplifier or the voltage-to-current converter (Sect. 1.4). The circuit is shown in Fig. 3.4.1 with the source and load circuit.

The nominal transadmittance and error terms are presented in the matrix of Eq. 3.4.1.

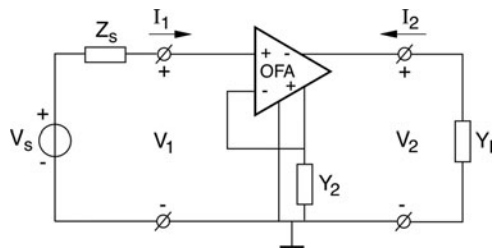


**Fig. 3.4.1** Voltage-to-current converter or transadmittance amplifier with source and load circuits

$$\begin{vmatrix} V_1 \\ I_1 \end{vmatrix} = \begin{vmatrix} 1/Y_{tn} + 1/Y_{te} & 1/A_{ve} \\ 1/A_{ie} & 1/Z_{te} \end{vmatrix} \begin{vmatrix} -I_2 \\ V_2 \end{vmatrix} + \begin{vmatrix} V_{1offs} \\ I_{1offs} \end{vmatrix}; \quad (3.4.1)$$

with:

$$\begin{aligned} 1/Y_{tn} &= -1/Y_2 \\ 1/Y_{te} &\simeq -1/Y_t - Y_{id}/Y_t Y_2 - 1/H_i Y_2 + Y_{ic2}/Y_2 Y_2 - 2/H_o Y_2 + Y_{oc2}/Y_2 Y_2 \\ 1/A_{ve} &\simeq -Y_{od}/Y_t - Y_{id} Y_{od}/Y_t Y_2 - 2Y_{od}/Y_t H_o Y_2 - Y_{oc1}/Y_2 \\ 1/A_{ie} &\simeq -Y_{id}/Y_t - Y_{ic1}/Y_2 \\ 1/Z_{te} &\simeq -Y_{id} Y_{od}/Y_t \\ V_{1offs} &\simeq V_{ioffs} + I_{ioffs}/Y_2 + I_{ibias}/Y_2 + 2I_{obias}/Y_2 \\ I_{1offs} &\simeq I_{ioffs} + I_{obias} \end{aligned}$$

The reciprocal value of the nominal transadmittance is  $1/Y_{tn} = -1/Y_2$ . All other terms are error terms caused by non-idealities. Each error term is the sum of partial errors which can have six origins (see Sect. 2.4): firstly  $V_{id} = f(-I_2, V_2)$ , secondly  $I_{id} = f(-I_2, V_2)$ , thirdly  $V_{id} = f(V_{ic})$ , fourthly  $I_{ic} = f(V_{ic})$ , fifthly  $I_{oc} = f(-I_2)$ , and lastly  $I_{oc} = f(V_{oc})$ . We neglected  $Y_{od}$  against  $Y_2$ .

The partial errors are placed in six columns according to the above sequence. The partial errors have already been explained in the preceding sections of this chapter. There is an extra entrance noise caused by the noise voltage  $V_{Y2n}$  of the admittance  $Y_2$ .

### Inverting Current Amplifier

An inverting current amplifier or current mirror can be made by adding an entrance admittance  $Y_1$  to the transadmittance amplifier (Fig. 3.4.1). The entrance admittance  $Y_1$  converts the entrance current  $I_1$  into a voltage  $V_1$  which is in turn converted into the exit current  $I_2$  by the transadmittance amplifier containing  $Y_2$ . A special case

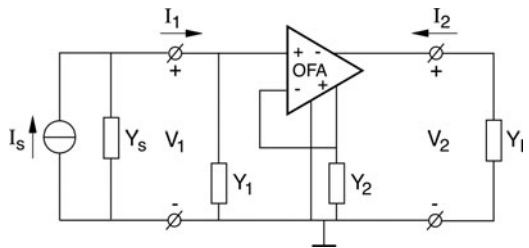


Fig. 3.4.2 Inverting current amplifier with source and load circuits

appears if  $Y_1 = Y_2$ . In that case the circuit is known as the “current mirror”. The circuit is drawn in Fig. 3.4.2 while the matrix is given by Eq. 3.4.2.

$$\begin{vmatrix} I_1 \\ V_1 \end{vmatrix} = \begin{vmatrix} 1/A_{in} + 1/A_{ie} & 1/Z_{te} \\ 1/Y_{te} & 1/A_{ve} \end{vmatrix} \begin{vmatrix} -I_2 \\ V_2 \end{vmatrix} + \begin{vmatrix} I_{1offs} \\ V_{1offs} \end{vmatrix}; \tag{3.4.2}$$

with:

$$\begin{aligned} 1/A_{in} &= -Y_1/Y_2 \\ 1/A_{ie} &\simeq -Y_1/Y_t - Y_{id}/Y_t \\ &\quad - 1/H_i A_{in} - Y_{ic1}/Y_2 + Y_{ic2}/Y_2 A_{in} \\ &\quad - 2/H_o A_{in} + Y_{oc2}/Y_2 A_{in} \\ 1/Y_{te} &\simeq -1/Y_2 \end{aligned}$$

The first term is the reciprocal nominal value of the current amplification factor. The other terms are error terms, as has been explained earlier. A disadvantage of the inverting current amplifier is the relatively high entrance voltage  $V_1 = -I_2/Y_{te} = I_2/Y_2$  which is not present in the non-inverting current amplifier of Fig. 3.2.1.

### Differential Voltage-to-Current Converter

The floating character of the input of an OFA together with the current-source character of the output of an OFA having series feedback at its output can be applied to obtain the CM-voltage isolation needed for the entrance circuit of an instrumentation amplifier. This is shown by the instrumentation transadmittance amplifier of Fig. 3.4.3 [3.3]. Two OFAs, connected as voltage and current followers

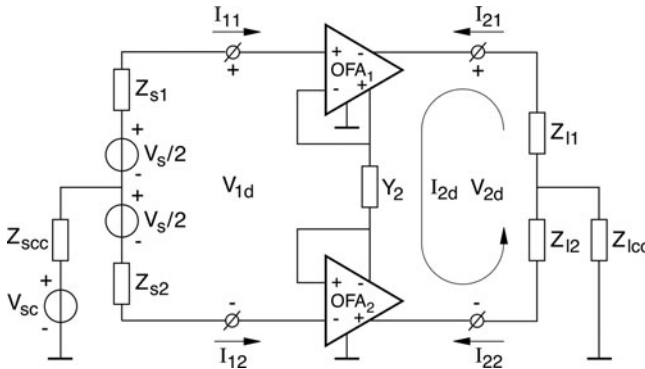


**Fig. 3.4.3** Instrumentation voltage-to-current or transadmittance amplifier with source and load circuits

(VCFs), firstly, transfer the DM entrance voltage  $V_{id}$  at unity gain to the terminals of a conductance  $Y_2$ , and secondly, transfer the current  $-I_{2d} = -V_1 Y_2$  through  $Y_2$  towards the output terminals. The CM input voltage only affects the output current through the non-ideal properties of the OFAs, as described by the matrix equation (3.4.3).

$$\begin{pmatrix} V_{1d} \\ I_{1d} \\ I_{1c} \\ I_{2c} \end{pmatrix} = \begin{pmatrix} 1/Y_m + 1/Y_{te} & 1/A_{ve} & 1/H_e & \cdot \\ & 1/A_{ie} & 1/Z_{te} & \cdot \\ \cdot & \cdot & 1/Z_{ice} & \cdot \\ \cdot & \cdot & 1/Z_{tce} & 1/Z_{oce} \end{pmatrix} \begin{pmatrix} -I_{2d} \\ V_{2d} \\ V_{1c} \\ V_{2c} \end{pmatrix} \begin{pmatrix} V_{1offs} \\ I_{1offs} \\ I_{1bias} \\ I_{2bias} \end{pmatrix}; \quad (3.4.3)$$

with:

$$\begin{aligned} 1/Y_m &= -1/Y_2 \\ 1/Y_{te} &\simeq -2/Y_t - Y_{id}/Y_t Y_2 - 1/2H_{i1}Y_2 + 1/2H_{i2}Y_2 + Y_{ic}/2Y_2 Y_2 \\ &\quad - 1/H_{o1}Y_2 + 1/H_{o2}Y_2 + Y_{oc}/2Y_2 Y_2 \\ 1/H_e &\simeq Y_{od1}/Y_{i1} + Y_{od2}/Y_{i2} + Y_{id1}Y_{od1}/Y_{i1}Y_2 + Y_{id2}Y_{od2}/Y_{i2}Y_2 \\ &\quad - 1/H_{i1} + H_{i2} + Y_{ic12}/Y_2 - Y_{ic21}/Y_2 + Y_{oc12}/Y_2 - Y_{oc21}/Y_2 \\ 1/Z_{tce} &\simeq +Y_{id}Y_{od}/Y_t - Y_{ic} - Y_{oc} \end{aligned}$$

and with:  $V_{1d} = V_{11} - V_{12}$ ,  $V_{1c} = (V_{11} + V_{12})/2$ ,  $I_{1d} = (I_{11} - I_{12})/2$ ,  $I_{1c} = (I_{11} + I_{12})/2$ ; idem for the exit voltages and currents; all OFA parameters without OFA number are average values.

The nominal value of the reciprocal admittance is  $1/Y_m = -1/Y_2$ . All other terms are error terms which have been explained in the preceding part of this chapter. The common-mode crosstalk ratio (CMCR), or the reciprocal value of the common-mode rejection ratio (CMRR), is  $1/H_i$ .

A complete instrumentation voltage amplifier arises if we include the current-to-voltage conversion function of the load impedances  $Z_{L1}$  and  $Z_{L2}$ . In that case the reciprocal nominal overall voltage gain  $1/A_{vm}$  and the overall CMCR  $1/H_i$  are given by Eq. 3.4.4.

$$\begin{aligned} 1/A_{vm} &= -1/Y_2 Z_{1d} \\ 1/H_i &\simeq 1/H_e + 1/F_e H_{iL} \end{aligned} \quad (3.4.4)$$

with:  $Z_{1d} = Z_{L1} + Z_{L2}$ ,  $1/H_{iL} = \Delta Z_{L1}/Z_{1d}$ ,  $\Delta Z_{L1} = Z_{L1} - Z_{L2}$ .

The reciprocal value of the discrimination factor is defined as:  $1/F_e = (I_{2c}/V_{ic})/I_{2d}(V_{id}) = 1/Z_{tce} Y_m$ .

From the above expression we see that a low overall CMCR  $1/H_i$  can only be obtained if the amplifier has a low CMCR  $1/H_e$  as well as a low reciprocal discrimination factor  $1/F_e$ . The effect of the latter term is further reduced by a low CMCR  $1/H_{iL}$  of the load circuit.

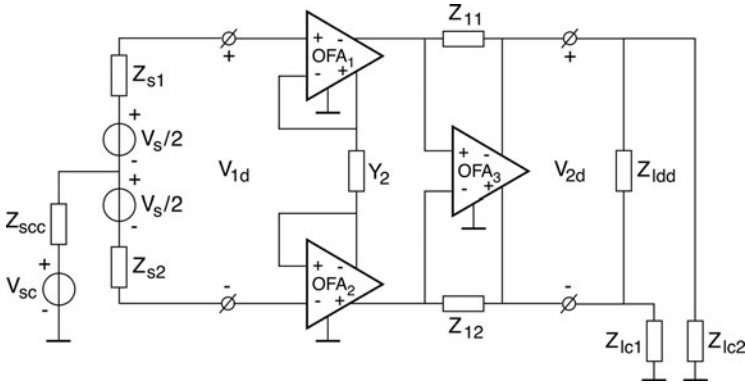


Fig. 3.4.4 Instrumentation voltage amplifier with source and load circuits

### Instrumentation Voltage Amplifier

An instrumentation voltage amplifier with a voltage-source character between the output terminals arises if we insert a balanced floating impedance amplifier with an OFA and two impedances  $Z_{11}$  and  $Z_{12}$  between the preceding example's instrumentation transadmittance amplifier and its load circuit [3.3, 3.4].

The complete instrumentation voltage amplifier circuit is drawn in Fig. 3.4.4 together with the source and load circuits.

The reciprocal nominal overall differential voltage gain and the CMCR of the complete amplifier are described by Eq. 3.4.5.

$$\begin{aligned} 1/A_{vm} &= -1/Y_2 Z_{1s} \\ 1/H_i &\simeq 1/H_e + 1/F_e H_i \end{aligned} \quad (3.4.5)$$

with:  $Z_{1s} = Z_{11} + Z_{12}$ ,  $1/H_i = \Delta Z_1 / Z_s$ ,  $\Delta Z_1 = Z_{11} - Z_{12}$

The instrumentation amplifier has a floating entrance port and an independently floating exit port. It measures the differential entrance voltage at nominal zero entrance currents. The differential exit port has a voltage source character.

### Instrumentation Current Amplifier

If we change the sequence of the transadmittance and transimpedance amplifiers of the preceding example we obtain an instrumentation current amplifier. This circuit is drawn in Fig. 3.4.5 together with the source and load circuits.

The overall reciprocal nominal current gain is given by Eq. 3.4.6.

$$1/A_{vm} = -1/Y_2 Z_{1s} \quad (3.4.6)$$

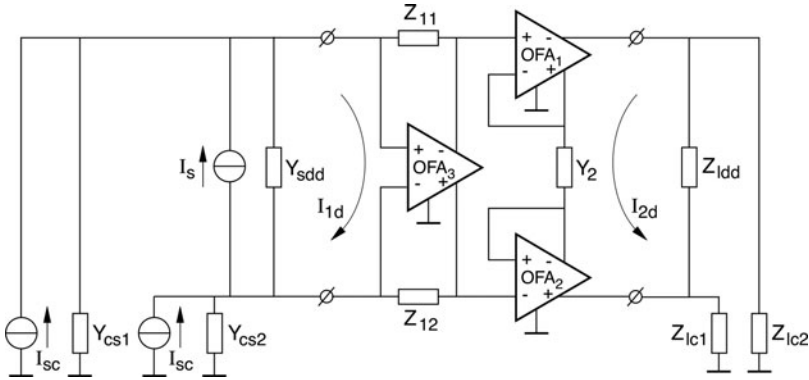


Fig. 3.4.5 Instrumentation current amplifier

The instrumentation current amplifier has a floating entrance port and an independently floating exit port. It measures the differential entrance current at nominal zero differential entrance voltage. The exit port has a current source character.

### Gyrator Floating

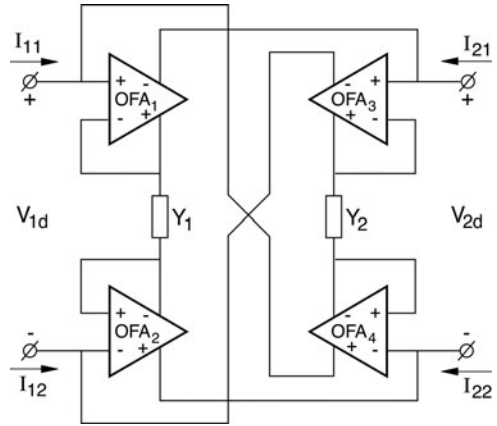
From among the applications of the OFA the gyrator should not be left out. A fully floating gyrator can be composed of two instrumentation transadmittance amplifiers as shown in Fig. 3.4.6 [3.5, 3.6]. The nominal and error terms of the transfer are given in Eq. 3.4.7.

$$\begin{pmatrix} I_{1d} \\ I_{1c} \\ I_{2d} \\ I_{2c} \end{pmatrix} = \begin{pmatrix} 1/Z_{t21n} + 1/Z_{t21e} & \cdot & 1/Z_{1de} & \cdot \\ \cdot & \cdot & \cdot & 1/Z_{1ce} \\ 1/Z_{2de} & \cdot & 1/Z_{t21n} + 1/Z_{t21e} & \cdot \\ \cdot & 1/Z_{2ce} & \cdot & \cdot \end{pmatrix} \begin{pmatrix} V_{2d} \\ V_{2c} \\ V_{1d} \\ V_{1c} \end{pmatrix}; \quad (3.4.7)$$

with:

$$\begin{aligned} 1/Z_{t21n} &= -Y_2 \\ 1/Z_{t21e} &= Y_2 \\ 1/Z_{t21e} &\simeq 2Y_2 \cdot 2Y_2/2Y_t + Y_{id} \cdot 2Y_2/2Y_t \\ &\quad - Y_{ic}/2 + 1/H_i Y_2 - Y_{oc}/2 + 2/H_o Y_2 \\ 1/Z_{t21e} &\simeq -2Y_2 \cdot 2Y_1/2Y_t - Y_{id} \cdot 2Y_1/2Y_t + Y_{ic}/2 \\ &\quad - 1/H_i Y_2 + Y_{oc}/2 - 2/H_o Y_2 \\ 1/Z_{1de} &\simeq 2Y_2 Y_{od}/2Y_t + Y_{id} \cdot 2Y_1/2Y_1 + Y_{ic}/2 + Y_{oc}/2 \\ 1/Z_{2de} &\simeq 2Y_1 Y_{od}/2Y_t + Y_{id} \cdot 2Y_2/2Y_t + Y_{ic}/2 + Y_{oc}/2 \end{aligned}$$

**Fig. 3.4.6** Floating gyrator



and with average OFA parameters.

The nominal resonant frequency  $\omega_o$  circuit which is composed of a gyrator with  $Y_1 = Y_2 = 1/R$  and loaded on both sides with a capacitance  $C_1 = C_2 = C$  is given in Eq. 3.4.8.

$$\omega_n = I/RC \tag{3.4.8}$$

$$1/Q \simeq 2R/R_d - 2C_t/C$$

with:  $1/R_d = \text{real}(1/Z_{de})$ ,  $\omega_n C_t = \text{im.}(1/Z_{te})$ ,  $Z_{de} \simeq Z_{1de} \simeq Z_{2de}$ ,  $Z_{te} \simeq Z_{t21e} \simeq Z_{t21e}$

The second term in the expression of  $1/Q$  describes the phase-lag in admittance amplifiers. This phase-lag undamps the circuit at higher resonant frequencies.

### Conclusion

The application examples given in this section have shown the relation between the specifications of the active devices and the accuracy of the applications mentioned. This is necessary for determining how far we have to go in improving the specifications of the active devices whose designs will be the subjects of the following chapters. The important overall specification of dynamic range brings about special requirements, as we will see in the next section.

### 3.5 Dynamic Range

The total amount of information that can be processed in an analog signal-processing step is determined by the product of dynamic range and bandwidth. The dynamic range over power limitations will be evaluated in this section,

while the bandwidth over power limitations will be extensively covered in Sect. 6.2.

The fundamental specification of low power is in contradiction to the fundamental specification of dynamic range. Therefore, it is important to see how these specifications relate in several OVA applications. An optimum for low power and dynamic range can be found if the output stage and input stage possess a rail-to-rail voltage range. This will be shown in this section, in which the OVA will simply be called Operational Amplifier (OpAmp).

### Dynamic Range Over Supply-Power Ratio

The trend towards smaller dimensions in VLSI circuits firstly leads to smaller break-down voltages across isolation barriers. The supply voltages will go down from 5 through 3 to 2 V or even 1 V. Secondly, the high density of circuit cells on a chip limits the power that can be dissipated per circuit cell. Moreover, the increased use of batteries or solar power in wireless applications emphasise the above trend. As a consequence, the dynamic range (DR) of analog signals is squeezed down between a lower supply-voltage ceiling and a higher noise-voltage floor. The latter is a consequence of a lower supply current.

The maximum top value of a single-phase signal voltage is equal to half the supply voltage  $V_{sst} = V_{sup}/2$ , as is shown in Fig. 3.5.1a. Its RMS value is  $V_{ss} = V_{sup}/2\sqrt{2}$ . If this signal is present across a signal-processing resistor  $R_s$ , the supply power needed to drive this resistor in class-B mode is  $P_{sup} = V_{sup}I_{av} = V_{sup}^2/2\pi R_s$ . The thermal noise voltage across this resistor equals:  $V_N = (4kTB_e R_s)^{1/2}$ , in which k is Boltzman’s constant, T the absolute temperature, and  $B_e$  the effective bandwidth. The maximum dynamic range as a function of the supply power can now be calculated as

$$DR_{max} = \frac{V_{ss}^2}{V_N^2} = \frac{\pi}{4} \cdot \frac{P_{sup}}{4kTB_e} \tag{3.5.1}$$

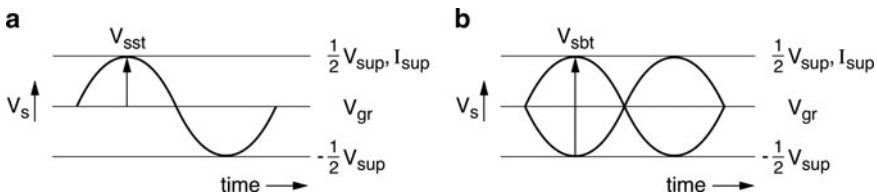


**Fig. 3.5.1** (a) and (b) Single and Balanced rail-to-rail voltage  $V_{sst} = V_{sup}/2$  and  $V_{sbt} = V_{sup}$ , respectively, across a class-B driven signal-processing resistor has a maximum  $DR = (\pi/4)P_{sup}/4kTB_e$  ( $= 89$  dB at  $P_{sup} = 16 \mu W$ ,  $B_e = 1$  MHz)



from which we can find the dynamic-range over supply-power ratio as

$$\frac{DR_{max}}{P_{sup}} = \frac{\pi}{4} \cdot \frac{1}{4kTB_e} \quad (3.5.2)$$

Exactly the same expressions are found for the balanced case, where the top value of a balanced signal voltage is equal to the full supply voltage  $V_{sbt} = V_{sup}$ , instead of half the supply voltage in the single case, see Fig. 3.5.1b. To consume the same power, the value of the balanced resistor  $R_b$  must be taken four times that of the single one:  $R_b = 4R_s$ .

### Voltage-to-Current Converter

A simple example is shown in the single and balanced voltage-to-current converter shown in Fig. 3.5.2a, b with a single resistor of  $R_s = 10 \text{ k}\Omega$  or balanced resistor of  $R_b = R_{b1} + R_{b2} = 40 \text{ k}\Omega$  respectively, at a supply voltage  $V_{sup} = V_{SP} - V_{SN}$  of 1 V, in a bandwidth of 1 MHz. In this case the supply power  $P_{sup}$  is  $16 \text{ }\mu\text{W}$  at a maximum sinusoidal signal. The result is a maximum dynamic range  $DR_{max}$  of 89 dB. This maximum can only be obtained if the signal processing resistors can be driven in class-B and rail-to-rail, and when the amplifier is noise free.

If the output stage is biased in class-A instead of in class-B, the bias current must be equal to the maximum current and the  $DR/P_{sup}$  ratio loses minimally a factor of  $\pi$ , or 5 dB from its maximum value. This loss for class-A in regard to class-AB may easily be a factor of 100, or 40 dB, in the many cases where the signals are much lower than their maximum values most of the time. This is the case in audio, telecommunications, hearing aids, etc. If the output voltage range is restricted to one-third of the supply voltage, for instance when a diode voltage  $V_{BE}$  is lost at a supply voltage of 1 V, the  $DR/P_{sup}$  ratio loses another factor 3, or 5 dB.

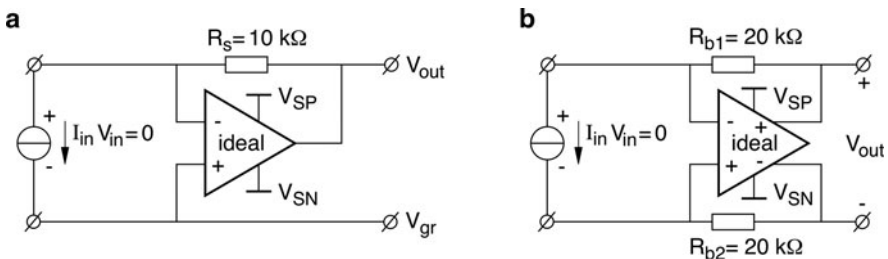


**Fig. 3.5.2** (a) and (b) Single and balanced voltage-to-current converter with  $R_s = 10 \text{ k}\Omega$  and  $R_{b1} = R_{b2} = 20 \text{ k}\Omega$ , respectively, with a  $DR = 89 \text{ dB}$  at  $V_{sup} = V_{SP} - V_{SN} = 1 \text{ V}$ ,  $P_{sup} = 16 \text{ }\mu\text{W}$ , R-R class-B output stage, and a bandwidth of 1 MHz

### Inverting Voltage Amplifier

The inverting voltage amplifier of Fig. 3.5.3a, firstly, loses a factor of 2, or 3 dB in its  $DR/P_{sup}$  ratio because an additional input buffer is needed to supply the power in the resistor  $R_1$ . Otherwise, this power has to be supplied by the source. Secondly, another factor 2, or 3 dB, is lost because of the noise of the two resistors. The resulting  $DR_{max}$  is 83 dB at a supply voltage of 1 V and a bandwidth of 1 MHz.

When we would choose a gain of 10 in the inverting voltage amplifier of Fig. 3.5.3a with  $R_1 = 2 \text{ k}\Omega$  and  $R_2 = 20 \text{ k}\Omega$ , we firstly lose a factor of 2, or 3 dB into the input buffer, and secondly another factor of 10, or 10 dB because resistor  $R_1$  only uses one-tenth of the supply voltage range. This means that the  $\sqrt{10}$  times larger current noise of resistor  $R_1 = 2 \text{ k}\Omega$  will be reflected into the ten times larger resistor  $R_2 = 20 \text{ k}\Omega$ , which gives rise to a ten times larger noise power. The resulting  $DR_{max}$  is 76 dB. The same result is obtained with the balanced version given in Fig. 3.5.3b.

### Non-Inverting Voltage Amplifier

The non-inverting voltage amplifiers shown in Fig. 3.5.4a, b with a gain of 10 do better than the inverting one(s). We only lose a factor of 10, or 10 dB, proportional

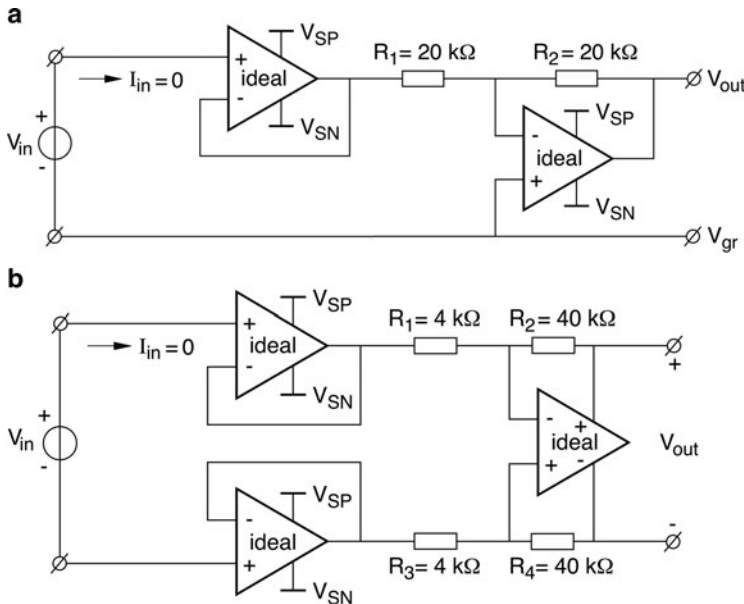
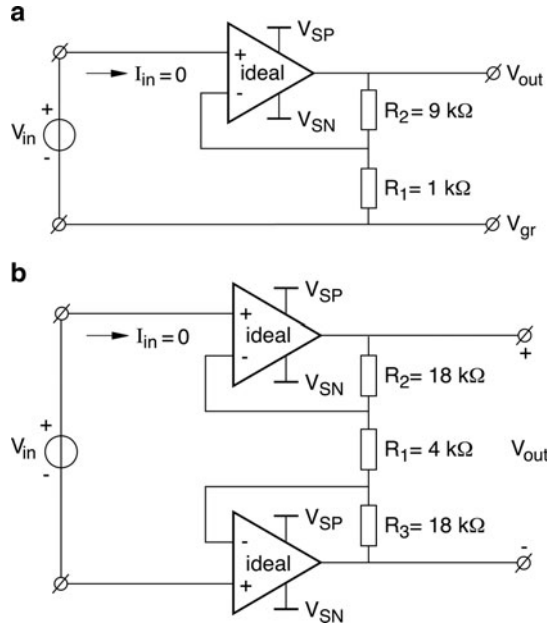


**Fig. 3.5.3** (a) Inverting amplifier with  $A = -R_2/R_1 = -1$ , with a  $DR = 89 - 3 - 3 = 83 \text{ dB}$ , at a supply voltage  $V_{sup} = V_{SP} - V_{SN}$  of 1 V,  $P_{sup} = 16 \text{ }\mu\text{W}$ , R-R, class B, 1 MHz. If  $R_1 = 2 \text{ k}\Omega$ ,  $R_2 = 20 \text{ k}\Omega$ , we obtain  $A = -10$ , with a  $DR = 89 - 3 - 10 = 76 \text{ dB}$ . (b) Balanced inverting amplifier with  $A = -(R_2 + R_4)/(R_1 + R_3) = -10$ , with a  $DR = 89 - 3 - 10 = 76 \text{ dB}$ , at a supply voltage  $V_{sup} = V_{SP} - V_{SN}$  of 1 V,  $P_{sup} = 16 \text{ }\mu\text{W}$ , R-R, Class-B, and 1 MHz

**Fig. 3.5.4** (a) Non-inverting voltage amplifier with  $A = (R_2 + R_1)/R_1 = +10$ , with a  $DR = 89 - 10 = 79$  dB, at a supply voltage  $V_{sup} = V_{SP} - V_{SN}$  of 1 V,  $P_{sup} = 16 \mu\text{W}$ , R-R, Class-B, and 1 MHz. (b) Balanced non-inverting voltage amplifier with  $A = (R_3 + R_2 + R_1)/R_1 = +10$ , with a  $DR = 89 - 10 = 79$  dB, at a supply voltage  $V_{sup} = V_{SP} - V_{SN}$  of 1 V,  $P_{sup} = 16 \mu\text{W}$ , R-R, Class-B, and 1 MHz



to the gain because  $R_1$  only uses one-tenth of the supply voltage range. We do not lose the factor 2, or 3 dB, because we do not need an additional input buffer. The  $DR_{max}$  is 79 dB in a frequency band of 1 MHz and a supply voltage of 1 V.

### Inverting Voltage Integrator

The balanced inverting voltage integrator shown in Fig. 3.5.5 only loses the factor 2, or 3 dB, because of the use of input buffers. The capacitors do not add to the noise.

Within the effective bandwidth of  $B_e = 1/2\pi RC$ , with  $R = R_1 = R_2 = 40 \text{ k}\Omega$  and  $C = C_1 = C_2$ , at a supply voltage of 1 V, the  $DR_{max}$  is 86 dB. The resistor values have been chosen such that the supply power is again  $16 \mu\text{W}$  at a maximum sinusoidal signal [3.7].

The dynamic range of an inverting voltage integrator is generally large:

$$\begin{aligned}
 DR &= (\pi/4)P_{sup}/4kTB_e = (\pi^2/2)P_{sup}RC/4kT \\
 &DR = \pi V_{sup}^2 C/4kT
 \end{aligned}
 \tag{3.5.3}$$

with:  $B_e = 1/(2\pi RC)$ ,  $R = R_1 = R_2$ ,  $C = C_1 = C_2$

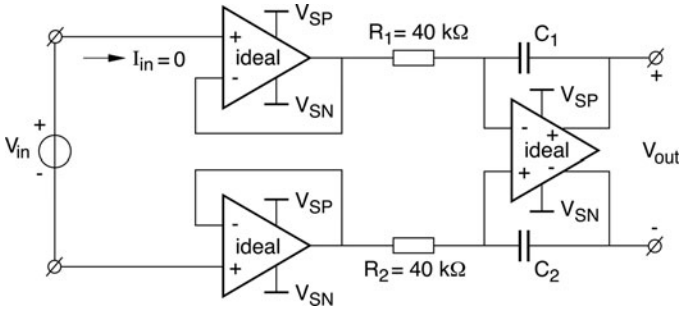


**Fig. 3.5.5** Balanced inverting voltage integrator with  $A = -(1/j\omega C_1 + 1/j\omega C_2)(R_1 + R_2)$  with a  $DR = 89 - 3 = 86$  dB, at  $V_{sup} = V_{SP} - V_{SN} = 1$  V,  $P_{sup} = 16$   $\mu$ W, R-R, Class-B, and 1 MHz

### Current Mirror

A very severe loss of the DR is found in current mirrors. The current mirror of Fig. 3.5.6 firstly, loses a factor  $\pi$ , or 5 dB in the  $DR_{max}$  because the circuit operates in class-A and not in class-AB, and, secondly, a factor 40, or 16 dB with bipolar transistors because the signal is compressed in a voltage range of  $V_T \approx kT/q = 25$  mV across the gain-setting base-emitter resistors. These resistors are small in regard to  $V_{sup}/I_{sup}$  and therefore their noise current is unnecessarily large. The resulting DR is only 68 dB. This is a factor 30, or 15 dB lower than the DR of the inverting voltage amplifier. Emitter degeneration resistors will help in decreasing the loss. A CMOS mirror will also do better, because a better use of the supply-voltage range is made because of the larger intrinsic source resistances.

The dynamic range of a current mirror is generally:

$$DR = (n/(n + 1)^2)(V_T/V_{sup})P_{sup}/4kTB_e \tag{3.5.4}$$

$$DR = (1/4)(1/40)P_{sup}/4kTB_e = 89 - 5 - 16 = 68 \text{ dB}$$

with:  $V_T = kT/q = 1/40$ ,  $n = 1$ ,  $V_{sup} = 1$  V,  $P_{sup} = 16$   $\mu$ W, class - A, and 1 MHz

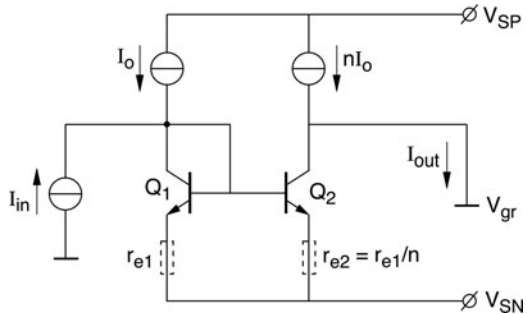


**Fig. 3.5.6** Bipolar current mirror with  $I_{out}/I_{in} = -n$ , with a  $DR = 89 - 5 - 16 = 68$  dB, with  $n = 1$ ,  $V_{sup} = V_{SP} - V_{SN} = 1$  V,  $P_{sup} = 16$   $\mu$ W, class-A, and 1 MHz

### ***Conclusion Current Mirror***

From this equation it follows that in all amplifier realizations, in which the signal has to pass through a current mirror, the dynamic range over power ratio is quite low. This is the case in so-called “current-mode” amplifiers. Moreover, in these current-mode solutions, where the signal passes through one or more internal current mirrors, the accuracy of the transfer is limited to that of the matching of non-linear transistor characteristics of the internal current mirrors. Further, current-mode active network elements do not fit the basic and accurate nullor approach of Chap. 1. Instead, they have more complicated network models and cannot describe the overall transfer function more accurately than of the order of 0.5%.

Another approach, the so-called current-mode feedback does have a better high-frequency behavior than the normal approach, due to the elimination of a pole in the feedback network. However, this solution has higher noise and offset due to the feeding of an emitter or source bias current through the feedback network. And again it does not fit the basic nullor approach of Chap. 1. For these reasons, so-called “current-mode” solutions, like current-mode amplifiers, and current-mode feedback are not discussed in this book.

### ***Non-Ideal Operational Amplifiers***

If we take into account the non-idealities of the amplifiers, then the  $DR/P_{sup}$  ratio is further reduced. Important non-idealities are caused by the input noise voltage and a restricted output voltage range.

The problem at the input is that we do not want to spill supply current in the input stage, while on the contrary, we need a large bias current for the active input devices in order to lower the input voltage noise. The input voltage noise can easily be estimated by the equivalent input series noise resistance  $R_{neqs}$ . For bipolar transistors  $R_{neqs} = r_e/2 = kT/2qI_e = V_T/2I_e$ , with  $V_T \approx 25$  mV at room temperature. For field-effect transistors we find  $R_{neqs} = \gamma/g_m = \gamma/(2\mu C_{ox}(W/L)I_D)^{1/2}$ , which is of the order of  $R_{neqs} = 10\gamma/(I_D)^{1/2}$  for transistors with a W/L ratio of 100, while  $\gamma$  is of the order of 2. The W/L ratio has been chosen as large for analog applications to increase  $g_m$  and lower noise and offset input voltages.

An optimal solution would be to choose no separate input transistors, but to use one-stage amplifiers in which the input transistors are used as output transistors as well. This interesting realization will be shortly evaluated here. In Fig. 3.5.7a, b, a single and balanced current-to-voltage application is shown with a one-stage single or balanced class-A transistor amplifier. The transistors  $T_1$  and  $T_2$  symbolize either bipolar or field-effect transistors.

Because of the class-A operation, we lose at least 5 dB. With bipolar transistors the equivalent input noise resistor will be  $R_{neqs} \approx 700 \Omega$  for the single and 1,500  $\Omega$  for the balanced version at a total supply current of 16  $\mu$ A. The resulting extra noise is much lower than 1 dB. With CMOS transistors, the equivalent input noise resistor will be

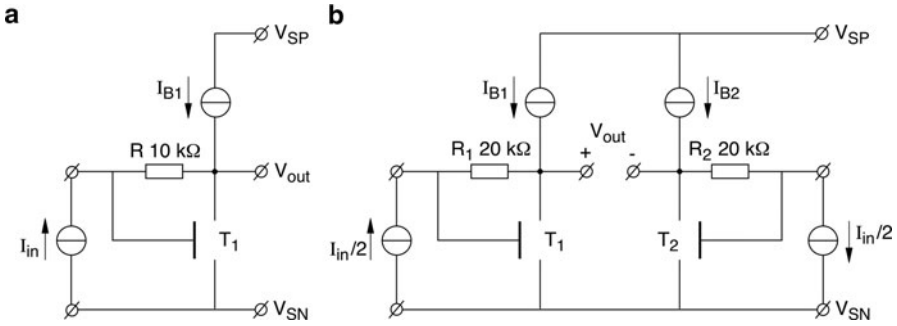


**Fig. 3.5.7** (a) and (b) Single and balanced current-to-voltage converter in a single-stage class-A realization with a  $DR = 89 - 5 - 1 = 83$  dB for bipolar transistors, and  $DR = 89 - 5 - 2 = 82$  dB for CMOS transistors,  $R$ -R,  $V_{sup} = 1$  V,  $P_{sup} = 16$   $\mu$ W,  $I_B = 16$   $\mu$ A, and 1 MHz

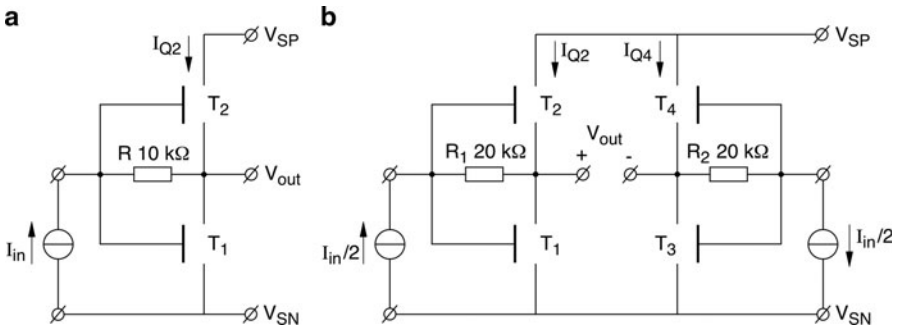


**Fig. 3.5.8** (a) and (b) Single and balanced current-to-voltage converter in a single-stage class-AB realization with a  $DR = 89 - 2 = 87$  dB for bipolar transistors and  $DR = 89 - 5 = 84$  dB for CMOS transistors at  $V_{sup} \approx 1.2$  V,  $P_{sup} = 20$   $\mu$ W, 1 MHz

$R_{neqs} = 5,000 \Omega$  for the single and 7,000  $\Omega$  for the balanced version. The resulting extra noise is of the order of 2 dB. At the output the signal cannot reach the rail within 100 mV. This results in a loss of 1 dB for bipolar as well as CMOS transistors.

We can avoid the  $-5$  dB loss of class-A biasing if we choose a class-AB push-pull configuration as shown in Fig. 3.5.8a, b.

The push-pull transistors have been connected with the emitters or sources between the rails, while their bases or gates are connected. To ensure proper class-AB biasing the supply rail voltage has to be regulated at two diode voltages at a proper quiescent current  $I_Q$ . The circuit may function at roughly 1.2 V. While we have now avoided the  $-5$  dB loss of the class-A circuit with a class-AB approach, the input noise voltage has been increased because the quiescent current has been reduced strongly with no signal. If we choose the quiescent current at one-tenth of the maximum current, the extra noise reduces the  $DR$  by 2 dB for bipolar transistors and 5 dB for CMOS transistors. The result is still better than in class-A. However, we have to build an additional supply-voltage regulator which easily takes away another 1 dB from the dynamic range. Moreover, the solution is only valid for a fixed low voltage and for the inverting OpAmp type.

If we also have to take the DC offset into account, the dynamic range becomes even lower. At DC the dynamic range is  $DR_{max\ DC} = V_{sup}^2/V_{offs}^2$ . With bipolar transistors we may expect an offset of 0.3 mV, which results in  $DR_{max\ DC} = 70$  dB, at a supply voltage of 1 V. For field-effect transistors with an offset of 3 mV the result is  $DR_{max\ DC} = 50$  dB. Only chopping can elevate this limit.

## Conclusion

We have shown that the thermal noise in the gain-setting resistors principally limits the dynamic-range over supply-power ratio of an analog signal operation to  $DR_{max}/P_{sup} = (4/\pi)/4kTB_e$ . At a supply voltage of 1 V and a gain setting resistor of 10 k $\Omega$  in a current-to-voltage converter, the supply power is 16  $\mu$ W for sinusoidal signals and the dynamic range in a bandwidth of 1 MHz can never be better than  $DR_{max} = 89$  dB, even for an ideal Operational Amplifier.

This maximum can only be obtained if the Operational Amplifier is able to, firstly, efficiently feed the full supply voltage range from rail-to-rail (R-R) to the load, and secondly, efficiently feed the supply current in a class-AB mode to the load or feedback resistor. In some cases, for instance in a voltage buffer input application, the Operational Amplifier must also be able, thirdly, to efficiently allow a common-mode signal from rail-to-rail. These three requirements impose the important requirements in the design of the input stages of Chap. 4 and output stages of Chap. 5.

In amplifiers where the above requirements can not be met, the dynamic range over power ratio is lower. For instance, when a diode prevents the output to go from rail-to-rail, but only allows an output voltage swing of 0.3 V at a supply voltage of 1 V, the dynamic range loses 10 dB. When the biasing is not class-AB, but class-A, we lose at least 5 dB or much more at low signal levels.

When we process analog signals through a bipolar current mirror without emitter degeneration, we lose 16 dB of dynamic-range over power ratio. With degenerated or CMOS current mirrors the loss is still 10 dB or more. Moreover, the accuracy and linearity of the overall transfer function is only as good as the matching of highly non-linear internal transistor-diode characteristics. For these reasons we will leave out current-mode amplifiers from this book.

## 3.6 Problems

### Problem 3.1

The circuit in Fig. 3.2.1 shows a non-inverting voltage amplifier built around the operational amplifier model explained with Fig. 2.2.1. The impedances in the external circuit are  $Z_S = 10$  k $\Omega$ ,  $Z_I = 10$  k $\Omega$  and  $Z_2 = 40$  k $\Omega$ .  $Z_I$  is the load

impedance and has a value of 50 k $\Omega$ . The parameters for the operational amplifier macromodel are:  $V_{ioffs} = 10$  mV,  $I_{ioffs} = 10$  nA,  $I_{ibias} = 50$  nA,  $Y_{id} = 1/20$  M $\Omega$ ,  $Y_{ic1} = Y_{ic2} = 1/100$  M $\Omega$ ,  $H_i = 80$  dB,  $Y_t = 100$  S and  $Y_o = 1/1$  k $\Omega$ . Calculate the output voltage for an input voltage of  $V_S = 10$  mV, 100 mV, 1 V.

### Solution

The matrix equation (3.2.1) shows the relations between input/output voltages and currents for the application circuit. Solution starts by calculating the parameters  $A_{vn}$ ,  $A_{ve}$ ,  $Y_{te}$ ,  $Z_{te}$ ,  $A_{ie}$ .

These values can be used to calculate the nominal and error terms in Eq. 3.2.1:

$$\begin{aligned}
 \frac{1}{A_{vn}} &= \frac{Z_1}{Z_1 + Z_2} = 0.2 \\
 \frac{1}{A_{ve}} &= \frac{Y_o + Y'_s}{Y_t} + \frac{Y_{id}(Y_o + Y'_s)}{Y_p Y_t} + \frac{1}{A_{vn} H_i} - \frac{Y_{ic1}}{Y_p A_{vn}} = 13.5 \times 10^{-6} \\
 \frac{1}{Y_{te}} &= \frac{1}{Y_t} + \frac{Y_{id}}{Y_p Y_t} = 0.010004 \\
 \frac{1}{Z_{te}} &= \frac{Y_{id}(Y_o + Y'_s)}{Y_t} + \frac{Y_{ic2}}{A_{vn}} = 2.10^{-9} \\
 \frac{1}{A_{ie}} &= \frac{Y_{id}}{Y_t} = 5.10^{-10} \\
 I_{loffs} &= I_{ibias} = 50 \text{ nA} \\
 V_{loffs} &= V_{ioffs} + \frac{I_{loffs}}{Y_p} + \frac{I_{ibias}}{Y_p} = 10.48 \text{ mV}
 \end{aligned} \tag{3.6.1}$$

With these values replaced in the matrix equation (3.2.1), and considering the voltage-current relations at the input and output

$$\begin{aligned}
 V_S - V_1 &= Z_S I_1 \\
 V_2 &= Z_l I_2
 \end{aligned} \tag{3.6.2}$$

With these values replaced in the matrix equation (3.2.1), and considering the voltage-current relations at the input and output

$$\begin{aligned}
 V_S - V_1 &= Z_S I_1 \\
 V_2 &= Z_l I_2
 \end{aligned} \tag{3.6.3}$$



the following equation is obtained for  $V_2$ :

$$V_2 \frac{V_S - Z_S I_{1offs} - V_{1offs}}{\frac{1}{A_{vn}} + \frac{1}{A_{ve}} - \frac{1}{Z_t Y_{te}} + \frac{Z_S}{Z_{te}} - \frac{Z_S}{Z_t A_{ie}}} \quad (3.6.4)$$

Replacing the values for circuit parameters and signal source voltage, the three output voltage values result:

$$\begin{aligned} V_2(10 \text{ mV}) &= -4.9 \text{ mV} \\ V_2(10 \text{ mV}) &= 445 \text{ mV} \\ V_2(1 \text{ V}) &= 4.94 \text{ V} \end{aligned} \quad (3.6.5)$$

### Problem 3.2

Figure 3.4.1 shows a voltage-to-current converter built around the OFA macromodel explained with Fig. 2.4.1. The external components are  $Z_S = 10 \text{ k}\Omega$ ,  $Y_2 = 1/50 \text{ k}\Omega$ ,  $Y_t = 1/50 \text{ k}\Omega$ . The macromodel parameters have the following values:  $V_{ioffs} = 10 \text{ mV}$ ,  $I_{ioffs} = 10 \text{ nA}$ ,  $I_{ibias} = 100 \text{ nA}$ ,  $Y_{idd} = 1/10 \text{ M}\Omega$ ,  $Y_{ic1} = Y_{ic2} = 1/100 \text{ M}\Omega$ ,  $H_i = 80 \text{ dB}$ ,  $Y_t = 0.1 \text{ S}$ ,  $Y_{odd} = 1/1 \text{ M}\Omega$ ,  $I_{obias} = 100 \text{ nA}$ ,  $Y_{oc1} = Y_{oc2} = 1/100 \text{ M}\Omega$ ,  $H_o = 60 \text{ dB}$ . Calculate the output current  $I_2$  for a signal voltage  $V_S = 100 \text{ mV}$ ,  $1 \text{ V}$ ,  $5 \text{ V}$ .

### Solution

The matrix equation (3.4.1) shows the relations between input/output voltages and currents for the application circuit. Solution starts by calculating the parameters  $Y_{in}$ ,  $Y_{te}$ ,  $A_{ve}$ ,  $A_{ie}$ ,  $Z_{te}$ .

$$\begin{aligned} \frac{1}{Y_{in}} &= -\frac{1}{Y_2} = -50 \cdot 10^3 \\ \frac{1}{Y_{te}} &= -\frac{Y_2 + Y_{odd}}{Y_2 Y_t} - \frac{Y_{idd}(Y_2 + Y_{odd})}{Y_2^2 Y_t} - \frac{1}{H_i Y_2} + \\ &\quad \frac{Y_{ic1}}{Y_2^2} - \frac{2}{H_o Y_2} + \frac{Y_{oc2}}{Y_2^2} = -65.55 \\ \frac{1}{A_{ve}} &= -\frac{Y_{odd}}{Y_t} - \frac{Y_{idd} Y_{odd}}{Y_t Y_2} - \frac{2 Y_{odd}}{Y_t H_o Y_2} - \frac{Y_{oc1}}{Y_2} = -1.51 \cdot 10^{-3} \\ \frac{1}{A_{ie}} &= \frac{Y_{idd}(Y_{odd} + Y_2)}{Y_2 Y_t} - \frac{Y_{ic1}}{Y_2} = -5.01 \cdot 10^{-4} \\ \frac{1}{Z_{te}} &= -\frac{Y_{idd} Y_{odd}}{Y_t} = -1 \cdot 10^{-12} \\ V_{1offs} &= V_{ioffs} + \frac{I_{ioffs}}{Y_2} + \frac{I_{ibias}}{Y_2} + \frac{2I_{obias}}{Y_2} = 0.025 \text{ V} \\ I_{1offs} &= I_{ioffs} + I_{ibias} = 110 \text{ nA} \end{aligned} \quad (3.6.6)$$

With these values replaced in the matrix equation (3.4.1) and considering the voltage-current relations at the input and output

$$\begin{aligned} V_S - Z_S I_1 &= V_1 \\ I_2 &= -Y_1 V_2 \end{aligned} \quad (3.6.7)$$

the following equation is obtained for  $I_2$ :

$$I_2 = -\frac{V_S - Z_S I_{1offs} - V_{1offs}}{\frac{1}{Y_{in}} + \frac{1}{Y_{te}} + \frac{1}{Y_{tA_{ve}}} + \frac{Z_S}{A_{ie}} + \frac{Z_S}{Z_{te} Y_1}} \quad (3.6.8)$$

Replacing the values for circuit parameters and signal source voltage, the three output voltage values result:

$$\begin{aligned} I_2(10 \text{ mV}) &= -1.47 \text{ } \mu\text{A} \\ I_2(1 \text{ V}) &= -19.4 \text{ } \mu\text{A} \\ I_2(5 \text{ V}) &= -99.18 \text{ } \mu\text{A} \end{aligned} \quad (3.6.9)$$

### Problem 3.3

The instrumentation amplifier shown in Fig. 3.5.3b relies on a differential input buffer and an inverting differential amplifier. Using the resistor nominal values  $R_1 = R_3 = 4 \text{ k}\Omega$ ,  $R_2 = R_4 = 40 \text{ k}\Omega$ , a supply voltage  $V_{SP} = 3 \text{ V}$ ,  $V_{SN} = 0 \text{ V}$  and non-ideal operational amplifiers with input common mode voltage range  $\Delta_{VIN} = (V_{SP} - 1 \text{ V}; V_{SN} - 0.5 \text{ V})$ , output voltage range  $\Delta_{VOUT} = (V_{SP} - 0.2 \text{ V}; V_{SN} + 0.2 \text{ V})$  and  $V_{ioffs} = 10 \text{ mV}$ , calculate the maximum input signal which can be amplified without distortion. Using this value, calculate the ratio of dynamic range over dissipated power which can be obtained with this amplifier over a bandwidth  $\Delta f = 1 \text{ MHz}$  if each operational amplifier draws  $I_d = 100 \text{ } \mu\text{A}$  and has an input noise of  $S_f = 10 \text{ nV}/\sqrt{\text{Hz}}$ . The resistors have a precision of  $\Delta R = 2\%$ . Boltzmann's constant is  $K = 1.38 \times 10^{-23}$ , temperature  $T = 300 \text{ K}$ .

### Solution

The first limit is introduced at the input by the differential buffer, as both input operational amplifiers are connected as repeaters, thus not allowing all of the input voltage range to be used:

$$\begin{aligned} V_{imin} &= V_{ioffs} + V_{VOUTmin} = V_{SN} + 0.2 \text{ V} + V_{ioffs} = 0.210 \text{ V} \\ V_{imax} &= V_{VINmax} - V_{ioffs} = V_{SP} - 1.0 \text{ V} - V_{ioffs} = 1.990 \text{ V} \end{aligned} \quad (3.6.10)$$

Another factor of  $R_2/R_1$  is lost in order not to saturate the output, which limits the input signal to

$$V_{imax} - V_{imin} = \frac{(V_{VOUTmax} - V_{VOUTmin})}{10} = 0.26 \text{ V} \quad (3.6.11)$$

Considering also the maximum gain

$$A_{Vmax} = \frac{R_2(1 + \Delta R)}{R_1(1 - \Delta R)} = 10.4 \quad (3.6.12)$$

$$V_{imax} - V_{imin} = \frac{(V_{VOUTmax} - V_{VOUTmin})}{A_{Vmax}} = 0.25 \text{ V}$$

this voltage range is reduced furthermore by the unwanted effect of the third operational amplifier input offset voltage:

$$V_{imax} - V_{imin} = \frac{(V_{VOUTmax} - V_{VOUTmin})}{A_{Vmax}} - 2V_{ioffs} = 0.248 \text{ V} \quad (3.6.13)$$

The dynamic range of the circuit is limited by the noise power and the maximum input signal. The input referred noise power is

$$P_n = 3S_f^2\Delta f + 4KTR_1\Delta f + 4KTR_3\Delta f \quad (3.6.14)$$

and is composed from buffer noise and equivalent resistor noise (virtually the equivalent resistors are equal with  $R_1, R_3$ ). The dynamic range can now be calculated

$$DR = 10\log_{10} \frac{(V_{imax} - V_{imin})^2}{P_n} = 81.5 \text{ dB} \quad (3.6.15)$$

The ratio of dynamic range over dissipated power is

$$\frac{DR}{P_d} = 112 \text{ dB} \quad (3.6.16)$$

### 3.7 References

- [3.1]. J.G. Graeme et al., *Operational Amplifiers Design and Applications* (McGraw Hill Book Company, New York, 1971)
- [3.2]. C.D. Motchenbacher, F.C. Fitchen, *Low-Noise Electronic Design* (John Wiley and Sons, New York, 1973)
- [3.3]. J.H. Huijsing, Instrumentation amplifiers: a comparative study on behalf of monolithic integration. *IEEE Trans. Instrum. Meas.* **IM-25**, 227–231 (1976)

- [3.4]. B.J. Dool, J.H. Huijsing, Indirect current feedback instrumentation amplifier with a common-mode input range that includes the negative rail. *IEEE J. Solid-St. Circ.* **28**(7), 743–749 (1993)
- [3.5]. J.D. Voorman, The gyrator as a monolithic circuit in electronic systems, Thesis, Katholieke Universiteit Nijmegen, Gema B.V., Eindhoven, June 1977
- [3.6]. K.M. Adams, E.F.A. Deprettere, J.O. Voorman, The gyrator in electronic systems in *Advances in Electronics and Electron Physics*, Vol. **37** (Academic Press, Inc., San Francisco, 1975), 79–179
- [3.7]. G. Groenewold, Optimal dynamic range integrated continuous-time filters, PhD thesis, Delft University of Technology, Delft, The Netherlands, 1992



## 4. Input Stages

The input stage of an Operational Amplifier has the task of sensing the differential input voltage. This process is disturbed by interference signals such as: offset, bias, drift, noise and common-mode crosstalk. The modeling of these signals has been given in Chap. 2. The level of these additive interference signals determines the useful sensitivity of the amplifier. The design of the input stage should aim at low values of these interference signals, while the current consumption should be low, and a large portion of the rail-to-rail range should be available for common-mode signals.

The discussion of input stages will be divided into aspects of: offset, bias, and drift in Sect. 4.1, noise in Sect. 4.2, common-mode crosstalk in Sect. 4.3; and the design of rail-to-rail input stages in Sect. 4.4.

### 4.1 Offset, Bias, and Drift

The quiescent input voltage and current, which are needed to drive the active elements at the input of an amplifier into their normal working range, result in equivalent offset and bias quantities at the input of an amplifier (see Chap. 2). Variations in these quantities as a function of time, supply voltage, or ambient temperature are referred to as drift.

The product of differential input voltage and input current is the input sensing power which must be supplied by the external source circuit. It is clear that a high sensitivity requires a low input sensing power in order to distinguish the differential DC signal from offset, bias, and drift.

Generally, the lowest input sensing power, or product of input voltage and current, is achieved if the active elements at the input are connected in the general-amplifier (GA) connection (common-emitter or common-source connection). This is the reason why all effective input stages have a GA connection.

One can apply two general techniques to reduce the effect of quiescent input voltages and currents: isolation and balancing. We will review these techniques.

## ***Isolation Techniques***

The input offset and bias quantities are the manifest results of the quiescent voltages and currents of the active elements in the input circuit. One of the most successful ways of reducing offset and bias is to apply active elements whose input is electrically isolated from the internal quiescent voltages and/or currents.

Examples of this electrical isolation can be found in the group of parametric amplifiers, such as the magnetic amplifier and the vibrating capacitor electrometer. A monolithically integrable variant of the latter is the varactor electrometer amplifier with varactor diodes as voltage-dependent capacitances. With a varactor amplifier an input offset current as low as 10 fA can be obtained, while the offset voltage is of the order of 1 mV [4.1].

Another elaboration of the principle of isolation is the separation of useful frequency regions from frequency bands where additive interference signals such as offset, drift and 1/f-noise can be expected. This idea is realized in the chopper amplifier or in the chopper-stabilized amplifier [4.2] (see Chap. 10 of this book). The residual offset quantities are mainly caused by capacitive crosstalk of the chopper driving signals. With CMOS chopper switches offset values of 1 $\mu$ V and 1 nA can be obtained.

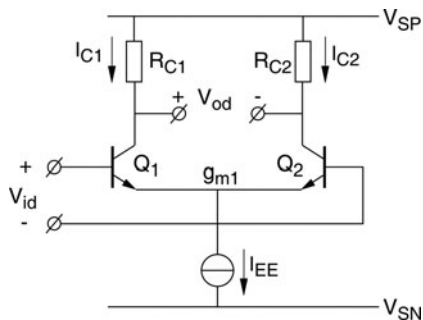
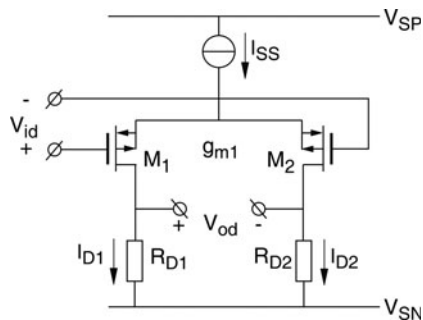
The principle of isolation can also be applied to reduce the effects of variations in the environmental conditions. Some examples are: stabilizing the supply voltages, isolating the chip from changes in the ambient temperature or stabilizing the chip temperature, isolating the chip from mechanical vibrations, and avoiding the influence of chemical reactions by the use of stable materials or an effective shielding.

A design which aims at a low value of the offset and drift must generally have an input stage with a sufficient amount of gain to shield the influence of offset and drift of stages behind the input stage.

Basically, isolation, shielding, or stabilization can be applied to any degree of perfection by increasing the “isolation barrier”. This is in contrast to balancing where the result is limited by the accuracy with which components can be matched, which is in turn dependent on the precision of the integration process. However, the above-mentioned isolation techniques can not always be applied. Then, we must rely on balancing techniques, which is the subject of the following section.

## ***Balancing Techniques***

Balancing techniques reduce the input offset voltage and current of a single device into those of a differential transistor pair. This will be expressed for bipolar transistors in the Eqs. 4.1.1, 4.1.2 and 4.1.3 for the balanced stage of Fig. 4.1.1 and for CMOS transistors in the Eqs. 4.1.4, 4.1.5 and 4.1.6 for the balanced stage of Fig. 4.1.2 respectively.

**Fig. 4.1.1** Balanced bipolar-transistor input stage**Fig. 4.1.2** Balanced CMOS-transistor input stage

For the single bipolar transistor [4.3] the input bias voltage and current is:

$$V_{BE} = \frac{kT}{q} \ln \frac{I_C W_b}{A_e K} + V_G, \quad (4.1.1)$$

$$I_B = I_C / \beta_F;$$

in which:  $k$  is the Boltzmann constant,  $T$  the absolute junction temperature,  $q$  the absolute value of the charge of an electron,  $I_C$  the collector current,  $W_b$  the base width,  $A_e$  the effective emitter area,  $K$  a constant proportional to  $T^{-4}$  and dependent on the doping profile,  $\beta_F$  the large signal current gain, and  $V_G$  the bandgap voltage which is about 1.2 V in silicon [4.4].

For the balanced configuration of Fig. 4.1.1 the input offset voltage, offset current and bias current are:

$$V_{IOFFS} = V_{BE1} - V_{BE2} = \frac{kT_1}{q} \ln \frac{I_{C1} W_{b1}}{A_{e1} K_1} - \frac{kT_2}{q} \ln \frac{I_{C2} W_{b2}}{A_{e2} K_2} + V_{G1} - V_{G2}$$

$$\simeq \frac{kT}{q} \left( \frac{\Delta R_C}{R_C} + \frac{\Delta W_b}{W_b} - \frac{\Delta A_e}{A_e} - \frac{\Delta K}{K} \right) + \Delta T \frac{k}{q} \ln \frac{I_C W_b}{A_e K} + \Delta V_G \quad (4.1.2)$$

$$I_{IOFFS} = (I_{B1} - I_{B2})/2 \simeq \frac{I_C}{2\beta_F} \left( \frac{-\Delta R_C}{R_C} - \frac{\Delta \beta_F}{\beta_F} \right)$$

$$I_{BIAS} = (I_{B1} + I_{B2})/2 \simeq \frac{I_C}{\beta_F}$$



in which

$$\begin{aligned}
 I_{C1} &= (V_{SP} - V_{REF})/R_{C1}, \quad I_{C2} = (V_{SP} - V_{REF})/R_{C2}, \\
 I_C &= (I_{C1} + I_{C2})/2, \quad \Delta R_C = R_{C1} - R_{C2}, \quad R_C = (R_{C1} + R_{C2})/2, \\
 \Delta W_b &= W_{b1} - W_{b2}, \quad W_b = (W_{b1} + W_{b2})/2, \quad \Delta K = K_1 - K_2, \quad K = (K_1 + K_2)/2, \\
 \Delta A_e &= A_{e1} - A_{e2}, \quad A_e = (A_{e1} + A_{e2})/2, \\
 \Delta T &= T_1 - T_2, \quad T = (T_1 + T_2)/2, \quad \Delta V_G = V_{G1} - V_{G2}, \quad \Delta \beta_F = \beta_{F1} - \beta_{F2}, \\
 \beta_F &= (\beta_{F1} + \beta_{F2})/2
 \end{aligned}$$

Balancing greatly reduces the offset voltage to a value of the order of 0.2 mV. The balancing owes its success to the well-determined voltage and current relations of bipolar transistors. The offset voltage of the balanced stage consists of three terms. The first term  $(kT/q)(-\Delta R_C/R_C + \Delta W_b/W_b - \Delta A_e/A_e - \Delta K/K)$  represents layout mismatches and doping inequalities of the two transistors  $Q_1$  and  $Q_2$ . This term is the dominating one. It has a value of the order of 0.2 mV for the present state of the art. The second term  $(\Delta T k/q) \ln(I_C W_b / A_e K)$  can be rated lower than 20  $\mu$ V if the difference between the junction temperatures is supposed to be lower than 0.01 K [4.5]. The third term  $\Delta V_G$  involves differences between the bandgap voltages, which can arise from differences in the mechanical strains of the two junctions. For two transistors situated close together in the centre of the chip the voltage difference  $\Delta V_G$  can be estimated lower than 20  $\mu$ V [4.3].

A way to reduce the bias currents for bipolar transistors is to compensate these currents with internal current sources, see Fig. 6.1.6b. Here the matching accuracy is limited to a value of the order of the offset current. This method raises the input noise current minimally with a factor  $\sqrt{2}$ . To further lower the offset and bias current super- $\beta$  transistors can be applied [4.6], although, this requires an additional step in the integration process.

The temperature drift of the balanced bipolar circuit of Fig. 4.1.1 can be expressed as (for definitions see Eqs. 4.1.1 and 4.1.2):

$$\begin{aligned}
 \frac{\partial V_{IOFFS}}{\partial T} &\simeq \frac{k}{q} \ln \frac{R_{C2} A_{e2} K_2 W_{b1}}{R_{C1} A_{e1} K_1 W_{b2}} \simeq \frac{V_{IOFFS}}{T}, \\
 \frac{\partial I_{IOFFS}}{\partial T} &\simeq \frac{\partial \beta_F}{\partial T} \frac{I_{IOFFS}}{\beta_F}.
 \end{aligned} \tag{4.1.3}$$

Note that if the offset of a bipolar pair is trimmed to zero, also the offset drift is zero. With CMOS transistors the offset voltage and drift behave more complicatedly. There are two basic operation ranges: Weak inversion at low current densities, with an exponential  $V_{GS}-I_D$  function like that of bipolar transistors, and strong inversion at high current densities, with a quadratic  $V_{GS}-I_D$  function. For most input stages operation in moderate inversion close to weak inversion is chosen, as that

results in the highest transconductance  $G_M$  at a given tail current [4.20], while the paracitic capacitors are still relative small. But sometimes, for a better linearity or better high frequency behavior, even smaller transistors with small input capacitors are choosen to operate in strong inversion. In contrast to bipolar transistors, where the NPN is often better than the PNP transistor, in CMOS the P-channel trnsistor is often better for an input stage at low frequencies than the N-channel transistor. The P-channel one has lower  $1/f$  noise and in most processes the back gate can be connected to the source, which improves the CMRR of the input stage (see Sect. 4.3).

In weak inversion the  $V_{GS}-I_D$  function can be expressed as:

$$V_{GS} = V_{TH} + \frac{nkT}{q} \ln \frac{I_D I}{I_{DO} W} \quad (4.1.4a)$$

in which  $V_{TH}$  is the threshold voltage,  $n$  is a factor of approximatly 1.6 in weak inversion,  $I_{DO}$  is a leakage current, and  $W/L$  is the width over length ratio of the CMOS transistor. The resulting  $V_{GS}$  is roughly 60 mV above the threshold voltage  $V_{TH}$  in moderate inversion close to weak inversion. This value represents a reasonable compromise between a small transistor size  $W \times L$  and a large as possible  $G_M$ .

The offset voltage can be expressed like that of the bipolar transistor as:

$$V_{IOFFS} \simeq \Delta V_{TH} + \frac{nkT}{q} \left( \frac{\Delta R_D}{R_D} - \frac{\Delta I_{DO}}{I_{DO}} + \frac{\Delta L}{L} - \frac{\Delta W}{W} \right) + \Delta T \frac{nk}{q} \ln \frac{I_D L}{I_{DO} W} \quad (4.1.5a)$$

Unlike the offset voltage of the bipolar transistor pair, the offset voltage of a CMOS transistor pair has a large threshold voltage offset term  $\Delta V_{TH}$  in addition to the geometric offset voltage term [4.21]. The difference in threshold voltage  $\Delta V_{TH}$  is most difficult to control. This voltage difference depends on irregularities of the channel doping and charge inclusion in the gate oxide of CMOS transistors. Therefore, in weak inversion the threshhold offset voltage is dominating and can be of the order of 2 mV, which is ten times larger than the offset of bipolar transistors.

The drift over temperature in weak inversion is:

$$\frac{\partial V_{IOFFS}}{\partial T} \simeq \frac{\partial V_{TH}}{\partial T} + \frac{nk}{q} \ln \frac{R_{D2} I_{D02} W_2 L_1}{R_{D1} I_{D01} W_1 L_2} \simeq \frac{\partial V_{TH}}{\partial T} + \frac{V_{IOFFS}}{T} \quad (4.1.6a)$$

Unlike the temperature drift of a bipolar transistor pair, the temperature drift of a CMOS transistor pair in weak inversion is not zero if the offset is zero, but the additional drift term due to the threshold voltage is present.

In strong inversion the gate-source voltage  $V_{GS}$  of a single CMOS transistor stage is a square-root function of the current:

$$V_{GS} = V_{TH} + \sqrt{2I_D/K} \quad (4.1.4b)$$

in which  $V_{TH}$  is the threshold voltage;  $I_D$  is the drain current;  $K = \mu C_{ox}W/L$  a main CMOS transistor parameter;  $W/L$  is the width over length ratio of the channel;  $C_{ox}$  is the normalized gate-oxide capacitance;  $\mu$  is the mobility of the charge carriers in the channel, which is about a factor 3 more for N doped channels than for P doped ones.

For the balanced input stage of Fig. 4.1.2 in strong inversion the offset is:

$$\begin{aligned} V_{I\text{OFFS}} &= V_{GS1} - V_{GS2} = \Delta V_{TH} + \frac{1}{2} \left( \frac{-\Delta R_D}{R_D} + \frac{\Delta K}{K} \right) \sqrt{2I_D/K} \\ V_{I\text{OFFS}} &= \Delta V_{TH} + \frac{1}{2} \left( \frac{-\Delta R_D}{R_D} + \frac{\Delta K}{K} \right) (V_{GS} - V_{TH}) \end{aligned} \quad (4.1.5b)$$

in which:  $\Delta V_{TH} = V_{TH1} - V_{TH2}$ ;  $\Delta R_D = R_{D1} - R_{D2}$ ;  $\Delta K = K_1 - K_2$ ; and  $\sqrt{(2I_D/K)} = V_{GS} - V_{TH}$ , and average values  $I_D, K, V_{GS}, V_{TH}$ .

The offset voltage clearly consists of two terms. The difference in threshold voltage  $\Delta V_{TH}$  in the left-hand term is nearly a constant voltage, while the two components  $\Delta R_D/R_D$  and  $\Delta K/K$  in the right-hand term are proportional to the square root of the drain current  $I_D$ , or directly proportional to  $(V_{GS} - V_{TH})$ .

In strong inversion, at relative high currents, the right-hand term may dominate the offset.

The bias and offset current is very low. With junction FETs the bias current is equal to that of the saturation current  $I_S$  of a bipolar diode, of the order of nA. With CMOS the bias current is equal to the leakage current of the gate oxide, of the order of pA to fA.

The temperature drift of the offset voltage in strong inversion is

$$\begin{aligned} \frac{\delta V_{I\text{OFFS}}}{\delta T} &= \frac{\delta \Delta V_{TH}}{\delta T} - \frac{1}{2} \left( \frac{\Delta R_D}{R_D} + \frac{\Delta K}{K} \right) \left( \frac{\delta I_D}{I_D \delta T} - \frac{\delta K}{K \delta T} \right) \sqrt{\frac{2I_D}{K_9}} \\ &= \Delta \alpha - \frac{3}{4} \frac{1}{T} \left( \frac{\Delta R_D}{R_D} + \frac{\Delta K}{K} \right) (V_{GS} - V_{TH}) \end{aligned} \quad (4.1.6b)$$

with:  $V_{TH} = V_{TH,THo} - \alpha(T - T_o)$ ,  $\Delta \alpha = \alpha_1 - \alpha_2$ ,  $\mu = k_\mu T^{-3/2} I_D = \text{constant}$ , and

$$K = \mu C_{ox}W/L.$$

The effect of gradients in doping, temperature and strain can be canceled in first-order approximation by using double-balanced transistors in a crosscoupled quad layout [4.6]. This method is visualized in Fig. 4.1.3a, b. For linear gradients the internal pair  $M_{12}M_{21}$  or  $Q_{12}Q_{21}$  and external pair  $M_{11}M_{22}$  or  $Q_{11}Q_{22}$  cancel each other's effects.

An additional consideration related to doping profiles is to give all transistors the same orientation. For equal stress the aluminium and oxide profiles should be equal around all transistors.

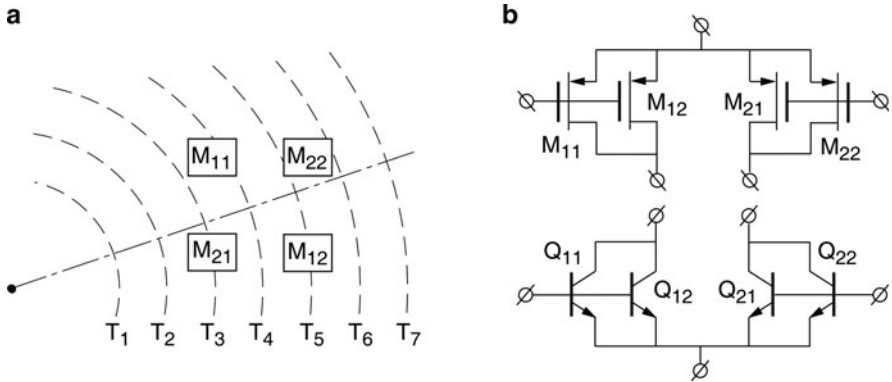


**Fig. 4.1.3** (a) Four transistors in a crosscoupled layout subjected to a temperature gradient. (b) Balanced input circuit with four transistors in the crosscoupled quad layout of Fig. 4.1.1 and 4.1.2

### Offset Trimming

For bipolar transistors (4.1.2), we can draw the conclusion that if we trim the ratio  $R_{C2}/R_{C1}$  such that  $R_{C2}/R_{C1} = A_{e1}K_1W_{b2}/A_{e2}K_2W_{b1}$ , then both the main term of the offset voltage  $V_{ioffs} \approx (kT/q)\ln(R_{C2}A_{e2}K_2W_{b1}/R_{C1}A_{e1}K_1W_{b2})$  (see Eq. 4.1.2) and the temperature drift of the offset voltage will be zero. We can regard the two transistors of the balanced stage and their collector resistors as a kind of geometric bridge circuit. Once the bridge balance is set to zero, its temperature drift will also be set to zero. A basic trim circuit for a bipolar input stage is drawn in Fig. 4.1.4 with a potentiometer. The potentiometer can be trimmed i.e., with laser trimming or zener zapping, or by a multiplying DAC. The stage behind should not disturb this balance.

For trimming a CMOS stage we encounter the difficulty that the temperature coefficient of the left-hand threshold term differs from the temperature coefficient of the right-hand geometric term in (4.1.5a, b). So, two trim actions are needed. The left-hand threshold offset term can be trimmed by inserting an adjustable voltage in series with the gate-source circuit, as shown in Fig. 4.1.5. Or alternatively, by adding a parallel input stage with same current density but lower bias current and with a trim voltage at its input. The right-hand geometric term can be resistively trimmed in the same way as the bipolar circuit such that  $\Delta R_D/R_D$  compensates  $\Delta K/K$  over temperature voltage. In weak inversion at low bias current the voltage trim is dominant, while in strong inversion at high bias current the resistive trim is dominant.

A well-trimmed bipolar input stage may have a temperature coefficient of the offset voltage lower than  $1 \mu\text{V/K}$  [4.8], while a junction-FET or CMOS stage has a coefficient lower than  $10 \mu\text{V/K}$  [4.7, 4.14].

The supply voltage dependence of the input offset voltage is equivalent to the terms of the common-mode voltage crosstalk if these terms are separated for

**Fig. 4.1.4** A basic trimming circuit for a bipolar input stage

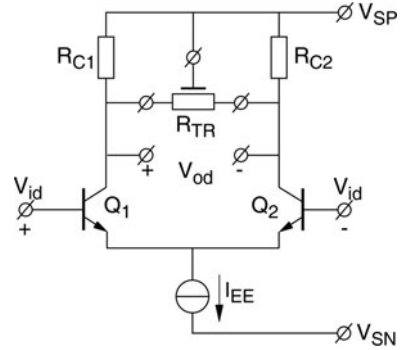
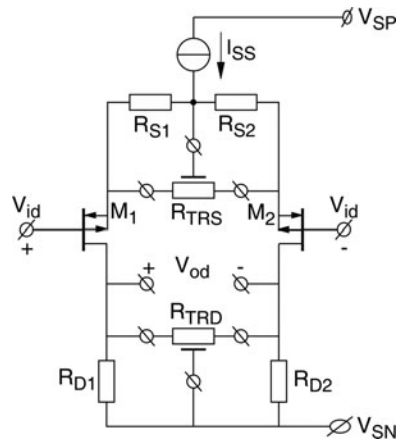


**Fig. 4.1.5** A basic trimming circuit for a CMOS input stage



parasites connected to the positive and negative supply voltages. This will be treated in Sect. 4.3.

With a balanced input stage one can only profit from a low offset voltage  $V_{IOFFS}$  and offset current  $I_{IOFFS}$  if the source circuit is also balanced to cancel the bias current  $I_{BIAS}$ . This is particularly important for a bipolar input stage. Figure 4.1.6 shows a balanced source circuit connected to the input of an OpAmp, whose offset and bias quantities are shown. Both bias currents of the OpAmp must flow back into ground via the source circuit. This results in two error voltages  $-aR_{sd}I_{BIAS}$  and  $+(1-a)R_{sd}I_{BIAS}$  of opposite polarities in series with the input terminals of the OpAmp. These error voltages cancel each other if the two parts  $aR_{sd}$  and  $(1-a)R_{sd}$  of the differential source resistance  $R_{sd}$  are equal, i.e., if  $a=1/2$ . Hence, when a balanced source circuit is used only the offset current  $I_{IOFFS}$  results in an error voltage of  $R_{sd}I_{IOFFS}$ . But, when an asymmetric source circuit is used with  $a=1$ , we get the much larger error voltage of  $R_{sd}I_{BIAS}$ . We can expect the offset current to be a factor of ten or more lower than the bias current.

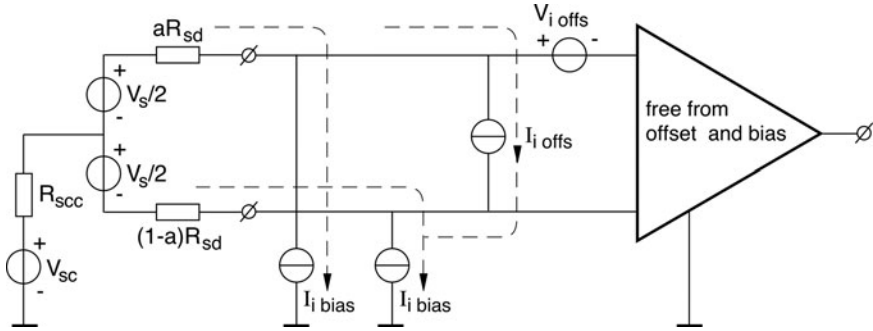


**Fig. 4.1.6** A balanced source circuit connected with the input of an OpAmp whose offset and bias quantities are shown separately

### Biasing for Constant Transconductance $G_m$ Over Temperature

The transconductance  $G_m$  of a bipolar differential transistor pair is  $I_Cq/kT$ , and of a CMOS transistor pair in weak inversion is  $I_Dq/nkT$ , with about  $n = 2.4$ . If these stages are biased by a constant current their  $G_m$  would decrease proportionally to the absolute temperature. This would not only affect the gain of an OpAmp equipped with one these stages, but also make the frequency compensation (see Chap. 6) inefficient. Therefore, it is better to bias these input stages by a current that is proportional to the absolute temperature (PTAT).

For a CMOS pair biased in strong inversion the  $G_m$  is  $2I_D/(V_{GS}-V_{TH}) = \mu C_{ox}(W/L)(V_{GS}-V_{TH}) = \mu C_{ox}(W/L)\sqrt{(2I_D/K)}$ . This function is proportional with the mobility  $\mu$ . The sensitivity of  $\mu$  to the absolute temperature is less than inverse proportional. But, if we want a constant  $G_m$  over the temperature range, we have to bias the stage by a current that is proportional to the inverse mobility (PTIM).

The question is of course: how to build a biasing circuit that can handle the different requirements?

The idea is to just force a constant  $G_m$  on a model pair by feedback, and use the same current generated in the model pair for the input stage. The situation is shown in Fig. 4.1.7.

Firstly, we look at the model stage with an artificial input voltage source  $V_{id2}$  and an artificial output current source  $I_{od2}$ , while the value of the asymmetrical source resistor  $R_{S22}$  is zero and  $M_{22}$  is equal to  $M_{21}$ , so  $N_x$  is 1x. The OVA regulates the tail current in such a way that the boundary conditions of input voltage and output current are met. This forces the  $G_m$  of the model to be:

$$G_m = I_{od2}/V_{id2} \tag{4.1.7}$$

for relative small signals of  $V_{id2}$  and  $I_{od2}$ . The transconductance  $G_m$  has a non-linear slanted S-shaped function of the input voltage. But, it is quite linear in the middle

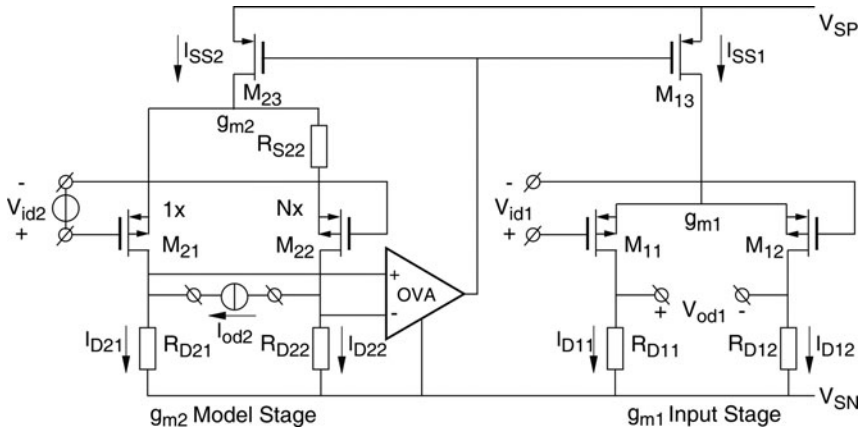


Fig. 4.1.7 Input stage with constant  $G_m$  over temperature by model bias generator

(see Sect. 6.4). If we do not take too large signals, than the value of  $G_m$  is approximately valid for input voltages with a maximum of 50 mV for bipolar and 100 mV for CMOS transistors.

When we apply the same tail current of the model stage for the input stage we can expect the same  $G_m$ , under the condition of equal type of transistors and same current densities as those of the model. If the input voltage  $V_{id2}$  is derived from a voltage across a resistor  $R_m$  through which a current is flowing equal to the output current  $I_{od2}$ , the transconductance  $G_m$  becomes  $G_m = 1/R_m$ . This result is approximately independent of the proces and even independent of the type of transistor. Measures have to be taken to ensure start-up of the bias circuit.

Secondly, we try to avoid the use of an artificial input voltage  $V_{id2}$  and output current  $I_{od2}$ . So, we give them a zero value. This means a shortcircuit input and open output. Instead, we take the transistor  $M_{22}$   $N$  times larger (wider) than  $M_{21}$  and insert a resistor  $R_{S22}$  in series with the source of  $M_{22}$ . The result is that the output currents  $I_{D21}$  and  $I_{D22}$  are regulated to be equal, supposedly  $R_{D21}$  and  $R_{D22}$  are equal. This means that  $1/G_{m22} + R_{S22} = 1/G_{m21}$ . In Other words: an  $N$  times wider  $M_{22}$  in regard to  $M_{21}$  has to catch up for the voltage loss across  $R_{S22}$ . Derived we get for the transconductance of the model:

$$G_m = V_{id2}/(I_{D21} - I_{D22}) = (N - 1)R_{S22}. \quad (4.1.8)$$

This result is again approximately independent of the proces and even independent of the type of transistor. If we bias the input stage with the same tail current as that of the model the input stage will have the same transconductance  $G_m$  as that of the model, under the condition of equal type of transistors and same current densities as those of the model [24].

The model circuit can be simplified [24] to that of Fig. 4.1.8. The model contains four transistors  $M_{21}$  through  $M_{24}$  in a nearly unity gain positive feedback loop. The

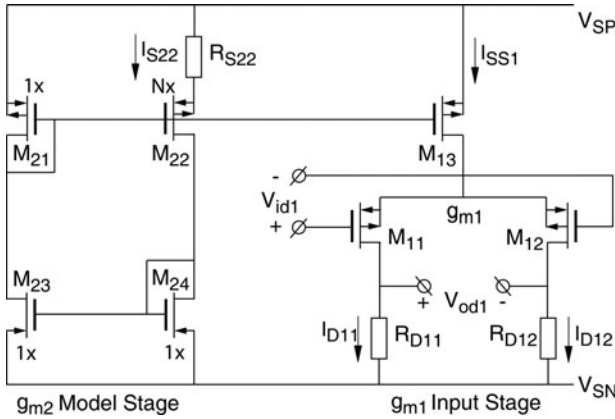


Fig. 4.1.8 Simple bias circuit for an input stage with constant  $G_m$

transistor  $M_{22}$  is  $N$  times larger than  $M_{21}$ . The resistor  $R_{S22}$  determines the current  $I_{S22}$ . If the current is smaller than the nominal one, the transistor  $M_{22}$  dominates by its multiple  $N$  and the current increases. If the current is larger than the nominal one, the source resistor  $R_{S22}$  reduces the current of transistor  $M_{22}$  and the current decreases. If the tail current  $I_{SS1}$  of the input stage is biased by two times the current  $I_{ang1024 S22}$  in the model, so  $I_{SS1} = 2I_{S22}$ , the  $G_m$  of the input stage is described by (4.1.8). This is under the condition of equal type of transistors and same current densities as those of the model.

A disadvantage of the simple bias circuit of Fig. 4.1.8 is that the progressive Early voltages of the transistors in the loop deteriorate its accuracy and supply-voltage rejection. A measure we can take is to aid the transistors of the bias circuit and the tail current of the input stage with cascode transistors. A disadvantage of this measure is that the minimum supply voltage is lowered.

A circuit that can work at very low supply voltage is drawn in Fig. 4.1.9.

The circuit has two loops: Firstly, a fast but not dominating loop through transistors  $M_{25}$ ,  $M_{26}$ , and  $M_{23}$  with positive feedback. This can become oscillative. Therefore a small capacitor  $C_2$  is placed across the gate and source of  $M_{25}$ . Secondly, a dominating loop through transistors  $M_{25}$ ,  $M_{26}$ ,  $M_{24}$ ,  $M_{22}$ , and  $M_{21}$  with negative feedback. The advantage of this circuit is that all current-determining transistors have equal Early voltages for all supply voltages [23]. The minimum supply voltage is equal to one  $V_{GS}$  and one saturation voltage  $V_{SAT}$ , which can be totally of the order of 1 V. If the tail current  $I_{SS1}$  of the input stage is biased by two times the current  $I_{S22}$  in the model, so  $I_{SS1} = 2I_{S22}$ , the  $G_m$  of the input stage is described by (4.1.8). This is under the condition of equal type of transistors and same current densities as those of the model.

The bias circuits for input stages with constant  $G_m$  over temperature have to be given some support circuitry to start up reliably [22].



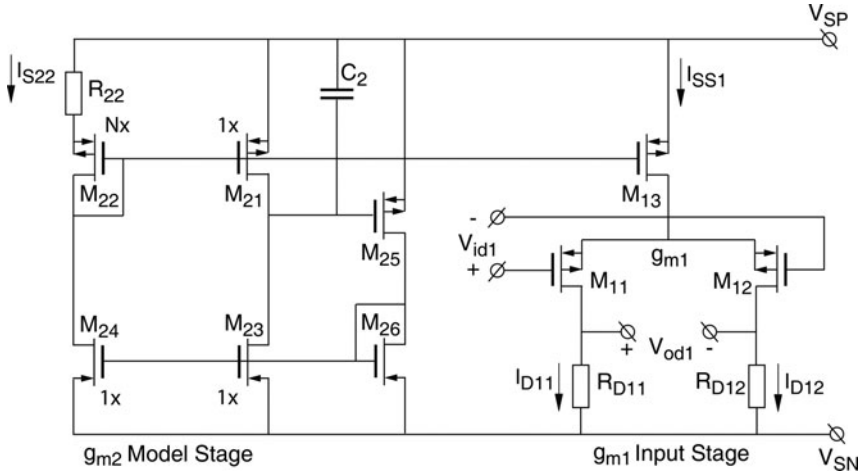


Fig. 4.1.9 Low voltage bias circuit for an input stage with constant  $G_m$

## 4.2 Noise

Noise can be regarded as a fluctuation of the input bias and offset quantities. Therefore, the same techniques can be applied as with bias, viz. isolation and balancing. Balancing will help less with noise because of the random character of noise.

### Isolation Techniques

An equivalent series spectral noise voltage source  $V_n$  and an equivalent parallel spectral noise current source  $I_n$  at the input port of an amplifier represent all noise sources of a linear amplifier, as shown in Fig. 4.2.1 a. Often it gives us more feeling for the amount of noise, if we compare the noise with that of a resistor. Therefore, we translate the noise voltage into that of an equivalent series noise resistance  $R_{eqs} = V_n^2/4kT$  and the noise current into that of an equivalent parallel noise resistance  $R_{eqp} = 4kT/I_n^2$ .

The first step for low-noise design is to make the noise voltage and current as low as possible by themselves. This means  $R_{eqs}$  low and  $R_{eqp}$  high.

With bipolar transistors the values of the equivalent noise resistors are  $r_{eqs} \simeq r_e/2 + r_{bb}$  and  $r_{eqp} \simeq 2\beta r_e$  in which  $r_e$  is the small-signal emitter resistance,  $r_{bb}$  the ohmic base resistance and  $\beta$  the small-signal current amplification factor. A practical value of  $r_{eqs}$  is between 1 and 10,000  $\Omega$  or higher, and of  $r_{eqp}$  between 0.1 and 1000  $k\Omega$  or higher depending on the quiescent current. With junction FETs we find an equivalent series noise resistance  $Z_{eqs} = \delta/g_m$ , with  $\delta \approx 2/3$ . The equivalent parallel

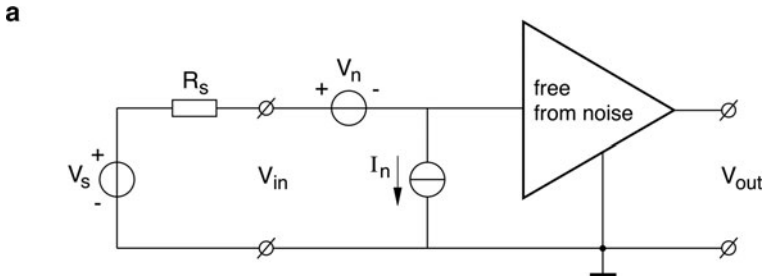


Fig. 4.2.1 (a) Noise sources in a single input stage

noise resistor represents the isolation of the gate by the gate oxide. This resistance is very high. A practical value of  $r_{eqs}$  is of the order of  $500\Omega$  and of  $r_{eqp}$  is of  $100M\Omega$  at low frequencies. In addition to the given noise values, we must regard  $1/f$ -noise which dominates with bipolar transistors in the frequency range roughly below  $100\text{ Hz}$  [4.8].

With CMOS transistors the value of the  $1/f$ -noise below  $10\text{ kHz}$  is so high that these transistors are not used in the input stage of low-noise amplifiers, unless a chopper amplifier configuration is used to convert the low-frequency signals into a high-frequency band, as explained in Chapter 10. The noise voltage of CMOS transistors is inverse proportional to the root of their gate area.

The second step in low-noise design is to optimally adapt the ratio of  $V_n$  and  $I_n$  to the signal-source resistance  $R_s$ .

The overall noise behavior may be described by the noise figure  $F$  [4.8]. This figure  $F$  can be calculated as the total available noise power of the source  $P_{ns}$  increased by the equivalent noise power  $P_n = V_n I_n$  of the amplifier divided by the noise power of the source  $P_{ns}$ .

$$F = \frac{P_{ns} + P_n}{P_{ns}} = \frac{(V_{ns}^2 + V_n^2 + I_n^2 R_s^2)/4R_s}{V_{ns}^2/4R_s}$$

$$F = 1 + (V_n^2/4R_s + I_n^2 R_s/4)/kT = 1 + R_{eqs}/R_s + R_s R_{eqp} \tag{4.2.1}$$

$$F_{\min} = 1 + V_n I_n / 2kT = 1 + 2\sqrt{R_{eqs} R_{eqp}}$$

at :  $R_{s\text{ opt}} = V_n / I_n = \sqrt{R_{eqs} R_{eqp}}$

The minimum value of  $F$  can be found by choosing an optimum value for the source resistance

$$R_{s\text{ opt}} = V_n / I_n = \sqrt{R_{eqs} R_{eqp}} \tag{4.2.1a}$$

with an equivalent series and parallel noise resistance, respectively  $R_{eqs} = V_n^2 / 4kT$  and  $R_{eqp} = 4kT / I_n^2$ . This only makes sense under the condition that the source power  $P_s = V_s^2 / R_s$  itself does not decrease. So, optimization by adding a series

resistance or applying a parallel resistor to the source only deteriorates the available signal power of the source.

As an example in which the source resistance may be enlarged or reduced while maintaining the same available signal power, one may choose a pick-up coil of a microphone with a larger or a lower number of windings, but with the same volume of copper.

As another example we may choose the bias current of the active input devices larger or smaller in such a way that a better optimization can be obtained.

### Balancing Techniques

The noise figure of a balanced input stage of Fig. 4.2.1.b is described by Eq. 4.2.2 in the case of a symmetrical source circuit ( $a = 1/2$ ).

$$F = 1 + (V_n^2/2R_{sd} + I_n^2 R_{sd}/8)/kT = 1 + 2R_{eqs}/R_{sd} + R_{sd}/2R_{eqp'} \quad (4.2.2)$$

$$F_{min} = 1 + V_n I_n / 2kT = 1 + 2\sqrt{R_{eqs} R_{eqp'}}$$

at :  $R_{sd\ opt} = 2V_n/I_n = 2\sqrt{R_{eqs} R_{eqp'}}$

For an asymmetrical source ( $a = 1$ ) with a balanced input circuit we find:

$$F = 1 + (V_n^2/2R_{sd} + I_n^2 R_{sd}/4)/kT = 1 + 2R_{eqs}/R_{sd} + R_{sd}/2R_{eqp'} \quad (4.2.3)$$

$$F_{min} = 1 + V_n I_n / 2kT = 1 + 2\sqrt{2R_{eqs} R_{eqp'}}$$

at :  $R_{sd\ opt} = \sqrt{2}V_n/I_n = \sqrt{2R_{eqs} R_{eqp'}}$

In the asymmetrical case ( $a = 1$ ) the noise contribution of one noise current source is multiplied by the full source resistance. While in the symmetrical case the noise currents of both sources is multiplied by half the source resistance and then added as the root of the squares. This results in a factor  $\sqrt{2}$  lower noise.

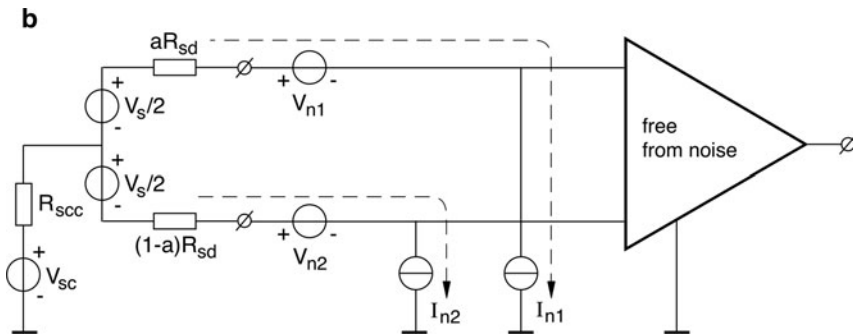


Fig. 4.2.1 (b) Noise sources of the balanced input stage

Low-noise operation with  $F < 2$  is possible at values of  $R_{sd}$  between the equivalent series noise resistance  $R_{eqs}$  and the equivalent parallel noise resistance  $R_{eqp}$ .

### Conclusion

From the Eqs. 4.2.1 – 4.2.3 we can draw the conclusions that the minimum noise figure  $F_{min}$  of the balanced input stage with a symmetrical source circuit equals that of a single transistor stage, while the use of an asymmetrical source circuit together with a balanced input stage leads to a  $\sqrt{2}$  larger value of the minimum noise figure. This conclusion is only relevant if the available signal power of the source circuit is equal in both cases.

More important than balancing is a proper choice of the type of input transistors and their bias currents, so that their equivalent series and parallel noise resistances  $R_{eqs}$  and  $R_{eqp}$  are positioned geometrically around the source resistance  $R_s$ . Finally, low 1/f noise can be obtained by using a chopper amplifier configuration, as explained in Chapter 10.

Low-noise design implies that the input stage will have a sufficiently high gain so that the noise of other stages will have a negligible influence on the equivalent input noise sources.

### 4.3 Common-Mode Rejection

The common-mode rejection ratio (CMRR)  $H$  (used here without index  $i$ ) or the supply-voltage rejection ratio (SVRR) describe the influence of a common-mode (CM) input voltage or supply-voltage variation on the differential-mode (DM) driving of the amplifier. In Chap. 2 the common-mode crosstalk ratio (CMCR) was defined as the inverse ratio  $1/H$ . This is the ratio of an equivalent DM input voltage and the CM input voltage, which brings it about.

Chapter 3 showed that a low value of the CMCR  $1/H$  is needed in all those applications in which an accurate equation is needed between the two input voltages. A low CMCR can be obtained by two methods: by isolation techniques and by balancing techniques. These two methods are symbolized in Figs. 4.3.1 and 4.3.2 respectively, and will be discussed in this section.

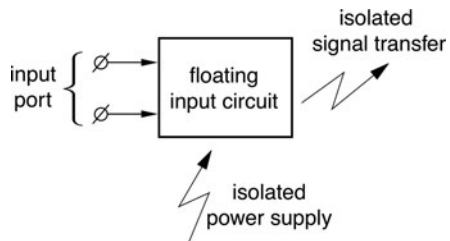


**Fig. 4.3.1** Common-mode rejection by isolation techniques

## Isolation Techniques

Electrical isolation of the input circuit is a basic method for obtaining a low common-mode crosstalk ratio (CMCR). Electrical isolation naturally adapts to the requirement of a floating input port, because if we isolate the input circuit, a common-mode voltage cannot influence the current distribution in the circuit. Imperfections of the isolation determine the value of the CMCR. Isolation can principally be realized to any large degree of perfection.

Isolated signal transfer and power supply (Fig. 4.3.1) can be obtained by all kinds of energy carriers. One can envision coupling by optical energy, magnetic energy, by the magnetic field energy of a transformer, or flow of voltage-isolated electrical charge. The last method is the most obvious to cope with both signal transfer and power supply on a chip. There are two different ways in which this method can be applied.

Firstly, floating capacitors can be switched to and from the isolated input circuit to the other parts of the amplifier. The capacitors can carry energy and signal values. Secondly, electronic current sources can continuously carry power and signal without making a voltage-dependent connection. The latter way of isolation by electronic current sources will be discussed in more detail in combination with balancing.

## Balancing Techniques

Balancing of the input circuit is another method for obtaining a low common-mode crosstalk ratio (CMCR). Figure 4.3.2 shows a basic configuration of grounded amplifiers with the gain factors of  $A_1$  and  $A_2$ . The CMCR  $1/H$  of the balanced circuit equals the relative inaccuracy of the matching of the amplification factors:

$$1/H = A_c/A_d = \Delta A/A \quad (4.3.1)$$

with:  $A_c A_1 - A_2 = \Delta A$ ,  $A_d = (A_1 + A_2)/2 = A$

If only balancing techniques were used in a monolithically integrated amplifier without trimming, the CMCR could not be guaranteed to be lower than of the order of  $1/1,000$  because the integrated resistors cannot be matched better than of the order of  $0.1\%$ . This is in contrast to isolating techniques which can basically be applied to any grade of perfection at low frequencies. At high frequencies parasitic coupling capacitors limit the isolation quality.

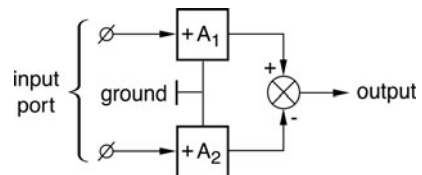
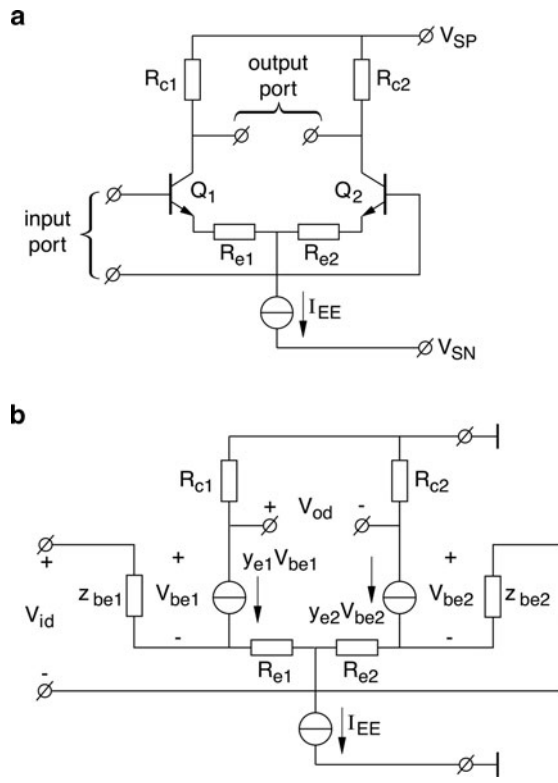


Fig. 4.3.2 Common-mode rejection by balancing techniques

### Combination of Isolation and Balancing

We conclude that a low common-mode crosstalk ratio (CMCR) which is inverse to the CMRR can best be achieved by using both techniques together. Current-source isolation provides the main step on the way to a low CMCR. Balancing further reduces the CMCR.

The combination of electronic current-source isolation and balancing is depicted in the long-tailed bipolar transistor pair of Fig. 4.3.3a. The simplified equivalent circuit of Fig. 4.3.3b clearly shows that if the tail contains an electronic current source  $I_{EE}$ , and if the input transistors have a current-source output, the complete input circuit is only connected by current sources with the surrounding parts. This means that the common-mode input voltage has no influence on the distribution of the current in the input circuit. With the ideal current sources of Fig. 4.3.3b it does not even matter whether the circuit is balanced or not.



**Fig. 4.3.3** (a) Bipolar long-tailed-pair input stage. (b) Simplified equivalent circuit of the bipolar long-tailed-pair input stage which shows the current-source isolation of the CM input voltage

### Common-Mode Cross-Talk Ratios

In practice, the equivalent circuit must be made complete by adding parasitic impedances in parallel with the current sources. This is shown in Fig. 4.3.4 where each transistor is represented by its hybrid- $\pi$  equivalent circuit. The hybrid- $\pi$  model for bipolar transistors has been chosen because it can easily be adapted to represent the HF behavior or to symbolize JFETs and CMOS transistors. The tail current source has also been provided with its parallel impedance  $Z_{ee}$ . At the input side any externally grounded feedback or bias impedances or stray capacitances have been represented by  $Z_{p1}$  and  $Z_{p2}$ .

The values of the parasitic impedances determine the degree of isolation, and the mutual inequalities of the parasitic impedances determine the degree of balancing. Together they determine the common-mode crosstalk ratio (CMCR).

The effect of the parasitic impedances on the CMCR will be discussed separately for each of the parasitic types. A new calculation method will be presented which distinguishes the aspect of isolation from that of balancing. With this method a better estimation of the crosstalk ratio as a function of a certain design aspect can be made than with preceding calculation methods.

### Parallel Input Impedance

The effect of the parallel input impedances  $Z_{p1}$  and  $Z_{p2}$  on the CMCR will be discussed in detail, while other effects are dealt with only briefly. The common-mode crosstalk ratio (CMCR) is defined as the ratio of the equivalent DM input voltage which is evoked by the CM input voltage. Hence, let us supply a CM input voltage  $V_{ic}$  and see what is the effect on the DM input voltage  $V_{id}$ . If we suppose

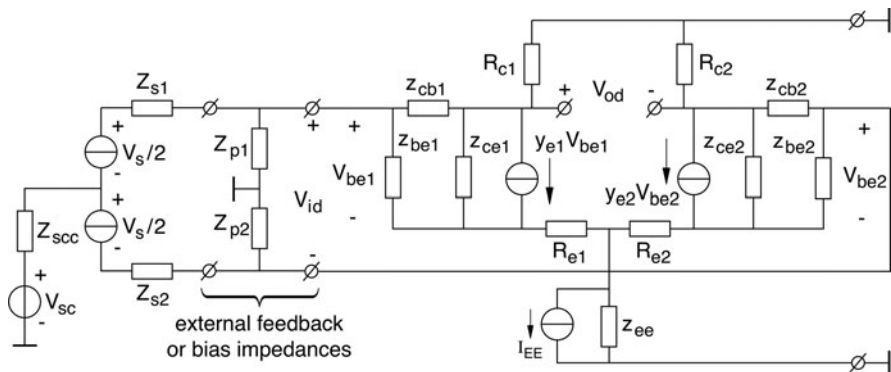


Fig. 4.3.4 Small-signal equivalent circuit of a bipolar long-tailed transition pair with parasitic impedances across the current sources

that the parallel impedances  $Z_{p1}$  and  $Z_{p2}$  are much larger than the source impedances  $Z_{s1}$  and  $Z_{s2}$ , the CM currents  $I_{s1}$  and  $I_{s2}$  through these impedances will be mainly determined by the parallel impedances, so:  $I_{s1} \approx V_{ic}/Z_{p1}$  and  $I_{s2} \approx V_{ic}/Z_{p2}$ . These currents cause a differential input voltage  $V_{id}$  across the source impedances of:  $V_{id} = -Z_{s1}I_{s1} + Z_{s2}I_{s2} \approx V_{ic}(-Z_{s1}/Z_{p1} + Z_{s2}/Z_{p2})$ .

The CMCR  $1/H_I$  is  $1/H_I = V_{id}/V_{ic} = -Z_{s1}/Z_{p1} + Z_{s2}/Z_{p2}$ . On inspection of the last expression three aspects can be distinguished: firstly, the average ratio of  $Z_s/Z_p$  with  $Z_s = (Z_{s1} + Z_{s2})/2$  and  $1/Z_p = Y_p = (1/Z_{p1} + 1/Z_{p2})/2$ , secondly, the imbalance of the source resistances  $\Delta Z_s = Z_{s1} - Z_{s2}$ , and thirdly, the imbalance of the parallel admittances  $\Delta Y_p = 1/Z_{p1} - 1/Z_{p2}$ . We can now express the CMCR with these three aspects as follows:

$$1/H_I \approx (Z_s/Z_p)(-\Delta Z_s/Z_s - \Delta Y_p/Y_p) \tag{4.3.2}$$

The first factor of the CMCR ( $Z_s/Z_p$ ) will be called the ‘‘isolation factor’’. It expresses the relative isolation of the source when loaded by the parallel impedances. The second factor ( $\Delta Z_s/Z_s - \Delta Y_p/Y_p$ ) will be called the ‘‘balancing factor’’. It expresses the relative imbalance of the source and parallel impedances. These impedances are connected in the form of a bridge circuit. Overall, the expression for the CMCR has a clear structure and can be easily understood. In the extreme situation of a fully unbalanced source or parallel load circuit, when one of the source impedances equals zero or one of the parallel impedances infinity, the balancing factor equals plus or minus two. In that situation the suppression of the crosstalk fully relies on the isolation factor ( $Z_s/Z_p$ ).

To depict the frequency dependency, the CMRR  $H_I$  is drawn in Fig. 4.3.5 as a function of the frequency in the case in which both source impedances amount to 1 kΩ and each of both parallel or grounded impedances consists of only one capacitance whose values differ by 1 pF. The example gives an idea about which values are attainable as a function of the frequency.

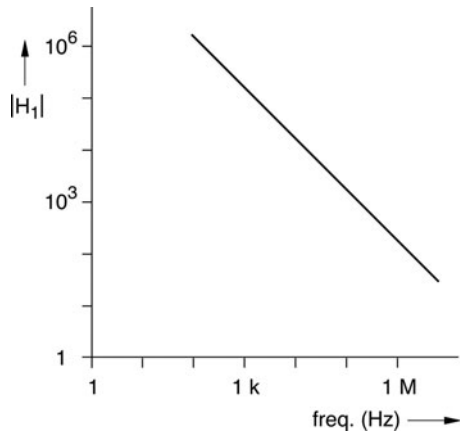


**Fig. 4.3.5** CMRR of a balanced source circuit with two series resistors of 1 kΩ and an imbalance of 1pF in the grounded load capacitors



The effects of the other parasitic impedances will be treated in the same way as has just been seen. However, the explanation will be shortened because of their similarity, the definitions for average values and unbalanced values will not be repeated.

### ***Collector or Drain Impedance***

All effects are supposed ideal except for the collector-emitter impedance.

The collector-emitter impedances  $z_{ce1}$  and  $z_{ce2}$  carry the full input CM voltage  $V_{ic}$ . This results in equivalent base-emitter voltages  $V_{be1} = -V_{ic}z_{e1}/z_{ce1}$  and  $V_{be2} = -V_{ic}z_{e2}/z_{ce2}$ . The equivalent differential input voltage  $V_{id} = V_{be1} - V_{be2} = V_{ic}(-z_{e1}/z_{ce1} + z_{e2}/z_{ce2})$  represents a CMCR:

$$1/H_2^* = (z_e/z_{ce})(-\Delta z_e/z_e - \Delta y_{ce}/y_{ce}) \quad (4.3.3)$$

The reciprocal gain ratio  $(1/\mu) = (z_e/z_{ce})$  of transistors of the same type tends to match better than their  $z_e$  and  $z_{ce}$  values separately. This holds for bipolar transistors, where  $z_e$  and  $z_{ce}$  are both inversely proportional to the quiescent emitter current, as well as for JFETs and CMOS transistors, where the  $1/g_m$  and  $z_{ds}$  are both likewise dependent on the quiescent source current and on the length-to-width ratio. For this reason, it is realistic to replace (4.3.3) for (4.3.4):

$$1/H_2 = (1/\mu)(-\Delta\mu/\mu) \quad (4.3.4)$$

A lower CMCR can only be obtained by cascoding the input stage while the reference base or gate voltage of the cascode stage is bootstrapped by the CM input voltage.

### ***Tail Impedance***

The tail impedance  $Z_{ee}$  also carries the full CM input voltage  $V_{ic}$ . This causes a tail current  $I_{ee} = V_{ic}/Z_{ee}$ . This current brings about a crosstalk if the emitter circuit or the collector circuit is unbalanced:

$$1/H_3^* = \{(R_e + z_e)/2Z_{ee}\}\{-\Delta(R_e + z_e)/(R_e + Z_e) + \Delta R_c/R_c\} \quad (4.3.5)$$

When a tail current source is used with a transistor  $Q_3$  in a common base connection with an emitter resistance  $R_{e3}$ , the value of  $1/Z_{ee}$  is  $1/Z_{ee} = 1/\mu(R_{e3} + z_{e3}) + 1/\beta_3 r_{ce3} + 1/r_{cb3}$ . Taking only the first term of this expression into account, we obtain:

$$1/H_3 = \{(R_e + z_e)/2\mu(R_{e3} + z_{e3})\}\{-\Delta(R_e + z_e)/(R_e + Z_e) + \Delta R_c/R_c\} \quad (4.3.6)$$

A lower CMCR can only be obtained by cascoding the tail-current source, or if the tail-current source can be actively regulated for a constant output current.

### ***Collector-Base Impedance***

All other effects are supposed ideal, except for the collector-base impedance. The collector-base impedances  $Z_{cb1}$  and  $Z_{cb2}$  contribute firstly to the crosstalk ratio like the parallel input impedances in the preceding case. This contribution is:

$$1/H_{41} = (Z_s/z_{cb})(-\Delta Z_s/Z_s - \Delta y_{cb}/y_{cb}) \quad (4.3.7)$$

Secondly, the collector-base impedances cause a direct signal transfer from the input towards the output. The collector-base impedances and the collector load resistances  $R_{c1}$  and  $R_{c2}$  make up a bridge circuit. The CMCR can be calculated by dividing the transfer of that bridge by the differential-to-differential voltage gain factor  $A_{dd} \approx R_c/(R_e + z_e)$ . This results in:

$$1/H_{42} = \{(R_e + z_e)/z_{cb}\}(-\Delta R_c/R_c - \Delta y_{cb}/y_{cb}) \quad (4.3.8)$$

This CMCR component is absent in CMOS at low frequencies.

### ***Base Impedance***

The base-emitter impedances  $z_{be1}$  and  $z_{be2}$  connect the input terminals with the emitter circuit. Via these connections the base currents can reach the input terminals. The common-mode base currents are a factor of  $1/\beta = z_e/z_{be}$  lower than the CM tail current  $I_{ee} = V_{ic}/Z_{ee}$  and the collector current  $I_c = V_{ic}/z_{ce}$ . These base currents load the source circuit and a CMCR arises:

$$1/H_5 = (Z_s/\beta z_{ce} + Z_s/\beta 2Z_{ee})\{-\Delta Z_s/Z_s - \Delta(1/\beta)/(1/\beta)\} \quad (4.3.9)$$

This CMCR component is absent if the tail-current source is ideal.

### ***Back-Gate Influence***

N-channel CMOS input stages have a strong disadvantage regarding CMCR. Figure 4.3.6a shows the situation. Besides the normal gate, there is the back-gate, which is connected to the substrate in most CMOS processes for the N-channel transistor. The back-gate has a transconductance  $g_{mb}$  of the order of 10 times smaller than the normal transconductance  $g_m$ . This limits the isolation factor  $g_{mb}/g_m$  to about  $10^{-1}$ .

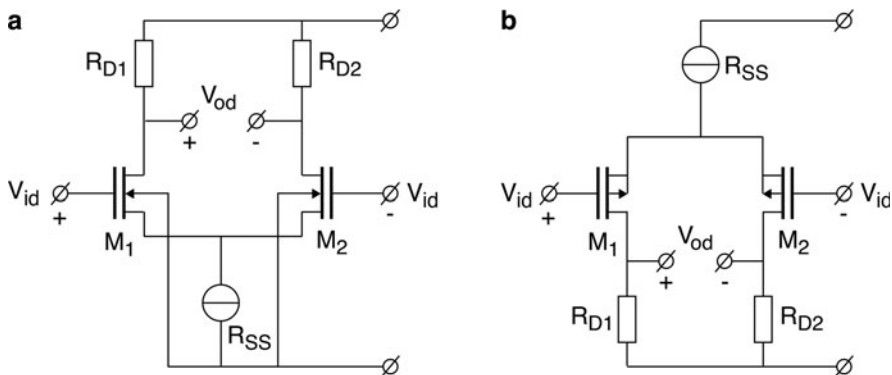


**Fig. 4.3.6** (a) N-channel CMOS input stage with substrate-connected back-gate bias. (b) P-channel CMOS input stage with source-connected back-gate bias

If we estimate differences in back-gate transconductances of the order of  $\Delta g_{mb}/g_{mb} = 1\%$ , then an additional partial crosstalk ratio will be added

$$1/H_{N\text{ CMOS}} = g_{mb}/g_m \cdot \Delta g_{mb}/g_{mb} \quad (4.3.10)$$

which is of the order of  $10^{-3}$  or  $-60$  dB.

This severely limits the minimum CMCR of N-channel CMOS stages. With P-channel CMOS stages of Fig. 4.3.6b the situation is better, because we have access to the back-gate and are able to connect this to the source. The remaining CMCR of P-channel CMOS input stages in strong inversion is maximally  $10^{-4}$  or  $-80$  dB, which is still a factor of 10 worse than that of bipolar transistors because the internal gain factor  $\mu$  of FETs is lower than that of bipolar transistors. However, the lower the bias current is taken, or the larger the W/L ratio, the more the FET approaches the gain factor of bipolar transistors, because the  $g_m$  is proportional to the root of the current and W/L ratio. In weak inversion the  $g_m$  is only roughly a factor of about 2 lower than that of the bipolar transistor. Again, cascoding of the input stage with bootstrapping of the cascode gate voltage by the CM input voltage can strongly improve the CM crosstalk.

## Total CMCR

The total crosstalk ratio  $1/H_t$  can be found when we superimpose all partial crosstalk ratios. In the worst case, the total crosstalk ratio is the sum of the absolute values of the partial crosstalk ratios:

The most dominating partial crosstalk ratios are  $1/H_2$  and  $1/H_3$ . The ratio  $1/H_2$  is a

$$|1/H_t| \leq |1/H_1| + |1/H_2| + |1/H_3| + |1/H_{41}| + |1/H_{42}| + |1/H_5| \quad (4.3.11)$$

consequence of the finite value of the collector-emitter impedance  $z_{ce}$  or drain-source impedance  $Z_{ds}$ . This ratio is determined by the finite value of the internal

voltage gain  $\mu = r_{ce}/r_e$  or  $\mu = r_{ds}g_m$  of the input transistors. The ratio  $1/H_3$  is the result of the finite value of the tail current-source impedance  $Z_{ee}$  or  $Z_{ss}$ . Also this ratio is mainly determined by the finite value of the internal voltage gain  $\mu_3$  of the current source transistor  $Q_3$  or  $M_3$  and its degeneration emitter or source resistor  $R_3$ .

With the bipolar circuit of Fig. 4.3.2 isolation factors of  $2 \cdot 10^{-4}$  and balancing factors of  $5 \cdot 10^{-2}$  can be obtained, leading to a CMCR of  $10^{-5}$ . With CMOS we obtain a CMCR of  $10^{-4}$ . At low frequencies, a practically unlimited improvement of the isolation can be obtained by using composite transistors for the input pair as well as for the tail-current source. Cascoding is one of the basic options.

To obtain a low overall CMCR  $1/H$  of a complete OpAmp the input or first stage should have a low total CMCR  $1/H_1$  (the index number refers to the stage number here) as well as a low reciprocal discrimination factor  $1/F_1$ . This reciprocal factor is defined as the ratio of the CM-to-CM and the DM-to-DM voltage gains. The reciprocal discrimination factor for the input circuit of Fig. 4.3.4 is:

$$1/F_1 = (R_e + z_e)(-1/2Z_{ee} + 1/\beta r_{ce} + 1/r_{cb}) \quad (4.3.12)$$

This expression shows that isolation is the only method to obtain a low reciprocal discrimination factor. A low reciprocal discrimination factor reduces the contribution of the CMCR  $1/H_2$  of the second amplifier stage to an overall value of  $1/F_1 H_2$ . It further reduces the extra crosstalk which arises if one of the stages is used single-ended, as is required in an OVA. If the second stage with a reciprocal discrimination factor  $1/F_2$  is used single-ended, the contribution to the crosstalk is  $1/F_1 F_2$ . The overall CMCR is in that case:

$$|1/H_o| \leq |1/H_1| + |1/F_1 H_2| + |1/F_1 F_2|. \quad (4.3.13)$$

## Conclusion

From the preceding discussion we can conclude that the common-mode crosstalk ratio (CMCR) of an input stage can be made low by isolation and balancing. Partial crosstalk ratios, as a result of each kind of parasitic current-source impedances, can be expressed as a product of an isolation factor and a balancing factor. Isolation can be performed practically to any degree of perfection at low frequencies by using composite transistor combinations. Balancing depends on the matching inaccuracies of integrated components. The minimum dominating crosstalk is limited by the internal gain of the transistors and is  $1/H_2 = (1/\mu)(\Delta\mu/\mu)$ .

For bipolar transistors this is of the order of  $10^{-5}$ , for P-channel CMOS transistors with source-connected back-gate  $10^{-4}$ , and for N-channel CMOS transistors  $10^{-3}$  because of the influence of the back-gate. Cascoding of the input transistors and the tail current source can drastically improve the CMRR. The CMRR further decreases as a function of the frequency because of the influence of parasitic parallel capacitors.

#### 4.4 Rail-to-Rail Input Stages

The trend in lower voltages, going from 30, 12, 5, 3, 1.8, and 1.2 V or 0.9 V, forces us to design input stages which maximally utilize the voltage range between the negative and positive supply rails. For instance, a large input range is required for a voltage follower buffer application with a high input impedance, as shown in Sects. 3.2 and 3.4.

Looking at the usable input range of input stages of Fig. 4.4.1 we find that the common-mode input voltage range of a P-channel input pair,

$M_3$ – $M_4$ , is limited between:

$$-V_{GS} + V_{Dsat} + V_{R3,4} + V_{SS} < V_{CM} < V_{DD} - V_{GS} - V_{Dsat} \quad (4.4.1)$$

where  $V_{CM}$  is the common-mode input voltage,  $V_{GS}$  is the gate-source voltage,  $V_{Dsat}$  is the saturation voltage across a current-source,  $V_{DD}$  and  $V_{SS}$  are the positive and the negative supply-rail respectively.

The common-mode input voltage range of an N-channel input pair,  $M_1$ – $M_2$ , is given by:

$$V_{SS} + V_{GS} + V_{Dsat} < V_{CM} < V_{DD} + V_{GS} - V_{sat} - V_{R1,2} \quad (4.4.2)$$

The CM range of the P pair may downwards exceeds the negative rail by  $-V_{GS} + V_{sat} + V_{R3,4}$ . Similarly, the CM range of the N pair may upwards exceeds the positive rail by  $V_{GS} - V_{sat} - V_{R1,2}$ . This will not be the case if the load resistances are replaced by diodes for current mirrors. For this reason current mirrors can not be used behind the input stage, but rather folded cascodes.

If the N-channel and P-channel input pairs are placed in parallel, as is shown in Fig. 4.4.2, the common-mode input voltage range becomes:

$$-V_{GS} + V_{Dsat} + V_{R3,4} + V_{SS} < V_{CM} < V_{DD} + V_{GS} - V_{Dsat} - V_{R1,2} \quad (4.4.3)$$

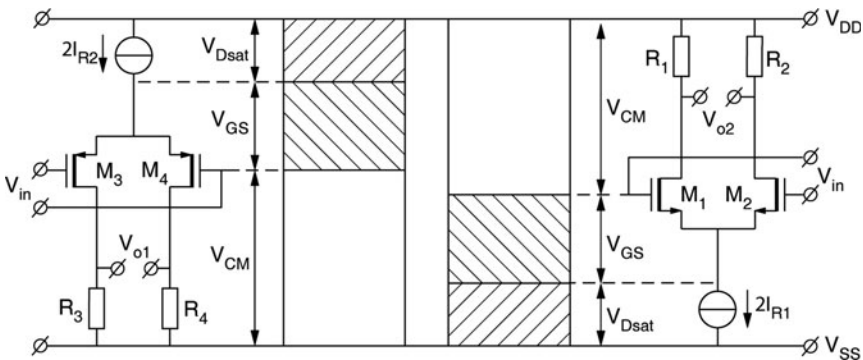


Fig. 4.4.1 Common-mode input voltage range of a P-channel and an N-channel input stage

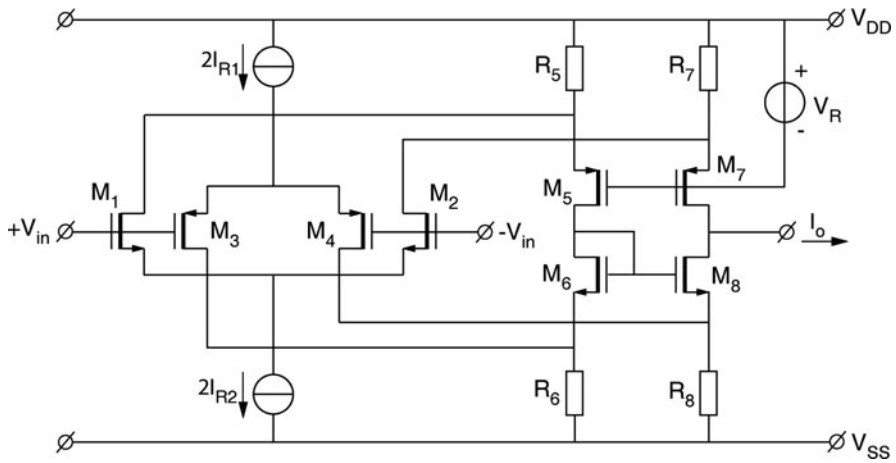


Fig. 4.4.2 Rail-to-rail CMOS complementary input stage

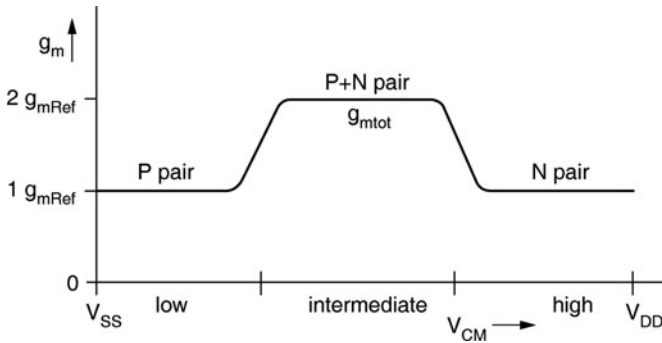


Fig. 4.4.3 The transconductance  $g_{mtot}$  versus the common-mode input voltage for a rail-to-rail complementary input stage

To avoid a forbidden voltage range in the middle of the rail-to-rail voltage range of the complementary input stage [4.1] the supply-voltage should have a minimum value of:

$$V_{sup,min} = 2V_{GS} + 2V_{Dsat} \tag{4.4.4}$$

Using standard CMOS technology, the minimum supply voltage for full rail-to-rail operation is approximately 1.8 V, depending on the bias-current level and the threshold voltage of the transistors. In many CMOS processes transistors are available with much smaller threshold voltages. In bipolar technology a minimum supply voltage of 1.6 V can be obtained.

The folded cascode transistors  $M_5$ – $M_8$ , together with the current-mirror connection of  $M_6$  and  $M_8$  add the output currents of the complementary input pairs.

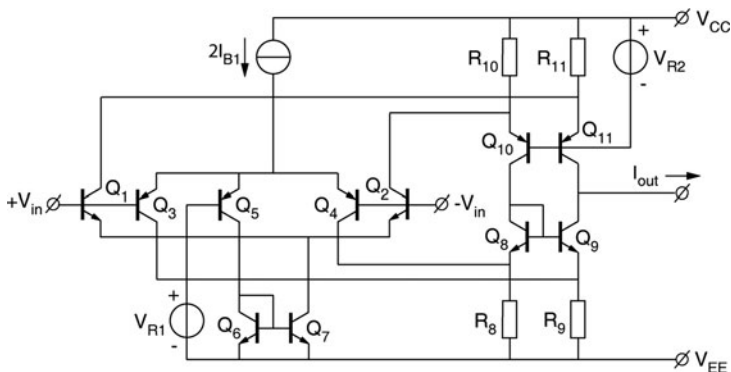


**Fig. 4.4.4** Rail-to-rail complementary bipolar or weak-inversion CMOS input stage with switch  $Q_5$  and 1:1 current mirror  $Q_6, Q_7$  to keep the sum of the tail currents constant, and hence the  $g_{m_{tot}}$  constant

A drawback of the simple complementary input stage of Fig. 4.4.2 is that the transconductance  $g_{m_{tot}}$  varies a factor two over the whole common-mode input range depending on the saturating of tail current sources, as is shown in Fig. 4.4.3 supposedly that the  $g_m$  of each of the N en P channel pairs is equal to  $g_{m_{Ref}}$ . This impedes an optimal frequency compensation of the amplifier [4.9], as we will see in Chap. 6.

### Constant $g_m$ by Constant Sum of Tail-Currents

In bipolar technology and in weak-inversion CMOS, the  $g_m$  of a transistor is proportional to the collector or drain current. Therefore, a constant  $g_{m_{tot}}$  can be obtained by keeping the sum of the tail-currents of the complementary input stages constant. A realization is shown in Fig. 4.4.4. Depending on the common-mode input voltage, the current switch  $Q_5$  directs the tail-current  $2I_{B1}$  to either one of the input stages [4.10]. The result is a constant  $g_{m_{tot}}$  over the whole common-mode input range, as is shown in Fig. 4.4.5.

This result for bipolar and weak-inversion CMOS transistors is clear from:

$$g_{m_{tot}} = g_{mN} + g_{mP} = \frac{I_{B1}}{V_T}; \tag{4.4.5}$$

with:  $V_T = kT/q$  for bipolar and about  $V_T = 60$  mV for weak-inversion CMOS.

There is an undesirable property of a complementary rail-to-rail input stage. The input offset voltage changes between that of the NPN and PNP pair when the CM input voltage crosses the turnover range. The turnover range is stretching out for about 100 mV for bipolar transistors, centered around the reference voltage  $V_{R1}$ .

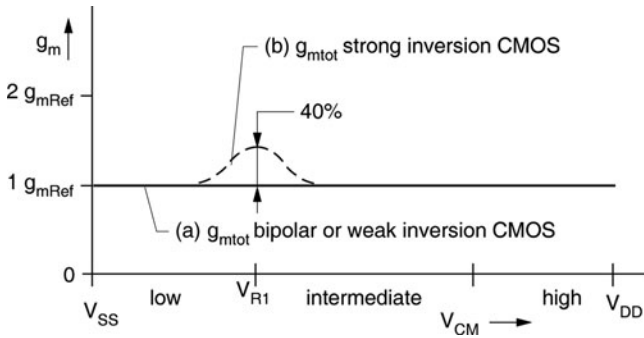


**Fig. 4.4.5** The transconductance  $g_{m\text{tot}}$  versus common-mode input voltage  $V_{cm}$  for the rail-to-rail complementary input stage with a 1:1 current mirror for bipolar technology, and CMOS technology in weak and strong inversion

Proper circuit layout with a cross-coupled quad for each input pair can typically keep the untrimmed offset voltage change in the order of 0.1 mV for bipolar transistors.

This means that the CMRR in the turnover CM range is:

$$1/H = 0.1/100 = 1/1200, \text{ or } 60 \text{ dB} \tag{4.4.6}$$

The CMCR can be improved by a factor of 10 or 20 dB by inserting a resistor in series with the emitter of  $Q_5$  because this spreads the turn-over range. However, this somewhat increases the minimum supply voltage for rail-to-rail operation.

In CMOS technology, the  $g_m$  of a transistor is also proportional to the drain-current if the transistor operates in weak-inversion. This biasing has the advantage that it gives CMOS transistors the highest transconductance of about  $g_m = I_{B1}/60 \text{ mV}$  (4.4.5) for a given bias current. Another advantage is that the  $g_{m\text{tot}}$  can be kept constant in the rail-to-rail input circuit of Fig. 4.4.4 as in bipolar technology. It is assumed that the P-channel transistors have a  $W/L$  that is about three times larger than that of the N-channel transistors, to compensate a three-times smaller mobility  $\mu$  of the P-channel transistors.

In strong-inversion however, this scheme leads to a  $g_{m\text{tot}}$  which increases approximately 40% in the middle of the common-mode range in regard to that in the side ranges, as shown in Fig. 4.4.5. This is because we have two times the  $g_m$  at half the current, while the  $g_m$  of a MOS transistor in strong-inversion is proportional to the square-root of the drain-current, according to:

$$g_m = K(V_{GS} - V_{TH}) = \sqrt{2KI_D} \tag{4.4.7}$$

with:  $K = \mu C_{ox}W/L$ ,  $\mu$  is the mobility of the charge carriers,  $C_{ox}$  is the normalized gate-oxide capacitance, and  $W/L$  is the width over length ratio of the channel.

A P-N complementary circuit is shown in the rail-to-rail input stage of Fig. 4.4.6. If both input pairs operate equally in the middle of the common-mode (CM) range,



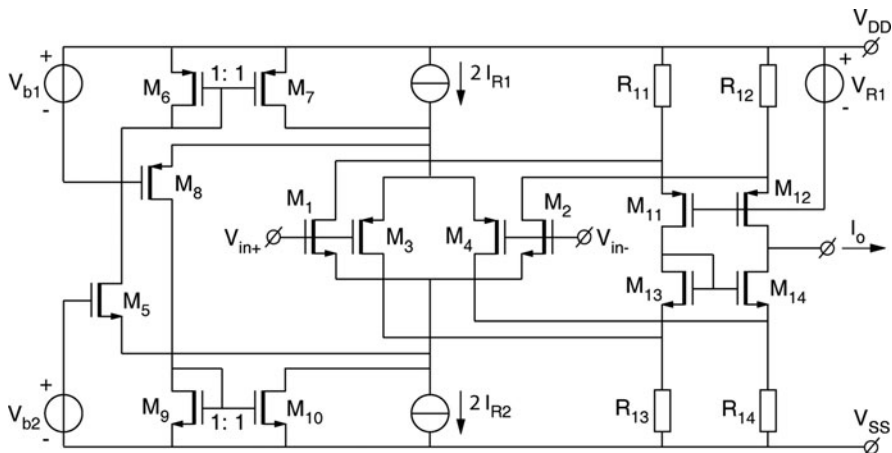


**Fig. 4.4.6** Rail-to-rail CMOS input stage with 1:1 current mirrors to keep the  $g_{mtot}$  constant in weak inversion

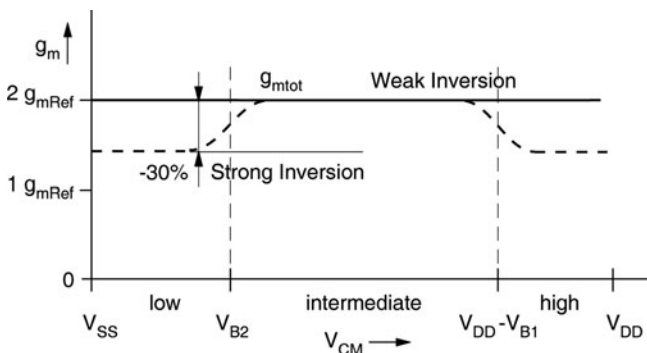


**Fig. 4.4.7** The transconductance  $g_{mtot}$  versus the common-mode input voltage  $V_{CM}$  for the rail-to-rail complementary input stage with 1:1 current mirrors of Fig. 4.4.6 for CMOS in weak inversion

the tail-currents of both input pairs are equal and have a value of  $2I_{Ref}$ . If only one input pair operates, the current-switches  $M_5$  and  $M_8$ , and the 1:1 current mirrors  $M_6$ - $M_7$  and  $M_9$ - $M_{10}$ , increase the tail-current of the active input pair by a factor 2 by adding the tail current of the inactive pair. Thus, the tail-current of the actual active input pair has a value of  $4I_{Ref}$ . The result is a constant  $g_{mtot} = 2I_{B1}/V_T$  for bipolar transistors, and about  $g_{mtot} = 2I_{B1}/60 \text{ mV}$  for CMOS in weak inversion, see (4.4.5).

The R-R input circuit of Fig. 4.4.6 has two transition ranges in the CM voltage range centered around  $V_{B2}$  and  $V_{DD}-V_{B1}$ . We estimate a total offset change of 1 mV for CMOS with a carefully designed circuit layout. Then, the CMRR in both the transition ranges of 200 mV for CMOS is:

$$1/H = 1/(2 \times 200), \text{ or } 53 \text{ dB} \quad (4.4.8)$$

Outside the transition ranges the CMRR is much higher, depending on the CMRR of the single P and N channel pairs.

### ***Constant $g_m$ by Multiple Input Stages in Strong-Inversion CMOS***

If the CMOS input transistors have to operate in strong inversion for high speed or an other reason, the proportionality of  $g_m$  to the root of the bias current (4.4.7) will cause a 30% lower total transconductance  $g_{mtot}$  outside the switching voltage levels  $V_{B2}$  and  $V_{DD}-V_{B1}$  of the input CM range than the transconductance of  $2g_{mRef}$  in the middle, see Fig. 4.4.7.

This reduction in  $g_{mtot}$  at the extremes can be changed into two hills of 14% at the switching voltages if the mirrored tail currents are not added to the tail of the active transistor pair, but instead given to one of the tails of an additional parallel N and P CMOS pair. In this way not only the current doubles in the active pairs, but also the total transistor width doubles. Thus the total transconductance comes back at  $2g_{mRef}$  at the high and low ends of the transient CM range [4.11] [4.14] [4.15].

### ***Constant $g_m$ by Current Spillover Control***

Another simple and robust approach to an R-R complementary input stage with a reasonable constant  $g_{mtot}$  by means of “current spillover control” [4.12] is shown in Fig. 4.4.8. The control transistors  $M_5$  and  $M_6$  spill the current which is not needed by the input pairs  $M_1M_3$  and  $M_2M_4$  into the supply rails.

The transistors  $M_5$  and  $M_6$  together with the input pairs  $M_1M_3$  and  $M_2M_4$  shape a voltage translinear loop:

$$V_{GS1,3} + V_{GS2,4} = V_{GS5} + V_{GS6} \quad (4.4.9)$$

We choose the W/L ratio of  $M_5$  and  $M_6$  two times that of  $M_1$  through  $M_4$  for biasing in weak inversion. And, we choose all P-channel transistors roughly three times wider than the N-channel transistors for compensating the  $g_m$ s for the mobility differences between the P and N complementary pairs.

$$\begin{aligned} I_{S1,3} \cdot I_{S2,4} &= I_{S5} \cdot I_{S6} \\ I_{S1,3} \cdot I_{S2,4} &= (2I_{Ref} - I_{S1,3}) \cdot (2I_{Ref} - I_{S2,4}) \\ I_{S1,3} + I_{S2,4} &= 2I_{Ref} \\ g_{mP} + g_{mN} &= 2g_{mRef} \end{aligned} \quad (4.4.10)$$

In the middle position of the CM voltage at  $V_{CM} = V_{B2}$  the currents through both pairs are equal  $I_{S1,3} = I_{S2,4} = I_{Ref}$ , and  $I_{S5} = I_{S6} = 2I_{Ref}$ . The transconductance of the two pairs in parallel equals  $g_{mP} + g_{mN} = 2g_{mRef}$ .

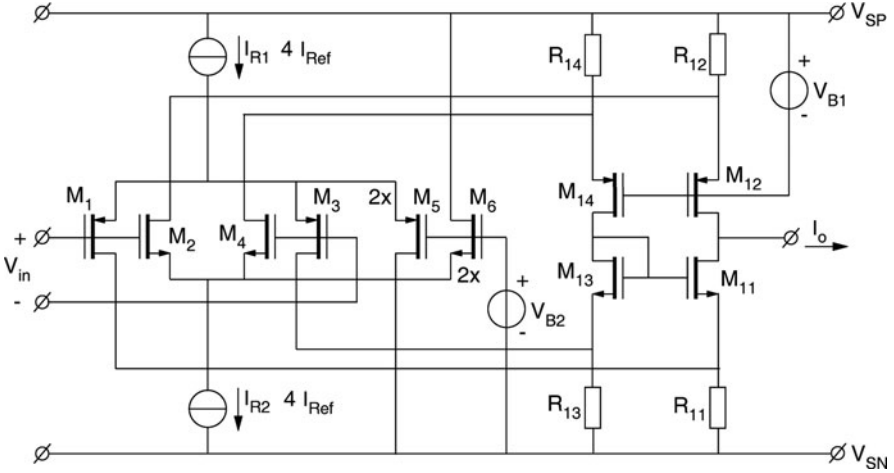


**Fig. 4.4.8** Constant- $g_{m\text{tot}}$  rail-to-rail input stage with current spillover control

At the end of the CM range we have  $I_{S1,3} = 0$  and  $I_{S2,4} = 2I_{\text{Ref}}$ , or  $I_{S1,2} = 2I_{\text{Ref}}$  and  $I_{S2,4} = 0$  resulting in  $g_{m\text{tot}} = 2g_{m\text{Ref}}$  according to (4.4.10).

When we choose to bias the input transistors in strong inversion, the sum of the voltages is proportional to the sum of the roots of the currents in strong inversion, with  $g_{m\text{Ref}} = \sqrt{2KI_{\text{Ref}}}$ ,  $K = \mu C_{\text{ox}}W/L$ . Then the total transconductance of the two pairs in parallel equals  $g_{m\text{tot}} = 2\sqrt{2}g_{m\text{Ref}}$  in the middle. This is 40% larger than the  $2g_{m\text{Ref}}$  of the left and right hand side position.

The input stage with current spillover control is simpler than that with the mirror current control. Moreover, the circuit can switch faster because there are no mirrors. The circuit with current spillover control is very robust and can be adapted to obtain other features [4.12]. A disadvantage is that it takes two times more bias current than without spillover control (Fig. 4.4.9).

One of the disadvantages of most R-R input stages is that the CM output drain currents of each pair varies from 0 to  $4I_{\text{Ref}}$  as a function of the CM input voltage. The summing circuit has to cope with this variation and may produce a CM voltage dependent offset. It is also difficult to optimize the summing circuit for noise and offset in combination with a rail-to-rail CM input range, as the voltage across  $R_{11}-R_{14}$  can not become larger than some hundreds of mV. To help solve this problem, the circuit with current spillover control can be adapted to produce a constant CM output current. Therefore, we split up the switching transistor  $M_5$  and  $M_6$  into two transistors each  $M_5, M_7$  and  $M_6, M_8$  and connect the drains with the outputs of the input pairs, as shown in Fig. 4.4.10.

Current spillover control can also be used to the advantage of a bipolar input stage as shown in Fig. 4.4.11. The translinear loop keeps the total  $g_{m\text{tot}}$  theoretically constant as calculated by (4.4.11) and (4.4.12) [4.12].

$$V_{BE1,3} + V_{BE2,4} = V_{BE5} + V_{BE6} \quad (4.4.11)$$

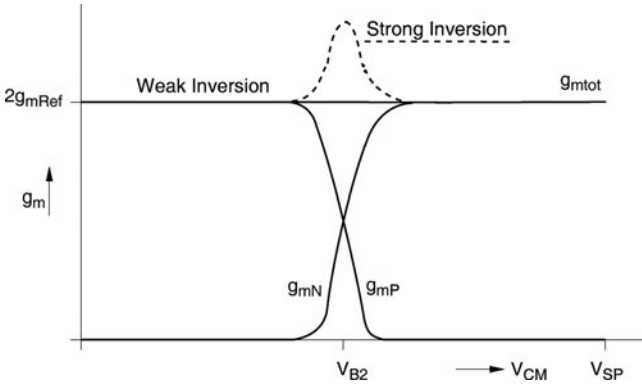


**Fig. 4.4.9** The transconductance  $g_{mtot}$  of the rail-to-rail input stage with current spillover control of Fig. 4.4.8

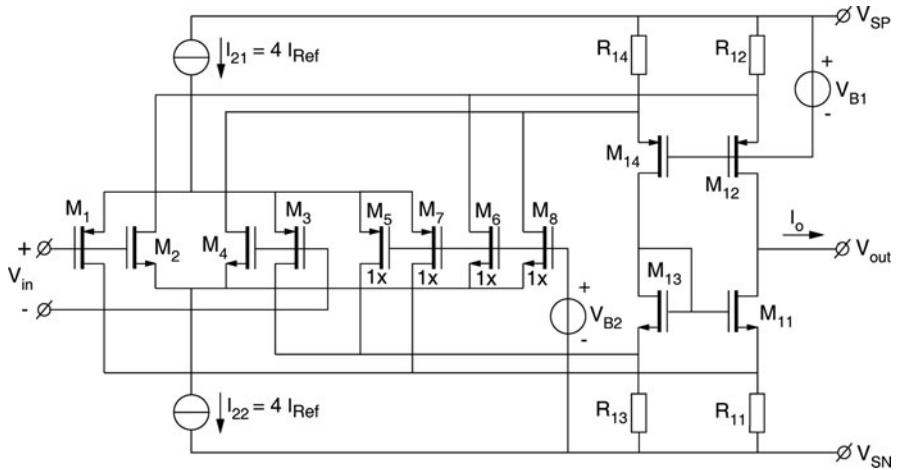


**Fig. 4.4.10** Current spillover switches keep the CM output current of the input pairs constant as well as the  $g_{mtot}$  in weak inversion

When we suppose emitter areas for  $Q_5$  and  $Q_6$  two times larger than that of  $Q_1$ ,  $Q_3$ , and  $Q_2$ ,  $Q_4$ , respectively, we find:

$$\begin{aligned}
 I_{E1,3}, I_{E2,4} &= I_{E5}, I_{E6} \\
 I_{E1,3}, I_{E2,4} &= (2I_{Ref} - I_{E1,3})(2I_{Ref} - i_{E2,4}) \\
 I_{E1,3}, I_{E2,4} &= 2I_{Ref} \\
 g_{mP} + g_{mN} &= 2g_{mRef}
 \end{aligned}
 \tag{4.4.12}$$

The sum of the  $g_m$ 's is depicted in Fig. 4.4.12 as a function of the CM input voltage.

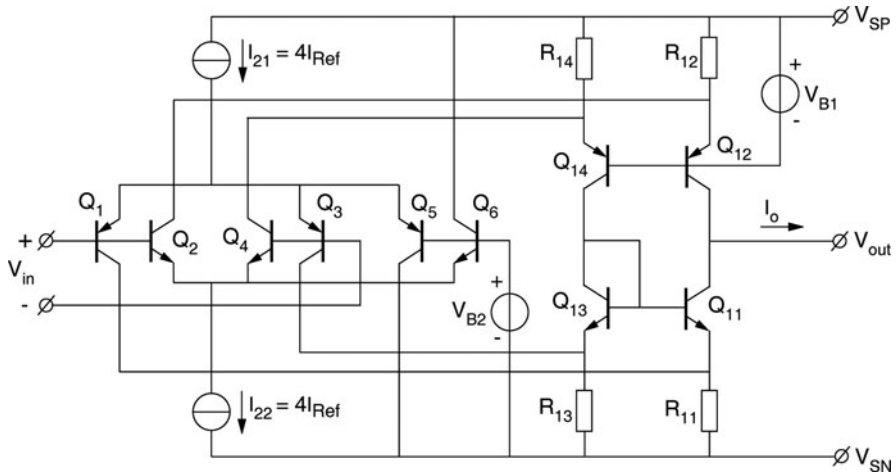


Fig. 4.4.11 Bipolar rail-rail input stage with current spillover control

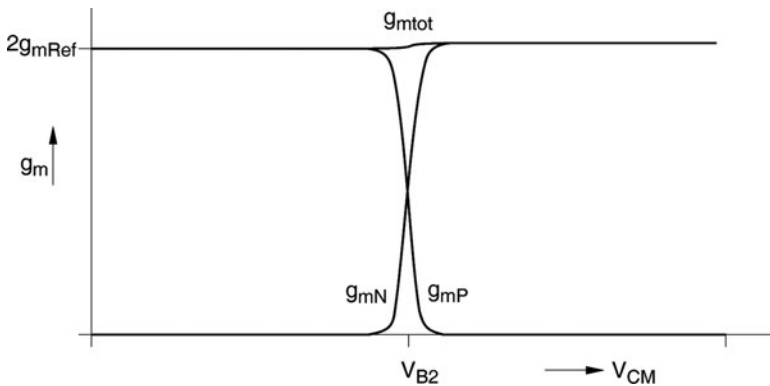
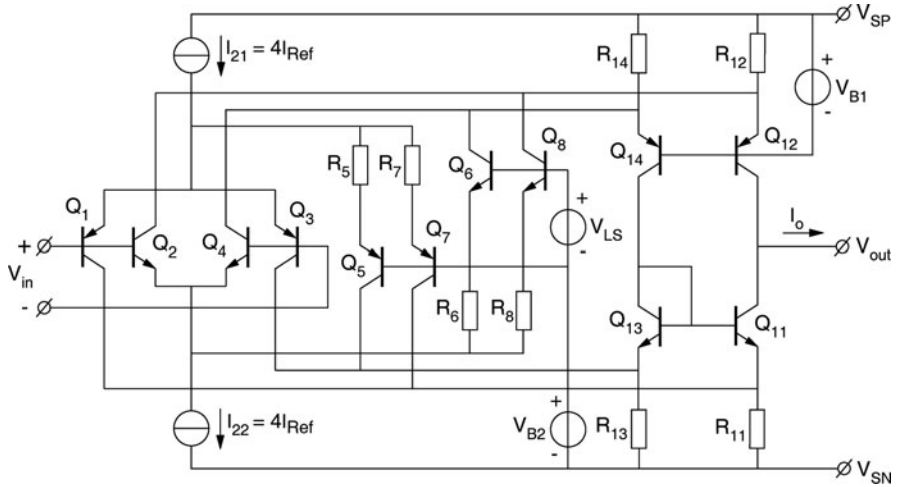


Fig. 4.4.12 The transconductance  $g_{mtot}$  of the bipolar or weak inversion CMOS input stage with current spillover control of Fig. 4.4.11

The R-R input stage with bipolar transistors and current spillover control can also be adapted to deliver a constant CM output current by splitting  $Q_5$  and  $Q_6$  into  $Q_5, Q_7$  and  $Q_6, Q_8$ .

As we have seen in Fig. 4.4.12 the transient from P to N is rather sharp with bipolar transistors. In order to improve the CMCR [4.12] in the transient range we can insert a voltage difference  $V_{LS}$  between the bases of control transistors  $Q_5, Q_7$  and  $Q_6, Q_8$  and degenerate the emitters of these transistors with resistors  $R_5$  through  $R_8$ , with a value of  $R = V_{LS}/I_{Ref}$ . This extends the CM input transient range of going from the offset of one input pair to the other by  $V_{LS}$ . The circuit with bipolar with split switching tra is shown in Fig. 4.4.13. It's total  $g_{mtot}$  as a function of the CM input voltage is shown in Fig. 4.4.14. This method can, of course, also be used for



**Fig. 4.4.13** Rail-rail input stage with bipolar transistors with splitted and degenerated switching transistors for spillover control having a constant CM output current

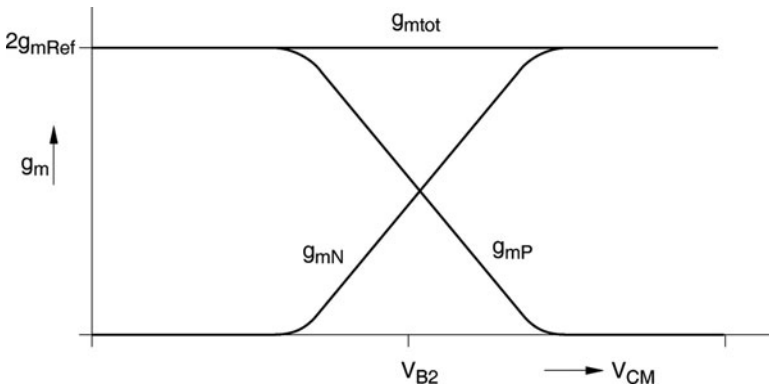


**Fig. 4.4.14** The transconductance  $g_{mtot}$  as a function of the input CM voltage of the R-R input stage with degenerated bipolar transistors of Fig. 4.4.13

CMOS transistors in weak inversion. The absence of current mirrors makes this circuit fast in a response on a large CM swing.

**Constant  $g_m$  in CMOS by Saturation Control**

An alternative approach is to use the saturation of CMOS current-source transistors to control the tail currents of the complementary transistors. The circuit is given in Fig. 4.4.15 [4.13].

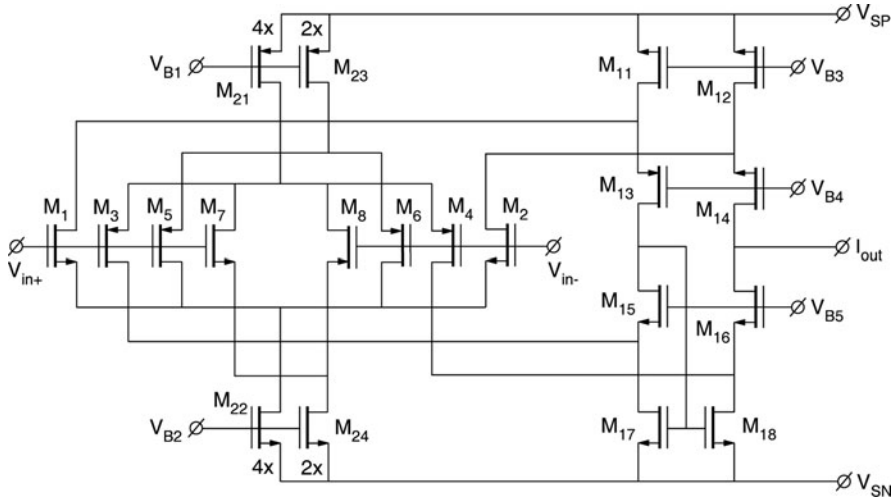


Fig. 4.4.15 Rail-to-rail input stage with controlled  $g_{m\text{tot}}$  by the use of saturation CMOS transistors

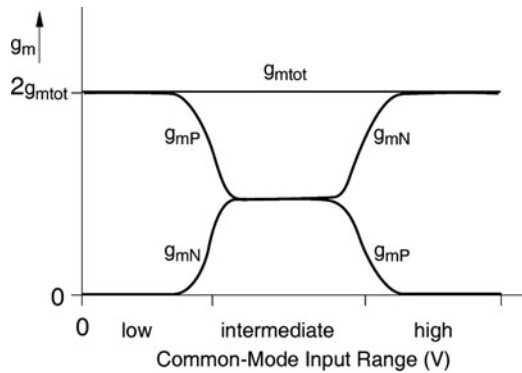


Fig. 4.4.16 The transconductance  $g_{m\text{tot}}$  of the R-R input stage of Fig. 4.4.15 with saturation control

The main tail current sources have a value of  $4I_{Ref}$ . However, a compensating current source from the other side with a value of  $2I_{Ref}$  brings the total tail current back to  $2I_{Ref}$ , which results in one  $g_{mRef}$  at one side.

When the CM range is in the middle both tails get  $4I_{Ref} - 2I_{Ref} = 2I_{Ref}$ . This is  $I_{Ref}$  per transistor. This leads to a total  $g_{m\text{tot}} = g_{mN} + g_{mP} = 2g_{mRef}$  for CMOS in weak inversion.

At the end of each range both current sources at one side are cut off. This results in one active pair with a tail current of  $4I_{Ref}$ . This results in  $g_{m\text{tot}} = 2g_{mRef}$ , which is equal to the value in the middle situation.

In the case where the current sources at one top or bottom partly saturates, the main tail current source with a nominal value of  $4I_{Ref}$  will partly saturate because it

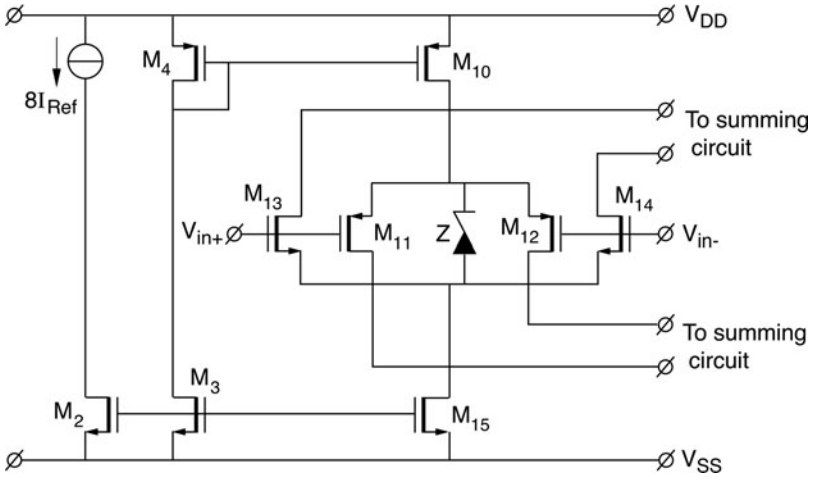


Fig. 4.4.17 Rail-to-rail input stage. The zener diode Z makes the  $g_{m\text{tot}}$  of the input pairs constant

is kept at the value of  $2I_{\text{Ref}}$  of the compensation source from the other side. The compensation current source at that side simultaneously partly saturates from its nominal value of  $2I_{\text{Ref}}$ . The result is that the complementary input pairs keep the sum of their  $g_m$ s constant as shown in Fig. 4.4.16 [4.13].

### Constant $g_m$ in Strong-Inversion CMOS by Constant Sum of $V_{GS}$

Probably the most essential way to achieve a constant  $g_{m\text{tot}}$  over the rail-to-rail CM voltage range with a CMOS circuit in strong inversion is to keep the sum of the gate-source voltages constant, as this keeps the sum of the  $g_m$ s constant [4.11]:

$$V_{GSN} + V_{GSP} = V_{THN} + V_{THP} + 2\sqrt{2I_{\text{Ref}}/K} = V_C \quad (4.4.13)$$

$$g_{mN} + g_{mP} = 2\sqrt{2KI_{\text{Ref}}} = g_{m\text{tot}} \quad (4.4.14)$$

with:  $V_{GSN}$  is the gate-source voltage of the N-channel pair,  $V_{GSP}$  that of the P-channel pair,  $V_{THN}$  the threshold voltage of the N-channel transistors,  $V_{THP}$  that of the P-channel transistors,  $g_{mN}$  the transconductance of the N-channel pair,  $g_{mP}$  that of the P-channel pair  $K = \mu C_{ox}W/L$ , and supposed is that we have compensated 1 difference in  $\mu_P$  and  $\mu_N$  by their W/L ratios, and  $g_m = K(V_{GS} - V_{TH}) = \sqrt{(2KI_D)}$ .

The implementation of a constant sum of the gate-source voltages of the N-channel and P-channel pair can be obtained by an electronic zener diode Z, as shown in Fig. 4.4.17 [4.11].

A realization of the electronic zener diode is presented in Fig. 4.4.18. The diode-connected transistors  $M_{21}$  and  $M_{25}$  form a reference chain. The current through this



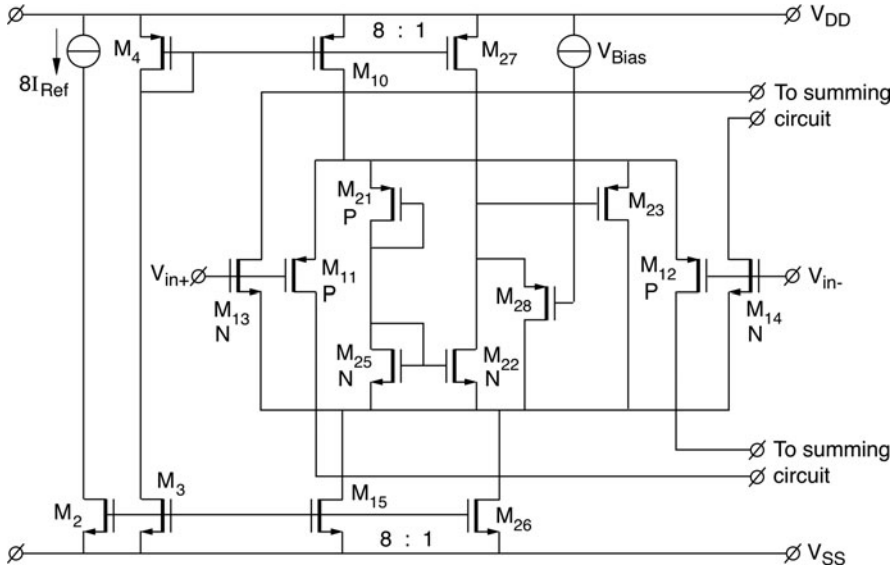


**Fig. 4.4.18** Constant- $g_m$  rail-to-rail input stage with an electronic zener diode, N and P are the W over L ratios of an N-channel and a P-channel input transistor, respectively [4.11]

chain is set by the W over L ratios of the diode- connected transistors and the voltage across the chain.  $M_{22}$  and  $M_{23}$  form the two transistor gain stages. Transistor  $M_{22}$  is biased by the constant current source,  $M_{27}$ , which has a value of  $I_{Ref}$ . The current source,  $M_{26}$ , drains the extra current of  $M_{27}$ . The transistor stage  $M_{23}$  controls the tail-currents, and therefore the gate-source voltages of the input pairs.

The principle of the circuit can be best understood by dividing the common-mode input range into three parts.

If low common-mode input voltages are applied, only the P-channel input pair operates. In this range the currents through the reference chain,  $M_{21}$  and  $M_{25}$ , and the regulator transistor  $M_{23}$ , are zero because  $M_{15}$  saturates and the sum of the voltages across  $M_{21}$  and  $M_{25}$  is too small.  $M_{28}$  prevents the saturation of  $M_{27}$ . Thus the tail-current of the P-channel input pair is equal to  $8I_{Ref}$  of  $M_{10}$ .

If intermediate common-mode input voltages are applied, the P-channel as well as the N-channel input pair operates. In this range  $M_{27}$  biases  $M_{22}$ .

The current through  $M_{22}$  is regulated to be equal to  $I_{Ref}$  of  $M_{27}$ . If  $M_{22}$  and  $M_{25}$  have the same W over L ratios, then the current in the reference chain is also set to  $I_{Ref}$ . Consequently, the tail-currents of both input pairs are equal to  $2I_{Ref}$ . The regulator transistor  $M_{23}$  takes the residual current  $8I_{Ref} - 2I_{Ref} - I_{Ref} = 5I_{Ref}$ .

If high common-mode input voltages are applied, only the N-channel input pair operates. In this range the current through the reference chain and  $M_{22}$  and  $M_{23}$  is zero.  $M_{28}$  takes away the current of  $M_{27}$  and feeds it to the drain of  $M_{26}$ . Now, it can be concluded that the tail-current of the N-channel input pair is equal to  $8I_{Ref}$  of  $M_{15}$ .

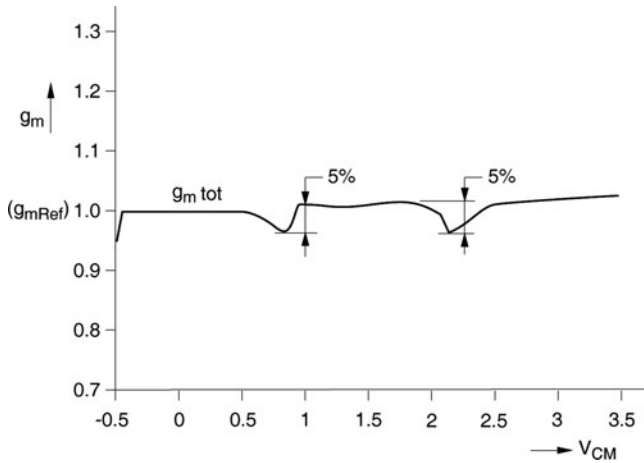


**Fig. 4.4.19** Total transconductance  $g_{m\text{tot}}$  versus the common-mode input voltage for the constant- $g_{m\text{tot}}$  input stage with the electronic zener circuit of Fig. 4.4.18

The total transconductance  $g_{m\text{tot}}$  versus the common-mode input voltage is shown in Fig. 4.4.19. From this figure it can be concluded that the  $g_{m\text{tot}}$  is nearly constant over the common-mode input range. In the transition regions the current through transistor  $M_{23}$  gradually changes from zero to  $5I_{\text{Ref}}$ , or vice versa. The result is a 5% variation of the  $g_m$ , due to the fact that the voltage across the electronic zener is slightly current dependent.

### ***Rail-to-Rail in CMOS by Back-Gate Driving***

An alternative approach to a 1-Volt rail-to-rail input stage is depicted in Fig. 4.4.20 [4.16].

The back gates of the input transistors are used as input terminals. The  $g_{m\text{tot}}$  of this stage is roughly a factor 10 lower than the  $g_{m\text{tot}}$  of a normal differential pair. Therefore, the offset and noise will be reflected a factor of 10 larger than that of a normal driven pair.

### ***Extension of the Common-Mode Input Range***

Besides techniques to provide input stages with a rail-to-rail common-mode range, other techniques have been developed to provide input stages with common-mode ranges far below the negative rail voltage or far above the positive rail voltage [4.17], [4.18], [4.19].

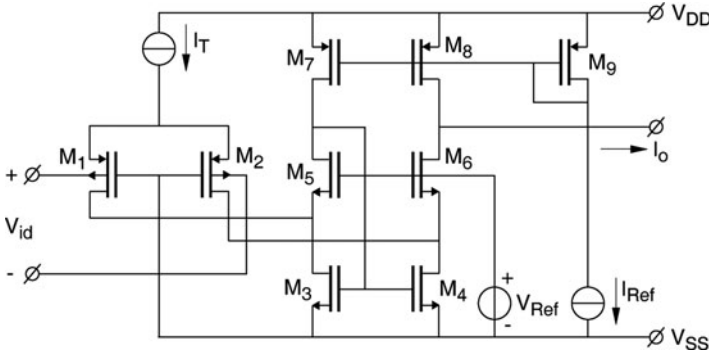


Fig. 4.4.20 Rail-to-rail 1-V CMOS input stage with back-gate input connection

**Conclusion**

It can be concluded that low-voltage complementary rail-to-rail input stages are feasible in bipolar as well as in CMOS technology. In bipolar technology and in weak-inversion CMOS the  $g_{m\text{tot}}$  can be kept constant by mainly keeping the sum of the tail currents constant, while in strong-inversion CMOS the  $g_{m\text{tot}}$  can be kept constant by mainly keeping the sum of the gate-source voltages constant. In the transition regions the common-mode rejection ratio is degraded because of the transition of the offset of one pair to that of the other pair. Many variations on these themes have been successfully realized. In Chapter 10 it is shown how R-R input stages can be given a very high CMRR by chopping. Also, CM input ranges far beyond the supply rail voltages can be achieved by chopper capacitive coupling at the input.

**4.5 Problems and Simulation Exercises**

**Problem 4.1**

The circuits in Fig. 4.4.1 show two input stages which use NMOS and PMOS devices. Considering the tail current in both circuits  $I_{\text{tail}} = 40 \mu\text{A}$ , load resistors  $R_1 = R_2 = R_3 = R_4 = 10 \text{ k}\Omega$  and supply voltage  $V_{DD} - V_{SS} = 3 \text{ V}$ , calculate the common-mode input range for both circuits. Using these ranges, determine the minimum supply voltage so there is no gap between the common-mode input range of the PMOS and NMOS input pairs. At the minimum supply voltage, how far can the supply rails be exceeded by the common-mode input range? The parameters of MOS devices are:  $V_{\text{THN}} = 0.7 \text{ V}$ ,  $V_{\text{THP}} = -0.8 \text{ V}$ ,  $K_P = 22 \mu\text{A}/\text{V}^2$ ,  $K_N = 75 \mu\text{A}/\text{V}^2$ . All devices have  $W/L = 100 \mu/1 \mu$ . The saturation voltage of  $I_{\text{tail}}$  current source is  $V_{\text{Dsat}} = 0.2 \text{ V}$ .

### Solution

As the circuits are balanced, the DC current through all transistors will be

$$I_D = \frac{I_{tail}}{2} = 20 \mu\text{A} \quad (4.5.1)$$

This in turn produces the gain-source voltage for MOS transistors to be

$$\begin{aligned} V_{GSN} &= V_{THN} + \sqrt{\frac{2I_D}{K_N \frac{W}{L}}} = 0.773 \text{ V} \\ V_{GSP} &= V_{THP} + \sqrt{\frac{2I_D}{K_P \frac{W}{L}}} = 0.934 \text{ V} \end{aligned} \quad (4.5.2)$$

The common mode input range for the NMOS pair is limited by  $ITAL$

$$\begin{aligned} V_{iminN} &= V_{SS} + V_{GSN} + V_{Dsat} = V_{SS} + 0.973 \text{ V} \\ V_{imaxN} &= V_{DD} - R_1 I_D - (V_{GSN} - V_{THN}) + V_{GSN} = V_{DD} + 0.5 \text{ V} \\ V_{imaxN} - V_{iminN} &= V_{DD} - V_{SS} R_1 I_D - (V_{GSN} - V_{THN}) = 2.527 \text{ V} \end{aligned} \quad (4.5.3)$$

and for the PMOS pair:

$$\begin{aligned} V_{iminP} &= V_{SS} + R_1 I_D - (V_{GSP} - V_{THP}) + V_{GSP} = V_{SS} - 0.6 \text{ V} \\ V_{imaxP} &= V_{DD} - V_{Dsat} + V_{GSP} = V_{DD} - 1.134 \text{ V} \\ V_{imaxP} - V_{iminP} &= V_{DD} - V_{SS} - R_1 I_D + (V_{GSP} - V_{THP}) = 2.466 \text{ V} \end{aligned} \quad (4.5.4)$$

Note that the range for PMOS devices is smaller than the corresponding input range for NMOS devices, due to operating identical sized transistors of both types at the same current. The minimum supply voltage can be calculated by forcing equal values for  $V_{iminN}$  (Eq. 4.5.3) and  $V_{imaxP}$  (Eq. 4.5.4)

$$V_{SS} + 0.973 \text{ V} = V_{DD} - 1.134 \text{ V} \quad (4.5.5)$$

which produces the minimum supply voltage

$$V_{DD} - V_{SS} = 2.1 \text{ V} \quad (4.5.6)$$

Independently of supply voltage value, the supply rails are exceeded by common-mode input voltage range with

$$\begin{aligned} V_{imaxN} - V_{DD} &= 0.5 \text{ V} \\ V_{SS} - V_{iminP} &= 0.6 \text{ V} \end{aligned} \quad (4.5.7)$$

### Problem 4.2

For the input stage shown in Fig. 4.4.2, design the output transistors  $M_5$ – $M_8$  so they work with  $I_D = 20\mu\text{A}$  at  $V_{GS\text{eff}} = V_{sat} = 0.2\text{ V}$  and the biasing source  $V_R$  for maximal output range. Then calculate the equivalent  $G_m$  of this input stage at common-mode input voltage for which only one of the input pairs or both of them are working, for input devices sized  $W/L_{NMOS} = 50\mu/2\mu$ ,  $W/L_{PMOS} = 175\mu/2\mu$  and operated with tail currents  $I_{R1} = I_{R2} = 40\mu\text{A}$  from sources with the saturation voltage  $V_{Dsat} = 0.2\text{ V}$ . Estimate the output impedance of this transconductance amplifier. Transistors have parameters:  $V_{THN} = 0.5\text{ V}$ ,  $V_{THP} = -0.6\text{ V}$ ,  $K_P = 16\mu\text{A}/\text{V}^2$ ,  $K_N = 56\mu\text{A}/\text{V}^2$ ,  $\lambda_P = \lambda_N = 0.1\text{ V}^{-1}$ ,  $\lambda$  parameters representing the channel-length modulation of the transistors. The resistors are all equal to  $10\text{ k}\Omega$ , and the supply voltages are  $V_{DD} = -V_{SS} = 2\text{ V}$ .

### Solution

The complete expression of  $I_D(V_{GS}, V_{DS})$  for a MOS transistor working in saturation is

$$I_D = \frac{K}{2} \frac{W}{L} (V_{GS} - V_{th})^2 (1 + \lambda V_{DS}) \quad (4.5.8)$$

The equation above shows the role of channel length modulation by drain-to-source voltage and can be used to derive the drain-to-source conductance

$$g_{ds} = \frac{dI_D}{dV_{DS}} = \lambda I_D \quad (4.5.9)$$

Sizing of transistors  $M_5$ – $M_8$  can be made knowing their drain current and gate overdrive voltage

$$\begin{aligned} \frac{W}{L_{M6,M8}} &= \frac{2I_D}{K_N V_{GS\text{eff}}^2} = 18 \\ \frac{W}{L_{M5,M7}} &= \frac{2I_D}{K_P V_{GS\text{eff}}^2} = 62 \end{aligned} \quad (4.5.10)$$

This provides the current through the resistors and the  $V_{GS}$  for cascode transistors, so  $V_R$  should be at least

$$V_R = I_7 R_7 + V_{GS7} = \left( \frac{I_{R2}}{2} + I_{D7} \right) R_7 - V_{THP} + V_{GS\text{eff}} = 1.2\text{ V} \quad (4.5.11)$$

Calculating the equivalent  $G_m$  can be reduced to calculating the input pair  $g_m$  and the common mode input range domains where each of the input pairs is active. Using Eqs. 4.4.1 and 4.4.2, these domains can be calculated based on

$$\begin{aligned}
 V_{GS\ M_1,M_2} &= V_{THN} - \sqrt{\frac{2I_D}{K_N \frac{W}{L}}} = -0.619\text{ V} \\
 V_{GS\ M_3,M_4} &= V_{THP} - \sqrt{\frac{2I_D}{K_P \frac{W}{L}}} = -0.719\text{ V} \\
 V_{sat\ N,P} &= 0.119\text{ V} \\
 V_R &= R_5 I_5 = 0.4\text{ V} \\
 V_{Dsat} &= 0.2\text{ V}
 \end{aligned} \tag{4.5.12}$$

Using these values, with  $V_{GS\ M_3,M_4}$  taken in absolute value, the CM input range limits for the PMOS and NMOS pairs become

$$\begin{aligned}
 V_{iminP} &= V_{GS\ M_3,M_4} + V_{sat\ N,P} + V_R + V_{SS} = -2.2\text{ V} \\
 V_{imaxP} &= V_{DD} - V_{GS\ M_3,M_4} - V_{Dsat} = 1.08\text{ V} \\
 V_{iminN} &= V_{SS} - V_{GS\ M_1,M_2} - V_{Dsat} = 1.18\text{ V} \\
 V_{imaxN} &= V_{DD} - V_{GS\ M_1,M_2} - V_{sat\ N,P} - V_R = 2.1\text{ V}
 \end{aligned} \tag{4.5.13}$$

Due to transistor sizing, which is proportional with  $K_N/K_P$ ,  $g_m$  of input pairs are equal

$$g_{mN,P} = \frac{2I_D}{V_{sat\ N,P}} = 336\ \mu\text{S} \tag{4.5.14}$$

The equivalent  $G_m$  is given by

$$\begin{aligned}
 G_m(V_{iminP} < V_{in} < V_{iminN}) &= g_{mN,P} = 336\ \mu\text{S} \\
 G_m(V_{iminP} < V_{in} < V_{imaxP}) &= g_{mN,P} = 672\ \mu\text{S} \\
 G_m(V_{imaxP} < V_{in} < V_{imaxN}) &= g_{mN,P} = 336\ \mu\text{S}
 \end{aligned} \tag{4.5.15}$$

The impedance of the cascoded output stage is given by the voltage gain of cascode transistors and biasing resistors

$$\begin{aligned}
 \mu_7 &= \frac{g_{m7}}{g_{ds7}} = \frac{1}{\lambda V_{GS\ eff}} = 50 \\
 Z_o &= \left( \mu_7 R_7 + \frac{1}{g_{ds7}} \right) \parallel \left( \mu_8 R_8 + \frac{1}{g_{ds8}} \right) = 250\ \text{k}\Omega
 \end{aligned} \tag{4.5.16}$$

### Problem 4.3

Design the circuit in Fig. 4.4.8 for a transconductance gain  $Y = 400\ \mu\text{A/V}$ . The transistor parameters, transistor sizes, resistor values and output transistors drain currents are the same as in Problem 4.2.

### ***Solution***

The transconductance gain is given by the input  $g_m$

$$Y = 2g_{m1,2} = 2\sqrt{2K_N \frac{W}{L_2} I_{D2}} \quad (4.5.17)$$

which in turn makes the drain current of the input devices to be

$$I_{D2} = \frac{\left(\frac{Y}{2}\right)^2}{2K_N \frac{W}{L_2}} = 14 \mu\text{A} \quad (4.5.18)$$

The transistors  $M_5$  and  $M_6$  are sized to be six times larger than the input devices

$$\begin{aligned} \frac{W}{L_5} &= 6 \frac{W}{L_{1,3}} = \frac{1050\mu}{2\mu} \\ \frac{W}{L_6} &= 6 \frac{W}{L_{2,4}} = \frac{300\mu}{2\mu} \end{aligned} \quad (4.5.19)$$

and the tail current sources must supply eight times more current than needed for each input device

$$I_{21} - I_{22} = 8I_{D2} = 112 \mu\text{A} \quad (4.5.20)$$

$V_{B1}$  differs from the one calculated in exercise (2) because the current through resistor  $R_{12}$  has changed

$$V_{B1} = I_{12}R_{12} + V_{GS12} = (I_{D2} + I_{D12})R_{12} - V_{THP} + V_{GS\text{eff}} = 1.14 \text{ V} \quad (4.5.21)$$

$V_{B2}$  can be calculated knowing the  $V_{GS6}$  is equal with  $V_{GS2}$  as for transistors operated at currents proportional to their size

$$V_{B2} = V_{GS6} + V_{D\text{sat}} = 0.819 \text{ V} \quad (4.5.22)$$

As a matter of fact,  $V_{B2}$  can have any value in the region of common mode input range where both input pairs are active. The other limit for  $V_{B2}$  can be easily calculated considering the results of Problem 4.2.

### ***Simulation Exercise 4.1***

The input stage shown in Fig. 4.5.1 is a rail-to-rail input stage which can also be considered a single-stage operational amplifier. Using a circuit as the one shown

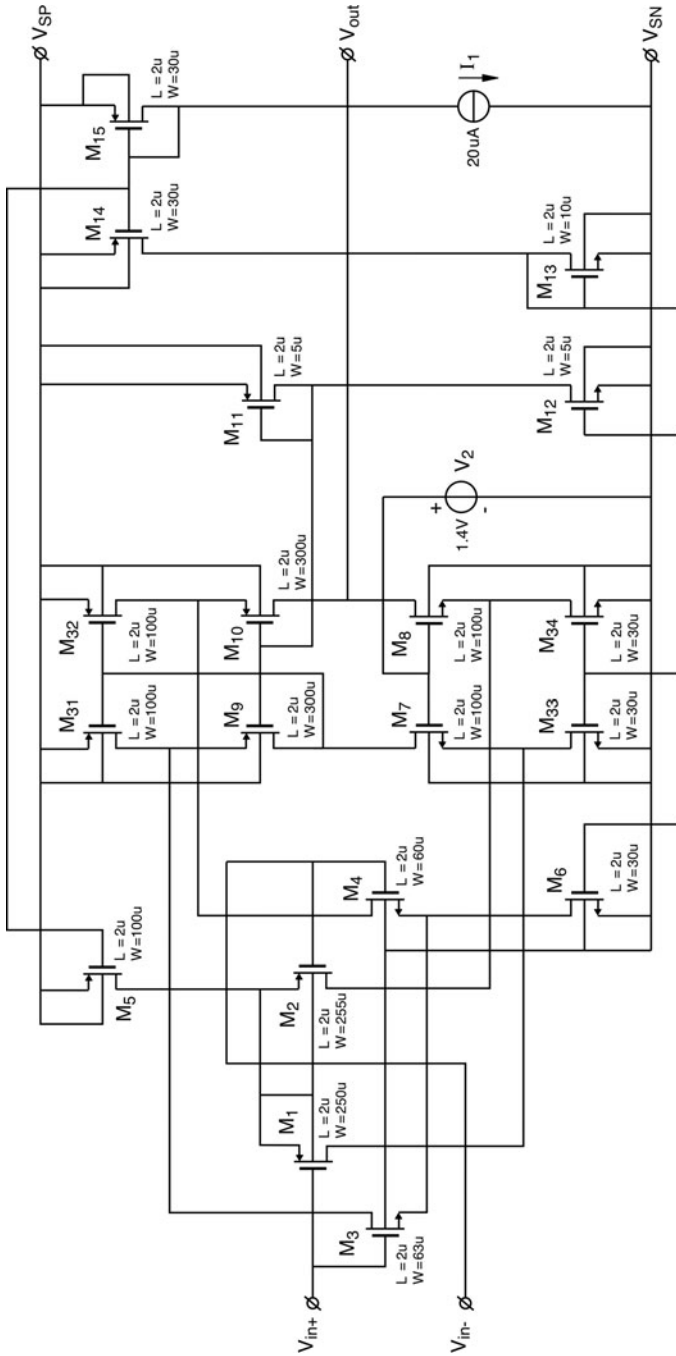


Fig. 4.5.1 Rail-to-rail input stage with summing circuit



in Fig. 2.8.2, simulate the AC behavior of this input stage. If using the same RC load, intended for an output stage, the gain and frequency behavior of the input stage will be strongly degraded. What is the usual load driven by a CMOS input stage?

### ***Simulation Exercise 4.2***

A transient analysis circuit for the rail-to-rail input stage is shown in Fig. 4.5.2. This circuit can be used to plot the  $g_m(V_{CM})$  curve which can affect the stability of an entire amplifier if not known in advance. The 10 mV DC input signal is used to obtain a current at the output of the input stage while the  $V_3$  0 V DC voltage source keeps the output of the stage at constant voltage for appropriate biasing. Simulate the  $g_m(V_{CM})$  curve for the circuit in Fig. 4.5.1 and calculate the percentage of  $g_m$  change over the whole  $V_{CM}$  range. How large can the input voltage  $V_2$  be and what limits this value?

### ***Simulation Exercise 4.3***

For the rail-to-rail input stage in Fig. 4.5.3 use the circuit depicted in Fig. 4.5.2 to simulate the  $g_m(V_{CM})$  behavior. A 0 V DC voltage source inserted near the source or drain of  $M_{20}$  and  $M_{21}$  can be used to plot the drain current of these transistors as a function of  $V_{CM}$ . What is the ratio of these currents to the drain current of  $M_6$  and  $M_5$  respectively?

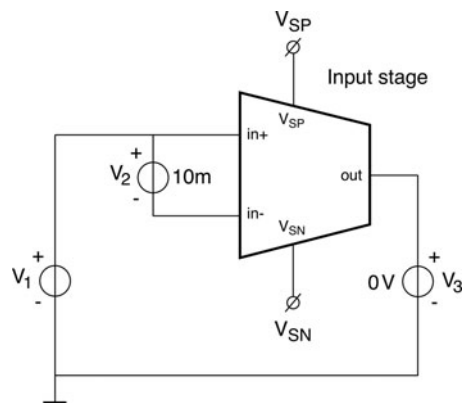


**Fig. 4.5.2** Input stage simulation circuit for transient analysis

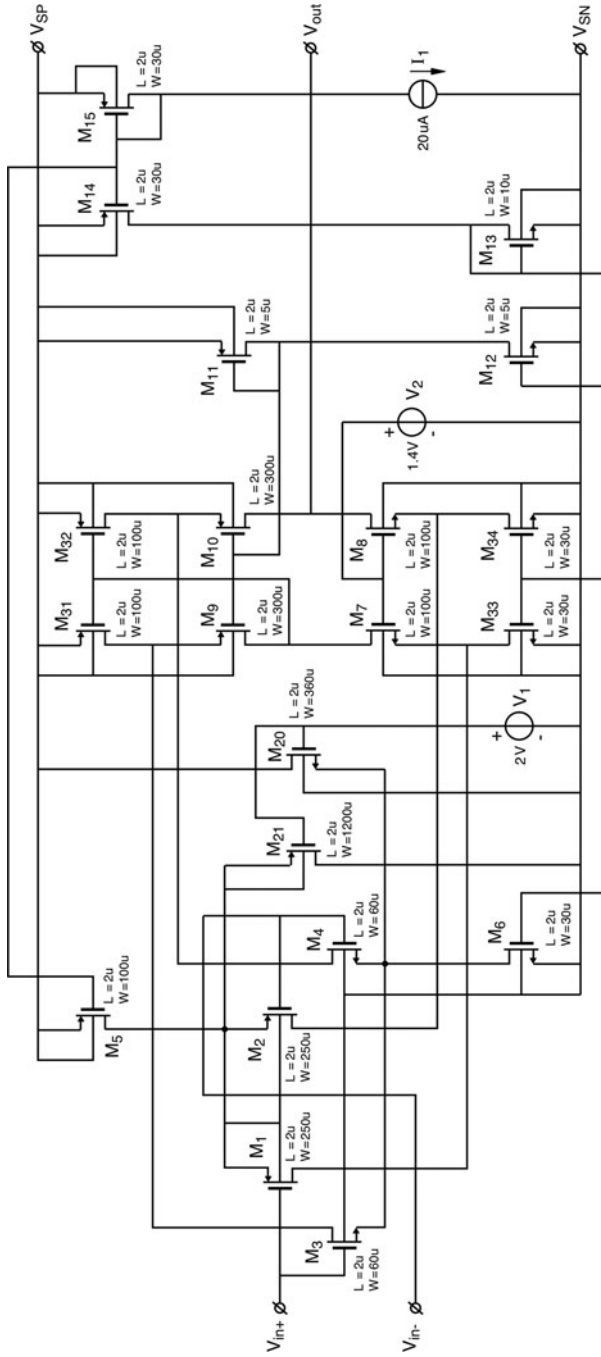


Fig. 4.5.3 Rail-to-rail input stage with  $G_m$  regulation

## 4.6 References

- [4.1]. Data sheet, Varactor-bridge operational amplifiers, Model 310 and 311 Analog Devices, 1974
- [4.2]. E.A. Goldberg, Stabilization of wideband amplifiers for zero and gain, *RCA Revue*, June 1950, pp. 298
- [4.3]. R.J. Veen, Piezjunction effect on a planar n-p-n transistor for transducer aims. *Electron. Lett.* **15**(12), 333–334 (1979)
- [4.4]. R.M. Warner Jr., J.N. Fordemwalt, Integrated circuits, design principles and fabrication in *Motorola Series Solid-State Electronics* (Mc Graw Hill, New York, 1965)
- [4.5]. J.E. Solomon, The monolithic opamp: a tutorial study. *IEEE J. Solid-St. Circ.* **SC-9**, 314–332 (1974)
- [4.6]. M.A. Maidigne, A high precision monolithic super beta operational amplifier. *IEEE J. Solid-St. Circ.* **SC-7**, 482–483 (1972)
- [4.7]. G.R. Wilson, A monolithic junction FET-NPN operation amplifier. *IEEE J. Solid-St. Circ.* **SC-3**, 341–348 (1968)
- [4.8]. C.D. Motchenbacher, F.C. Fitchen, in *Low-Noise Electronic Design* (Wiley, New York, 1973)
- [4.9]. R. Blauschild, Differential amplifier circuit with rail-to-rail capability, US Patent 4,532, 479, 30 July 1985
- [4.10]. J.H. Huijsing, D. Linebarger, Low-voltage operational amplifier with rail-to-rail input and output ranges. *IEEE J. Solid-St. Circ.* **SC-20**(6), 1144–1150 (1985)
- [4.11]. R. Hogervorst, J.P. Tero, R.G.H. Eschauzier, J.H. Huijsing, A compact power-efficient 3 V CMOS rail-to-rail input/output operational amplifier for VCSI cell libraries. *IEEE J. Solid-St. Circ.* **29**(12), (1994)
- [4.12]. K.J. de Langen, R. Hogervorst, J.H. Huijsing, Translinear circuits in low-voltage operational amplifiers in *Analog Circuit Design* (Kluwer, Boston, 1996), pp. 357–385
- [4.13]. D.L. Knee, C.E. Moore, General-purpose 3 V CMOS operational amplifier with a new constant-transconductance input stage. *Hewlett-Packard J.* **Aug**, 114–120 (1997)
- [4.14]. R. Hogervorst, J.H. Huijsing, J.P. Tero, Rail-to-rail input stages with  $g_m$ -control by multiple input pairs, US Patent 5,561,396, Oct 1996
- [4.15]. W. Redman-White, A high bandwidth constant  $g_m$  and slew-rate rail-to-rail CMOS input circuit and its application to analog cells for low-voltage VLSI systems. *IEEE J. Solid-St. Circ.* **32**(5), 701–712 (1997)
- [4.16]. B.J. Blalock, P.E. Allen, G.A. Rincon-Mora, Designing 1-V OpAmps using standard digital CMOS technology. *IEEE T. Circuits-II* **45**(07), 769–781 (1998)
- [4.17]. G. van der Horn, J.H. Huijsing, Extension of the common-mode range of bipolar input stages beyond the supply rails of operational amplifiers and comparators. *IEEE J. Solid-St. Circ.* **28**(7), 750–757 (1993)
- [4.18]. J.F. Witte, K.A.A. Makinwa, J.H. Huijsing, A current feedback instrumentation amplifier with 5  $\mu$ V offset for bidirectional high-side current sensing, *IEEE Solid-State Circuits Conference 2008*, San Francisco, Session 3.5, 4–6 Feb 2008
- [4.19]. J.F. Witte, K.A.A. Makinwa, J.H. Huijsing, *Dynamic Offset Compensated CMOS Amplifiers*. (Springer, New York, 2009), 250pp. ISBN:978-1-4020-8163-7
- [4.20]. D.J. Comer, D.T. Comer, Using the weak inversion region to optimize input stage design of CMOS OpAmps. *IEEE T. Circuits-II* **51**(1), 8–14 (2004)
- [4.21]. M.J.M. Pelgrom, H.P. Tuinhout, M. Vertregt, Transistor matching in analog CMOS applications, *IEDM 98*–915, 1998
- [4.22]. K.J. de Langen, J.H. Huijsing, Compact low-voltage PTAT-current source and bandgap-reference circuits, *Solid-State Circuits Conference, ESSCIRC '98, Proceedings of the 24th European*, pp. 109–111, 22–24 Sept 1998
- [4.23]. H.C. Nauta, E.H. Nordholt, New class of high-performance PTAT current sources. *Electron. Lett.* **21**, pp. 384–386 (1985)
- [4.24]. R.F. Wassenaar, Analysis of analog CMOS circuits, Fig. 5.9, PhD Thesis, Twente University, 31 Oct 1996

## 5. Output Stages

The output stage of an operational amplifier has to provide the load impedance  $Z_L$  with the desired output voltage  $V_O$  and current  $I_O$ , resulting in an output power  $P_O = V_O I_O$ . The main requirements of the output stage are: the ability to deliver negative and positive output currents at a high current efficiency, an output voltage range that efficiently utilizes the range between the negative supply rail voltage and the positive one, a high power efficiency, a low distortion, and good high-frequency (HF) performance.

Section 5.1 explains some issues of power efficiency. Section 5.2 presents a systematic classification of potential class-AB biased output circuits with a good compromise of power efficiency and distortion. Such a classification enables us to choose one which best matches the requirements of the output stage in combination with the restrictions of a given integration process. The design of output stages is divided into Sect. 5.3 for feedforward-biased class-AB output stages, and Sect. 5.4 for feedback-biased class-AB output stages. Finally, Sect. 5.5 evaluates several current and saturation limiters for bipolar output stages.

### 5.1 Power Efficiency of Output Stages

Obtaining a high power efficiency is one of the main objects of designing a general-purpose output stage. Power efficiency can be defined as the ratio of output power  $P_o$  delivered to the load and the supply power  $P_s$  taken from the supply rails. The difference between  $P_s$  and  $P_o$  is dissipated by the output stage. Power dissipation in the output transistors causes the chip's temperature to rise, while the heat that flows from the dissipating sources towards the cooling surface brings about temperature differences on the chip. Both the temperature rise and differences may deteriorate the amplifier characteristics, as will be discussed shortly.

Above a temperature of 450 K, too many thermally generated electrons appear in the conducting band of extrinsic silicon. This causes excessive diode leakage currents, which double at each 6 K temperature increase.

In order to keep the temperature of the chip  $T_c$  below the maximum value  $T_{cmax}$  of about 150°C, the product of the dissipated heat on the chip  $P_d$  and the thermal

resistance  $R_{TH}$  between the chip and the ambience must be lower than the temperature difference  $\Delta T$  between  $T_{cmax}$  and the ambient temperature  $T_a$ . So,

$$P_d R_{TH} \leq (T_{cmax} - T_a). \tag{5.1.1}$$

This cooling problem is present not only in large-power amplifiers but also in micro-power amplifiers. In the latter case, the dissipated heat per amplifier determines how many OpAmps can be placed on a single VLSI chip and which measures must be taken to avoid thermal crosstalk to sensitive points on the chip.

The thermal coupling on the chip between the output and input stages causes internal feedback which limits the useful low-frequency gain of the OpAmp [5.1]. This effect can be divided into two parts. Firstly, there are changes in the temperature of the input transistors which modulate the offset quantities of the amplifier via the temperature drift of these quantities (Sect. 4.1). Secondly, there are temperature gradients which can introduce additional variations in the offset quantities. The first effect can be minimized by placing the output transistors as far away from the critical input transistors as possible. The second effect can be reduced by placing the output transistors on the line of symmetry of the critical transistors, and by precisely balancing or crosscoupling the critical transistors of the input stage as shown in Fig. 5.1.1.

An output stage for a universal operational amplifier should be able to provide an output voltage and current of both polarities. This leads to the general supply configuration of Fig. 5.1.2 for an operational amplifier. The ground connection has

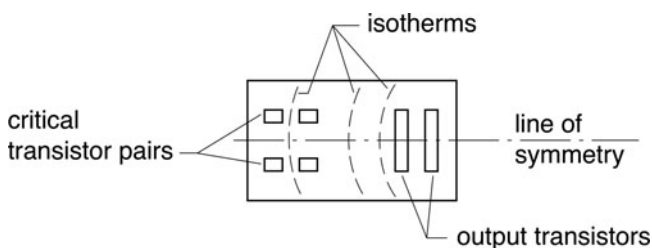


Fig. 5.1.1 Layout which balances out thermal feedback

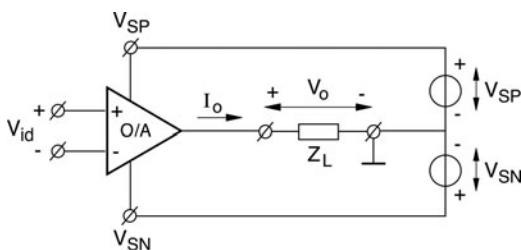


Fig. 5.1.2 General supply configuration of an operational amplifier

been shown between two external supply voltages  $V_{sp}$  and  $V_{sn}$  of opposite polarity. This is according to the general description in Chaps. 1–3. However, with a single supply source, the ground connection is mostly placed at the negative supply rail. In that case, the right-hand side of the load impedance  $Z_L$  needs an artificial supply connection in between the supply rails  $V_{sp}$  and  $V_{sn}$ .

We will now explore several types of possible output circuits with regard to the power efficiency and handling of both output polarities at a low distortion. The efficiency is strongly dependent on the biasing mechanism of the output transistors. Several possibilities of biasing are exemplified by five voltage-follower circuits of Fig. 5.1.3. These circuits are depicted with CMOS transistors but may also be equipped with bipolar transistors. For this reason we have named these transistors  $T$ . The diodes are of the same kind as the transistors.

The single-sided circuits of Fig. 5.1.3a, b handle their power very uneconomically. The first circuit is not even capable of driving the output down to the negative supply voltage. For a symmetrical sine-wave output of maximally half the supply voltage, its power efficiency is 20% with a resistor  $R_2 = R_L$ .

This circuit is much more fit for asymmetrically driving a load resistor connected to the negative supply rail. Like an open collector or drain output, such an open emitter or source output then has a power efficiency of nearly 100% for a rail-to-rail output block wave, disregarding the voltage loss of the base-emitter or gate-source diode.

The second circuit has a power efficiency of 35% for a rail-to-rail output sine-wave driving a symmetrical load resistor using a current source  $I_2 = 1/2 V_S / R_L$  connected to the negative rail.

The push-pull circuits of Fig. 5.1.3c–e handle their power much more efficiently. Neither of these circuits dissipate power if the output is driven against the positive or negative supply voltage, apart from power loss in the base-emitter or gate-source diodes of the output transistors and the auxiliary components.

The class-A circuit of Fig. 5.1.3c has a maximum sine-wave efficiency of 50%. The sum of the push and pull currents is constant:

$$I_1 + I_2 = \frac{1}{2} \frac{V_S}{R_L} \quad (5.1.2)$$

with  $V_S = V_{SP} - V_{SN}$ . It has a maximum power loss at zero output current. In this point the class-C circuit of Fig. 5.1.3e is better with a zero power loss at zero output current, as the product of the push and pull currents is zero:

$$I_1 \times I_2 = 0 \quad (5.1.3)$$

A disadvantage of the class-C stage is its dead band in the transfer function. This can theoretically be reduced to zero by overall feedback with a large loop gain. In that case, the circuit would behave as an ideal class-B amplifier with zero quiescent current in the output transistors and a max. sine-wave

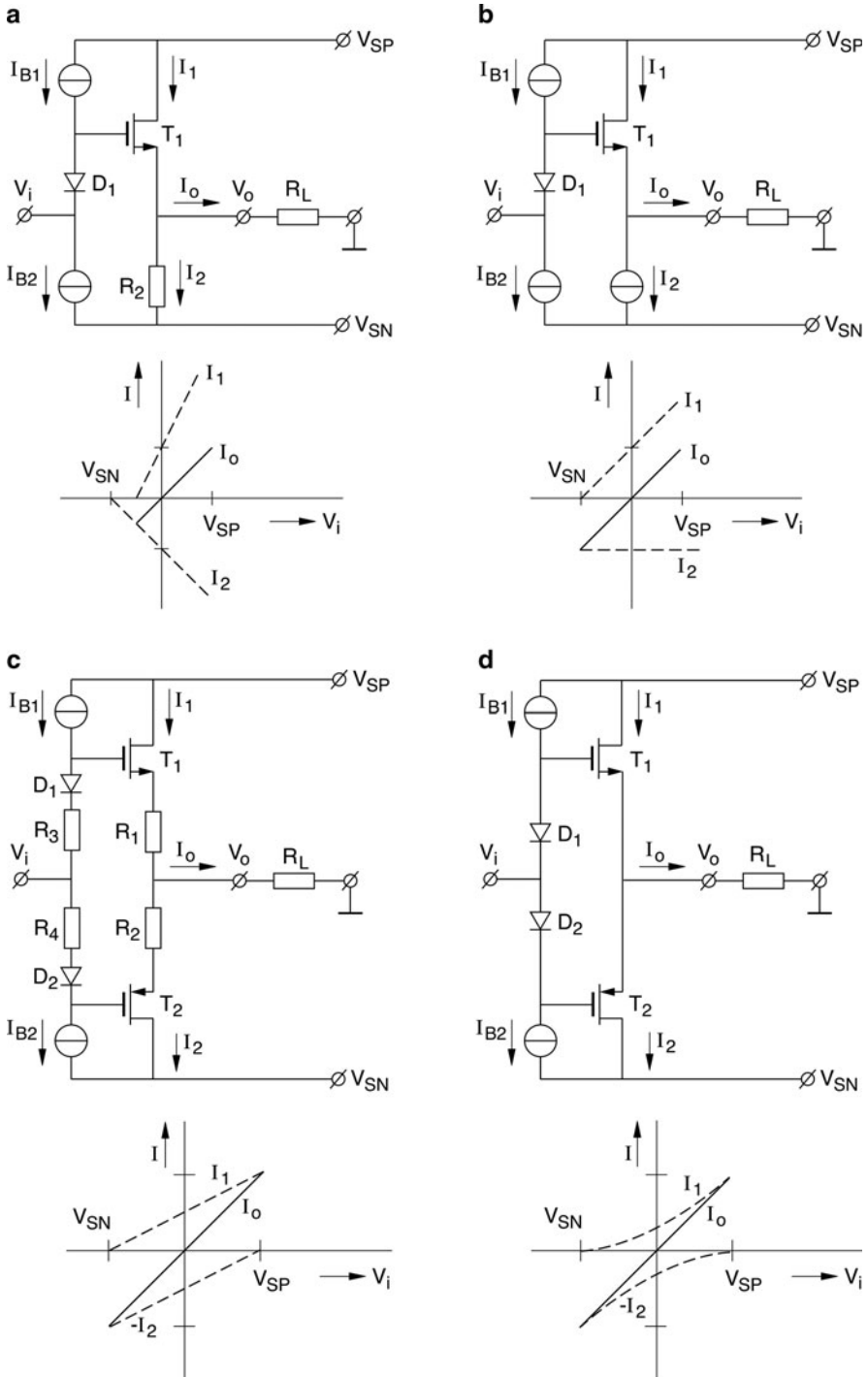
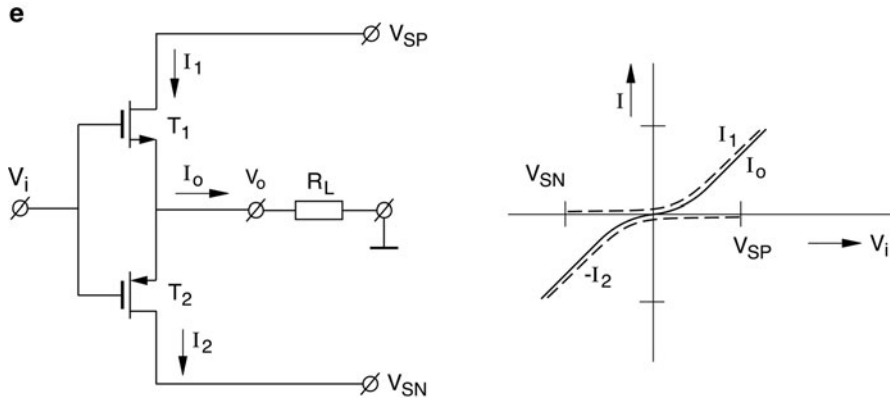


Fig. 5.1.3 (continued)



**Fig. 5.1.3** (a) Single resistor-loaded voltage follower with:  $R_2 = R_L$  and  $V_S = V_{SP} - V_{SN}$  Sine-wave efficiency 20%. (b) Single current-source-loaded voltage follower with:  $I_2 = 1/2 V_S / R_L$  and  $V_S = V_{SP} - V_{SN}$  Sine-wave efficiency 35%. (c) Push-pull class-A voltage follower:  $I_1 + I_2 = 1/2 V_S / R_L$  Sine-wave efficiency 50%. (d) Push-pull class-AB voltage follower with:  $I_B = I_{B1} = I_{B2}$  Sine-wave efficiency nearly 78%. (e) Push-pull class-C voltage follower with a dead current zone around  $V_i = 0$ , Sine-wave efficiency 78%

efficiency of 78%. However, the limited slew rate of the preceding driver stage causes the class-C output stage to have a distorted dynamic cross-over response. For that reason the compromise of a class-AB output stage with a smooth cross-over response is commonly required in analog systems. The class-AB circuit of Fig. 5.1.3d has push and pull currents whose product is relatively small. It has a smooth cross-over behavior. It's sine-wave efficiency is a little below 78%.

The maximum square-wave response efficiency of the three circuits of Fig. 5.1.3c–e is nearly 100%, except that the output voltage cannot completely reach the supply rail voltage due to the diode-voltage loss of the voltage-follower and the saturation voltage of the bias current source. It would be better to connect the output transistors in a common-emitter or common-source configuration, as we will see later on. Then only one saturation voltage would be lost.

In conclusion: The maximum sine-wave efficiency of a pure class-A push-pull stage is 50%, while that of a pure class-B or class-C stage is 78% [5.2]. The sine-wave efficiency of a class-AB stage lies a little below 78%.

Figure 5.1.4 gives an overview of the power dissipation as a function of the output voltage of the three push-pull circuits.

A higher efficiency can principally be reached when the supply voltages could be dynamically adapted to the output waveform, i.e., with switchable taps on the supply sources. Another potential way of obtaining a higher efficiency is a class-D amplifier in which the output is switched between zero and both supply voltages and whose sampled output waveform is smoothed by a low-loss filter. These possibilities are not described in this book.



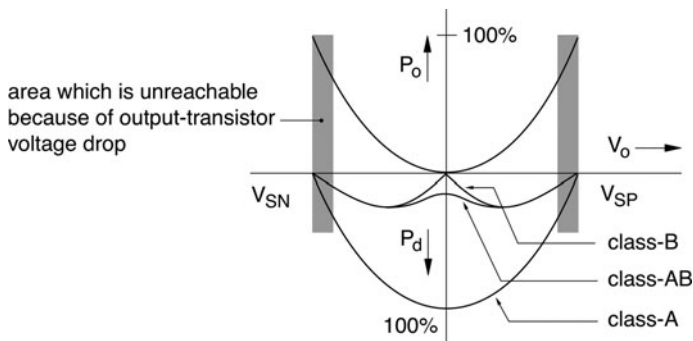


**Fig. 5.1.4** Power dissipation  $P_d$  and output power  $P_o$  as a function of the output voltage  $V_o$  at various biasing classes, disregarding bias currents

## 5.2 Classification of Output Stages

A systematic classification of potential output stages will be given in this section. This provides the designer with the ability to choose that which best suits the requirements and process parameters.

Output transistors can generally be connected in three different ways: firstly, in a general-amplifier (GA) connection (common-emitter or common-source), secondly, in a voltage-follower (VF) connection (common-collector or common-drain), and thirdly, in a current-follower (CF) connection (common-base or common-gate).

A CF-connected transistor may be inserted as a cascode transistor in the collector or drain lead of a GA-connected output transistor, for instance, to increase the output impedance of the stage. This transistor combination does not change the basic GA configuration of the output stage. A CF-connected transistor may also be inserted in the emitter or source lead of a VF-connected output transistor. This results in a transistor combination which has properties similar to a normal GA-connected transistor. The transistor combination will be classified as a GA-connected circuit. For this reason we may leave the CF-connection out of the classification of output stages, leaving two possible connections: the VF and the GA-connection.

All possible combinations of VF and GA-connected output transistors give rise to three main push-pull configurations: the VF/VF stage or fully VF stage, the compound VF/GA stage or GA/VF stage, and the GA/GA stage or fully GA stage. The VF/GA stage will not be distinguished from an GA/VF stage (Table 5.2.1).

The three main types are shown in Fig. 5.2.1a–c.

Figure 5.2.2 shows the desired class-AB output-current relations. For a large efficiency, the positive and negative maximum output currents should be much larger than the quiescent currents  $I_{MP,MN}$ . While for a good HF behavior, the minimum positive and negative currents should be as large as possible,  $I_{max,min} \approx < I_{quies}$ .

**Table 5.2.1** Classification of all possible push-pull output stages

Classification number	Connection of upper output transistor	Connection of lower output transistor
1	VF	VF
2	VF	GA
3	GA	GA

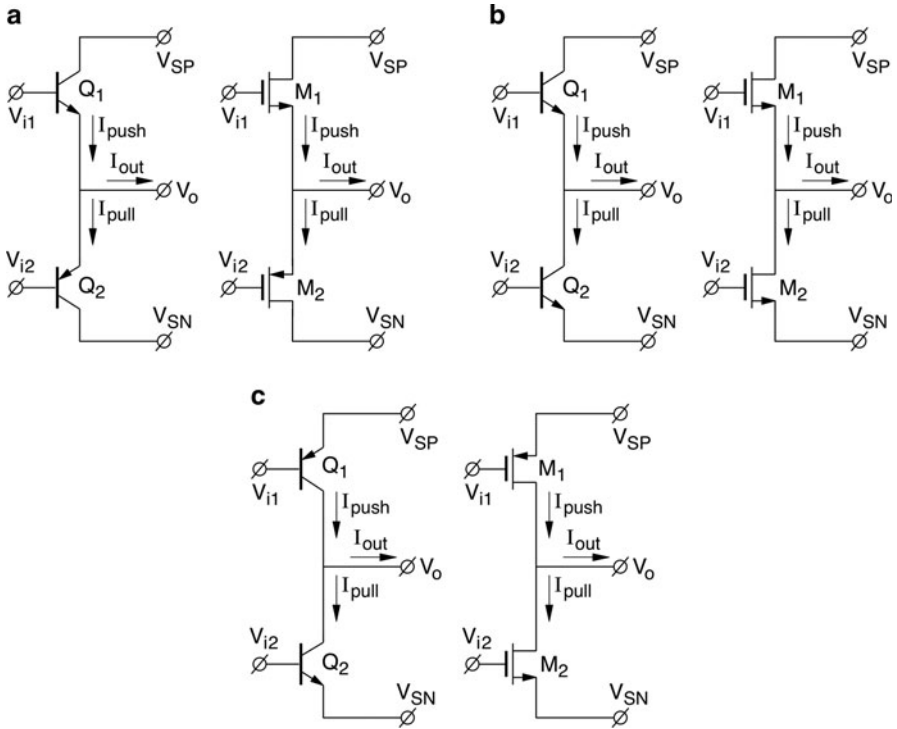


**Fig. 5.2.1** (a) Fully voltage-follower (VF) stage in bipolar and CMOS. (b) Compound (VF/GA) stage in bipolar and CMOS. (c) Fully general-amplifier (GA) stage in bipolar and CMOS

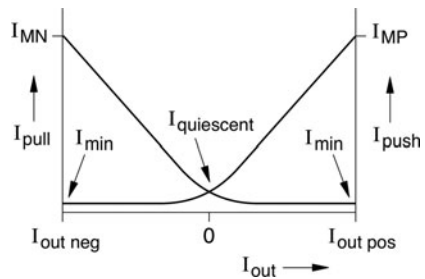


**Fig. 5.2.2** Desired class-AB output-current relations

Each basic circuit has a particular feature which makes it appealing. The VF stage can be biased most easily in class-AB. The VF/GA stage can be provided with the best type of transistor which can be made in a certain fabrication process for both push and pull sides. This is important for high output currents or high-frequency capabilities. The GA stage has the largest power gain.

Its output can almost reach both supply rails. This is very important for low-voltage rail-to-rail applications.

In Sects. 5.3 and 5.4, we will see how these three basic output stages can be efficiently biased in class-AB. This can be done by feedforward techniques and feedback techniques.

### 5.3 Feedforward Class-AB Biasing (FFB)

The term “feedforward biasing” is used if the biasing is fixed by components in series or in parallel with the signal path. This, in distinction to feedback biasing. Here a feedback loop is used to fix the class-AB biasing, which will be discussed in Sect. 5.4.

#### *FFB Voltage Follower Output Stages*

For a long time, the voltage follower (VF) configuration has been the most popular feedforward class-AB biasing scheme for its simplicity and robustness. The basic circuit is shown in Fig. 5.3.1a with complementary bipolar transistors and in Fig. 5.3.2a with CMOS transistors.

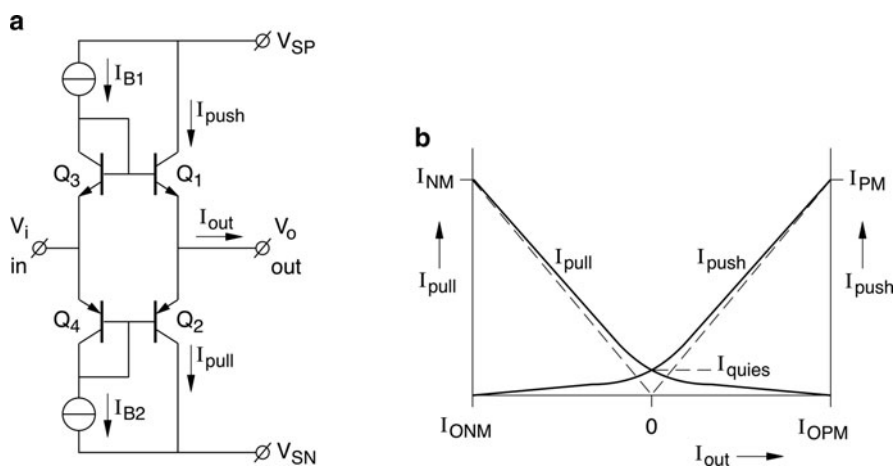


**Fig. 5.3.1** (a) VF output stage with complementary bipolar transistors. (b) Push and pull currents  $I_{push}$  and  $I_{pull}$  as a function of the output current  $I_{out}$

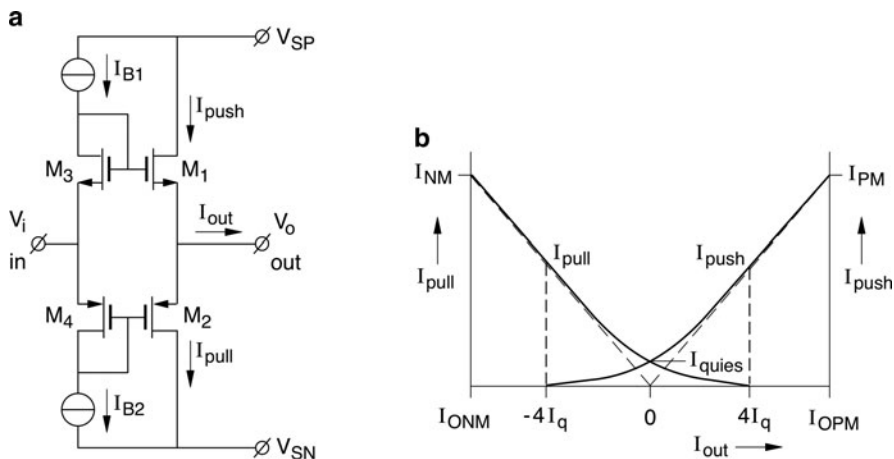


**Fig. 5.3.2** (a) VF output stage with CMOS transistors. (b) Push and pull current  $I_{push}$  and  $I_{pull}$  as a function of the output current  $I_{out}$

For the bipolar circuit of Fig. 5.3.1a the product of the push and pull currents  $I_{push}$  and  $I_{pull}$  is approximately constant. This is because of the logarithmic relation between base-emitter voltage and collector current of bipolar transistors, and the constant sum voltage across the base-emitter voltages, which is set by the diode connected transistors  $Q_3$  and  $Q_4$  in a translinear loop.

So we have:

$$\begin{aligned} V_{BE1} + V_{BE2} &= V_{BE3} + V_{BE4} \\ I_{push} \times I_{pull} &= I_{quies}^2 \end{aligned} \quad (5.3.1)$$

with  $I_{quies} = I_{B1} = I_{B2}$ , and  $V_{BE} = V_T \ln(I_c/I_{sat}) + V_G$ , in which  $V_T = kT/q$ ,

$I_{sat}$  is the saturation current,  $V_G$  is the band gap voltage of silicon, and equal parameters for all transistors are supposed.

The CMOS circuit of Fig. 5.3.2a has a square root characteristic between drain current and gate-source voltage of the output transistors in strong inversion at high current. This, and the constant voltage across the diodes  $M_3$  and  $M_4$  cause the sum of the square roots of the push and pull currents  $I_{push}$  and  $I_{pull}$  to be constant in a voltage translinear loop. So:

$$\begin{aligned} V_{GS1} + V_{GS2} &= V_{GS3} + V_{GS4} \\ \sqrt{I_{push}} + \sqrt{I_{pull}} &= 2\sqrt{I_{quies}} \end{aligned} \quad (5.3.2)$$

with  $I_{quies} = I_{B1} = I_{B2}$ , and  $V_{GS} = V_{TH} + \sqrt{2I_0/K}$  and equal parameters for all transistors are supposed. For low output currents the stage behaves in weak inversion like a bipolar stage.

Both VF stages with bipolar or CMOS transistors show a smooth cross-over behavior. In the bipolar circuit the maximum output current is  $I_{OPM} = \beta_1 I_{B1}$ , and  $I_{ONM} = \beta_2 I_{B2}$ . No output transistor is ever cut off. In the CMOS circuit the maximum output current is determined by the allowable input voltage drive. The output transistor with the lowest current will be smoothly cut off if the transistor with the highest current has a current larger than  $I_O = 4I_B = 4I_{quies}$ .

The low-impedance of the two-diode coupling between the input nodes of the transistors in the VF stages makes the relation between the push and pull currents strongly fixed in class-AB. This class-AB biasing is insensitive to wide changes in supply voltages, temperatures and process parameters. The bipolar VF stage has an output impedance in quiescent situation

$$z_o = \frac{1}{2} z_e, \quad (5.3.3)$$

with  $z_e = V_T/I_e$ ,  $V_T = kT/q$ . The CMOS VF stage has an output impedance

$$z_o = \frac{1}{2g_m}, \quad (5.3.4)$$

with  $g_m = K(V_{GS} - V_{TH} \text{ (index)})$ , and  $K = \mu C_{ox} W/L$  in strong inversion, and  $g_m = I_D/(V_{DS} - V_{TH})$  with  $(V_{DS} - V_{TH}) = 60\text{mV}$  in weak inversion.

The successful way of biasing VF stages in class-AB is the basis of a number of further developments, which will be discussed in the next part.

The coupling between the input nodes of the upper and lower output transistors is so firm that the circuit can also be driven asymmetrically. This has been practised in the bipolar circuits of Figs. 5.3.3 and 5.3.4.

The circuit of Fig. 5.3.3 is the most popular circuit. It can be found in the classic operational amplifier  $\mu\text{A}741$  of Fairchild Semiconductor [5.3], and in a number of other OpAmp realizations. In this circuit the VF output stage is asymmetrically driven with an GA-connected NPN transistor. The driver and upper-output transistor are of the NPN type. This type of transistor has the best qualities in terms of

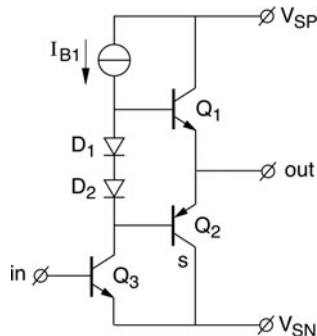


**Fig. 5.3.3** VF complementary FFB output stage with an asymmetric GA-connected NPN driver transistor, ( $\mu\text{A}741$ )

current gain, HF-response, and current capability. The lower-output transistor is a substrate PNP, which is the next best transistor with regard to the qualities of an NPN transistor. The maximum positive output current is  $I_{OPM} = \beta_1 I_{B1}$ .

The circuit of Fig. 5.3.4 has not often been implemented in the general purpose OpAmp. In this case the output stage is asymmetrically driven by a VF-connected NPN transistor. Its negative output current is limited to  $I_{ONM} = \beta_2 I_{B2}$ . This is lower than the maximum positive output current of the preceding stage because  $\beta_2 < \beta_1$ . The output voltage cannot reach the positive rail voltage within two diode voltages and a saturation voltage. The linearity of the current transfer of both previous configurations suffers from the difference in current gains  $\beta_1$  and  $\beta_2$  of the two output transistors.

Next, we will look at the group of ‘‘Darlington’’ bipolar variants of the VF output stage in which an emitter follower is inserted in front of the output transistor. The different ways in which a combination of two transistors can be connected allows for more freedom in the circuit configuration than the single VF output stage.

The conventional-Darlington VF output stage of Fig. 5.3.5 applies a Darlington NPN in the upper half and a Darlington substrate PNP in the lower half. This has the

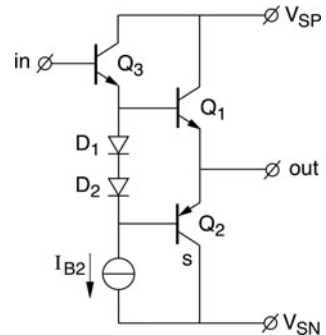


**Fig. 5.3.4** VF complementary FFB output stage with an asymmetric VF-connected NPN driver transistor

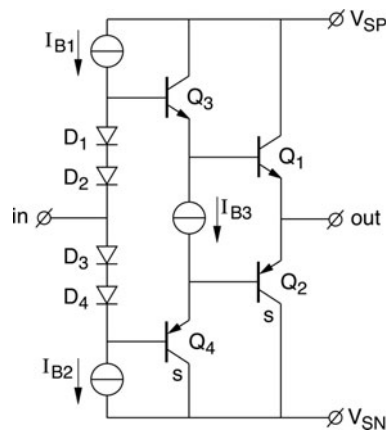


**Fig. 5.3.5** VF conventional-Darlington FFB output stage

disadvantage that the lower half has a significantly lower current gain (order:  $30 \times 30 = 900$ ) than the upper half (order  $100 \times 100 = 10,000$ ). Moreover, the output cannot reach the supply voltages within two diode voltages and a saturation voltage of the bias current sources. An advantage is the large ratio of maximum output current and bias current. This stage has only sporadically been implemented.

The folded-Darlington variant of Fig. 5.3.6 uses an NPN and a substrate PNP in both halves, which results in nearly equal current gains for both halves. This results in a more linear current gain than the preceding circuit of Fig. 5.3.5. It is also simpler and it can reach the supply within only one diode voltage. For these reasons the later stage has frequently been used, for instance in the general-purpose wide-band OpAmp described in [5.4]. A disadvantage is the larger bias current  $I_{B2}$  needed to drive the lateral PNP  $Q_2$  with a low  $\beta$ .

Another way of increasing the current gain of a bipolar VF output stage, is to add an GA output booster, as is shown in Fig. 5.3.7. This stage uses lateral PNP transistors for  $Q_1$  and  $Q_4$  which have poorer qualities for bandwidth and current

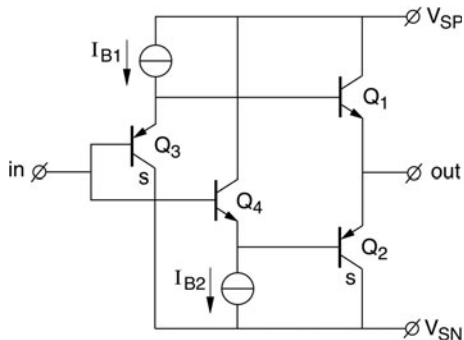


Fig. 5.3.6 VF folded-Darlington FFB output stage

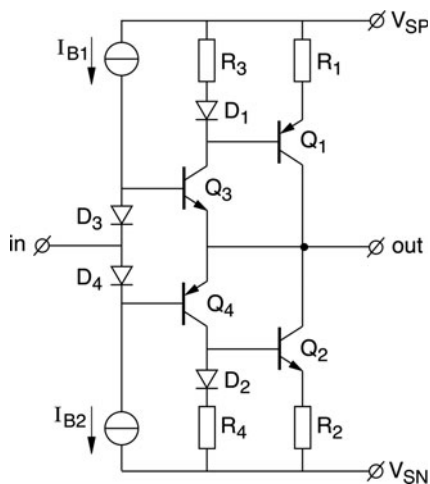


Fig. 5.3.7 GA boosted VF FFB output stage (LH0021)

gain than those of the substrate PNPs. Moreover, their current gain  $\beta$  rapidly goes down at higher output currents. Consequently, a practical implementation with discrete output transistors can be considered, as in the hybrid GA power OpAmp LH0021 of National Semiconductor [5.5].

A disadvantage of this stage, in comparison to the previous Darlington stages, is that the GA output transistors  $Q_1$  and  $Q_2$  are driven by current sources. This means that the biasing of the output transistors is dependent on their current gain  $\beta$ . To reduce this disadvantage, additional parallel-base diode chains  $D_1, D_2$  with resistors  $R_3, R_4$  and series-emitter resistors  $R_1, R_2$  have to be inserted. Such resistors reduce the current gain.

### FFB Compound Output Stages

In particular, the combination of the GA boosted VF pair in the lower half and the conventional or folded-Darlington pair in the upper half brings about a group of successful compound (VF/GA) stages. This success is due to the presence of an NPN output transistor in the upper and lower halves. Members of this group will be discussed next.

A realization of this compound Darlington output stage is shown in Fig. 5.3.8 and has been described in [5.6] for application in a monolithic power OpAmp which can deliver an output current of the order of 1A. This is possible because the push and pull output transistors are both of the NPN type. The use of a lateral PNP ( $Q_4$ ) limits the HF response to some MHz. The biasing stability of this stage is much better than that of the preceding stage in Fig. 5.3.7. The reason is that the upper half controls its own current due to the inclusion of the  $V_{BE}$  of the output transistor  $Q_1$  in its translinear bias loop. And, the overall feedback makes that the upper half also controls the biasing of the lower output transistor  $Q_2$ . Hence, no low impedance

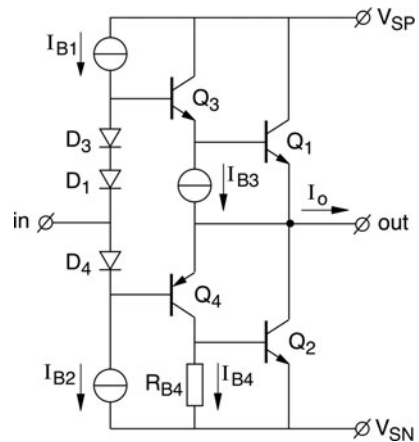
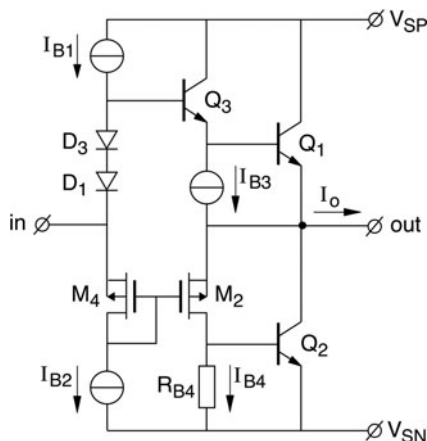


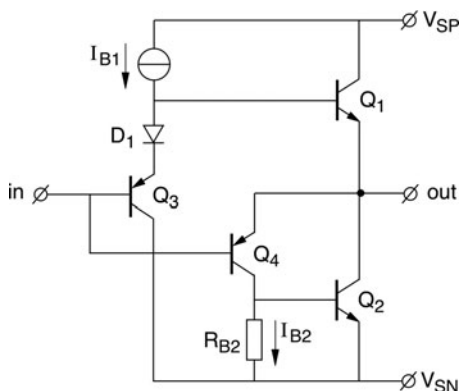
Fig. 5.3.8 VF/GA compound Darlington FFB output stage with a lateral PNP transistor



**Fig. 5.3.9** VF/GA compound Darlington output stage with P MOS FETs (CA3100)



**Fig. 5.3.10** VF/GA compound folded Darlington FFB output stage (LM101)



emitter resistor and diode chain has to be included in the lower half, as was the case in the preceding circuit, except for a relatively large bias current-source resistor  $R_{B4}$ .

Another realization of the compound Darlington output stage is shown in Fig. 5.3.9 and has been described in [5.7] for application in the (50 MHz) OpAmp CA 3100 of RCA. The wideband application could be obtained by replacing the lateral PNPs of the preceding circuit with P MOS FETs. Again the biasing is controlled by the upper half.

The GA boosted VF pair in the lower half combined with the folded Darlington pair in the upper half results in the relatively simple compound output stage of Fig. 5.3.10. It has been realized in the general-purpose OpAmp LM101 of National Semiconductor and has been described in [5.8]. This stage also has a good output-current capability, although its frequency response is limited to some MHz by the lateral PNP transistor  $Q_4$ .

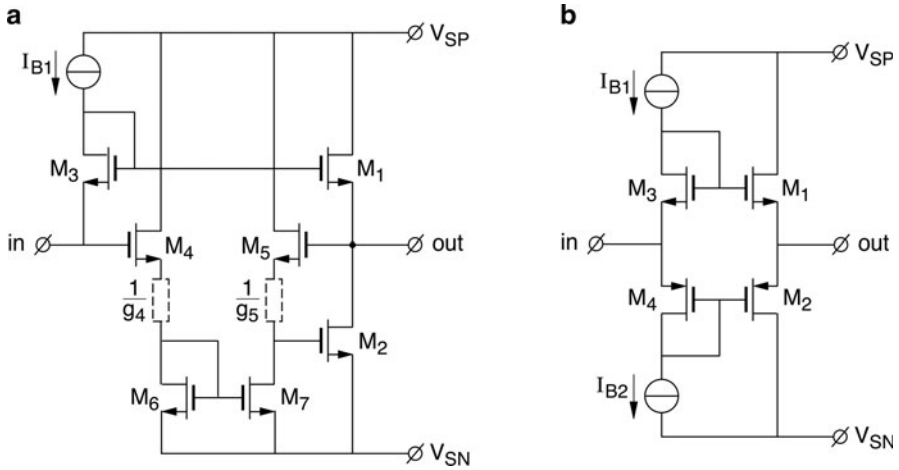


Fig. 5.3.11 (a) VF/GA all N MOS compound output stage. (b) Equivalent circuit of Fig. 5.3.11a

A resistor voltage-level shifter has been used in the lower half of Fig. 5.3.11a to obtain the compound stage with two equal output N-MOS FETs. The circuit is described in [5.9]. The VF-connected N-MOS FETs  $M_4$  and  $M_5$  function as two equal and large source resistances  $1/g_4$  and  $1/g_5$ . These resistors, together with the current mirror  $M_6M_7$ , function as a voltage-level shifter. Because the voltage transfer of the level shifter has a negative polarity, the lower output functions as if it were its complementary counterpart. The equivalent VF circuit of the stage is shown in Fig. 5.3.11b.

### FFB Rail-to-Rail General-Amplifier Output Stages

After the VF and VF/GA feedforward biasing schemes, we now have to examine the feedforward class-AB biasing of inverting amplifier (GA) output stages. The GA configuration is particularly important for low-voltage operation because the output voltage can utilize the full rail-to-rail voltage range except for two small saturation voltage ranges near each rail. This is in contrast with the VF configuration, where the output range loses two diode voltages plus two saturation voltages. Even the compound VF/GA stage loses at least one diode voltage and a saturation voltage at the VF side.

The simplest configuration is the digital inverter circuit of Fig. 5.3.12a.

The relation between the push and pull currents is shown in Fig. 5.3.12b. The quiescent current  $I_{quies}$  is difficult to control, as it is strongly dependent on variations of the supply voltage  $V_S = V_{SP} - V_{SN}$  and the threshold voltages of the transistors  $V_{THP}$  and  $V_{THN}$ , according to:

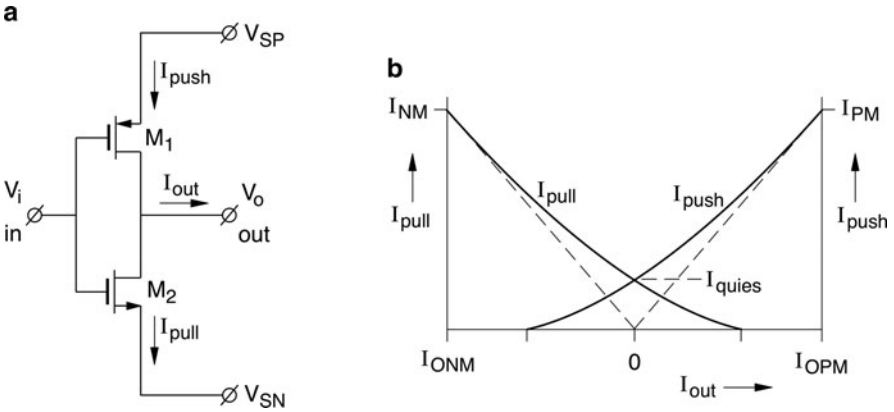


**Fig. 5.3.12** (a) GA FFB R-R class-AB CMOS output stage. (b) Push and pull currents  $I_{push}$  and  $I_{pull}$  as a function of the output current  $I_{out}$

$$I_{quies} = \frac{1}{2} \left( K_P^{-1/2} + K_N^{-1/2} \right)^{-2} (V_S - V_{THP} - V_{THN})^2 \quad (5.3.5)$$

To obtain a low sensitivity to supply-voltage variations and to process-dependent variations of the transistor characteristics, these characteristics must have a shallow curve. For this reason the biasing is chosen more A than AB by choosing a low W/L ratio in this configuration. Bipolar transistors have such steep characteristics that they can not generally be used in this configuration, unless the supply voltage  $V_{SP} - V_{SN} = V_S$  is regulated at two diode voltages. The main parameter of the CMOS GA stage is the voltage gain  $A_u \simeq g_m z_{ds}$ , which is of the order of 100. The maximum output current is restricted because of the required shallow driving characteristic. So the digital inverter stage is a rather poor analog GA output stage.

What we really would like to obtain is a behavior that is independent of the supply-voltage and transistor-parameter variations, like the behavior of the VF configuration. To develop this idea, we start with the conventional VF circuit of Fig. 5.3.13a. Next, we cut this circuit in an upper and lower half, and place these halves reversely on each other in Fig. 5.3.13b. To this end we have to insert a floating supply voltage source  $V_S$ , which is connected at its half to the input. This restores the voltage translinear loop  $V_{GS1} + V_{GS2} = V_{GS3} + V_{GS4}$ .

A first implementation of the idea is shown in Fig. 5.3.14a. The desired voltage source between the gates of the output transistors must be of the format  $V_B = V_S - V_{GS1} - V_{GS2}$ , with  $V_S = V_{SP} - V_{SN}$ . Such a voltage is available in the reference chain of Fig. 5.3.14a as  $V_{B2}$ .

This chain  $M_5, R_2$  and  $M_6$  between the supply rails generates a current  $I_{B2} = V_{B2}/R_2$ , with  $V_{B2} = V_S - V_{GS5} - V_{GS6}$  and  $V_S = V_{SP} - V_{SN}$ . This current is re-produced by the current mirrors  $M_5, M_3$  and  $M_6, M_4$ . The reproduced current  $I_{B1}$  generates the desired floating voltage  $V_{B1} = I_{B1}R_1$  between the gates of the output transistors [5.10]. The high-frequency behavior of the output stage is excellent because the

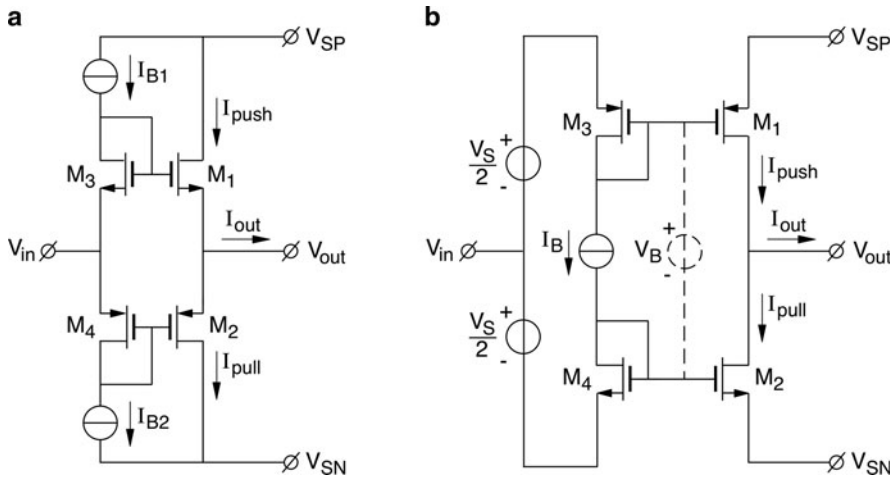


**Fig. 5.3.13** (a) VF feedforward biased class-AB CMOS output stage. (b) GA feedforward biased class-AB CMOS output stage

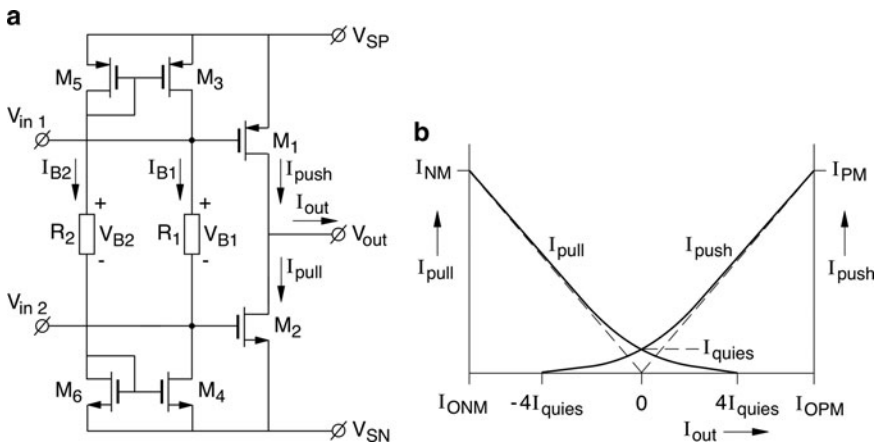


**Fig. 5.3.14** (a) GA FFB R-R class-AB CMOS output stage with common resistive coupling. (b) Push and pull currents  $I_{push}$  and  $I_{pull}$  as a function of the output current  $I_{out}$

output transistors are directly accessible at their gates. A capacitor across  $R_1$  may improve the HF coupling between the gates, particularly when the stage is driven from one side of  $R_1$  only. The push and pull currents behave similarly to those of the VF feedforward biased CMOS circuit of Fig. 5.3.2a and is depicted again in Fig. 5.3.13a. The equation for the quiescent current is given by (5.3.2). The circuit of Fig. 5.3.14a is quite useful. The minimum supply voltage equals that of two gate-source or base-emitter diode voltages  $2 V_D$ .

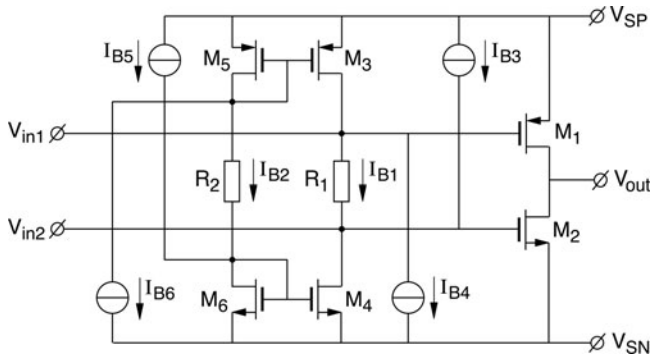


**Fig. 5.3.15** Low-voltage version of the GA feedforward biased rail-to-rail class-AB CMOS output stage with common resistive coupling with a minimum supply voltage of  $V_{SMin} = V_{GS} + V_{sat}$

For a supply voltage lower than that of two diodes, the resistive level shift voltage  $V_{B1} = I_{B1}R_1$  can be prebiased with a negative voltage by crosscoupled bias current sources  $I_{B3}$  through  $I_{B6}$ . This is shown in Fig. 5.3.15.

When the bias currents  $I_{B3}$  through  $I_{B6}$  are equal to  $I_B$ , and  $R_1$  and  $R_2$  are equal to  $R$ , the value of the bias current can be chosen equal to  $I_B = (V_{GS} - V_{sat})/R$ , to obtain a minimum supply voltage  $V_{SMin} = V_{SP} - V_{SN}$  equal to  $V_{SMin} = V_{GS} - V_{sat}$ , with  $V_{GS}$  equal to the gate source voltage of the output transistors, and  $V_{sat}$  equal to the saturation voltage of the current-source transistors.

A disadvantage of the two previous stages is that the quiescent current of the output transistors  $I_{quies}$  is proportional to the supply voltages minus two diode voltages according to:  $V_{B2} = V_S - V_{GS5} - V_{GS6}$ .

This can be overcome by decoupling the diode connection of the drain of  $M_5$  and driving a model output transistor  $M_8$  like  $M_1$ , by the drain of  $M_5$ , and comparing the drain current  $I_{D8}$  with a reference, current  $I_{ref}$ , and controlling the common gate of  $M_5$  and  $M_3$  so that  $I_{D8} = I_{ref}$ . Now the quiescent current is fixed at  $I_{ref}$  independent at the supply voltage.

The same circuit can be implemented in bipolar technology. The circuit for supply voltages of two diodes or higher is shown in Fig. 5.3.16a.

The result is similar to that of the circuit of Fig. 5.3.1a. The product of the push and pull currents should be constant according to Eq. 5.3.1, except for an asymmetric behavior of the currents below the quiescent value  $I_{quies}$  and that one output transistor is cut off when the other is driven. This is because the base currents of the output transistors with different current gains  $\beta_P$  and  $\beta_N$  disturb the constant voltage  $V_B$  across  $R_1$ . This results in a non-linear dynamic behavior. The resistive coupling for bipolar transistors is not strong enough so that  $R_1$  can be driven from one side only. The minimum supply voltage is that of two diode voltages  $2V_{BE} \approx 1.4$  V.

A different way to bias an GA output stage is to individually relate the driving voltages to the rail voltages. This is shown in a very elementary way with resistive coupling of bipolar transistors in Fig. 5.3.17 [5.15].

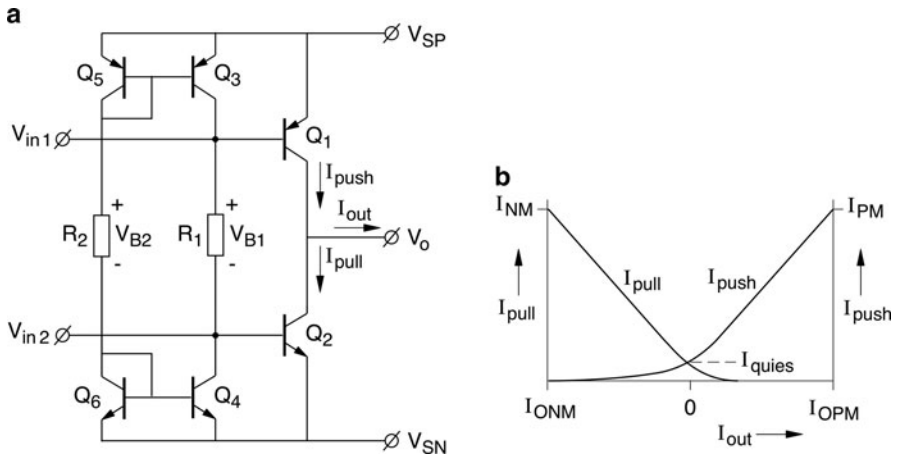
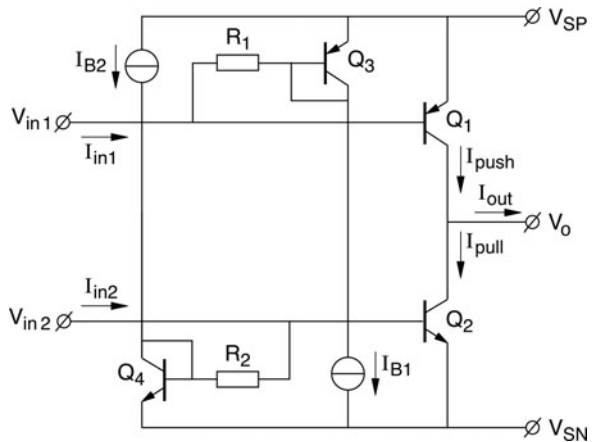


**Fig. 5.3.16** (a) GA FFB R-R class-AB bipolar output stage with CM resistive coupling. (b) Push and pull currents  $I_{push}$  and  $I_{pull}$  as a function of the output current  $I_{out}$

**Fig. 5.3.17** GA feedforward biased class-AB bipolar output stage with separate resistor and diode biasing



The idea is that the sum of the base-emitter voltages  $V_{SUM} = V_{BE1} + V_{BE2}$  remains constant and equal to the sum of the voltages across the diode-connected transistors  $Q_3$  and  $Q_4$ ,  $V_{SUM} = V_{BE3} + V_{BE4}$ , because the driving currents  $I_{in1}$  and  $I_{in2}$  generate equal but opposite voltages across  $R_1$  and  $R_2$ . The result is that the product of the push and pull currents remains constant, as expressed with the bipolar VF circuit of Fig. 5.3.1a and by Eq. 5.3.1. However, the base currents in the output transistors disturb this relation because they also generate currents in the biasing resistors  $R_1$  and  $R_2$ . To reduce this disturbance the resistors must be small. On the other hand, these resistors may not be taken too small or their conductances would take away too much of the input currents, and the current

gain of the output stage becomes too small. An advantage of the circuit of Fig. 5.3.17 is that the total supply voltage may be as low as one diode plus one saturation voltage, or about 0.9 V.

We certainly would not try to use CMOS in this circuit. Their high input impedance would be completely destroyed by the driving current of the low conductance of the resistors. But, what we can do to prevent the loss of driving current in the separate coupling elements  $R_1$  and  $R_2$ , is to collect the lost currents and add them again in a positive coupling loop. This principle is shown in Fig. 5.3.18 [5.10].

The transistor strings  $Q_1, Q_3, Q_5, Q_7$  and  $Q_2, Q_4, Q_6, Q_8$  are separate translinear loops that fix the bias current of the output transistors. To allow for a 100 mV voltage drop across the bias current sources  $I_{B3}$  and  $I_{B4}$ , a similar voltage-level shift is created across  $R_1$  and  $R_2$ . To compensate for this level shift in the translinear loops, the output transistor  $Q_1$  and  $Q_2$  should be small. The currents which are lost in the diode connected biasing transistors  $Q_3$  and  $Q_4$  are collected by the emitters of  $Q_5$  and  $Q_6$  respectively, and are returned as a driving current to the complementary side. The transistors  $Q_3, Q_5, Q_4, Q_6$  form a positive coupling loop with a current gain of slightly lower than one, which keeps this loop stable. All input current which is not used to drive one output transistor is used to drive the other. So, the gain decrease due to the class-AB biasing circuit is eliminated. In fact, the positive loop-gain coupling is a way to implement a class-AB bias circuit with high input impedance. The circuit needs a supply voltage of that of one diode and two saturation voltages, which is about 1 V.

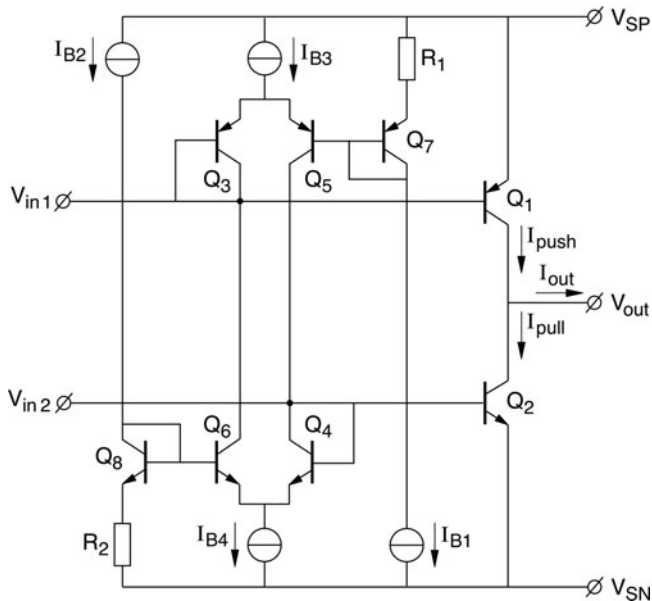


**Fig. 5.3.18** GA feedforward biased class-AB bipolar output stage with separate diode string biasing and positive loop gain coupling

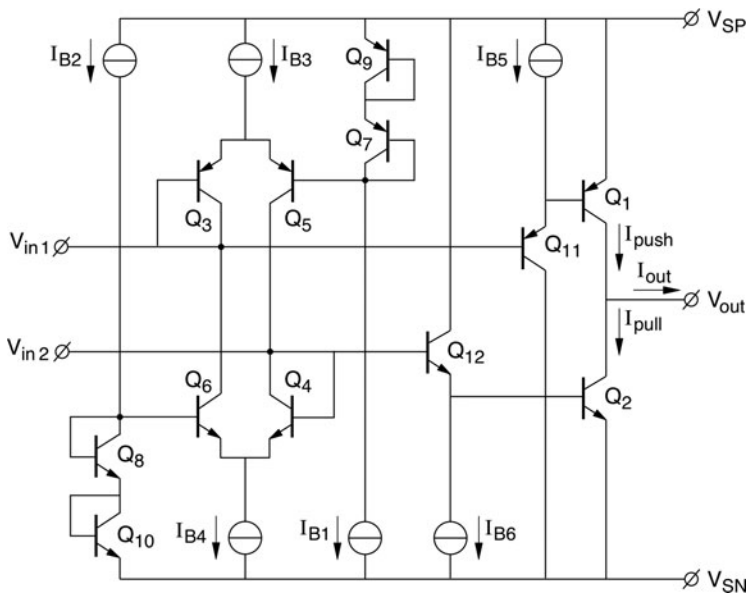


Fig. 5.3.19 GA FFB R-R class-AB Darlington output stage with CM transistor coupling

One way to eliminate the problem with the voltage drop needed for the bias current sources is to use Darlington output transistors  $Q_{11}$  and  $Q_{12}$  in combination with extra diodes in series with  $Q_7$  and  $Q_8$ . The result is shown in Fig. 5.3.19 [5.10].

The result is an GA feedforward biased class-AB rail-to-rail Darlington output stage. The stage may be driven by a single input terminal. The GA Darlington output stage can be made very current efficient, because the currents in the class AB loops may be chosen  $\beta_p^2$  lower than the maximum output currents; which may be a factor 1,000. However, the circuit needs a minimum supply voltage of that of three diodes and a saturation voltage, which is about 2.4 V.

A very robust feedforward biasing in class-AB arises if we simplify the translinear loops such that the diode coupled transistors  $Q_3$  and  $Q_4$  and the Darlington transistors  $Q_{11}$  and  $Q_{12}$  are taken away, as shown in Fig. 5.3.20a [5.10].

The translinear loops  $Q_1, Q_3, Q_5$  and  $Q_2, Q_4, Q_6, Q_8$  strongly fix the biasing in class-AB. The behavior of the push and pull currents  $I_{push}$  and  $I_{pull}$  in relation to the output current  $I_{out}$  is described as:

$$\begin{aligned}
 (I_{push} - 1/2 I_{quies})(I_{pull} - 1/2 I_{quies}) &= (1/2 I_{quies})^2 \\
 I_{out} &= I_{push} - I_{pull} \\
 I_{MIN} &= 1/2 I_{quies} = 1/2 I_{B1} = 1/2 I_{B2} = 1/2 I_{B3} = 1/2 I_{B4}
 \end{aligned}
 \tag{5.3.6}$$

with equal emitter areas for  $Q_1, Q_3, Q_5, Q_7$  and  $Q_2, Q_4, Q_6, Q_8$ .



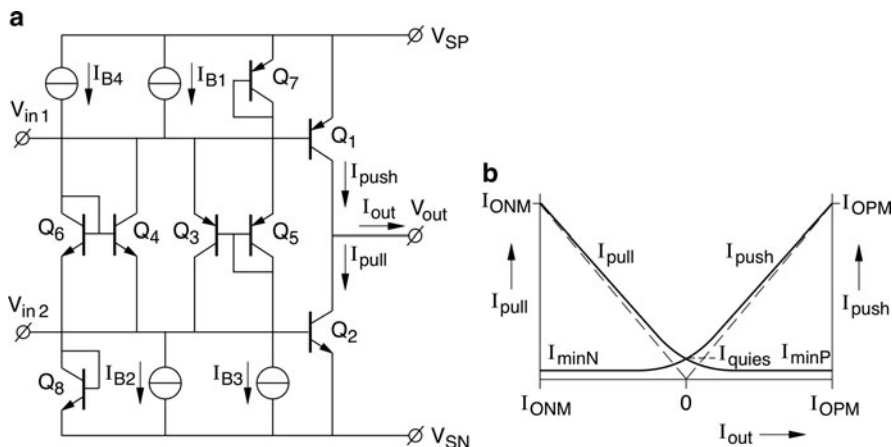


**Fig. 5.3.20** (a) GA FFB R-R class-AB bipolar output stage with CM transistor coupling. (b) Push and pull currents  $I_{push}$  and  $I_{pull}$  as a function of the output current  $I_{out}$

In the quiescent state, half the current of the current sources  $I_{B1}$  and  $I_{B2}$  flow through transistor  $Q_3$  and the other half through  $Q_4$ . But when one of the output transistors, say  $Q_1$ , draws a large current, all of the current of the current sources  $I_{B1}$  and  $I_{B2}$  flow through  $Q_4$ . This means that the current through  $Q_4$  is doubled. And, consequently, the current through the output transistor  $Q_2$  is halved, and is not reduced further. This situation is in favour of the simpler VF circuit of Fig. 5.3.1, whose behavior was described by Eq. 5.3.1. There the push or pull current did approach zero at full output current.

Since the output transistors always stay into their normal working conditions, a low distortion can be achieved by this circuit.

Another advantage of this circuit is the simplicity of the coupling circuit between the upper and lower output transistors. The coupling circuit consists of a mesh of two head-to-tail connected transistors  $Q_3$  and  $Q_4$ . This mesh shapes a positive feedback loop with a gain just below one. Therefore, the mesh has a high input resistance for CM input currents. Except for the base currents, no driving current is lost from this mesh. All input current, which is not used to drive one output transistor, is automatically rerouted to the other output transistor. Firstly, this means that the class-AB coupling is so strong that the output stage can easily be driven from a single upper or lower input terminal, without losing control of the biasing. Secondly, the straight coupling through  $Q_3$  or  $Q_4$  from one side to the other means that the driving currents may far exceed the bias currents  $I_{B1}$  and  $I_{B2}$ . This implies a large ratio between the maximum output currents and the bias currents of the circuit.

A final advantage is the good high-frequency behavior, firstly, because the output transistors are directly accessible by their inputs, and secondly, when the input current is rerouted to the complementary output transistor, the signal has only to pass one transistor  $Q_3$  or  $Q_4$  in a common-base connection.

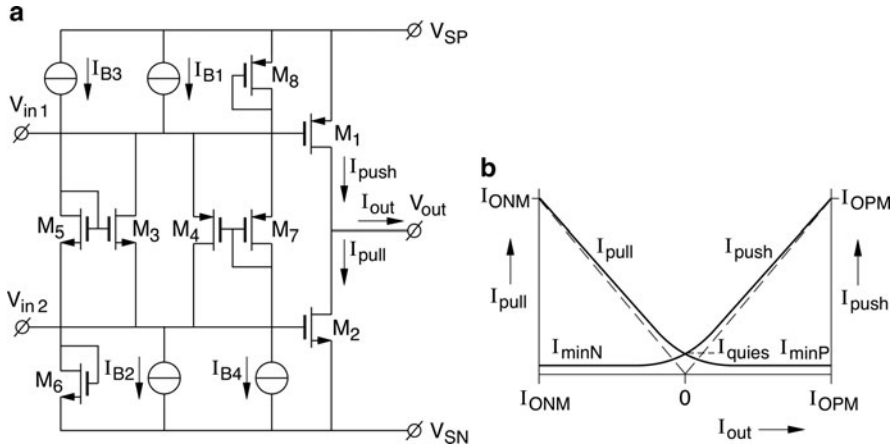


**Fig. 5.3.21** (a) GA FFB R-R class-AB CMOS output stage with CM transistor coupling. (b) Push and pull currents  $I_{push}$  and  $I_{pull}$  as a function of the output current  $I_{out}$

The only disadvantage of this GA output stage is that it needs at least a supply voltage of two diodes plus a saturation voltage, which amounts together to about 1.6 V.

The last described circuit also has excellent properties in CMOS technology. The GA feedforward biased CMOS output circuit with a simple common-mode transistor coupling is depicted in Fig. 5.3.21a [5.11] [5.12].

We take all  $(W/L)_P$  of the P-channel transistors three times larger than the  $(W/L)_N$  of the N-channel transistors to compensate for the one-third ratio of the mobilities  $\mu_P$  and  $\mu_N$  in order to keep the transconductances of the N-channel and P-channel transistors equal at equal currents. For simplicity, we take all  $(W/L)_N$  equal for the N-channel transistors and all  $(W/L)_P$  equal for the P-channel transistors, except for the output transistors which are scaled a factor  $\alpha$  larger. If we choose the quiescent currents through the translinear loop transistors equal, we need the following relation between the bias currents:  $1/2 I_{B1} = 1/2 I_{B2} = I_{B3} = I_{B4} = I_B$ . When we describe the CMOS transistors with  $V_{GS} = V_{th} + \sqrt{2I_D/K}$ , and  $\beta = \mu C_{ox}W/L$ , the following relation between the push and pull currents results:

$$\begin{aligned}
 & (\sqrt{I_{push}} - 2\sqrt{I_{quies}})^2 + (\sqrt{I_{pull}} - 2\sqrt{I_{quies}})^2 = 2I_{quies} \\
 & I_{quies} = \alpha I_B, \text{ and } I_{MIN} = (2 - \sqrt{2})^2 I_q = 0.34 I_q, \text{ at } I_{MAX} = 4 I_{quies}
 \end{aligned}
 \tag{5.3.7}$$

When one of the push or pull currents becomes four times as large as the quiescent current, the other one becomes  $(2 - \sqrt{2})^2 = 0.34$  times the quiescent current  $I_{quies}$ . At this value the full bias current of  $I_{B1} = I_{B2}$  flows through one of the transistors  $M_3$  or  $M_4$ , while the other is cut off.

The smallest one of the push or pull currents will not become any smaller and stays at  $0.34 I_{quies}$ , while the largest one is allowed to increase far above  $4 I_{quies}$ .

Again, this class-AB regulation is very robust because none of the output transistors is ever cut off, but stays largely within the normal bias conditions.

It is interesting to note that the mesh with  $M_3$  and  $M_4$  on one hand fixes the differential-mode voltage movement at the gates of the output transistors in robust class-AB biasing conditions, but, on the other hand, does not present any resistance to the common-mode voltage movement at the gates. Though the source impedance of  $M_3$  and  $M_4$  present a normal value, the head-to-tail connection of these transistors form a positive feedback loop for currents with a gain of nearly perfect unity, which cancels the influence of the source resistance on the common-mode voltage movement. Or otherwise described, no common-mode driving current can flow out of the mesh  $M_3, M_4$ . All input current is either used to drive one or the other output transistor.

The same advantages of the bipolar stage are present with the CMOS GA feedforward biased class-AB output stage. The circuit may easily be driven from one input terminal. All current which is not needed to drive one output transistor is automatically rerouted to drive the other output transistor. The high-frequency behavior is excellent, because the output transistors are directly accessible from their input, and, when one input drives the other output transistor, only one transistor in a common-gate connection is in series with the signal. The only disadvantage is that the output stage needs two diode voltages and one saturation voltage as a minimum supply voltage, which is about 1.8 V.

## *Conclusion*

We have discussed feedforward biased class-AB output stages. The simplest ones were the voltage follower (VF) configurations. These are the classic solution for class-AB biasing. Several circuits with Darlington output transistors have been shown. The compound (VF/GA) derivations are of particular interest because of the use of solely NPN transistors as output transistors. This makes these circuits suitable for large currents or high frequency responses. The inverting-amplifier configurations (GA) are of importance at low supply voltages, because the output can utilize nearly the full supply voltage. Several robust bipolar and CMOS GA circuits have been shown.

## **5.4 Feedback Class-AB Biasing (FBB)**

In the preceding section, a systematic classification has been given of output stages which are feedforward-biased. We have investigated voltage-follower (VF), compound voltage-follower/inverting amplifier (VF/GA), and general-amplifier (GA) feedforward configurations. In all these stages the biasing and driving functions are processed by the same components. This often leads to compromises. In this

section, output stages are discussed in which the biasing function is separated from the driving in what we will call feedback biasing (FBB). The push and pull output currents are measured and compared with a bias reference. If the biasing is not correct in a class-AB relation, the output transistors receive a correction signal by a feedback signal. In this way, we obtain more freedom to design the class-AB output stage in the GA, VF or VF/GA mode according to the derived specifications in a certain IC process.

Basically, there are two possible places to measure the push and pull currents. Firstly, a voltage measurement transistor can be connected with its base-emitter or gate-source in parallel to the base-emitter or gate source of the output transistor. Secondly, a current-measurement diode may be inserted in the collector or drain of the output transistor with a measurement transistor with its base-emitter or gate-source connected across the diode.

In any case, the currents of the measurement transistors have to be related to each other in a translinear loop which controls the class-AB biasing of the output transistors.

### FBB Voltage-Follower Output Stages

The simplest feedback-biased VF circuits are drawn in Fig. 5.4.1 a, b. The transistors  $Q_3$  and  $Q_4$  measure the sum of the base voltages of  $Q_1$  and  $Q_2$  and regulate this sum at a constant value so that the product of the push and pull currents remains constant, according to Eq. 5.3.1 with bipolar transistors.

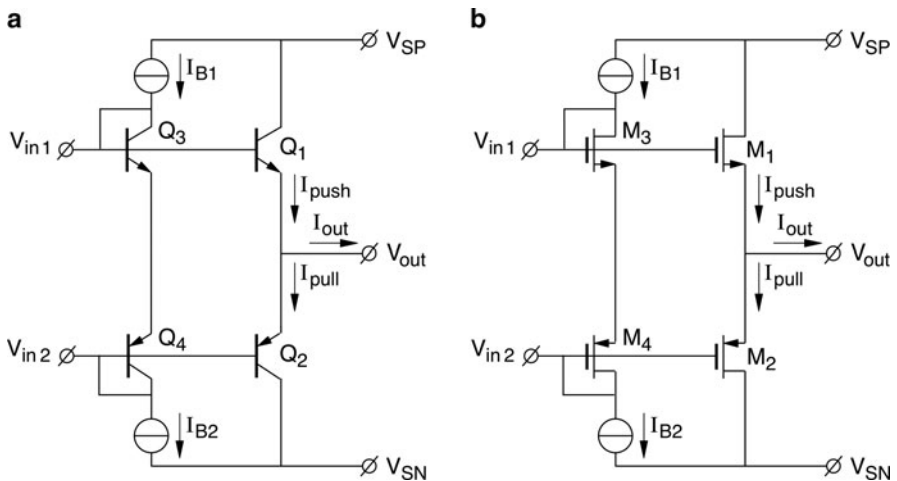


**Fig. 5.4.1** (a) VF FBB class-AB bipolar output stage with parallel transistor measuring. (b) VF FBB class-AB CMOS output stage with parallel transistor measuring

With CMOS the sum of the square roots of the push and pull drain currents is controlled at a constant value according to Eq. 5.3.2. In fact, there is no difference between the feedback-biased circuits of Fig. 5.4.1a, b and the feedforward-biased circuits of Figs. 5.3.1a and 5.3.2a, except that the input connections are drawn immediately at the bases or gates of the output transistors instead of in between the diode-connected transistors  $Q_3$  and  $Q_4$  or  $M_3$  and  $M_4$ . Because of this similarity we will not discuss VF feedback-biased stages further.

### FBB Compound Output Stages

A compound output stage with equal N-type push and pull output transistors is particularly important for bipolar output stages because of the much better properties of NPN transistors than PNP ones. For that reason, the examples of this paragraph are given with bipolar transistors, but the ideas extend to other transistor types as well. A compound output stage can be obtained by combining a feedforward-biased VF upper half with a feedback-biased GA complementary lower half, as is shown in the bipolar circuit of Fig. 5.4.2a. The diode  $D_2$  measures the collector current of  $Q_2$ .

The transistor  $Q_3$  and series diode  $D_1$  measure the sum of the voltages across  $Q_1$  and  $D_2$  and regulate the input signals directly on the base of  $Q_1$ , and indirectly through the mirror  $D_3Q_4$  on the base of  $Q_2$ .

The class-AB biasing is so strong that the circuit can easily be asymmetrically driven at the inverting input, as is shown in Fig. 5.4.2b.

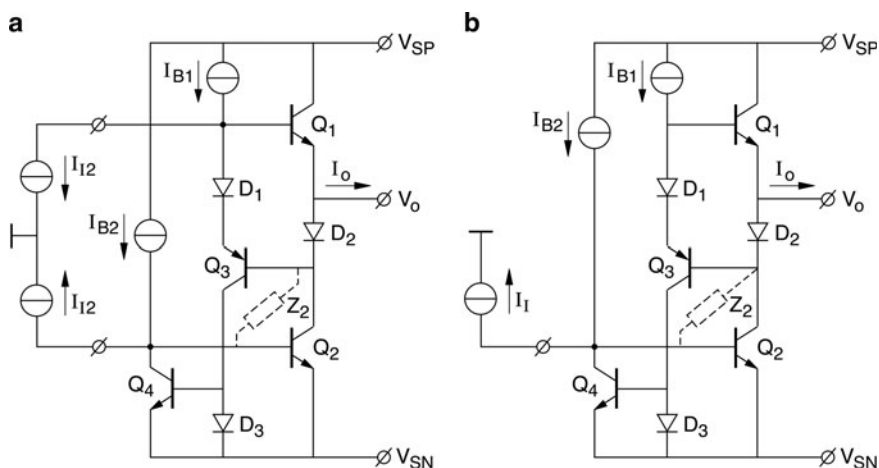


**Fig. 5.4.2** (a) VF/GA compound mixed FFB and FBB class-AB output stage. (b) VF/GA compound mixed FF and FB biased class-AB output stage with asymmetrical driving at the inverting input

The VF/GA circuit may alternatively be driven as if it were a feedforward biased stage by connecting the input symmetrically between the emitter of  $Q_3$  and diode  $D_1$ .

If the transistor  $Q_3$  is replaced by a diode  $D_3$  and the feedback is removed, a strongly simplified feedforward-biased compound output stage arises, which no longer has a linear current transfer. This circuit and its current transfer characteristic are shown in Fig. 5.4.3a, b. A practical realization of this circuit is found in the power OpAmp  $\mu A791$  of Fairchild [5.13] with a maximum output current of 1.2 A. The most important properties of this compound stage are that it uses push and pull output transistors of only one kind (NPN), and that it is simple. The transimpedance of the circuit can be linearized by inserting a dominating Miller feedback impedance  $Z_2$  across the natural collector-base impedance of  $Q_2$ .

More gain can be obtained by the application of Darlington transistor combinations.

The mixed-biased combination of a feedforward-biased Darlington VF upper half with a feedback-biased GA-boosted VF lower half shown in Fig. 5.4.4 is of interest. The stage has a smoother cross-over behavior, a better bias stability and a higher gain at low output currents than those of the feedforward-biased equivalent of Fig. 5.3.8. This Darlington stage has a high ratio between maximum output-current and input-bias currents  $I_{B1}$  through  $I_{B4}$ . The output-voltage range is four diodes and two saturation voltages lower than the supply voltage range.

Combining the feedforward-biased folded Darlington in the upper half with the feedback-biased GA-boosted folded-VF lower half results in the rather simple VF/GA mixed-biased stage of Fig. 5.4.5 with an output-voltage range that loses only two diodes and two saturation voltages of the supply voltages. The accurate feedback biasing gives the circuit a smooth class-AB cross-over behavior.

Feedback biasing provides us with the freedom to use any output transistor configuration because driving and biasing functions can be chosen independently.

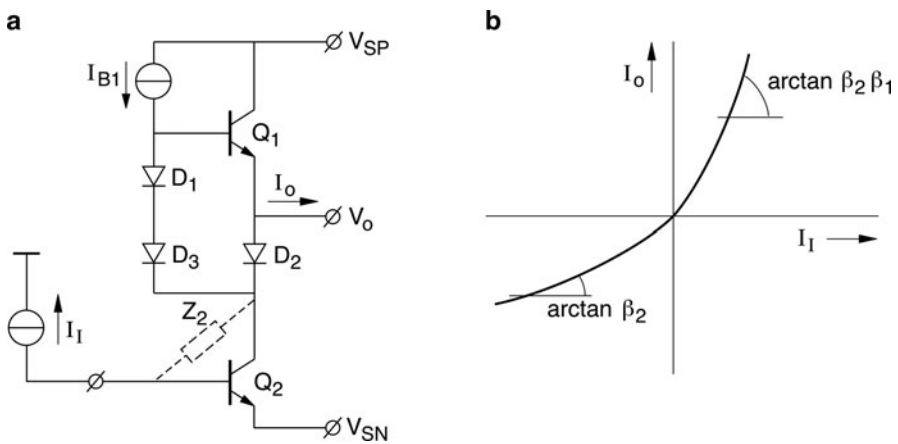
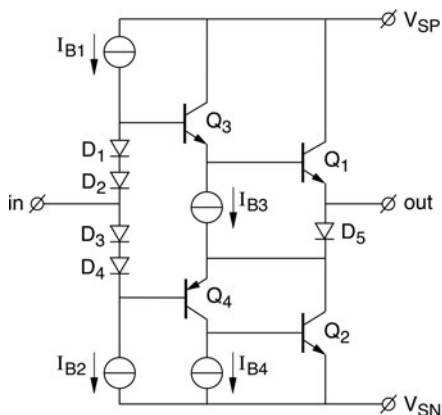
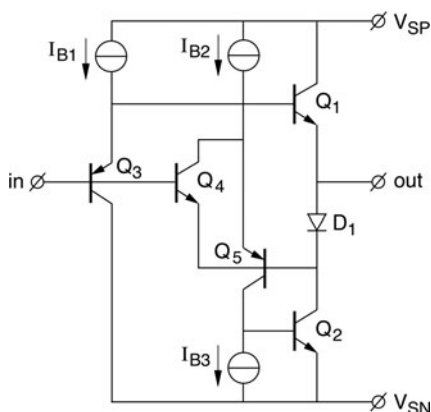


Fig. 5.4.3 (a) VF/GA compound simplified mixed FFB and FBB class-AB output stage driven at the inverting input ( $\mu A791$ ). (b) Non-linear current amplification of the circuit of Fig. 5.4.3a

**Fig. 5.4.4** VF/GA compound mixed-biased Darlington class-AB output stage



**Fig. 5.4.5** VF/GA compound mixed-biased folded-Darlington class-AB output stage



For instance, for high current gain and high bandwidth we can choose to use all NPN Darlington transistors in a compound VF/GA output stage as shown in Fig. 5.4.6. The output transistors are feedforward-driven by the input signals without going through other transistors.

Independently of this driving, the class-AB feedback biasing is settled by the measurement transistors  $Q_6$  and  $Q_7$  with diodes  $D_2$  and  $D_3$ , respectively, in series with the emitters. These transistor-diode combinations measure the sum of the voltages across the base-emitter junction of  $Q_1$  carrying the push current, and the diode  $D_1$  carrying the pull current. The biasing current for the lower half is fed via a folded CF-connected PNP transistor  $Q_5$ . The all-pass network  $R_f$ ,  $C_f$  passes the low-frequency currents through  $Q_5$ , while frequencies above  $\omega_f = 1/R_f C_f$  are directly fed to the lower half. The good HF properties of the feedback bias path is essential for the HF stability of the feedback loop.

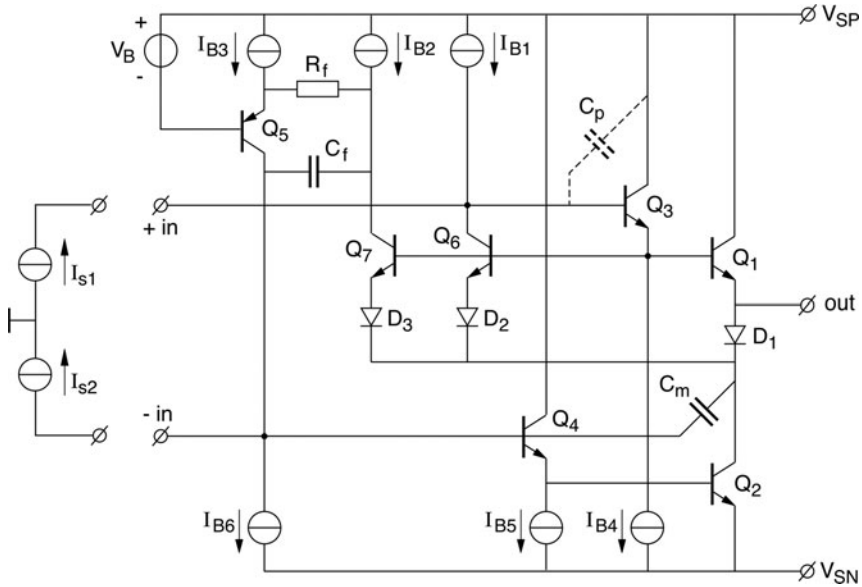


Fig. 5.4.6 VF/GA compound FBB All-NPN class-AB Darlington output stage

The circuit may be driven asymmetrically at the upper input terminals as a voltage follower, or at the lower input terminal as an inverter. In both of these cases, the internal biasing circuitry provides a correct class-AB behavior of the whole output stage.

The circuit may ideally be driven with two input currents having opposite signs. These currents can be obtained at the two output terminals of a longtailed transistor pair having a tail current source, or at the collector and emitter terminals of a transistor connected as a voltage and current follower (VCF).

The transimpedance of the upper output half is roughly equal to the parasitic parallel impedance  $Z_p$  between the upper input terminal and the supply or substrate terminals, while that of the lower half is equal to the Miller impedance  $Z_m$  between the collector and base nodes of the lower Darlington transistor. The high-frequency behavior and slew rate of both halves can be balanced by adding a Miller capacitor  $C_m$  to the lower half which is as large as the natural parasitic capacitor  $C_p$  in the upper half.

The circuit has been realized in a 30 MHz operational amplifier [5.14], see Sect. 7.5.

A disadvantage of the series connection of a measuring diode and the lower output transistor is the loss of one extra diode voltage in the output voltage swing. In order to eliminate this loss, measurement transistors  $Q_3$  and  $Q_4$  are placed with their base-emitter connections in parallel to those of the output transistors  $Q_1$  and  $Q_2$  respectively, as in Fig. 5.4.7.



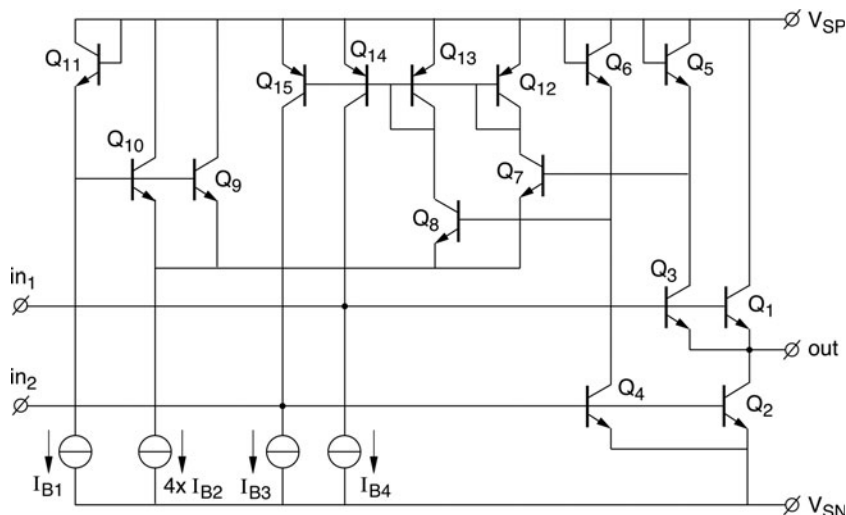


Fig. 5.4.7 VF/GA compound FBB All-NPN output stage with minimum selector

The currents of the measurement transistors are brought in a class-AB relation by the translinear loop [5.15] with  $Q_5$  through  $Q_{11}$  and controlled by the output currents of  $Q_7$ ,  $Q_8$  through the mirrors  $Q_{12}$ ,  $Q_{14}$  and  $Q_{13}$ ,  $Q_{15}$ . Alternatively, the controlling could be done by the output currents of  $Q_9$  and  $Q_{10}$  through folded cascode with an all pass RC network as shown in Fig. 5.4.6, if the HF stability of the feedback loop with the PNP controlling transistors  $Q_{14}$  and  $Q_{15}$  appears to be insufficient. We suppose that all emitter areas are equal for the NPN transistors and equal for the PNP transistors, except that the output transistors are  $n$  times scaled up. We also suppose that all transistors  $Q_5$ – $Q_{11}$  have an equal current in quiescent state.

The translinear loop  $Q_5$  through  $Q_{11}$  has several segments. The diode connected transistors  $Q_5$  and  $Q_6$  model the base emitter voltages of the output transistors  $Q_1$  and  $Q_2$ , respectively. The transistors  $Q_7$  and  $Q_8$  function like an and-gate, passing on the lowest of the two diode ( $Q_5$ ,  $Q_6$ ) voltages to their common emitter connection. Thus, the lowest of the two output currents is regulated. If the lowest current is half the quiescent current,  $Q_7$  or  $Q_8$  already take over the full current of both transistors in the quiescent-state. So the lowest of the push or pull currents never comes below half the quiescent current according to:

$$(I_{push} - 1/2 I_{quies})(I_{pull} - 1/2 I_{quies}) = (1/2 I_{quies})^2 \quad (5.4.1)$$

This is equal to the expression (5.3.6) of the GA feedforward biased output stage of Fig. 5.3.20a. This robust biasing scheme is realized in a 100 MHz precision operational amplifier [7.16], a 1 GHz operational amplifier, and in a 100 mA voltage and current efficient operational amplifier [5.23].

### FBB Rail-to-Rail General Amplifier Output Stages

Finally, we will see how the flexibility of the feedback class-AB biasing will turn the push-pull inverting-amplifier output stage into a robust rail-to-rail GA output stage which can function well at a low supply voltage.

Firstly, we will show how feedback biasing can mimic the classic class-AB control of the VF output stage with two diodes. Figure 5.4.8 shows how this is done [5.16].

The circuit has GA Darlington output transistors which are directly accessible from the input. The upper folded Darlington structure has an extra current boost  $Q_4, D_3, Q_6$  to compensate the low current gain of the lateral upper output transistor  $Q_2$ . The base-emitter voltage  $V_{BE2}$  of the upper output transistor  $Q_2$  is converted into a current by the base-emitter diode of  $Q_7$  in series with  $R_7$  and regenerated into a voltage across the base-emitter diode of  $Q_{10}$  in series with  $R_{10}$ . The base of  $Q_{10}$  is connected to the base of the lower output transistor  $Q_1$ . In this way the sum voltage  $V_{BEsum} = V_{BE1} + V_{BE2}$  of the two output transistors is modeled. This sum is compared to the sum of two diode voltages  $V_{Dsum} = V_{D1} + V_{D2}$  by a differential amplifier  $Q_8, Q_9$ . When the sum of the base-emitter voltages  $V_{BEsum}$  is lower than the sum of the diode voltages  $V_{Dsum}$ , the transistor  $Q_8$  draws more current and  $Q_9$  less current than half the tail current  $I_{B4}$ . This differentially engages both output transistors, by which the sum of the base-emitter voltages grows until

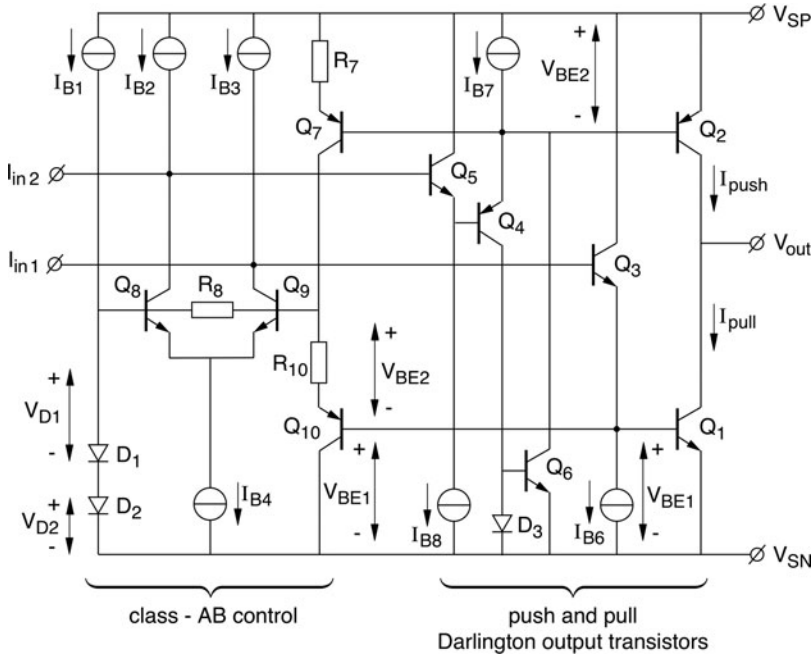


Fig. 5.4.8 GA FBB R-R class-AB Darlington output stage with control amplifier (NE5230)

$V_{BEsum} = V_{Dsum}$ . With equal quiescent currents and emitter areas for all NPN transistors and diodes, as well as for all PNPs, and  $R_{I0} = R_7$  the push and pull currents are controlled as to obey:

$$I_{push} \cdot I_{pull} = I_{quies}^2 = I_{B1}^2 \tag{5.4.2}$$

This behavior is equal to the VF circuit of Fig. 5.3.1a, as described by (5.3.1).

The minimum supply voltage is two diodes and a saturation voltage, which is about 1.8 V. The circuit is utilized in the Signetics NE5230 low-voltage operational amplifier and described in [5.16].

A weak spot of this circuit is the high impedance at the emitter of  $Q_{10}$  when the upper output transistor is nearly cut off and the current through  $Q_{10}$  is low. This deteriorates the HF behavior of the feedback loop. To prevent this, a shunt resistor  $R_8$  has been placed across the bases of the differential control amplifier to lower the impedance on the emitter of  $Q_{10}$ .

The class-AB control can be improved by using a minimum selector [5.15]  $Q_{10}, Q_{11}$  as shown in Fig. 5.4.9. The minimum selector is placed on top of the base-emitter voltages  $V_{BE1}$  of  $Q_1$  and  $V_{BE2}$  of  $Q_2$ . The last voltage is modeled by the diode-connected  $Q_4$ . With equal quiescent currents and emitter areas for the NPN and PNP transistors respectively, the relation between the push and pull currents is:

$$(I_{push} - 1/2 I_{quies})(I_{pull} - 1/2 I_{quies}) = (1/2 I_{quies})^2 = (1/2 I_{B1})^2 \tag{5.4.3}$$

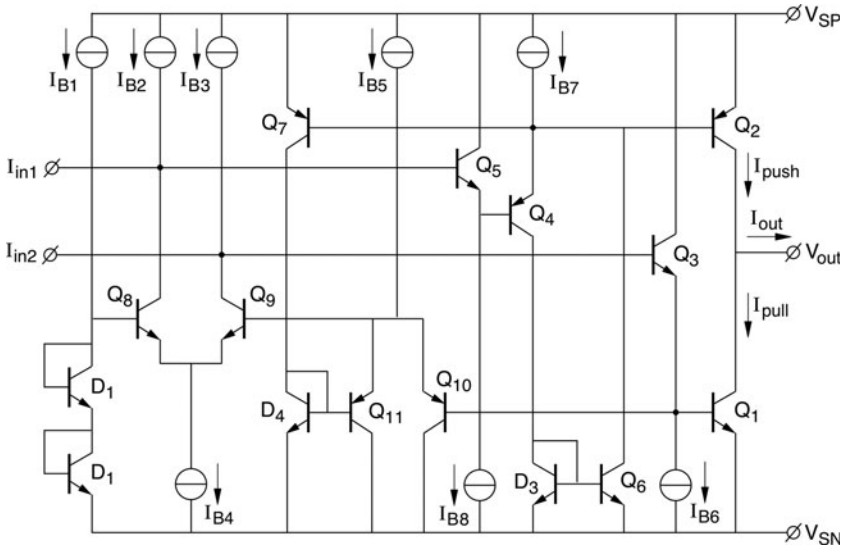


Fig. 5.4.9 GA FBB R-R class-AB output stage with Darlington output transistors and minimum selector (NE 5234)

The low impedances anywhere at the emitters of the control circuit ensure a good HF behavior of the class-AB loop. The differential amplifier  $Q_8, Q_9$  controls the class-AB behavior in a robust way.

The push and pull output currents do not go below  $1/2 I_{quies}$ . The amplifier has a similar relation between the push and pull currents as the circuit of Fig. 5.3.20a with Eq. 5.3.6. The circuit of Fig. 5.4.9 can be found in the quad OpAmp NE5234 and is described in [5.17].

It is interesting to note that if, in these circuits, only one input terminal is used to drive the circuit, the regulator amplifier automatically drives the other input terminal correctly. Half of the input current is used to drive one output transistor. Whereas, through the collector-emitter loop of the differential amplifier the other output transistor receives the other half of the input current. Further, if one output transistor is regulated at a constant value of  $1/2 I_{quies}$ , the other output transistor gets all the input driving current of both inputs. This guarantees a very linear signal transfer.

A low voltage version of the previous circuit is shown in Fig. 5.4.10. The base-emitter voltages of the output transistors are modeled in a reduced form across  $R_2$  and  $R_3$ . The minimum selector  $Q_{10}, Q_{11}$  takes the lowest of these voltages and the differential control amplifier  $Q_8, Q_9$  regulates this minimum equal to a reference voltage across a reference network. The circuit has the capability to work down to one diode voltage and two saturation voltages, which amounts to about 1.0 V. The circuit is described in [5.17].

A similar circuit can be obtained in CMOS. A CMOS GA feedback- biased class-AB output stage is shown in Fig. 5.4.11.

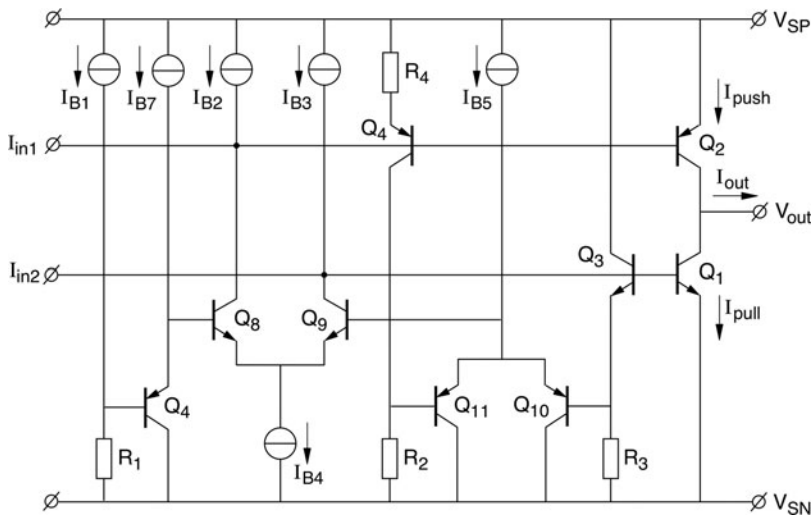


**Fig. 5.4.10** GA FFB R-R class-AB bipolar output stage with minimum selector for a 1 V supply voltage

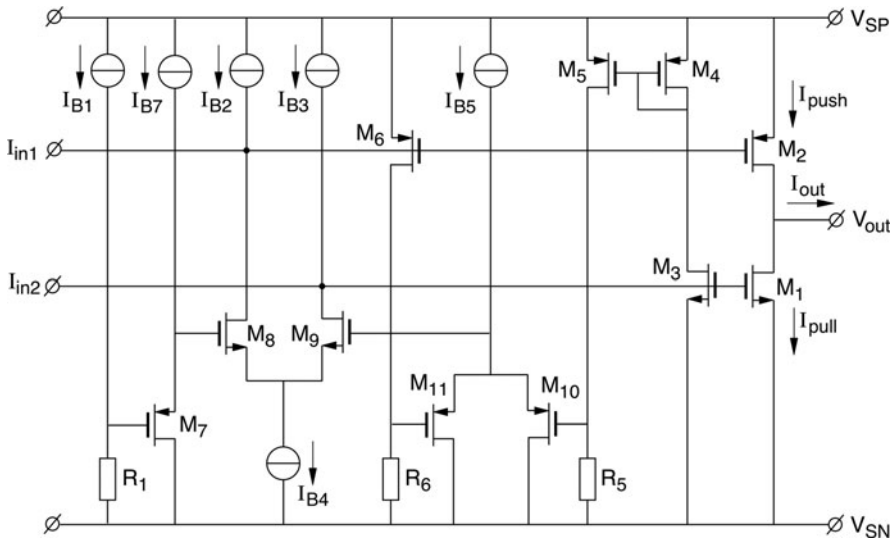


**Fig. 5.4.11** GA FBB R-R class-AB CMOS output stage with minimum selector for 1.2 V supply voltage

The measuring of the lower output transistor  $M_1$  cannot be done in the same way as in Fig. 5.4.10, because the threshold voltage of CMOS transistors cannot be scaled by the  $W/L$  ratio's. Only the current can be scaled down. This is done with the aid of two current mirrors  $M_1, M_3$  and  $M_4, M_5$ .

The voltage across  $R_5$  carries a model of the current in the lower output transistor  $M_1$ , while the voltage across  $R_6$  carries a model of the current of the upper output transistor  $M_2$ . The minimum selector  $M_{10}, M_{11}$  takes the lowest of these voltages. The differential amplifier  $M_8, M_9$  compares the lowest voltage with the voltage across a reference circuit  $M_7, R_1$ , which is biased by  $I_{B1}$ . For equal transconductance of the P-channel and N-channel output transistors, the  $W/L$  ratio of all P-channel transistors is taken three times that of the N-channel ones, to compensate for a lower charge mobility  $\mu_p$ . The resulting behavior is roughly similar to that of the circuit of Fig. 5.3.21a and Eq. 5.3.7.

The circuit is described in [5.18]. It works down to a supply voltage of one diode and two saturation voltages, which amounts to about 1.2 V.

A GA feedback-biased class-AB output stage which avoids resistors in a CMOS process is shown in Fig. 5.4.12 [5.19]. It can easily be scaled with the  $W/L$  ratios of the CMOS transistors. The minimum selector is composed of two inverters  $M_{11}, M_{21}, M_{23}, M_{15}$  and  $M_{12}, M_{14}$ , followed by a maximum selector  $M_{18}$  and  $M_{17}, M_{16}$  which functions as a differential control amplifier as well. The reference is set by  $M_{19}$ . The inverters invert the minimum output currents of the output transistors to a maximum. The differential amplifier is controlled at the right-hand side by the highest of the two voltages at the gates of  $M_{17}$  or  $M_{16}$  respectively.

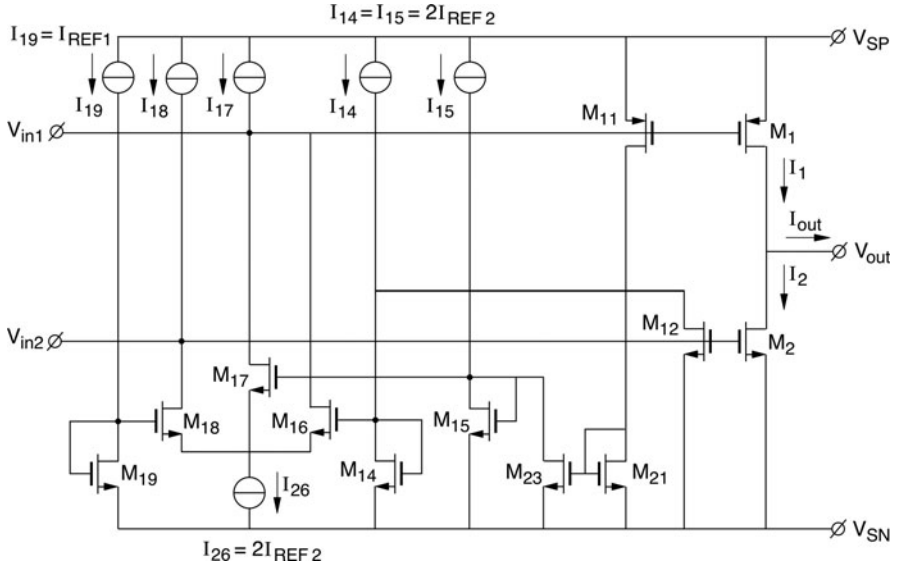


**Fig. 5.4.12** GA FBB R-R class-AB CMOS output stage with a maximum selector for 1.2 V supply voltage

The quiescent current is:

$$I_q = 2 \frac{W_1 W_2}{L_1 L_2} \frac{L_{11} L_{12}}{W_{11} W_{12}} (2I_{ref2} - I_{ref1}) \tag{5.4.4}$$

The minimum current stays at about two-thirds of the quiescent current. The application of feedback-biasing allows a minimum supply voltage of that of one diode and two saturation voltages, which amounts to about 1.2 V.

A very simple minimum selector without resistors in CMOS technology is shown in Fig. 5.4.13 [5.20].

The minimum selector is composed of two measuring transistors  $M_{11}$  and  $M_{12}$ , and a mirror  $M_{22}$ ,  $M_{24}$ . If  $M_1$  carries the lowest output current,  $M_{24}$  is biased in triode mode and  $M_{11}$  roughly measures the minimum current of  $M_1$ . If  $M_2$  carries the lowest current,  $M_{11}$  acts as a cascode which passes on the current of the measuring transistor  $M_{12}$  which is fed through the mirror  $M_{22}$ ,  $M_{24}$ . The quiescent current and minimum currents are:

$$I_q = 2 \frac{W_1 W_2}{L_1 L_2} \frac{L_{11} L_{12}}{W_{11} W_{12}} I_{ref}$$

$$I_{min} = \frac{1}{2} I_q \tag{5.4.5}$$

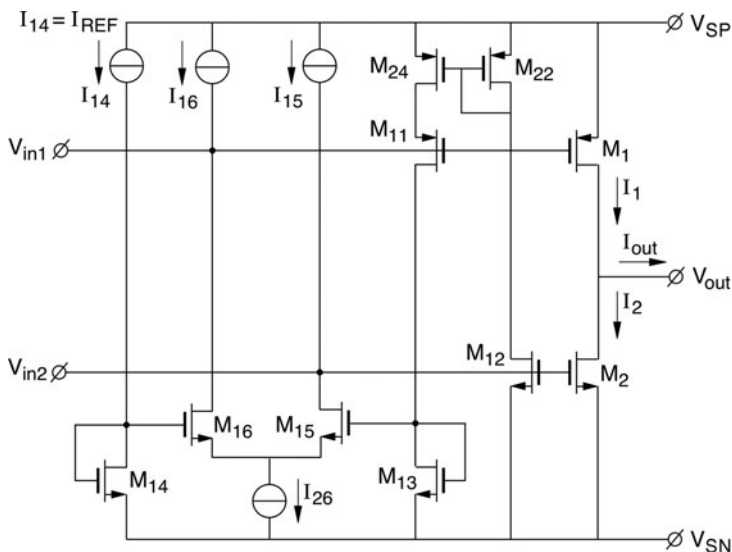


**Fig. 5.4.13** GA FBB R-R class-AB CMOS output stage with simple minimum selector for 1.2 V supply voltage

The circuit excels by its simplicity. The minimum voltage is equal to that of one diode and two saturation voltages, which amounts to about 1.2 V.

## Conclusion

We have discussed feedback-biased class-AB output stages in a voltage follower (VF), compound (VF/GA), and inverting amplifier (GA) configurations. The VF circuits are similar to those with feedforward-biasing. Though they are the simplest, their output voltage range loses at least two diode voltages and two saturation voltages in regard to the supply voltage range.

The VF/GA stages are of particular interest in “all-NPN” output stages, where large output currents must be drawn, or where the highest frequency response of the NPN transistors must be utilized. These circuits lose minimally one diode voltage and two saturation voltages in their output swing. The GA output stages are of particular importance at low supply voltages, as their output voltage can swing nearly from rail-to-rail, except for a saturation voltage at each rail. The feedback-biasing robustly controls these stages in class-AB and leaves much flexibility to the designer. The minimum supply voltage may be of the order of one diode voltage and two saturation voltages.

### 5.5 Saturation Protection and Current Limitation

Output stages that have to deliver large output currents and high bandwidth may advantageously be equipped with bipolar transistors. This is possible in bipolar and BiCMOS processes. However, if the output voltage becomes so low or high that respectively the NPN or PNP output transistor saturates, the bandwidth of these transistors may easily become so low that the amplifier starts to oscillate. Moreover, the substrate parasitic transistors become activated so that a large substrate current may cause unexpected latch-up problems. For this reason we need a saturation-protection circuit. This is presented in the section “Output Saturation Protection Circuits”. Bipolar output transistors can also be easily overloaded when the output has to supply heavy loads or is being short circuited. For that reason a current limitation circuit is needed. Several limiters are presented in the section “Output Current Limitation Circuits”.

#### Output Saturation Protection Circuits

When the collector-emitter voltage of an GA-connected bipolar output transistor becomes lower than about 200 mV, the collector-base junction becomes forward biased. This causes several undesired effects. The situation is depicted in Fig. 5.5.1 for a push-pull GA/GA configuration. But the effect is also present in the lower side of a VF/GA connected all-NPN output stage.

Firstly, if one of the transistors  $Q_1$  or  $Q_2$  becomes saturated, the collector-base junction is activated and a large reverse current may flow back from the collector into the emitter. This must be compensated by a further increase of the forward

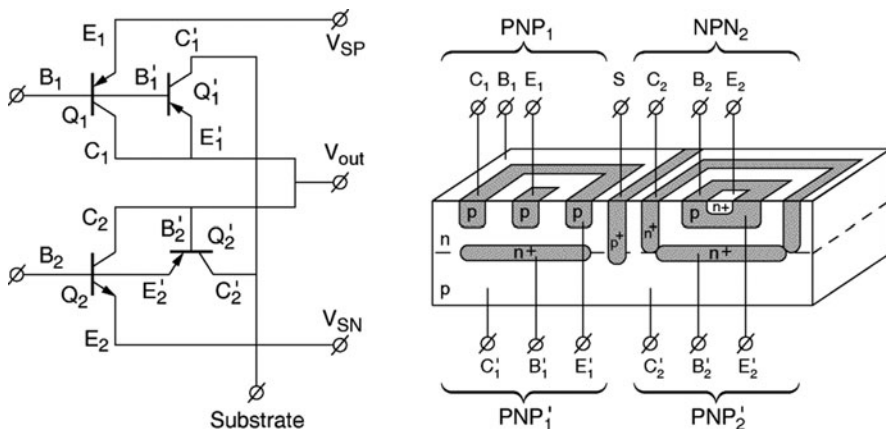


Fig. 5.5.1 A push-pull GA/GA output stage with a  $PNP_1$  and  $NPN_2$  transistor and their  $PNP'_1$ , and  $PNP'_2$  parasitic transistors



current. The result is a decrease of  $\beta$  and an increase of the diffusion capacitors. The bandwidth of the output stage may decrease so much that the frequency compensation may easily become unstable. Ringing is the result.

Secondly, the parasitic substrate PNP transistor  $Q'_1$ , or  $Q'_2$  of the concerned PNP transistor  $Q_1$  or NPN transistor  $Q_2$  becomes active. This may cause a large current to flow into the substrate. Particularly, in BiCMOS processes with a lightly doped substrate, a large voltage drop in the substrate may be the result so that even reverse biased diodes may turn on. This may cause unexpected latch-up problems in the circuit.

The saturation voltage may be modeled by using the Ebers-Moll model [5.21]. When we suppose that while saturated the ratio between the collector and base currents is in the order of the square root of the forward current gain  $\beta_F$ , the saturation voltage can be simply expressed as:

$$V_{CEsat} \approx I_c r_c + \frac{kT}{q} \ln \left( \frac{1}{\beta_F} \frac{I_c}{I_B} \right) \quad (5.5.1)$$

The first term is caused by the internal resistive collector resistance  $r_c$ . This term can be of the order of several 100 mV. The second term maybe of the order of 20–50 mV.

For detection of saturation, we could use the actual collector voltage if we are sure that the resistive collector voltage drop is sufficiently under control. This gives rise to the saturation protection circuit of the Darlington output transistor of Fig. 5.5.2 for example.

A disadvantage of the clamp transistor  $Q_3$  is that the emitter can easily get too high a reverse voltage, so that it could become zenering and be destroyed. Therefore, it is better to interchange its emitter and collector connections and use it reversed. If we further connect the base of  $Q_3$  to the base of  $Q_1$ , the collector-base junction of  $Q_3$  perfectly matches the collector-base junction of  $Q_1$  in voltage, doping profile, and process variations. The only detection error that remains is the resistive collector voltage drop. To largely avoid this, we may use an output transistor with a second emitter. So, we obtain the robust saturation protection circuit of Fig. 5.5.3 [5.22].

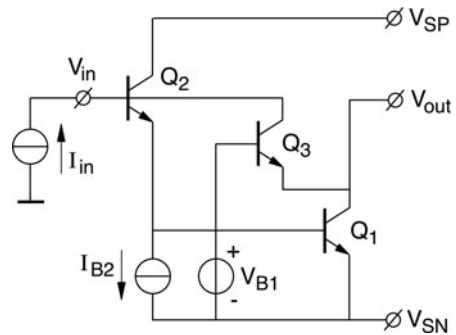
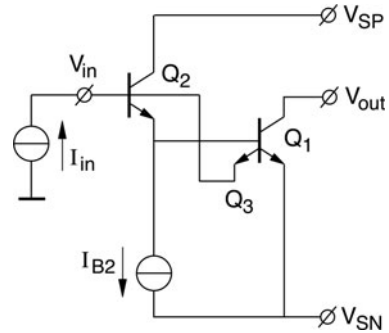


**Fig. 5.5.2** Saturation protection with clamp transistor  $Q_3$

**Fig. 5.5.3** Robust saturation protection with a second emitter  $Q_3$  of the output transistor  $Q_1$



Another important feature of the protection circuit of Fig. 5.5.2 is that the control loop through  $Q_2$  and  $Q_1$  is very short and naturally HF stable. A complementary circuit can be used with the complementary PNP output transistor if applicable.

### ***Output Current Limitation Circuits***

The high bandwidth  $f_T$  and current gain  $\beta_F$  of the NPN transistor makes it perfectly suitable for a high quality output stage in a bipolar or BiCMOS process. But these very attributes also make the NPN output transistor vulnerable for overloading at heavy load currents or at short circuit conditions. Therefore, a current limitation circuit has to be applied. Many existing limiter circuits have control paths that are too long, so that these circuits tend to oscillate when they have to limit the output current. In the next three circuits, this has been avoided. There are two ways to detect over-currents in output transistors that do not make the circuit too complicated or do not cost too much voltage loss in the output range. The first detection method is to measure the collector current of a transistor connected with its base-emitter contacts in parallel with those of the output transistor. The second detection method is to insert a small resistor into the emitter lead of the output transistor and to measure the voltage drop over that resistor. The latter is more accurate of course, as we measure the real current through the output transistor.

The first limiter circuit is divided from the successful saturation limiter circuit with a reversed connected detection transistor  $Q_4$  in combination with a model transistor  $Q_3$  in parallel with the output transistor  $Q_1$ . The circuit is given by Fig. 5.5.4 [5.22].

The resistor  $R_3$  together with the base-emitter voltage of  $Q_3$  set the threshold current. A disadvantage of the resistor connection to the base of  $Q_1$  is its damping action on the current gain of  $Q_1$ .

But this can be overcome by some extra elements. Another drawback of the circuit is that the reverse connected transistor  $Q_4$  has a low reverse current gain in modern processes. This slightly weakens the limitation action.

**Fig. 5.5.4** Output current limitation circuit with a model transistor  $Q_3$  in parallel with the output transistor  $Q_1$  and with its collector current through a reversed connected detection transistor  $Q_4$  and a threshold current provided by  $R_3$

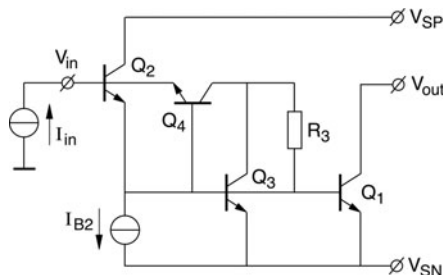
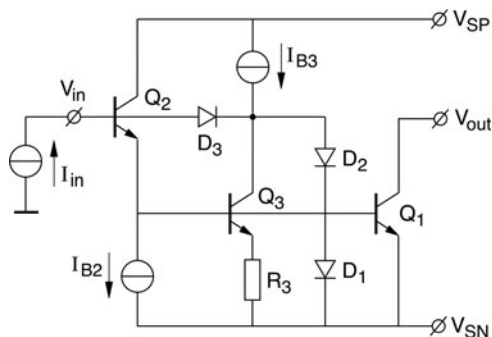


**Fig. 5.5.5** Output current limitation circuit with a model transistor  $Q_3$  in parallel with the output transistor  $Q_1$  and with its collector connected through a diode  $D_3$  to the input and a threshold bias current source  $I_{B3}$



A limiter circuit that alleviates the above mentioned disadvantages is shown in Fig. 5.5.5. It uses a model transistor  $Q_3$  in parallel with the output transistor and a separate threshold bias current  $I_{B3}$  in its collector circuit. The circuit further incorporates diodes for clamping purposes. The limiting action is strong enough so that a current limitation series resistor  $R_3$  may be used in series with the emitter of  $Q_3$ . The limitation function may be sharpened by using a fixed voltage instead of  $R_3$ .

One disadvantage still remains: if the output transistor tends to go into avallange breakdown at high output voltages, the model  $Q_3$  does not detect this. Only the current source  $I_{B2}$  can absorb some the avallange current.

If we really want to measure the output current through  $Q_1$ , an emitter resistor  $R_1$  can be connected in series with the emitter of  $Q_1$ .

The current can be measured by  $Q_3$  through a voltage level shifter  $Q_4$  and biased by a threshold current source  $I_{B3}$ , as shown in Fig. 5.5.6 [5.22].

The diodes  $D_1$  through  $D_3$  perform clamping functions. The maximum voltage across the measuring resistor  $R_1$  need only to be of the order of 50 mV, so that not much of the output current range is being sacrificed.

The limitation functions starts at a value of:

$$I_{out\ lim} = \frac{kT}{R_1 q} \ln \left( \frac{I_{B3}}{I_{B4}} \frac{A_4}{A_3} \right) \tag{5.5.2}$$

**Fig. 5.5.6** Output current limitation circuit with an emitter-current measuring resistor  $R_1$ , a level-shift transistor  $Q_4$ , and a regulator transistor  $Q_3$  biased with a threshold current  $I_{B3}$

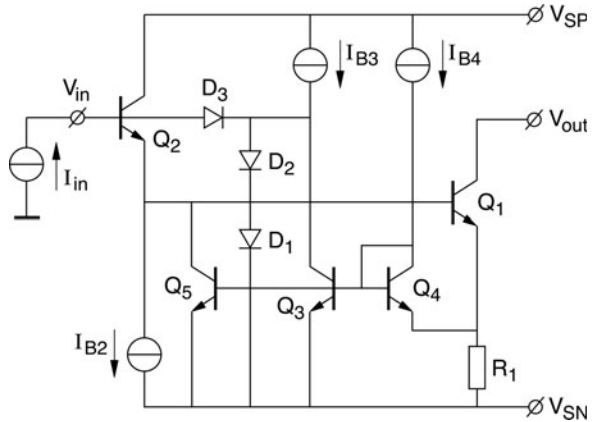
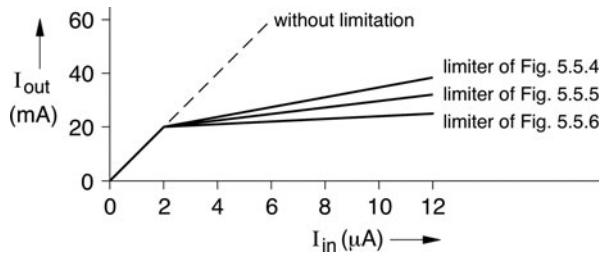


**Fig. 5.5.7** Output current versus input current of the limiter circuits of Figs. 5.5.4, 5.5.5, and 5.5.6



where  $A_4/A_3$  is the ratio of the emitter areas of  $Q_4$  and  $Q_3$ .  $Q_5$  has further been added to increase the current by which the output transistor is being cut off. This may be needed in case of avalanche breakdown of  $Q_1$ .

As a conclusion the operation characteristics of the three limiter circuits as discussed are shown in Fig. 5.5.7.

Further information can be found in [5.23].

## 5.6 Problems and Simulation Exercises

### Problem 5.1

The voltage-follower output stage shown in Fig. 5.3.2a is biased with  $I_{B1} = I_{B2} = 20 \mu\text{A}$ , with transistors sized  $W/L_1 = 175$ ,  $W/L_2 = 50$ ,  $W/L_3 = 35$ ,  $W/L_4 = 10$ . The MOS devices are modeled by  $V_{THN} = 0.5$ ,  $V_{THP} = -0.6$ ,  $K_N = 56 \mu\text{A}/\text{V}^2$ ,  $K_P = 16 \mu\text{A}/\text{V}^2$  and the current sources are saturating at  $V_{Dsat} = 0.2 \text{V}$ .

Calculate the maximum output current so no transistor operates at zero drain current and the output voltage range which does not introduce distortion in the signal. The supply voltages are  $V_{DD} = -V_{SS} = 1.5 \text{ V}$ .

### **Solution**

The quiescent current of the output stage is given by the all- $V_{GS}$  loop formed by the four MOS devices. Noting that the size of these devices obey

$$\frac{\frac{W}{L_3}}{\frac{W}{L_1}} = \frac{\frac{W}{L_4}}{\frac{W}{L_2}} \quad (5.6.1)$$

the solution is

$$I_{D1} = I_{D2} = 5I_{D3} = 100 \mu\text{A} \quad (5.6.2)$$

According to Eq. 5.3.2, the maximum output current which still allows the both transistors to operate is

$$I_{Omax} = 4I_{quies1,2} = 400 \mu\text{A} \quad (5.6.3)$$

The limits for output voltage can be calculated considering the fact that both pairs of NMOS and PMOS transistors operate at the same saturation voltages, but the diode connected transistors are drastically limiting the input voltage range. When approaching one voltage limit, the current through the limiting transistor is also decreasing, a convenient limit being  $I_D = 0$  which corresponds to a  $V_{GS} = V_{th}$

$$\begin{aligned} V_{Omax} &= V_{imax} = V_{SP} - V_{Dsat} - V_{GS3} \\ &= V_{SP} - V_{Dsat} - V_{THN} = 0.8 \text{ V} \\ V_{Omin} &= V_{imin} = V_{SN} + V_{Dsat} - V_{GS4} \\ &= V_{SN} + V_{Dsat} - V_{THP} = -0.7 \text{ V} \end{aligned} \quad (5.6.4)$$

### **Problem 5.2**

Figure 5.3.7 shows the schematic of a bipolar IA/VF output stage. The diodes  $D_1$  through  $D_4$  have an area  $A_{ref}$  and a saturation current  $I_S = 10^{-16} \text{ A}$ . The other

transistors are upsized:  $Q_1$  and  $Q_2$  ten times,  $Q_3$  and  $Q_4$  two times. The resistor  $R_1$  and  $R_2$  are  $100 \Omega$  while  $R_3 = R_4 = 1 \text{ k}\Omega$ . The biasing sources  $I_{B1} = I_{B2} = 10 \mu\text{A}$  and the transistors have large current gain and a saturation voltage  $V_{sat} = 0.2 \text{ V}$ . Calculate the minimum supply voltage which allows the output to reach  $2V_{PP}$  without distorting the signal. Consider  $kT/q = 25 \text{ mV}$ .

### Solution

In order to calculate the limits of the output voltage, the biasing currents must be known for all transistors and diodes. The biasing of  $Q_3$  and  $Q_4$  can be easily calculated based on the translinear loop  $Q_3 - Q_4 - D_4 - D_3$

$$I_{C3} = I_{C4} = \frac{I_{SQ3}}{I_{SD3}} I_{B1} = \frac{A_{Q3}}{A_{D3}} I_{B1} = 20 \mu\text{A} \quad (5.6.5)$$

The biasing of  $Q_1$  and  $Q_2$  can be calculated by observing that in the  $Q_1 - R_1 - R_3 - D_1$  loop, the ratio of sizes for both resistors and transistors is 10, so

$$I_{C1} = 10I_{D1} = 200 \mu\text{A} \quad (5.6.6)$$

This value satisfies the equation

$$\frac{kT}{q} \ln \frac{I_{C1} I_{SD1}}{I_{D1} I_{SQ1}} = R_3 I_{D1} - R_1 I_{C1} \quad (5.6.7)$$

Alternatively a numerical solver can be used to find the solution of this equation. The maximum output signal which is not saturating any transistor is

$$V_{Omax} = V_{SP} - \max(V_{BE3} + V_{sat1B1}, V_{satQ3} + V_{D1} + R_3 I_3, V_{satQ1} + R_1 I_1) \quad (5.6.8)$$

Obviously, the second term in the list above has the largest value, as it adds a  $V_{BE}$  to a saturation voltage and the voltage on a resistor. This makes the value of the maximum output voltage to be

$$V_{Omax} = V_{SP} - V_{satQ3} - \frac{kT}{q} \ln \frac{I_{D1}}{I_{SD1}} - R_3 I_3 = V_{SP} - 650.8 \text{ mV} \quad (5.6.9)$$

As the requested range of the output signal is  $2 \text{ V}$  peak-to-peak, the supply voltage should be

$$V_{SP} - V_{SN} = 2 \text{ V} + 2 * 650.8 \text{ mV} = 3.3 \text{ V} \quad (5.6.10)$$

### Problem 5.3

The class-AB output stage depicted in Fig. 5.3.14a operates at  $V_{SP} = V_{SN} = 1.5$  V and the MOS devices are sized  $W/L_3 = W/L_5 = 35$ ,  $W/L_4 = W/L_6 = 10$ ,  $W/L_1 = 100$  and  $W/L_2 = 350$ . Resistor values are  $R_1 = R_2 = 50$  k $\Omega$ . Considering the MOS parameters  $V_{THN} = 0.5$  V,  $V_{THP} = -0.6$  V,  $K_P = 16$   $\mu\text{A}/\text{V}^2$ , and  $K_N = 56$   $\mu\text{A}/\text{V}^2$  calculate the maximum push and pull currents of the output such that no transistor operates at zero drain current.

### Solution

The biasing of the output stage is set by the current leg  $M_5 - R_2 - M_6$

$$V_{SP} - V_{SN} = V_{GS5} + R_2 I_{B2} + V_{GS6} \quad (5.6.11)$$

Replacing the  $V_{GS}$  expression as functions of drain currents, the following second order equation results

$$-V_{THP} + \sqrt{\frac{2I_{B2}}{K_P} \frac{W}{L_5}} + R_2 I_{B2} + V_{THN} + \sqrt{\frac{2I_{B2}}{K_N} \frac{W}{L_6}} - V_{SP} + V_{SN} = 0 \quad (5.6.12)$$

which has the only positive solution

$$\sqrt{I_{B2}} = \frac{-b + \sqrt{b^2 - 4R_2(-V_{THP} + V_{THN} - V_{SP} + V_{SN})}}{2R_2} \quad (5.6.13)$$

with

$$b = \frac{1}{\sqrt{\frac{K_P}{2} \frac{W}{L_5}}} + \frac{1}{\sqrt{\frac{K_N}{2} \frac{W}{L_6}}} \quad (5.6.14)$$

Numerically, these equations produce

$$I_{B2} = 26 \mu\text{A} \quad (5.6.15)$$

The quiescent current for output transistors  $M_1, M_2$  is given by the equal voltage on  $R_1$  and  $R_2$  and the  $W/L$  ratios of  $M_1$  and  $M_5$  and for  $M_2$  and  $M_6$ , respectively.

$$I_{D1} = I_{D2} = I_{D5} \frac{W}{L_1} \frac{L_5}{W} = 260 \mu\text{A} \quad (5.6.16)$$

As explained with Fig. 5.3.2, the maximum push and pull output current at which the transistor driving the lower current is still on is

$$I_{pushmax} = -I_{pullmax} = 4I_{D1} = 1.04 \text{ mA} \quad (5.6.17)$$

### Problem 5.4

Figure 5.3.21a shows a class-AB output stage with common-mode transistor coupling which allows operation at lower supply voltages compared to the common-mode resistor coupling version. Such an output stage operates at  $V_{SP} = -V_{SN} = 1.0 \text{ V}$ , the NMOS devices are sized  $W/L_3 = 2.5$ ,  $W/L_5 = 5$ ,  $W/L_6 = 20$ , and  $W/L_2 = 100$  and all the PMOS counterparts are sized  $K_N/K_P$  larger. Considering the MOS parameters  $V_{THN} = 0.5 \text{ V}$ ,  $V_{THP} = -0.6 \text{ V}$ ,  $K_P = 16 \mu\text{A}/\text{V}^2$ , and  $K_N = 56 \mu\text{A}/\text{V}^2$ , calculate the output transistors quiescent current, the maximum push and pull currents and the minimum currents which are kept flowing through output devices. The biasing currents are  $I_{B1} = I_{B2} = I_{B3} = I_{B4} = 10 \mu\text{A}$ .

### Solution

The quiescent current of transistors  $M_1$  and  $M_2$  results from the translinear loop

$$V_{GS2} + V_{GS3} = V_{GS5} + V_{GS6} \quad (5.6.18)$$

All the threshold voltages being equal for all PMOS devices, the equation above can be translated to a drain current and sizes equation

$$\sqrt{\frac{I_{D2}}{W/L_2}} + \sqrt{\frac{I_{D3}}{W/L_3}} = \sqrt{\frac{I_{D5}}{W/L_5}} + \sqrt{\frac{I_{D6}}{W/L_6}} \quad (5.6.19)$$

Solution of the equation becomes

$$\begin{aligned} \sqrt{I_{D2}} &= \sqrt{W/L_2} \left( \sqrt{\frac{I_{D5}}{W/L_5}} + \sqrt{\frac{I_{D6}}{W/L_6}} - \sqrt{\frac{I_{D3}}{W/L_3}} \right) \\ I_{D2} &= 50 \mu\text{A} \end{aligned} \quad (5.6.20)$$



The maximum push and pull currents are equal because of the complete symmetry of the circuit related to NMOS and PMOS devices. The pull current reaches its largest value when all of the  $I_{B1}$  current is flowing through  $M_4$ , thus operating  $M_3$  at  $V_{GS3} = V_{THN}$ . Starting again from the translinear loop Eq. 5.6.18, the drain currents equation can be re-written for the maximum pull current

$$\sqrt{I_{pullmax}} = \sqrt{W/L_2} \left( \sqrt{\frac{I_{D5}}{W/L_5}} + \sqrt{\frac{I_{D6}}{W/L_6}} \right) \quad (5.6.21)$$

$$I_{pullmax} = 450 \mu\text{A}$$

The minimum current, which is kept flowing through one of the output devices while the other is driving the maximum push/pull current, will also be identical for both PMOS and NMOS output transistors. For  $M_2$ , this current is reached when all of the  $I_{B1}$  current flows through  $M_3$ , reducing the available  $V_{GS2}$  to a minimum. The value of this current is

$$\sqrt{I_{D2min}} = \sqrt{W/L_2} \left( \sqrt{\frac{I_{D5}}{W/L_5}} + \sqrt{\frac{I_{D6}}{W/L_6}} - \sqrt{\frac{I_{B1}}{W/L_3}} \right) \quad (5.6.22)$$

$$I_{D2min} = 1.3 \mu\text{A}$$

### Problem 5.5

For the class-AB output stage in Fig. 5.4.13, calculate the quiescent and the minimum current through the output transistors  $M_1$  and  $M_2$ , if the sizes of active devices are  $W/L_{14} = W/L_{13} = 10$ ,  $W/L_{15} = W/L_{16} = 20$ ,  $W/L_{11} = 0.2 W/L_1 = 70$ ,  $W/L_{12} = 0.1 W/L_2 = 10$ , and  $W/L_{22} = W/L_{24} = 70$ . The biasing currents are  $I_{B14} = I_{B15} = I_{B16} = 20 \mu\text{A}$ ,  $I_{B26} = 40 \mu\text{A}$ .

### Solution

Because of the comparator built with devices  $M_{15}$  and  $M_{16}$  the feedback loop makes the devices  $M_{13}$  and  $M_{14}$  work at the same gate-source voltage, which in turn makes the current through  $M_{13}$  to be

$$I_{D13} = \frac{W}{L_{13}} \frac{L_{14}}{W} I_{D14} = 20 \mu\text{A} \quad (5.6.23)$$

This current is also the drain current for  $M_{11}$ , as well as the drain current for  $M_{12}$  because the current mirror  $M_{22}$ :  $M_{24}$  has a current gain equal to unity. The quiescent current through the output transistor is then given by

$$I_{D2} = \frac{W}{L_2} \frac{L_{J2}}{W} I_{D12} = 200 \mu\text{A} \tag{5.6.24}$$

Identical drain current can be obtained for  $M_1$  knowing the current through  $M_{11}$ ,  $M_{24}$  and the fact that at quiescent biasing the two transistors  $M_{11}$ ,  $M_{24}$  act like one transistor with double channel length compared to  $M_{11}$ .

$$I_{D1} = \frac{W}{L_1} \frac{2L_{11}}{W} I_{D11} \tag{5.6.25}$$

The minimum current in the output devices is limited to

$$I_{D2min} = \frac{1}{2} I_{D2} = 100 \mu\text{A} \tag{5.6.26}$$

### Simulation Exercise 5.1

The feedforward-biased class-AB output stage shown in Fig. 5.6.1 uses  $V_{GS}$  voltage loops for AB-biasing of output transistors  $M_4$  and  $M_8$ . A circuit shown in Fig. 5.6.2 can be used to put the signal currents at the input of such a stage while keeping the output at a constant voltage.

Simulate this circuit and plot the drain currents of  $M_4$  and  $M_8$  as a function of the input current.  $I_6$  and  $I_7$  in the simulation circuit must supply equal current at all

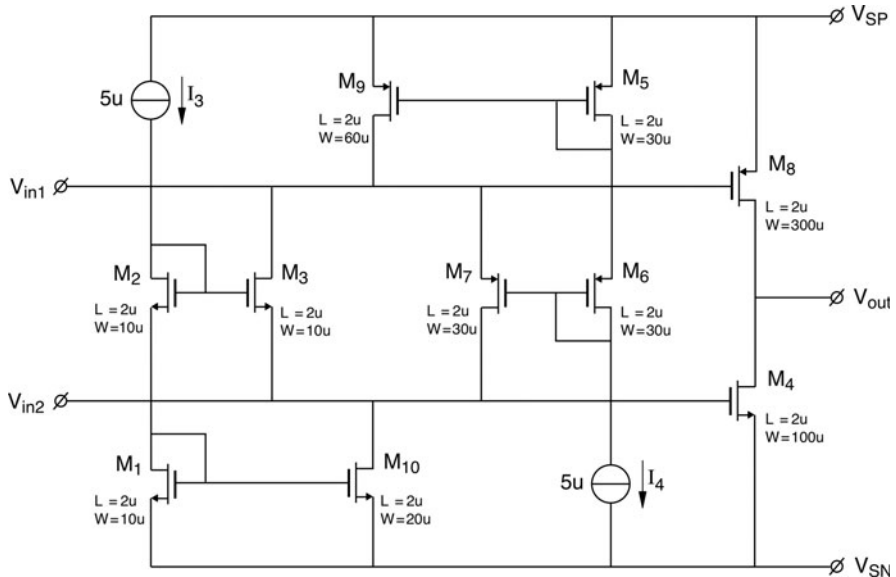


Fig. 5.6.1 Class-AB output stage with feedforward biasing



## 5.7 References

- [5.1]. J.E. Solomon, The monolithic op amp: a tutorial study. *IEEE J. Solid-St. Circ.* **SC-91**, 314–332 (1974)
- [5.2]. P.R. Gray, R.G. Meyer, *Analyses and Design of Analog Integrated Circuits* (Wiley, New York, 1984)
- [5.3]. D. Fullager, A new high performance monolithic operational amplifier, Fairchild Semiconductor, Application Briefing, May 1968 ( $\mu\text{A}$  741)
- [5.4]. Y. Nishikawa, J.E. Solomon, A general-purpose wideband operational amplifier, *IEEE ISSCC 73, Digest of Technical Papers*, pp. 144, 145, 212, 213
- [5.5]. Data sheet, LH-0021 operational amplifier, National Semiconductor, April 1972
- [5.6]. F.L. Long, A dual monolithic power operational amplifier, *IEEE ISSCC 1973, Digest of Technical Papers*, pp. 178, 179, 221
- [5.7]. O.H. Shade Jr., A new generation of MOS/Bipolar operational amplifiers. *RCA Rev.* **37**, 204–224 (1976)
- [5.8]. R.J. Widlar, Monolithic op amp with simplified frequency compensation. *IEEE* **15**, 58–63 (1967)
- [5.9]. D. Senderowicz, D.A. Hodges, P.R. Gray, High performance N-MOS operational amplifier. *IEEE J. Solid-St. Circ.* **SC-13**, 760–766 (1978)
- [5.10]. W.C.M. Renirie, K.J. de Langen, J.H. Huijsing, Parallel feedforward class-AB control circuits for low-voltage bipolar rail-to-rail output stages of operational amplifiers. *Analog Integr. Circ. S.* **8**, 37–48 (1995)
- [5.11]. D.M. Montecelli, A quad CMOS single-supply op amp with rail-to-rail output swing. *IEEE J. Solid-St. Circ.* **SC-21**, 1026–1034 (1986)
- [5.12]. R. Hogervorst, J.P. Tero, R.G.H. Eschauzier, J.H. Huijsing, A compact power-efficient 3V CMOS rail-to-rail input/output operational amplifier for VLSI cell libraries. *IEEE J. Solid-St. Circ.* **29**(12), 1505–1513 (1994)
- [5.13]. P.R. Gray, A 15-W monolithic power operational amplifier. *IEEE J. Solid-St. Circ.* **SC-7**, 478–480 (1972)
- [5.14]. J.H. Huijsing, F. Tol, Monolithic operational amplifier design with improved HF behaviour. *IEEE J. Solid-St. Circ.* **SC-11**, 323–328 (1976)
- [5.15]. E. Seevinck et al., A low-distortion output stage with improved stability for monolithic power amplifiers. *IEEE J. Solid-St. Circ.* **23**(3), 794–801 (1988)
- [5.16]. J.H. Huijsing, D. Linebarger, Low-voltage operational amplifier with rail-to-rail input and output ranges. *IEEE J. Solid-St. Circ.* **SC-20**, 1144–1150 (1985)
- [5.17]. J. Fonderie, J.H. Huijsing, Operational amplifier with I-V rail-to-rail multipath-driven output stage. *IEEE J. Solid-St. Circ.* **26**(12), 1817–1824 (1991)
- [5.18]. R. Hogervorst et al., CMOS low-voltage operational amplifiers with constant- $g_m$  rail-to-rail input stage. *Analog Integr. Circ. S.* **5**, 135–146 (1994)
- [5.19]. R.G.H. Eschauzier, R. Hogervorst, J.H. Huijsing, A programmable 1.5 V CMOS class-AB operational amplifier with hybrid-nested Miller compensation for 120 dB gain and 6 MHz UGF. *IEEE J. Solid-St. Circ.* **29**(12), 1497–1504 (1994)
- [5.20]. K.J. de Langen, J.H. Huijsing, Compact low-voltage power-efficient operational amplifier cells for VLSI. *IEEE J. Solid-St. Circ.* **33**(10), 1482–1496 (1998)
- [5.21]. I. Getreu, *Modelling the Bipolar Transistor* (Tektronix, inc., Beaverton, 1976)
- [5.22]. K.J. de Langen, J. Fonderie, J.H. Huijsing, Limiting circuits for rail-to-rail output stages of lowvoltage bipolar operational amplifiers, *ISCAS 95, Seattle*, vol. 3, pp. 1728–1731
- [5.23]. K.J. de Langen, J.K. Huijsing, *High-frequency and Low-voltage Bipolar, BiCMOS, and CMOS Operational Amplifier Techniques* (Kluwer Academic Publishers, Boston, 1999)



## 6. Overall Design

The previous chapters dealt with two important stages of OpAmps. With the design of the input stage the aspects of bias, offset, drift, noise, common-mode rejection, and rail-to-rail input range were covered. With the design of the output stage power efficiency, classification of the fully VF, compound VF/GA, and rail-to-rail fully GA output stages with feed forward and feedback class-AB biasing were presented. The remaining attributes of gain, high-frequency response, slew rate, and linearity have to be performed by the whole of the input, intermediate, and output stages. That is the subject of this chapter.

This chapter discusses the overall design of Operational Amplifiers.

Firstly, we will investigate how a large gain can be achieved. Therefore, an inventory will be made of nine main overall configurations in Sect. 6.1. Secondly, a systematic overview of HF compensation techniques will be presented in Sect. 6.2. Finally, aspects of slew rate and linear distortion are surveyed in Sects. 6.3 and 6.4 respectively.

### 6.1 Classification of Overall Topologies

One of the most important requirements of an Operational Amplifier is a large voltage gain  $A_V$  and current gain  $A_i$  (defined as  $A_V = -Y_i/Y_o$  and  $A_i = Y_i/Y_i$  in Chap. 2). The larger the voltage and current gain, the lower the errors which are made in OpAmp applications by a non-zero input voltage and current, as calculated in Chap. 3. For obtaining a large amount of voltage and current gain, several amplifier stages can be connected in cascade. The choices of these stages and the ways they are connected determines the main topology of the Operational Amplifier. Therefore, we will first make an inventory of possible configurations. After that some gain-boosting and compensation techniques will be reviewed.

## Nine Overall Topologies

A general purpose OpAmp must have a common-mode (CM) input and output voltage range which extends from nearly the negative supply-rail voltage  $V_{SN}$  to nearly the positive supply-rail voltage  $V_{SP}$ .

We have seen that good input stages must be connected in the GA mode, and push-pull output stages can be chosen from the fully VF, compound VF/GA or fully GA modes. These basic connections for input and output stages are shown in Figs. 6.1.1 and 6.1.2.

In the input stage the NPN bipolar and P-channel CMOS versions are shown, because these ones are generally the best of their kind. The NPN transistor has the highest bandwidth and current gain. The P-channel transistor has a floating back-gate, which can be bootstrapped by the source, so that the CMRR is high.

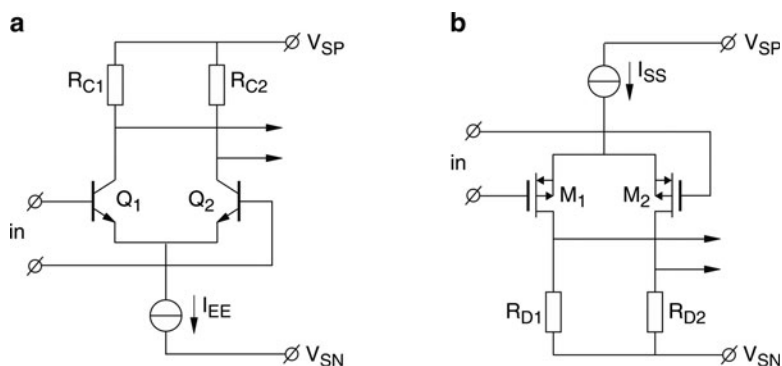


Fig. 6.1.1 Basic GA connections of input stages in (a) bipolar and (b) CMOS technology

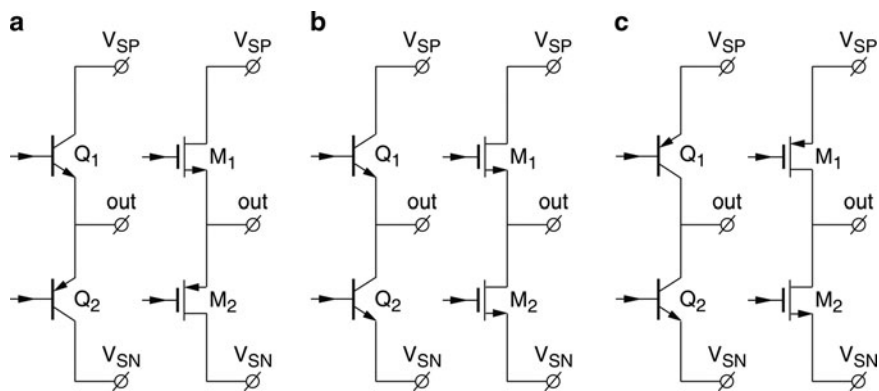


Fig. 6.1.2 Basic connections of the push-pull output stages in bipolar and CMOS technology: (a) Fully VF, (b) VF/GA and (c) GA connections

Moreover, the P-channel transistor generally has a lower  $1/f$  noise than the N-channel one. But, of course, complementary versions in both technologies are also possible.

In the output stage the full VF and GA versions are already complementary in nature. The output voltage range of the full VF stage cannot reach the rail within one diode voltage and one saturation voltage of the driver transistor, which all together amounts to about 1 V at each side. The full GA stage is much better in this respect. It only fails to reach the rails within one saturation voltage, which amounts to some hundreds of mV at each side. We call it a rail-to-rail output stage. The weakest spot in the full GA connection is the lateral PNP transistor  $Q_1$  if we cannot dispose of an IC process with vertical PNPs. This transistor has a low current gain at higher current densities, so it has to be chosen very large in regard to the NPN transistor  $Q_2$  to preserve some gain. Also its bandwidth is very low. For these reasons this transistor  $Q_1$  may be replaced by a NPN transistor in the compound VF/GA version. We then have to accept an asymmetrical output voltage range. If the output swing must be rail-to-rail,  $Q_1$  of the GA stage is sometimes replaced by a P-channel CMOS transistor when a BiCMOS process is at hand.

The question is now how to connect the input and output stages. A GA input transistor can only be directly connected with an GA output transistor if the latter is complementary to the former. No direct connection can be made with a VF or non-complementary GA output transistor. So, we must conclude that a level-shift stage or an intermediate stage is always necessary to connect input and output stages of a general-purpose Operational Amplifier. Otherwise the output voltage cannot swing from close to the negative rail to close to the positive rail voltage.

An inventory of level-shift stages is given in Figs. 6.1.3 and 6.1.4.

The folded-cascode current mirror (CM) level-shift stages in Fig. 6.1.3a can also be regarded as folded-cascode current follower (CF) stages in the classification. They are able to subtract the differential output currents of the input stage and bring the result out at a single terminal. The bipolar version has emitter degeneration resistors to lower the current offset and noise, and thus to lower the equivalent input offset and noise voltage of the connected input stage. The bipolar folded-cascode current follower (CF) stage in Fig. 6.1.3b is able to connect an NPN GA input stage with any output stage at a large bandwidth. The all-pass current networks  $R_F C_F$  lead the low-frequency signal components through the PNP transistors, and the high-frequency components through the NPN transistors [6.1]. If the turnover frequencies  $f_F$  of the  $R_F C_F$  networks are higher than the cut-off frequencies  $f_T$  of the PNP transistors, there is no loss in the PNP transistors, and all of the input current is collected again at the output. This results in a flat frequency response of the current transfer from DC up to the  $f_T$  of the NPN transistors. The CMOS CF stage of Fig. 6.1.3c may have a large voltage gain due to the full cascoded structure.

The GA stages of Fig. 6.1.4 are useful as level-shift stages between an GA PNP or P-channel input stage and any output stage, and provide voltage and current gain at the same time.



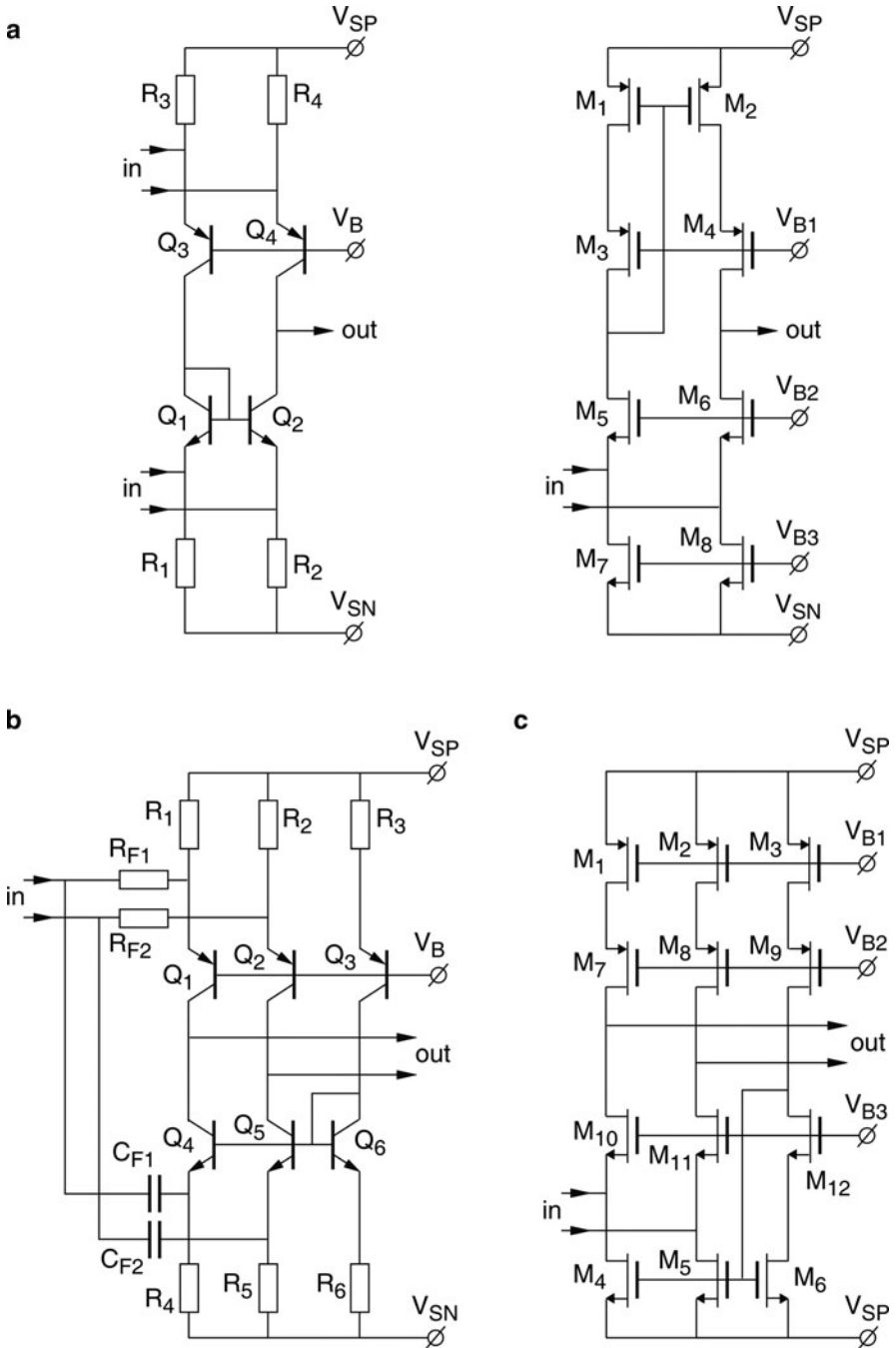


**Fig. 6.1.3** Intermediate CF level-shift stages in bipolar and CMOS technology: (a) Folded-cascode current mirror (CM), and (b/c) folded-cascode current follower (CF)

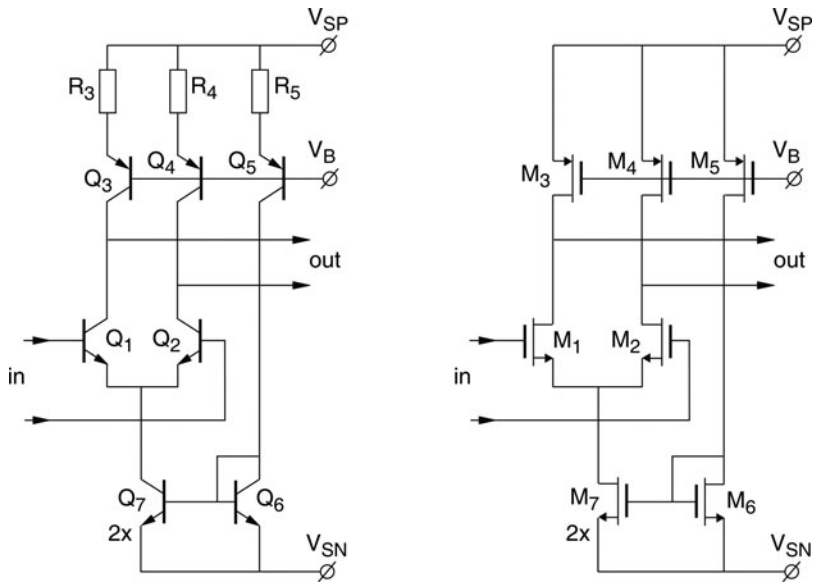


**Fig. 6.1.4** Intermediate GA level-shift stages or intermediate amplifier stages in bipolar and CMOS technology

**Table 6.1** Classification of Operational Amplifiers according to their main overall topology

Configuration number	Input stage	Level-shift or intermediate stage	Output stage
1	GA	CF	–
2	GA	GA	–
3	GA	CF	VF
4	GA	GA	VF
5	GA	CF	VF/GA
6	GA	GA	VF/GA
7	GA	CF	GA
8	GA	GA	GA
9	GA	GA + GA	GA

It stands to reason that these stages may all be of their complementary counterparts also. Further, there is no need to mention a straight cascode CF stage after a GA stage, because such a cascode stage does not change the overall topology. Similarly, there is no need to mention a VF Darlington stage before a GA stage.

The conclusion may be drawn now, that we have only one type of input stage: the GA type; three types of output stages: the VF, VF/GA, and the GA types; and, finally, we have two types of level-shift stages: the folded-cascode current mirror (CM) or the current follower CF (both denoted as CF in Table 6.1) type, and the GA types.

From all these possibilities we can make six three-stage combinations. We may add two possible two-stage combinations without a push-pull output stage.

Also, we may add a group of multistage GA combinations with more than three GA, stages as the number of GA stages generally determines the complexity of the frequency compensation structure. Then, we have divided all Operational Amplifiers in nine main overall configurations. These are given in Table 6.1.

The design of these nine overall topologies together with their realization examples are further elaborated in Sects. 7.1–7.9.

### Voltage and Current Gain Boosting

An alternative to the cascading of more GA stages is to apply voltage or current boosting to increase the gain.

Figure 6.1.5a shows a CF transistor  $M_1$ , used to increase the voltage gain of  $M_3$  by the voltage-gain factor  $\mu_1$  of  $M_1$ . When we now artificially regulate the gate of  $M_1$  with an amplifier  $M_2$  such that the potential at the drain of  $M_3$  remains constant, the output current is not dependent anymore on its output voltage and the output impedance at the drain of  $M_1$  is increased [6.2]. The voltage gain of  $M_1$  is boosted by the voltage-gain factor  $\mu_2$  of  $M_2$ . The total unloaded voltage gain is now  $A_v = \mu_1\mu_2\mu_3$ .

Figure 6.1.5b shows a VF transistor  $Q_1$  used as a Darlington combination with  $Q_3$  to increase the current gain of  $Q_3$  by a factor  $\beta_1$ . We now artificially regulate the collector current of  $Q_1$  at a constant value  $I_B$  by using  $Q_2$  to boost the current gain of  $Q_1$  by a factor  $\beta_2$  of  $Q_2$  [6.3]. The total current gain is now  $A_i = \beta_1\beta_2\beta_3$ .

### Input Voltage and Current Compensation

A third method to increase the gain, besides cascading more GA stages or boosting, is compensation. Two examples are shown in Fig. 6.1.6a, b.

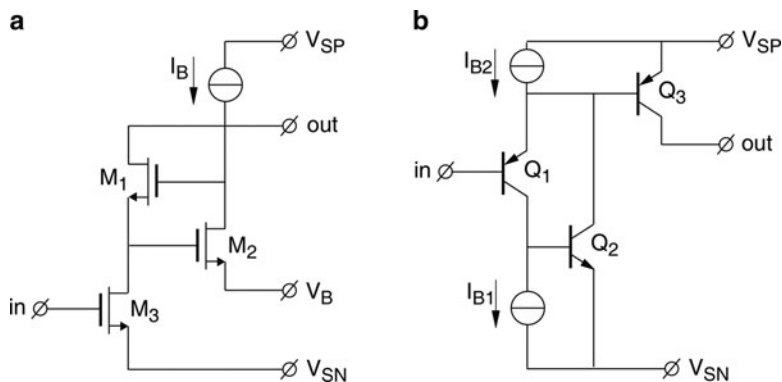
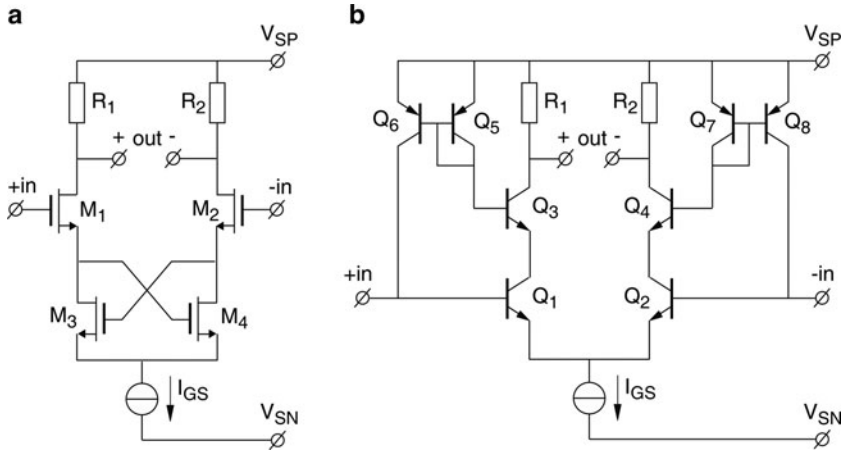


Fig. 6.1.5 (a) Voltage boosting of a CF transistor  $M_1$  and (b) current boosting of a VF transistor  $Q_1$



**Fig. 6.1.6** (a) Compensation of the input voltage across of the source impedance  $1/g_{m1,2}$  of  $M_{1,2}$  by the negative source impedance  $-1/g_{m3,4}$  of  $M_{3,4}$ . (b) Compensation of the input base current of  $Q_{1,2}$  by the negative base currents of  $Q_{3,4}$

In the example of Fig. 6.1.6a, the relatively large source resistances  $1/g_{m1,2}$  of the CMOS transistors are compensated by the equal but negative source resistances  $-1/g_{m3,4}$  in a positive feedback loop [6.4]. The result is an overall transconductance  $g_m = 1/(1/g_{m1,2} - 1/g_{m3,4})$ . The transistors  $M_3$  and  $M_4$  must be taken slightly smaller in their W/L ratio than  $M_1$  and  $M_2$ , to make sure that the positive conductances  $g_{m1,2}$  dominate the negative ones  $g_{m3,4}$  so that the circuit remains stable. In the bipolar version, small degeneration resistors  $R_3$  and  $R_4$  have to be inserted in the emitters of  $Q_3$  and  $Q_4$  to keep the circuit stable. In the example of Fig. 6.1.6b, the base current of transistors  $Q_1$  and  $Q_2$  are compensated by duplicating these currents in  $Q_3$  and  $Q_4$  and mirroring them back into the bases of  $Q_1$  and  $Q_2$ .

It should be clear that the above compensation methods to increase the gain by a positive feedback loop are limited by the matching accuracy of components. This is in contrast to the methods of cascading or boosting, where there is no limit in gain increase at low frequencies.

However, there are two fundamental limits to the overall gain: thermal feedback and frequency compensation. Thermal feedback on the chip going from the output stage into the input stage sets a limit to the maximum useful low-frequency voltage gain  $A_{V0}$  which can be obtained. The maximum useful value depends on the amount of dissipated power in the output stage and on the symmetry of the layout of the input stage in regard to the output stage, as was discussed with Fig. 5.1.1. A maximum useful value of the order of  $10^5$  or  $10^6$  can be obtained on a single chip. The other gain limitation is given by the high-frequency characteristic. This will be discussed in the next paragraph.

## 6.2 Frequency Compensation

The phase lag of the signal when going through the several stages of an OpAmp determines the limit to the useful gain at high frequencies. At the frequency where the phase lag exceeds  $180^\circ$ , the open loop gain must be dropped below unity. Otherwise, the feedback system will become self-oscillating [6.5]. Moreover, a certain amplitude and phase margin must be adopted to obtain a response without peaking in the frequency domain [6.6] or without overshoot in the time domain [6.7]. In Fig. 6.2.1 the desired frequency characteristic of the open-loop amplifier is presented. It contains the amplitude characteristic (amplitude  $|A_v|$  versus frequency) and the phase characteristic (phase  $\nu(A_v)$  versus frequency), combined in a Bode diagram. It represents an amplifier with one dominating pole  $P_2 = 2\pi f_2$  and a limiting pole  $P_1 = 2\pi f_1$ . Parasitic poles situated above  $P_1$  are disregarded.

For a Butterworth pole position of the unity-gain feedback amplifier with a flat frequency response and with an overshoot in the step response of 5%, the two pole frequencies of the open loop must be separated at a distance of two times the DC gain:

$$\frac{f_1}{f_2} \geq 2A_{v0} \tag{6.2.1}$$

A larger separation of the poles is also allowed. In that case the phase margin of the open loop gain is larger than  $60^\circ$ . But this may represent a waste of bandwidth or current.

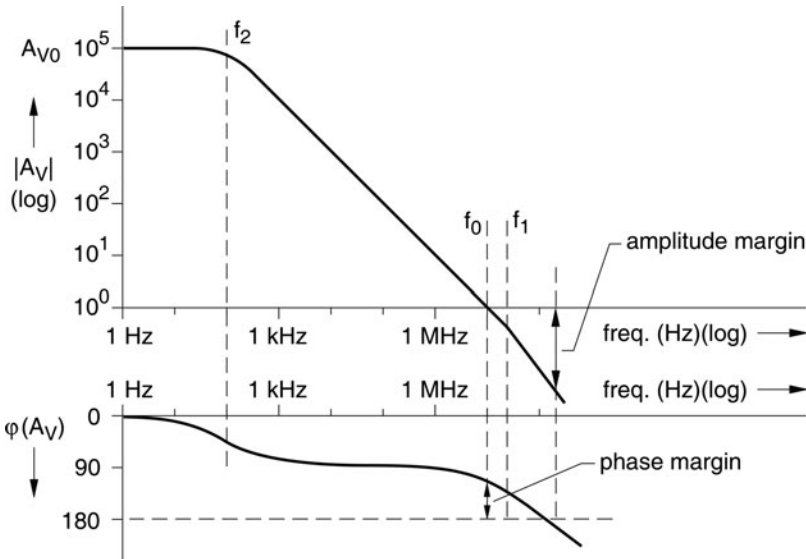


Fig. 6.2.1 Frequency response of an Operational Amplifier

From Eq. 6.2.1 it follows that the frequency  $f_0 = \omega_0/2\pi$  where the amplitude characteristic crosses zero must be a factor two below the limiting pole frequency  $f_1 = P_1/2\pi$ , so

$$f_0 \leq \frac{1}{2}f_1 \quad (6.2.2)$$

The frequency  $f_0$  is called the 0 dB bandwidth of the open loop amplifier. The dominating-pole frequency  $f_2$  is situated a factor equal to the DC gain  $A_{V0}$  lower than the 0 dB frequency:

$$f_2 = f_0/A_{v0} \quad (6.2.3)$$

If the amplitude characteristic between  $f_0$  and  $f_2$  is not straight, but curved by a pole-zero doublet, the step response of the unity-gain feedback amplifier can be expected to have a slow settling overshoot or undershoot component [6.7]. This is undesirable in amplifiers which need a fast and accurate settling after a step signal. Hence, a general-purpose OpAmp needs a straight 6 dB per octave slope between the 0 dB frequency  $f_0$  and the dominating frequency  $f_2$ .

An overview of how to obtain the desired frequency response will be presented now. The way this is done is called frequency compensation. The complexity of the frequency compensation is mainly determined by the number of GA stages in the loop. We start with a configuration of one GA stage and end with four GA stages.

### One-GA-Stage Frequency Compensation

A one-GA-stage GA-CF Operational Amplifier is shown in Fig. 6.2.2b. A CF stage has been used as a cascode, to increase the voltage gain of the input GA transistor pair. The output is loaded by a capacitor  $C_1$  and a resistor  $R_1$ , including all parasitics at this point. The tail current  $I_{T1}$  has a value of twice the bias current  $I_{B1}$ .

The DC gain is  $A_{v0} = g_{m1}R_1$ , with  $g_{m1} = 2/(1/g_{m11} + 1/g_{m12}) \approx g_{m11}$ . Hence, the transconductance of the whole stage with mirror is equal to that of one of the input transistors. If there is no resistive load besides those of the transistors, and if we suppose that the current mirror  $M_{23}$  through  $M_{26}$  is ideal, the DC gain for a bipolar circuit is maximally  $A_{V0M} \approx r_{cb2}/r_{e1} \approx (r_{cb2}/r_{ce2})(r_{ce1}/r_{e1}) \approx \beta_2\mu_1$ , with average values for transistors in the cascoded stages  $g_{m1}$  and  $g_{m2}$  and for a CMOS circuit  $A_{V0M} = g_{m1}r_{d1}g_{m2}r_{d2} = \mu_1\mu_2$ , which may be of the order of  $10^5$  and  $10^4$ , respectively. In CMOS the input stage should be biased in weak inversion, as this gives the highest ratio of  $g_{m1}/I_{B1}$ .

The amplifier has a limiting frequency  $f_1$  caused by the transit frequency  $f_{T2}$  of the cascode transistors  $M_{21}$  and  $M_{21}$ , so  $f_1 = f_{T2}$ . The dominating frequency  $f_2$  is caused by the load circuit, so  $f_2 = 1/(2\pi R_1 C_1)$ .

The 0 dB bandwidth is for bipolar input transistors:

$$f_0 = \frac{g_{m1}}{2\pi C_1} = \frac{I_{B1}}{2\pi C_1 V_T} \quad (6.2.4)$$

and for CMOS input transistors biased in weak inversion:

$$f_0 = \frac{g_{m1}}{2\pi C_1} \approx \frac{I_B}{2\pi C_1 (V_{GS} - V_{TH})} \tag{6.2.5}$$

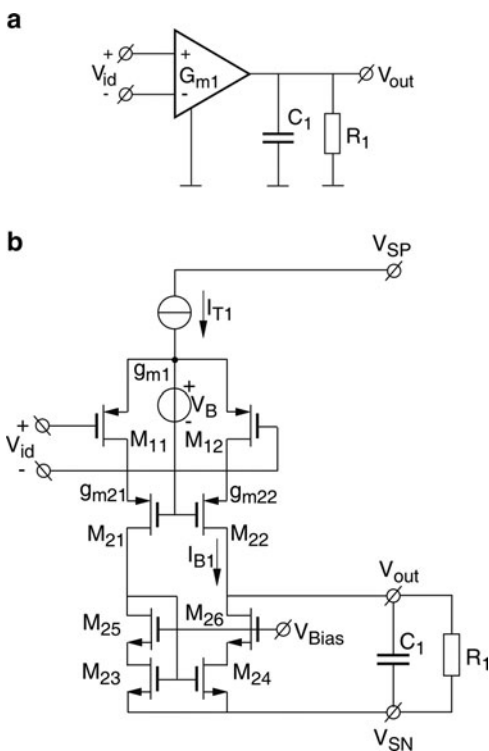


**Fig. 6.2.2** (a) Block diagram of GA-CF Operational Amplifier. (b) Simplified one-GA-stage GA-CF Operational Amplifier

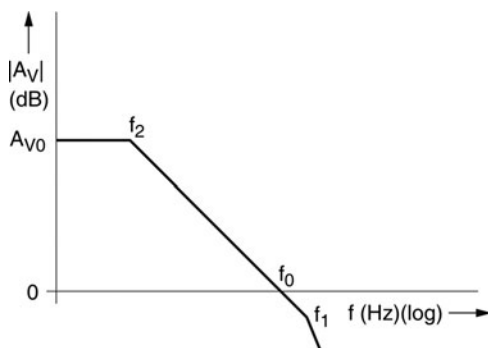


**Fig. 6.2.3** Frequency characteristic of a GA-CF Operational Amplifier

in which

$$V_T = kT/q \approx 25 \text{ mV}$$

$$(V_{GS} - V_{TH}) \approx 60 \text{ mV}$$

For a load capacitor of  $C_l = 10 \text{ pF}$  and a bias current  $I_{BI}$  of  $100 \text{ }\mu\text{A}$ , the bipolar circuit has a bandwidth of  $f_0 = 30 \text{ MHz}$ , and the CMOS circuit  $f_0 = 12 \text{ MHz}$ .

The maximum bandwidth  $f_0$  must be kept half of that of the limiting pole frequency  $f_0 = 2f_l = 2f_{T2}$  by the choice of  $C_l$ . For bipolar transistors the transit frequency  $f_T$  ranges from  $300 \text{ MHz}$  up to  $60 \text{ GHz}$ , and for CMOS from  $100 \text{ MHz}$  up to  $20 \text{ GHz}$ . In fact, the load capacitance  $C_l$  functions as well as an HF compensation capacitor.

When we divide the bandwidth by the supply power needed  $f_0/P_s$ , with  $P_s = V_s I_s$ , we obtain a figure of merit which is reverse to the well-known power delay product used in digital circuits. For the bipolar circuit:

$$f_0/P_s = \frac{I_{BI}}{2\pi C_l V_T V_s 2I_{BI}} = \frac{1}{2} \frac{1}{2\pi C_l V_T V_s} \quad (6.2.6)$$

and for the CMOS circuit:

$$f_0/P_s = \frac{1}{2} \frac{1}{2\pi C_l (V_{GS} - V_{TH}) V_s} \quad (6.2.7)$$

The bandwidth over power ratio is inverse proportional to the supply voltage  $V_s$  with bipolar as well as with CMOS transistors, so the supply voltage should be as small as possible. With CMOS in weak inversion the term  $(V_{GS} - V_{TH})$  may be replaced by some 20% more than two times the thermal voltage  $2V_T = 2kT/q \approx 50 \text{ mV}$ , which is about  $60 \text{ mV}$ . The optimum choice CMOS transistor has the smallest possible length  $L$ , and a width  $W$  so that the transistor is on the verge of weak inversion. In that case the ratio between  $g_m$  and  $C$  parasitic is the highest.

### ***No Internal Poles Without Cascodes!***

If we would eliminate the cascode transistors  $M_{21}$  and  $M_{22}$  in Fig. 6.2.2, there would be no limiting pole, supposing the mirror is ideal.

This would mean that we may use the circuit up to its transit frequency  $f_T$ . In that case the bandwidth over power ratio will be doubled. This is already an important conclusion. Moreover, if the OpAmp would be used in filter applications, the non-existence of internal limiting poles means that there is no extra phase shift involved. The external poles at the input and output can be made part of the intentional filter poles. This situation is highly desirable for wideband filters [6.8]. On the other



hand, omitting the cascode transistors  $M_{21}$  and  $M_{22}$  will reduce the maximum voltage gain  $A_{VOM}$  to that of a single CMOS or bipolar transistor. Parallel compensation by an artificial negative resistance equal to the output resistance is an option [6.8]. But such compensation is limited by the inequality of both parasitic resistances and takes extra power again. Yet, it is worthwhile looking for system architectures that allow low-gain amplifier stages. Then such simple stages as mentioned with Figs. 3.5.7 and 3.5.8 of Chap. 3 could be used.

### Two-GA-Stage Frequency Compensation

Next we look at the two-stage GA-GA Operational Amplifier of Fig. 6.2.4. Its frequency response is given in Fig. 6.2.5.

The DC voltage gain is  $A_{V0} = g_{m2}R_2g_{m1}R_1$ . When there is no external load resistor the maximum gain is  $A_{V0} = \mu_2\mu_1$ , which value is in the order of  $10^6$  for the bipolar circuit and  $10^4$  for the CMOS version. The pole frequencies  $f_1 = 1/2\pi R_1C_1$  at the output, and  $f_2 = 1/2\pi R_2C_2$  at the output of the input stage probably do not obey the rule  $f_1/f_2 \geq 2A_{V0}$ . Hence, frequency compensation has to be applied.

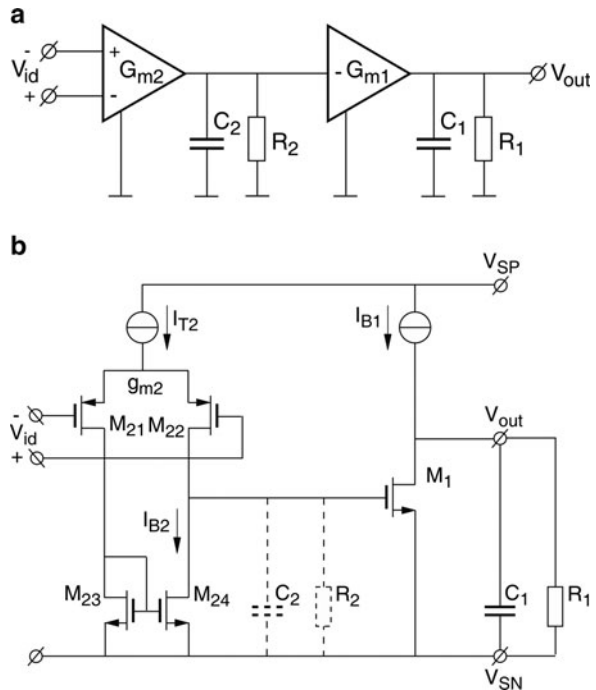
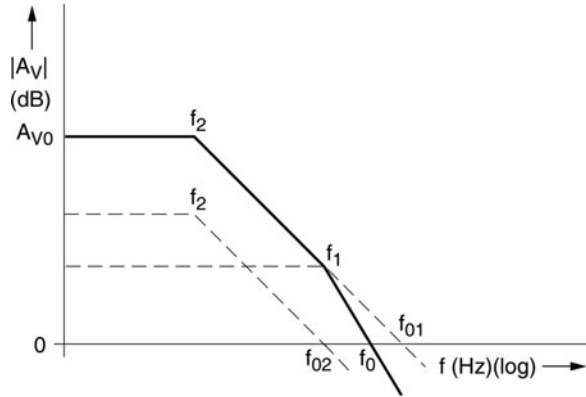


**Fig. 6.2.4** (a) Block diagram of two-stage GA-GA Operational Amplifier. (b) Simplified two-stage GA-GA Operational Amplifier ( $C_2$  and  $R_2$  are usually parasitic transistor parameters)

**Fig. 6.2.5** Uncompensated frequency response of a two-stage GA-GA Operational Amplifier



The 0 dB bandwidth  $f_0$  of the non-compensated amplifier is the geometric mean of the 0 dB bandwidths  $f_{01}$  and  $f_{02}$  of the two composing GA stages, which can be understood from Fig. 6.2.5 with its log. scales:

$$f_0 = \sqrt{f_{01}f_{02}} = \sqrt{\frac{g_{m1}g_{m2}}{2\pi C_1 2\pi C_2}} \tag{6.2.8}$$

Note, that the 0 dB bandwidth is independent of the resistor values. Also note, that we have drawn in Fig. 6.2.5 the output stage with a higher 0 dB frequency  $f_{01}$  than that of the input stage  $f_{02}$ . This is often not the case. For this moment the sequence does not change our reasoning. When it will with Miller compensation, we come back to it. Two ways of frequency compensation can be used for a two stage GA-GA amplifier: parallel compensation and Miller compensation.

### ***Two-GA-Stage Parallel Compensation (PC)***

The parallel compensated amplifier is shown in Fig. 6.2.6, and its frequency characteristic in Fig. 6.2.7. The natural load elements of the input stage  $C_2$  and  $R_2$  are usually parasitic elements. The parallel compensation network is composed of the series connection of  $C_p$  and  $R_p$ .

The parallel compensation network  $C_p R_p$  can best be placed in between the two stages. Going from lower to higher frequencies, the capacitor  $C_p$  in “parallel” with the parasitic capacitor  $C_2$ , firstly, decreases the dominating-pole frequency  $f_2$  to  $f'_2$ . Secondly, the reduction of gain is gradually terminated by  $R_p$  above  $f_1$ .  $R_p$  must be chosen equal to  $R_p = 1/2\pi f_1 C_p$ .

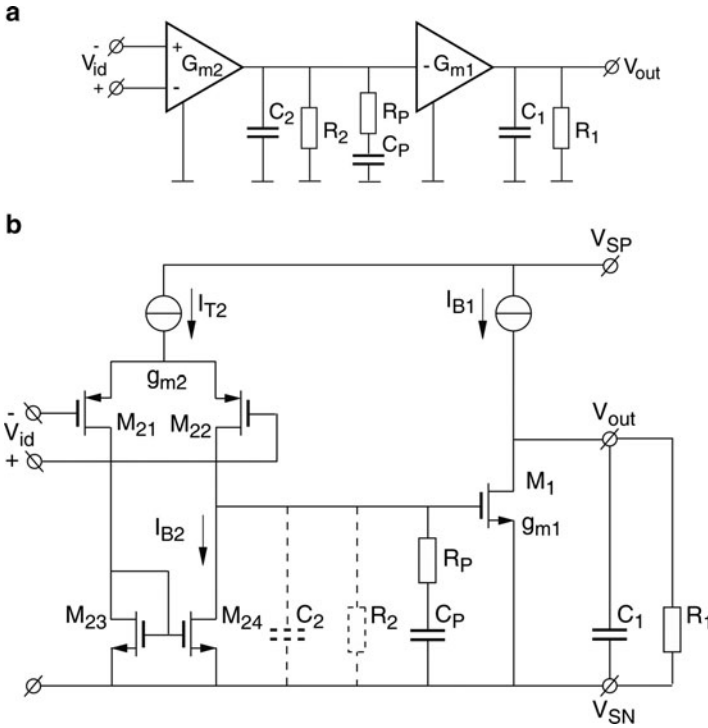


**Fig. 6.2.6** (a) Block diagram of parallel-compensated two-stage GA-GA amplifier ( $C_2$  and  $R_2$  are usually parasitic elements). (b) Simplified parallel-compensated two-stage GA-GA amplifier ( $C_2$  and  $R_2$  are usually parasitic transistor parameters)

When we choose the components such that:

$$\begin{aligned}
 C_P &= R_1 \sqrt{2C_1 C_2 g_{m1} g_{m1}} \\
 R_P &= \sqrt{C_1 / (2C_2 g_{m1} g_{m2})}
 \end{aligned}
 \tag{6.2.9}$$

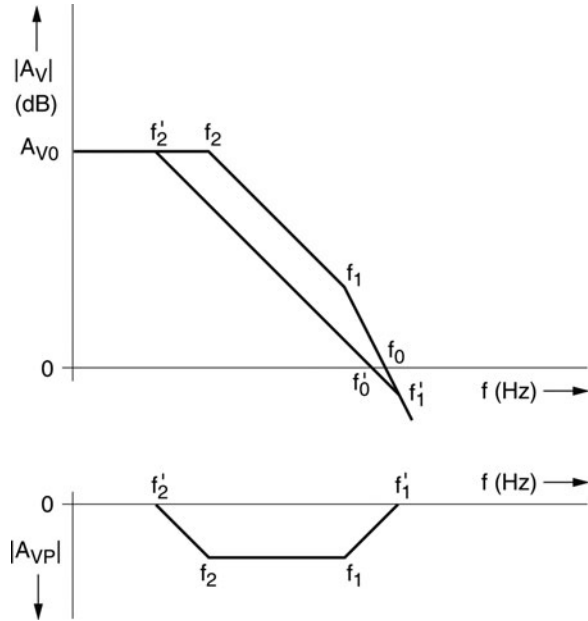
we find the desired new straight 6 dB frequency roll-off from  $f'_2$  up to  $f'_1$ , with a new 0 dB bandwidth  $f'_0$  positioned a factor 2 below  $f'_2$ :

$$f'_0 = \sqrt{\frac{1}{2} \frac{g_{m1}}{2\pi C_1} \frac{g_{m2}}{2\pi C_2}}
 \tag{6.2.10}$$

The parallel compensation shows a remarkably good result. The new 0 dB frequency  $f'_0$  lies only a factor  $\sqrt{2}$  lower than the theoretical maximum of  $f_0$ . Particularly at heavy capacitive loads, when the bandwidth  $f_{01}$  of the output stage is much lower than the  $f_T$  of the transistors, the bandwidth  $f_{02}$  of the input stage helps to broaden the bandwidth.

When we calculate the bandwidth over power ratio for a bipolar amplifier and CMOS amplifier in weak inversion with  $(V_{GS} - V_{TH}) = 60$  mV, we find respectively:

**Fig. 6.2.7** Frequency characteristic of a parallel compensated two-stage GA-GA amplifier and its parallel attenuation



$$\frac{f'_0}{P_S} = \frac{1}{2\pi V_T} \sqrt{\frac{1}{2} \frac{I_{B1}}{C_1} \frac{I_{B2}}{C_2}} / V_S (I_{B1} + 2I_{B2}) \tag{6.2.11}$$

$$\frac{f'_0}{P_S} \approx \frac{1}{2\pi (V_{GS} - V_{TH})} \sqrt{\frac{1}{2} \frac{I_{B1}}{C_1} \frac{I_{B2}}{C_2}} / V_S (I_{B1} + 2I_{B2}) \tag{6.2.12}$$

We find a broad optimum for equal currents in the output and input stage around  $I_{B1} = 2I_{B2}$ .

When we substitute  $I_{B1} = 2I_{B2}$  at the optimum, we obtain for bipolar and CMOS transistors, respectively:

$$\frac{f'_0}{P_S} = \frac{1}{4} \frac{1}{2\pi \sqrt{C_1 C_2} V_T V_S} \tag{6.2.13}$$

$$\frac{f'_0}{P_S} = \frac{1}{4} \frac{1}{2\pi \sqrt{C_1 C_2} (V_{GS} - V_{TH}) V_S} \tag{6.1.14}$$

Unfortunately, there are a number of serious disadvantages associated with parallel compensation. The main problem is that the compensation cannot be made anywhere close to the desired value because the transconductance  $g_{m1}$  changes signal-dependently. When the output current changes from the quiescent value up to 100 times larger, the  $g_m$  varies with a factor 100. A second problem is that the

compensation depends on process parameters which are different from those to be compensated. This means that the choices given by (6.2.9) are not accurately met and that a pole-zero doublet will occur resulting in a slow settling component.

For class-A operation and for applications where a large slow settling signal component is not a problem, parallel compensation can be considered. However, the relative large parallel compensation capacitor  $C_p$  that is needed may take an excessive large chip area. These are the reasons that other means of compensation have to be explored.

### Two-GA-Stage Miller Compensation (MC)

Miller compensation is the other possibility. Figure 6.2.8 shows a two-stage GA-GA amplifier with Miller compensation [6.9]. And, Fig. 6.2.9 shows the frequency response of it.

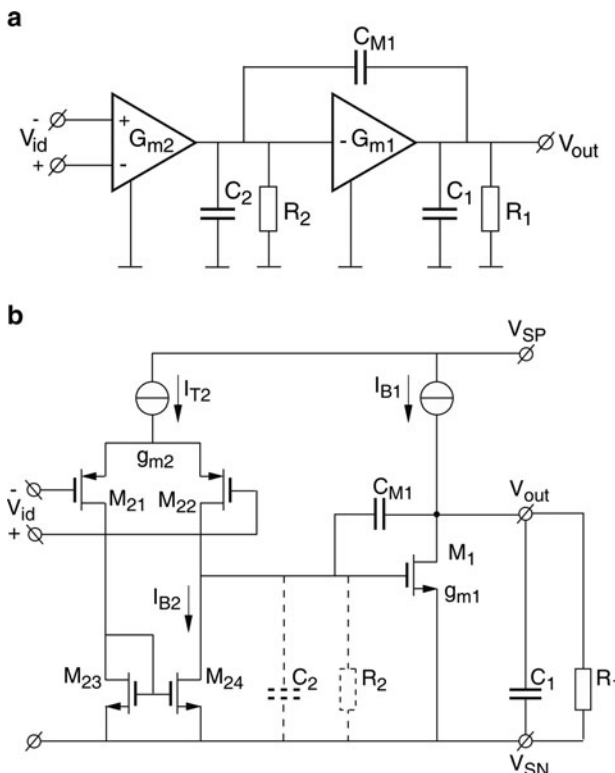
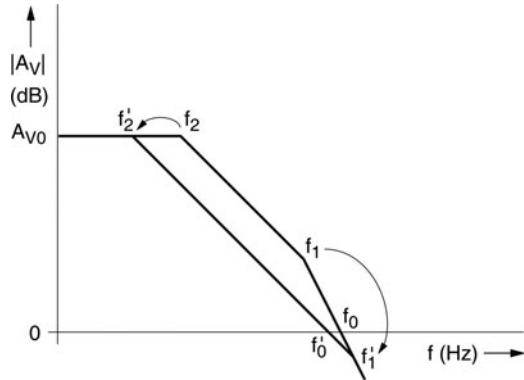


**Fig. 6.2.8** (a) Block diagram Miller-compensated two-stage GA-GA Operational Amplifier ( $C_2$  and  $R_2$  are usually parasitic elements). (b) Simplified Miller-compensated two-stage GA-GA Operational Amplifier ( $C_2$  and  $R_2$  are usually parasitic transistor parameters)

**Fig. 6.2.9** Pole-splitting by Miller compensation of a two-stage GA-GA amplifier



The output stage with a Miller capacitor  $C_{M1}$  around it behaves as an integrator with a transimpedance  $1/2\pi f C_{M1}$ . It integrates the output current  $I_{O2}$  of the input stage and presents it as the output voltage  $V_{out}$ .

The transfer of the Miller-compensated output stage is:

$$\frac{V_{out}}{I_{O2}} = \frac{1}{2\pi f C_{M1}} \tag{6.2.15}$$

The voltage gain of the whole amplifier, including the input stage with a transconductance  $g_{m2}$ , becomes:

$$\frac{V_{out}}{V_{in}} = \frac{g_{m1}}{2\pi f C_{M1}} \tag{6.2.16}$$

The new 0 dB bandwidth  $f'_0$  of the amplifier is determined for  $V_{out}/V_{in} = 1$ , as:

$$f'_0 = \frac{g_{m1}}{2\pi C_{M1}} \tag{6.2.17}$$

The Miller capacitor, on one hand, reduces the dominant pole frequency  $f_2$  to  $f'_2$  by its integrator function, but, on the other hand, provides feedback by which the bandwidth increases from  $f_1$  to  $f'_1$ . It looks as if the pole frequencies  $f_1$  and  $f_2$  are split apart, as is clearly shown in Fig. 6.2.9. The maximum obtainable bandwidth  $f'_0$  for a  $60^\circ$  phase margin must lie a factor 2 below the new pole frequency  $f'_1$ , or a factor  $1/2$  below the uncompensated 0 dB frequency  $f_0$ , just as with parallel compensation.

So, the maximum 0 dB bandwidth  $f'_0$  is:

$$f'_0 \leq \frac{1}{\sqrt{2}} f_0 = \sqrt{\frac{1}{2} f_{01} f_{02}} = \sqrt{\frac{1}{2} \frac{g_{m1}}{2\pi C_1} \frac{g_{m2}}{2\pi C_2}} \tag{6.2.18}$$

This implies a minimal choice for  $C_{M1}$ :

$$C_{M1} \leq \sqrt{2C_1C_2 \frac{g_{m2}}{g_{m1}}} \quad (6.2.19)$$

This result is as good as with parallel compensation.

### **Remark on the Order of Pole Positions**

We have assumed that the 0 dB frequency  $f_{01}$  of the output stage lies above the frequency  $f_{02}$  of the input stage in Fig. 6.2.5. This may not always be the case, as the output may be loaded with a large capacitor  $C_1$ , and is also loaded by the Miller capacitor  $C_{M1}$ .

With parallel compensation the sequence of  $f_{01}$  and  $f_{02}$  did not matter, but now it does. The Miller effect is based on feedback around one stage [6.9]. Feedback is only effective if the loop gain around that stage is higher than unity. At frequencies where the loop gain is unity or lower the Miller effect is not present anymore. This is the case when we try to split the output pole frequency  $f_1$  beyond the point  $f_{01}$  where the gain of the output stage is lower than unity. The situation is drawn in Fig. 6.2.10.

The splitting of the output pole frequency  $f_1$  stops at the limiting pole frequency  $f_{01}$ .

$$f'_1 \approx f_{01} = \frac{g_{m1}}{2\pi C_1} \quad (6.2.20)$$

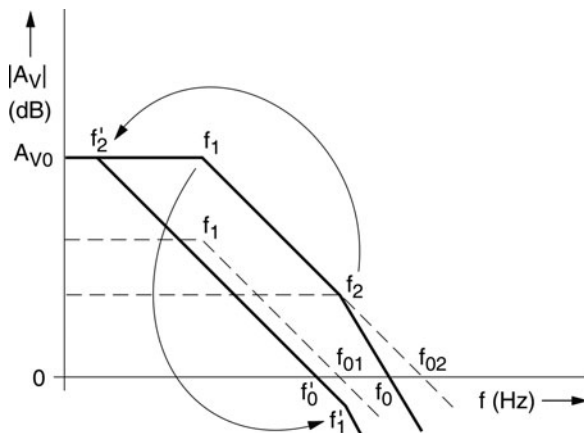


**Fig. 6.2.10** Frequency characteristics of a Miller-compensated two-stage GA-GA amplifier with a 0 dB frequency of the output stage  $f_{01}$  lower than that of the input-stage pole frequency  $f_{02}$

Further lowering of  $f_2$  by further increasing  $C_{MI}$  must be carried on until the 0 dB frequency is two times lower than  $f'_1$  for a phase margin of  $60^\circ$ . Hence, the 0 dB frequency  $f'_0$  must be chosen:

$$f'_0 = \frac{1}{2}f'_1 \approx \frac{1}{2}f_{01} \quad (6.2.21)$$

The lowering of  $f'_2$  by increasing  $C_{MI}$  without increasing  $f'_1$  beyond  $f_{01}$  is inefficient. We could as well have started with a lower bandwidth  $f_{02}$  of the first stage to save power. For the moment it can be concluded that the 0 dB bandwidth of the whole amplifier is limited by half that of the output stage  $2f_{01}$ . This is the reason why we are counting the stages from the output back to the input. For applications where  $f_{01}$  is lower than  $f_{02}$  due to heavy capacitive output loads we can follow the methods described with Figs. 6.2.24–6.2.30. This ends the remark.

The Eqs. 6.2.17 and 6.2.21 determine the minimum choice of  $C_{MI}$ :

$$C_{MI} = \frac{g_{m2}}{2\pi f'_0} \quad (6.2.22)$$

The Miller compensation capacitor  $C_{MI}$  must be calculated at the lowest current through  $M_1$  which is  $I_{B1}$  where  $g_{m1}$  has the lowest value and at the highest expected value of the load capacitance  $C_1$ .

The dominating pole frequency becomes:

$$f'_2 = \frac{f'_0}{A_{v0}} \quad (6.2.23)$$

with  $A_{v0} = g_{m2}R_2g_{m1}R_1$ .

The cut-off frequency  $f_T$  of the output transistor  $M_1$  may pose a further restriction on the bandwidth. The Miller feedback is attenuated by the voltage divider  $C_{MI}/(C_{MI} + C_2)$ . By this value the limiting pole frequency  $f'_1$  and the bandwidth  $f'_0$  are lowered:

$$f'_0 = \frac{1}{2}f'_1 = \frac{1}{2} \frac{g_{m1}}{2\pi C_1} \frac{C_{MI}}{C_{MI} + C_2} \quad (6.2.24)$$

For bipolar transistors with  $C_{MI} = C_2 = C_{BE1}$ , and for CMOS transistors with the width  $W$  set so that  $C_{MI} = C_2 = C_{GS1}$ , and the length  $L$  at the minimum, the bandwidth is practically limited to:

$$f'_0 = \frac{1}{2}f'_1 = \frac{1}{2} \frac{g_{m1}}{2\pi C_1} \frac{C_{MI}}{C_{MI} + C_2} \approx \frac{1}{4}f_T \quad (6.2.25)$$

Coming back to the case of Figs. 6.2.5 and 6.2.9 with  $f_{02} < f_{01}$ , the bandwidth  $f_{02}$  of the input stage need not be higher than  $f_{02} = \frac{1}{2}f_{01} = f'_0$ . The result is



a bandwidth over power ratio of the whole amplifier for bipolar and CMOS transistors of respectively:

$$\frac{f'_0}{P_S} = \frac{1}{2} \frac{1}{2\pi(C_1 + 2C_2)V_T V_S} \quad (6.2.26)$$

$$\frac{f'_0}{P_S} = \frac{1}{2} \frac{1}{2\pi(C_1 + 2C_2)(V_{GS} - V_{TH})V_S} \quad (6.2.27)$$

When we compare these results with those of parallel compensation we find a somewhat lower bandwidth over power ratio. With  $C_1 = C_2$  the ratio is  $3/\sqrt{2} \approx 2.1$  lower, and with  $C_1 = 10C_2$  the ratio is  $12/\sqrt{20} \approx 2.7$  lower than that of parallel compensation. Although, this is a disadvantage of Miller compensation, there are many advantages.

The main advantage of the Miller-compensated amplifier over the parallel-compensated version is the straight 6 dB/oct. roll-off of the frequency characteristic, without pole-zero doublets from pole-zero cancellation techniques. This makes the amplifier suitable for fast settling step responses without slow settling components.

Another important advantage of Miller compensation is that all gain which is attenuated by the compensation capacitor  $C_{MI}$  is used to lower the output impedance and the linear distortion of the output stage. With parallel compensation the attenuated gain is lost for any use!

A final advantage is that the compensation capacitor  $C_{MI}$  is much smaller compared to that which is needed with parallel compensation. That means a much smaller chip.

The obvious choice with Miller compensation for unity-gain feedback and relatively heavy capacitive load is to utilize most of the supply power in the output stage.

It should be kept in mind that if the amplifier need not be unity-gain feedback, but has for instance a closed-loop gain of 10, the supply current of the output transistor can be taken 10 times lower, and so the supply power will strongly be reduced.

A disadvantage of Miller compensation is that a zero appears in the right-half complex plane at a frequency  $f'_z$ :

$$f'_z = \frac{g_{m1}}{2\pi C_{MI}} \quad (6.2.28)$$

The additional zero frequency  $f'_z$  in the right half of the complex plane causes a reduction of the phase margin for values of  $f'_z$  above but still close to  $f'_1$ . If  $f'_2$  is below  $f'_1$ , even nearly a reversal of the phase occurs. This effect can easily be understood if we consider that the Miller capacitor  $C_{MI}$  functions as a feed forward path across the output transistor. At frequencies of  $f'_z$  lower than the limiting pole frequency  $f'_1 = g_{m1}/2\pi C_1$  the output transistor is no longer effective and the transistor does not invert anymore.

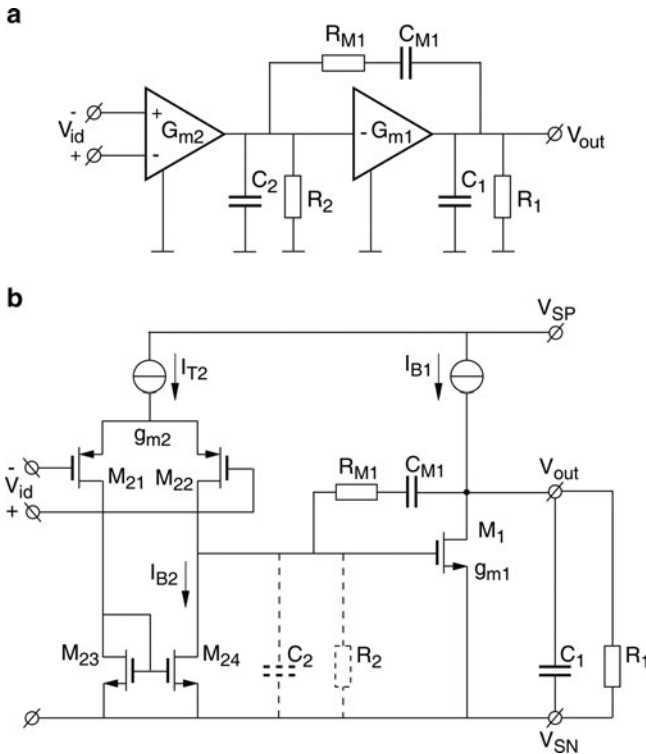


**Fig. 6.2.11** (a) Block diagram of resistive Miller-zero cancellation with a resistor  $R_{M1} = 1/g_{m1}$  in series with  $C_{M1}$  ( $C_2$  and  $R_2$  are usually parasitic elements). (b) Simplified circuit with resistive Miller-zero cancellation with a resistor  $R_M = 1/g_{m1}$  in series with  $C_{M1}$  ( $C_2$  and  $R_2$  are usually parasitic transistor parameters)

Many techniques have been used to overcome this effect. The best ways are shown in Figs. 6.2.11–6.2.13.

Resistive Miller Zero Cancellation with a resistor  $R_{M1} = 1/g_{m1}$  is shown in Fig. 6.2.11. The resistor  $R_{M1}$  must attenuate the feed forward path through  $C_{M1}$  by the same amount as by which the  $g_{m1}$  of the output transistor provides gain.

The value of  $R_{M1}$  must be matched with  $1/g_{m1}$ . For large variations in output current resistive Miller Zero Cancellation is poor. For a high current  $R_{M1}$  must be small to match a high  $g_{m1}$ . This means that at low output current the cancellation is not effective, just when it is most needed at a low  $g_{m1}$ . So, this solution functions well when the output transistor is biased in class-A, but is less useful for class-AB biasing.

Another popular solution is Active Miller Zero Cancellation using a cascode transistor  $M_{32}$  in series with the Miller loop, as shown in Fig. 6.2.12 [6.10, 6.11]. The zero cancellation is most needed with CMOS, because of a relatively low  $g_{m1}$ .

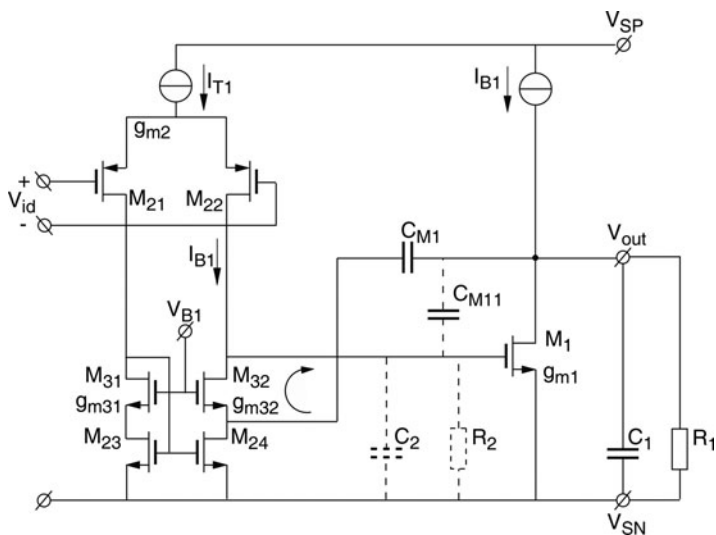
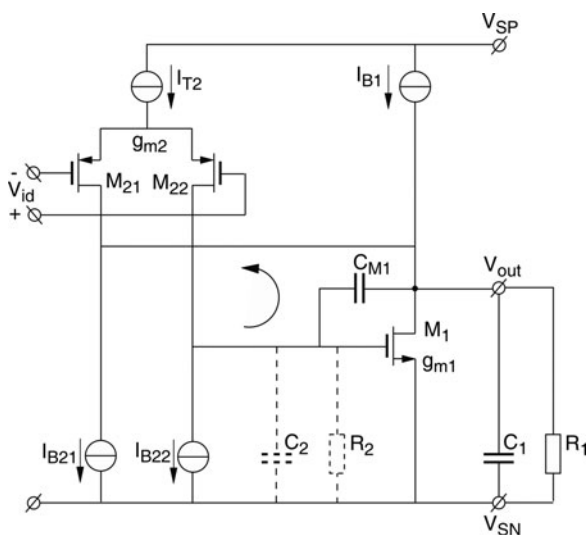


Fig. 6.2.12 Active Miller-zero cancellation with a cascode in series with the Miller loop

Fig. 6.2.13 Multipath Miller-zero cancellation with an additional feed forward path of opposite polarity



With CMOS a cascode is often already present in the input stage for increasing its gain. In Fig. 6.2.12 the mirror in the input stage is cascoded. The cascode has two advantages:

Firstly the Miller feedback circuit has more loop gain, viz.  $C_{M1}/C_2$ , instead of that of the conventional configuration which amounts  $C_{M1}/(C_{M1} + C_2)$ .

This means that the limiting pole frequency  $f'_1$  can be increased by roughly a factor 2 from  $\frac{1}{2}f_{01}$  to  $1f_{01}$ , with  $C_{M1} = C_2$ , or even more [6.10, 6.11]. Hence the bandwidth of the whole amplifier can be a factor 2 larger at the same supply current or even more.

Secondly, the Miller capacitor feeds back to a point at the emitter or source of  $M_{32}$  with a much smaller voltage movement than at the base or gate of the output transistor  $M_1$ . This improves the linearity of the OpAmp in the frequency range where  $C_{M1}$  is active.

However, at high output currents the loop gain can become so high, because of a high  $g_{m1}$ , that the phase margin within the Miller loop, having a second pole at the input of  $M_{32}$  with a value of  $f_3 = g_{m32}/C_{M1}$ , becomes too low. This is particularly the case with CMOS transistors. In that case,  $C_2$  can be intentionally enlarged. Alternatively, we can choose a nested combination of a part of  $C_{M1}$  through the cascode transistor  $M_{32}$  and another part  $C_{M11}$  directly to the gate of  $M_1$ . [6.11]. A ratio of 2 between  $C_{M1}$  and  $C_{M11}$  is usually taken. Note that the cascode stage is capacitive balanced by  $C_{P1} = C_{M1}$  so that there is no pole-zero doublet in the cascode stage at high frequencies.

Finally, the Miller zero can be cancelled by adding a feed forward path across  $C_{M1}$ , as shown in Fig. 6.2.13. This precisely cancels the current at the right-hand side of  $C_{M1}$  which causes the zero of the feed forward path through  $C_M$ . The equal but opposite currents are precisely available at the outputs of  $M_{21}$  and  $M_{22}$  of the differential pair. This technique is called Multipath Miller Zero Cancellation [6.12, 6.13].

A disadvantage of this technique is that this feed forward path is not always available. Nor can its voltage always swing from rail-to-rail.

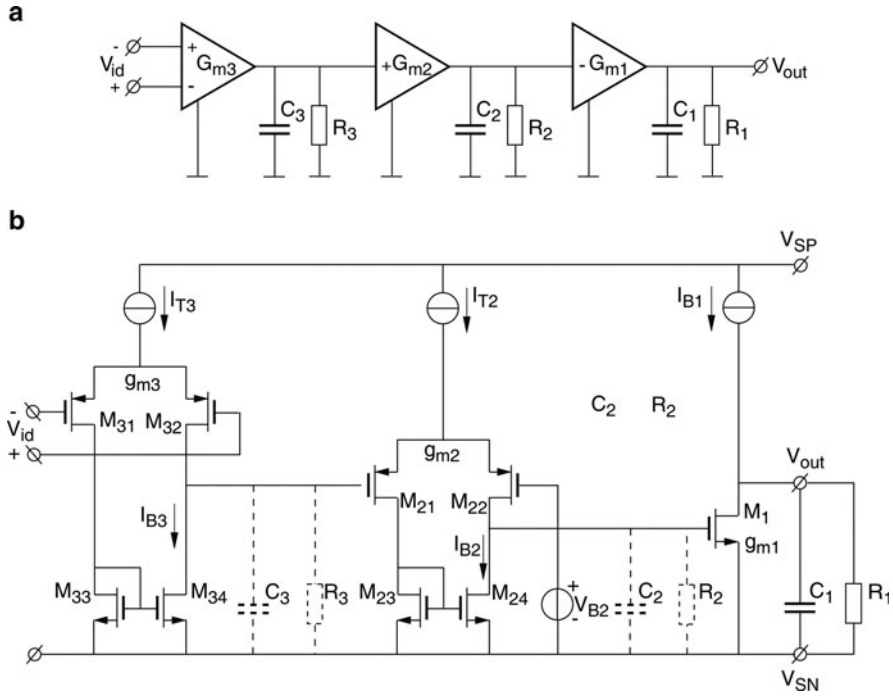
### ***Three-GA-Stage Frequency Compensation***

Figure 6.2.14 shows the basic circuit of a three-GA-stage Operational Amplifier.

The way of frequency compensation of a three-GA-stage Operational Amplifier is to: firstly, compensate the two-stage output and intermediate stages as was done in previous sections by parallel or Miller compensation; and secondly, compensate the whole amplifier again with parallel or Miller compensation as if the intermediate and output stages were one new output stage.

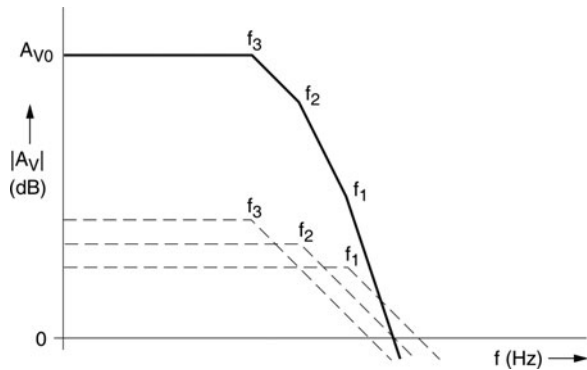
Though parallel compensation may lead to a slightly higher bandwidth over power ratio, its pole-zero cancellation is very dependent on parameter spreading of the IC process and current variations.

Moreover, parallel compensation leads to large compensation capacitors. For these reasons we will only choose the overall Miller compensated structure of an already Miller compensated intermediate and output stage. This is called nested Miller compensation [6.3, 6.14] (Fig. 6.2.14).



**Fig. 6.2.14** (a) Block diagram of three-GA-stage Operational Amplifier. (b) Simplified three-GA-stage Operational Amplifier

**Fig. 6.2.15** Frequency characteristic of the three-GA-stage amplifier of Fig. 6.2.14



### Three-GA-Stage Nested Miller Compensation (NMC)

A nested Miller compensated amplifier is drawn in its basic structure in Fig. 6.2.16 [6.3, 6.14].

We firstly split apart  $f_1$  and  $f_2$  by a regular Miller compensation capacitor  $C_{M1}$  to new positions  $f'_1$  and  $f'_2$ . Next, we split again  $f'_2$  and  $f_3$  apart by a nested Miller

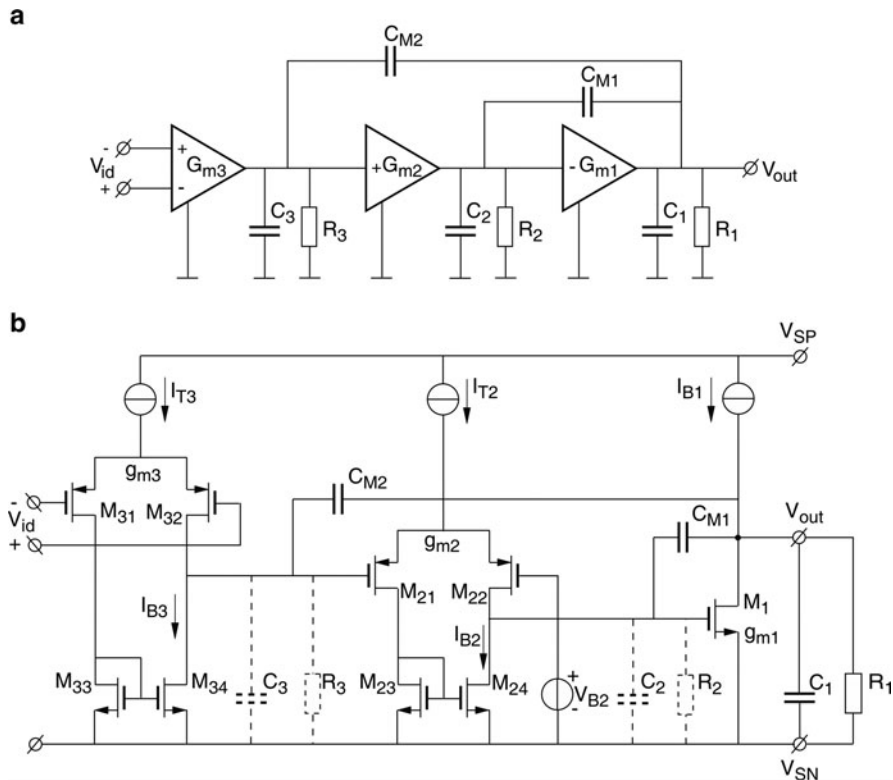


**Fig. 6.2.16** (a) Block diagram of nested Miller compensation of a three-GA-stage Operational Amplifier. (b) Simplified nested Miller compensation of a three-GA-stage Operational Amplifier

compensation capacitor  $C_{M2}$  to final positions  $f''_2$  and  $f'_3$ . The second splitting by  $C_{M2}$  has been made possible by the choice of a non-inverting intermediate stage  $g_{m2}$ .

The combination of a non-inverting intermediate stage  $g_{m2}$  and inverting output stage  $g_{m1}$  results in an inverting two-stage amplifier combination, which can be compensated by a nested Miller capacitor  $C_{M2}$  again. The frequency characteristic is shown in Fig. 6.2.17.

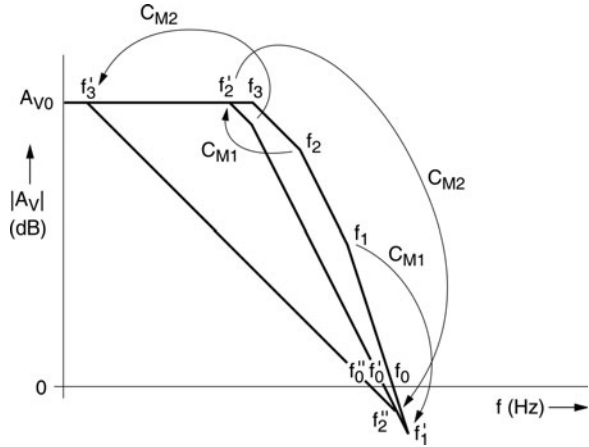
The choices of Miller Capacitors  $C_{M1}$  and  $C_{M2}$  are determined by the limiting pole frequency  $f'_1$ , which amounts again:

$$f'_1 = \frac{g_{m1}}{2\pi C_1} \tag{6.2.29}$$

The 0 dB bandwidth  $f'_0$  of the intermediate and output stage must be taken half of  $f'_1$  for a 60° phase margin:

$$f'_0 = \frac{1}{2}f'_1 \tag{6.2.30}$$

**Fig. 6.2.17** Frequency characteristics of the nested Miller compensated three-GA-stage Operational Amplifier of Fig. 6.2.16



From this the value of  $C_{M1}$  follows as:

$$C_{M1} = \frac{g_{m2}}{2\pi f'_0} \quad (6.2.31)$$

$C_{M1}$  must be calculated at the lowest value of the bias current  $I_{B1}$  through  $M_1$  at which  $g_{m1}$  is minimal and at the highest value of the load capacitance  $C_l$ . Next we split again by the outer Miller capacitor  $C_{M2}$ . The 0 dB bandwidth  $f''_0$  of the whole amplifier must be again taken half of  $f'_0$  for a  $60^\circ$  phase margin:

$$f''_0 = \frac{1}{2}f'_0 = \frac{1}{4}f'_1 \quad (6.2.32)$$

From this the value of  $C_{M2}$  follows as:

$$C_{M2} = \frac{g_{m3}}{2\pi f''_0} \quad (6.2.33)$$

The low-frequency gain  $A_{v0}$  and the dominating pole frequency  $f'_3$  are:

$$A_{v0} = g_{m3}R_3g_{m2}R_2g_{m1}R_1 \quad (6.2.34)$$

$$f'_3 = f''_0/A_{v0} \quad (6.2.35)$$

Nested Miller compensation is a robust way to compensate a three-GA-stage Operational Amplifier. The load capacitor  $C_l$  may be chosen smaller than the upper supposed value, but not larger.

No pole-zero cancellation techniques are needed. An abundance of gain can be obtained with three GA stages. The penalty is that the bandwidth is half that of the version with two GA stages and that we need extra current for the input stage.

An optimal choice for the currents of the three stages is roughly determined by:

$$f_{03} = \frac{1}{2}f_{02} = \frac{1}{4}f_{01}, \quad \text{or} \quad (6.2.36)$$

$$\frac{g_{m3}}{2\pi C_3} = \frac{1}{2} \frac{g_{m2}}{2\pi C_2} = \frac{1}{4} \frac{g_{m1}}{2\pi C_1} \quad (6.2.37)$$

So, the contribution to the total supply current of the current of the input stage is relatively low. And the bandwidth over power ratio is about two times lower than that of the two-GA-stage amplifier.

### ***Three-GA-Stage Multipath Nested Miller Compensation (MNMN)***

A way to regain the factor 2 again is to use the multipath nested Miller compensated (MNMN) circuit of Fig. 6.2.18. [6.14, 6.15].

The circuit has a second input stage with a transconductance of  $g_{m32}$ , additional to the first input stage with  $g_{m31}$ . The second input stage forms an independent parallel path across the first input stage and intermediate stage. The output of the second input stage is connected to the input of the output stage. In fact, we have an additional two-stage amplifier in parallel to a three-stage amplifier. At low frequencies the three-stage amplifier dominates by its large low-frequency gain. But at high frequencies the two-stage amplifier dominates. In the middle range both paths have equal transfer functions, without adding their transfers. Adding would have resulted in a pole-zero doublet. Adding would have happened if we had a simple capacitive parallel path across the intermediate stage, for example as in the NE5534 (see Sect. 7.6). The intermediate stage  $g_{m2}$  allows for a separation between the two paths if its transconductance is relatively weak, as expressed by (6.2.44), or if we artificially increase the parasitic ground capacitance  $C_3$  at the input of  $G_{m2}$ . The internal feedback loop around  $G_{m2}$  through  $C_{M2}$  suppresses the two-stage's frequency characteristic from the dominating pole frequency  $f'_3$  up to  $f''_2$ , where that loop breaks down because of lack of gain, and the two-stage amplifier takes over [6.26]. The separation of the two paths makes it possible that we obtain a straight frequency characteristic under the condition that the mid-range gains of the three-stage path  $g_{m31}/C_{M2}$  and that of the two-stage path  $g_{m32}/C_{M1}$  are equal, as expressed by (6.2.41).

The frequency characteristics of MNMN are drawn in Fig. 6.2.19. The main requirement is that the two-stage and three-stage amplifier's amplitude characteristics touch each other at mid range so that one takes over from the other without pole-zero doublet, independent from the load capacitor  $C_L$ .



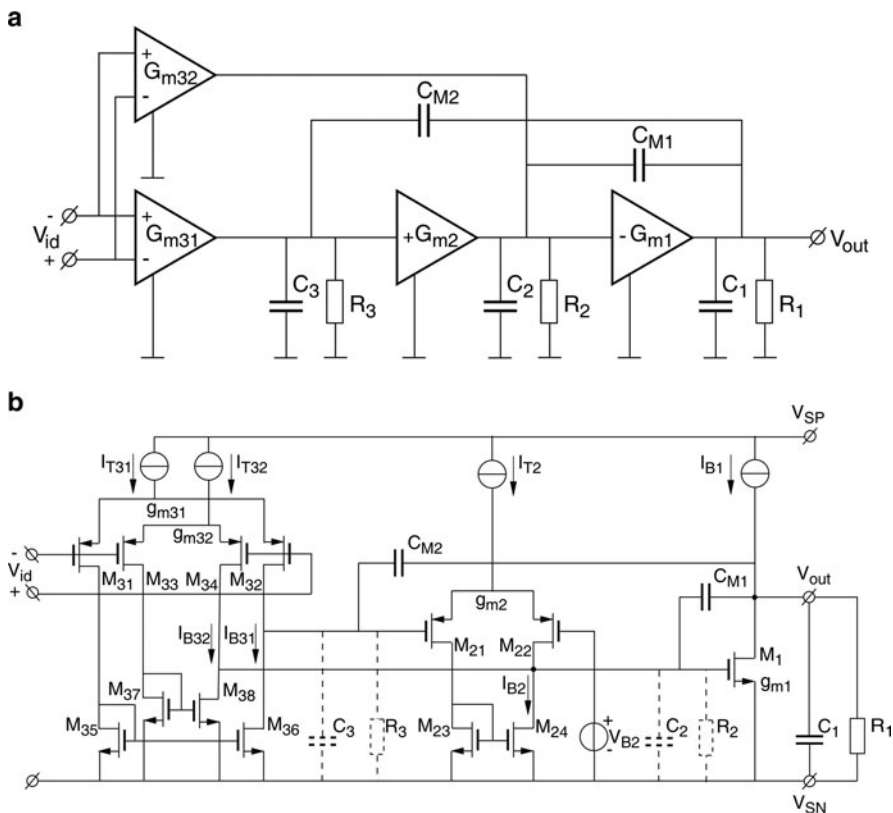


**Fig. 6.2.18** (a) Block diagram of multipath nested Miller compensation of a three-GA-stage Operational Amplifier. (b) Simplified multipath nested Miller compensation of a three-GA-stage Operational Amplifier

This leads to the following relations and choices:

$$f'_1 = \frac{g_{m1}}{2\pi C_1} \quad (6.2.38)$$

$$f'_0 = \frac{1}{2}f'_1 \quad (6.2.39)$$

$$C_{M1} = \frac{g_{m32}}{2\pi f'_0} \quad (6.2.40)$$

$$f''_0 = f'_0 = \frac{1}{2}f'_1 \quad (6.2.41)$$

$$C_{M2} = \frac{g_{m31}}{2\pi f''_0} \quad (6.2.42)$$

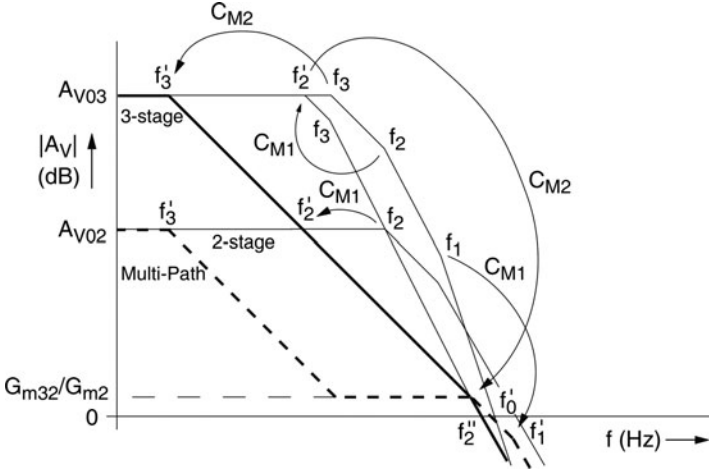


**Fig. 6.2.19** Frequency characteristics of a multipath nested Miller compensated (MNMC) three-stage Operational Amplifier

$$f'_3 = f''_0 / A_{v0} \tag{6.2.43}$$

$$g_{m2} < \frac{1}{3} g_{m32} \tag{6.2.44}$$

The limiting pole frequency  $f'_1$  is set again by the output stage according to (6.2.38). The 0 dB bandwidth  $f'_0$  is chosen half of  $f'_1$ . The additional input stage with  $g_{m32}$  and  $f'_0$  is compensated as if it were the first stage of a two-stage amplifier combination with  $C_{M1}$  according to (6.2.40).

The original input stage with  $g_{m31}$  is now compensated with  $C_{M2}$  according to (6.2.42), at the same 0 dB frequency  $f'_0$  as  $g_{m32}$  with  $C_{M1}$  has been done. This implies that the compensated characteristics of the two and three-stage amplifiers touch each other for a wide frequency range. At the high frequency end the two-stage amplifier extends up to the limiting pole frequency  $f'_1$ . At low frequencies the three-stage amplifier goes down to  $f'_3 = f'_0 / A_{v0}$ . The overall characteristic is straight from  $f'_1$  down to  $f'_3$  with a 6 dB/oct roll-off. There is no summing of the two characteristics in the middle range because of the independent nature of the two characteristics separated by a weak  $g_{m2}$ . The two-stage amplifier must have a 0 dB frequency  $f'_0 \approx g_{m32} / 2\pi C_{M1}$  equal to that of the three-stage amplifier  $f'_0 \approx g_{m31} / 2\pi C_{M2}$ .

The matching of  $g_{m31} / C_{M2} = g_{m32} / C_{M1}$  determines the pole-zero cancellation in the overall characteristic. Accurate matching can be realized because  $C_{M2}$  and  $C_{M1}$  can be made by the same type of integrated MOS capacitors, and  $g_{m31}$  and  $g_{m32}$  are the result of two equal stages, biased with equal current sources.

The accurate controllable matching of the two characteristics in IC technology is a major advantage of the multipath nested Miller compensation technique over other pole-zero cancellation schemes.

The value of  $g_{m2}$  of the intermediate stage is still undetermined. We want the frequency characteristic to be determined by the second input stage  $g_{m32}$  at the 0 dB frequency  $f'_0$  and not by the intermediate stage  $g_{m2}$ . For this reason we take  $g_{m2} < g_{m32}$ , as prescribed by (6.2.44). Later, at Fig. 6.2.24 we will see that a quenching capacitor  $C_3$  at the input of  $g_{m2}$  to ground can be used to solve this issue.

The result is a three-stage OpAmp with a large amount of gain and nearly the same bandwidth over power ratio as the two-stage Miller compensated Operational Amplifier. The extra costs are the addition of the second input stage and its addition to the supply power.

### ***Four-GA-Stage Frequency Compensation***

When we need more gain we can add a fourth stage or even more stages. The question is how to compensate these stages reliably. Besides parallel compensation, which becomes very impractical with four or more stages, the nested Miller compensation method can be extended. However, without multipath, we lose a factor 2 in bandwidth each time we nest. With many multipaths the circuit becomes complex. For instance, with a four-stage amplifier, already three input stages are needed in front of the circuit of Fig. 6.2.18. To simplify the nesting, and not lose a factor 2 each nest, we can use hybrid nested Miller compensation.

### ***Four-GA-Stage Hybrid Nested Miller Compensation (HNMC)***

The circuit of a hybrid nested Miller compensated (HNMC) four-GA-GA-GA-GA stage Operational Amplifier is shown in Fig. 6.2.20 [6.16, 6.13]. The circuit is maximally simple for a four-stage amplifier because no differential stages are needed for the second and third stage.

The driving of the output stage can nearly be done from rail-to-rail. No cascodes are needed because there is an abundance of gain. This means that this HNMC is suitable for the lowest possible supply voltage with one  $V_{GS}$  plus one  $V_{SAT}$  [6.16].

Three invertors are connected in cascade: The first and second stages, counted from the output, are compensated by the Miller capacitor  $C_{M1}$ . The new pole positions  $f_1$  and  $f_2$  are split to  $f'_1$  and  $f'_2$ .

The third and fourth stages with  $f_3$  and  $f_4$  are split by the Miller capacitor  $C_{M3}$  into the new pole positions  $f'_3$  and  $f'_4$ . The frequency characteristics are drawn in Fig. 6.2.21. The two two-stage Miller-compensated amplifiers  $g_{m1,2}$  and  $g_{m3,4}$  are cascaded into one amplifier with two dominating poles  $f'_2$  and  $f'_4$ . The phase of the

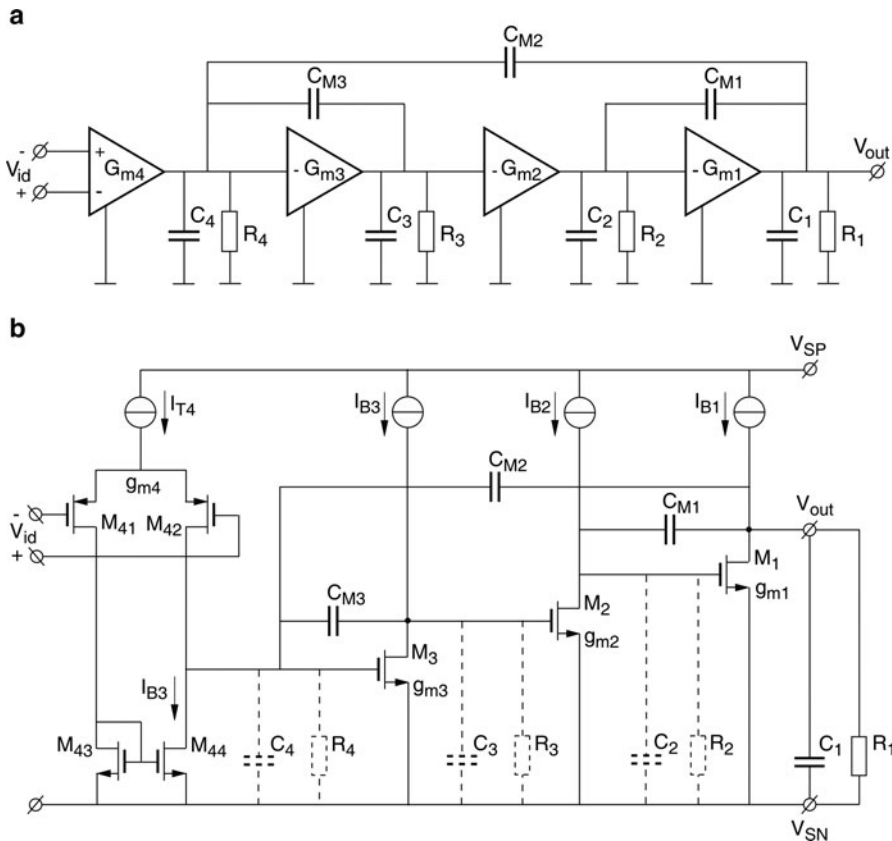


**Fig. 6.2.20** (a) Block diagram of hybrid nested Miller compensated four-GA-stage Operational Amplifier. (b) Simplified hybrid nested Miller compensated four-GA-stage Operational Amplifier

three cascaded inverting amplifiers is just right so that the poles  $f'_2$  and  $f'_4$  can be split by an overall Miller capacitor  $C_{M2}$  into the final pole positions  $f''_2$  and  $f''_4$ . The following choices have been made:

The limiting-pole frequency  $f'_1$  is:

$$f'_1 = \frac{g_{m1}}{2\pi C_1} \tag{6.2.45}$$

The 0 dB frequency  $f'_0$  of the driver and output stage multiplied by the loop gain  $C_{M2}/C_{M3}$  of the intermediate inverting stage  $M_3$  must be half  $f'_1$ , so:

$$f'_0 \frac{C_{M2}}{C_{M3}} = \frac{1}{2} f'_1 \tag{6.2.46}$$

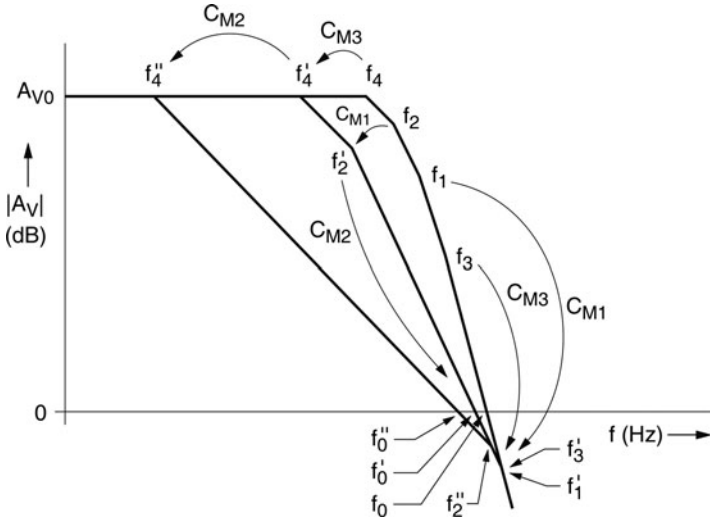


**Fig. 6.2.21** Frequency characteristics of hybrid nested Miller compensated four-GA-stage Operational Amplifier

This leads to the choice of  $C_{M1}$ :

$$\frac{g_{m2}}{2\pi C_{M1}} \frac{C_{M2}}{C_{M3}} = \frac{1}{2} f'_1 \tag{6.2.47}$$

This is only true if the limiting pole frequency  $f'_3$  of the intermediate inverting stage  $M_3$  is equal or larger than  $f'_1$ , which means a choice for  $g_{m3}$ :

$$\frac{g_{m3}}{2\pi C_{M2}} \geq f'_1 \tag{6.2.48}$$

The overall bandwidth  $f''_0$  must be taken a quarter of  $f_1$ , hence:

$$f''_0 = \frac{1}{4} f'_1 \tag{6.2.49}$$

This leads to a choice for  $C_{M2}$ :

$$\frac{g_{m4}}{2\pi C_{M2}} = \frac{1}{4} f'_1 \tag{6.2.50}$$

The hybrid nested Miller compensation is a robust way to handle the stability of a four-GA-stage Operational Amplifier. The 0 dB bandwidth is four times lower than that of the limiting-pole frequency  $f'_1 = g_{m1}/2\pi C_1$ , of the output stage and its capacitive load. The load capacitor  $C_1$  may be taken smaller, but not larger than given by the above formulas.

### Four-GA-Stage Multipath Hybrid Nested Miller Compensation (MHNMC)

We can improve the bandwidth of the HNMC amplifier with a factor 2 if we add a multipath input stage according to the multipath hybrid nested Miller compensated (MHNMC) amplifier of Fig. 6.2.22 [6.16, 6.13].

In that case, we do not have to take the 0 dB bandwidth  $f''_0$  of the whole amplifier a quarter of  $f'_1$  but equal to half  $f'_1$ . So the overall 0 dB bandwidth  $f''_0$  becomes equal to half  $f'_1$ , without losing a factor 2:

$$f''_0 = \frac{1}{2}f'_1 \tag{6.2.51}$$

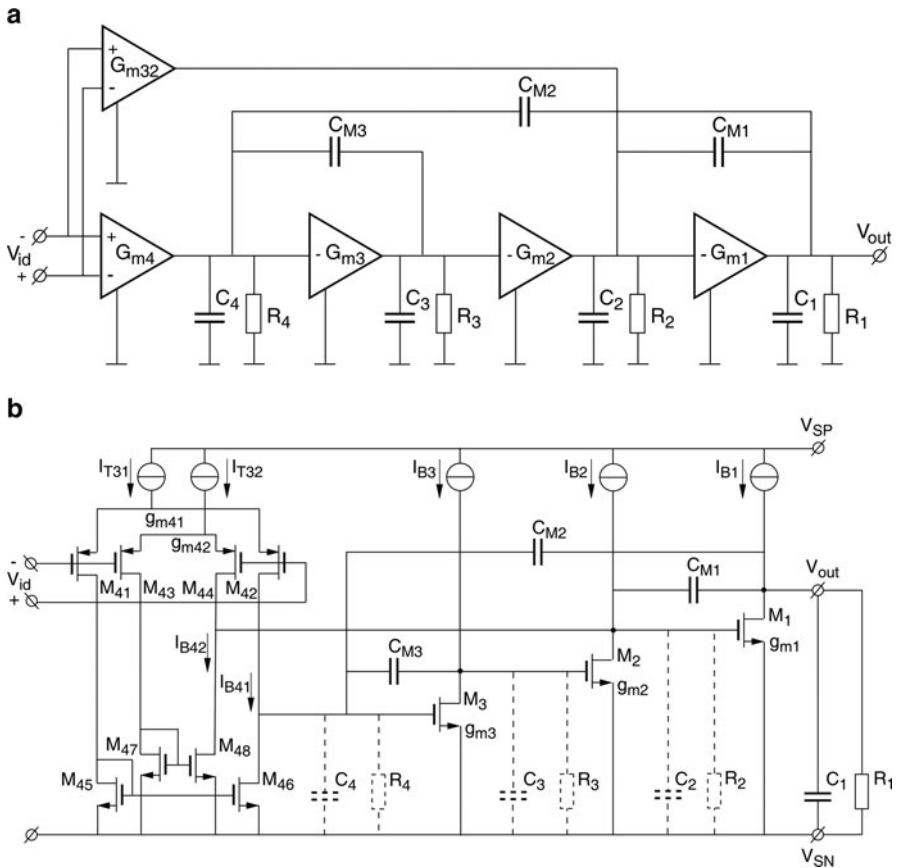


Fig. 6.2.22 (a) Block diagram of multipath hybrid nested Miller compensated four-GA-stage Operational Amplifier. (b) Simplified multipath hybrid nested Miller compensated four-GA-stage Operational Amplifier

This leads to the choice for  $C_{M2}$ :

$$\frac{g_{m41}}{2\pi C_{M2}} = \frac{1}{2}f'_1 \tag{6.2.52}$$

Further, domination of the HF path by the gain path should be prevented at high frequencies. This means that the gain through the driver stage must be lower than that of the direct path. This leads to the choice:

$$\frac{C_{M2}}{C_{M3}} \frac{g_{m2}}{2\pi C_{M1}} \leq \frac{1}{3} \frac{g_{m42}}{2\pi C_{M1}} \tag{6.2.53}$$

This also means that the limiting-pole frequency  $f'_3$  of the intermediate stage may be lower:

$$\frac{g_{m3}}{2\pi C_{M2}} \leq \frac{1}{3}f'_1 \tag{6.2.54}$$

The gain reduction of the driver and intermediate stage can be prevented by using a quenching capacitor to ground, as we will see with Fig. 6.2.25.

Finally, we must match the 6 dB roll-off of the gain path with that of the HF path, in order to avoid a pole-zero doublet. This leads to the important choice of:

$$\frac{g_{m41}}{2\pi C_{M2}} = \frac{g_{m42}}{2\pi C_{M1}} \tag{6.2.55}$$

The frequency characteristics are shown in Fig. 6.2.23. The result is a robust compensated four-stage amplifier with an abundance of gain and nearly the same

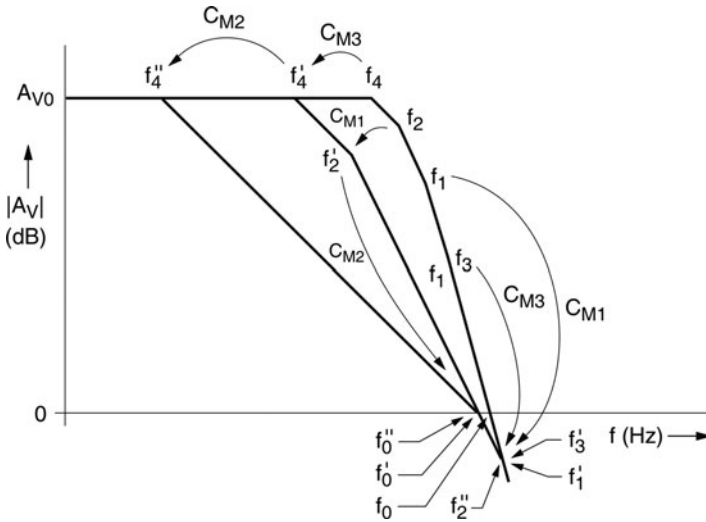


**Fig. 6.2.23** Frequency characteristic of the multipath hybrid nested Miller compensated four-GA-stage Operational Amplifier

bandwidth over supply power ratio as the two-stage Miller compensated amplifier. Only the currents of the third and fourth stages add to the supply power consumption.

### ***Four-GA-Stage Conditionally Stable MHNMC***

An interesting simplification can be made of the MHNMC amplifier. If we eliminate  $C_{M2}$ , a conditionally stable MHNMC amplifier arises [6.13]. This can be of advantage in audio amplifiers to increase the loop gain of the feedback amplifier up to 20 kHz for a lower distortion, while a slow settling component can be tolerated. The gain is allowed to roll off above the 20 kHz at a higher rate than 6 dB/oct. In this case it is 12 dB/oct. However, at the 0 dB frequency this must be slowed down again to 6 dB/oct. The independent nature of the multipath makes that this can be robustly realized, only depending on the multipath parameters. The frequency characteristic of the conditionally stable MHNMC amplifier without  $C_{M2}$  can be derived from Fig. 6.2.23.

Starting with the DC gain flat from the right until  $f'_4$ , then with 6 dB/oct down until  $f'_2$ , following with 12 dB/oct down until it hits the curve of the compensated two-stage amplifier  $g_{m42}/2\pi C_{M1}$ , which equals the overall characteristic of the MHNMC amplifier. The overall characteristic is determined in this range by the second input stage  $g_{m42}$  and the output stage which take the frequency response down by 6 dB/oct through the 0 dB line.

### ***Multi-GA-Stage Compensations***

Many variations and combinations can be made in the HF compensation of Operational Amplifiers. With MNMC and MHNMC more than four stages can reliably be compensated without too much loss in bandwidth over power ratio [6.13].

### ***Compensation for Low Power and High Capacitive Load***

Low power consumption in combination with high capacitive load becomes more important in many cases than a straight 6 dB per octave open-loop frequency response with fast settling close-loop behaviour. Particularly in low-frequency applications, low-dropout power regulators and headphone amplifiers with unpredictable high capacitive load a low quiescent current consumption is very important.



In the previous Miller compensated amplifiers a phase margin of  $60^\circ$  was required for fast settling. This implied an output stage with enough current to allow a capacitive load  $C_l$  at the limiting pole frequency  $f'_l$ , according to:

$$f'_l = \frac{g_{ml}}{2\pi C_l} \quad (6.2.56)$$

A first relieve is that we may lower the limiting pole frequency of the output transistor and thus its current consumption if there is a high closed-loop gain  $A_{v0}$ . If we know that the closed-loop gain is not unity but higher, the bandwidth is lower and we can lower the limiting-pole frequency of the output stage in a two-stage Miller compensated amplifier.

### ***Active Miller Compensation***

But what happens with the stability when we do not obey the rules at all? Let we again look at the two-stage active Miller compensated amplifier of Fig. 6.2.24a.

Suppose we give the output stage of the OpAmp enough current for a phase margin  $S$  of  $60^\circ$  at a capacitive load  $C_l$  of 30 pF and a limiting pole frequency  $f'_l$  of 2 MHz, so that the bandwidth  $f'_o$  for unity gain stability is 1 MHz according to (6.2.18). If we now increase the load capacitor  $C_l$  the phase margin will decrease. But, if we increase the load capacitor further the phase margin will increase again. The situation is sketched in Fig. 6.2.24b.

According to [6.17] the minimum phase margin  $S_{Min}$  obeys the following rule:

$$S_{Min} = \frac{4}{g_{m2}R_2} \frac{C_{M1}}{C_2} \quad (6.2.57)$$

If the voltage gain  $A_{v2} = g_{m2}R_2$  of the input stage is 10 and if the ratio  $C_{M1}/C_2$  is 50, the phase margin will not get below about  $20^\circ$ . This result is even independent of  $g_{ml}$  and hence independent of the current consumption of the output transistor  $M_l$ . The bandwidth will reduce, though.

### ***RC or Distributed RC Compensation Network***

The reduction of the voltage gain of the input stage is a disadvantage, as this reduces the loop gain and the accuracy. To allow more gain in the input stage a resistor  $R_{M1}$  can be inserted in series with  $C_{M1}$ , as shown in the Low-Drop-Out amplifier [6.18] of Fig. 6.2.25a. The resulting phase margin with a resistor  $R_{M1}$  in series with  $C_{M1}$  is shown in Fig. 6.2.25b.

The best result is obtained when  $R_{M1}$  is chosen  $0.5xR_2$ . Still there are two points where the phase margin is low, about  $20^\circ$ . The phase margin can be further

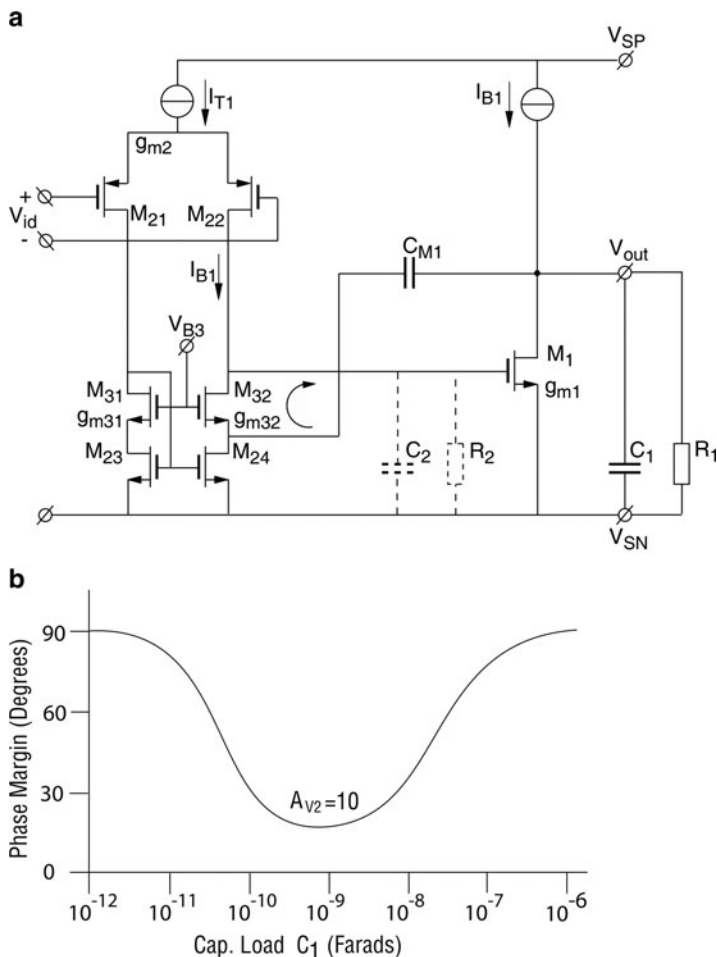


**Fig. 6.2.24** (a) Two-stage active Miller compensated OpAmp. (b) Phase Margin versus load capacitance for an active Miller-compensated OpAmp with a voltage gain  $A_{V2}$  of 10 of the input stage

improved by using a distributed  $R_{MI}C_{MI}$  network. This result is also shown in Fig. 6.2.25b. Theoretically, the phase margin does not sink below  $45^\circ$ . The main idea is to obtain a frequency characteristic with 3 dB per octave roll-off over a wide frequency range.

In our search for a combination of high gain and stability at high capacitive load or to lower current consumption of the output stage we now look at the three-stage OpAmp. By itself the nested Miller compensated OpAmp can not be made stable for a wide range of load capacitances at a low bias current of the output transistors. The reason is that, if the limiting pole frequency  $f'_1 = g_{m1}/2\pi C_1$  falls within the frequency band where the closed-loop gain of the amplifier is higher than one, the nested Miller compensation around the output stage breaks down.

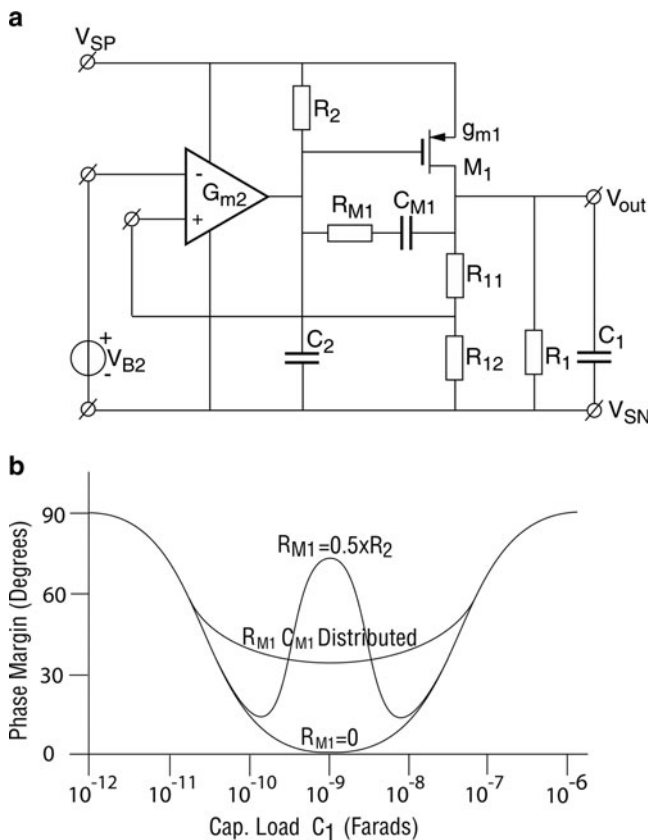


**Fig. 6.2.25** (a) Low-Drop-Out regulator with a resistor  $R_{M1}$  in series with  $C_{M1}$  or with a purposefully distributed  $R_{M1}C_{M1}$  network. (b) Phase margin as a function of the load capacitance of a Low-Drop-Out regulator of Fig. 6.2.25a with a resistor  $R_{M1} = 0.5xR_2$  in series with  $C_{M1}$  or with a distributed  $R_{M1}C_{M1}$  network

However, if we are able to reduce the three-stage amplifier into a two-stage amplifier for high frequencies then the compensation can fall back on the two-stage stability presented above. Two solutions will be presented in the following: one with pole-zero damping of the intermediate stage and one with high-frequency quenching of the intermediate stage in a multipath topology.

### ***Damping Compensation Network***

Several solutions with damping of the intermediate stage by pole-zero cancellation schemes have been proposed to stabilize three-stage amplifiers with high capacitive load at low quiescent currents. Important ones are described in [6.19, 6.20]. But

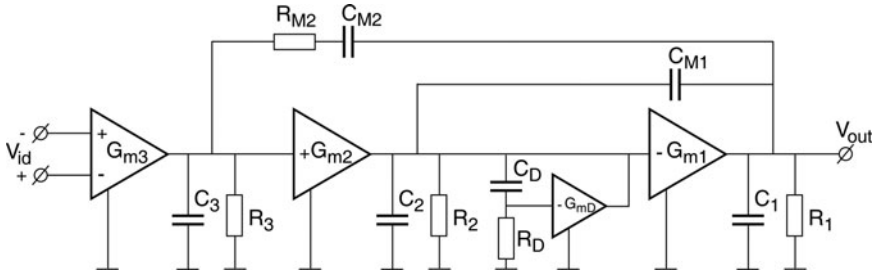


**Fig. 6.2.26** Three-stage nested Miller compensated OpAmp with damping network

they are designed for a certain range of the load capacitances and may become unstable when loaded by a small capacitance. In [6.21] a solution is presented where the gain of the intermediate stage is reduced and made broadband by a pole-zero damping network  $R_D, C_D$ , and  $g_{mD}$ . That solution is depicted in Fig. 6.2.26.

The inner-nested Miller capacitor  $C_{M1}$  is made inactive by the low impedance of the damping network. The outer Miller capacitor  $C_{M2}$  takes the place of a single Miller compensation capacitor. Only for small capacitive loads, where the gain of the output stage is high, the inner-nested Miller capacitor  $C_{M1}$  comes into functioning again. Hence the circuit largely mimics a two-stage amplifier at high frequencies that can be made stable for all capacitive loads either by limiting the gain of  $g_{m3}$ , or a resistor  $R_{M2}$  in series with  $C_{M2}$ , or by the use of a distributed  $R_{M2}C_{M2}$  network, as described before. The following choices have been made:

$$f''_0 = \frac{g_{m3}}{2\pi C_{M2}} = f'_0 = \frac{g_{m2}}{2\pi C_{M1}} = \frac{1}{2}f'_1 = \frac{1}{2} \frac{g_{m1}}{2\pi C_1} \tag{6.2.58}$$

$$\frac{1}{2} \frac{1}{2\pi R_D C_2} = \frac{g_{m2}}{2\pi C_{M1}} = \frac{1}{2}f'_1 \tag{6.2.59}$$

### Quenching Capacitor Network

The next solution is the multipath nested Miller compensated three-stage amplifier that can be made stable by itself. The multipath two-stage path makes the three-stage path stable when we quench the three-stage path by a quenching capacitor  $C_Q$  to ground in parallel with  $C_3$  [6.22], so that the two-stage path is dominating at high frequencies, see Fig. 6.2.27a, b.

For the two-stage path the same measures have to be taken as explained above. These either pose a limitation on the voltage gain of  $G_{m32}$ , or let us insert a resistor  $R_{M1}$  in series with  $C_{M1}$ , or use a distributed  $R_{M1}C_{M1}$  network.

If the transconductance  $g_{m31}$  is large the quenching capacitor  $C_Q$  may also become large for high capacitive loads. This disadvantage is not present in the four-stage hybrid nested Miller compensated amplifier of Fig. 6.2.28.

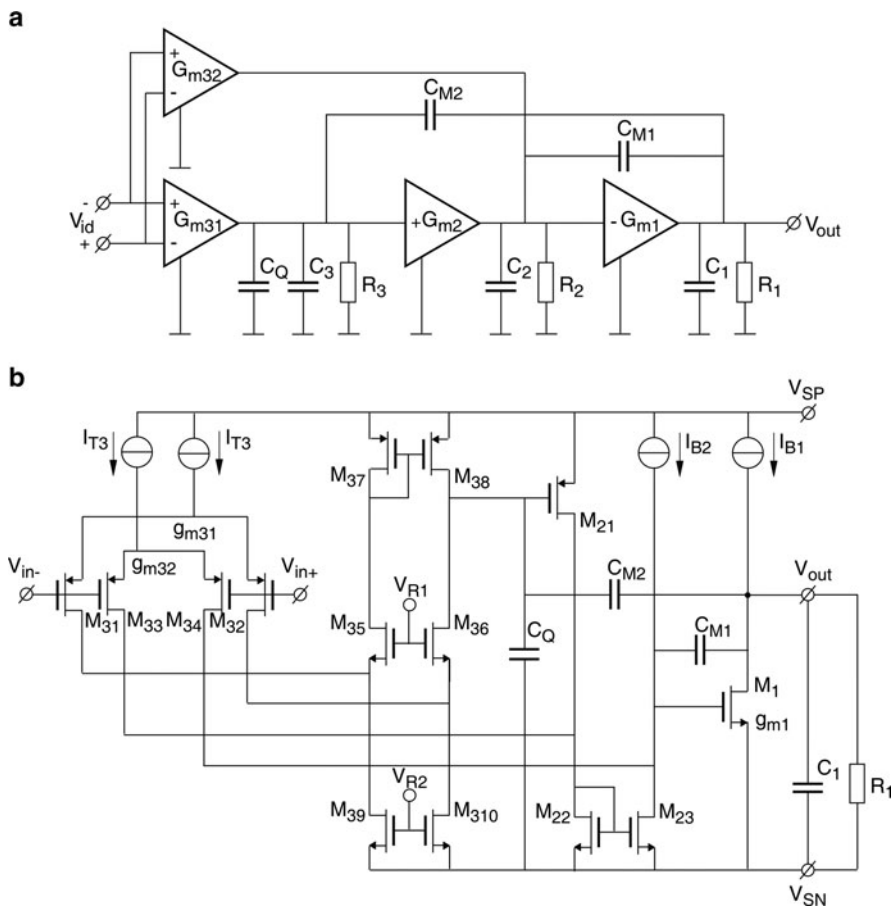


**Fig. 6.2.27** (a) Block diagram of a multipath nested Miller compensation with quench capacitor  $C_Q$  that can be made stable for all capacitive loads. (b) Circuit for a multipath nested three-stage OpAmp with a quenching capacitor  $C_Q$  to ground at the input of the intermediate stage  $M_{21}$  of the three-stage gain path

The most important result of the quenched multipath three-stage solution is that we do not anymore have to lower the transconductance of the intermediate stage  $g_{m2}$  as required earlier in formula (6.2.44). We just use a small quench capacitor  $C_Q$  in any multipath three-stage amplifier to allow a large  $g_{m2}$  of the intermediate stage and make it more stable at high load capacitances.

A circuit for a multipath nested three-stage OpAmp that has a minimum phase margin of  $20^\circ$  for all capacitive loads with a relative small voltage gain of  $g_{m32}$  is shown in Fig. 6.2.27b.

In search for more gain the Multipath Hybrid Nested Miller compensation of a four-stage OpAmp is a good candidate for stability at all capacitive loads if we use a quenching capacitor  $C_Q$  [6.22] across  $C_{M3}$ , as shown in Fig. 6.2.28.

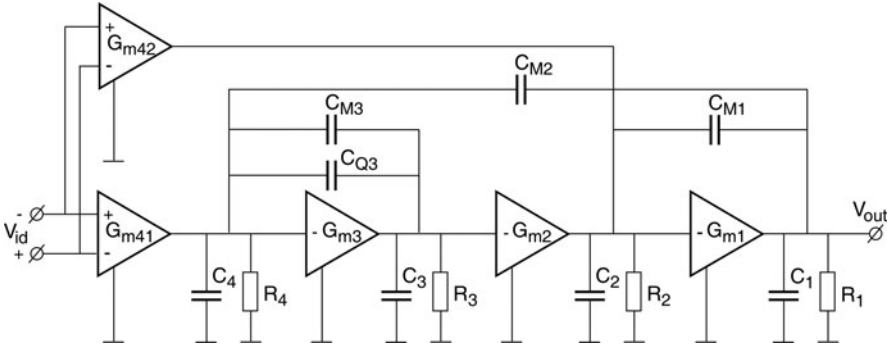


**Fig. 6.2.28** Block diagram of a multipath hybrid nested four-stage OpAmp with a quenching capacitor  $C_Q$  across  $C_{M3}$  that is stable for all capacitive loads

The circuit has a minimum phase margin of  $20^\circ$  for all capacitive loads if the voltage gain of  $g_{m42}$  is restricted. The phase margin can be improved by using a resistor  $R_{M1}$  in series with  $C_{M1}$  or a distributed  $R_{M1}C_{M1}$  network. The quenching capacitor is now part of the Hybrid Nested Miller Compensation scheme across  $g_{m3}$  which amplifies the influence of the quenching capacitor. Therefore it can be taken smaller for the same task than the quenching capacitor to ground in the three-stage amplifier. Stability requirement for normal capacitive loads was already indicated by Eq. 6.2.53. But now  $C_{M3}$  is further increased by  $C_Q$  to obtain stability for all capacitive loads and for a larger  $g_{m2}$ .

***Reversed Nested Miller Compensation (RNMC) for Low Power and High Capacitive Load***

A most interesting way of compensation is the forward nested Miller compensation (RNMC) in which high load capacitances can be facilitated at low quiescent current and low power [6.13] under certain conditions. In the original patent of 1985 [6.23] this method was called Forward Nested Miller Compensation (FNMC). With reverse or forward nesting a stage close to the input stage is used as the centre of nesting, while the nesting is extended in the direction to the output. An example is RNMC around the inverting intermediate stage of a three-GA-stage amplifier. The situation is sketched in Fig. 6.2.29a.

The strength of this architecture for heavy capacitive loads is based on two attitudes: Firstly, to the capacitive load it looks like a two-stage amplifier with one Miller capacitor  $C_{M1}$ . As we have seen earlier this one can be made suitable for a large capacitive load in regard to the quiescent current of the output stage. Secondly, the intermediate stage makes extra loop gain around the output stage to boost its limiting pole frequency if the ratio  $C_{M1}/C_{M2}$  larger than 1. It can be easily seen that the intermediate stage is connected in a feedback loop around the output stage as an inverting amplifier with input impedance  $C_{M1}$  and feedback impedance  $C_{M2}$ .

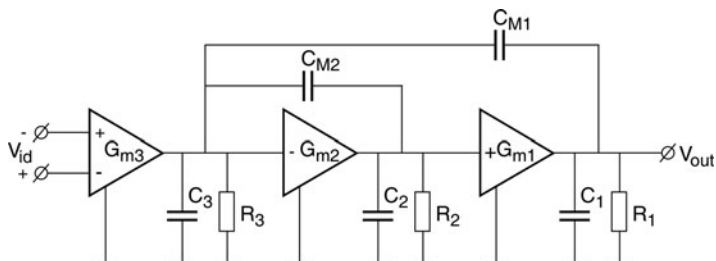


**Fig. 6.2.29** Block diagram of a reverse or forward nested Miller compensated three-stage OpAmp

The limiting pole frequency  $f'_2 = g_{m2}/2\pi C_2$  is now situated at the output of the intermediate stage. This pole is not loaded by the output capacitance. Hence, the limiting pole frequency can be high at a low current consumption of the intermediate stage. The limiting pole frequency is:

$$f'_2 = g_{m2}/2\pi C_2 \quad (6.2.60)$$

For  $60^\circ$  phase margin the outer Miller capacitor  $C_{M1}$  must be taken as given in (6.2.61):

$$f'_1 = \frac{1}{2} C_{m1} g_{m1} / C_{m2} 2\pi C_1 \quad (6.2.61)$$

In [6.24] the topology of a three-stage RNMC is presented in which refinements are introduced to facilitate high capacitive load at low current consumption. The topology is shown in Fig. 6.2.30a, b.

A voltage buffer  $A_v$  with a voltage gain of 1 is inserted in the inner Miller loop in order not to load the intermediate stage by the capacitor  $C_{M2}$ . Therefore the HF gain of the intermediate stage stays high. Further two resistors  $R_{M1}$  and  $R_{M2}$  have been inserted to null right-hand-plane zeros and to improve phase margin. Potentially, this topology is able to facilitate stability at all capacitive load.

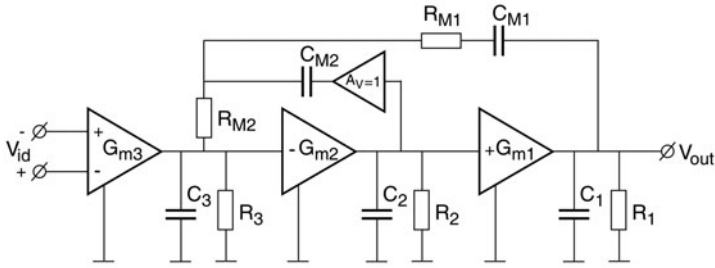
A transistor circuit diagram of this topology [6.25] is shown in Fig. 6.2.30b.

The circuit has a bandwidth of 3 MHz with phase margin of  $70^\circ$  at a load capacitor  $C_l$  of 1 nF while it only consumes 33  $\mu\text{A}$ . Thanks to the feed forward path through  $M_{22}$  the amplifier gets a pseudo class-AB biasing with a negative slew-rate as large as the positive slew-rate of nearly 2 V/ $\mu\text{V}$ .

## Conclusion

We have seen that frequency compensation is needed with amplifiers having more than one stage. Parallel compensation leads to the highest bandwidth over supply-power ratio. However, strong pole-zero doublets can be expected, because of

**a**



**b**

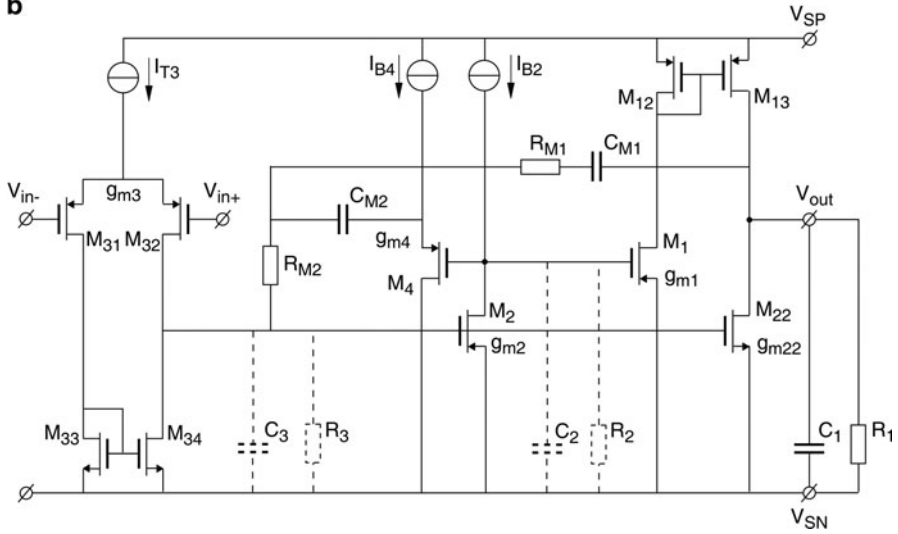


**Fig. 6.2.30** (a) Topology of a reverse nested Miller compensated three-stage OpAmp with voltage buffer and nulling resistors  $R_{M1}$  and  $R_{M2}$ . (b) Circuit diagram of a reverse nested Miller compensated three-stage OpAmp with voltage buffer and nulling resistors  $R_{M1}$  and  $R_{M2}$

unmatched IC process parameters. This makes parallel compensation unfit for amplifiers used to obtain a fast step response without slow settling components. Miller compensation is very robust and has by nature no pole-zero doublets. However, with normal Miller compensation the bandwidth is limited by that of the output stage and its capacitive load. Derivations of normal Miller compensation (MC), such as NMC, MNMC, HNMC, and MHNMC for amplifiers with more than two-GA-stages can successfully be compensated without losing too much of the bandwidth over power ratio. For a combination of high capacitive load and low power consumption several techniques can be used, such as a distributed RC network in combination MC of a two-stage amplifier, or damping control of the intermediate stage of a three-stage MC amplifier, or quenching of the gain path of a HNMC four-stage amplifier, or finally RNMC which relieves the amplifier of its limiting pole frequency at the output.



### 6.3 Slew Rate

The currents and voltages in an Operational Amplifier are limited. Each stage has its own limitation. The two-stage amplifier of Fig. 6.3.1 has two current limitations: one at the output of the output stage  $I_{B1}$ , and one at the output of the input stage  $I_{B2}$ . These currents limit the speed at which the output voltage  $V_{out}$  can change. This speed is called slew rate  $S_r = dV_{out}/dt$ .

When the limitation at the output dominates, the output voltage  $V_{out}$  cannot slew faster than:

$$S_{r1} = \left( \frac{dV_{out}}{dt} \right)_{\max} = I_{B1}/C_1 = V_{2\max}g_{m1}/C_1 = V_{2\max}2\pi f_{01} \tag{6.3.1}$$

for linear or sinusoidal waveforms, with  $V_{2\max}$  as the maximum linear approximated voltage swing at the input of  $M_1$ , which amounts to  $V_{2\max} = V_T = kT/q$  for bipolar, or  $V_{2\max} = (V_{GS} - V_{TH})$  for CMOS, and  $f_{01} = g_{m1}/2\pi C_1$  is the 0 dB frequency of the output stage.

However, the above is seldom the case, because when the output is biased in class-AB, it has basically no current limitation.

Moreover, when feedback is applied the voltage gain is strongly reduced. The limitation will be almost certain in the input stage. Its output is attenuated by the parallel or Miller compensation network, which is dotted in Fig. 6.3.1.

If the frequency of the input signal is raised above the dominating pole frequency  $f_d$  of the compensation network, the signal is attenuated proportionally to the frequency, while the output voltage remains constant because of the feedback.

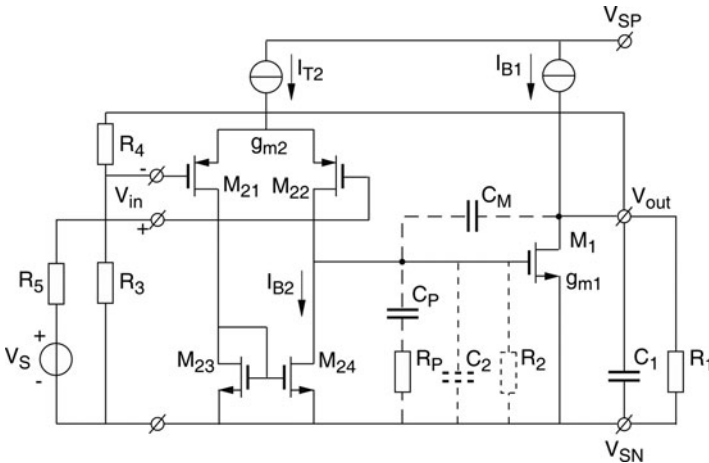


**Fig. 6.3.1** Two-stage Operational Amplifier with parallel or Miller compensation and feedback resistor

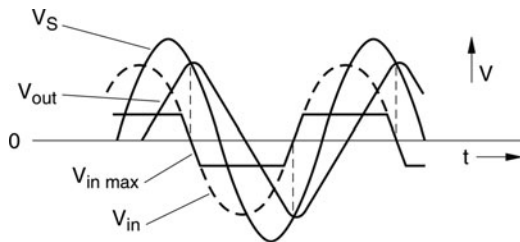


**Fig. 6.3.2** Time responses of various signals in the circuit of Fig. 6.3.1 showing slewing with  $\beta = R_3/(R_3 + R_4) = 1$ , at unity gain

The increase of the output current of the input stage goes on until the maximum current of  $I_{B2} = I_{M2}$  is reached. At higher frequencies, the returning part  $\beta = R_3/(R_3 + R_4)$  of the output voltage  $V_{out}$  cannot follow the source voltage  $V_S$  any more. Figure 6.3.2 shows the various response voltages in Fig. 6.3.1 with  $\beta = 1$ , at unity gain feedback. The input stage is blocking if the input voltage  $V_{in} = V_S - \beta V_{out}$  is larger than  $V_{in\ max}$ , which is  $V_{in\ max} \approx 2 V_T = 2 kT/q$  for a bipolar differential input pair and  $V_{in\ max} \approx 2(V_{GS} - V_{TH})$  for a CMOS differential input pair.

So, normally the slew rate  $S_r$  is dominated by the input stage, and can then be calculated for parallel and Miller compensation as:

$$S_r = \left( \frac{dV_{out}}{dt} \right)_{\max} = \frac{I_{T2}}{C_p} g_{m1} R_1 = \frac{I_{T2}}{C_M} = V_{in\ max} 2\pi f'_0 \tag{6.3.2}$$

for parallel compensation with  $f'_0 = g_{m2} g_{m1} R_1 / 2\pi C_p$ , or for Miller compensation with  $f'_0 = g_{m2} / 2\pi C_M$ , respectively.

We can now compare the slewing of the output stage with that of the input stage. Normally we choose  $f'_0$  of the whole amplifier half of  $f_{o1}$  of the output stage so that the slewing of the input stage dominates. This is also valid for a well-designed Operational Amplifier with more than two stages.

The relation between slew rate and bandwidth makes it possible to calculate one from the other. For a bipolar input pair  $V_{in\ max} = 2 kT/q = 50$  mV. For CMOS,  $V_{in\ max} = 2(V_{GS} - V_{TH})$  may be from 100 mV up to 1 V.

$$(S_r)_{bipolar} \approx 0.3 f'_0 \tag{6.3.3}$$

$$(S_r)_{CMOS} \approx (0.6 \text{ to } 6) f'_0 \tag{6.3.4}$$

Apparently, CMOS transistors have a higher slew rate than bipolar transistors, and more so when they are in stronger inversion. However, this is only seemingly true. The same results as those with CMOS are obtained with bipolar transistors if we use degeneration resistors in series with the emitters to lower the  $g_{m2}/I_{T2}$  ratio. A compromise must be chosen between slew rate and offset and noise.

A general approach to increase the slew rate is to make the bias currents signal dependent with a class-AB input stage. This will be discussed in an example in Sect. 7.1

## 6.4 Non-Linear Distortion

We encounter two types of non-linear distortion when using Operational Amplifiers: firstly, distortion caused by the input stage close to slewing, and secondly, distortion caused by the output stage.

To investigate the distortion caused by the input stage close to slewing, we have to have a closer look at the transconductance  $g_{m2}$  for large signals of the input stage of Fig. 6.3.1. This is depicted in Fig. 6.4.1.

When we looked at slewing, we treated the input stage as if it had a straight transconductance  $g_{m2}$  over the maximum useful input range from  $-V_{in\ max}$  up to  $+V_{in\ max}$  at which values the output current  $I_2$  changed from  $-I_{T2}$  up to  $+I_{T2}$ . In reality we find a lying “S” shaped function. For a bipolar and a CMOS pair we have, respectively:

$$I_2 = I_{T2} \tanh(V_{in} q / 2kT) \quad (6.4.1)$$

$$I_2 \approx I_{T2} \tanh(V_{in} / (V_{GS} - V_{TH})) \quad (6.4.2)$$

With  $V_{GS} - V_{TH} \approx 60\text{ mV}$  for CMOS input transistors in weak inversion.

It is interesting to note that by the balanced nature of the input pair all even order distortion components have disappeared. Only odd harmonic distortion remains. At plus and minus half  $V_{in\ max}$ , which corresponds with half the slew rate, the third-order distortion voltage component  $(V_{in\ 3rd})_{sr/2}$  referred to the input voltage is about 10% of  $V_{in}$  or 2.5 mV for bipolar, and 5% of  $V_{in}$  or 5–50 mV for CMOS transistors. This distortion component can be seen as an additional voltage source  $V_{in\ D}$  in series with the differential input voltage  $V_{in}$ .

Though the input distortion voltage is larger with CMOS than with bipolar transistors, the relative frequency at which half the slew rate occurs is much larger with CMOS than with bipolar transistors. This over-compensates the larger distortion with CMOS, as we will see in the following calculation.

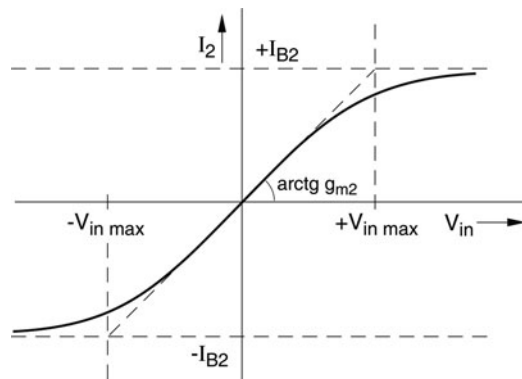


**Fig. 6.4.1** Transconductance  $g_{m2}$  of the input stage for large signals

The signal-to-distortion ratio is:

$$\frac{S}{D} = \frac{V_S}{V_{inD}} = \frac{V_{out}}{AV_{inD}} \quad (6.4.3)$$

For an output voltage of  $V_o \approx 1$  V, and a closed loop gain  $A = 1$ , the S/D ratio is in the order of 400 for bipolar transistors and between 200 and 20 for CMOS at the frequency where the amplifier is excused at half the slew rate.

The bandwidth  $f_{sr/2}$  at half the slew rate is:

$$f_{sr/2} = \frac{1}{2} S_r / 2\pi V_{out} = \frac{1}{2} f'_o V_{in\ max} / V_{out} \quad (6.4.4)$$

For an output voltage of 1 V, the bandwidth  $f_{sr/2}$  is  $f'_o/40$  for bipolar transistors, and  $f'_o/20$  to  $f'_o/2$  for CMOS. Above this frequency the distortion rises sharply, but below  $f_{sr/2}$  the third-order distortion  $V_{in\ 3rd}$  reduces with about the square of the ratio ( $fV_{out}/2f'_oV_{in\ max}$ ) [6.13]:

$$V_{\in 3rd} \approx (V_{in\ 3rd})_{sr/2} \left( fV_o / \frac{1}{2} f'_o V_{in\ max} \right)^2 \quad (6.4.5)$$

We can now take this in consideration for the signal-to-distortion ratio S/D, and obtain:

$$\frac{S}{D} = \frac{V_S}{V_{inD}} = \frac{V_{out}}{AV_{inD}} \approx \frac{1}{A} \frac{V_{in\ max}^2}{V_{out}(V_{in\ 3rd})_{sr/2}} \left( \frac{\frac{1}{2} f'_o}{f} \right)^2 \quad (6.4.6)$$

For bipolar and CMOS transistors this can be roughly estimated when slewing below half the slew rate:

$$\left( \frac{S}{D} \right)_{bipolar} \approx \frac{1}{A} \frac{1}{V_{out}} \left( \frac{\frac{1}{2} f'_o}{f} \right)^2 \quad (6.4.7)$$

$$\left( \frac{S}{D} \right)_{CMOS} \approx \frac{1}{A} \frac{2\ to\ 20}{V_{out}} \left( \frac{\frac{1}{2} f'_o}{f} \right)^2 \quad (6.4.8)$$

The result is that for a signal-to-distortion ratio of better than 0.1%, at  $V_{out} = 1$  V, and  $A = 1$ , we have a bandwidth of about  $f'_o/60$  for bipolar transistors, and between  $f'_o/40$  and  $f'_o/13$  for CMOS transistors.

The slack characteristic of CMOS transistors in strong inversion is in favour of the steep one of bipolar transistors for distortion. The more the CMOS transistors

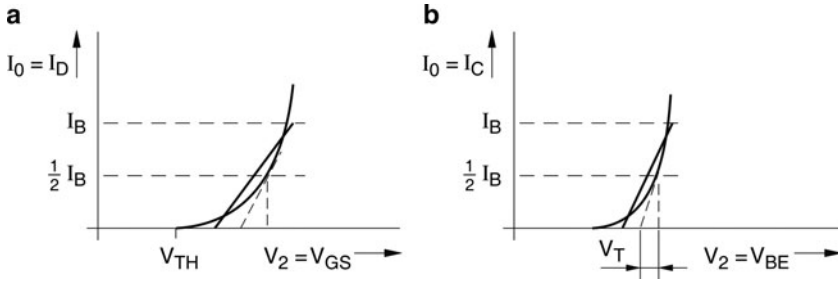


**Fig. 6.4.2** Transconductance of (a. to the left) CMOS transistors and (b. to the right) bipolar transistors

are in strong inversion, the better. But again, with emitter degeneration of bipolar transistors we can obtain the same results as with CMOS (Fig. 6.4.2).

Unequal slew rate for up and down CM input voltage movements is caused by the parasitic capacitance at the tail of the input stage. This can generate excessive distortion in unity-gain feedback amplifiers.

The distortion caused by the output stage can be modeled by the transconductance of the output transistor  $g_{m1}$ . The output current  $I_0$  is distorted as a function of the drive voltage  $V_2$  at the output of the second stage.

The distortion to signal ratio D/S cannot generally be expressed by a function of the ratio of the output current to the maximum output current  $I_{B1}$ :

$$\frac{D}{S} = f(I_0/I_{B1}) \tag{6.4.9}$$

because this function may have several types of non-linearity.

For CMOS with  $I_D = \frac{1}{2}\beta(V_{GS} - V_{TH})^2$  the distortion at a maximum sinusoidal output current can be estimated at 10%, and is of the second order. For bipolar transistors with  $I_c = I_s \exp(V_{BE}/V_T)$  the distortion can be estimated at 20% totally, including even and odd order components. For a complementary transistor pair in a push-pull class-AB configuration with a high ratio between the maximum output current  $I_{OM}$  and the quiescent output current  $I_{oquis}$ , the second order harmonic distortion disappears but the odd harmonics increase. This is depicted in Fig. 6.4.3.

The distortion with CMOS transistors is estimated at 10%, when we have adapted the W/L ratios of both transistors so that their Ks are equal for the P channel and N channel transistor. For bipolar transistors the distortion is estimated at 30%.

Until now we have assumed that the transistors are voltage driven. But if we drive with a current, which is the case at low frequencies, or if there is no parallel compensation, a bipolar transistor determines the value of  $R_2$  and  $C_2$  at its input. If we replace  $R_2$  for  $\beta_1 r_{e1}$ , and  $I_{c1} = \beta_1 I_2$ , the bipolar transistor becomes fairly linear with a distortion of 1% for a single transistor.

For a class-AB push-pull complementary pair, the distortion may be 20% because of a large difference between the current gain  $\beta_1$  and  $\beta_2$  of the PNP and NPN transistors. The situation is drawn in Fig. 6.4.4.

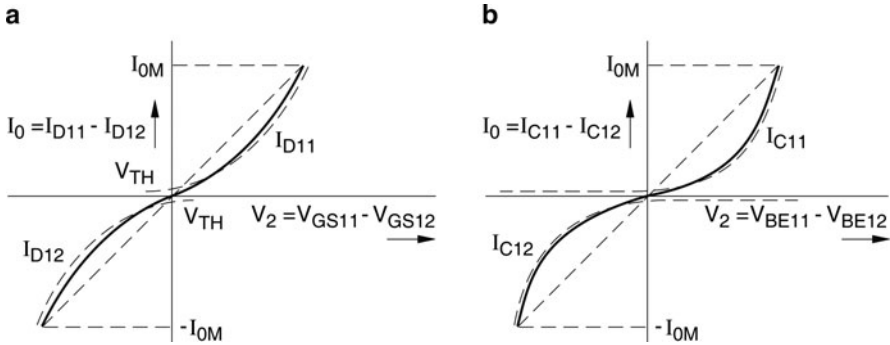
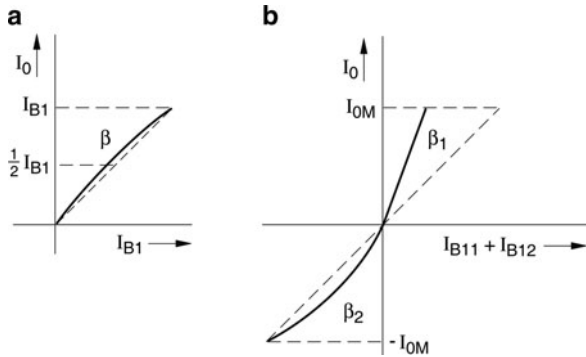


**Fig. 6.4.3** Transconductance of (a. to the left) CMOS class-AB push-pull complementary pair, and (b. to the right) of a bipolar pair

**Fig. 6.4.4** The current transfer characteristic of (a. to the left) a single bipolar output transistor, and (b. to the right) a class-AB push-pull complementary bipolar pair



The main advantage of feedback with an Operational Amplifier is that the distortion of the output stage is strongly reduced by the return difference or loop gain  $A_V \beta_V$ , in which  $A_V$  is the open loop gain of the amplifier and  $\beta_V$  the attenuation of the feedback network in the loop.

The closed-loop gain  $A_V$  is determined by the feedback network

$$A_V = \frac{A_{VC}}{1 + A_{VC} \beta_V} = \frac{1}{\beta_V} \frac{A_{VC} \beta_V}{1 + A_{VC} \beta_V} \approx \frac{1}{\beta_V} \tag{6.4.10}$$

with:  $\beta_V = R_3 / (R_3 + R_4)$

The sensitivity  $S_{A_{VC}}^{A_V}$  of the closed-loop gain  $A_V$  to changes in the open loop gain  $A_{VC}$  is reduced by the loop gain  $A_{VC} \beta_V$ , as is calculated in Eq. 6.4.11.

$$S_{A_{VC}}^{A_V} = \frac{\delta A_V}{\delta A_{VC}} \frac{A_{VC}}{A_V} = \frac{1}{1 + A_{VC} \beta_V} \approx \frac{1}{A_{VC} \beta_V} \tag{6.4.11}$$

With the same value as that of the loop gain the distortion is reduced. Figure 6.4.5 shows the loop gain  $A_{VC}\beta_V$  of the compensated and  $A_{VNC}$  of the non-compensated amplifier.

At low frequencies the loop-gain is  $A_{VO}\beta_V = g_{m2}R_2g_{m1}R_1\beta_V$ . This is normally a large value and the distortion is mostly reduced by it. At low frequencies bipolar transistors can be regarded as current driven along with their specific distortion. The reduction of the distortion at high frequencies depends on the way the amplifier is compensated.

With parallel compensation using  $C_P$  and  $R_P$  the return difference is unity  $A_{VC}\beta_V = 1$  at the bandwidth of the feedback amplifier  $f_B = f'_0\beta_V$ .

Hence, at this frequency the full distortion of the output transistor appears at the output. The shaded area of the loop gain in Fig. 6.4.5 is lost and cannot be used for reducing the distortion. At a frequency 10 times lower than  $f_B$  the distortion is only reduced with a factor 10.

With Miller compensation using  $C_M$  the linearity is much better than with parallel compensation. The reason is that the Miller capacitor internally provides feedback across the output transistor reducing its distortion. It can be regarded as if the gain of the non-compensated amplifier is still available to reduce the distortion. At the bandwidth  $f_B = f'_0\beta_V$  of the feedback amplifier, the return difference is still  $A_{VNC}\beta_V = f_2/f'_2$ , which might easily be of the order of 100. At a frequency 10 times lower than  $f_B$  the distortion is reduced by a factor 1,000. With a closed-loop bandwidth near  $f'_0$  at unity gain, the advantage of the Miller compensation over parallel compensation is lower.

With nested Miller compensation around the output stage of a three- stage amplifier, the advantage is even more pronounced as the uncompensated gain is larger than that of a two-stage amplifier.

There is one distortion component which is added with Miller compensation. The Miller capacitor is connected to the diode voltage at the input of the output transistor as a virtual ground. The non-linear voltage characteristic of this diode appears in series with the output. The non-linearity of this diode voltage is only reduced by the return difference  $A_{VC}\beta_V$  of the compensated amplifier. To eliminate this effect, the Miller capacitor can be connected to the input of a cascode transistor inserted between the input and output stage, as shown in Fig. 6.2.12.

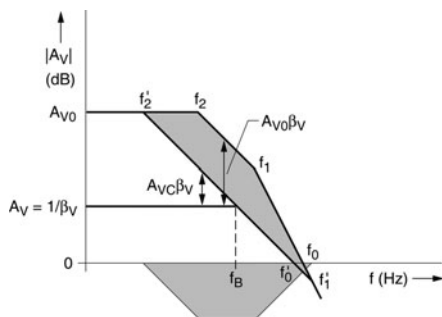


**Fig. 6.4.5** Frequency characteristics of the closed-loop gain ( $A_{VC}$ ) and open-loop gain ( $A_{V0}$ ) two-stage amplifier of Fig. 6.3.1

## Conclusion

We have seen that the distortion of the Operational Amplifier originates from the input stage and the output stage. The distortion of the input stage is lower than 1 percent in regard to a signal voltage of 1 V. It is reduced by the ratio of the signal frequency  $f$  and the frequency  $f_{sr}$  at which the amplifier slews. The distortion of the output stage is in the order of 10%. It is reduced by the compensated loop gain with parallel compensation and with the uncompensated open loop with Miller compensation. Miller compensation and particularly nested Miller compensation strongly reduces the distortion of the output stage.

## 6.5 Problems and Simulation Exercises

### Problem 6.1

Using NMOS devices for the one-stage amplifier in Fig. 6.2.2, sized  $W/L_{11,12} = 200\mu/2\mu$ ,  $W/L_2 = 50\mu/1\mu$ , draw the Bode amplitude characteristic if the devices have  $V_{THN} = 0.5$  V,  $K_N = 56 \mu\text{A}/\text{V}^2$ ,  $\lambda_N = 0.1 \text{ V}^{-1}$ , and  $f_{T2} = 30$  MHz. Biasing currents are  $I_{M1} = 100 \mu\text{A}$ ,  $I_{B1} = 50 \mu\text{A}$  and the load capacitor is  $C_l = 10$  pF. How does the Bode characteristic change if a load resistor  $R_l = 500 \text{ k}\Omega$  is added in the circuit?

### Solution

The DC gain of the amplifier can be calculated for no external resistive load as the product of input stage  $g_m$  and the output impedance of the cascoded transistor  $M_{11}$

$$A_{DC} = \frac{1}{2} g_{m11} r_{ds11} g_{m2} r_{ds2} = \frac{1}{2} \mu_{11} \mu_2 \quad (6.5.1)$$

For saturated MOS transistors, the voltage gain  $\mu$  can be calculated

$$\begin{aligned} \mu_{11} &= \frac{1}{\lambda_N \sqrt{2I_{D11} K_N W/L_{11}}} = 75 \\ \mu_2 &= \frac{1}{\lambda_N \sqrt{2I_{D2} K_N W/L_2}} = 53 \end{aligned} \quad (6.5.2)$$

The DC voltage gain of a one-stage NMOS amplifier becomes

$$A_{DC} = \frac{1}{2} g_{m11} r_{ds11} g_{m2} r_{ds2} = \frac{1}{2} \mu_{11} \mu_2 = 2000 \quad (6.5.3)$$



The second non-dominant pole of the amplifier is given by the transit frequency of  $M_2$

$$f_1 = f_{T2} = 30 \text{ MHz} \quad (6.5.4)$$

The unity gain bandwidth is set by the ratio of the input stage  $g_m$  and the load capacitor  $C_l$

$$f_0 = \frac{1}{2} \frac{g_{m11}}{2\pi C_l} = 11.9 \text{ MHz} \quad (6.5.5)$$

at  $g_{m11} = 750 \mu\text{S}$ . Note that the second pole frequency is more than two times larger compared to the unity gain bandwidth, so the phase margin will be higher than  $60^\circ$ . The dominant pole frequency is obtained as the division of unity gain bandwidth to DC voltage gain value

$$f_2 = \frac{f_0}{A_{DC}} = 5.6 \text{ kHz} \quad (6.5.6)$$

The changes produced by the presence of a load resistor are related to a reduced output impedance, which in turn reduces to voltage gain and the unity gain bandwidth. If the load resistance is much smaller than the amplifier output impedance

$$R_l = 500 \text{ k}\Omega \gg r_{ds11} g_{m2} r_{ds2} = 10.25 \text{ M}\Omega \quad (6.5.7)$$

then the two equations above, which are dependent on DC voltage gain, are affected by the load resistance alone

$$\begin{aligned} A_{DC} &= \frac{1}{2} g_{m11} R_l = 187 \\ f_2 &= \frac{f_0}{A_{DC}} = 63.6 \text{ kHz} \end{aligned} \quad (6.5.8)$$

The decrease in voltage gain is dramatic because a single stage MOS amplifier obtains the biggest part of its voltage gain by using a high output impedance

### **Problem 6.2**

A two-stage amplifier using parallel compensation is depicted in Fig. 6.2.6. Considering an all-NMOS circuit, with transistors sized  $W/L_{21,22} = 100\mu/2\mu$  and  $W/L_l = 200\mu/2\mu$ , and loaded with  $C_l = 20 \text{ pF}$ ,  $R_l = 50 \text{ k}\Omega$ , compensate the circuit by calculating the values of  $C_p$ ,  $R_p$ . Also calculate the unity gain bandwidth of the compensated amplifier and the bandwidth over dissipated power ratio if the

circuit is biased at  $V_{SP} - V_{SN} = 2$  V. The transistors have  $V_{THN} = 0.5$  V and  $K_N = 56 \mu\text{A}/\text{V}^2$  and are biased with  $I_{M2} = 50 \mu\text{A}$ ,  $I_{B1} = I_{B2} = 25 \mu\text{A}$ . The internal components are  $C_2 = 1$  pF and  $R_2 = 1$  M $\Omega$ .

### Solution

According to Eq. 6.2.9, the parallel compensation network should be designed with

$$\begin{aligned} C_P &= R_I \sqrt{2C_1 C_2 g_{m1} g_{m2}} \\ &= R_I \sqrt{2C_1 C_2 \sqrt{2K_N \frac{W}{L_1} I_{B1}} \frac{1}{2} \sqrt{2K_N \frac{W}{L_2} 2I_{B2}}} = 118 \text{ pF} \\ R_P &= \sqrt{\frac{C_1}{C_2 g_{m1} g_{m2}}} = 8.4 \text{ k}\Omega \end{aligned} \quad (6.5.9)$$

With this compensation the unity gain bandwidth of the amplifier is, according to Eq. 6.2.10,

$$f'_0 = \sqrt{\frac{g_{m1}}{2\pi C_1} \frac{g_{m22}}{2\pi C_2}} = 18.8 \text{ MHz} \quad (6.5.10)$$

Noting that  $I_{B1} = I_{B2}$  and all transistors operate at the same  $V_{GS} - V_{THN}$ , Eq. 6.1.14 can be used to find the bandwidth over power ratio

$$\frac{f'_0}{P_S} = \frac{1}{8\pi \sqrt{2C_1 C_2} (V_{GS} - V_{THN}) (V_{SP} - V_{SN})} = 4.7 \times 10^{10} \quad (6.5.11)$$

### Problem 6.3

Using the same device parameters and resistor and capacitor values as in problem 6.2, calculate the Miller capacitor  $C_{MI}$  and the Miller zero cancellation resistor  $R_{MI}$  for maximum unity gain bandwidth of the amplifier shown in Fig. 6.2.11. What is the frequency of the dominant pole?

### Solution

Since the relationship between the uncompensated amplifier's poles is important, with the Miller cancellation techniques the values of these poles should be calculated first

$$\begin{aligned} f_{01} &= \frac{g_{m1}}{2\pi C_1} = 6 \text{ MHz} \\ f_{02} &= \frac{g_{m2}}{2\pi C_2} = 30 \text{ MHz} \end{aligned} \quad (6.5.12)$$

Noting that  $f_{01} < f_{02}$ , the attainable unity gain bandwidth will be

$$f'_0 = \frac{1}{2}f_{01} = 3 \text{ MHz} \quad (6.5.13)$$

and the corresponding Miller capacitor value becomes

$$C_{MI} = \frac{g_{m2}}{2\pi f'_0} = \frac{g_{m22}}{4\pi f'_0} = 10 \text{ pF} \quad (6.5.14)$$

according to Eq. 6.2.22. The Miller zero cancellation resistor results from Eq. 6.2.24 which states the value of the Miller zero frequency

$$R_{MI} = \frac{1}{g_{m1}} = 1.3 \text{ k}\Omega \quad (6.5.15)$$

The dominating pole frequency produced by Miller compensation becomes

$$f'_2 = \frac{f'_0}{A_{v0}} = \frac{f'_0}{g_{m2}R_2g_{m1}R_1} = 426 \text{ Hz} \quad (6.5.16)$$

The bandwidth over power ratio for this amplifier is

$$\frac{f'_0}{P_S} = \frac{1}{8\pi(C_1 + 2C_2)(V_{gs} - V_{th})(V_{SP} - V_{SN})} = 1.7 \times 10^{10} \quad (6.5.17)$$

### **Problem 6.4**

The three-GA-stage amplifier in Fig. 6.2.16 is designed with NMOS transistors sized  $W/L_{31,32} = 100\mu/2\mu$ ,  $W/L_{21,22} = 10\mu/1\mu$ , and  $W/L_1 = 100\mu/1\mu$  biased at  $I_{M3} = 2I_{B3} = 50 \mu\text{A}$ ,  $I_{M2} = 2I_{B2} = 20 \mu\text{A}$ , and  $I_{B1} = 50 \mu\text{A}$ . The internal nodes are loaded with  $C_3 = 0.5 \text{ pF}$ ,  $R_3 = 300 \text{ k}\Omega$ ,  $C_2 = 1 \text{ pF}$ ,  $R_2 = 200 \text{ k}\Omega$  while the output is loaded with  $C_1 = 10 \text{ pF}$ ,  $R_1 = 100 \text{ k}\Omega$ . Calculate the nested Miller compensation network, the unity gain bandwidth frequency and the dominant pole frequency. The NMOS devices have  $V_{THN} = 0.5 \text{ V}$  and  $K_N = 56 \mu\text{A}/\text{V}^2$ .

### **Solution**

The 0 dB bandwidth  $f''_0$ , of the Miller compensated intermediate and output stages should be, according to Eq. 6.2.30,

$$f'_{0} = \frac{1}{2}f'_{1} = \frac{1}{2} \frac{g_{m1}}{2\pi C_1} = \frac{1}{2} \frac{\sqrt{2K_N \frac{W}{L_1} I_{B1}}}{2\pi C_1} = 6 \text{ MHz} \quad (6.5.18)$$

which takes a Miller capacitor  $C_{M1}$  sized

$$C_{M1} = \frac{g_{m2}}{2\pi f'_{0}} = \frac{g_{m22}}{4\pi f'_{0}} = 1.3 \text{ pF} \quad (6.5.19)$$

The unity gain bandwidth of the nested Miller compensated amplifier will be half  $f'_{0}$ .

$$f''_{0} = \frac{1}{2}f'_{0} = 3 \text{ MHz} \quad (6.5.20)$$

which needs a nested Miller capacitor  $C_{M2}$

$$C_{M2} = \frac{g_{m3}}{2\pi f''_{0}} = \frac{g_{m32}}{4\pi f''_{0}} = 10 \text{ pF} \quad (6.5.21)$$

The dominant pole frequency is obtained by combining Eqs. 6.2.34 and 6.2.35

$$f'_3 = \frac{f''_{0}}{A_{v0}} = \frac{4f''_{0}}{g_{m32}R_3 g_{m22}R_2 g_{m1}R_1} = 70 \text{ Hz} \quad (6.5.22)$$

### Problem 6.5

A multipath nested Miller compensated amplifier designed with the schematic shown in Fig. 6.2.18 and using NMOS transistors sized  $W/L_{31,32} = W/L_{33,34} = 100\mu/2\mu$ ,  $W/L_{21,22} = 10\mu/1\mu$  and  $W/L_1 = 100\mu/1\mu$  is driving a load capacitor  $C_1 = 10$  pF with an output impedance of  $R_1 = 100$  k $\Omega$ . The biasing currents are  $I_{M32} = I_{M31} = 2I_{B32} = 2I_{B31} = 50$   $\mu$ A,  $I_{M2} = 2I_{B2} = 20$   $\mu$ A and  $I_{B1} = 50$   $\mu$ A. The internal nodes are loaded with  $C_3 = 0.5$  pF,  $R_3 = 300$  k $\Omega$ ,  $C_2 = 1$  pF,  $R_2 = 200$  k $\Omega$ . Calculate the nested Miller compensation network  $C_{M1}$  and  $C_{M2}$ . The NMOS devices have  $V_{THN} = 0.5$  V and  $K_N = 56$   $\mu$ A/V<sup>2</sup>.

### Solution

$$f'_{0} = \frac{1}{2}f'_{1} = \frac{1}{2} \frac{g_{m1}}{2\pi C_1} = \frac{1}{2} \frac{\sqrt{2K_N \frac{W}{L_1} I_{B1}}}{2\pi C_1} = 6 \text{ MHz} \quad (6.5.23)$$

The 0 dB bandwidth  $f'_{0}$  after first compensation with  $C_{M1}$

which in turn makes the Miller capacitor  $C_{M1}$  to be

$$C_{M1} = \frac{g_{m32}}{2\pi f'_0} = \frac{g_{mT34}}{4\pi f'_0} = 1.3 \text{ pF} \tag{6.5.24}$$

Because of the existing multipath, the overall unity gain bandwidth

$$f''_0 = f'_0 = 6 \text{ MHz} \tag{6.5.25}$$

$$C_{M2} = \frac{g_{m31}}{2\pi f''_0} = \frac{g_{mT32}}{4\pi f''_0} = 10 \text{ pF} \tag{6.6.26}$$

will be equal to  $f'_0$  after the second compensation by  $C_{M2}$  which according to Eq. 6.2.42 needs a Miller capacitor  $C_{M2}$

The dominant pole frequency is given by Eq. 6.2.43

In order to obtain a phase margin larger than  $55^\circ$ , the condition in Eq. 6.2.44 should be checked

$$f'_3 = \frac{f''_0}{A_{v0}} = \frac{4f''_0}{g_{mT34}R_3g_{m22}R_2g_{m1}R_1} = 140 \text{ Hz} \tag{6.5.27}$$

$$g_{m2} = \frac{1}{2}g_{m22} = 51 \mu\text{A/V} < \frac{1}{3}g_{m32} = \frac{1}{6}g_{mT34} = 62.5 \mu\text{A/V} \tag{6.5.28}$$

### Simulation Exercise 6.1

The three-GA-stage operational amplifier in Fig. 6.5.1 is shown in a setup for AC differential gain simulation. The amplifier is Miller compensated by  $C_8$  and  $C_9$ . Remove the Miller capacitors and simulate the circuit to calculate the phase margin, unity gain bandwidth and dominant pole frequency, then repeat the previous step

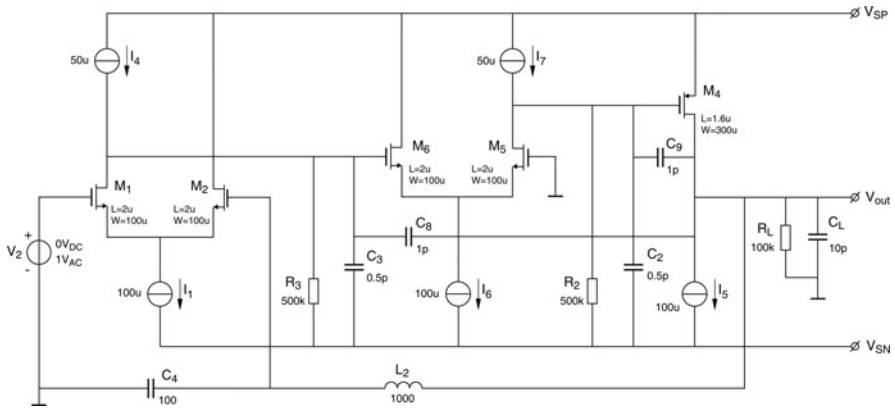


Fig. 6.5.1 Three-stage Miller compensated amplifier

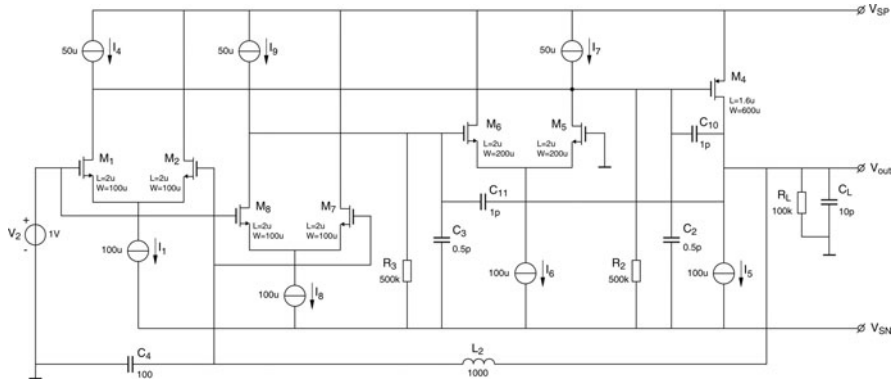


Fig. 6.5.2 Multipath nested Miller compensated amplifier

with the Miller capacitors in the circuit. Considering the fact that some transistor models do not model accurately the moderate inversion region of a MOS device, resize the transistors to place them in strong inversion by checking the  $V_{GS} - V_{TH}$  to be at least 0.2 V. Considering a threshold voltage variation of 40 mV (the actual  $V_{TH}$  variation can be calculated dividing this value by transistor width) for all devices, compensate the amplifier for 60° phase margin in the worst case combination of the mismatch mentioned above.

### Simulation Exercise 6.2

The operational amplifier shown in Fig. 6.5.2 can provide a large DC gain due to the dual input stage. Compare the gain and phase characteristics of this amplifier with the ones from the previous exercise, after removing the Miller capacitors in both circuits and after making the output stage transistors  $M_4$  of equal size  $W/L_4 = 300/1.6$ . The three-stage gain characteristic is now shown by the results from the previous circuit and can be compared with the results for the multipath version. Add the Miller capacitors and compare the two results again. Note the bandwidth increase for the multipath circuit.

## 6.6 References

- [6.1]. J.H. Huijsing, F. Tol, Monolithic operational amplifier design with improved HF behavior. IEEE J. Solid-St. Circ. **SC-11**, 323–328 (1976)
- [6.2]. K. Bult, G.J.G.M. Gielen, A fast settling CMOS op amp for SC-circuits with 90 dB gain. IEEE J. Solid-St. Circ. **SC-25**(12), 1379–1383 (1990)
- [6.3]. J.H. Huijsing, D. Linebarger, Low-voltage operational amplifier with rail-to-rail input and output ranges. IEEE J. Solid-St. Circ. **SC-20**(6), 1144–1150 (1985)
- [6.4]. R. Caprio, Precision differential voltage-current converter. Electron. Lett. **9**, 147–148 (1973)

- [6.5]. H. Nyquist, Regeneration theory. *Bell Syst. Tech. J.* **11**, 126–147 (1932)
- [6.6]. H.W. Bode, *Network Analysis and Feedback Amplifier Design*. (D. van Nostrand Company Inc., New York, 1949)
- [6.7]. B.Y. Kamath, R.G. Meyer, P.R. Gray, Relationship between frequency response and settling time of operational amplifiers. *IEEE J. Solid-St. Circ.* **SC-9**(6), 347–352 (1974)
- [6.8]. B. Nauta, A CMOS transconductance-C filter technique for very high frequencies. *IEEE J. Solid-St. Circ.* **27**(2), 142–153 (1992)
- [6.9]. J.M. Miller, Dependence of the input impedance of a three-electrode vacuum tube upon the load in the plate circuit. *Sci. Paper Bur. Stds.* **15**(351), 367–385 (1920)
- [6.10]. R. Hogervorst et al., A compact power-efficient 3 V CMOS rail-to-rail input/output operational amplifier for VLSI cell libraries. *IEEE J. Solid-St. Circ.* **29**(12), 1505–1513 (1994)
- [6.11]. R. Hogervorst, J.H. Huijsing, *Design of Low-Voltage Low-Power Operational Amplifier Cells* (Kluwer Academic Publishers, Boston, 1996)
- [6.12]. R.G.H. Eschauzier, J.H. Huijsing, An operational amplifier with multipath Miller zero cancellation for RHP zero removal, Proceedings ESSCIRC 1993, Editions Frontières, Gif-sur-Yvettes, France
- [6.13]. R.G.H. Eschauzier, J.H. Huijsing, *Frequency Compensation Techniques for Low-Power Operational Amplifiers* (Kluwer Academic Publishers, Boston, 1995)
- [6.14]. M.J. Fonderie, J.H. Huijsing, *Design of Low-Voltage Bipolar Operational Amplifiers* (Kluwer Academic Publishers, Boston, 1993)
- [6.15]. M.J. Fonderie, J.H. Huijsing, Operational amplifier with 1-V rail-to-rail Multipath-Driven output stage. *IEEE J. Solid-St. Circ.* **26**(12), 1817–1824 (1991)
- [6.16]. R.G.H. Eschauzier, R. Hogervorst, J.H. Huijsing, A programmable 1.5 V CMOS class-AB operational amplifier with Hybrid Nested Miller compensation for 120 dB gain and 6 MHz UGF. *IEEE J. Solid-St. Circ.* **29**(12), 1497–1504 (1994)
- [6.17]. R.J. Reay, G.T.A Kovacs, An unconditionally stable two-stage CMOS amplifier. *IEEE J. Solid-St. Circ.* **30**(5), 591–594 (1995)
- [6.18]. A. Bakker, Low-dropout voltage regulator with improved stability for all capacitive loads, U.S. Patent 6,373,233 B2, 16 April 2002
- [6.19]. K.N. Leung, P.K.T. Mok, W.H. Ki, J.K.O. Sin, Three-stage large capacitive load amplifier with damping-factor-control frequency compensation. *IEEE J. Solid-St. Circ.* **35**(2), 221–230 (2000)
- [6.20]. X. Peng, W. Sansen, Transconductance with capacitances feedback compensation for multistage amplifiers. *IEEE J. Solid-St. Circ.* **40**(7), 1514–1520 (2005)
- [6.21]. V. Dhanasekaran, J.S. Martinez, E. Sanchez-Sinenco, Design of three-stage class-AB 16 Ohm headphone driver capable of handling wide range of load capacitance. *IEEE J. Solid-St. Circ.* **44**(6), 1734–1744 (2009)
- [6.22]. J. Hu, J.H. Huijsing, K.A.A. Makinwa, A three-stage amplifier with quenched multipath frequency compensation for all capacitive loads. *IEEE international symposium on circuits and systems, ISCAS 2007*, 27–30 May 2007, pp. 225–228
- [6.23]. J.H. Huijsing, (as misspelled in US Patent 4,559,502), Multi-stage amplifier with capacitive nesting for frequency compensation, U.S. Patent 4,559,502, filed by Signetics Corporation (Sunnyvale, CA), 17 Dec 1985
- [6.24]. D. Marano, G. Palumbo, S. Pennisi, Improved Power-Efficient RNMC technique with voltage buffer and nulling resistors for low-power high-load three-stage amplifiers. *JCS* **18**(7), 1321–1331 (2009)
- [6.25]. A.D. Grasso, D. Marano, G. Palumbo, S. Pennisi, Improved reversed Nested Miller frequency compensation technique with voltage buffer and resistor. *IEEE Trans. Circ. Syst. 2: Express briefs* **54**(5), 382–386 (2007)
- [6.26]. K.L. de Langen, J.H. Huijsing, *Compact Low-Voltage and High-Speed CMOS, BiCMOS and Bipolar Operational Amplifiers* (Kluwer Academic Publishers, Boston, 1999), 200 pp

# 7. Design Examples

We have made a classification of Operational Amplifiers in Chap. 6. Nine main topologies have been listed as in a periodic system.

## Nine Overall Topologies

For a good input stage only the GA type is suited, as shown in Chap. 4. For level-shift or intermediate stages there are two possible types, the CM or CF (both denoted as CF), and the GA stage, as shown in Chap. 6. Three push-pull output stages exist, the fully VF, VF/GA, and fully GA stages, as shown in Chap. 5. The combination of these possibilities create two two-stage configurations without a push-pull output stage, six three-stage configurations, and one multistage configuration with four GA stages or more. These nine main topologies are inventoried again in Table 7.1.

We will give practical examples of each of these nine overall topologies in the following nine paragraphs and end with conclusions. We will see that the first configuration is mainly useful for capacitive loads. Configurations 3–6 are mostly useful in bipolar technology. While the configurations 7–9 with rail-to-rail output stage are particularly useful for low-voltage CMOS technology, but may also be used in some low-voltage bipolar and BiCMOS applications.

### 7.1 GA-CF Configuration

The most simple topology for an Operational Amplifier is the GA-CF configuration.

#### *Operational Transconductance Amplifier*

The simple class-A complete general OpAmp is called operational transconductance amplifier (OTA). The OTA has besides the GA-input stage, a current-mirror (CM) or a folded-cascode current-follower (CF) stage for providing an output-voltage



**Table 7.1** Classification of nine main overall topologies for operational amplifiers

Configuration number	Input stage	Level-shift or intermediate stage	Output stage
1	GA	CF	–
2	GA	GA	–
3	GA	CF	VF
4	GA	GA	VF
5	GA	CF	VF/GA
6	GA	GA	VF/GA
7	GA	CF	GA
8	GA	GA	GA
9	GA	GA + GA	GA

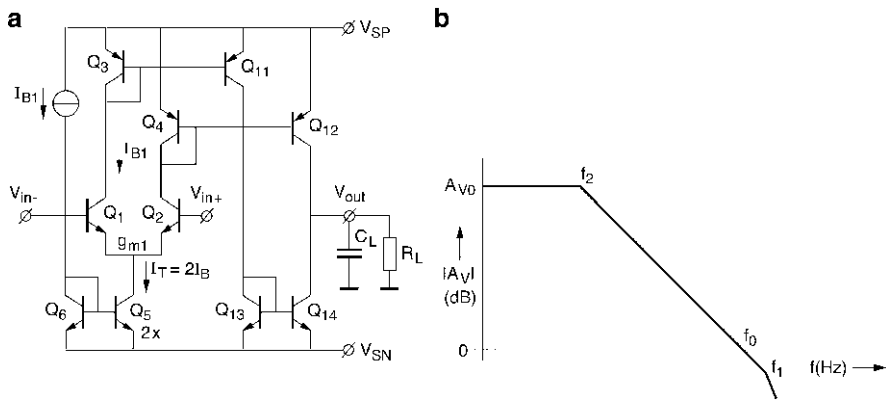


**Fig. 7.1.1** (a) Class-A operational transconductance amplifier (OTA) with GA-CM configuration and (b) frequency characteristic of the GA-CF configuration

swing independent of the CM input voltage. This type of amplifier is mainly used to drive capacitive loads  $C_L$ . The transconductance, which is provided by the GA input stage, is too low to provide a large DC gain with a resistive load  $R_L$ . A typical structure in bipolar technology is shown in Fig. 7.1.1a.

The OTA of Fig. 7.1.1a has a transconductance  $G_m$  equal to the transconductance of the input stage  $g_{m1}$  which is proportional to the bias current  $I_{B1}$ . The series connection of the two emitters of the input stage halves the transconductance of the input transistors  $g_{m1,2}$ . The current mirror  $Q_{13}, Q_{14}$  doubles the transconductance again, so that  $G_m$  of the whole OTA equals that of one of the input transistors  $g_{m1,2}$ . The emitter-area ratios have been chosen such that all transistors have a quiescent current of  $I_{B1}$ . With  $V_T = kT/q$  the total  $G_m$  becomes:

$$G_m = g_{m1} = g_{m1,2} = \frac{I_{B1}}{V_T} \tag{7.1.1}$$

Formula (7.1.1) shows that the transconductance  $G_m$  is constant over temperature if the bias current  $I_{B1}$  is proportional to the absolute temperature  $T$  (PTAT).

The limiting pole frequency  $f_l$  results from the mirrors. Their transit frequency  $f_l$  is half that of a single transistor  $f_T$  because of the double base-emitter capacitor  $2c_{be}$  parallel to one diode resistor  $r_e = 1/g_m$ . The PNP transistors usually limit the bandwidth by their low  $f_{TP}$ . So the limiting pole frequency  $f_l$  is:

$$f_l \approx \frac{1}{2} f_{TP} \quad (7.1.2)$$

The load capacitor  $C_L$  must be so large that the zero-dB frequency  $f_0$  lies a factor 2 below  $f_l$  for a  $60^\circ$  phase margin:

$$f_0 = \frac{G_m}{2\pi C_L} \leq \frac{1}{2} f_l \approx \frac{1}{4} f_{TP} \quad (7.1.3)$$

The dominating pole frequency  $f_2$  is:

$$f_2 = \frac{1}{2\pi R_L C_L} \quad (7.1.4)$$

The DC voltage gain is:

$$A_{V0} = G_m R_L \quad (7.1.5)$$

The GA-CM configuration is often used without load resistor  $R_L$  to drive a capacitive load.

The maximum obtainable gain without  $R_L$  is limited by the parallel ( $\parallel$ ) output resistance  $r_o$  of the PNP and NPN current mirrors  $^{1/2} r_{cep}$  and  $^{1/2} r_{cen}$ :

$$A_{VOM} = G_m R_o = G_m \left( \frac{1}{2} r_{cep} \parallel \frac{1}{2} r_{cen} \right) \approx G_m \frac{1}{4} r_{ce} \approx \frac{1}{4} \mu \quad (7.1.6)$$

The value of  $\mu = g_m r_{ce} = r_{ce}/r_E$  may be of the order of  $10^3$  or 60 dB. When we would have cascoded the output stage with bipolar transistors, the output impedance  $r_o$  will be limited by the collector-base resistance  $r_{cb} \approx \beta r_{ce}$ , and the maximum obtainable gain would become:

$$A_{VOM} = G_m (r_{cbp} \parallel r_{cbn}) \approx G_m \frac{1}{2} r_{cb} \approx \frac{1}{2} \beta \mu \quad (7.1.7)$$

### ***Folded-Cascode Operational Amplifier***

To obtain a high output impedance in CMOS, a cascode stage can be placed straight on the output of the input pair, as will later be discussed with the telescopic cascode of Fig. 7.1.3, or a folded cascode can be placed in cascade, as shown in the circuit of Fig. 7.1.2a, b.

**Fig. 7.1.2 (a)** Class-A folded-cascode operational amplifier with GA-CF configuration

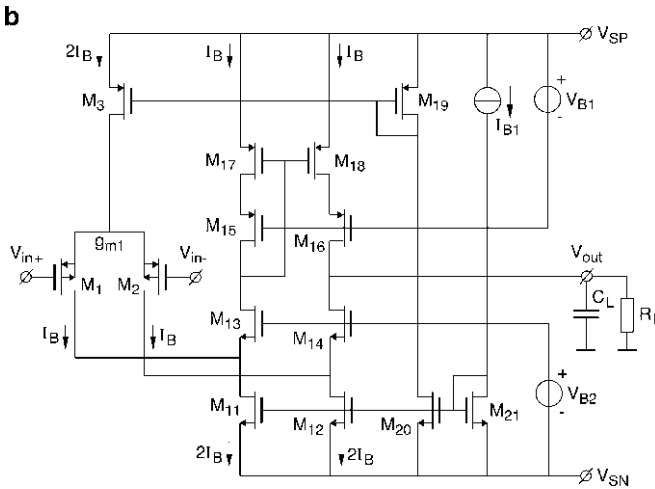
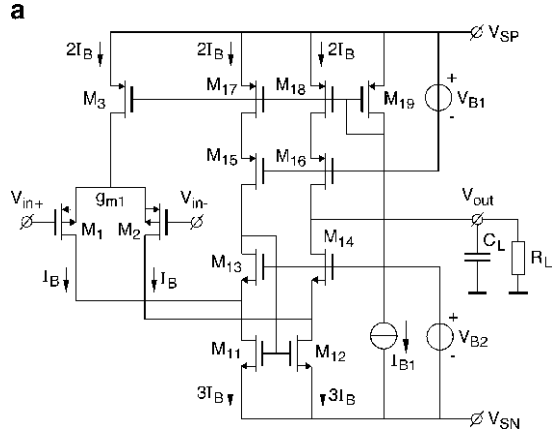


**Fig. 7.1.2 (b)** Class-A folded-cascode operational amplifier (OpAmp) with GA-CF configuration and the current-mirror connection at the P-channel side

The CMOS folded-cascode amplifier of Fig. 7.1.2a has a transconductance  $G_m = g_{m1,2}$  equal to that of one input transistor  $g_{m1,2}$ . The series connection of the two input transistors halves the transconductance. But, the mirror-connected transistors  $M_{11}, M_{12}$  sum the differential currents of the input transistors, so that the transconductance is doubled again. We have chosen relative wide input transistors, so that these become biased in weak inversion at  $I_{B1}$ . That provides the highest  $G_m$  at the given tail current of  $2I_{B1}$ . This means that all offset and noise sources of the input stage and the following stage are minimally reflected in the input offset voltage  $V_{inoff}$ . In weak inversion the CMOS transistors function like bipolar transistors in an exponential way. But the transconductance is  $n$  times smaller. The transconductance of the whole amplifier is:

$$G_m = g_{m1,2} = \frac{I_{B1}}{nV_T} \quad (7.1.8)$$

with  $V_T = kT/q$ , and  $nV_T$  is chosen about 60 mV at room temperature, which is in moderate inversion close to weak inversion.

The W/L ratios of all current-source transistors  $M_3$ ,  $M_{17}$  and  $M_{18}$  are chosen such that their output currents are all equal to  $2I_{B1}$ . This provides a maximum symmetrical output current at a minimal supply power. The current sources need to have low noise, low offset, and a high output resistance. Therefore, relatively long CMOS transistors have been chosen for these current sources such that they become biased in strong inversion at an effective gate-source voltage  $V_{GS} - V_{TH}$  of about 300 mV. The  $G_m$  is:

$$G_m = g_{m1,2} = K(V_{GS} - V_{TH}) = \sqrt{2KI_{B1}} = \frac{2I_{B1}}{(V_{GS} - V_{TH})} \quad (7.1.8a)$$

with:  $K = \mu C_{ox}W/L$ .

Some times the mirror connection is chosen at the bottom at the gates of the lower N-channel transistors  $M_{11}$  and  $M_{12}$  as in Fig. 7.1.2a. This gives the highest frequency response because the gate capacitors of the N-channels are smaller than that of the P-channels. The P-channel transistors are usually chosen three times larger to compensate the  $g_m$  for a three times lower mobility. With the current mirror connection at the lower side, the current sources  $M_{17}$  and  $M_{18}$  at the upper side must provide two times the bias current of one input transistor, to fully excure the output. As a consequence, the mirror-connected transistors  $M_{11}$  and  $M_{12}$  must carry three times the bias current of one input transistor. Only then the maximum positive and negative output current, equal to two times that of one input transistor, can be provided at the output to the load.

The bottom mirror transistors  $M_{11}$ ,  $M_{12}$  carry three times more current than the input transistors do. Their noise and offset would be reflected three times stronger at the input if these transistors would be biased in weak inversion like the input transistors are. To avoid this large amount of noise and offset, the bottom mirror transistors have to be biased in very strong inversion. But there is a limit. If the input CM range need to include ground, the maximum effective gate-source voltage can not be much larger than 300 mV.

The additional noise and offset caused by the mirror connection in the bottom of the folded cascode CF stage can be reduced, as well as its supply power, by making the mirror connection at the top instead of in the bottom, as shown in Fig. 7.1.2b. This can be allowed for OpAmps where high frequency behavior is not the most critical issue.

If we choose the mirror connection at the upper side as drawn in Fig. 7.1.2b, the current sources  $M_{11}$  and  $M_{12}$  have only to provide two times the bias current of one input transistor. Then, the current mirror transistors carry only one times the bias current of an input transistor. Still, the current mirror at the top allows the output to provide the maximum positive and negative current of two times the bias current of one input transistor. The lower currents in the bottom current-source transistors and upper mirror transistors allow to choose these transistors with a lower W/L ratio in

strong inversion at the same saturation voltages as in the previous case. The lower bias currents and the lower W/L ratios result in a substantially lower  $g_m$  of the transistors  $M_{11}$ ,  $M_{12}$ ,  $M_{17}$  and  $M_{18}$ . Hence, their noise and offset currents are lower, which results in lower input noise and offset voltages.

An alternative to strong inversion is the use of resistive degenerated transistors in weak inversion. That might take more area in the layout. But the degeneration resistors can be accurately matched and their  $G_m$  is two times smaller than that of transistors in strong inversion at the same bias current and voltage loss. This results in a lower noise and offset. This alternative can also be applied to the lower current sources  $M_{11}$  and  $M_{12}$  and upper current mirror  $M_{17}$  and  $M_{18}$ . The alternatives are shown in Fig. 7.1.2c.

The limiting pole frequency  $f_l$  in the folded cascode of Fig. 4.1.2a results from the folded current follower  $M_{14}$  and mirror  $M_{11}$ ,  $M_{12}$ . The transit frequency of the N-channel mirror  $f_l = 1/2 f_{TN}$  roughly limits the bandwidth:

$$f_l = \frac{1}{2} f_{TN} \tag{7.1.9}$$

The load capacitance  $C_L$  must be large enough so that the zero-dB frequency  $f_0$  lies a factor 2 below  $f_l$ :

$$f_0 = \frac{g_m l}{2\pi C_L} \leq \frac{1}{2} f_l = \frac{1}{4} f_{TN} \tag{7.1.10}$$

The dominating pole frequency  $f_2$  is:

$$f_2 = \frac{1}{2\pi R_L C_L} \tag{7.1.11}$$

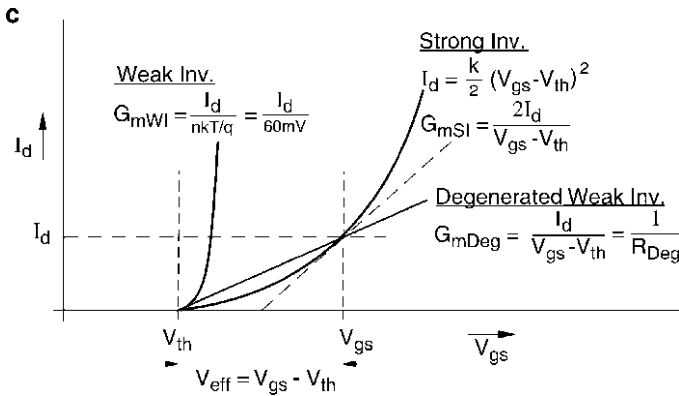


Fig. 7.1.2 (c) Comparison of the  $G_m$  of a CMOS transistor in weak inversion, strong inversion, and degenerated weak inversion

The maximum DC voltage gain (without load resistance  $R_L$ ) is limited by the parallel ( $\parallel$ ) output resistance  $R_o$  of the cascodes  $M_{14}$  and  $M_{16}$  and can be estimated at  $R_o \approx \mu_{14}r_{ds12} \parallel \mu_{16}r_{ds18} \approx 1/2 \mu r_{ds}$ :

$$A_{VOM} = G_m R_o \approx g_m \frac{1}{2} \mu r_{ds} \approx \frac{1}{2} \mu_P \mu_N \tag{7.1.12}$$

The maximum value of of the voltage gain  $\mu_P$  or  $\mu_N$  for P-channel or N-channel CMOS transistors, respectively, may vary from 30 to 300, depending on the chosen W/L ratio and on the current level.

### Telescopic-Cascode Operational Amplifier

In cases where the common-mode input voltage range need not be large, for instance in an inverting integrator (see Fig. 3.5.5), a telescopic cascode may be used instead of a folded cascode output stage. This OpAmp is shown in Fig. 7.1.3.

A very important feature is that the telescopic OpAmp only needs half the supply current of the folded version for the same maximum output current and  $G_m$ . Moreover, the extra noise and offset of the extra currents sources in the folded cascode stage are not present here. A disadvantage, though, is that the minimum supply voltage is one saturation voltage higher than that of the folded version. For the folded version of Fig. 7.1.2a the minimum supply voltage is:  $V_S = V_{SP} - V_{SN} = V_{diode11} + V_{sat15} + V_{sat17}$ , while the minimum supply voltage for the telescopic version is  $V_S = V_{sat9} + V_{sat1,2} + V_{sat3,4} + V_{diode5}$ .

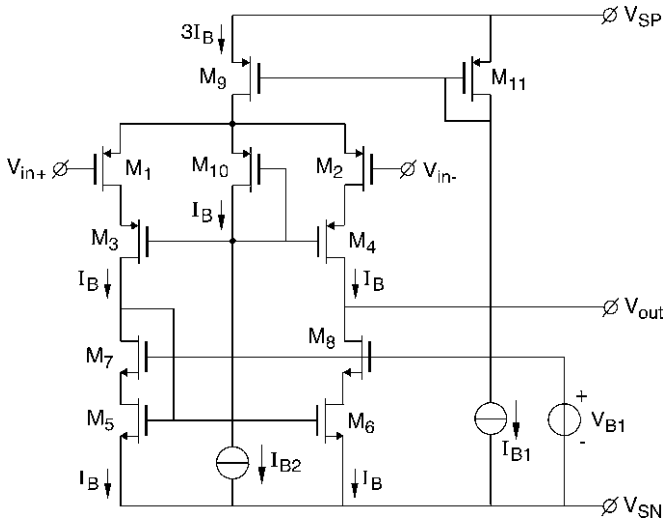


Fig. 7.1.3 Telescopic cascoded class-A operational amplifier with GA-CF configuration

A disadvantage of the telescopic OpAmp is that the common-mode input voltage range of the telescopic version can not include the negative rail voltage at all. Nor can the common-mode input voltage cover much of the output voltage range. The output CM voltage can not come higher than a threshold voltage minus two saturation voltages above the input CM voltage.

### Feedforward HF Compensation

The main advantage of the preceding simple GA-CM or CF circuits is that the zero-dB bandwidth lies only a factor 4 below the  $f_T$  of the transistors. Ways to improve the bandwidth are based on bypassing the mirrors or cascodes by an  $R_F C_F$  all pass network [7.1, 7.2]. This eliminates the PNPs from the HF path in the OTA in Fig. 7.1.4 so that the limiting pole frequency  $f_l$  is equal to  $1/2 f_{TN}$  of an NPN mirror. Note that the HF feedforward network has been crosscoupled to match the negative transfer of the mirrors.

Moreover, the HF feedforward network provides a direct HF path from the collector of  $Q_1$  to the output without a limiting-pole frequency.

This same HF path, but not crosscoupled, is provided in the CMOS folded cascode amplifier of Fig. 7.1.5. The partly elimination of the dominating pole makes that the zero-dB bandwidth  $f_0$  may approach  $1/2 f_T$ , or even  $f_T$ , by the HF-bypassing of the internal connection. Note that the elimination is only at one half and that the output load also influences the existence of a pole-zero doublet in the frequency characteristic.

A disadvantage of the simple circuits of Figs. 7.1.1 and 7.1.2 is the relatively low transconductance  $G_m$  and DC gain  $A_{V0}$ . Many approaches have been made to increase the  $G_m$  or  $A_{V0}$ . Some of these approaches will be discussed in the following sections.

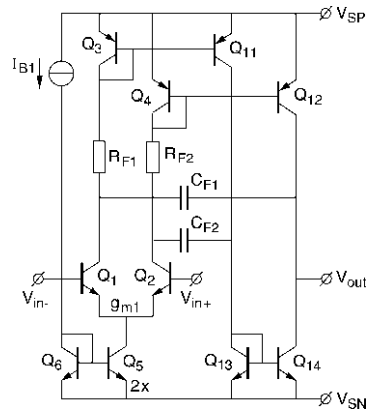
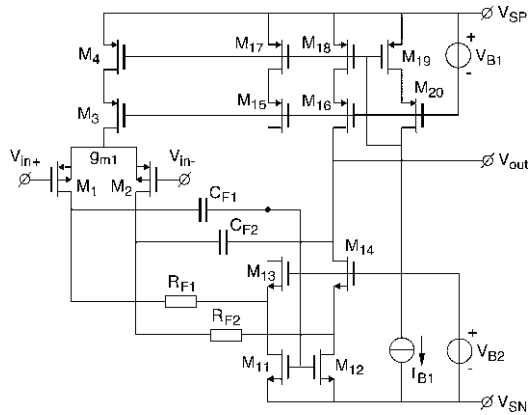


**Fig. 7.1.4** OTA with GA-CM configuration and a crosscoupled HF feedforward network  $R_{F1}C_{F2}$  and  $R_{F2}C_{F1}$

**Fig. 7.1.5** Folded-cascode amplifier with GA-CF configuration and a straight HF feedforward network  $R_{F1}C_{F1}$  and  $R_{F2}C_{F2}$



### Input Voltage Compensation

The most important attribute of an input stage is its transconductance  $g_m$ . Bipolar transistors provide the largest  $g_m$  at a certain quiescent current in nature. Their  $g_m = I_E/V_T$  with  $V_T = kT/q$  is determined by the Boltzmann statistics for distribution of charge carriers in a semiconductor. There is no motive for charge carriers in a junction to react more sensitively to a voltage than according to the Boltzmann statistics law. Tunneling or other quantum effects may break this law. Yet, there is a demand to improve the  $g_m$  without enlarging the quiescent current. A network approach to do something is to compensate one source or emitter resistance with another of the same value but with a negative sign by positive feedback. A basic circuit is drawn for a bipolar and CMOS circuit in Figs. 7.1.6 and 7.1.7 [7.3].

The cross-coupled transistors  $Q_3$  and  $Q_4$  create a positive feedback loop. The currents of  $Q_1$  and  $Q_3$  are equal to  $I_{C1}$ , and those of  $Q_2$  and  $Q_4$  equal to  $I_{C2}$ , if we disregard the base currents. This means that the base-emitter voltages of  $Q_1$  and  $Q_3$  are equal:  $V_{BE1} = V_{BE3}$ , and even so those of  $Q_2$  and  $Q_4$ :  $V_{BE2} = V_{BE4}$ . The sum of the base-emitter voltages of  $Q_1$  and  $Q_4$  are equal to the sum of those of  $Q_2$  and  $Q_3$ . Hence the input voltage appears unattenuated across  $R_3$  and  $R_4$ . If  $R_3$  and  $R_4$  are chosen zero, the circuit may oscillate uncontrollably due to parasitic capacitances. The value of  $1/R_{3,4}$  may not be chosen larger than 30 times  $g_{m1,2} = 1/r_{e1,2}$  to insure stability. With non-zero  $R_3$  and  $R_4$  the transconductance  $G_m$  is:

$$G_m = \frac{\Delta I_{out}}{V_{in}} = \frac{I_{C1} - I_{C2}}{V_{in}} = \frac{-2}{R_3 + R_4} = \frac{-1}{R_{3,4}} \tag{7.1.13}$$

Note that the input stage does not inverse the signal like it does in a conventional input stage. This effect appears as a negative value of  $g_m$ . The positive feedback in  $Q_{3,4}$  does not work above the transit frequency  $f_T$  of the transistors, so the bandwidth cannot be increased by this method. But the  $g_m$  at lower frequencies can be enlarged by a factor 30, and so can the voltage gain  $A_{vo}$ .



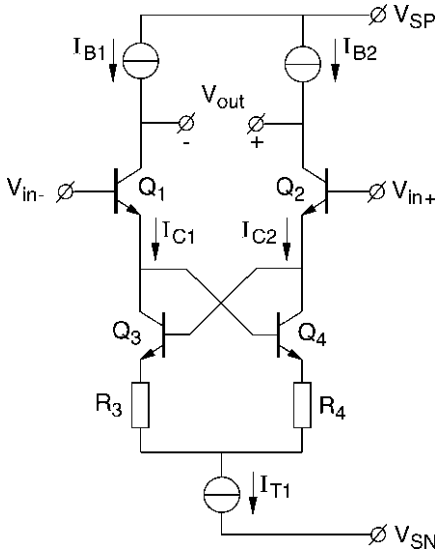


**Fig. 7.1.6** Bipolar input stage with enlarged  $g_m$  by compensation

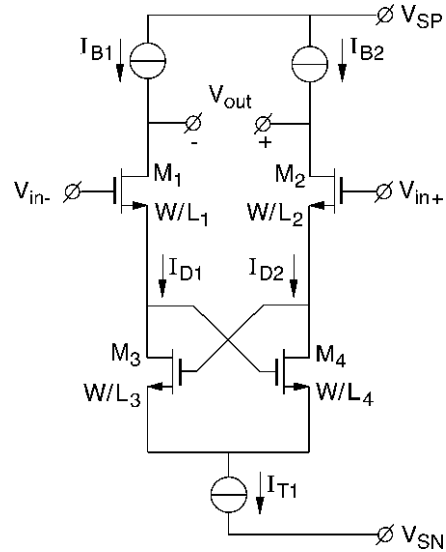


**Fig. 7.1.7** CMOS input stage with enlarged  $g_m$  by compensation and  $W/L_{3,4} < W/L_{1,2}$

The CMOS circuit in weak inversion can also be kept stable by series resistors. But by choosing the  $W/L_{3,4}$  ratio of  $M_3, M_4$  smaller than  $W/L_{1,2}$  of  $M_1, M_2$  the stability may also be assured in strong inversion

$$g_m = \frac{\Delta I_{out}}{V_{in}} = \frac{1}{1/g_{m1,2} - 1/g_{m3,4}} = g_{m1,2} \left( 1 - \sqrt{\frac{W/L_{1,2}}{W/L_{3,4}}} \right)^{-1} \quad (7.1.14)$$

When  $W/L_{3,4}$  equals  $W/L_{1,2}$  the circuit is uncontrolled. We may not choose  $W/L_{3,4}$  less than 5% smaller than  $W/L_{1,2}$  to assure stability over variations in transistor parameters. This means an increase of  $g_m$  of 20 times.

### **Input Class-AB Boosting**

Many approaches have been made to improve the slew rate and settling time of the GA-CM configuration by using a class-AB input stage. Its output current may be much larger than the quiescent current. A first approach is shown in Fig. 7.1.8a [7.4].

The input pair  $M_1 M_2$  is cross-coupled with the complementary pair  $M_3 M_4$ . Transistors  $M_5$  and  $M_6$  serve as level shifters. The translinear loop through  $M_1-M_6$

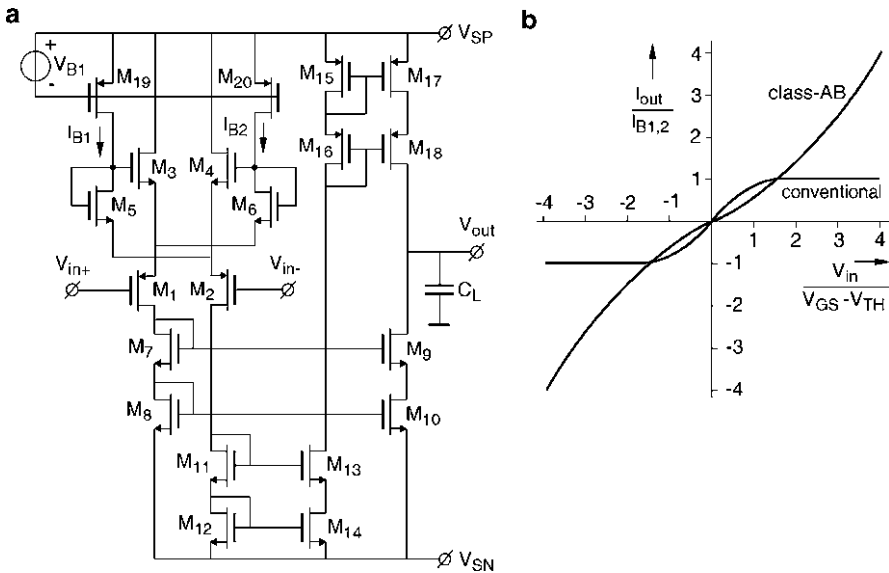


**Fig. 7.1.8** (a) Class-AB cascode current-mirrored (CCM) amplifier and (b) transconductance of the class-AB input stage

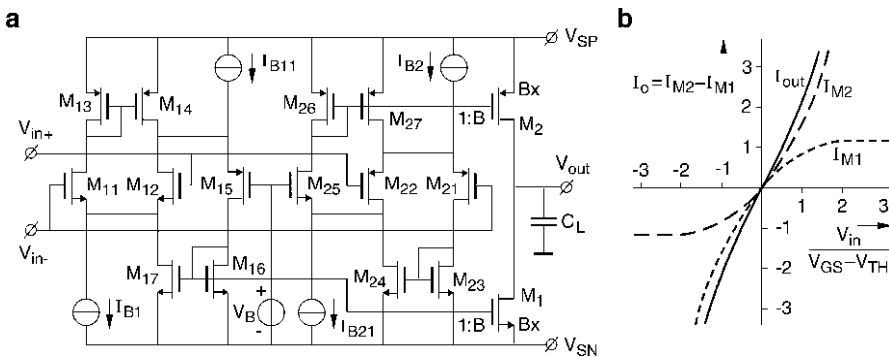


**Fig. 7.1.9** (a) OTA with class-AB biasing and (b) transconductance of the class-AB OTA of (a)

biases the transistors in class-AB as shown in Fig. 7.1.8b. A slew rate has been reported of 80 V/ $\mu$ s at a supply-power consumption of 1 mW.

A disadvantage of the above circuit is that it needs a supply voltage larger than three diodes and two saturation voltages. A circuit that can function at one diode and two saturation voltages is shown in Fig. 7.1.9 [7.5].

The first input stage  $M_{11} M_{12}$  drives its own tail current through  $M_{15} M_{16} M_{17}$  and also drives the output transistor  $M_1$ . The second stage  $M_{21} M_{22}$  does the same and drives the output transistor  $M_2$ . When the first stage has a negative input voltage the tail current boosts itself with the output current.

The current in  $M_{11}$  increases strongly, while the current in  $M_{12}$  stays nearly constant. In this way much larger signals can be processed than the quiescent current. The class-AB boost has a stable loop gain independent of the device dimensions and bias currents [7.5]. The P-channel transistors have a W/L ratio three times larger than that of the N-channel transistors to compensate the  $g_m$  for a lower mobility  $\mu$ . The output transistors  $M_1$  and  $M_2$  are scaled  $Bx$  to provide a large output current. The ratio between maximum output current  $I_{OM}$  and quiescent current  $I_Q$  is limited by the supply voltage available to  $M_{11}$  and  $M_{21}$  according to

$$\frac{V_{OM}}{V_Q} = \frac{1}{4} \left( 1 + \frac{V_{SP} - V_{SN}}{V_{GS11,21} - V_{TH}} \right)^2 \quad (7.1.15)$$

The circuit was used to drive a large capacitive load at a reasonable slew rate and settling time.

Many other approaches to class-AB input stages have been made to combine a low quiescent power consumption with a high current drive capability, slew rate, and settling time.

### ***Voltage-Gain Boosting***

The open-loop low-frequency voltage gain of the GA-CF Operational Amplifier of Fig. 7.1.2a, b can be increased by voltage gain boosting [7.6, 7.7]. The idea is to boost the voltage gain of the cascode transistors  $M_{14}$  and  $M_{16}$  by measuring their source voltages and regulating them at a constant value by actively controlling their gate voltages. The circuit is drawn in Fig. 7.1.10.

The amplifier without gain boosting had a voltage gain according to (7.1.12):  $A_{VOM} = 1/2\mu_p\mu_n$ . This gain is now boosted with the voltage gain of the differential amplifiers  $M_{21}, M_{22}$  and  $M_{31}, M_{32}$ , which is  $1/2g_m r_{ds} = 1/2\mu_p$  or  $1/2\mu_n$  multiplied by the voltage gain of the folded cascodes  $M_{25}, M_{35}$ , which is  $\mu_n$  or  $\mu_p$ . The total DC gain then becomes:

$$A_{VOM} = \frac{1}{4} \mu_p^2 \mu_n^2 \quad (7.1.16)$$

A voltage gain has been reported of 90 dB in combination with a zero-dB frequency of 116 MHz at a load capacitor of 16 pF and a power consumption of 52 mW [7.6].

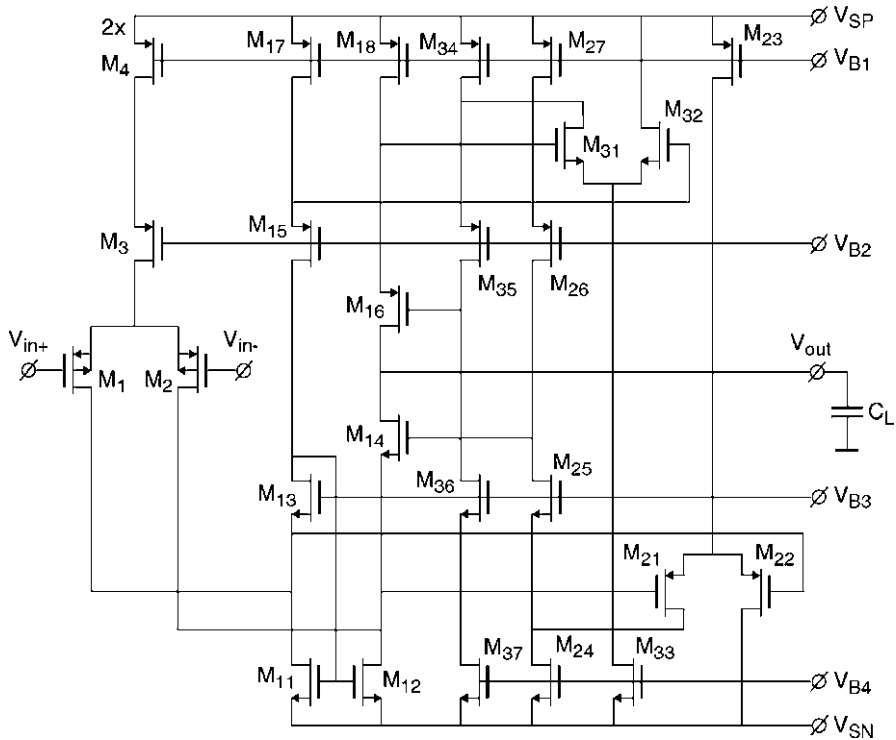


Fig. 7.1.10 Voltage-gain boosting in a class-A GA-CF operational amplifier

**Conclusion**

The GA-CF configuration has a high bandwidth  $f_0$  with a value in the order of a factor 4 lower than the transit frequency  $f_T$  of the transistors. The limited  $g_m$  and the class-A biasing makes that no significant resistive loads can be driven at a reasonable gain. The main application of this type of Operational Amplifier is to drive capacitive loads, as in integrator filters, switched capacitor filters, and sample and hold circuits. A capacitive load does not endanger HF stability, but improves it.

We have seen that the GA-CF configuration can be improved in various ways. Feedforward compensation can improve the bandwidth by a factor 2. Class-AB biasing of the input stage results in a high slew rate and fast settling. Transconductance compensation with an equal but negative value results in a higher low-frequency  $g_m$  but no larger bandwidth. Voltage boosting may greatly enlarge the DC voltage gain with pure capacitive loads.

The GA-(CM or) CF configuration will further be used as a basis for the GA-CF-VF configuration in Sect. 7.3.

### 7.2 GA-GA Configuration

The GA-GA configuration is the first step to profit from a second transconductance gain factor after the input stage. As a result, resistive loads  $R_L$  can be driven at a reasonable voltage gain, besides capacitive loads  $C_L$ . A direct consequence of two cascaded GA stages is that we have two poles and that one pole has to be compensated by an HF compensation network, which is often a Miller capacitor.

#### Basic Bipolar R-R-Out Class-A Operational Amplifier

A basic GA-GA bipolar operational amplifier is shown in Fig. 7.2.1.

The frequency characteristic of the basic GA-GA bipolar operational amplifier of Fig. 7.2.1 is given in Fig. 7.2.3.

The limiting pole frequency with the highest specified load capacitor  $C_L$  and the tranconductance  $g_{m1}$  at  $Q_{11}$  is roughly:

$$f'_1 = \frac{g_{m1}}{2\pi C_L} \tag{7.2.1}$$

The zero-dB bandwidth  $f'_0$  must be chosen half  $f'_1$  for a  $60^\circ$  phase margin by choosing the right value for  $C_{m1}$ :

$$f'_0 = \frac{g_{m2}}{2\pi C_{M1}} = \frac{1}{2} f'_1 = \frac{1}{2} \frac{g_{m1}}{2\pi C_L} \tag{7.2.2}$$

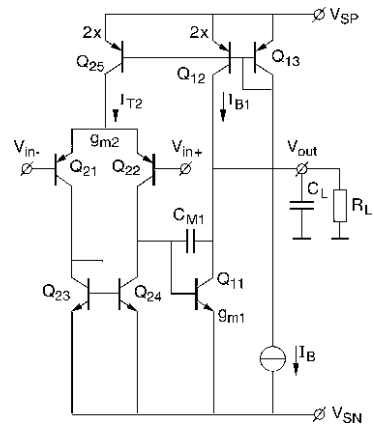


**Fig. 7.2.1** Basic bipolar R-R-out class-A GA-GA configuration in bipolar technology

The value for  $C_{M1}$  must be chosen at a value:

$$C_{M1} = 2g_{m2} \frac{C_L}{g_{m1}} = C_L \frac{I_{T2}}{I_{B1}} \quad (7.2.3)$$

The voltage gain of the amplifier is:

$$A_{V0} = g_{m2} \beta_{11} R_L \quad (7.2.4)$$

The maximum voltage gain obtained without  $R_L$  is:

$$A_{VOM} \approx g_{m2} \beta_{11} (r_{ce11} || r_{ce12}) \approx \frac{1}{4} \beta_{\mu} \quad (7.2.5)$$

The dominating pole frequency without  $R_L$  is:

$$f'_2 = \frac{f'_0}{A_{VOM}} \quad (7.2.6)$$

We have now roughly dimensioned the Operational Amplifier of Fig. 7.2.1. We are better to choose the current  $I_{B1}$  through  $Q_{11}$  equal to the tail current  $I_{T2}$  of the input stage. In that case, the base current of  $Q_{11}$ , which loads  $Q_{22}$ , compensates the offset of the base currents of  $Q_{23}$  and  $Q_{24}$ , which loads  $Q_{21}$ . This choice is also close to the optimum for a maximum bandwidth over power ratio as expressed in (6.2.27). Because of this choice the value for  $C_{M1}$  must be equal to  $C_L$ , as follows from (7.2.3).

### ***Improved Basic Bipolar R-R-Out Class-A Operational Amplifier***

Now we will try to improve the basic amplifier of Fig. 7.2.1 as shown in Fig. 7.2.2. The main improvement is to use a Darlington second stage. This enlarges the gain by roughly a factor  $\beta_{12}$  to:

$$A_{V0} \approx g_{m2} \beta_{12} \beta_{11} R_L \quad (7.2.7)$$

The extra Darlington transistor  $Q_{12}$  also requires some extra measures. An important consequence is that there is the extra pole frequency  $f_{12}$  in the Miller loop at the emitter of  $Q_{12}$ , which is loaded by the base-emitter capacitor  $C_{be11}$  of  $Q_{11}$ . Its frequency is  $f_{12} = 1/(r_{bb11} + r_{e12})2\pi C_{be11}$ . In 1975 James Solomon touched

**Fig. 7.2.2** Improved basic bipolar R-R-out class-A GA-GA configuration in bipolar

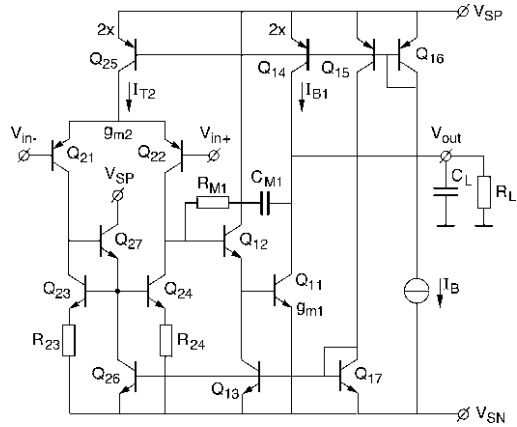
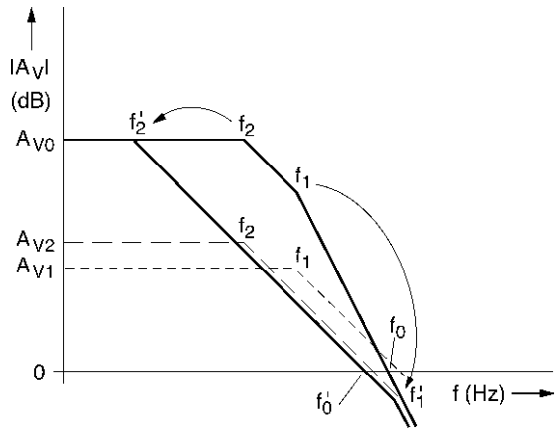


**Fig. 7.2.3** Frequency characteristic of the GA-GA operational amplifier of Fig. 7.2.1



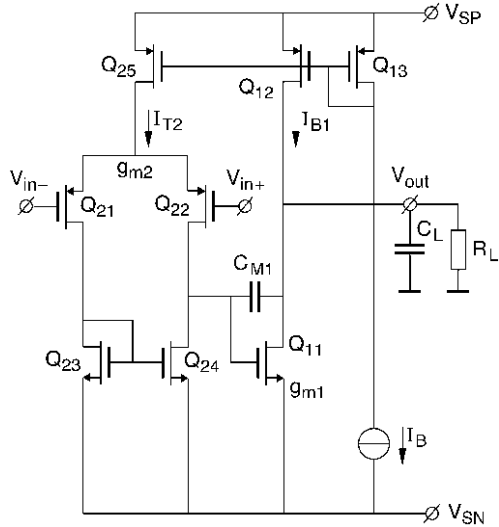
this problem in his famous OpAmp tutorial [7.10]. To place this pole frequency  $f_{12}$  at least at  $f'_1$  the current through  $Q_{12}$  must at least be  $I_{B12} = I_{B1}f'_1/f_{T1} = I_{B1}C_{be2}/C_L$ , and the bulk base resistance  $r_{bb11}$  of  $Q_{11}$  must be made small by a fingered structure of the emitter of  $Q_{11}$ .

To eliminate the extra phase shift by the right-half-plane zero  $f'_z = g_{m1}/2\pi C_{M1}$  (6.2.24), a resistor  $R_{M1}$  is placed in series with  $C_{M1}$ . Its value is chosen such that the feedforward path through  $C_{M1}$  is canceled by the  $g_m$  of  $Q_{11}$ :

$$R_{M1} = r_{e11} = 1/g_{m11} \tag{7.2.8}$$

To balance the asymmetrical load current  $i_{B12}$  at one side of the input stage, an equal load  $i_{B27}$  of the Wilson mirror transistor  $Q_{27}$  is used at the other side. The bias currents through  $Q_{12}$  and  $Q_{27}$  must be equal to prevent an induced input voltage

**Fig. 7.2.4** Basic class-A R-R-out GA-GA configuration in CMOS



offset. To further prevent the full offset and noise of  $Q_{23}$  and  $Q_{24}$  being added to the input offset and noise voltage, the emitter resistors  $r_{e23}$  and  $r_{e24}$  of these transistors have to be degenerated by  $R_{23}$  and  $R_{24}$ .

### Basic CMOS R-R-Out Class-A Operational Amplifier

In CMOS the situation is different. The voltage gain of the basic circuit of Fig. 7.2.4 is:

$$A_{VOM} = g_{m2}(2r_{ds22} || r_{ds24})g_{m1}R_L \approx \mu_2 g_{m1}R_L \tag{7.2.9}$$

The maximum voltage gain without  $R_L$  is  $\mu_2\mu_1$ .

### Improved Basic CMOS R-R-Out Class-A Operational Amplifier

The current gain can not be improved by a Darlington, but the voltage gain can be enlarged by cascoding the output transistors.

This is shown by the circuit of Fig. 7.2.5.

Inserting the cascodes  $M_{12}$  and  $M_{13}$  improves the maximum voltage gain without  $R_L$  with a factor  $\mu_3$ :

$$A_{VOM} = \mu_2\mu_1\mu_3 \tag{7.2.10}$$



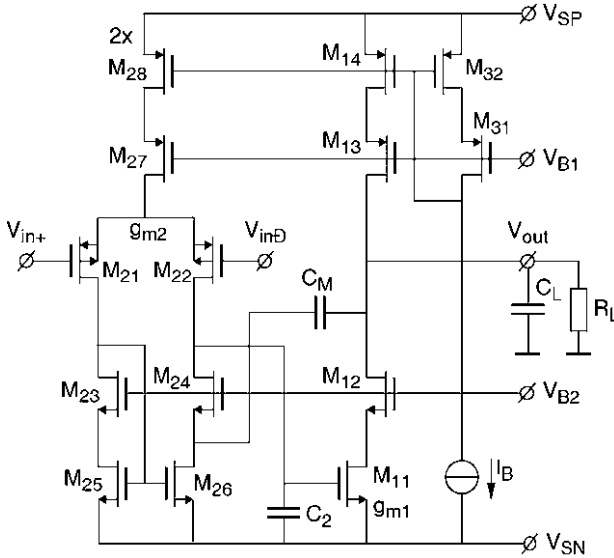


Fig. 7.2.5 Improved class-A R-R-out GA-GA configuration in CMOS

With CMOS low-capacitive loads are often applied. This increases the influence of  $C_M$  and its corresponding right-half plane zero  $f'_z$ , as discussed with Fig. 6.2.12.

To solve this problem we have connected the left-hand side of  $C_M$  to the cascode transistor  $M_{24}$  of the mirror. This cuts the feedforward path through  $C_M$  so that  $f'_z$  is eliminated. However, the limited  $g_{m24}$  of  $M_{24}$  causes another zero at  $f'_z = g_{m24}/2\pi C_M$  in the Miller loop as the current through  $C_M$  is hindered to flow through  $M_{24}$  in order to counteract the driving current from  $M_{22}$ . Several measures can be taken to repair this zero. One of them is to split  $C_M$  into two parts of which one is used as a regular Miller capacitor. One other is to use a parallel capacitor  $C_P = C_M$  from the gate of  $M_{26}$  to ground to help reducing the driving of the output transistor  $M_{11}$ .

The connection of  $C_M$  to the cascode transistor  $M_{24}$  introduces a voltage gain  $C_M/C_2$  in the Miller loop, with  $C_2$  as the parasitic capacitance at the gate of  $M_{11}$ . This loop consists of three poles, one at each output of  $M_{24}$ ,  $M_{11}$ , and  $M_{12}$ . The pole at the gate-source capacitance  $C_2$  of  $M_{11}$  dominates. If the HF stability of the loop is insufficient,  $C_2$  can artificially be enlarged.

If we had not used the cascoded current mirror to connect the left-hand side of  $C_m$  but rather a separate folded cascode chain in parallel to the input stage as in Fig. 7.1.2b (which has often been done to lower the minimum supply voltage from  $3V_{SAT} + 1V_{TH}$  to  $2V_{SAT} + 1V_{TH}$  [7.8]), all offset and noise of this chain would be added to the input voltage. To lower the additional noise and offset of  $M_{25}$ ,  $M_{26}$  these transistors must have a low  $g_m$  at a low W/L ratio in relation to those of the input pair.

## Conclusion

The bandwidth  $f'_0$  of the GA-GA configuration with Miller compensation lies roughly a factor 2 below  $f'_0$  of the GA-CF configuration at the same bias current. This is caused by the fact that we have to stay away by a factor 2 from the zero-dB frequency of the Miller loop gain for a  $60^\circ$  phase margin. The main advantage of the GA-GA configuration over the GA-CF one is a  $\beta$  or  $\beta^2$  increased transconductance of the bipolar or Darlington bipolar circuit, and a  $\mu$  improved transconductance of the CMOS circuit. This helps keeping the voltage gain high with resistive loads.

The GA-GA configuration will further be used as a basis for the description of the GA-GA-VF configuration in Sect. 7.4.

## 7.3 GA-CF-VF Configuration

The lack of a reasonable transconductance of the GA-CF configuration of Sect. 7.1 and the reduction of bandwidth of the GA-GA configuration of Sect. 7.2 makes us look to the combination of the GA-CF configuration with an output VF buffer for a larger current gain, while maintaining as much of the high bandwidth of the GA-CF topology as possible.

### *High-Speed Bipolar Class-AB Operational Amplifier*

An example of a high-speed bipolar circuit is shown in Fig. 7.3.1. It has a class-AB VF output stage with folded Darlington transistors [7.9].

The current gain  $\beta_n\beta_p$  of this VF stage is linear and fairly symmetric because each push and pull path has an NPN and a substrate PNP transistor in cascade, the total transconductance is:

$$g_{tot} = g_{m3} \beta_n \beta_p = g_{m3} \beta^2 \quad (7.3.1)$$

The limiting pole frequency  $f_I$  lies at the output, and has a value of:

$$f_I = \frac{g_{mI}}{2\pi C_L} = \frac{2I_{BI}q}{2\pi C_L kT} = \frac{I_{BI}}{\pi C_L V_T} \quad (7.3.2)$$

with:  $g_{mI} = g_{mI1} + g_{mI2}$ .

The two transconductances of the output transistors  $g_{mI1}$  and  $g_{mI2}$  are in parallel to each other. This helps to keep the quiescent current  $I_{BI}$  a factor 2 lower for a certain bandwidth than with a single VF transistor.

Moreover, the phase shift of the VF output stage is reduced by the feedforward path of its base-emitter capacitances. This means a zero in the left-hand plane at the

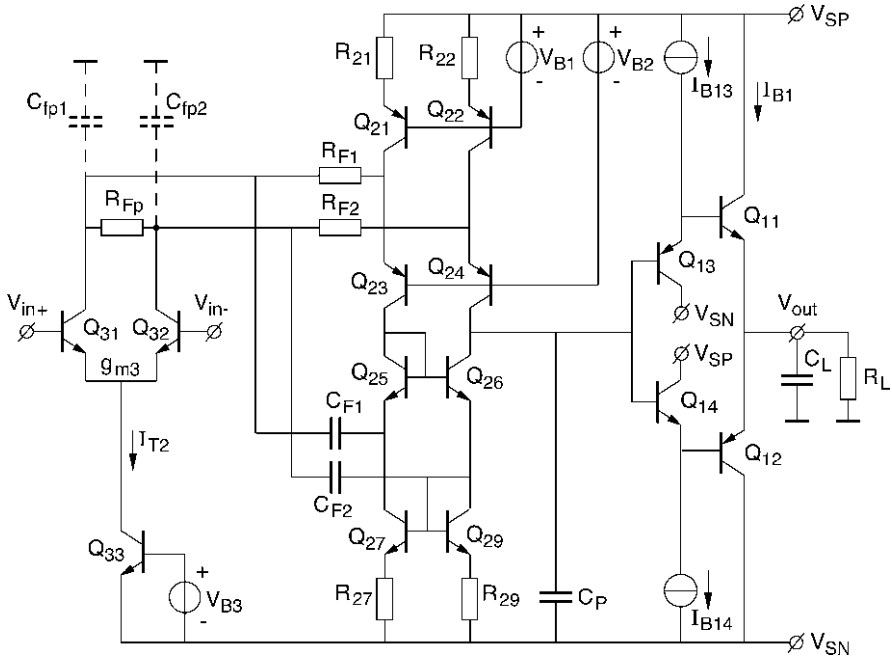


Fig. 7.3.1 High-speed GA-CF-VF configuration with a class-AB folded Darlington output stage

$f_T$  of these transistors. We do have to keep the bulk base resistors  $r_{bb}$  low by a fingered layout of the emitter. The zero-dB bandwidth  $f'_0$  of the whole amplifier must be chosen again at half of  $f_l$  by the choice of  $C_p$ .

$$f'_0 = \frac{g_{m3}}{2\pi C_p} = \frac{1}{2} f_l = \frac{g_{m1}}{4\pi C_L} = \frac{I_{B1}}{2\pi C_L V_T} \tag{7.3.3}$$

$$C_p = C_L = \frac{2g_{m3}}{g_{m1}} \tag{7.3.4}$$

The quiescent currents through the Darlington transistors  $Q_{13}$  and  $Q_{14}$  should be at least  $I_{B13} \geq I_{B11} C_{be11}/C_L$ , and  $I_{B14} \geq I_{B12} C_{be12}/C_L$ , to avoid a second limiting pole in the Darlington output stage, with  $I_{B11}$  and  $I_{B12}$  the bias currents of the output transistors  $Q_{11}$  and  $Q_{12}$ , respectively.

A disadvantage of the class-AB VF output buffer is that its non-linear diode voltage characteristic is outside the grip of the compensation capacitor  $C_p$ . Therefore, at high frequencies below  $f'_0$ , where the external loop gain is low, the distortion will be relatively high.

Another disadvantage of the Darlington VF output buffer is that it might peak or even oscillate at high frequencies when the amplifier is heavily capacitively loaded. Solomon calls this the output bump [7.10]. The situation is depicted in Fig. 7.3.2.

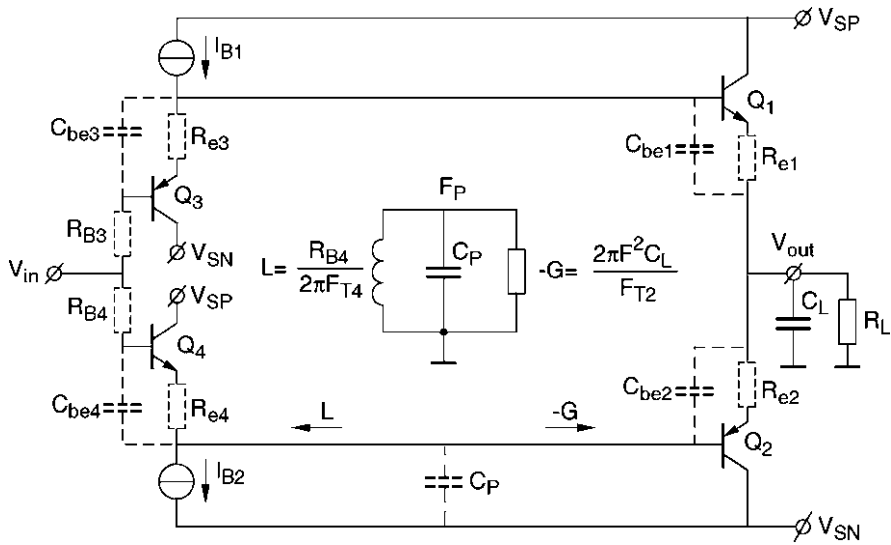
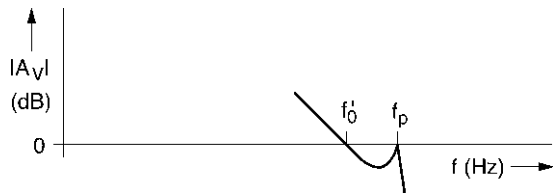


Fig. 7.3.2 Frequency peaking of the VF Darlington output stage

Fig. 7.3.3 Amplitude characteristic of the frequency peaking in a Darlington VF output buffer



The PNP output emitter follower \$Q\_2\$ shows a negative input conductance \$-G\_T = 2\pi f^2 C\_L / f\_{T2}\$. While the Darlington emitter follower \$Q\_4\$ shows an inductive output \$L = R\_{B4} / 2\pi f\_{T4}\$. Together with the interstage capacitor \$C\_P\$ the circuit gives rise to a resonance LC circuit at a resonance frequency of \$f\_p = (1/2\pi)\sqrt{LC\_P}\$ with a poor damping. The effect is shown in the amplitude characteristic of Fig. 7.3.3. The design parameters must be chosen such that the top of the peak remains sufficiently below 0 dB, by choosing a fingered layout for the emitter of \$Q\_4\$ to lower \$R\_{B4}\$.

The input and folded-cascode stages have been sufficiently described in Sect. 7.1. It will be noted that into the all-pass current network \$R\_F C\_F\$ behind the input stage a parallel resistor \$R\_{fp}\$ has been inserted. This is used to compensate at low frequencies the attenuation caused by the parasitic substrate capacitors \$C\_{fp1}\$ and \$C\_{fp2}\$ at the left-hand side of \$C\_{F1}\$ and \$C\_{F2}\$ which take away about 20% of the HF current. The resulting pole-zero doublet has a value of one or two percent. It is important that the remaining pole-zero doublet is small as this appears in the overall frequency characteristic of the whole amplifier and results in a slow settling component in the step response of the OpAmp.

The turn-over frequency of \$R\_F C\_F\$ must be made more than three times lower than the \$f\_T\$ of the PNP cascode. The bandwidth of the level shift stage is equal to that of

the  $f_T$  of the NPN transistors, loaded with the parasitic parallel capacitors  $C_{fp1}$  and  $C_{fp2}$  of the capacitors  $C_{F1}$  and  $C_{F2}$ , respectively.

The all-pass network and its pole-zero doublet can be completely eliminated when the bipolar process allows for vertical PNPs with high  $f_T$ . This is of advantage for a short settling time. A settling time to 0.1% of 100  $\mu$ s was reported [7.9] with a slew rate of 375 V/ $\mu$ s, and a GBW of 60 MHz. CMOS versions of the GA-CF-VF configuration have been made in early years, but the relatively low  $g_m$  of the VF output buffer results in a low limiting pole frequency. Moreover, the large voltage loss across the diodes of the VF buffer makes the CMOS variant less attractive.

### High-Slew-Rate Bipolar Class-AB Voltage-Follower Buffer

A very special simplification of the GA-CF-VF configuration is the high slew-rate voltage follower of Fig. 7.3.4 with an GA-VF configuration. Because the input is always connected to the output, there is no need for a level shift stage. When we replace the compensation capacitor  $C_P$  with  $C_C$  between the collector and emitter of  $Q_{21}$ , the compensation still functions, but the slew rate is not reduced by  $C_C$  because it is bootstrapped with the CM signal voltage. The slew rate is limited by the parasitic capacitance  $C_P$ .

An asymmetric slew-rate can be observed in all OpAmps connected as voltage followers by the effect of the parasitic tail capacitor  $C_T$  of the input stage. If the input voltage goes down, the capacitor decreases the tail current  $I_{T2}$  and the slew rate decreases. But if the input voltage goes up, the slew rate increases. The downwards slew rate of the voltage follower is limited to:

$$S_{r\text{down}} = I_{B2}/(C_P + C_T) \tag{7.3.5}$$

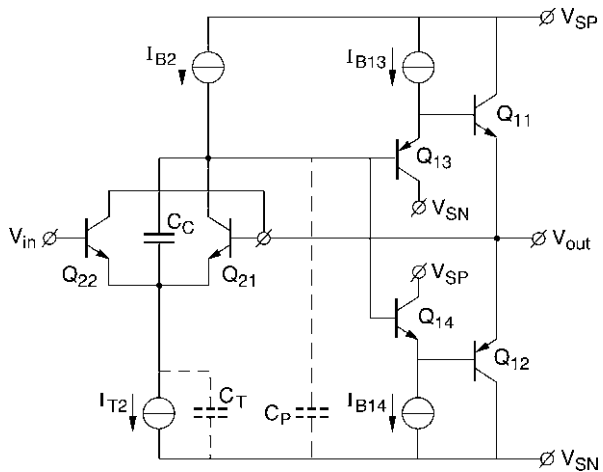


Fig. 7.3.4 High-slew-rate voltage follower in GA-VF configuration

## Conclusion

The high bandwidth of the GA-CF configuration combined with a high bipolar transconductance VF output buffer raises an excellent bipolar amplifier with an GA-CF-VF configuration. The bandwidth and slew rate can be chosen high. The settling time is particularly high when the bipolar process allows for complementary vertical PNPs with high  $f_T$ , so that the all-pass network and its pole-zero doublet can be eliminated. But still a high bandwidth can be obtained. CMOS versions of the GA-CF-VF configuration are less attractive because of the high voltage loss and relative low transconductance of the VF buffers at high output currents.

## 7.4 GA-GA-VF Configuration

Most of the favourite classic bipolar Operational Amplifiers have been made in the GA-GA-VF configuration. These include the  $\mu A741$  [7.11], and many others.

It was about this configuration that James E. Solomon wrote his famous tutorial study in 1974 [7.10]. It is still a good overview paper about this type of OpAmp in bipolar technology.

### *General Bipolar Class-AB Operational Amplifier with Miller Compensation*

The general topology is shown in Fig. 7.4.1. It is composed of the GA-GA circuit of Fig. 7.2.2 and the basic VF output stage of Fig. 5.3.1a. Most of the HF behaviour is already described with the GA-GA stage, except for the addition of the limiting pole frequency of the output stage, which is described with the GA-CF-VF circuit of Fig. 7.3.1.

In overviewing the HF behavior we have two limiting pole frequencies. One at the capacitive loaded VF stage:

$$f_1 = \frac{g_{m1}}{2\pi C_L} = \frac{I_{B1}}{\pi C_L V_T} \quad (7.4.1)$$

with:  $g_{m1} = g_{m11} + g_{m12}$ .

And the other limiting frequency at the Miller compensated output of the intermediate stage:

$$f_2 \approx \frac{g_{M2}}{2\pi(C_{p2} + C_{M1})} = \frac{I_{B2}}{2\pi(C_{p2} + C_{M1})V_T} \quad (7.4.2)$$

with  $g_{m2} = g_{m21}$ .

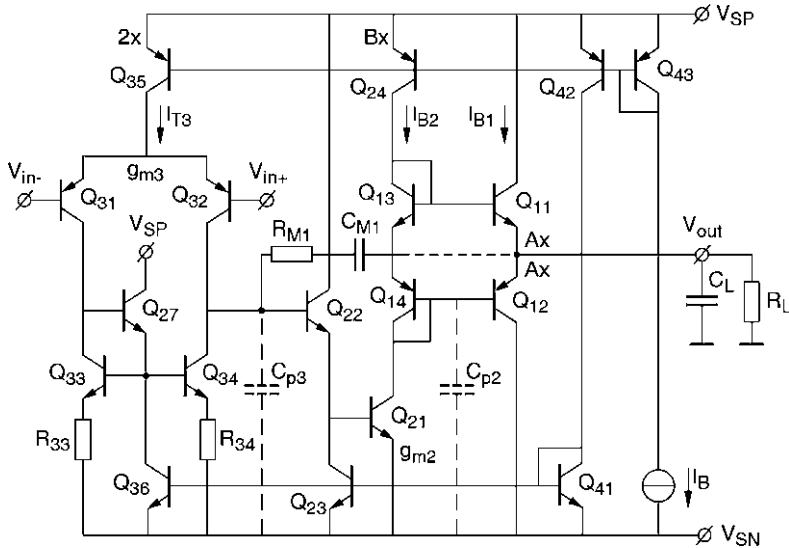


**Fig. 7.4.1** General class-AB GA-GA-VF configuration in bipolar technology with Miller compensation (MC)

When we choose to let the load capacitance set the limiting frequency,  $f_l$ , the other one  $f_2$  must be made at least twice  $f_l$ :

$$f_2 \geq 2f_l \tag{7.4.3}$$

The zero-dB frequency must be chosen half of  $f_l$ :

$$f'_0 = \frac{1}{2}f_l = \frac{I_{B1}}{2\pi C_L V_T} \tag{7.4.4}$$

And the value of  $C_{MI}$  becomes:

$$C_{MI} = \frac{g_{m3}}{2\pi f'_0} = \frac{I_{T3}/2}{I_{B1}} C_L \tag{7.4.5}$$

The parasitic pole in the Darlington pair  $Q_{21}, Q_{22}$  must be coped with, as described with the GA-GA stage. The value of  $R_{MI}$  must be chosen closely to  $1/g_{m21}$  to eliminate the zero in the right half complex plane along with its extra phase shift.

An important drawback of the connection of the Miller capacitor to the input of the VF output stage is that the non-linearity of the output-stage's voltage transfer is not suppressed by the Miller loop. For that reason a relatively high non-linear signal component can be found at high frequencies where the external loop gain is low. This was also the case with the GA-CF-VF configuration. However, now we can try

to incorporate the output buffer into the active Miller loop, by connecting  $C_{ml}$  to the final output  $V_{out}$  (see dotted line in Fig. 7.4.1). Stability of the Miller loop must now be ensured while the limiting pole frequency  $f_l$  is incorporated into the Miller loop. The Miller loop becomes an GA-VF stage in itself, which must be compensated to:

$$f'_{02} = \frac{1}{2} f_l \quad (7.4.6)$$

For this purpose the parasitic capacitor  $C_{p2}$  must be artificially enlarged to:

$$C_{p2} = \frac{2g_{m2}}{2\pi f_l} = \frac{I_{B2}}{I_{B1}} C_L \quad (7.4.7)$$

The bandwidth of the whole amplifier must now again be reduced a factor 2 for a phase margin of  $60^\circ$  to:

$$f'_0 = \frac{1}{2} f'_{02} = \frac{1}{4} f_l \quad (7.4.8)$$

This leads to a choice of  $C_{ml}$ :

$$C_{Ml} = \frac{g_{m3}}{2\pi f'_0} = \frac{I_{T3}}{I_{B1}} C_L \quad (7.4.9)$$

Though the external loop gain is reduced by a factor of 2, the loop gain around the output buffer is roughly increased by a factor  $C_{Ml}/C_{p2}$  at high frequencies. This may improve the HF linearity by factor 2 to 10. It must be noted, however, that the slew-rate is reduced by a factor 2, according to the reduction of the bandwidth. So, the non-linearity due to the input stage increases at high frequencies (see also Sect. 6.4, and [7.33]).

An alternative solution to enlarging the parasitic capacitor  $C_{p2}$  is to split  $C_{ml}$  at it's right hand, for instance, partly 2/3 to the final output, and partly 1/3 to the input of the output stage, like in forward nested Miller compensation (see Fig. 6.2.29). This solution does not reduce the bandwidth by a factor 2.

### ***$\mu$ A741 Operational Amplifier with Miller Compensation***

An equivalent circuit of the  $\mu$ A741 Operational Amplifier of Fairchild [7.10, 7.11] is shown in Fig. 7.4.2.

The VF-CF connected input pair functions like an GA stage, only it is non inverting (NIGA). The NPN VF pair  $Q_1, Q_2$  reduces the input bias current by its large current gain  $\beta$  to 80 nA at a collector bias current of 10  $\mu$ A. The  $g_m$  is half that of a regular pair because we have four emitters in series, instead of two emitters.



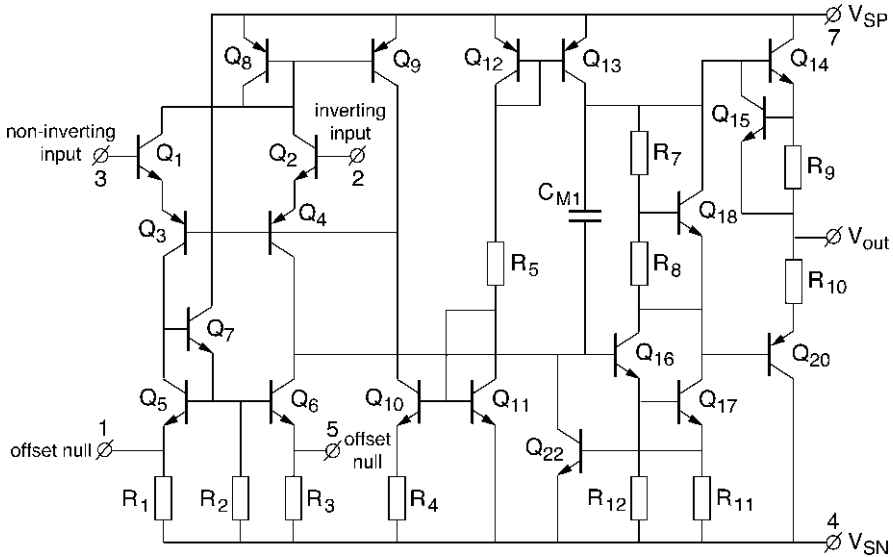


**Fig. 7.4.2** Equivalent circuit of the  $\mu\text{A741}$  GA-GA-VF operational amplifier with Miller compensation (MC)

A common-mode feedback loop senses the sum of the collector currents of the NPN pair and compares it through a current mirror  $Q_8, Q_9$  with the current of a current source  $Q_{10}$ . By this loop the common-base point of the PNP CF pair  $Q_3, Q_4$  is controlled. In this way the voltage of the common base point follows the CM input voltage at the right bias.

The resistors  $R_1$  and  $R_3$  degenerate the current mirror load in order to lower its offset and noise contribution. The DC load current of the input stage is balanced by equal base currents through  $Q_7$  and  $Q_{16}$  in order to avoid offset.

The biasing of the output transistors is performed by a current source  $Q_{13}$  and a transistor  $Q_{18}$  connected with  $R_7$  and  $R_8$  as a diode with about two  $V_{BE}$  voltages. The biasing current of the whole amplifier of  $70 \mu\text{A}$  is derived from  $R_5$ .

A short-circuit current limiting transistor  $Q_{15}$  compares its  $V_{BE}$  with the voltage across a resistor  $R_9$  which measures the upper output current. If the output current is larger than  $25 \text{ mA}$ , the driving of the upper output transistor  $Q_{14}$  is taken away.

The drive current of the lower output transistor  $Q_{20}$  is limited by transistor  $Q_{22}$  which similarly measures the current through  $R_{11}$ . The limited current gain  $\beta_{20}$  of the lower substrate output PNP  $Q_{20}$  further limits its current to  $25 \text{ mA}$ .

The intermediate Darlington stage  $Q_{16}, Q_{17}$  is Miller compensated by  $C_{ml}$  of  $30 \text{ pF}$ . The bandwidth  $f'_0$  is slightly less than  $1 \text{ MHz}$ . The double voltage compliance  $V_{in \max}$  of the VF-CF input stage allows a two times larger slew rate  $S_r$  of  $0.5 \text{ V}/\mu\text{s}$  than Eq. 6.3.3 indicates. The double voltage compliance, on the other hand, increases any input offset voltage with a factor 2.

The two GA stages in cascade provide an abundance of DC gain  $A_0$ , which is in the order of  $2 \cdot 10^5$ .

A well-elaborated realization with a class-AB input stage that provides a large slew rate is described by Widlar [7.12].

## ***Conclusion***

The GA-GA-VF configuration has been made in many variations and yields high gain, medium bandwidth, medium output current, in applications where no rail-to-rail output range is necessary. The topology combines well with bipolar transistors and it is a favourite classic OpAmp solution. The popular  $\mu$ A741 is based on this configuration.

## **7.5 GA-CF-VF/GA Configuration**

When we would like to avoid PNP transistors in the output stage in order to obtain a high output current drive capability and good HF behavior, we can apply an all-NPN compound VF/GA output stage and combine it with an GA-CF configuration.

An in-between approach towards the GA-CF-VF/GA configuration would be to use the GA-CF-VF configuration of Fig. 7.3.1 in combination with one of the many semi-complementary compound output stages with feedforward biasing of Figs. 5.3.8, 5.3.9, and 5.3.10, or with feedback biasing of Figs. 5.4.4 and 5.4.5.

However, the signal path through the PNP transistor, which is still present in these semi-complementary compound output stages, impairs the HF behavior of the lower output transistor and lowers its limiting pole frequency.

### ***High-Frequency All-NPN Operational Amplifier with Mixed PC and MC***

A better approach is to optimally utilize the large current and HF capability of the NPN transistors in an “all-NPN” GA-CF-VF/GA as shown in Fig. 7.5.1.

Figure 7.5.1 shows the combination of the GA-CF-VF configuration of Fig. 7.3.1 combined with the VF/GA output stage of Fig. 5.4.6. The high-frequency path is made up of only NPN transistors [7.1].

It is interesting to see how similarly the upper VF output Darlington pair  $Q_{11}$ ,  $Q_{13}$  functions in regard to the lower GA output Darlington pair  $Q_{12}$ ,  $Q_{14}$  when both these pairs are driven by current sources from the outputs of the CF intermediate stages. Their HF transadmittances are  $2\pi C_{P1}$  and  $2\pi C_{M1}$ , respectively, are equal if  $C_{P1} = C_{M1}$ . Their HF output impedances are  $1/g_{m11}$  and  $1/g_{m12}$ , which are equal if  $I_{11} = I_{12}$  in the quiescent situation.

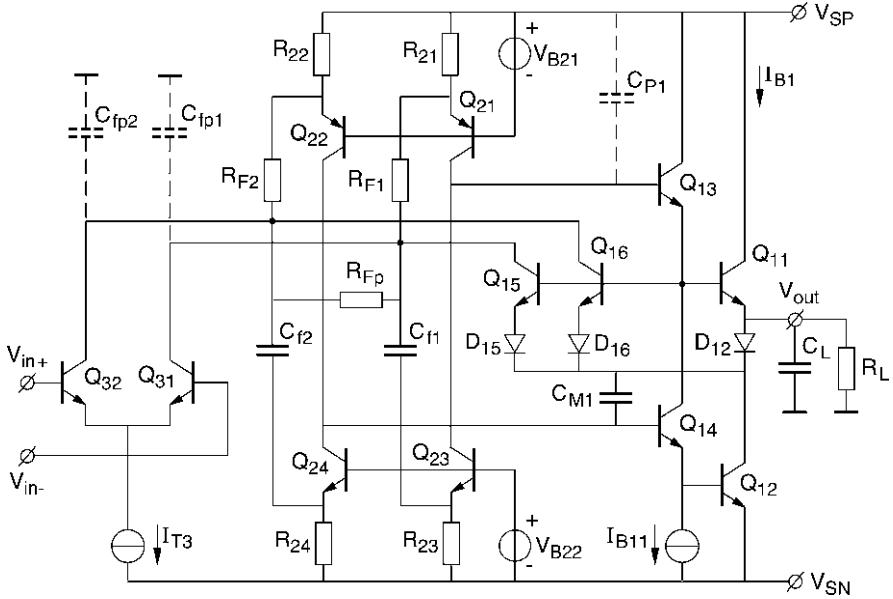


**Fig. 7.5.1** High-frequency “All-NPN” GA-CF-VF/GA configuration with parallel compensation (PC) and Miller compensation (MC)

The sum of the  $V_{BE}$  of  $Q_{11}$  and  $D_{12}$  is measured by  $Q_{15} D_{15}$  and  $Q_{16} D_{16}$  and regulated in a common-mode feedback loop. By this loop the product of the push and pull output currents is regulated at a constant value, as explained with Fig. 5.4.6.

The limiting pole frequency  $f_l$  is set by:

$$f_l = \frac{g_{m1}}{2\pi C_L} = \frac{I_{B1}}{\pi C_L V_T} \tag{7.5.1}$$

with  $g_{m1} = g_{m11} + g_{m12}$ .

At a bias current of the output transistors of  $I_B = 0.5$  mA and a load capacitance of  $C_L = 100$  pF, the limiting pole frequency is  $f_l \approx 60$  MHz. The zero-dB bandwidth must be chosen:

$$f'_0 = \frac{1}{2} f_l \approx 30 \text{ MHz} \tag{7.5.2}$$

When we choose a tail current of the input pair of  $I_{T3} = 100$   $\mu$ A, the  $g_{m3}$  of the input stage is 1/1,000 S. The value of  $C_{P1}$  and  $C_{M1}$  must then be chosen:

$$C_{P1} = C_{M1} = \frac{g_{m3}}{2\pi f'_0} = 6 \text{ pF} \tag{7.5.3}$$

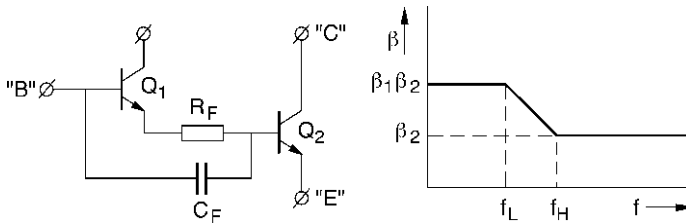


**Fig. 7.5.2** HF bypassing of the first transistor of a Darlington pair to cure the HF peaking

The currents must be chosen slightly higher than calculated. At the output, there is the extra series diode impedance of  $D_{I2}$  which lowers the limiting pole frequency of the lower Miller-compensated output transistor. So, the output bias current must be chosen about 30% larger to obtain the right  $g_{mI}$ .

The input tail current must be chosen 20% larger to overcome the leakage into the parasitic capacitors  $C_{fp1}$  and  $C_{fp2}$ . These are partly caused by the substrate sides of the feedforward capacitors  $C_{F1}$  and  $C_{F2}$ . At low frequencies the gain is equally reduced by a shunt resistor  $R_{FP}$ .

One of the problems of Darlington output transistors is their peaking, as we have shown with Fig. 7.3.2. This is particularly the case when we wish to deliver large output currents, i.e., 100 mA or higher. At high output currents, the output Darlington has a parasitic pole in between the two stages, caused by the emitter impedance of the first transistor and the diffusion capacitor  $C_{BE}$ , which becomes large at high currents.

To cope with this the bias current  $I_{B11}$  of the first transistors must be high, and the bulk base resistance of the first transistor low by a fingered layout.

A general cure is to bypass the first transistor of the Darlington pair for high frequencies, as is shown in Fig. 7.5.2.

The value of the upper turnover frequency  $f_H = 1/2\pi R_F C_F$ , and of the lower on  $f_L = 1/2\pi \beta_1 R_F C_F$ .

The offset and noise of the Operational Amplifier is somewhat degraded by the offset and noise of the current source resistors  $R_{21}$  through  $R_{24}$  and the class-AB regular transistors  $Q_{15}$  and  $Q_{16}$ , which add with their current offset and noise to the equivalent input voltage offset and noise.

### Conclusion

The “all-NPN” GA-CF-VF/GA configuration of Fig. 7.5.1 is an efficient circuit in regard to bandwidth/power ratio, disregarding the diode voltage losses at the output. It has a large programmable quiescent current range.

The amplifier works perfectly at very low quiescent currents in the order of 10  $\mu$ A, while the bandwidth depends on the load capacitor. Even at high quiescent currents of the order of 10 mA, without Darlington in the output stage, the

amplifier has been used up to 1 GHz in a  $50\ \Omega$  source and load environment [7.13]. However, at a  $50\ \Omega$  load and no Darlington transistors, the voltage gain is restricted to 40–50 dB. To provide a larger gain we have to insert an GA intermediate stage, as we will describe in the next chapter.

The input voltage noise of the amplifier is somewhat degraded by the extra noise of the current source resistors in the intermediate stage and the class-AB control transistors.

## 7.6 GA-GA-VF/GA Configuration

When we want more gain, lower voltage noise and a lower offset voltage than with the previous GA-VF-VF/GA configuration, it is better to shield the noise and offset sources of the output stage from the input stage by an GA intermediate gain stage. We then obtain the GA-GA-VF/GA configuration.

### *LM101 Class-AB All-NPN Operational Amplifier with MC*

The design of the famous LM101 was described by Widlar in 1967 as a monolithic OpAmp with simplified frequency compensation [7.14]. Before that time the architecture of Operational Amplifiers resembled some of the limitations of the early tube versions. Widlar reduced the high-frequency compensation scheme to a simple Miller compensation. Though the output stage principally has a compound VF/GA configuration with all-NPN output transistors  $Q_{16}$  and  $Q_{11}$ , the stage has the overall function of a semi-complementary full voltage-follower VF stage. At the lower output side the voltage-follower VF function of  $Q_{12}$  dominates, while being boosted by the GA slave-connected transistor  $Q_{11}$ . At the upper output side we have the folded-Darlington VF pair  $Q_{13}$ ,  $Q_{16}$ . The total compound stage has earlier been described with Fig. 5.3.10. The frequency compensation could be reduced to one Miller capacitor  $C_M$  which has been connected across the intermediate GA Darlington pair  $Q_9$  and  $Q_{10}$ . Its frequency compensation has already been described with Figs. 6.2.8. and 7.4.1.

The input stage consists of a non-inverting general amplifier (NIGA). It uses NPN input transistors  $Q_1$  and  $Q_2$  with good  $\beta$  for a low input bias current. These input transistors are connected as voltage followers. The complementary PNP transistors  $Q_3$  and  $Q_4$  function as cascodes to the emitters of the input transistors. The whole functions like a differential PNP input pair with an input bias current of that of an NPN pair. Only, the offset voltage is larger than that of a single differential pair because the offset of the NPN and PNP transistor pairs are summed. The input stage is biased by the diode-connected secondary collectors of  $Q_3$  and  $Q_4$  in combination with a current source  $Q_{21}$ . These diode-connected secondary collectors and the primary collectors of  $Q_3$  and  $Q_4$  can be seen as a pair of current mirrors.

These mirrors are biased at the “tail” of the diode connected secondary collectors by the collector current source of  $Q_{21}$ . The three-transistor mirror  $Q_5$  through  $Q_7$  provides for a single-ended output of the input stage. This structure provides for equal early voltages for the output of the input transistors at  $Q_3$  and  $Q_4$  and the mirror load current sources  $Q_5$  and  $Q_6$ . Also, the base current load of  $Q_9$  is compensated by the base current load of  $Q_7$ .

The other transistors provide bias and protection functions. The junction FET  $Q_{18}$  functions as a biasing resistor to the bias generators  $Q_{19}Q_{20}$ ,  $Q_{21}Q_{22}$ , and the multiple-collector transistor  $Q_{17}$ . The input transistors are protected against reverse base-emitter voltages by the reverse-connected diodes  $Q_{23}$  and  $Q_{24}$ .

Output current limitation is provided by the resistors  $R_{10}$  and  $R_{11}$  in combination with the translinear loop of  $Q_{11}Q_{12}Q_{14}Q_{16}$  for positive output currents and with the base-emitter voltage of  $Q_{15}$  for negative going output currents. The voltage divider  $R_7$ ,  $R_8$  in combination with  $Q_8$  limits the drive current of  $Q_{11}$ . This would otherwise become too large in regard to the drive current of the upper output transistor  $Q_{16}$ . The latter is limited by the bias current source provided by a collector of  $Q_{17}$ .

The LM101 has a bandwidth of about 1 MHz, and a straight 6 dB/oct roll-off from a DC gain of 100 dB (see Fig. 7.6.1).

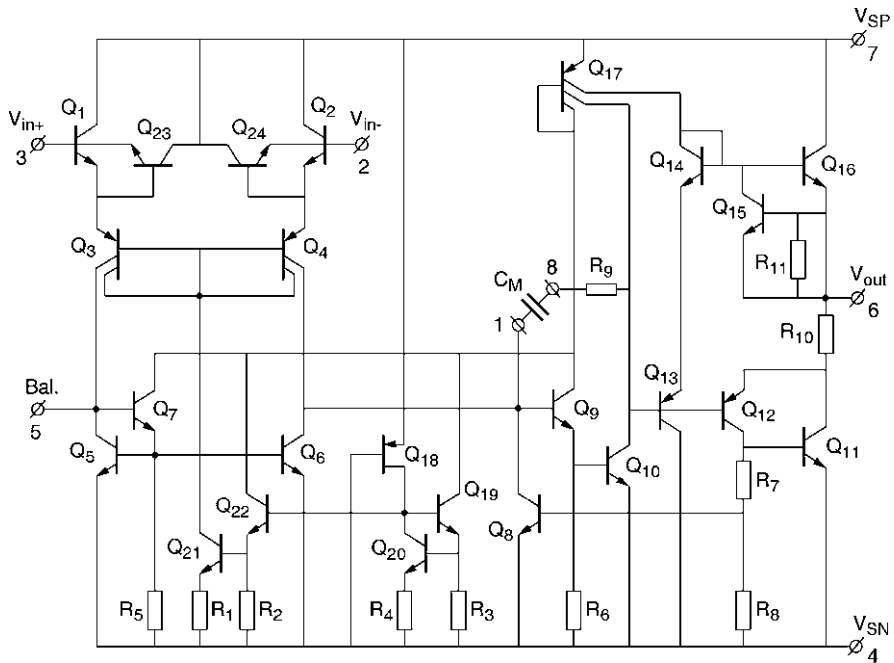


**Fig. 7.6.1** Equivalent circuit of the LM101 Class-AB all-NPN operational amplifier with GA-GA-VF/GA configuration and Miller compensation (MC)

### NE5534 Class-AB Operational Amplifier with Bypassed NMC

The classic NE5534 audio OpAmp with GA-GA-VF/GA configuration is depicted in Fig. 7.6.2a [7.15]. The input stage consists of  $Q_1$  and  $Q_2$ . The intermediate stage has emitter-resistor degenerated transistors  $Q_8$  and  $Q_{11}$  loaded with a mirror  $Q_{61}$ ,  $Q_{62}$ , and  $Q_{10}$  at  $E_2$ . The output stage at the GA side consists of the Darlington pair  $Q_{13}$ ,  $Q_{17}$ , while at the VF side  $Q_{21}$  is driven by  $Q_{17}$  through the class-AB biasing network  $D_4$ ,  $Q_{15}$  and  $D_5$ , as explained with Fig. 5.4.3. A direct HF path for driving  $Q_{21}$  is provided by the collector connection of  $Q_{13}$  to the base of  $Q_{21}$ . Transistors  $Q_{19}$  and  $Q_{20}$  limit the positive and negative output currents respectively. The limits are set by the resistor values of  $R_{18}$  and  $R_{19}$  respectively.  $Q_{10}$  at  $E_1$  and  $Q_{16}$  are clipping diodes, preventing the saturation of  $Q_{17}$  when overdriven.

Principally, the NE5534 is a GA-GA-GA configured OpAmp with a VF upper output transistor functioning as a slave. So we can regard this circuit as a special case of the GA-GA-GA configuration.

The HF compensation scheme can best be denoted by a capacitive feed-forward coupled nested Miller compensation. The latter has been described with Fig. 6.2.16. The inner nest is compensated by  $C_4$ . The outer nest is compensated by  $C_3$ . Capacitor  $C_1$  is a balancing capacitor for providing virtual ground to the reference input side of the differential intermediate stage to prevent a zero in the transfer of the Miller compensated intermediate stage far below its regular zero  $f_z = g_{m2}/2\pi C_3$ .

The nested Miller compensation would have been adequate in itself if the bandwidth of the intermediate stage with the lateral PNP transistors  $Q_8$  and  $Q_{11}$  was not so low.

To overcome this problem a multipath according to Fig. 6.2.18 should have been used. But instead an HF feedforward capacitor  $C_2$  has been inserted between the input and output of the intermediate stage so that this stage is overbridged at higher frequencies. The amplifier can now be compensated for a zero-dB bandwidth of

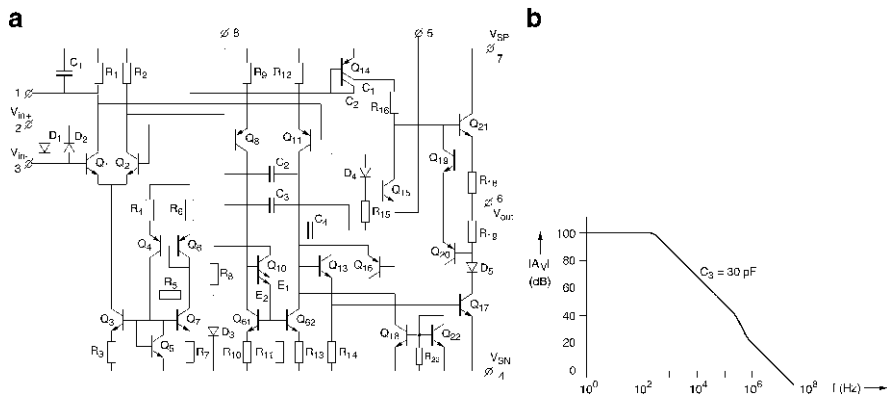


**Fig. 7.6.2** (a) The GA-GA-VF/GA configuration of the classic NE5534 OpAmp and (b) Frequency characteristic of the classic NE5534 OpAmp with pole-zero doublet

10 MHz. However, the overbridging of the intermediate stage changes the nested Miller compensation network at high frequencies into a single Miller compensated output stage, as  $C_3$  and  $C_4$  effectively become connected in parallel by  $C_2$ . This evokes a pole-zero doubled at 300 kHz where the gain is 30 dB in the frequency characteristic of the NE5534, as shown in Fig. 7.6.2b. This means that the amplifier has a low phase margin, if utilized at a feedback gain of about 30 dB where the roll-off of the amplitude characteristic is larger than 20 dB/dec. This makes the stability tricky in a tone-control circuit, where the feedback around the OpAmp is variable. Moreover, a slow settling component will distort the step response if used at a bandwidth above 300 kHz.

### Precision All-NPN Class-AB Operational Amplifier with NMC

A better approach is to insert an NPN GA intermediate stage into the “all-NPN” GA-CF-VF/GA configuration of Fig. 7.5.1 and to use a pure Nested Miller Compensation scheme, as explained with Fig. 6.2.16. The result is presented in the circuit of Fig. 7.6.3 [7.16].

The input stage consists of  $Q_{100}$  and  $Q_{110}$ . The intermediate stage has  $Q_{200}$  and  $Q_{210}$ . The “all-NPN” level-shift stage consists of  $Q_{300}$ – $Q_{360}$ , and was explained with Fig. 7.3.1. The all-NPN Darlington VF/GA output stage consists of  $Q_{400}$ ,  $Q_{410}$  and  $Q_{500}$ ,  $Q_{510}$ . The feedback-biasing class-AB regulating circuit consists of  $Q_{601}$ ,  $Q_{602}$ ,  $Q_{611}$ ,  $Q_{621}$  and  $Q_{650}$ ,  $Q_{660}$  together with the diode-connected transistors  $Q_{710}$ ,  $Q_{750}$ ,  $Q_{760}$ , and has been described with Fig. 5.4.7.

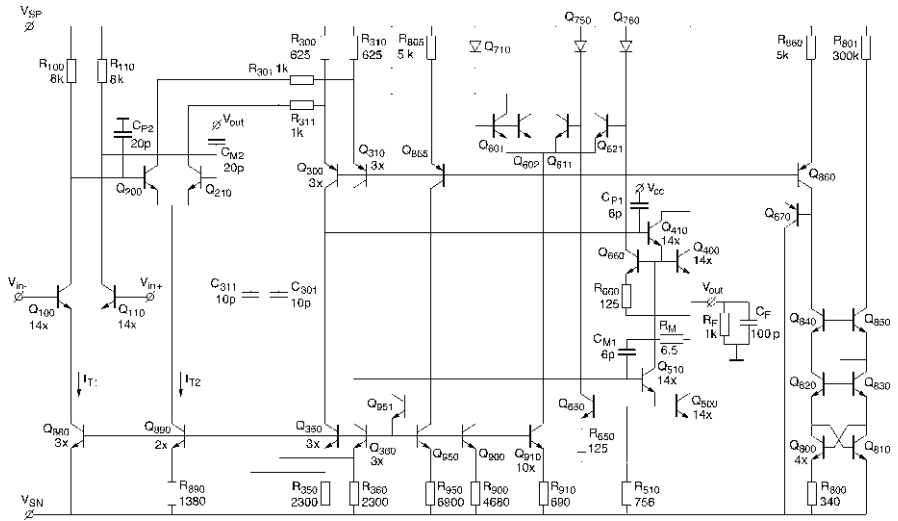


Fig. 7.6.3 Precision class-AB all-NPN operational amplifier with GA-GA-VF/GA configuration and nested Miller compensation



The Nested Miller Compensation has  $C_{M1}$  as an inner Miller capacitor on the GA output side, while  $C_{P1}$  balances  $C_{M1}$  for the VF output side. The outer nest consists of capacitor  $C_{M2}$ , while  $C_{P2}$  balances  $C_{M2}$  at the reference input of the intermediate stage. Without the capacitor  $C_{P2}$  a bypath for high frequency would exist, and a zero appears in the frequency characteristic. Starting out with a quiescent current of 2 mA through the output transistors  $Q_{400}$  and  $Q_{500}$ , both emitters have a resistance of  $r_e = 1/g_m = V_T/I_E = 12.5 \Omega$ . As both push and pull stages are in parallel regarding the load capacitor  $C_L = 100$  pF, we obtain a limiting pole frequency at the output of:

$$f_1 = \frac{g_{m1}}{2\pi C_L} \approx 250 \text{ MHz} \quad (7.6.1)$$

with  $g_{m1} = g_{m400} + g_{m500}$ .

The zero-dB frequency  $f'_0$  of the intermediate and Miller compensated output stage must be half  $f_1$  to obtain  $60^\circ$  phase margin when the loop is closed by the second nest. So, with  $g_{m2} = I/(r_{e200} + r_{e210})$  and  $C_{M1} = C_{P1}$ , we obtain:

$$f'_0 = \frac{g_{m2}}{2\pi C_{M1}} = \frac{1}{2} f_1 \approx 125 \text{ MHz} \quad (7.6.2)$$

We choose  $C_{M1} = C_{P1} = 6$  pF at a transconductance  $g_{m2} \approx 5$  mS, corresponding with a tail current of the intermediate stage of  $I_{T2} = 4g_{m2}V_T \approx 0,5$  mA. The overall zero-dB frequency  $f''_0$  must again be taken half of  $f'_0$  to ensure an overall phase margin of  $60^\circ$ . So, with  $g_{m3} = I/(r_{e100} + r_{e110})$  and  $C_{M2} = C_{P2}$  we obtain:

$$f''_0 = \frac{g_{m3}}{2\pi C_{M2}} = \frac{1}{2} f'_0 = \frac{1}{4} f_1 \approx 60 \text{ MHz} \quad (7.6.3)$$

In this case we choose a relative large capacitor value of  $C_{M2} = C_{P2} = 20$  pF for obtaining a low input noise voltage, at a relatively large transconductance of the input stage  $g_{m3} \approx 8$  mS, corresponding with a tail current of the input stage of  $I_{T1} = 4g_{m3}V_T = 0.8$  mA. The balancing capacitor  $C_{P2}$  is needed to block the HF path through  $Q_{200}$ . The result is a straight frequency response without pole-zero doublet with a zero-dB frequency of 60 MHz, when loaded with a capacitor  $C_L < 100$  pF, as shown in Fig. 7.6.4, and an input noise voltage of 2 nV/ $\sqrt{\text{Hz}}$ .

### ***Precision HF All-NPN Class-AB Operational Amplifier with MNMC***

Comparing the Nested Miller Compensated GA-GA-VF/GA configuration of Fig. 7.6.3 with the simpler Miller compensated GA-CF-VF/GA configuration of Fig. 7.5.1, we see an increased low-frequency gain, a lower offset and noise, but half the maximum obtainable bandwidth under the condition that the quiescent

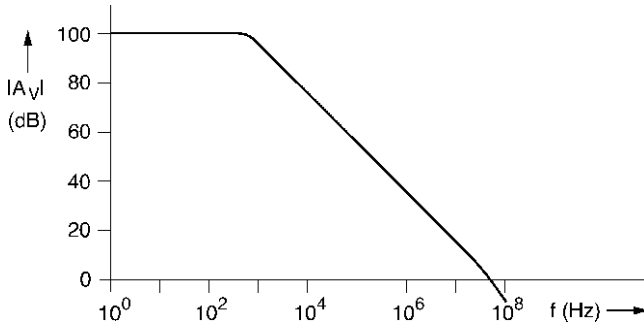


Fig. 7.6.4 Frequency response of the GA-GA-VF/GA configuration with nested Miller compensation of Fig. 7.6.3

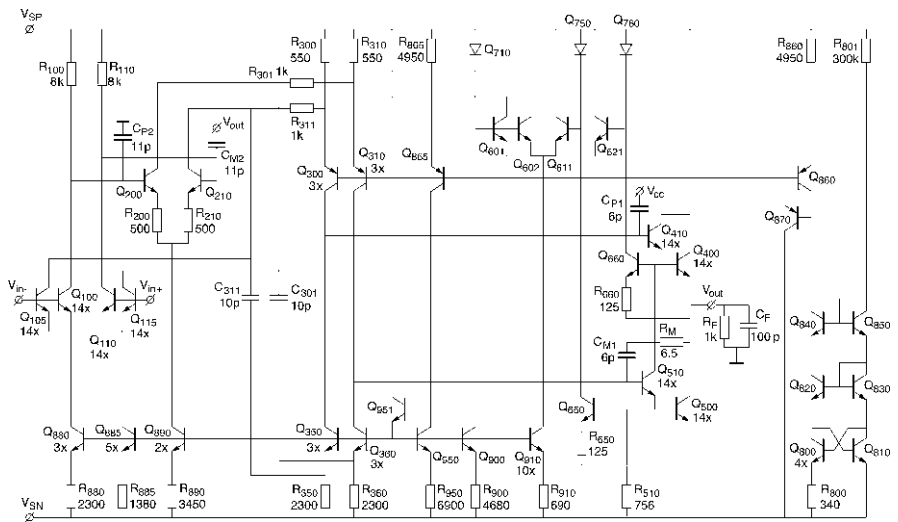
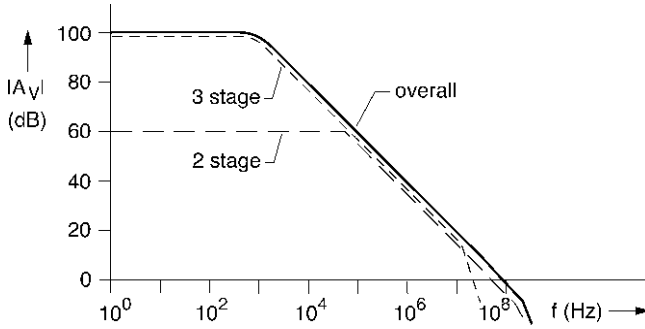


Fig. 7.6.5 Precision HF all-NPN class-AB operational amplifier with GA-GA-VF/GA configuration and Multipath nested Miller compensation (MNMC)

output currents were chosen equal. The question arises: is it possible to have the high gain and low noise of the three-stage amplifier, while maintaining the high bandwidth of the two-stage amplifier at an equal quiescent current? A feedforward capacitor which bridges the intermediate stage, as in the NE 5534, results in a strong pole-zero doublet, as shown with Fig. 7.6.2. So, then the Multi-path Nested Miller compensation technique (MNMC), as explained with Fig. 6.2.18, presents an adequate solution. The idea is to have a two-stage amplifier independently in parallel with a three stage amplifier. With this topology one can have the best of the two and three-stage amplifier without strong pole-zero doublets. The resulting circuit is shown in Fig. 7.6.5, together with its frequency characteristic in Fig. 7.6.6. [7.16].



**Fig. 7.6.6** Amplitude characteristic of the GA-GA-VF/GA configuration with a multipath nested Miller compensation

As with the circuit of Fig. 7.6.3, starting with a quiescent current of 2 mA in the output transistors, resulting in  $r_e = 1/g_m = V_T/I_e = 12.5 \Omega$  and a load capacitance of 100 pF, we obtain a limiting pole frequency of:

$$f_1 = \frac{g_{m1}}{2\pi C_L} \approx 250 \text{ MHz} \quad (7.6.4)$$

with  $g_{m1} = g_{m400} + g_{m500}$ .

The zero-dB frequency  $f'_0$  of the two-stage amplifier through the second input stage  $Q_{105}$ ,  $Q_{115}$  must be half  $f_1$ , so, with  $g_{m32} = 1/(r_{e105} + r_{e115})$  and  $C_{M1} = C_{P1}$ , we obtain:

$$f'_0 = \frac{g_{m32}}{2\pi C_{M1}} = \frac{1}{2} f_1 \approx 125 \text{ MHz} \quad (7.6.5)$$

We have chosen  $C_{M1} = C_{P1} = 6 \text{ pF}$ , and  $I_{T31} = 4g_{m32}V_T \approx 0.6 \text{ mA}$ .

The overall amplitude characteristic of the three-stage amplifier must run along with that of the two-stage amplifier. So, with  $g_{m31} = 1/(r_{e100} + r_{e110})$  and  $C_{M2} = C_{P2}$ , we obtain likewise for the first input stage:

$$f'_0 = \frac{g_{m31}}{2\pi C_{M2}} = \frac{1}{2} f_1 \approx 125 \text{ MHz} \quad (7.6.6)$$

We have chosen  $C_{M2} = C_{P2} = 11 \text{ pF}$ , and  $I_{T31} = 4g_{m31}V_T \approx 0.9 \text{ mA}$ .

Next we have to choose the  $g_{m2}$  of the intermediate stage with  $Q_{200}$  and  $Q_{210}$ . According to the reasoning with (6.2.44), by which we argued that with a unity overall feedback the second input stage becomes connected in parallel with the unity gain Miller feedback intermediate stage, which could endanger the phase margin of the inner loop, we have to choose  $g_{m2}$  much smaller than  $g_{m32}$ . This leads to:

$$g_{m2} < 1/3 g_{m32} \quad (7.6.7)$$

For this reason we degenerated the intermediate stage with emitter resistor  $R_{200}$  and  $R_{210}$  of  $500\ \Omega$  each, making  $g_{m2} \approx 1\ \text{mS}$ , which is much lower than  $g_{m32} \approx 6\ \text{mS}$ .

### ***1 GHz, All-NPN Class-AB Operational Amplifier with MNMC***

One of the disadvantages of the Darlington all-NPN output stage is that the upper output voltage range is limited to at least the voltage of two diodes plus a saturation voltage plus a current-source resistor voltage.

The three-stage GA-GA-VF/GA configuration has enough gain to leave out the Darlington VF driver transistors in the output stage. An example is shown in Fig. 7.6.7. It is a 1 GHz OpAmp powered at 5 Volt single supply and loaded with a  $50\ \Omega$  resistive load at a voltage gain of 76 dB. The circuit is almost equal to that of Fig. 7.6.5, except for the single output transistors instead of Darlington ones. Importantly the class-AB feedback is now connected in front of the all-pass feedforward network  $R_F C_F$  to accommodate class-AB control up to 1 GHz. The circuit is fully described in [7.13].

The 1 GHz amplifier has a supply-current consumption of 20 mA. But the bandwidth and supply current can easily be scaled down, while the resistor values are scaled up. At a bandwidth of 1 MHz, the supply current need only be  $20\ \mu\text{A}$ .

### ***2 V Power-Efficient All-NPN Class-AB Operational Amplifier with MDNMC***

When we do need more gain without losing the extra diode voltage of a Darlington transistor in the output stage of Fig. 7.6.3, we can take another GA driver while adding another nest to the nested HF compensation structure. This is shown in the power-efficient “all-NPN” OpAmp of Fig. 7.6.8.

In the circuit of Fig. 7.6.8 we easily distinguish, going from left to right, an GA input stage, an GA intermediate stage, an GA-VF/GA output stage, and a feedback biasing class-AB regulator. The GA-VF/GA output stage includes a Multipath Nested Miller compensation scheme. This multipath scheme allows the Darlington VF transistor to be replaced by an GA boost transistor with a current mirror,  $Q_{102}$ ,  $Q_{106}$ ,  $Q_{105}$  in the upper VF half, and  $Q_{104}$ ,  $Q_{106}$ ,  $Q_{107}$  in the lower half to drive the output transistors  $Q_{101}$  and  $Q_{103}$ , respectively. The primary Miller compensation capacitors are  $C_{M1}$  and  $C_{P1}$ . The secondary nested capacitors are  $C_{M2}$  and  $C_{P2}$ . The tertiary nested capacitors are  $C_{M3}$  and  $C_{P3}$ . Strictly, the topology is not a three-stage amplifier but a four-stage one GA-GA-(GA-VF)/(GA-GA). However, the resemblance with a three-stage amplifier is so strong that we like to place it in this chapter. Only the output transistors and the drivers have a multipath topology generated in the intermediate stage. The quiescent current of the whole OpAmp is 0.35 mA. The peak load current is 100 mA. The bandwidth is 1 MHz. The output-voltage range

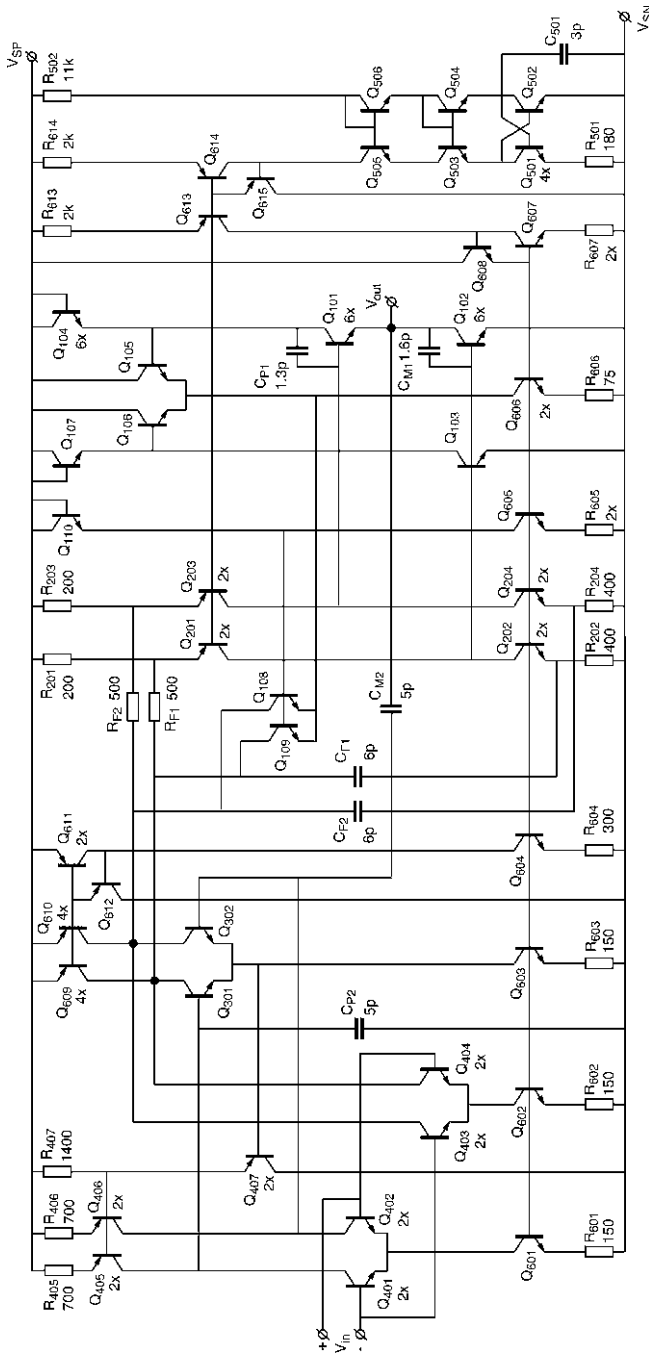
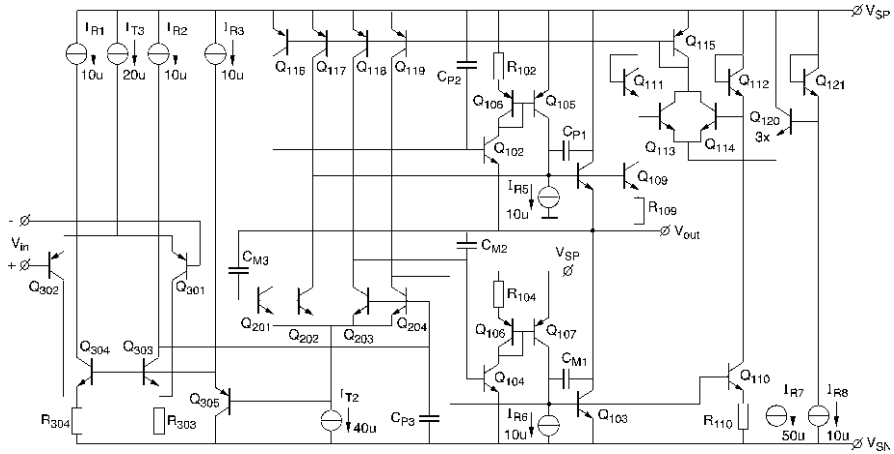


Fig. 7.6.7 1GHz 5V class-AB operational amplifier with all-NPN GA-GA-VF/GA configuration and a multipath nested Miller compensation



**Fig. 7.6.8** 2 V power-efficient “all-NPN” class-AB OpAmp with GA-GA-VF/GA configuration and a multipath double nested Miller compensation (MDNMC)

reaches from 0.2 V above the negative supply rail up to 1.0 V below the positive supply rail. The supply voltage must be larger than 2 V.

**Conclusion**

We have shown that the GA-GA-VF/GA configuration is ideally suited to high-quality bipolar OpAmps with an all-NPN topology.

The classic NE5534 with a capacitive feedforward bridged intermediate stage has a pole-zero doublet in the frequency characteristic.

The Nested Miller compensation provides a straight frequency characteristic combined with a large voltage gain. The Multipath Nested Miller compensation allows a two-times larger bandwidth-over-power ratio with a frequency characteristic having a straight 20 dB/dec roll-off.

The bandwidth can be taken up to the GHz range when we take out the Darlington VF driver transistors. Taking out the Darlington transistors also increases the effective usable output voltage range. When we cannot miss the current gain of the Darlington transistors, nor allow a reduction of the output voltage range, the Darlington VF transistor can be replaced by another nested GA transistor driver stage. This results in a power-efficient “all-NPN” output stage.

**7.7 GA-CF-GA Configuration**

The demand for lower supply voltages such as 3.0, 2.0 and eventually 1.0 V by very dense VLSI processes with sub-micron gate lengths necessitates an efficient use of the supply voltage range by the output voltage range. This can only be accomplished if we use a rail-to-rail.

(R-R) GA-output stage, because only then we avoid the loss of one or more diode voltages. The GA-CF-GA configuration is the simplest way to obtain this.

**Compact 1.2 V R-R-Out CMOS Class-A OpAmp with MC**

When we do not care about a current-efficient class-AB output stage but instead can live with a class-A version, the simple class-A compact 1.2 V CMOS OpAmp with an GA-CF-GA configuration of Fig. 7.7.1 results. Its behavior is comparable with the GA-GA circuit of Fig. 7.2.5, except that now we are using a folded cascode stage in between the two GA stages.

This enables the input CM voltage to include the negative rail. Further, we can choose between a direct (with  $C_{M1}$ ) or active (through the cascode, explained with Fig. 6.2.12) (with  $C_{M1A}$  dotted) connection of the Miller capacitor, depending on circumstances, or a combination of both.

P-channel transistors have been chosen for the differential input pair because the back-gate can be bootstrapped with the common-source voltage. This has the advantage that the input transistors are purely driven by the differential input voltage and not that much by a common-mode input voltage through the back-gates as would be the case with N-channel transistors. This results in the highest obtainable CMRR (see Sect. 4.3).

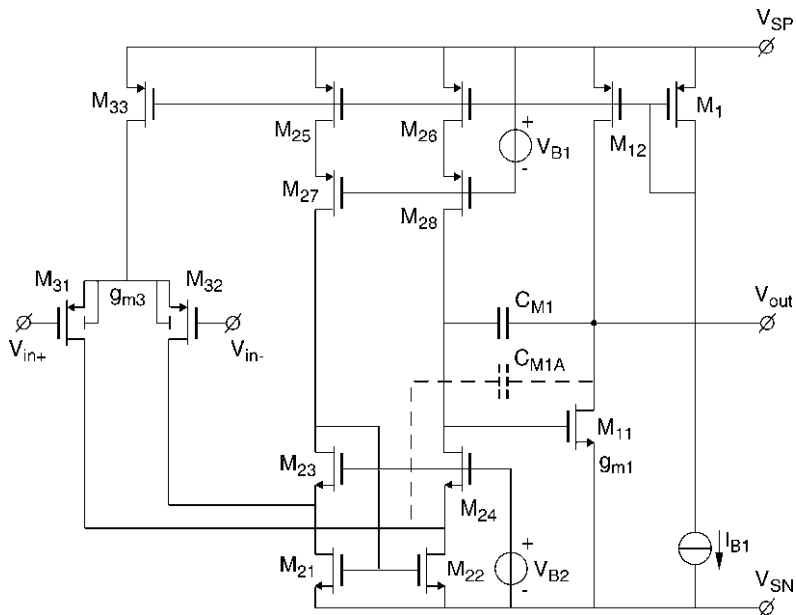


**Fig. 7.7.1** Compact 1.2 V R-R-out CMOS class-A OpAmp with GA-CF-GA configuration and Miller compensation. Compact 1.0 V OpAmp without the upper cascodes  $M_{27}$ ,  $M_{28}$

The folded-cascode intermediate stage functions in addition to a current mirror as a summing circuit for the differential signals from the input stage.

N-channel transistors are chosen for the folded cascode mirror connection because they have the highest  $f_T$ .

To keep the offset and noise contribution of the folded cascodes low, in regard to those of the input stage, the  $g_m$  or  $W/L$  ratio of the current-determining transistors in the folded cascodes must be lower than the  $g_m$  or  $W/L$  ratio of the input-stage transistors. Moreover, the input transistors as well as the current-determining transistors in the folded cascodes may have a cross-coupled quad layout to further reduce the offset. The upper bias current sources  $M_{25}$ ,  $M_{26}$  of the folded cascode branches must be chosen equal to the tail current of the differential input pair to ensure that the full differential output current of the input pair is available to drive the Miller capacitors  $C_{MI}$  and  $C_{MIA}$ . This is needed for a maximal slew-rate.

In respect to noise and offset the GA-CF-GA configuration of Fig. 7.7.1 has a disadvantage over the GA-GA configuration of Fig. 7.2.5. The intermediate summing and mirror CF stage adds its noise and offset to that of the input stage. This addition is more than the noise and offset of the “telescopic” current mirror load of the input stage of Fig. 7.2.5.

We may alternatively choose for a lower noise and offset as well as a lower power consumption instead of choosing a high-frequency behavior for the intermediate cascode and summing circuit. This can be realized by taking the mirror connection at the upper P-channel side instead of at the lower N-channel side. In that case, the lower current-source transistors  $M_{21}$  and  $M_{22}$  need to provide a current equal to the tail current of the differential input pair.

As a result, the two branches of the summing circuit would carry only a quiescent current equal to half of the tail current. Yet the output of the summing circuit would symmetrically deliver the maximum of plus or minus the full tail current of the input pair into the compensation capacitor. Thus proving full slew rate. This has been further explained with Fig. 7.1.2b.

The limiting pole frequency, if loaded with a load capacitance  $C_L$ , is roughly:

$$f'_1 = \frac{g_{m1}}{2\pi C_L} \quad (7.7.1)$$

with  $g_{m1} = g_{m11}$ .

The zero-dB bandwidth must be chosen half of  $f'_j$ :

$$f'_0 = \frac{g_{m3}}{2\pi C_{MI}} = \frac{1}{2} f'_1 = \frac{1}{2} \frac{g_{m1}}{2\pi C_L} \quad (7.7.2)$$

Hence the Miller capacitor has to be chosen roughly:

$$C_{MI} = 2C_L \frac{g_{m3}}{g_{m1}} \quad (7.7.3)$$



The bandwidth can be increased by roughly a factor 2 if we make use of the active-Miller connection (dotted) with  $C_{MIA}$ , as explained with Fig. 6.2.12. The maximum low-frequency voltage gain obtained without  $R_L$  is roughly:

$$A_{VOM} \approx g_{m3}r_{ds22}\mu_{24}\mu_{11} \quad (7.7.4)$$

with  $\mu_{24} = g_{m24}r_{ds24}$ ,  $\mu_{11} = g_{m11}r_{ds11}$ , and disregarding the output resistance of the upper cascoded current source.

A practical value is 80 dB.

If loaded with a load resistor  $R_L$  the gain  $A_{V0}$  is lowered by a load factor  $R_L/(R_L + r_{ds11})$ .

The dominating pole frequency without  $R_L$  is:

$$f'_2 = f'_0/A_{VOM} \quad (7.7.5)$$

The OpAmp of Fig. 7.7.1 has a minimum supply voltage of about 1.2 V as a result of the addition:  $V_{S\ min} = V_{diode\ 11} + V_{sat\ 28} + V_{sat\ 26}$ .

When we further simplify the circuit and leave out the upper cascode transistors  $M_{27}$ ,  $M_{28}$ , a very simple GA-CF-GA OpAmp remains that may be powered at the absolute minimum supply voltage of 1 V, made up by one diode voltage of  $M_{11}$  and one saturation voltage of  $M_{26}$ . However, the maximum voltage gain will drop to:

$$A_{VOM} \approx g_{m3}r_{ds26}\mu_{11} \quad (7.7.6)$$

A practical value then is in the order of 60 dB.

### **Compact 2 V R-R-Out CMOS Class-AB OpAmp with MC**

When we need a higher output current and still want a low quiescent current we need to incorporate a current efficient class-AB biasing of the output stage. A compact and robust OpAmp in an GA-CF-GA configuration [7.17] is shown in Fig. 7.7.2.

The GA output stage  $M_{11}$ ,  $M_{12}$  is feedforward biased in class-AB by a mesh of head-to-tail connected transistors  $M_{13}$ ,  $M_{14}$ . The output stage has been described with Fig. 5.3.21. At first sight, the bias connections to the sources of  $M_{13}$  and  $M_{14}$  seem to lower the impedance at the gates of the output transistors  $M_{11}$  and  $M_{12}$  and thus lower the gain. However, the drain connections of  $M_{13}$  and  $M_{14}$  cancel the low source impedances by a positive feedback loop for CM driving voltages. Meanwhile, the bias impedances for DM driving voltages are strongly fixed to accurately bias the output transistors an a class-AB characteristic, as has been described by Eq. 5.3.7.

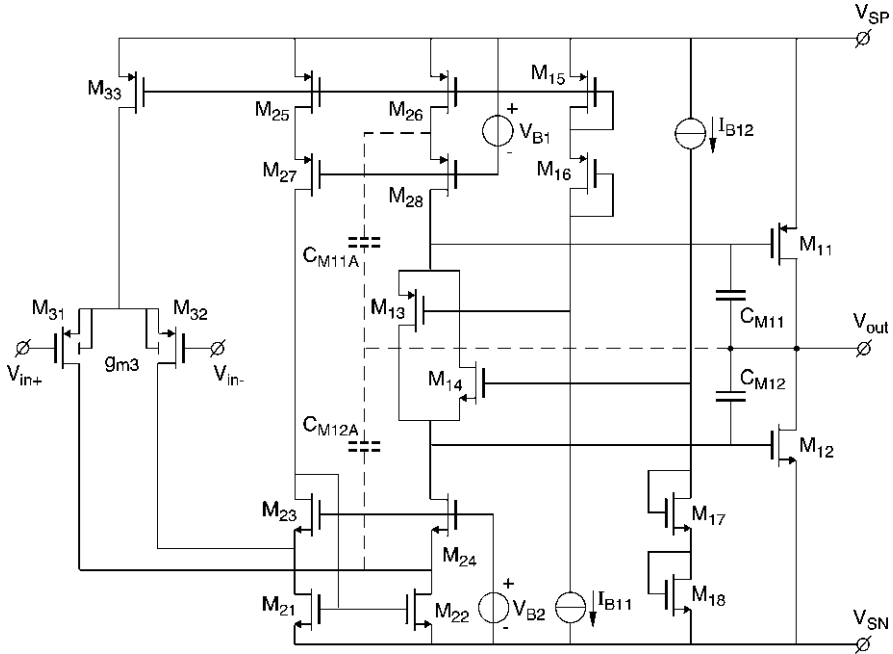


**Fig. 7.7.2** Compact 2 V R-R-out CMOS class-AB OpAmp with GA-CF-GA configuration having a R-R output stage with Miller compensation

The class-AB mesh with  $M_{13}$  and  $M_{14}$  has been incorporated into the folded cascode with  $M_{21}$  through  $M_{24}$ . This has the important advantage that no additional bias currents have to be used for class-AB biasing. The offset and noise of these extra bias currents would otherwise have been added to the offset and noise of the input stage. To further reduce the noise and offset contribution of the folded-cascode stage, one could have chosen for the mirror connection at the upper side instead as of at the lower side. By so doing, the currents in the folded cascodes can be reduced by a factor two. This has been extensively explained with Figs. 7.1.2b and 7.7.1.

The limiting pole frequency, if loaded with a load capacitance  $C_L$ , is roughly:

$$f'_1 = \frac{g_{m1}}{2\pi C_L} \tag{7.7.7}$$

with  $g_{m1} = g_{m11} + g_{m12}$ .

The zero-dB bandwidth must be chosen half of  $ff'$ :

$$f'_0 = \frac{g_{m3}}{2\pi C_{M1}} = \frac{1}{2} f'_1 = \frac{1}{2} \frac{g_{m1}}{2\pi C_L} \tag{7.7.8}$$

with  $C_{M1} = C_{M11} + C_{M12}$

Hence, the Miller capacitors have to be chosen roughly:

$$C_{M1} = 2C_L \frac{g_{m3}}{g_{m1}} \approx C_L \frac{g_{m3}}{g_{m11,12}} \tag{7.7.9}$$

with  $g_{m3} = g_{m31} = g_{m32}$  due to the mirror in the folded cascode and  $g_{m11,12} \approx g_{m11} \approx g_{m12}$ .

The bandwidth can increase by roughly a factor 2, if we make use of the active-Miller connection (dotted) with  $C_{M11A}$  and  $C_{M12A}$ , as explained with Fig. 6.2.12.

The maximum low-frequency voltage gain obtained without  $R_L$  is:

$$A_{VOM} \approx g_{m3}r_{ds22}\mu_{24}\mu_{11,12} \tag{7.7.10}$$

with:  $\mu_{24} = g_{m24}r_{ds24}$ ,  $\mu_{11,12} \approx \mu_{11} \approx \mu_{12}$ .

If loaded with a load resistor  $R_L$ , the gain is lowered by a load factor  $R_L/(R_L + r_{ds11}||r_{ds12})$ .

### Compact 2 V R-R-In/Out CMOS Class-AB OpAmp with MC

The minimum supply voltage of the circuit of Fig. 7.7.2 is set by two-diode voltages and a saturation voltage through the class-AB mesh  $M_{13}$ ,  $M_{14}$ , which is

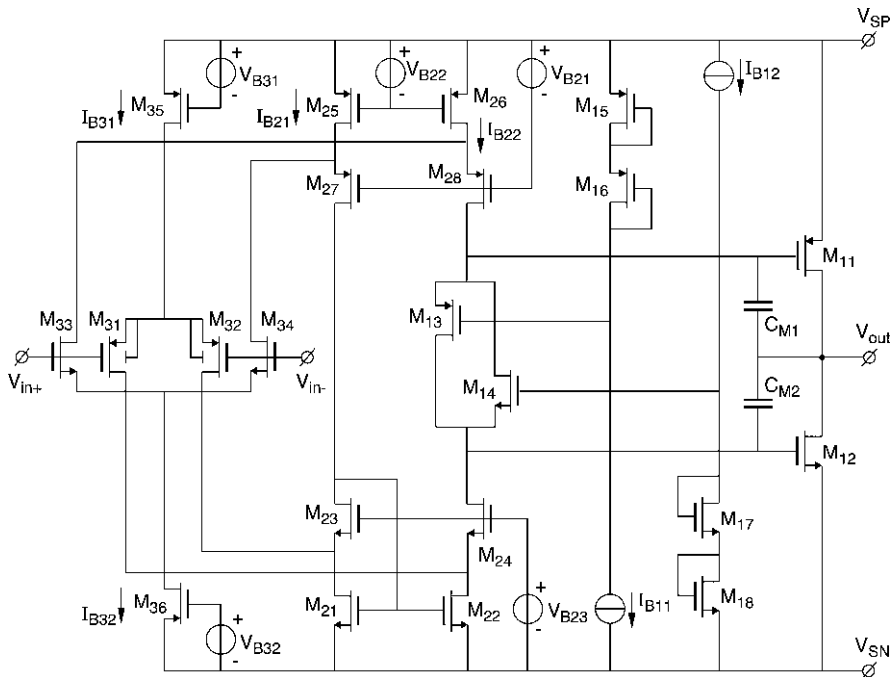
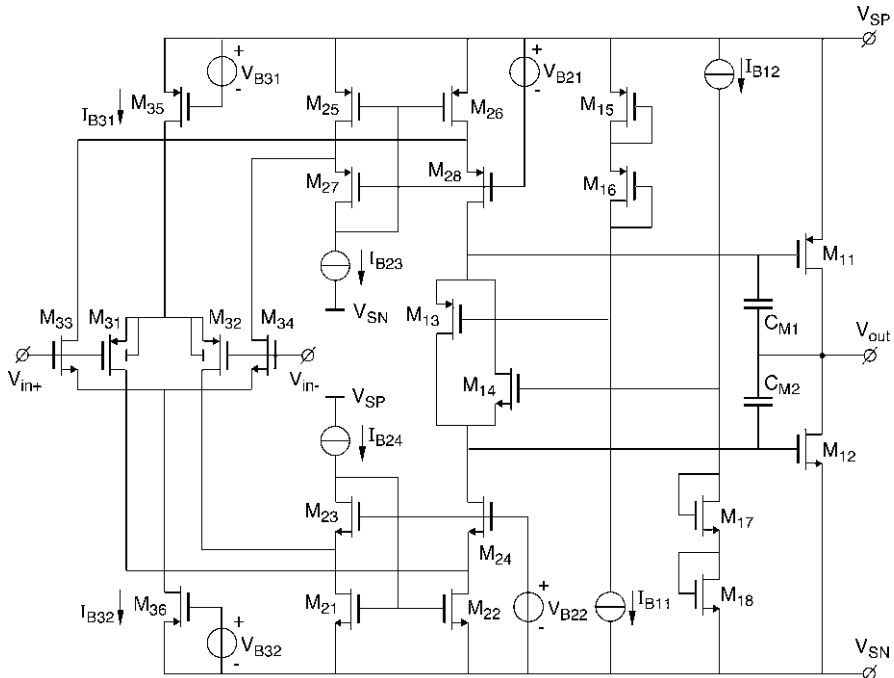


Fig. 7.7.3 Compact 2 V R-R-in/out CMOS class-AB OpAmp with GA-CF-GA configuration and Miller compensation (first approach)



**Fig. 7.7.4** Compact 2 V R-R-in/out CMOS class-AB OpAmp with GA-CF-GA configuration and Miller compensation (second approach)

of the order of 2 V. This allows for the addition of a rail-to-rail (R-R) input stage. As a first approach, we could extend the circuit of Fig. 7.7.2 with a R-R input stage as shown in Fig. 7.7.3. When the common-mode (CM) input voltage is at the negative supply rail voltage  $V_{SN}$ , the circuit behaves exactly like the circuit of Fig. 7.7.2, because the N-channel pair transistors  $M_{33}, M_{34}$  do not have enough gate-source voltage to conduct, and hence the current source  $M_{36}$  is being cut off.

When the input CM voltages rise above the threshold voltage  $V_{TH}$  of  $M_{33}, M_{34}$ , these transistors start conducting a current, and so does the tail-current source transistor  $M_{36}$ . When  $M_{36}$  conducts the full tail current, both input pairs function normally, as explained with Figs. 4.4.2 and 4.4.3 in Chap. 4. Now the total  $g_m$  of the R-R input stage is twice that of a single rail input stage. We suppose that  $I_{B32} = I_{B31}$ , and that the  $W/L$  ratios of both input pairs have been chosen such that they compensate the ratio of about three in the mobilities between the N and P-channel type, so that both input pairs have the same  $g_m$ .

Now two problems arise: firstly, the  $g_m$  of the input stage changes a factor 2 when the input CM voltage swings from rail-to-rail, and we cannot optimize the frequency compensation. We will address this problem later. Secondly, the changing of the currents through the N-channel input pair from 0 to half the tail

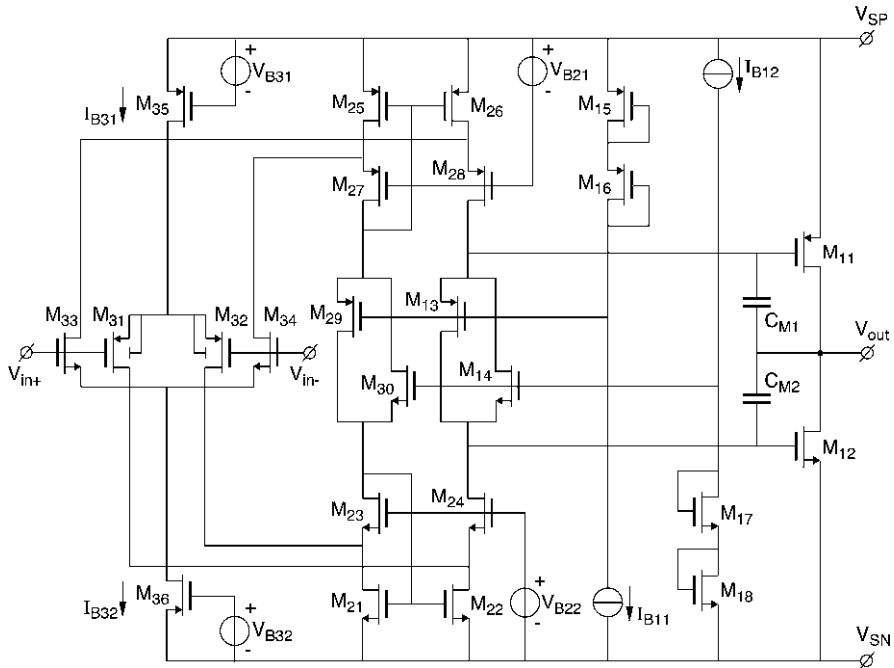


**Fig. 7.7.5** Compact 2 V R-R-in/out CMOS class-AB OpAmp with GA-CF-GA configuration and Miller compensation (third approach)

current  $I_{B32}$  also changes the currents through the upper folded cascodes  $M_{27}$  and  $M_{28}$ . And this changes the quiescent current of the class-AB output stage, which is undesirable.

The changing of the quiescent current as a function of the CM input voltage can be stopped by using current mirror connections both in the upper and lower folded cascodes. This is depicted in the second approach of Fig. 7.7.4. Both current mirrors are driven by an equal current source  $I_{B23}$  and  $I_{B24}$ , respectively. This means that each mirror has a constant output current, independent of whether there is a common-mode output current of one of the input stages or not.

However, there is a disadvantage with the circuit of Fig. 7.7.4, in that the two current sources  $I_{B23}$  and  $I_{B24}$  are physically different sources, which means that offset and noise of these current sources add to the offset and noise of the input stage. It would be much nicer if  $I_{B3}$  and  $I_{B4}$  were the two ends of one physical floating current source. In that case the offset and noise of one end cancels through one mirror the equal offset and noise of the other end through the other mirror. So the question arises of how to build a low-voltage floating current source. One solution at a higher supply voltage is given in [7.18]. The solution we prefer is given in [7.19] and is shown in Fig. 7.7.5.

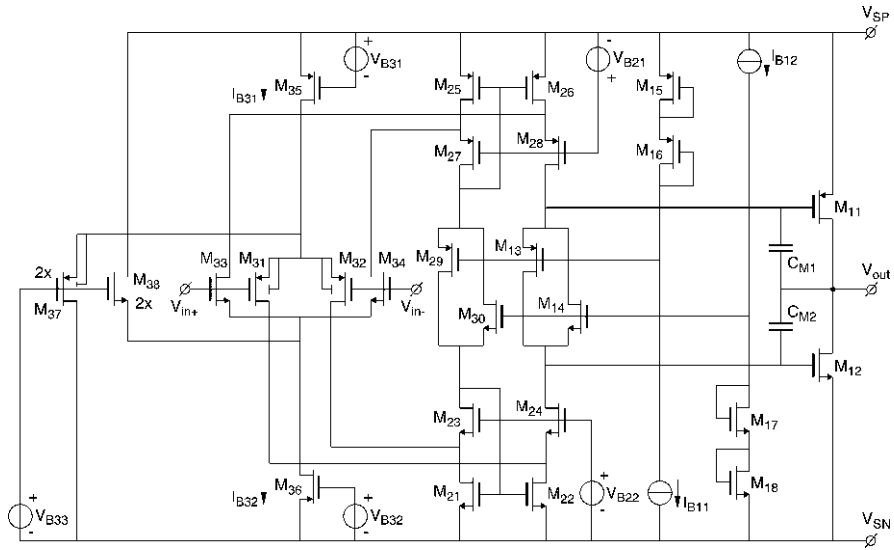


**Fig. 7.7.6** Compact 2 V R-R-in/out CMOS class-AB OpAmp with GA-CF-GA configuration and Miller compensation (final approach)

The floating-current source is composed of a similar mesh as is used for the class-AB biasing of the output transistors, and consists of the head-to-tail connected transistors  $M_{29}$  and  $M_{30}$ .

The bias current through this mesh is determined by the two translinear loops  $M_{25}$ ,  $M_{29}$ ,  $M_{15}$ ,  $M_{16}$  and  $M_{21}$ ,  $M_{30}$ ,  $M_{17}$ ,  $M_{18}$ . This current only slightly depends on changes of the CM current of the input pairs. It is interesting to see that the influence of supply voltage variations through the Early effect is limited. Early effect in both meshes cancel each other in their influence on the biasing of the output transistors [7.19].

For the final circuit, we have still to solve the problem of the changing  $g_m$  of the R-R input stage. For this purpose we choose one of the solutions of Sect. 4.4. For example we choose the solution with the current switches of Fig. 4.4.8, because of its simplicity [7.20, 7.21].

The final approach is shown in Fig. 7.7.6. The result is a compact circuit with excellent specifications and which is robust against device parameter variations. An example of specifications is a bandwidth of 2 MHz at a load capacitance of 20 pF and a quiescent current of 200  $\mu$ A. The DC gain is 85 dB at a resistive load of 10 k $\Omega$ , and the CMRR is 80 dB at a CM input voltage around the negative supply rail voltage, but 43 dB when just crossing the CM voltage level of  $V_{B33}$ . Most specifications can easily be programmed by a factor 1/10 or a factor 10 by choosing other  $W/L$  ratios and other voltages and currents.

The bandwidth may be enlarged by roughly a factor 2 without changing the bias currents nor the load capacitor by connecting the Miller capacitors, not directly to the gates of the output transistors, but indirectly through a connection at the sources

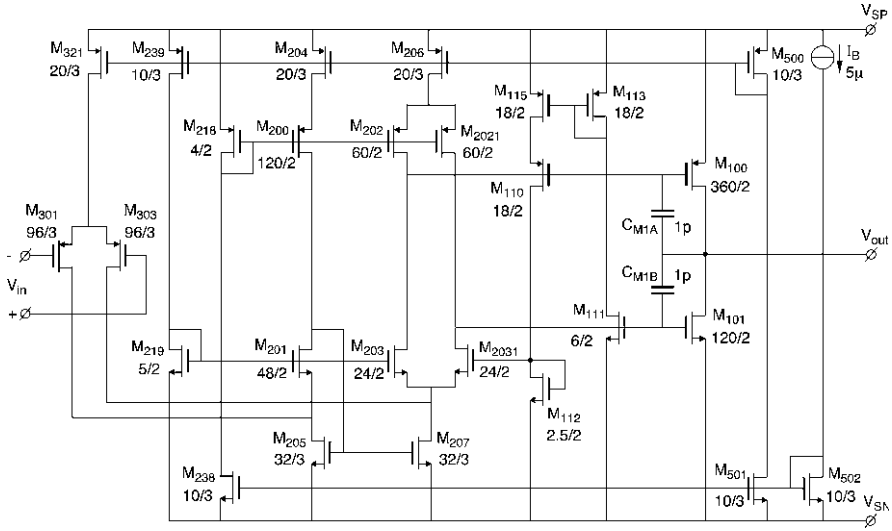


**Fig. 7.7.7** Compact 1.2 V R-R-out CMOS class-AB OpAmp with GA-CF-GA configuration and Miller compensation

of the folded cascode transistors  $M_{28}$  and  $M_{24}$ . This has been described in Sect. 6.2 with Fig. 6.2.12 [7.19]. At very low bias currents the transistors function in weak inversion. For a constant  $g_m$  the spill-over switches must be chosen two times wider than the inpt stages.

### **Compact 1.2 V R-R-Out CMOS Class-AB OpAmp with MC**

When we want to further reduce the supply voltage while maintaining a class-AB bias for the output stage, the feedforward class-AB biasing mesh cannot be used anymore, because its two stacked diode voltages can no longer be provided.

To avoid this problem the mesh has been folded, as shown in the compact 1.2 V CMOS OpAmp of Fig. 7.7.7 [7.22].

The folded mesh consists of  $M_{202}$ ,  $M_{201}$ ,  $M_{203}$ ,  $M_{2031}$ . Somewhat similar to the non-folded mesh, at first it does not seem that it has such a high output impedance because the folded mesh does not consist of two folded cascodes, but of two differential pairs. Their output impedance is only  $2r_{DS}$ . However, for CM signals that drive the output transistors, the folded mesh may be considered as a folded cascode. Even when the class-AB feedback control at the gates of  $M_{203}$ ,  $M_{2031}$  keeps the gate voltage of one output transistor constant at its minimum current, the regulation is such that the gate voltage of the other output transistor is fully driven at a high impedance. The class-AB control acts like a cascode 2-times boost circuit for CM driving voltages.

The DM driving is strongly controlled by the feedback class-AB measuring circuit. In this example, the minimum selector of Sect. 5.4 is used and is explained with Fig. 5.4.13 [7.23, 7.22].

The circuit needs one diode voltage and two collector-source saturation voltages, which allows a minimum supply voltage of about 1.2 V over temperature variations.

The circuit can be extended with a rail-to-rail input stage at 2 V supply voltage. The easiest way is with an input stage having constant  $g_m$  using spilling-over switches and adding the currents from the switches to obtain a constant output current [7.22]. A quiescent current of 200  $\mu\text{A}$  was needed for bandwidth of 4 MHz at a capacitive load of 5 pF, and a DC gain of 85 dB at a resistive load of 10 k $\Omega$ .

## ***Conclusion***

Robust and high-quality compact low-voltage CMOS VLSI OpAmp cells can be designed with the GA-CF-GA configuration. If the simple GA-CF configuration of Sect. 7.1 does not provide adequate LF gain, the GA-CF-GA configuration is the next best choice. The output may nearly swing from rail-to-rail at a minimum supply voltage as low as one diode and two saturation voltages, which is in the order of 1.2 V, or even 1V. The CM input voltage may include the negative supply voltage rail, and at a supply voltage of 2 V even from rail-to-rail. The bandwidth can roughly be designed up to  $f_T/4$ . The circuits stay relatively simple.

## **7.8 GA-GA-GA Configuration**

The previous GA-CF-GA configuration may not always deliver enough LF gain. This may particularly be the case when the supply voltage has to go down to the absolute minimum value of 1 V of one diode voltage plus one saturation voltage, or if we want to have a bipolar output stage. At such low voltages we can no longer use CMOS cascode or bipolar Darlington transistors. In those cases we have to take resource to another GA general amplifying stage instead of a CF intermediate stage, resulting in the GA-GA-GA configuration. In this section we will discuss a CMOS, a BiCMOS and a full bipolar design.

### ***1 V R-R-Out CMOS Class-AB OpAmp with MNMC***

When we have to drive relatively heavy output loads in CMOS at a low supply voltage, the GA-CF-GA configuration with a folded cascode intermediate stage no longer meets the needs. The folded cascode with its two saturation voltages in series



with a higher gate-source voltage at high currents may require a too high supply voltage. Moreover, we may need more power gain. To solve these two problems, a third GA stage may be needed instead of the CF intermediate stage. A design example is given in Fig. 7.8.1 [7.24].

The 1.0 V CMOS OpAmp with GA-GA-GA configuration of Fig. 7.8.1 has an input stage  $M_{301}, M_{302}$  and a folded-cascode mirror circuit  $M_{211}$  through  $M_{216}$ . The second stage  $M_{201}, M_{202}$ , drives through mirrors  $M_{203}, M_{205}$  and  $M_{204}, M_{206}$  the output push-pull stage  $M_{101}, M_{102}$ . The driver mirrors are needed to provide an equal phase to the intermediate and output stage in order to allow a nested Miller frequency compensation. The driver mirrors also separate the direct class-AB control amplifier  $M_{221}, M_{222}$  from the gates of the output transistors in order to allow these gates to be driven from rail-to-rail. For the same purpose we avoided folded cascodes to drive the output transistors. This whole architecture does not have any branch between the supply lines that contain more than one gate-source diode voltage plus one-drain-source saturation voltage. This makes the architecture of Fig. 7.8.1 suitable for operation at a supply voltage of 1.0 V, or over wide temperature and process variations 1.2 V.

The high-frequency compensation scheme has been multipath nested. The first nest across the output transistors is shaped by  $C_{M1A}$  and  $C_{M1B}$ . The second nest runs from the output to the input of the intermediate stage  $M_{201}, M_{202}$  through  $C_{M2A}$  and  $C_{M2B}$ . The gain path goes through the intermediate stage. The feedforward path has been tapped single-sidedly from the folded-cascode mirror connection and duplicated directly into the gates of the output transistors by  $M_{231}$  and  $M_{232}$ , by passing the intermediate stage.

The limiting-pole frequency is set by the output stage at its quiescent current by:

$$f'_1 \approx \frac{g_{m1}}{2\pi C_L} \quad (7.8.1)$$

with  $g_{m1} = g_{m101} + g_{m102}$ .

The zero-dB frequency of the two-stage direct amplifier path must be half of the limiting-pole frequency, so:

$$f'_0 = \frac{1}{2} f'_1 \approx \frac{1}{2} \frac{g_{m1}}{2\pi C_L} \quad (7.8.2)$$

The Miller capacitors of the first nest must be chosen:

$$C_{M1} = \frac{g_{m3}}{2\pi f'_0} = \frac{g_{m3}}{g_{m1}} C_L \quad (7.8.3)$$

with  $C_{M1} = C_{M1A} + C_{M1B}$ .

under the assumption that the W/L ratios of  $M_{215}, M_{216}, M_{231}, M_{232}$  are equal. On one hand we have half the  $g_{m3}$  of the input stage because the mirror only senses one input half, but on the other hand we double the current in two transistors  $M_{231}, M_{232}$ .

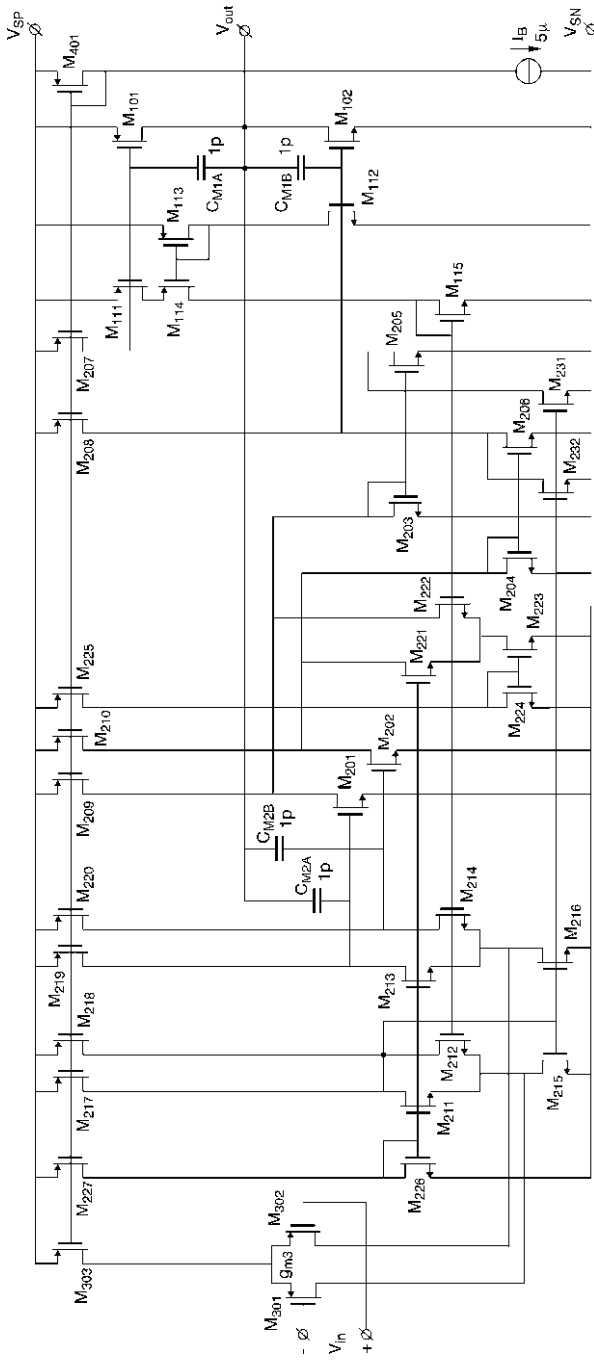


Fig. 7.8.1 1.0 V CMOS R-R-out class-AB OpAmp with GA-GA-GA configuration with multipath nested Miller compensation

The zero-dB frequency of the whole three-stage amplifier may be equal to that of the two-stage one because of the multipath nested Miller compensation structure, hence:

$$f_0'' = f_0' = \frac{1}{2} f_1 \quad (7.8.4)$$

which leads to the choice of the Miller capacitors of the second nest:

$$C_{M2} = \frac{g_{m3}}{2\pi f_0''} = \frac{g_{m3}}{g_{m1}} C_L \quad (7.8.5)$$

with  $C_{M2} = C_{M2A} + C_{M2B}$ .

The two-stage amplifier must dominate the high-frequency behavior at the amplifier's bandwidth, therefore the transconductance through the intermediate stage must be smaller than the transconductance through the feedforward path. This causes the requirement:

$$g_{m2} < \frac{1}{3} \frac{1}{2} g_{m3} \quad (7.8.6)$$

with  $g_{m2} = g_{m201} + g_{m202}$ .

The factor 1/3 stems from the explanation with Fig. 6.2.19. The factor 1/2 comes from the fact that only half of the input stage contributes through its mirror connection to the transconductance of the feedforward path through  $M_{231}$ ,  $M_{232}$ .

For measuring the class-AB relation between the push and pull currents we have chosen a variation to the Seevinck version, described with Fig. 5.4.13. Note that the functions of  $M_{111}$  and  $M_{114}$  have been interchanged in regard to Fig. 5.4.13.

The direct class-AB control loop is realized by the control amplifier  $M_{221}$ ,  $M_{222}$  which differentially controls the biasing of the output transistors via the mirrors  $M_{203}$ ,  $M_{205}$  and  $M_{204}$ ,  $M_{206}$ . The control amplifier has been referenced on the left side by  $M_{226}$ . The bandwidth of this first or direct class-AB loop is determined by the product of the  $g_m$  of the control amplifier and the impedance of a parallel compensation capacitor, which consists of the series connection of  $C_{M1A}$  and  $C_{M1B}$  in between the output of the mirrors. The bandwidth of the class-AB control loop must be stable and of the same order as the bandwidth of the whole amplifier.

The intermediate stage with the grounded transistors  $M_{201}$ ,  $M_{202}$  may provide such large driving currents that the direct class-AB control may be overruled. To avoid this, the class-AB control has been given a second, or gain path, through the intermediate stage in a multipath compensation topology. To this end, the folded cascode circuit between the input and intermediate stage has also been given a differential amplifier function by splitting the cascode transistors. In this way the intermediate stage is driven in parallel for input signals, and differentially for class-AB control signals. The transconductance of this extra gain path for class-AB control signals is determined by the product of the  $g_m$  of the differential amplifier  $M_{213}$ ,  $M_{214}$ ,

the impedance of a parallel compensation capacitor, which consists of the series connection of  $C_{M2A}$  and  $C_{M2B}$ , and the  $g_m$  of the intermediate stage  $M_{201}, M_{202}$ . This transconductance must be smaller than that of the direct path at the bandwidth of the direct path, otherwise the direct path does not dominate the stability of the class-AB loop at high frequencies.

A realized example of such a three-stage CMOS 1.0-voltage OpAmp has a bandwidth of 5 MHz at a load of 5 pF and 10 k $\Omega$ , at a quiescent current of only 200  $\mu$ A. The voltage gain is 80 dB. Over wide temperature and process variations the minimum supply voltage is 1.2 V [7.24, 7.26].

### ***Compact 1.2 V R-R-Out BiCMOS Class-AB OpAmp with MNMC***

At low supply voltages we can no longer use Darlington transistors to drive bipolar output transistors. An excellent solution for driving bipolar output transistors at low supply voltages is to use the low-voltage GA-CF-GA configuration of Fig. 7.7.6 as a class-AB driver. The result is shown in the 1.2 V BiCMOS OpAmp of Fig. 7.8.2 with an GA-GA-GA configuration [7.25].

The nested Miller compensation requires an equal phase across the first and second nested Miller capacitors. This forces us to place mirrors  $M_{203}, M_{204}$ , and  $Q_{205}, Q_{206}$  between the CMOS driver intermediate transistors  $M_{201}$  and  $M_{202}$  and the output transistors  $Q_{101}$  and  $Q_{102}$ . These mirrors allow the transfer of class-AB driving currents. This was not needed in the CMOS OpAmp of Fig. 7.8.1, in which case we could choose an all N-channel intermediate stage and N-channel mirror driver for best HF performance.

The complementary CMOS intermediate stage and mirror drivers may generate such large class-AB dominating currents, that a local class-AB control differential amplifier  $M_{207}, M_{208}$  is not sufficient. Therefore the class-AB regulation is extended with a multipath control amplifier  $M_{213}, M_{214}$  as to also control the intermediate stage. The control amplifier is made by splitting the cascode transistors of the folded cascode and mirror following the input stage.

The push and pull currents are sensed by the bipolar transistors  $Q_{111}$  and  $Q_{112}$ . To limit their currents, emitter resistors may be inserted. The minimum selector  $M_{116}, M_{115}$  senses the lowest of one of the two push or pull output currents across the measurement resistors  $R_{116}$  and  $R_{115}$ . The class-AB control amplifiers  $M_{207}, M_{208}$  and  $M_{213}, M_{214}$  are referenced at the left hand by the diode  $M_{231}$  and resistor  $R_{231}$ . The result is a robust class-AB regulation that keeps the lowest of the push or pull output currents above the minimum value.

The driving of the complementary intermediate stage by a folded cascode mesh  $M_{213}, M_{214}, M_{218}, M_{219}$ , as explained with Fig. 7.7.6, allows a minimum supply voltage of one diode voltage and two saturation voltages. The result is a minimum supply voltage of about 1.2 V, or over a wide range of temperature and process variations 1.4 V. The three transistor combination  $M_{207}, M_{208}, M_{209}$  can be regarded as a third folded cascode, to directly drive the output transistors. This allows the

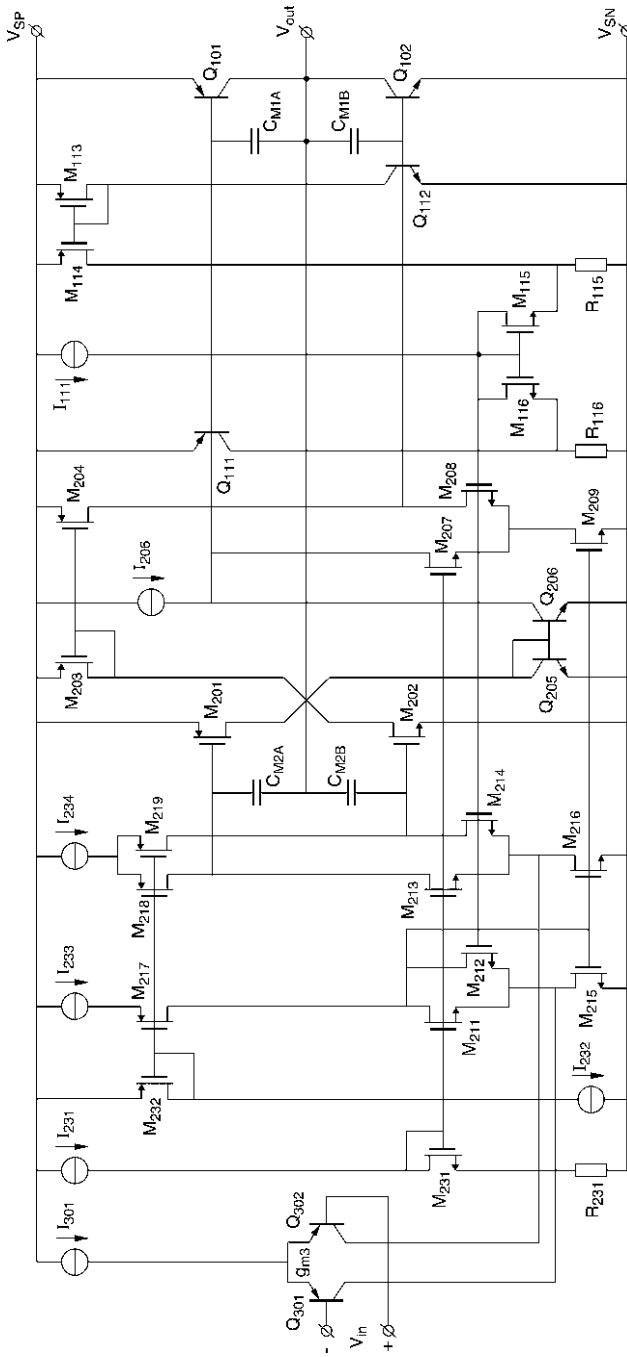


**Fig. 7.8.2** Compact 1.2 V BiCMOS class-AB OpAmp with GA-GA-GA configuration and multipath nested Miller compensation

combination of the direct class-AB control path through  $M_{207}$ ,  $M_{208}$  and the feedforward path through  $M_{209}$  from the input stage to the bases of the output transistors.

The multipath nested Miller frequency compensation is similar to that of Fig. 7.8.1 and has been described by the Eqs. 7.8.1–7.8.6. In the last formula  $g_{m231} + g_{m232}$  must be replaced for  $g_{m209}$ . The main differences to the circuit of Fig. 7.8.1 are that the output and input transistors are bipolar and that the second stage is driven by cascodes at the bottom as well as at the upper side. This means that a larger bandwidth can be obtained, and that the DC gain is larger than those of the circuit of Fig. 7.8.1. Moreover, the input offset voltage is lower.

By example, a 30 MHz bandwidth was obtained at a supply current of 800  $\mu\text{A}$  at a load of 5 pF and a supply voltage of 1.2 V, or 1.4 V over wide temperature and process variations. The DC gain is in the order of 100 dB at a load resistor of 10 k $\Omega$  [7.25].

### ***Bipolar Input and Output Protection***

When the amplifier is used at the input or output of a VLSI chip, the bipolar input or output must be protected. Firstly, ESD diodes must be used from each input and output to both power rails. Secondly, two antiparallel diodes across the input terminals are needed to protect the input transistors against large reverse bias voltages. Thirdly, to avoid HF ringing when the output transistors are drivers into saturation, saturation detection transistors must be connected across the output transistors, as was explained earlier with Fig. 5.5.2. These transistors must be of the same type as the concerned output transistors and with a base-to-base and collector-to-collector connection with the output transistors. The emitter in reverse mode is used as a collector and can be connected to the related gate of the CMOS driver transistor of the intermediate stage. This limits the drive current and keeps the output transistors from saturation. Fourthly, the output current must be limited to protect the output transistors from being destroyed. To this end the current-limiting topology of Fig. 5.5.5 can be used with a direct path to the base of the output transistor and a multipath to the gate of the related driver transistor of the intermediate stage [7.26]. These protection issues must be dealt with in all described circuits.

#### ***1.8 V R-R-In/Out Bipolar Class-AB OpAmp (NE5234) with NMC***

If we want to obtain a high output current capability in pure bipolar technology, Darlington output transistors offer the most simple solution. However, a Darlington output stage needs a supply voltage of minimally two diode voltages and one saturation voltage, which is 1.8 V over a wide range of temperature and process

variations. An example circuit of a fully bipolar OpAmp with an GA-GA-GA configuration and Darlington output transistors, the NE5234, is shown in Fig. 7.8.3. [7.27, 7.28]

The output stage consists of the complementary Darlington transistors  $Q_{11}$ ,  $Q_{12}$  on the NPN side and the folded Darlington transistors  $Q_{13}$ ,  $Q_{14}$ ,  $Q_{15}$  on the PNP side. The PNP side is current-boosted (see Sect. 6.1) by  $Q_{140}$ ,  $Q_{141}$ ,  $Q_{130}$ .

The class-AB control amplifier consists of a differential pair  $Q_{16}$ ,  $Q_{17}$  with a reference voltage across  $Q_{20}$ ,  $Q_{21}$  at the left-hand side and a minimum selector  $Q_{200}$ ,  $Q_{201}$  at the right-hand side, which gets its push and pull current information directly from the NPN output transistor  $Q_{11}$  and indirectly from the PNP output transistor  $Q_{13}$  through  $Q_{18}$  and  $Q_{19}$  (see Sect. 5.4.3).

The differential pair senses the differential voltage between the voltage reference and the minimum selector and regulates the difference in the ideal case at zero. When driving the current of one output transistor high, the current of the other output transistor will be regulated at half its quiescent current (see Sect. 5.4.3). If this happens, the driving current for the transistor with the lowest output current is channeled away from this transistor and fed to the other output transistor through the differential pair, thus doubling the drive current of the output transistor with the highest current. The result is that both currents from the intermediate stage are either used to drive both output transistors in parallel in the quiescent situation, or to jointly drive the output transistor that needs to drive the largest current, while the other is idle at half the quiescent current.

Bipolar output transistors must be protected against excess current, otherwise they can be destroyed, and against saturation, otherwise the bandwidth may drastically decrease and the circuit may start oscillating. Moreover, saturation of NPNs creates large amounts of charge carriers in the substrate, which may create unwanted signal paths. Current limiting is provided by the sense transistors  $Q_{63}$ ,  $Q_{64}$  for the NPN output side, and  $Q_{65}$ ,  $Q_{66}$  for the PNP output side. Saturation protection is provided by the sense transistors  $Q_{61}$  and  $Q_{62}$  for the NPN and PNP sides, respectively. These transistors are used in reverse mode. They match their base-collector diodes with those of the output transistors over process variations.

The R-R input stage has the two complementary differential input stages  $Q_{51}$ ,  $Q_{52}$  and  $Q_{53}$ ,  $Q_{54}$ . The current switch  $Q_{56}$  and mirror  $Q_{57}$ ,  $Q_{58}$  keeps the sum of the tail currents constant at the collector current of  $Q_{55}$ . The folded cascodes  $Q_{41}$ ,  $Q_{42}$ ,  $Q_{43}$ ,  $Q_{44}$  feed the output currents of the input long-tail-pairs to the second stage while these currents are being summed.

Bipolar input stages have the nasty property that their signal transfer is reversed when the transistors are driven into saturation. This is caused by conductance of the reverse base-collector diodes. Particularly for low-voltage amplifiers, input voltages can easily surpass the supply voltage. To protect the input stage from signal reversion each input transistor is paralleled with a two-times larger transistor, which is connected as a collector-base diode, while its collector is cross-coupled to the other transistor of the belonging input pair (see Sect. 4.4).

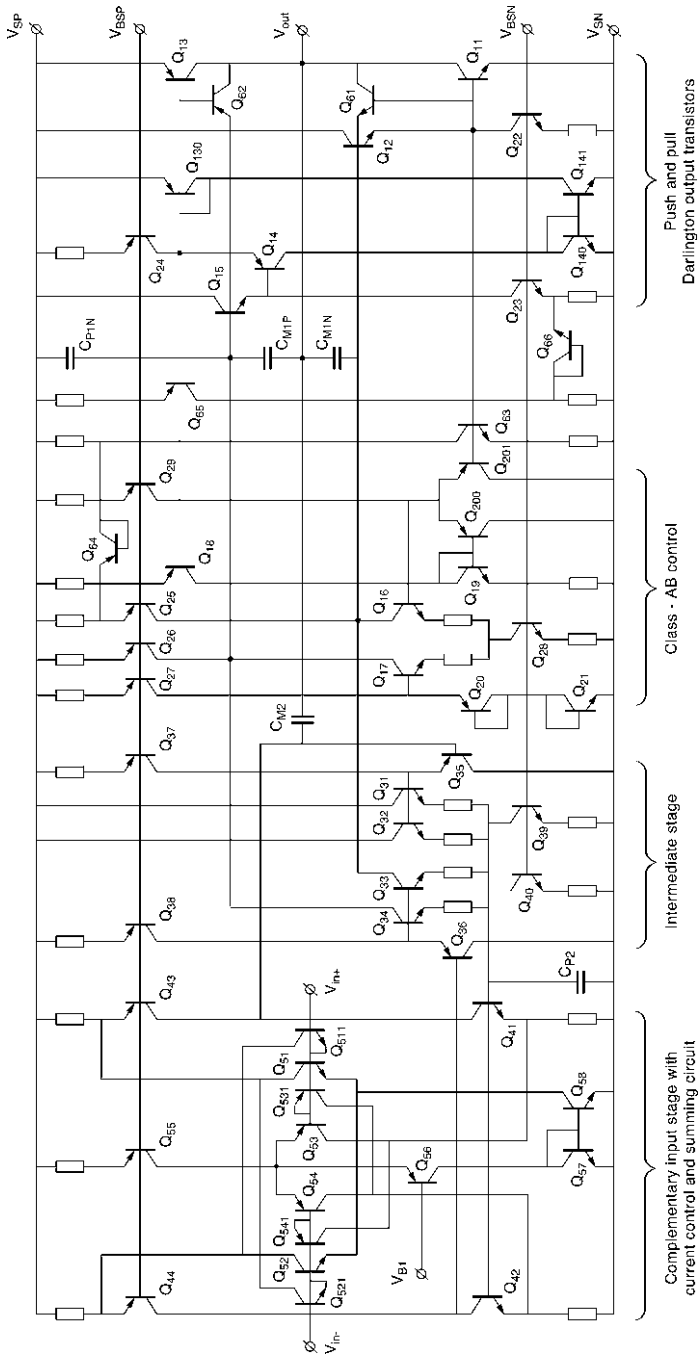


**Fig. 7.8.3** 1.8 V bipolar class-AB operational amplifier NES234 with R-R input and output ranges in GA-GA-GA configuration and nested Miller compensation



The intermediate stage consists of a folded Darlington differential structure with double output currents of the same signal polarity to drive the output stage push-pull in common-mode. The intermediate stage provides common-mode feedback to the input stage at its common-emitter connection to the bases of  $Q_{41}$  and  $Q_{42}$ .

The high-frequency behavior of the OpAmp is well determined by a nested Miller compensation structure (see Sect. 6.2.3). The capacitors of the first nest are  $C_{MIN}$  and  $C_{MIP}$ . To lower the loop gain at the PNP side a parallel capacitor  $C_{P1}$  is used. The capacitors of the second nest are  $C_{M2}$  and  $C_{P2}$ . Ground has been chosen as the virtual reference for the second Miller loop through  $C_{P2}$ .

Note that the stabilizing of the other internal loops must also be separately secured, as there are: the class-AB loop through both the positive and negative output transistors; the current booster loop of the positive output transistor; both output-current limiter loops; and finally the CM feedback loop through the input stage and intermediate stage.

The limiting-pole frequency at the PNP side is:

$$f'_1 = \frac{g_{m1}}{2\pi C_L(1 + C_{P1}/C_{MIP})} \quad (7.8.7)$$

with load capacitor  $C_L$  and transconductance of the output stage  $g_{m1}$ .

The zero-dB frequency of output and intermediate stages is:

$$f'_0 = \frac{f'_1}{2} = \frac{g_{m2}}{2\pi C_{M1}} \quad (7.8.8)$$

with  $g_{m2}$  as the transconductance of half the second stage, and  $C_{M1}$  the average of  $C_{MIN}$  and  $C_{MIP}$ .

The zero-dB bandwidth of the whole amplifier becomes:

$$f''_0 = \frac{f'_0}{2} = \frac{f'_1}{4} = \frac{g_{m3}}{2\pi C_{M2}} \quad (7.8.9)$$

with  $g_{m3}$  as the transconductance of the second stage, and  $C_{M2} = C_{P2}$  the second Miller-loop capacitors.

In the example of the NE5234, the overall bandwidth is 2 MHz at a total supply current of 700  $\mu$ A.

It is interesting to see how the intermediate stage functions like a mirror in adding the voltage across  $C_{P2}$  (in series) with the voltage across  $C_{M2}$ . This provides the factor 2 in gain comparable to that of a mirror in the output of an input stage in subtracting the two differential output currents, thus adding the absolute values into a single output.

The overall low-frequency gain is:

$$A_0 = g_{m1}R_L g_{m2}r_{p2} g_{m3}r_{p3} \quad (7.8.10)$$

in which  $r_{p2}$  is the parasitic parallel resistance at the output of the intermediate stage, and  $r_{p3}$  that at the output of the input stage. In the example of the NE5234, the DC gain is in the order of  $3 \times 10^5$  at a 10 k $\Omega$  load resistance.

The minimum supply voltage is set by the Darlington output transistors and the minimum selector, which take at least two diodes and a saturation voltage. Over the full temperature range the minimum single supply voltage is 1.8 V.

When we have to work at supply voltages down to 1 V, we can fold the Darlington output transistors and boost the bias currents as in the LM10 [7.29].

However, these stages have a poor HF behavior. Therefore, it is better to replace the VF-GA Darlington output stage for an GA-GA multipath nested output stage [7.30]. In fact, we then obtain a four-stage GA-GA-GA-GA configuration, which will be discussed in Sect. 7.9.

## ***Conclusion***

We have seen that the GA-GA-GA configuration may provide an abundance of gain. Therefore, it may be used for the design of precision low-voltage operational amplifiers and for heavy loads. Three important design examples have been evaluated.

## **7.9 GA-GA-GA-GA Configuration**

It is a general rule that if we cannot improve the gain of a single GA stage by a bipolar Darlington or a CMOS cascode connection because of lack of supply-voltage room, we have to cascade more GA stages. In this paragraph we will present two four-stage GA-GA-GA-GA OpAmps, the first in full bipolar technology and the second in CMOS technology.

### ***1 V R-R-In/Out Bipolar Class-AB OpAmp with MNMC***

If we need to work at supply voltages as low as 1 V, we can no longer use bipolar Darlington output transistor combinations with stacked diode voltages. Nor would we like to use the folded Darlington output stage with a current boost [7.29] because of its poor HF behavior. Hence, the way out is to replace the VF-GA Darlington output stage by an GA-GA output stage. This leads to a bipolar OpAmp design with the GA-GA-GA-GA configuration of Fig. 7.9.1 [7.31] with a simplified schematic, and Fig. 7.9.1a, b with a full schematic.

Starting at the output, we have the complementary output transistors  $Q_{110}$  and  $Q_{120}$ . They have first inner-nested Miller capacitors  $C_{M11}$  and  $C_{M12}$ , respectively. The output transistors are driven by complementary driver transistors and mirrors, respectively:  $Q_{210}$  through mirror  $Q_{230}$ ,  $Q_{240}$  and  $Q_{220}$  through mirror  $Q_{250}$ ,  $Q_{260}$ .

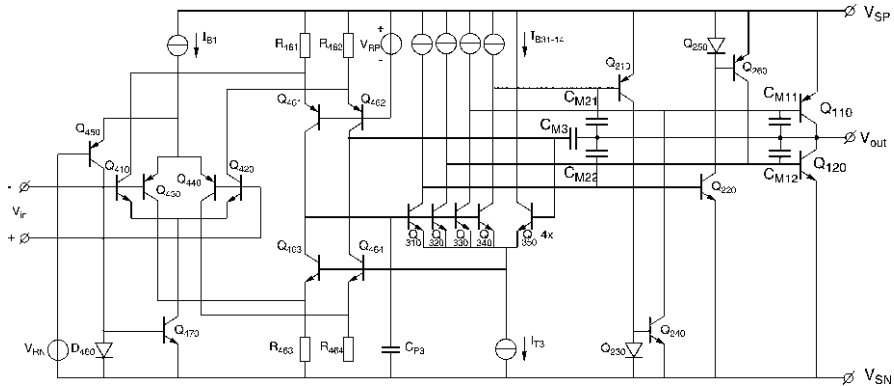


**Fig. 7.9.1** Simplified schematic of a 1 V bipolar class-AB OpAmp with R-R (in)/out, GA-GA-GA configuration, and multi-path nested Miller compensation

These drivers and Cascaded mirrors may provide the output transistors with an abundance of current, particularly because we can give the mirrors an extra gain.

The drivers combined with the mirrors have a non-inverting gain, so we may simply connect a second nest of Miller capacitors  $C_{M21}$  and  $C_{M22}$  to the inputs of the two drivers respectively.

We decided to apply a multipath to the nest so in order to regain a factor 2 in bandwidth. To this effect, we designed an intermediate stage that provides two output currents for each of the N and P output sides. The intermediate stage for the N output side  $Q_{310}$ ,  $Q_{320}$ ,  $Q_{360}$  has been terminated by two folded N-type mirrors  $Q_{380}$ ,  $Q_{381}$ ,  $Q_{382}$ . The folding has been done to give the mirror input side the same voltage level as the mirror output sides to balance out the effect of variations in the supply voltage through the Early effect. The intermediate stage for the P output side  $Q_{330}$ ,  $Q_{340}$ ,  $Q_{360}$  has been terminated by two P-type mirrors. This gives the mirror-input side the same voltage-level as the mirror-output side, which also balances the effect of supply voltage changes through the Early effect at the P-side. The current gain of the intermediate stage is further enhanced by folded Darlington transistors  $Q_{490}$ ,  $Q_{495}$ . The differential intermediate stage is HF compensated by a third nest  $C_{M3}$  and  $C_{P3}$ . The capacitor  $C_{P3}$  is needed to provide the intermediate stage with an HF ground terminal. Without  $C_{P3}$  the left input of the intermediate stage will not be a virtual ground, but terminated by  $R_{590}$ . This would provide an HF sneaky path, that keeps the frequency compensation from roll-off at 6 dB/oct above  $f_z = 1/2\pi R_{590} C_{P3}$ .  $C_{P3}$  must be equal to  $C_{M3}$  for balancing purposes. The level-shift resistor  $R_{596}$  has been inserted to make it possible for the whole amplifier to function at a supply voltage of 1 V between the positive and negative supply rails.

The input stage  $Q_{410}$ ,  $Q_{420}$ ,  $Q_{430}$ ,  $Q_{440}$  has been connected as a rail-to-rail input stage (see Sect. 4.4). The CM range is from rail to rail at a supply voltage of 1.8 V or higher, but at 1 V the circuit already functions with CM ranges around both rails. The switching between the PNP side and NPN side occurs at a voltage  $V_{R1}$ .

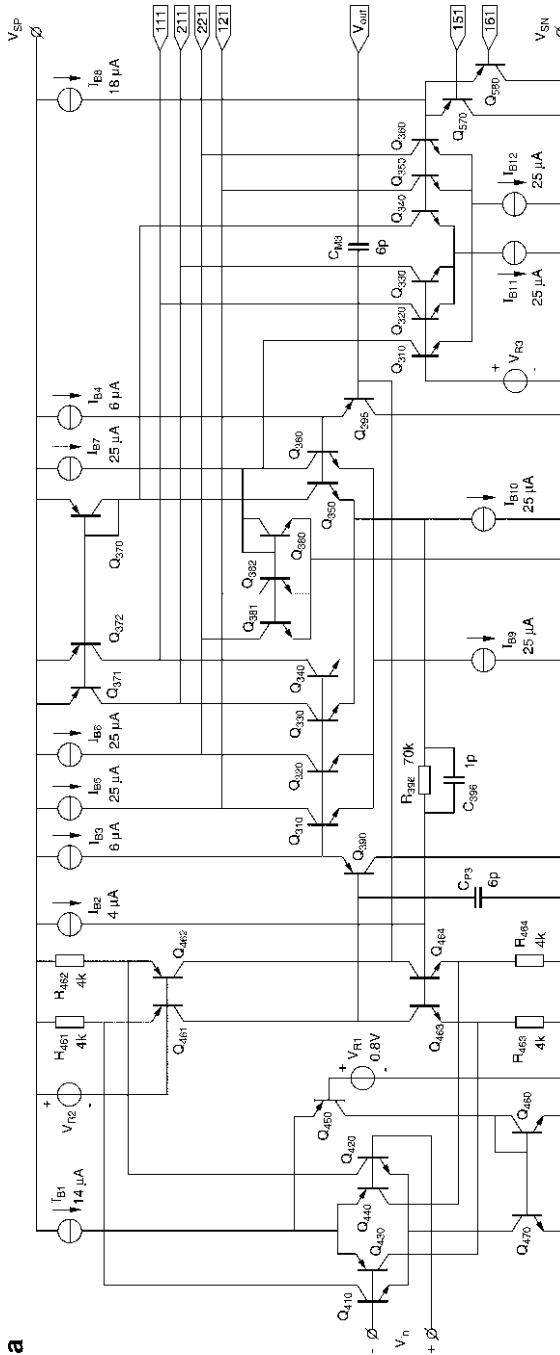
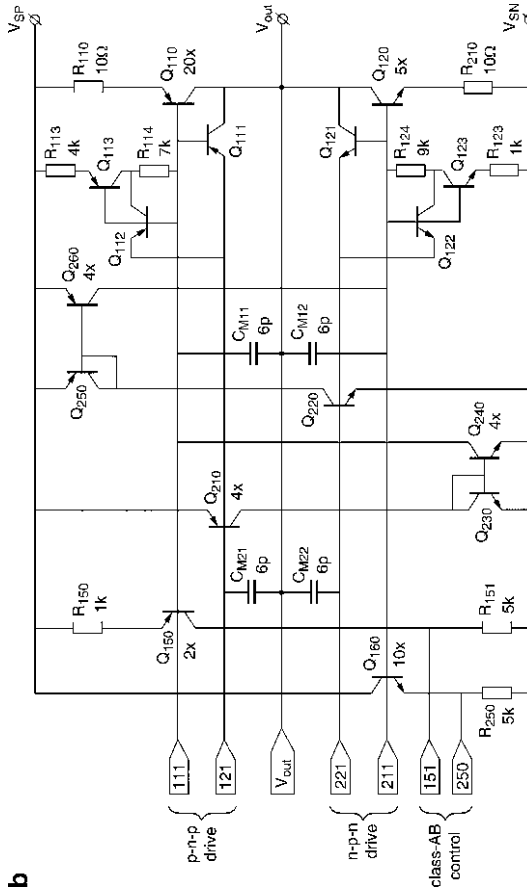


Fig. 7.9.1 (a) GA input stage, GA intermediate stage, and class-AB current control of a 1V R-R-(in)/out OpAmp with GA-GA-GA-GA configuration



**Fig. 7.9.1 (b)** GA output stage with multipath GA booster of a 1-V R-R-in/out OpAmp with GA-GA-GA configuration

The summing circuit  $Q_{461}$ ,  $Q_{462}$ ,  $Q_{563}$ ,  $Q_{464}$  functions as a folded cascode and has a differential output. The summing circuit receives its common-mode feedback at the bottom by the intermediate stages through the level shift resistor  $R_{396}$ .

The class-AB regulator amplifier  $Q_{510}$  through  $Q_{560}$  has been connected in parallel to the intermediate stage. The class-AB amplifier also provides a multipath output to directly drive the output transistors. The output currents are measured in parallel with the output transistors by  $Q_{150}$  and  $Q_{160}$  which have series emitter resistors. The lowest of the output current is sensed by the minimum selector  $Q_{570}$ ,  $Q_{580}$  and transferred to the class-AB regulator amplifier on its right-hand side. A reference voltage is offered on the left-hand side.

The limiting frequency  $f'_1$  is at the output transistors:

$$f'_1 = \frac{g_{m1}}{2\pi C_L} \quad (7.9.1)$$

with  $g_{m1} = g_{m110} + g_{m120}$ .

The  $g_m$  is taken at its quiescent current level. The zero-dB frequency of the feedforward path of the intermediate stage and output stage is:

$$f'_0 = \frac{1}{2} f'_1 = \frac{1}{2} \frac{g_{m1}}{2\pi C_L} \quad (7.9.2)$$

So, the choice of the first nest of Miller capacitors of the feedforward path should be:

$$C_{M1} = \frac{g_{m3}}{2\pi f'_0} = 2 \frac{g_{m3}}{g_{m1}} C_L \quad (7.9.3)$$

with  $C_{M1} = C_{M11} + C_{M12}$  and  $g_{m3} = g_{m330}$ .

The zero-dB frequency of the gain path of the intermediate stage, driver stage, and output stage is:

$$f''_0 = f'_0 = \frac{1}{2} f'_1 \quad (7.9.4)$$

This results in a choice for the second nest of Miller capacitors:

$$C_{M2} = \frac{g_{m3}}{2\pi f''_0} = 2 \frac{g_{m3}}{g_{m1}} C_L \quad (7.9.5)$$

with  $C_{M2} = C_{M21} + C_{M22}$  and  $g_{m3} = g_{m340}$ .

The zero-dB frequency of the whole amplifier is:

$$f'''_0 = \frac{1}{2} f''_0 = \frac{1}{2} f'_0 = \frac{1}{4} f'_1 \quad (7.9.6)$$

The factor  $1/2$  results from the third nest, in which we have not used a second multipath to make the amplifier less complicated. The bandwidth of the four-stage

amplifier with multipath output stage and driver stage is thus comparable with a three-stage amplifier without a multipath. The third nest of Miller capacitors is:

$$C_{M3} = \frac{g_{m4}}{2\pi f_0'''} = 4 \frac{g_{m4}}{g_{m1}} C_L \quad (7.9.7)$$

with  $g_{m4} = g_{m410}$ .

The transconductance  $g_{m4}$  is that of the R-R input stage with mirrored (through tail of intermediate stage) output of the summing circuit.

Care must be taken that the transconductance of the driver stage and current mirror is lower (see explanation with Fig. 6.2.19) than the transconductance of the feedforward path from the intermediate stage. Because at high frequencies the direct HF path must dominate the LF gain path. This results in:

$$4g_{m2} < g_{m3} \quad (7.9.8)$$

with  $g_{m2} = g_{m210} + g_{m220}$  and  $g_{m3} = g_{m340}$ .

At high output currents, this can become difficult to comply with. A solution can be to degenerate the emitters of the driver transistors  $Q_{210}$  and  $Q_{220}$ .

Bipolar output transistors have to be protected against saturation, otherwise their HF behavior drastically reduces and ringing may occur. They must also be protected against overdriving, otherwise these transistors can easily be destroyed. For this purpose, the saturation detectors  $Q_{111}$  and  $Q_{121}$  have been placed in parallel with the output transistors with their collectors and bases. If the output transistors saturate then the saturation detectors also saturate and feed the saturation current in reverse mode through their emitters to the bases of the regarding drivers. Current limitation is effected by a combination of small emitter-resistors in the output transistors, and sense transistors  $Q_{113}$  and  $Q_{123}$  with emitter resistors  $R_{113}$  and  $R_{123}$  with their bases in parallel with the output transistors. The collectors of the sense transistors have been connected through collector resistors  $R_{114}$  and  $R_{124}$  respectively, to the concerning bases. If the currents of these sense transistors become so large that they saturate, this saturation current is sensed by additional sense detectors  $Q_{112}$  and  $Q_{122}$ . Their emitter currents limit the current at the base of the driver transistors.

The result is a 1 V Bipolar OpAmp with a bandwidth of 3 MHz at a load of 100 pF and a total quiescent supply current of 700  $\mu$ A, a DC gain of 100 dB at a load of 10 k $\Omega$ , and a maximum current of 10 mA. These values can be scaled up or down easily by a factor 10 [7.31].

## 1.2 V R-R-Out CMOS Class-AB OpAmp with MHNMC

As a last example of the use of more than three GA-stages in cascade, a 1.2 V CMOS OpAmp with an GA-GA-GA-GA configuration will be given. It has

a multipath hybrid nested Miller compensation. The circuit has an abundance of gain and can drive low-impedance loads. Nowhere are more than one diode and two saturation voltages stacked. The output transistors are driven by transistors which need only one saturation voltage. This results in a supply voltage as low as 1.2 V over temperature and process variations. The circuit is shown in Fig. 7.9.2a [7.32] with a simplified schematic, and Fig. 7.9.2b with a full schematic.

The output stage  $M_{110}$  and  $M_{120}$  has a first Miller nest of capacitors  $C_{M11}$  and  $C_{M12}$ . The output stage is driven by a driver stage  $M_{210}$ ,  $M_{220}$ . The intermediate stage  $M_{310}$  and  $M_{320}$  has a second Miller nest of capacitors  $C_{M31}$  and  $C_{M32}$ . Across the intermediate, driver, and output stages the outer nest is made up by  $C_{M2}$ . The input stage  $M_{410}$  and  $M_{420}$  is followed by a folded cascode  $M_{431}$ ,  $M_{432}$  and loaded with a mirror  $M_{433}$ ,  $M_{434}$ . The mirror also produces two feedforward paths through  $M_{435}$  and  $M_{436}$ , which directly drive the output transistors in a multipath way. The mirror and intermediate stage-transistors are chosen of equal type, so that the mirror transistors have about equal drain-source voltages and do not contribute to supply-voltage dependent offset.

The class-AB regulator has output current sensors  $M_{560}$  with mirror  $M_{570}$ ,  $M_{580}$  and  $M_{590}$ . The sense currents are first subtracted from current sources  $M_{541}$  and  $M_{591}$ , and then fed into the measuring diodes  $M_{540}$  and  $M_{550}$ , respectively. By this action a minimum current in one of the output transistors is translated into a maximum current in one of the measuring diodes. A class-AB control amplifier  $M_{500}$  through  $M_{521}$  has been connected to the measuring diodes as an and-gate or “maximum selector” at its right-hand side. The four outputs of the control amplifier bias the driver-stage and output transistors in a multipath nested manner. This ensures a robust and stable class-AB biasing of the output transistors [7.32]. It has further been explained with Fig. 5.4.12.

The frequency compensation has been explained with Fig. 6.2.22 [7.33].

The limiting-pole frequency is:

$$f_1' = \frac{g_{m1}}{2\pi C_L} \quad (7.9.9)$$

in which  $C_L$  is the output load capacitor, and  $g_{m1} = g_{m110}$ .

The zero-dB frequency  $f_0'$  of the driver and output stage combination must be half that of the limiting-pole frequency, so:

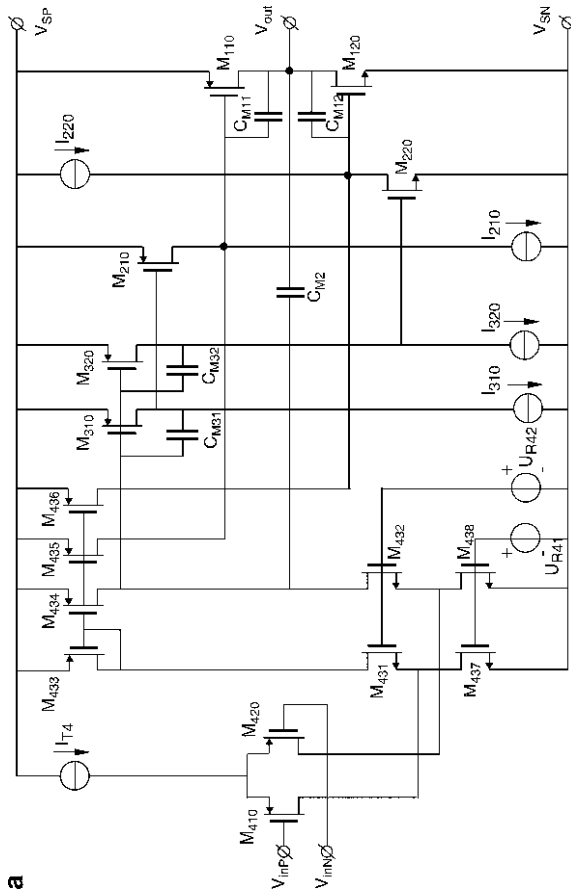
$$f_0' = \frac{1}{2} f_1' \quad (7.9.10)$$

The gain around the driver and output stage is determined by the inverting intermediate stage  $M_{310}$ ,  $M_{320}$  with a gain of  $C_{M2}/C_{M3}$ , which leads to the choice of:

$$\frac{g_{m2}}{2\pi C_{M1}} = \frac{1}{2} \frac{C_{M2}}{C_{M3}} \frac{g_{m1}}{2\pi C_L} \quad (7.9.11)$$

with  $g_{m2} = g_{m210} + g_{m220}$  and  $C_{M1} = C_{M11} + C_{M12}$  and  $C_{M3} = C_{M31} + C_{M32}$ .





**a**

**Fig. 7.9.2 (a)** Simplified schematic of a 1.2 V R-R-out CMOS class-AB OpAmp with GA-GA-GA configuration, and multi-path hybrid nested Miller compensation

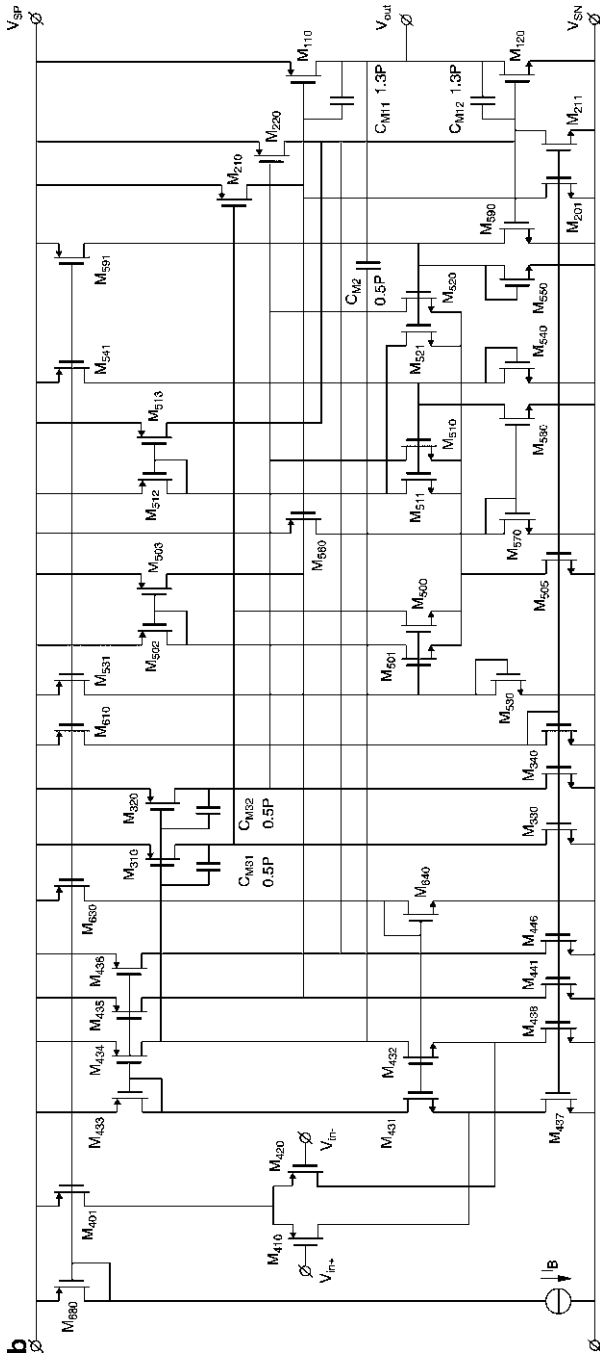


Fig. 7.9.2 (b) 1.2V R-R-out CMOS class-AB OpAmp with GA-GA-GA-GA configuration with multipath hybrid nested Miller compensation

When a multipath connection is made directly from the input stage to drive the output transistors, the overall bandwidth  $f_0''$  may be taken equal to  $f_0'$  or half  $f_1'$ , so:

$$f_0'' = f_0' = \frac{1}{2} f_1' \quad (7.9.12)$$

which leads to a choice for  $C_{M2}$ :

$$\frac{g_{m4}}{2\pi C_{M2}} = \frac{1}{2} \frac{g_{m1}}{2\pi C_L} \quad (7.9.13)$$

in which  $g_{m4}$  is the gain path of the transconductance of the input stage  $M_{410}$ ,  $M_{420}$  provided through the mirror  $M_{433}$ ,  $M_{434}$  to the overall nest  $C_{M2}$ , while the direct path of the transconductance  $1/2 g_{m4}$  is provided through  $M_{435}$  and  $M_{436}$  to the first nest  $C_{M1A}$  and  $C_{M1B}$  respectively.

It must be prevented that the gain-path dominates the HF path at high frequencies. This leads to the choice of a lower transconductance of the driver stage.

Hence:

$$\frac{C_{M2}}{C_{M3}} \frac{g_{m2}}{2\pi C_{M1}} \leq \frac{1}{3} \frac{1/2 g_{m4}}{2\pi C_{M1}} \quad (7.9.14)$$

As the gain path does not contribute much at high frequencies, the constraint for the bandwidth  $f_3'$  of the intermediate stage is also relaxed to  $f_3' \geq 1/3 f_1'$ . This leads to a choice:

$$\frac{g_{m3}}{2\pi C_{M2}} \leq \frac{1}{3} \frac{g_{m1}}{2\pi C_L} \quad (7.9.15)$$

with  $g_{m3} = g_{m310} + g_{m320}$ .

Finally, we must match the 6 dB roll-off of the gain path and the multipath, to avoid a pole-zero doublet.

This leads to the choice:

$$\frac{g_{m4}}{2\pi C_{M2}} = \frac{1/2 g_{m4}}{2\pi C_{M1}} \quad (7.9.16)$$

## Conclusion

The conclusion can be drawn that the hybrid nested Miller compensation technique leads to robust GA-GA-GA-GA amplifiers with an abundance of gain and, when provided with a multipath, a bandwidth comparable to that of a regular Miller compensated OpAmps. As an example two CMOS OpAmp were made, one with and one without a multipath. At a bias current  $I_B$  of 10  $\mu\text{A}$ , the total quiescent current was 300  $\mu\text{A}$  with a supply voltage of 1.5 V, a bandwidth was obtained of

2 MHz and 6 MHz, respectively for the non-multipath and the multipath version, at a load capacitance of 10 pF.

The open-loop voltage gain was 120 dB at a load resistor of 10 k $\Omega$ . The OpAmp does not use resistors and can be easily scaled up or down. At a bias current  $I_B$  of 1  $\mu$ A, a total supply current of only 15  $\mu$ A, a supply voltage of 1.2 V, and a bandwidth was obtained of 0.2 and 0.6 MHz, respectively [7.32].

## 7.10 Problems and Simulation Exercises

### Problem 7.1

Figure 7.1.2b shows a folded-cascode operational amplifier with class-A output stage. Considering the MOS devices sized  $W/L_{15} = W/L_{16} = 3.5W/L_{13} = 3.5W/L_{14} = 35\mu/1\mu$ ,  $W/L_{17} = W/L_{18} = 100\mu/3\mu$ ,  $W/L_{19} = 60\mu/3\mu$  and  $W/L_{20} = W/L_{21} = 20\mu/3\mu$  biased with the current source  $I_{B1} = 20 \mu$ A at a supply voltage of  $V_{SP} = -V_{SN} = 1.35$  V, design the input pair and the current sources  $M_3$ ,  $M_{11}$  and  $M_{12}$  so the gain of the amplifier will be 60 dB with capacitive load  $C_L = 1$  pF and resistive load  $R_L = 5$  M $\Omega$ , and under these conditions the slew-rate will be  $S_r = 40$  V/ $\mu$ s. Transistor parameters are  $V_{THN} = 0.5$  V,  $V_{THP} = -0.6$  V,  $K_N = 56\mu\text{A}/\text{V}^2$ ,  $K_P = 16\mu\text{A}/\text{V}^2$ ,  $\lambda_N = \lambda_P = 0.1$  V $^{-1}$ . Calculate the 0-dB frequency and the biasing voltages  $V_{B1}$ ,  $V_{B2}$ .

### Solution

The tail current of the input stage limits the slew rate of the whole amplifier under given capacitive load, the second stage being only a current follower

$$S_r = \frac{I_{D3}}{C_L} = \frac{2I_B}{C_L} \quad (7.10.1)$$

which for the given slew-rate value requires an  $I_B$  current of

$$I_B = \frac{S_r C_L}{2} = 20 \mu\text{A} \quad (7.10.2)$$

The corresponding sizes for the current source transistors are determined taking care to keep the same channel length for the current mirrors using  $M_{19}$  as reference

$$\frac{W}{L_3} = \frac{120 \mu}{3 \mu} \quad (7.10.3)$$

Transistors  $M_{I1}$  and  $M_{I2}$  are sized knowing their drain current equal to  $2I_B$

$$\frac{W}{L_{I1}} = \frac{W}{L_{I2}} = \frac{2I_B}{I_{B1}} \frac{W}{L_{21}} = \frac{40 \mu}{3 \mu} \quad (7.10.4)$$

Without load resistance, the DC voltage gain of the amplifier is

$$A_{V0} = g_{m1} (\mu_{I4} r_{ds12} \parallel \mu_{I6} r_{ds18} \parallel R_L) \quad (7.10.5)$$

For a saturated MOS transistor, the voltage gain  $\mu$  and  $r_{ds}$  above can be calculated based on device sizes and drain current

$$\begin{aligned} \mu &= \frac{1}{\lambda \sqrt{\frac{2I_D}{K'_L W}}} \\ r_{ds} &= \frac{1}{\lambda I_D} \end{aligned} \quad (7.10.6)$$

Numerically, using device sizes and the biasing given by 7.10.6, this allows calculating the amplifier output impedance

$$Z_0 = 31.2 M\Omega \quad (7.10.7)$$

which is much larger than the load resistance

$$Z_0 \gg R_L \quad (7.10.8)$$

Thus,  $g_{m1}$  can be calculated as

$$g_{m1} = \frac{A_{V0}}{R_L} = 200 \mu S \quad (7.10.9)$$

Using the value above in Eq. 7.1.8 the sizes of input pair transistors result

$$\frac{W}{L_{I,2}} = \frac{g_{m1,2}^2}{4K_P I_B} = 32 \quad (7.10.10)$$

For low input offset, the channel length of the input pair transistors is usually non-minimal, similar to the current mirrors

$$\frac{W}{L_{I,2}} = \frac{100 \mu}{3 \mu} \quad (7.10.11)$$

Because the input transistors are actually close to weak inversion, their size is usually large in real circuits. The 0-dB frequency of the amplifier designed above will be

$$f_0 = \frac{g_{m1}}{2\pi C_L} = 32 MHz \quad (7.10.12)$$

The biasing sources  $V_{B1}$ ,  $V_{B2}$  should be designed to keep  $M_{17,18}$  and  $M_{11,12}$  in saturation even when the input pair is slewing, sourcing all available current through one of the input transistors

$$\begin{aligned} V_{B1} &= (V_{GS16} + V_{sat18})|_{I_{D16}=2I_B} = 0.977 + 0.380 = 1.36 \text{ V} \\ V_{B2} &= (V_{GS14} + V_{sat12})|_{I_{D12}=2I_B} = 0.077 + 0.330 = 1.10 \text{ V} \end{aligned} \quad (7.10.13)$$

### Problem 7.2

Figure 7.2.5 shows a rail-to-rail output two-stage amplifier compensated by a Miller configuration which does not introduce a positive zero in its AC behavior. Considering the MOS devices sized as  $W/L_{28} = 2W/L_{14} = 10W/L_{32} = 80\mu/2\mu$ ,  $W/L_{27} = 2W/L_{13} = 10W/L_{31} = 100\mu/2\mu$ ,  $W/L_{21} = W/L_{22} = 60\mu/2\mu$ ,  $W/L_{23} = W/L_{24} = 20\mu/2\mu$ ,  $W/L_{25} = W/L_{26} = 10\mu/2\mu$ ,  $W/L_{12} = 40\mu/1\mu$  and  $W/L_{11} = 80\mu/1\mu$ , the biasing source  $I_B = 10\mu\text{A}$  and the amplifier loaded with only the capacitor  $C_L = 10 \text{ pF}$ , calculate the D-C voltage gain  $A_{V0}$  and the Miller compensation capacitor  $C_M$  for a phase margin of the compensated amplifier  $\phi_m = 60^\circ$ . Transistor parameters are  $V_{THN} = 0.5 \text{ V}$ ,  $V_{THP} = -0.6 \text{ V}$ ,  $K_N = 56 \mu\text{A}/\text{V}^2$ ,  $K_P = 16 \mu\text{A}/\text{V}^2$ ,  $\lambda_N = \lambda_P = 0.1 \text{ V}^{-1}$ .

### Solution

The biasing currents for  $M_{14}$  and  $M_{28}$  can be calculated knowing the reference current through  $M_{32}$ .

$$\begin{aligned} I_{D14} &= I_{D32} \frac{W}{L_{14}} \frac{L}{W_{32}} = 50 \mu\text{A} \\ I_{D28} &= I_{D32} \frac{W}{L_{28}} \frac{L}{W_{32}} = 100 \mu\text{A} \end{aligned} \quad (7.10.14)$$

The DC voltage gain with no resistive load is given by Eq. 7.2.10 as

$$A_{V0} = \mu_2 \mu_1 \mu_3 \quad (7.10.15)$$

each  $\mu$  voltage gain corresponding to  $M_{21}$ – $M_{22}$ ,  $M_{11}$  and  $M_{12}$  respectively

$$A_{V0} = \frac{1}{\lambda_P \sqrt{\frac{2I_{D22}}{K_P \frac{W}{L_{22}}}}} \frac{1}{\lambda_N \sqrt{\frac{2I_{D11}}{K_N \frac{W}{L_{11}}}}} \frac{1}{\lambda_N \sqrt{\frac{2I_{D12}}{K_N \frac{W}{L_{12}}}}} = 96 \text{ dB} \quad (7.10.16)$$

There is a huge gain which can be obtained with this amplifier structure. The price is the reduced input and output common-mode ranges.

The Miller compensation is calculated forcing the unity gain bandwidth to be half the value of the non-dominant pole introduced by the capacitive load

$$f_0 = \frac{1}{2} \frac{g_{m11}}{2\pi C_L} = 10.6 \text{ MHz} \quad (7.10.17)$$

As this frequency should be set by the transconductance of the input stage and the Miller capacitor, the value of  $C_M$  results

$$C_M = \frac{g_{m22}}{2\pi f_0} = 6.6 \text{ pF} \quad (7.10.18)$$

### Problem 7.3

The class-AB amplifier in Fig. 7.7.2 is designed with transistors sized  $W/L_{12} = 7.5\mu/2\mu$ ,  $W/L_{17} = W/L_{18} = 2\mu/2\mu$ ,  $W/L_{11} = 26\mu/2\mu$ ,  $W/L_{15} = W/L_{16} = 7\mu/2\mu$ ,  $W/L_{25} = W/L_{26} = W/L_{33} = 42\mu/2\mu$ ,  $W/L_{31} = W/L_{32} = 10\mu/2\mu$ ,  $W/L_{13} = 14\mu/2\mu$ ,  $W/L_{14} = 4\mu/2\mu$ ,  $W/L_{21} = W/L_{22} = 4\mu/2\mu$ ,  $W/L_{23} = W/L_{24} = 6\mu/2\mu$ ,  $W/L_{27} = W/L_{28} = 21\mu/2\mu$  and biased with  $I_{B11} = I_{B12} = 0.5 \mu\text{A}$ . For a capacitive load only,  $C_L = 10 \text{ pF}$ , calculate the Miller capacitors  $C_{M11}$  and  $C_{M12}$  so the phase margin becomes  $\varphi_m = 60^\circ$ . Calculate the unity gain bandwidth of the compensated amplifier. What is the maximum current which can be supplied by the class-AB output stage? Transistor parameters are  $V_{THN} = 0.5 \text{ V}$ ,  $V_{THP} = -0.6 \text{ V}$ ,  $K_N = 56 \mu\text{A/V}^2$ ,  $K_P = 16 \mu\text{A/V}^2$ ,  $\lambda_N = \lambda_P = 0.1 \text{ V}^{-1}$ .

### Solution

The drain currents for  $M_{33}$ ,  $M_{25}$  and  $M_{26}$  are all equal because of equal sizing of these transistors

$$I_{D33} = I_{D25} = I_{D26} = I_{D15} \frac{W}{L_{33}} \frac{L}{W_{15}} = 3 \mu\text{A} \quad (7.10.19)$$

The quiescent current of output transistors can be calculated using one of the translinear loops, for example  $V_{GS11} - V_{GS13} - V_{GS16} - V_{GS15}$

$$I_{D11} = W/L_{11} \left( \sqrt{\frac{I_{D15}}{W/L_{15}}} + \sqrt{\frac{I_{D16}}{W/L_{16}}} - \sqrt{\frac{I_{D13}}{W/L_{13}}} \right)^2 = 1.1 \mu\text{A} \quad (7.10.20)$$

This value is equal with  $I_{D12}$  at quiescent operating point. Knowing the drain current and the sizes of the transistors, the DC gain voltage can be calculated

$$A_{V0} = g_{m3} r_{ds22} \mu_{24} \mu_{12} = \frac{\sqrt{2K_P \frac{W}{L_{32}} I_{D32}}}{\lambda_N^3 I_{D22} \sqrt{\frac{2I_{D24}}{K_N \frac{W}{L_{24}}}} \sqrt{\frac{2I_{D12}}{K_N \frac{W}{L_{12}}}}} \quad (7.10.21)$$

The Miller capacitors result from Eq. 7.7.9

$$C_{M11} = C_{M12} = C_L \frac{g_{m3}}{g_{m12}} = 7.6 \text{ pF} \quad (7.10.22)$$

Unity gain bandwidth of the compensated amplifier can now be calculated as

$$f'_0 = \frac{g_{m3}}{2\pi C_L} = 246 \text{ KHz} \quad (7.10.23)$$

The maximum output push or pull current can be calculated if all the available current from  $M_{28}$  flows either through  $M_{13}$  or  $M_{14}$ . Using (7.10.20) under the assumption that  $I_{D13} = 0$ , the push current limit results

$$I_{D11} = W/L_{11} \left( \sqrt{\frac{I_{D15}}{W/L_{15}}} + \sqrt{\frac{I_{D16}}{W/L_{16}}} \right)^2 = 7.4 \mu\text{A} \quad (7.10.24)$$

### Problem 7.4

The compact amplifier shown in Fig. 7.7.7 can be tuned to operate at 1.2 V supply voltage and 10  $\mu\text{A}$  supply current. Considering the transistors sized as shown, adjust the bias current to the required value to operate the amplifier at the aforementioned supply current, then calculate the Miller compensation capacitors  $C_{M1A}$ ,  $C_{M2A}$  and the 0-dB bandwidth for a phase margin  $\phi_m = 60^\circ$  when the amplifier is loaded with a capacitor  $C_L = 10 \text{ pF}$ . The PMOS transistors have  $K_P = 16 \mu\text{A}/\text{V}^2$ .

### Solution

All the biasing currents are obtained from  $I_B$  in this circuit so the sum of all these currents can be obtained as a function of  $I_B$ .



$$\begin{aligned}
 I_{D321} &= I_{D204} = I_{D206} = 2I_B \\
 I_{D239} &= I_{D238} = I_{D501} = I_B \\
 I_{D112} &= I_{D113} = \frac{1}{2}I_{D219} = \frac{1}{2}I_B \\
 I_{D101} &= \frac{W}{L_{101}} \frac{L}{W_{111}} \frac{1}{2}I_B = 10I_B
 \end{aligned} \tag{7.10.25}$$

Summing all the currents calculated above except for the biasing current itself, the total supply current is

$$I_{supply} = 20I_B \tag{7.10.26}$$

which requires a bias current

$$I_B = \frac{10 \mu\text{A}}{20} = 0.50 \mu\text{A} \tag{7.10.27}$$

In order to calculate the Miller capacitors and the bandwidth of the compensated amplifier, two  $g_m$  values must be calculated

$$g_{m3} = g_{m301} = g_{m302} = \sqrt{2K_P \frac{W}{L_{301}} I_{D301}} = 22.6 \mu\text{A}/\text{V} \tag{7.10.28}$$

The above value seems to be too large, considering the level of drain current for the input transistors. The maximum  $g_m$  for a MOS transistor operated at a drain current  $I_D$  is attained when the transistor works in weak inversion and is typically limited to  $25I_D$  at room temperature, similar to a bipolar transistor. Therefore, the value of  $g_{m3}$  will be limited to

$$g_{m3} = 25I_{D301} = 12.5 \mu\text{A}/\text{V} \tag{7.10.29}$$

In the same manner, the output  $g_m$  can be calculated

$$g_{m1} = 2g_{m100} = 50I_{D100} = 250 \mu\text{A}/\text{V} \tag{7.10.30}$$

The Miller capacitors are compensating one output transistor each, so their value is

$$C_{M1A} = C_{M2A} = \frac{g_{m3}}{g_{m1}} C_L = 0.5 \text{ pF} \tag{7.10.31}$$

and the corresponding 0-dB frequency of the compensated amplifier becomes

$$f_0' = \frac{g_{m3}}{2\pi(C_{M1A} + C_{M2A})} = 2 \text{ MHz} \tag{7.10.32}$$



non-inverting configuration and using a pulsed voltage for input signal. Estimate the slew-rate of both versions. By changing the input signal to a variable amplitude sinusoidal voltage and running transient and Fourier analyses, a maximum limit can be obtained for the output voltage by imposing a limit for the accepted distortion  $\text{THD} = 0.1\%$ .

### ***Simulation Exercise 7.2***

The class-AB compact amplifier shown in Fig. 7.10.2 can be operated at a supply voltage as low as 1.2 V. Run AC simulation for gain and phase characteristic, then transient simulations for slew-rate and maximum output range in a manner similar to the one described in the previous exercise. During the slew-rate measurement, plot the drain currents of both the output transistors and observe the minimum current which is drawn by the inactive transistor.

## **7.11 References**

- [7.1]. J.H. Huijsing, F. Tol, Monolithic operational, amplifier design with improved HF behavior. *IEEE J. Solid State Circ.* **SC-11**, 323–328 (1976)
- [7.2]. M. Steyaert, W. Sansen, Opamp design towards maximum gain-bandwidth in *Analog Circuit Design*, ed. by J.H. Huijsing et al. (Kluwer Academic Publishers, Boston, 1993) pp. 63–85
- [7.3]. R. Caprio, Precision differential voltage-current converter. *Electron. Lett.* **9**, 147–148 (1973)
- [7.4]. B.W. Lee, B.J. Shen, A high-speed CMOS amplifier with dynamic frequency compensation. *J. Semicustom ICs* **8**(3), 42–46 (1991), Elsevier Science Publishers
- [7.5]. L.G.A. Callewaert, W. Sansen, Class AB CMOS amplifiers with high efficiency. *IEEE J. Solid State Circ.* **25**(3), 684–691 (1990)
- [7.6]. K. Bult, G.J.G.M. Geelen, A fast settling CMOS op amp for SC-circuits with 90-dBDC gain. *IEEE J. Solid State Circ.* **25**(3), 1379–1383 (1990)
- [7.7]. R. Hogervorst, et al., A programmable power-efficient 3-V CMOS rail-to-rail opamp with gain boosting for driving heavy resistive loads, in *Proceedings IEEE International Symposium on Circuits and Systems*, Seattle, USA, 30 Apr–3 May 1995, pp. 1544–1547
- [7.8]. P.R. Gray, R.G. Meijer, MOS operational amplifier design – a tutorial overview. *IEEE J. Solid State Circ.* **17**(6), 969–982 (1982)
- [7.9]. G.M. Cotreau Operational amplifiers and voltage regulators. *ISSCC 85*, in *Proceedings vol. 28, THAM 11.3*, pp. 138–139
- [7.10]. J.E. Solomon, The monolithic Op Amp: A tutorial study. *IEEE J. Solid State Circ.* **9**(6), 314–332 (1974)
- [7.11]. Fairchild Data Sheet of  $\mu\text{A}$  741 opamp
- [7.12]. R.J. Widlar, M. Yamatake, A fast-settling op amp with low supply current. *IEEE J. Solid State Circ.* **24**(3), 796–802 (1989)
- [7.13]. K.J. de Langen, et al., A 1-GHz bipolar class-AB operational amplifier with multipath nested Miller compensation for 76-dB gain. *IEEE J. Solid State Circ.* **32**(4), 488–498 (1997)
- [7.14]. R.J. Widlar, Monolithic op amp with simplified frequency compensation *IEEE* **15**, 58–63 (1967)

- [7.15]. Signetics/Philips Data Sheet NE 5534
- [7.16]. R.G.H. Eschauzier et al., A 100-MHz 100-dB operational amplifier with multipath nested Miller compensation structure. *IEEE J. Solid State Circ.* **27**(12), 1710–1717 (1992)
- [7.17]. D.M. Monticelli, A quad CMOS single-supply op amp with rail-to-rail output swing. *IEEE J. Solid State Circ.* **21**(6), 1026–1033 (1986)
- [7.18]. W.C.S. Wu et al., Digital-compatible high-performance operational amplifier with rail-to-rail input and output ranges. *IEEE J. Solid State Circ.* **29**(1), 63–66 (1994)
- [7.19]. R. Hogervorst et al., A compact power-efficient 3 V CMOS rail-to-rail input/output operational amplifier for VLSI cell libraries. *IEEE J. Solid State Circ.* **29**(12), 1505–1513 (1994)
- [7.20]. R. Hogervorst, J.H. Huijsing, in *Design of Low-Voltage Low-Power Operational Amplifier Cells* (Kluwer Academic Publishers, Boston, 1996), pp. 35–63, 147–203, 207
- [7.21]. K.J. de Langen, et al., Translinear circuits in low-voltage operational amplifiers in *Analog Circuit Design*, ed. by W. Sansen et al. (Kluwer Academic Publishers, Boston, 1996), pp. 357–386
- [7.22]. K.J. de Langen, J.H. Huijsing, Compact low-voltage power efficient operational amplifier cells for VLSI. *IEEE J. Solid State Circ.* **33**(10), pp. 1482–1496 (1998)
- [7.23]. E. Seevinck, et al., A low-distortion output stage with improved stability for monolithic power amplifiers. *IEEE J. Solid State Circ.* **23**(3), 794–801 (1988)
- [7.24]. K.J. de Langen, J.H. Huijsing, *Ultimate Low-Voltage Compact Three-Stage Operational Amplifiers Using Nested Miller and Mirrored Nested Miller Compensation* (Kluwer Academic Publishers, Boston, 1999), 249pp
- [7.25]. K.J. de Langen, J.H. Huijsing, *Compact Low-Voltage Three Stage BiCMOS Operational Amplifier Cell* (Kluwer Academic Publishers, Boston, 1999), 249pp
- [7.26]. K.J. de Langen, J.H. Huijsing, *Compact Low-Voltage and High-Speed CMOS, BiCMOS, and Bipolar Operational Amplifiers* (Kluwer Academic publishers, Boston, 1999), 249pp
- [7.27]. J.H. Huijsing, D. Linebarger, Low-voltage operational amplifier with rail-to-rail input and output ranges. *IEEE Solid State Circ.* **20**(6), 1144–1150 (1985)
- [7.28]. M.J. Fonderie, J.H. Huijsing, *Design of Low-Voltage Bipolar Operational Amplifiers* (Kluwer Academic Publishers, Boston, 1993), 193pp
- [7.29]. R.J. Widlar, Low-voltage techniques. *IEEE J. Solid State Circ.* **13**(6), 838–846 (1978)
- [7.30]. M.J. Fonderie et al., I-V operational amplifier with rail-to-rail input and output ranges. *IEEE J. Solid State Circ.* **24**(6), 1551–1559 (1989)
- [7.31]. M.J. Fonderie, J.H. Huijsing, Operational amplifier with 1-V rail-to-rail multipath driven output stage. *IEEE J. Solid State Circ.* **26**(12), 1817–1824 (1991)
- [7.32]. R.G.H. Eschauzier et al., A programmable 1.5 V Class-AB operational amplifier with hybrid nested Miller compensation for 120 dB gain and 6 MHz UGF. *IEEE J. Solid State Circ.* **29**(12), 1497–1504 (1994)
- [7.33]. R.G.H. Eschauzier, J.H. Huijsing, *Frequency Compensation Techniques for Low-Power Operational Amplifiers* (Kluwer Academic Publishers, Boston, 1995), 245pp



# 8. Fully Differential Operational Amplifiers

As the supply and signal voltages go down to lower values from 30, 12, 5, 3, 2, and finally 1 V, the signal-to-noise-and-interference ratio becomes increasingly worse. An important way to cope with this problem is to use fully differential signal paths. The differential peak-to-peak signal then becomes maximally twice the total supply voltage  $V_S = V_{SP} - V_{SN}$ . But even more important will be that the influence of substrate interference on the two balanced signals will largely cancel one another. All kinds of amplifiers, filters, sigma-delta converters, and other circuits using fully differential OpAmps may thus be designed in a fully balanced or differential way.

For this purpose, we have to design fully differential OpAmps which have two outputs of which the voltages accurately move opposite to each other in regard to a constant common output reference voltage.

The main additional problem is to design a common-mode output control circuit that is accurate and that can handle voltages that move close to the supply-rail voltages, so that the amplifier can function at low supply voltages. This will be elaborated in this chapter for the GA-CF, GA-CF-GA, and the GA-GA-GA-GA configuration with several different solutions.

The control of the differential output voltages of this chapter is in contrast with the OFA approach (see Chap. 9) in which the relation between the output currents is controlled in an accurate differential way.

## 8.1 Fully Differential GA-CF Configuration

The simplest OpAmp is the GA-CF configuration. It has been shown in Fig. 7.1.2b. with a single-ended output. To properly connect the differential input to the single output a mirror connection was needed. If we want a differential output this mirror connection must be removed and a common-mode output voltage control must be added.

### ***Fully Differential CMOS OpAmp with Linear-Mode CM-Out Control***

A very simple CM output control circuit arises when we use CMOS transistors in their linear mode as CM sensors. An example of a simple circuit is shown in Fig. 8.1.1a [8.1, 8.2].

The common mode output control consists of two transistors  $M_9$  and  $M_{10}$  biased in their linear resistive region and connected at their drains with an equal drain-source voltage  $V_{DS9} = V_{DS10} = V_{DS9,10}$  of only 100 mV, while the effective gate-source voltage  $V_{GT} = V_{GS} - V_{TH}$  is larger.

$$V_{GT} = V_{GS} - V_{TH} > V_{DS} \quad (8.1.1)$$

Under this condition, the channel is not pinched-off anywhere, and we can write for the drain current

$$I_D = \mu C_{ox} \frac{W}{L} V_{DS} \left( V_{GT} - \frac{1}{2} V_{DS} \right) \quad (8.1.2)$$

This relation is linearly dependent on  $V_{GT}$  or  $V_G$ . So, we connect one gate  $V_{G9}$  to one output  $V_{out-}$  and the other gate  $V_{G10}$  to the other output  $V_{out+}$ , and we keep the sum of the two drain currents  $I_{D9} + I_{D10} = I_C$  constant, and the drain voltages  $V_{DS9}$ ,  $V_{DS10}$  equal:  $V_{DS9} = V_{DS10}$ . The average gate voltage  $(V_{G9} + V_{G10})/2$  will now regulate itself at the common-mode level  $V_{CM}$  of the gate voltage  $V_{G4}$  of a model transistor  $M_4$  that is driven with the same current density as  $M_9$  and  $M_{10}$ .

This follows from:

When we choose  $I_C = 2 I_{D4}$ ,  $W_9/L_9 = W_{10}/L_{10} = W_4/L_4$ , and

$$I_C = I_{D9} + I_{D10} = \mu C_{OX} = \frac{W_{9,10}}{L_{9,10}} V_{DS9,10} (V_{GT9} + V_{GT10} - V_{DS9,10}) \quad (8.1.3)$$

$$2I_{D4} = \mu C_{OX} \frac{W_4}{L_4} V_{DS4} (2V_{GT4} - V_{DS4}) \quad (8.1.4)$$

with  $V_{DS9,10} = V_{DS4}$ , we find:

$$(V_{G9} + V_{G10})/2 = V_{G4} \quad (8.1.5)$$

and hence:

$$(V_{out-} + V_{out+})/2 = V_{CM} \quad (8.1.6)$$

The result is a robust common-mode regulation of the output. A condition therefore is that no common-mode output signal current  $I_{outCM} = (I_{out-} + I_{out+})/2$  is drawn

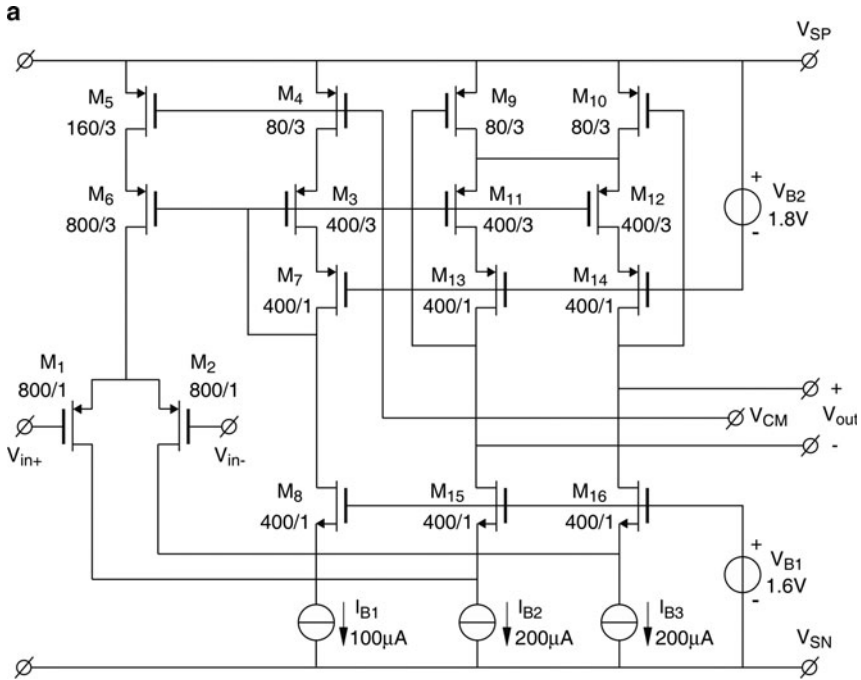


**Fig. 8.1.1 (a)** Fully differential operational amplifier with an GA-CF configuration having common-mod output-voltage control with CMOS transistors in their linear mode

from the output. Otherwise, we may no longer state that  $I_{D9} + I_{D10} = I_C = 2I_{D4}$ . This condition can normally be met by the application.

A bandwidth of 80 MHz was obtained with this simple fully differential OpAmp at load capacitors of 1 pF, an open DC gain of 70 dB, a maximum output current of 100 µA and a quiescent current of 500 µA [8.2].

A drawback of the circuit is that the output voltages cannot reach the positive supply-rail voltage within a threshold voltage  $|V_{TH}|$  of the p-channel transistors  $M_9$  and  $M_{10}$ . These transistors do not function for a negative effective gate-source voltage  $|V_{GT}| = |V_{GS}| - |V_{TH}|$ . To use the supply voltage range more effectively, we have to choose from the input CM feedback control of Fig. 8.1.3, or the rail-to-rail buffered resistive CM sensor of Fig. 8.1.4, or the resistive CM sensor of Fig. 8.2.1, or the switched-capacitor CM sensor of Fig. 8.3.1.

### **Fully Differential Telescopic CMOS OpAmp with Linear-Mode CM-Out Control**

A simple CMOS differential telescopic GA-CF OpAmp with linear-mode CM-output control is shown in Fig. 8.1.1b. It has been derived from the telescopic single-ended OpAmp of Fig. 7.1.3. The transistors  $M_9$  and  $M_{10}$  sense in linear-mode ( $V_{DS} \approx 50\text{--}100$  mV) the output voltages and control the CM output voltage at a



constant level  $V_{CM\ out}$  which is sensed by the model control transistor  $M_{17}$ . The telescopic cascoded differential version has the advantage of half the supply current over the folded cascoded version of Fig. 8.1.1a. A disadvantage is the somewhat limited input and output range, as described with the single-ended telescopic cascoded OpAmp of Fig. 7.1.3. The maximum positive output voltage should be limited to  $V_{SP} - V_{TH9,10}$ , or  $V_{in\ CM} + V_{TH1,2} - V_{sat\ 3,4}$ , whichever is lower.

**Fully Differential CMOS OpAmp with LTP CM-Out Control**

A set of two long-tail pairs (LTP) can also sense the common mode output voltage. An example of a simple circuit is shown in Fig. 8.1.2 [8.3, 8.4].

Two long-tail pairs  $M_{60}, M_{61}$  and  $M_{62}, M_{63}$  are connected with their gates between the desired CM voltage level  $V_{CM}$  and each of the output terminals  $V_{out+}$  and  $V_{out-}$ .

Each long-tailed pair has a non-linear transconductance. But if the non-linearities of both pairs is identical, we can still accurately measure differences in the input voltage of each pair. The sum of the output currents of the transistors  $M_{61}$  and  $M_{62}$ , whose gates are connected to  $V_{CM}$  is used to control the common-mode output voltages CM through  $M_{65}, M_{13}, M_{14}$ . This sum current is constant if the gate voltage of  $M_{60}$  moves opposite to that of the gate voltage of  $M_{63}$ . This results in:

$$V_{G60} - V_{G61} = V_{G62} - V_{G63} \tag{8.1.7}$$

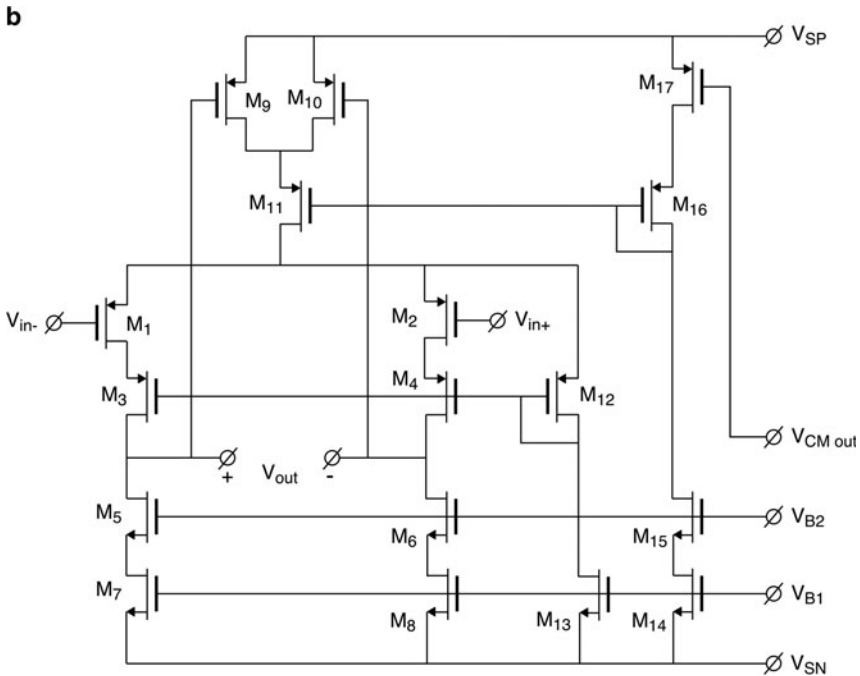


**Fig. 8.1.1 (b)** Fully differential telescopic operational amplifier with GA-CF configuration with common-mode output-voltage control with CMOS transistors in their linear mode

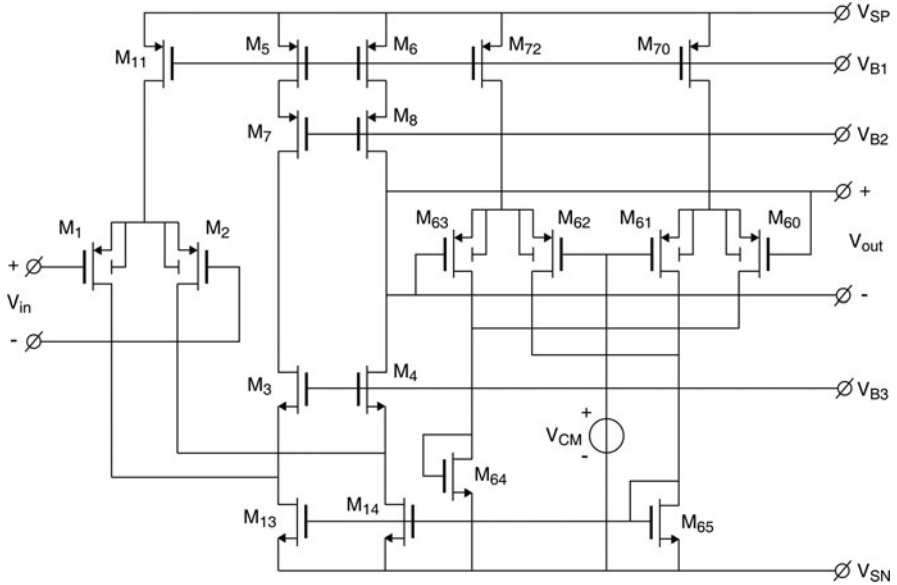


**Fig. 8.1.2** Fully differential operational amplifier with an GA-CF configuration having common-mode output voltage control with a set of two long-tail pairs

or

$$(V_{G60} + V_{G63})/2 = (V_{G61} + V_{G62})/2 = V_{CM} \tag{8.1.8}$$

Note that we certainly used P-channel pairs instead of N-channel ones to avoid differences in  $g_m$  by signal dependent back-gate modulation.

The CM regulation of the circuit naturally has the same bandwidth as the differential signal bandwidth.

The circuit of Fig. 8.1.2 with long-tail pair CM-output-voltage control works well in a certain output voltage range. The same drawback, or even a little worse, is present as with control by CMOS in the linear mode. The long-tail pair sensors do not work when one of the gate voltages is higher than one saturation voltage plus one threshold voltage below  $V_{SP}$ . So, the circuit cannot effectively use the full supply-voltage range at its output.

### ***Fully Differential GA-CF CMOS OpAmp with Output Voltage Gain Boosters***

In many cases, like in the first stage of a sigma-delta converter or passive integrator, a very large voltage gain is needed at a very large output impedance. This can be made by inserting gain boosters to regulate the gates of the output cascode transistors. The situation is depicted in Fig. 8.1.3 [8.5].



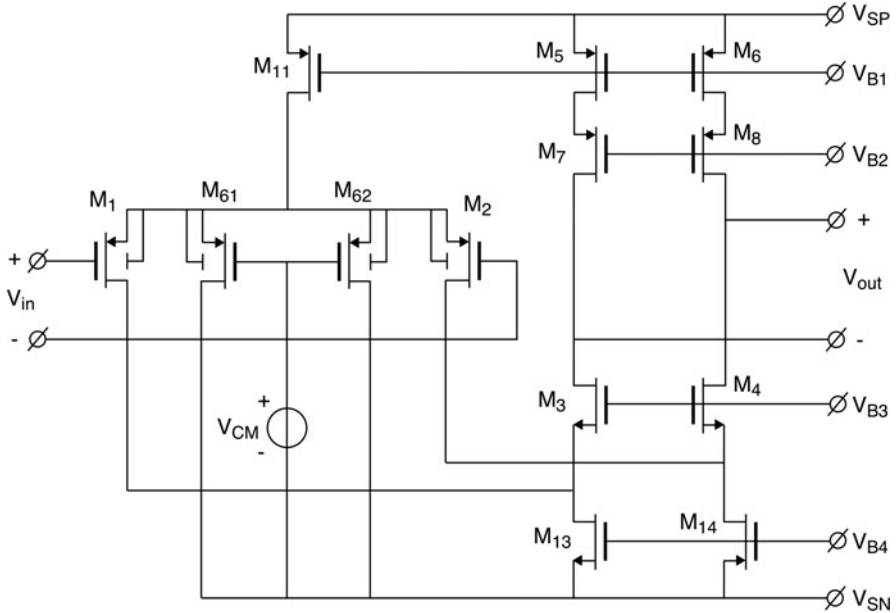


Fig. 8.1.3 (b) Fully differential operational amplifier with an GA-CF configuration and output CM control by input CM feedback

**Fully Differential CMOS OpAmp with R-R Buffered Resistive CM-Out Control**

If we could connect two equal resistors, one to each of the output voltages, and control the common mode level by sensing the centre connection voltage between the two resistors, a nearly rail-to-rail (R-R) output signal range would result. However, the connection of the resistors between both outputs will ruin the DC gain. In order to avoid this we can drive the resistors not directly by the outputs, but indirectly through R-R buffers. This is shown in Fig. 8.1.4a.

The voltage on the centre point in Fig. 8.1.4a of the CM resistors  $R_{CM1}$  and  $R_{CM2}$  is sensed by the differential pair  $M_{31}$ ,  $M_{32}$  and compared with the desired CM voltage level  $V_{CM}$ . The transistor  $M_{32}$  is connected as a diode.

A circuit example of an R-R voltage follower is shown in Fig. 8.1.4b, see also Chap. 4.

Two complementary differential, mirrored, and folded-cascode transconductance amplifiers  $M_{51}$ – $M_{58}$  and  $M_{61}$ – $M_{68}$  have been connected together at their outputs and connected as a unity-gain voltage follower. If the total supply voltage is larger than two saturation voltages and two diode voltages, which is normally the case at 2 V, at least one of the differential pairs is functioning, and the output will follow the input voltage nearly from rail-to-rail.

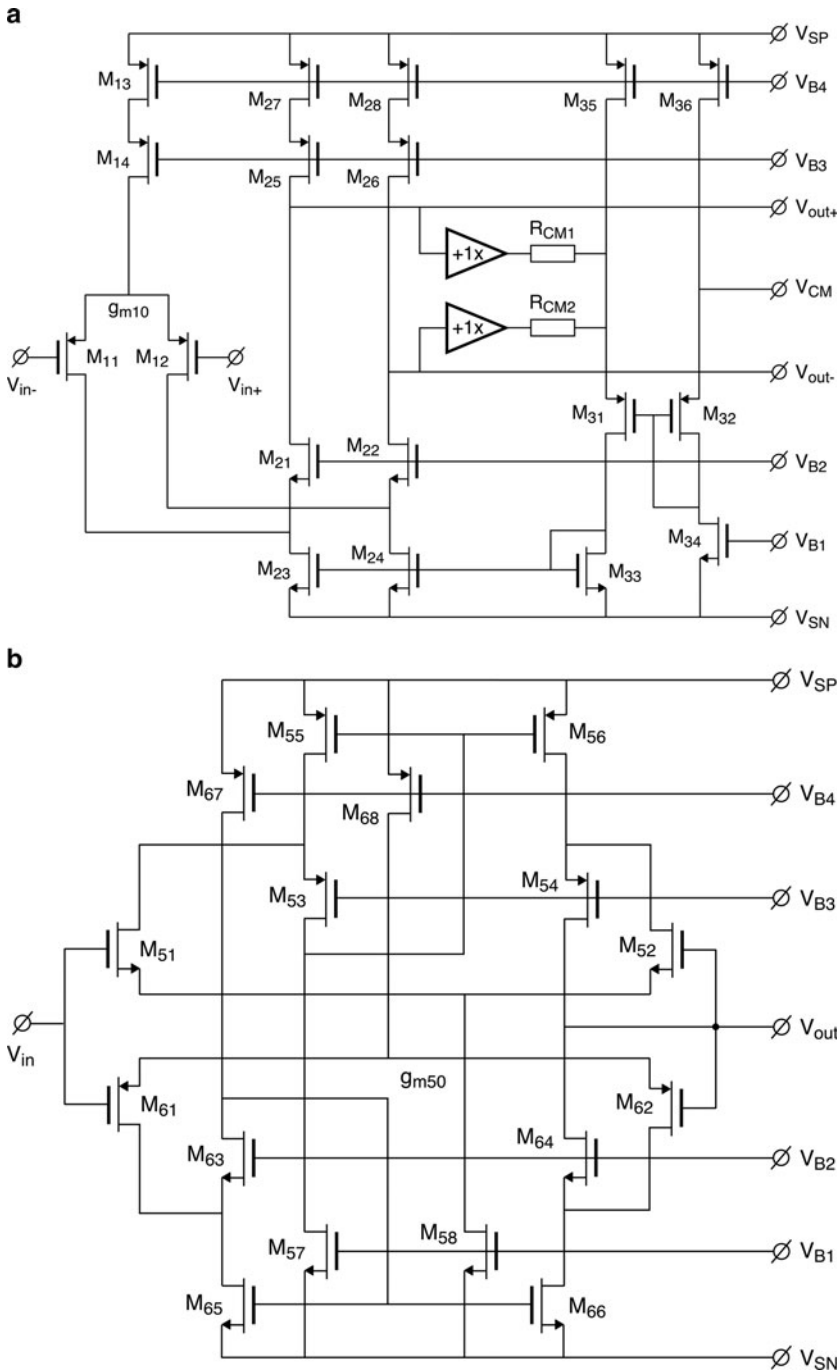


**Fig. 8.1.4** (a) Fully differential operational amplifier with an GA-CF configuration having CM output voltage control by an R-R buffered resistive sensor. (b) Rail-to-rail (R-R) voltage follower

The transconductances  $g_{m50}$  and  $g_{m60}$  are supposed to be equal. To this end the W/L ratios of the P-channel transistors have been corrected for their mobilities in regard to the N-channel transistors.

The transconductance of the circuit ( $g_{m50} + g_{m60}$ ) is a factor two larger, when the input voltage is in the middle between the supply voltages and both pairs are functioning, than when the input voltage is closer to one of the rail voltages and one pair  $g_{m50}$  or  $g_{m60}$  is cut off.

This results in a gain error change  $\Delta E_T$

$$\Delta E_T \approx -1/R_{CM1,2}(g_{m50} + g_{m60}) \quad (8.1.9)$$

This means that the product  $R_{CM1,2}(g_{m50} + g_{m60})$  must be chosen much larger than 1. However, if  $V_{CM}$  is chosen in the middle, the error of one buffer compensates that of the other, because both buffers switch from 2 to  $1g_m$  at the same time, so the requirements are relaxed.

For HF stability of the CM feedback loop, it may be necessary that  $R_{CM1}$  and  $R_{CM2}$  each are bridged by a small capacitor  $C_{CM1}$  and  $C_{CM2}$ . In general, the bandwidth of the CM loop must be chosen as large as the bandwidth for differential signals. This means that the inverse CM parallel resistance  $1/R_{CM1} + 1/R_{CM2}$  must have the same value as the transconductance  $g_{I0}$  of the input stage.

If the HF loads at the outputs are balanced, the HF output signals will stay balanced even if the CM loop is functioning only at lower frequencies than the differential bandwidth. In that case the CM parallel conductance  $1/R_{CM1} + 1/R_{CM2}$  may be much smaller than  $g_{I0}$ .

The CM control by an R-R buffered resistive sensor works fine for a total supply voltage larger than two saturation voltages and two threshold voltages, which is about 2 V. A drawback is the extra circuiting and extra supply current needed to do the job.

## 8.2 Fully Differential GA-CF-GA Configuration

When we need an amplifier with a higher transconductance than we can get with the GA-CF configuration, the GA-CF-GA configuration is a good choice at low supply voltages. It also has an R-R output range except for one saturation voltage at each rail. The high transconductance allows us to load the output directly with common-mode feedback resistors without losing too much gain.

### ***Fully Differential CMOS OpAmp with R-R Resistive CM-Out Control***

An example of a fully differential GA-CF-GA configuration with rail-to-rail resistive CM-out control is given in Fig. 8.2.1 [8.2].

The circuit is based on the compact CMOS OpAmp of Fig. 7.7.2. The two outputs  $V_{out+}$  and  $V_{out-}$  are sensed by a resistor string  $R_{CM1}$  and  $R_{CM2}$  and paralleled by two small capacitors  $C_{CM1}$  and  $C_{CM2}$  for HF stability of the CM loop. The voltage of the central sensing point is compared with a desired common-mode voltage  $V_{CM}$  by the transistors  $M_{51}$ ,  $M_{52}$  and  $M_{53}$ . The latter is connected as a diode. The CM output voltage is translated into a current by  $R_{CM1}$  and  $R_{CM2}$  and fed through cascodes  $M_{51}$  and  $M_{52}$  into the folded cascodes  $M_{45}$  and  $M_{46}$ . The bandwidth of the CM loop should be taken as large as that of the whole OpAmp. The latter one is:

$$f'_o = g_{m30}/2\pi(C_{M11} + C_{M12} + C_{M21} + C_{M22}) \tag{8.2.1}$$

The transconductance of the input stage  $g_{m30}$  has the same value as in Fig. 7.7.2, but now it drives four Miller capacitances instead of two. The transconductance of the CM loop circuit should therefore be taken equal to  $1/2g_{m30}$  to obtain the same bandwidth, so:

$$\frac{1}{2}g_{m30} = 1/(1/(g_{m51} + g_{m52}) + 1/(1/R_{CM1} + 1/R_{CM2})) \tag{8.2.2}$$

An example of the above circuit had a bandwidth of 7.5 MHz at a capacitive load of 5 pF, a DC gain of 86 dB at a load resistor of 10 kΩ, and a maximum output current of 5 mA at a quiescent current of 450 μA [8.2].

The circuit of Fig. 8.2.1 needs a supply voltage of two diode voltages and two saturation voltages, which is in the order of 2 V. If we would have taken the circuit of Fig. 7.7.6 with the folded cascode summing circuit as a basis for the differential

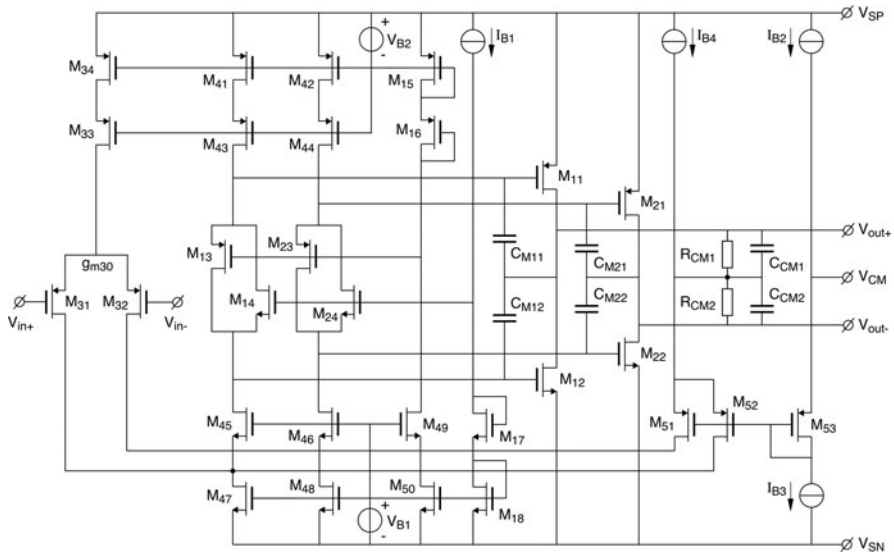


**Fig. 8.2.1** Fully differential operational amplifier with GA-CF-GA configuration and with a resistive CM output control





### 8.3 Fully Differential GA-GA-GA-GA Configuration

When more gain is needed, for example to linearize a heavy duty loudspeaker output stage a fully differential OpAmp with an GA-GA-GA-GA configuration can be used. Apart from CM output control with resistors, switched-capacitors can also be used, as shown next.

#### Fully Differential CMOS OpAmp with Switched-Capacitor CM-Out Control

As a final example, a circuit is presented of a fully differential OpAmp in an GA-GA-GA-GA configuration that has CM output control by switched-capacitors. The circuit is shown in Fig. 8.3.1 [8.7].

The purpose of the circuit is to provide low-distortion at a relatively high output power for audio applications. The large gain of four cascaded GA stages and the double nesting around the output stage provide a high loop gain around the output stage up to relatively high frequencies. The input stage  $M_1, M_2$  is connected to a differential folded cascode stage with  $M_3$  through  $M_9$ . The two balancing second stages  $M_{10}$  through  $M_{13}$  with indices A for the left-hand side and B for the right-hand side have a mirror output to bring the phase back to positive. The third stages  $M_{14}$  through  $M_{19}$  with indices A and B respectively also have a current mirror in the output. They drive the upper transistors. The lower output transistors are driven in parallel with the third stages. This provides for a multipath. This also provides a kind of very non-linear class-AB behavior. The gain of the three or four-stage amplifier is so high though, that the strong non-linear behavior of the output stage is sufficiently linearized. The Miller capacitors  $C_3, C_2$  and  $C_1$  shape the double-nested HF compensation structure.

The CM feedback circuit is shown in Fig. 8.3.1b.

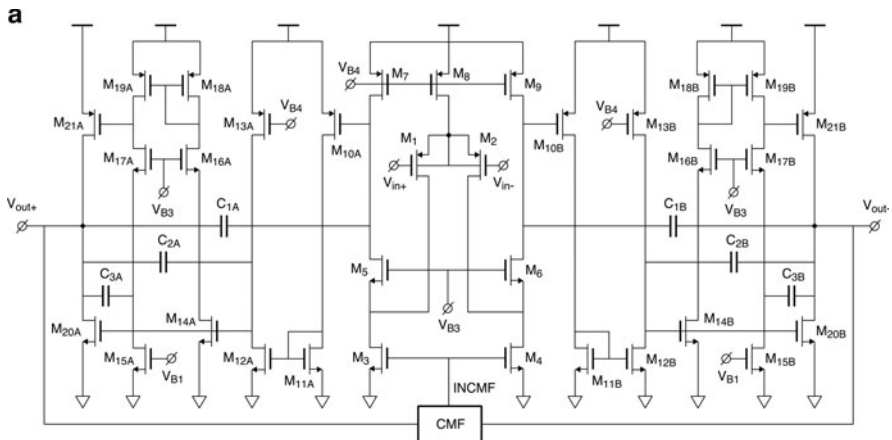


Fig. 8.3.1 (a) Fully differential operational amplifier with GA-GA-GA-GA configuration and CM output feedback control



### Solution

The common-mode output voltage, according to Eq. 8.1.5, equals the source-gate voltage of  $M_9$  and  $M_{10}$  when no input signal is present. The drain currents for  $M_9$  and  $M_{10}$  are equal to those of the current sources  $I_{B2}$  and  $I_{B3}$  minus the drain currents of  $M_1$  and  $M_2$ . The current mirror  $M_7$ - $M_3$ - $M_4$ - $M_5$ - $M_6$  makes the drain currents of  $M_1$  and  $M_2$  100  $\mu$ A each. Assuming  $M_9$  and  $M_{10}$  work in their linear region, the common-mode output voltage can be calculated by applying Eq. 8.1.2

$$V_{GS9} = V_{GS10} = \frac{I_{D9}}{K_P \frac{W}{L_9} V_{DS9}} - V_{THP} + \frac{1}{2} V_{DS9} \quad (8.4.1)$$

From the equation above it can be seen that a  $V_{DS}$  value is also needed in order to calculate  $V_{GS}$ . In this amplifier, the biasing circuit  $M_7$ - $M_3$ - $M_4$  sets the  $V_{DS}$  for  $M_9$  and  $M_{10}$  to

$$V_{DS9} = V_{GS9} - V_{GS11} \quad (8.4.2)$$

These two equations can be used to write a second order equation with only  $V_{GS9}$  as unknown parameter

$$V_{GS9} = \frac{I_{D9}}{K_P \frac{W}{L_9} (V_{GS9} - V_{GS11})} - V_{THP} + \frac{1}{2} (V_{GS9} - V_{GS11}) \quad (8.4.3)$$

$V_{GS11}$  can be calculated considering  $M_{11}$  saturated and knowing its drain current

$$V_{GS11} = \sqrt{\frac{2I_{D11}}{K_P \frac{W}{L_{11}}}} = 1.26 \text{ V} \quad (8.4.4)$$

Solving Eq. 8.5.3 and picking the positive solution

$$\begin{aligned} V_{GS9} &= 1.37 \text{ V} \\ V_{DS9} = V_{GS9} - V_{GS11} &= 0.11 \text{ V} < V_{GS9} + V_{THP} = 0.36 \text{ V} \end{aligned} \quad (8.4.5)$$

The results show that both  $M_9$  and  $M_{10}$  are working in the linear region and that the common-mode output voltage is close to the middle of the supply voltage. The differential DC voltage gain can be calculated taking into account that half the input signal is amplified to one of the outputs using half of the differential circuit, so

$$A_{V0} = g_{m1} r_{CS16}^{\mu} = \frac{\sqrt{2K_P \frac{W}{L_1} I_{D1}^r CS}}{\lambda_N \sqrt{\frac{2I_{D16}}{K_N \frac{W}{L_{16}}}}} = 93 \text{ dB} \quad (8.4.6)$$

The 0-dB frequency is given by the input  $g_{m1}$  and the load capacitor, for each side of the differential output

$$f_0 = \frac{g_{m1}}{2\pi C_L} = 300 \text{ MHz} \quad (8.4.7)$$

### Problem 8.2

For the fully differential depicted in Fig. 8.1.1b, the biasing voltages  $V_{B1}$  and  $V_{B2}$  together with transistors  $M_5$  through  $M_8$  and  $M_{13}$  through  $M_{15}$  are sized for drain currents  $I_{D1} = I_{D2} = 100 \mu\text{A}$ ,  $I_{D13} = 50 \mu\text{A}$  and  $I_{D14} = 50 \mu\text{A}$ . Design the common-mode control loop  $M_9$  through  $M_{11}$  and  $M_{16}$ ,  $M_{17}$  such that the output common-mode level is placed 1.5 V lower than  $V_{SP}$ .  $V_{THP} = -1.0 \text{ V}$ ,  $K_p = 22 \mu\text{A}/\text{V}^2$ .

### Solution

The output common-mode is set by transistors  $M_9$ ,  $M_{10}$  which should be forced to work in the linear region. For transistor  $M_{17}$ , which is the model transistor for common-mode control, the equation voltage-current is

$$V_{GS17} = \frac{I_{D17}}{K_P \frac{W}{L_{17}} V_{DS17}} - V_{THP} + \frac{1}{2} V_{DS17} \quad (8.4.8)$$

As this transistor should stay in its linear region even when noise or power voltages spikes are added, a safe margin for the difference between gate-source effective voltage and drain-source voltage is

$$V_{GS17} + V_{THP} = V_{DS17} + 350 \text{ mV} \quad (8.4.9)$$

Replacing the equality above in Eq. 8.5.8 and considering the requested common-mode voltage which is identical to  $V_{GS17}$ , the aspect ratio of transistor  $M_{17}$  can be calculated

$$\frac{W}{L_{17}} = \frac{I_{D17}}{(V_{GS17} + V_{THP} - \frac{1}{2} V_{DS17}) K_P V_{DS17}} = 35.6 \quad (8.4.10)$$

Sizing of  $M_9$  and  $M_{10}$  is made considering that in the linear region the drain current is proportional to  $W/L$  for the same  $V_{DS}$

$$\frac{W}{L_9} = \frac{W}{L_{10}} = \frac{I_{D9}}{I_{D17}} \frac{W}{L_{17}} = 178 \tag{8.4.11}$$

This will produce equal  $V_{GS}$  and  $V_{DS}$  values for all transistors working in their linear region, keeping the source voltage for the saturated current sources  $M_{16}$  and  $M_{11}$  at the same value, so sizing for these transistors must be in the ratio

$$\frac{W/L_{11}}{W/L_{16}} = \frac{I_{D11}}{I_{D16}} = 5 \tag{8.4.12}$$

The actual size for these transistors is calculated based on the needed common-mode input range, which provides a minimum size for  $M_{11}$ .

### Simulation Exercise 8.1

The differential output amplifier shown in Fig. 8.4.1 can be simulated for AC analysis using the circuit in Fig. 8.4.2. Run AC simulation for gain and phase using the test circuit. An important factor in the functioning of the circuit is the

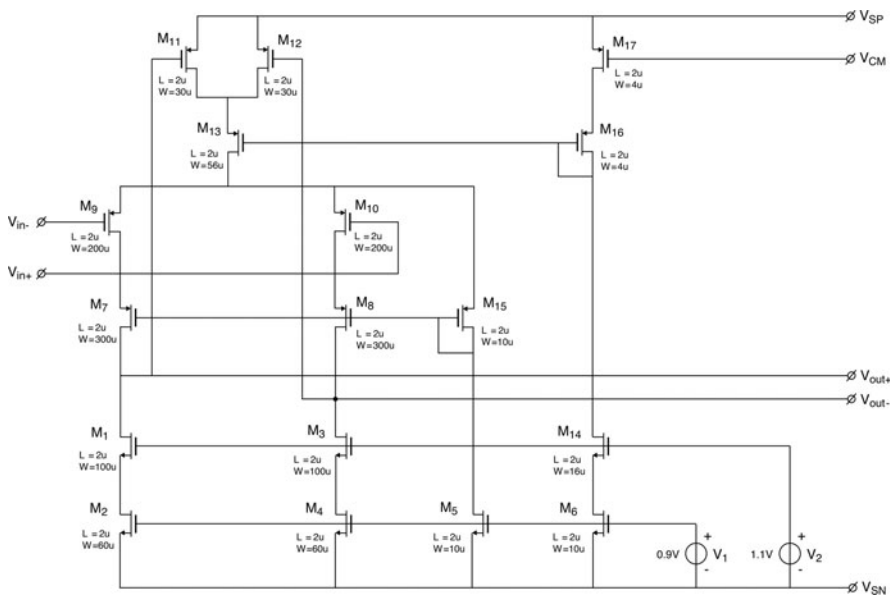


Fig. 8.4.1 Telescopic differential amplifier

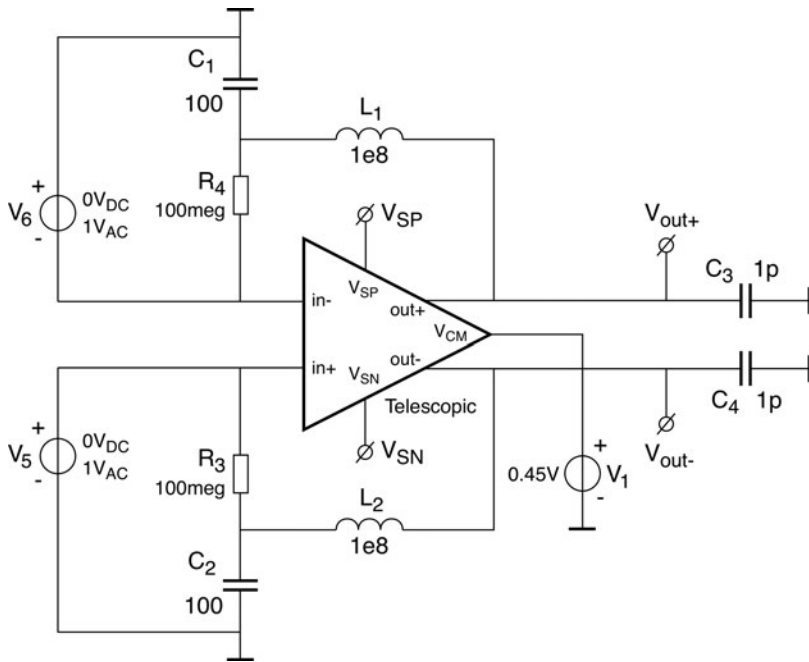


Fig. 8.4.2 AC simulation circuit for differential output amplifier

reference common-mode voltage  $V_I$  which has to be in a certain range to allow correct biasing of all devices. Use a stepped voltage for  $V_I$  to find the limits of this range by observing the biasing of all MOS transistors. Change the input AC signal from differential to common-mode and measure the common-mode to differential crosstalk. Change the test circuit to one suited for transient simulation, using two feedback resistors and two resistors as voltage-to-current converters at the input of the amplifier and simulate the resulted inverting amplifier using a sinus differential voltage input to analyze the output differential voltage range if a total harmonic distortion of 0.1% is allowed.

## 8.5 References

- [8.1]. T.C. Choi et al., High-frequency CMOS switched-capacitor filters for communications applications. *IEEE J. Solid State Circ.* **SC-18**(6), 652–664 (1983)
- [8.2]. R. Hogervorst, J.H. Huijsing, *Design of Low-Voltage Low-Power Operational Amplifier Cells* (Kluwer Academic Publishers, Boston, 1996), pp. 195–203
- [8.3]. G. Nebel, U. Kleine, H.J. Pfeleiderer, Large bandwidth BiCMOS operational amplifiers for SC-video-applications, in *Proceedings of ISCAS*, 1994, pp. 5.85–5.88
- [8.4]. J.H. Huijsing et al., Low-power low-voltage VLSI operational amplifier cells. *IEEE Trans. Circ. Sys. I, Fundam. Theory Appl.* **42**(11), 841–852 (1995)

- [8.5]. K. Bult, G.J.G.M. Geelen, A fast-settling CMOS op amp for SC circuits with 90-dB DC gain. *IEEE J. Solid State Circ.* **25**(6), 1379–1383 (1990)
- [8.6]. J.N. Babanezhad, A low-output-impedance fully differential op amp with large output swing and continuous-time common-mode feedback. *IEEE J. Solid State Circ.* **26**(12), 1825–1833 (1991)
- [8.7]. S. Pernici, G. Nicolini, R. Castello, A CMOS low-distortion fully differential power amplifier with double nested Miller compensation. *IEEE J. Solid State Circ.* **28**(7), 758–763 (1993)

# 9. Instrumentation Amplifiers and Operational Floating Amplifiers

With the definition of universal active devices in Chap. 1 we have seen that the operational floating amplifier (OFA) is the most universal active device, even more universal than the operational voltage amplifier (OVA), abbreviated to OA or OpAmp, because of its most wide usage. The OpAmp provides us with accurate output voltage control. Additionally, the OFA provides us with accurate control of an output current, independently of the output voltage. So, with the OFA we are able to create controlled current sources. These can be used for the transmission of current signals independent of ground or reference voltage differences and for instrumentation amplifier applications mentioned in Sect. 3.4 [9.1].

It may be as important to open up our mind to the more simple system approach which the OFA offers over the OpAmp approach in many cases [9.2]. Only after finding that the simple OFA system solution cannot be implemented because of lack of good OFA realizations, a more complicated system design with more OpAmps can be justified.

## 9.1 Introduction

The symbol for an OFA is shown again in Fig. 9.1.1.

Ideally, the OFA should obey the nullor requirements, as explained in Chap. 1:

$$V_{i1} - V_{i2} = V_{idiff} \approx 0, \quad \text{or} \quad V_{i2} \approx V_{i1} \tag{9.1.1}$$

$$I_{i1} + I_{i2} = 2I_{ibias} \approx 0 \tag{9.1.2}$$

$$I_{o1} + I_{o2} = 2I_{obias} + 2I_{o1}/H_o \approx 0, \quad \text{or} \quad I_{o2} \approx -I_{o1} \tag{9.1.3}$$

The equality of  $I_{o2} = -I_{o1}$  makes it possible to establish accurate external current relations, in the same way as that the equality of  $V_{i2} = V_{i1}$  makes it possible to establish accurate external voltage relations.



**Fig. 9.1.1** Symbol for an operational floating amplifier (OFA)

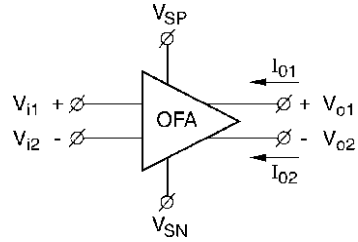
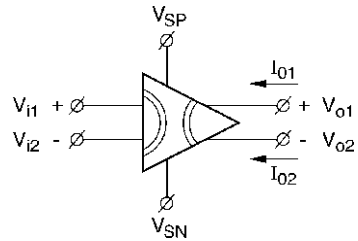


**Fig. 9.1.2** Isolation barriers in an OFA



Practically, we can approach this by the following four requirements: high gain, low input offset voltage and current, low input bias current, and a low bias current at the output. We have seen in Chap. 2 that we could obtain the dynamic input requirements by isolation of the input stage, while we need not depend on accurate internal components. Similarly, we will see that the dynamic output requirements too can be met by isolation of the output stage and that we need not depend on accurate internal components.

Isolation of the input and output stages is symbolized in Fig. 9.1.2. Current-source isolation is the way to go at the input stage as is shown in Chap. 4.

However, at the output stage current-source isolation is more complicated than at the input stage. This is because of the need to supply larger output currents. This is the topic of this chapter. In the first five sections, Sects. 9.1–9.5, we will explore ways to obtain accurate current signals without having to resource to a fully universal OFA. In Sects. 9.6–9.8 the design of fully universal class-A and class-B OFAs will be discussed.

Section 9.2 explains how simple unipolar three-terminal OFAs can be used to realize unipolar voltage-to-current converters. Section 9.3 shows the design of differential voltage-to-current converters using unipolar three-terminal OFAs. Section 9.4 discusses how differential voltage-to-current converters can be used to realize high-quality instrumentation amplifiers, without requiring universal OFAs.

Section 9.5 shows how an accurate universal voltage-to-current converter can be realized without an OFA by using an instrumentation amplifier. In Sect. 9.6 we see that current-source isolation can be used to realize class-A biased output stages for high-quality universal OFAs. Section 9.7 discusses how the problem of designing a class-AB output stage, that is isolated from ground, can be shifted to the use of

a floating power supply. Finally, Sect. 9.8 shows how difficult it is to design class-AB biased output stages for universal OFAs. Only the use of an instrumentation amplifier provides a high-quality solution.

## 9.2 Unipolar Voltage-to-Current Converter

In many cases we use the OFA as a three-terminal element. In those cases, the input nullator is connected with the output norator [9.2] to create a voltage-to-current converter as shown in Figs. 9.2.1 and 9.2.2.

The circuit functions as follows: at the input of the OFA the input voltage  $V_{IN}$  is carried over at no loss, or followed by the voltage  $V_G$  across a conductance  $G$ . The current  $I_G$  through  $G$  is carried over at no loss, or followed by the current at the output  $I_{out}$ . So:

$$\begin{aligned} V_G &= V_{in} \\ I_G &= V_{in} \cdot G \\ I_{out} &= I_G = V_{in} \cdot G \end{aligned} \tag{9.2.1}$$

The result is a voltage-to-current converter in which only one passive element  $G$  determines the V-I transfer.

The simplest realization of the previous idea is a single transistor. The Ebers-Moll [9.3] model of a forward biased bipolar transistor resembles the previous idea closely, see Fig. 9.2.3.

**Fig. 9.2.1** OFA connected as a three-terminal element used as a voltage-to-current converter

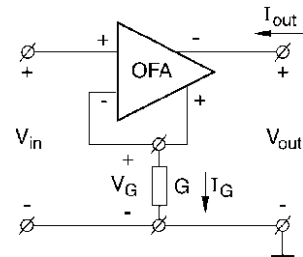


**Fig. 9.2.2** OFA dissected in its basic parts of a nullator and a norator as a three-terminal element used as a voltage-to-current converter

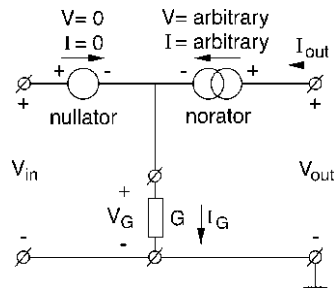


**Fig. 9.2.3** A three-terminal nullator/norator combination closely resembles the Ebers-Moll model for a forward-biased bipolar transistor, but may also be used to model a CMOS transistor in a generalized transistor model

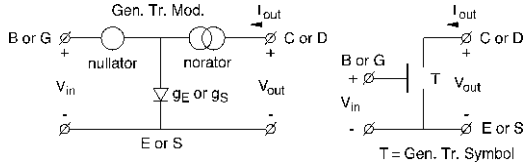
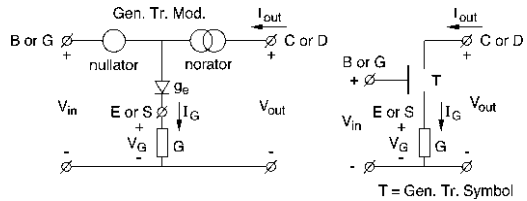


**Fig. 9.2.4** A unipolar voltage-to-current converter composed of a single generalised transistor and a transconductance of  $G$



The conductance  $g_e$  for a bipolar transistor or  $g_s$  for a CMOS transistor models the forward transconductance. At one supply-voltage polarity, the current is restricted to the regarding polarity. For this reason the transfer is unipolar. The idealized transfer is:

$$I_{out} = g_m V_{in} \tag{9.2.2}$$

with:  $g_m = g_e$ , or  $g_m = g_s$ .

The transfer is strongly non-linear, and depends on many process and environmental parameters, because we are using only one transistor. The model may be extended by the nodal parasitics.

### Unipolar Single-Transistor V-I Converter

When we want to use the previous single-transistor for a linear voltage-to-current converter, we may connect a conductance  $G$  in series with the emitter or source of the generalized transistor, as shown in Fig. 9.2.4.

The transfer of the circuit of Fig. 9.2.4 is:

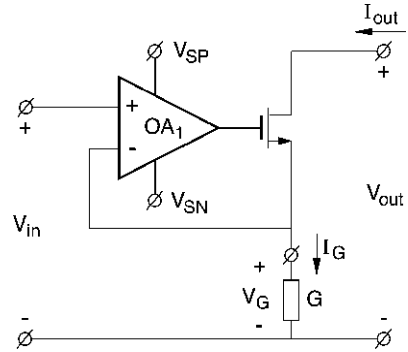
$$I_{out} = G \left( \frac{1}{1 + G/g_m} \right) V_{in} \tag{9.2.3}$$

If  $g_m \gg G$ , we may write:

$$I_{out} \approx G V_{in} \tag{9.2.4}$$

The transfer is unipolar. If the output voltage is positive, the output current can only be positive.

**Fig. 9.2.5** Accurate voltage-to-current converter consisting of an OpAmp gain-boosted CMOS transistor



### Unipolar OpAmp-Gain-Boosted Accurate V-I Converter

For a higher accuracy we need to increase the  $g_m$  of the transistors and lower their parasitic effects. This can be obtained by applying more internal gain in a composite transistor circuit. The first approach is to use an OpAmp in combination with a CMOS transistor, as shown in Fig. 9.2.5.

The elegance of the unipolar voltage-to-current converter in Fig. 9.2.5 is its clear accuracy. The input voltage  $V_{in}$  is accurately followed by the voltage  $V_G$  because of the high gain of the OpAmp  $OA_1$ . The current  $I_G$  is accurately followed by the output current  $I_{out}$  because of the good channel-to-gate isolation and a presumably low input current of the OpAmp. The  $g_m$  of the composite transistor is equal to the  $g_m$  of the CMOS transistor multiplied by the gain  $A$  of the OpAmp. So the V-I converter has an accurate transfer according to (9.2.5):

$$I_{out} = G \left( \frac{1}{1 + G/A_v g_m} \right) V_{in} \approx G V_{in} \tag{9.2.5}$$

If the input of the OpAmp is able to reach the negative rail the voltage and current through  $G$  may function down to zero. However, the polarity cannot be reversed. The transfer remains unipolar.

### Unipolar CMOS Accurate V-I Converter

The OpAmp used may be simple. When we use the GA-CF CMOS OpAmp of Fig. 7.1.2b, the voltage-to-current converter with an GA-CF-VF configuration of Fig. 9.2.6 arises.

The example of Fig. 9.2.6 has a high accuracy. The error in the voltage-follower function is low. It is equal to the reciprocal gain of the OpAmp, which is of the order of  $3 \cdot 10^3$ . The error in the current-follower function is very low, because the

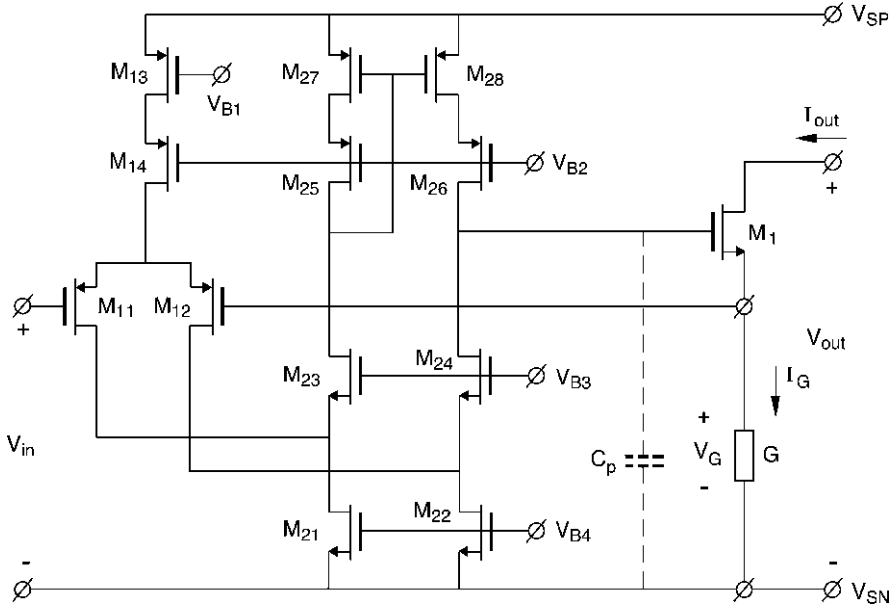


**Fig. 9.2.6** Accurate CMOS unipolar voltage-to-current converter design with GA-CF-VF configuration

channel of the output transistor is isolated from the rest of the circuit by gate oxide. The OpAmp will probably be sufficiently MF compensated by the parasitic stray capacitance at the gate of  $M_1$ .

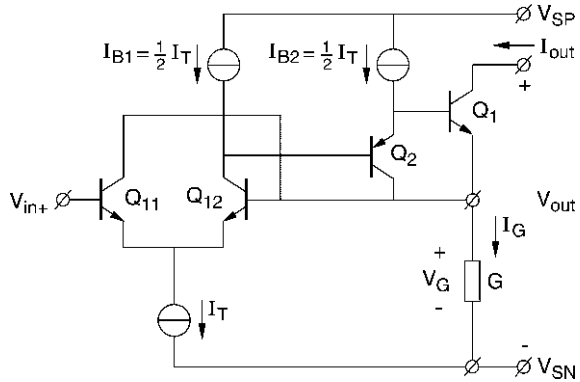
A unique attribute of the above voltage-to-current converter is that it fully functions down to the voltage of negative rail. This allows voltages and currents to be processed from zero.

### *Unipolar Bipolar Accurate V-I Converter*

The bipolar counterpart can be derived from the GA-VF voltage follower of Fig. 7.3.4 by eliminating the lower half of the output stage as shown in Fig. 9.2.7.

The voltage-to-current converter of Fig. 9.2.7 has several interesting features. The collector current of the input transistor  $Q_{11}$  has been used as bias current for the output driver  $Q_2$ . At the same time the collector of  $Q_{11}$  has been nicely bootstrapped at the same voltage of the collector of  $Q_{12}$ , so that the offset by the Early effect of the input stage is low. The base current of the output transistor  $Q_1$ , which is normally lost, has been retrieved again by adding it through the driver  $Q_2$  back into the output. Even the base current of  $Q_2$  has been retrieved again by adding it through  $Q_{12}$  and  $Q_{11}$  back into the output. This adding-what-is-missing operation takes care of a highly accurate current-follower function of the

**Fig. 9.2.7** Accurate unipolar bipolar voltage-to-current converter with GA-VF configuration



current in  $G$  through the output. So, the high current gain of the three-cascaded bipolar transistors  $Q_{11}$ ,  $Q_2$  and  $Q_1$  is not only used in the voltage-following feedforward path, but also in the current-following path. Only the voltage across  $G$  cannot reach the negative rail.

### Unipolar OpAmp Accurate V-I Converter

An interesting general approach to a unipolar voltage-to-current converter arises if we use a low-voltage rail-to-rail (R-R) input/output OpAmp in one of the following connections [9.4], see Fig. 9.2.8a, b.

The choice between the connection of Fig. 9.2.8a on the left and Fig. 9.2.8b on the right depends on the way the frequency compensation has been organized. The internal frequency compensation capacitors should not be shortcircuited by the external connections of input, supply, and output. So, if the virtual ground of the frequency compensation is sitting on the bottom (normally  $V_{SN}$  connection) then we should choose the right-hand circuit of Fig. 9.2.8b. If it is sitting at the top (normally  $V_{SP}$  connection) then we should choose the left-hand circuit of Fig. 9.2.8a. The functionality should not forbid a shortcut of the output to one of the supply rails. If so, we can avoid a full shortcut by the connection of a diode, for example, in between the output and one of the supply lines. See the application note of the NE 5230 [9.4].

Regarding the accuracy aspect, it is clear that the only errors are: the input offset voltage  $V_{ioffs}$  for the voltage-follower function, and the bias current  $I_{ibias}$  for the current-follower function. These errors may be very low, so that (9.2.5) is accurately true.

The output current is down-limited by the quiescent current of the OpAmp, which also flows through  $G$ . If this is a hindrance, one has to go back to the basic topology of Fig. 9.2.5.

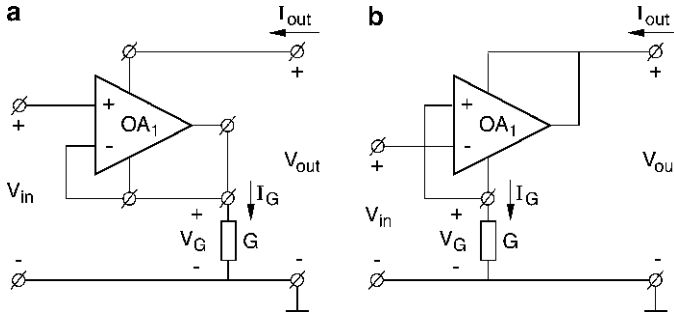


**Fig. 9.2.8** (a) and (b) Accurate unipolar R-R-in/out OpAmp voltage-to-current converter using different OpAmps connections

### ***Conclusion***

The design of several accurate unipolar voltage-to-current converters have been shown. Basically they consist of an OpAmp boosted transistor. CMOS and bipolar realizations have been shown as well as a single OpAmp realization. The restriction of these solutions is that the V-I conversion can only be performed on physical unipolar signals. Physical bipolar current signals may be processed by differential V-I converters, see Sect. 9.3, and by using an instrumentation amplifier, see Sects. 9.4 and 9.5.

## **9.3 Differential Voltage-to-Current Converters**

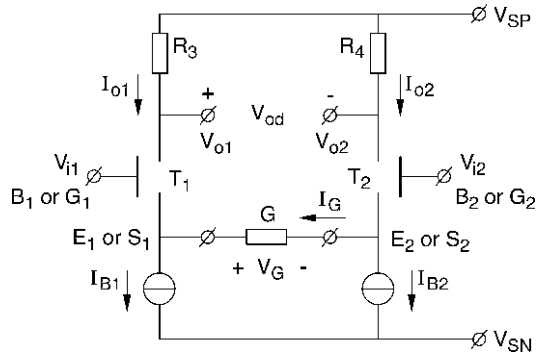
When we need to provide bipolar current signals instead of unipolar signals, we may apply the unipolar voltage-to-current converters of the previous Sect. 9.2 in a differential way.

### ***Differential Simple V-I Converter***

The simplest unipolar voltage-to-current converter can be made with the single transistor as a three-terminal OFA, as we have seen with Fig. 9.2.4.

If we balance the voltage-to-current converter, and bias it with current sources so that the transconductance  $G$  may be used floating or isolated from ground, the differential voltage-to-current converter of Fig. 9.3.1 arises.

**Fig. 9.3.1** A simple differential voltage-to-current converter with two transistors as two three-terminal unipolar OFAs



If  $g_{m1}$  and  $g_{m2} \gg G$ , the transfer is roughly:

$$I_{od} = G \left( \frac{1}{1 + 2G/g_m} \right) V_{id} \approx G V_{id} \tag{9.3.1}$$

$$V_{od} \approx -G(R_3 + R_4)V_{id} \tag{9.3.2}$$

with  $I_{od} = I_{o1} - I_{o2}$ ,  $V_{id} = V_{i1} - V_{i2}$ .

### Differential Accurate V-I Converter

For a high accuracy we have to increase the  $g_m$  of the transistors by artificial internal voltage gain. This can be realized by an OpAmp as shown in Fig. 9.3.2.

The circuit is closely related to the principle of Fig. 3.4.3.

The transfer is:

$$I_{od} = G \left( \frac{1}{1 + 2G/g_m A_v} \right) V_{id} \approx G V_{id} \tag{9.3.3}$$

$$V_{od} = G \left( \frac{1}{1 + 2G/g_m A_v} \right) (R_3 + R_4)V_{id} \approx -G(R_3 + R_4)V_{id} \tag{9.3.4}$$

With a relative error of:

$$E_{rel.} = \left( \frac{1}{1 + 2G/g_m A_v} \right) \tag{9.3.5}$$



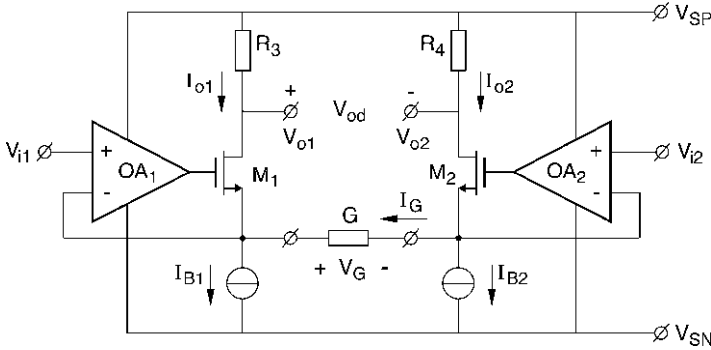


**Fig. 9.3.2** Accurate differential voltage-to-current converter with two OpAmp-boosted unipolar voltage-and-current followers

The common-mode crosstalk ratio  $CMCR = 1/H$  may be high. It is the product of the isolation factor and the balancing factor (see Sects. 3.4 and 4.3). The overall CMCR is:

$$\frac{1}{H} = \left| \frac{G_B}{G} \times \frac{\Delta G_B}{G_B} \right| + \left| \frac{1}{H_1} \right| + \left| \frac{1}{H_2} \right| \tag{9.3.6}$$

with:

$G_B$  = average in the parasitic conductances of  $I_{B1}$  and  $I_{B2}$ .

$\Delta G_B$  = difference in the parasitic conductances of  $I_{B1}$  and  $I_{B2}$ .

$H_{1,2}$  = common-mode rejection ratio of OpAmp 1 and 2, respectively.

### ***Differential CMOS Accurate V-I Converter***

The differential voltage-to-current converter of Fig. 9.3.2 can be realized using the OpAmp circuit as shown for the unipolar voltage-to-current converter in Fig. 9.2.6. This is shown in Fig. 9.3.3. However, insertion of the bias current sources  $I_{B1}$  and  $I_{B2}$  prevent the common-mode input voltages from reaching the negative rail.

This is not an obstacle, for instance if we want to read out a sensor like a bridge circuit, which has its common-mode voltage level between the negative and positive rail. But, if we need to read out a sensor like a thermocouple which is grounded, then we need to adapt the circuit.

For instance, a level-shift can be built-in on both sides by inserting a diode  $M_{13}$  and  $M_{23}$  in series with the source of  $M_{11}$  and  $M_{21}$ , respectively [9.5]. This allows differential voltage sensing around the negative rail voltage.

The circuit functions at a minimum supply voltage of 2.5 V, has a bandwidth of 3 MHz, and a CMRR > 90 dB [9.5].

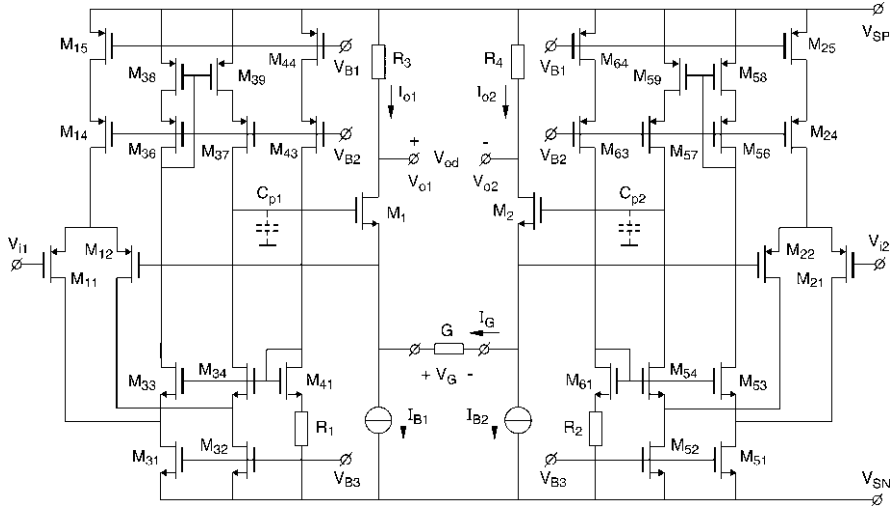


Fig. 9.3.3 Accurate differential CMOS V-I converter based on two accurate unipolar voltage-to-current followers [9.5]

### 9.4 Instrumentation Amplifiers

The design of high-quality instrumentation amplifiers requires the basic function of an OFA, as we have seen in Sect. 3.4. However, interestingly, we do not need a general-purpose OFA with physical bipolar voltages and currents: a differential voltage-to-current converter (see Sect. 9.3) is sufficient to meet our needs. But firstly we will see what we can do with just Operational Amplifiers.

#### *Instrumentation Amplifier (Semi) with Three OpAmps*

When we need to design an instrumentation amplifier for the readout of small differential signals with a large common-mode voltage, we would probably first think of using the three OpAmp semi-instrumentation amplifiers of Fig. 9.4.1. It has a bridge output amplifier  $OA_3$  preceded by a balanced preamplifier with  $OA_1$  and  $OA_2$ .

The three-OpAmp semi-instrumentation amplifier has a voltage gain:

$$A_V = A_{V1,2} A_{V3} \tag{9.4.1}$$

with:  $A_{V1,2} = (R_{21} + R_{22} + R_1)/R_1$ , and  $A_{V3} = R_5/R_3$ .

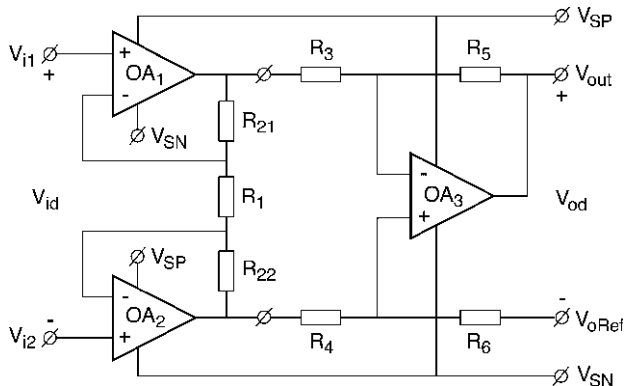


**Fig. 9.4.1** Semi-instrumentation amplifier with a bridge amplifier  $OA_3$  preceded by a balanced preamplifier with two amplifiers  $OA_1$  and  $OA_2$

The common-mode crosstalk  $1/H$  depends on matching of the bridge resistors and on the voltage gain:

$$1/H = -\Delta R_B/R_B(-A_{V3} + 1)A_{V1,2} \tag{9.4.2}$$

with:  $\Delta R_B/R_B = 1 - R_5R_4/R_6R_3$ .

For the explanation see [3.4] in Sect. 3.2.

The semi-instrumentation amplifier will probably work fine together with a bridge-type sensor circuit. If the preamplifier stage  $OA_{1,2}$  has enough gain  $A_{V1,2}$ , the common-mode crosstalk  $1/H$  of the bridge amplifier  $OA_3$  will probably be negligible in regard to that of the sensor bridge itself. But, if we do not need a high gain, and we do not want to trim the bridge resistors, we have to find other solutions for designing high-quality instrumentation amplifiers. The OpAmps themselves may have a high CMRR because of the current-source isolation applied to the input stage (see Sect. 4.3). But, OpAmps do not have an accurate fixed gain. For this reason the three OpAmp instrumentation amplifier has feedback resistors around its OpAmps. These feedback resistors are crossing the current-source isolation barrier. And the value of the CMRR falls back on the accuracy of matching (see Sect. 4.3).

If we want to design real instrumentation amplifiers without having to cross the isolation barrier by feedback resistors, we have to make use of voltage-to-current converters which have a built-in current-source isolation barrier at their output. This will be described next.

### ***Instrumentation Amplifier with a Differential V-I Converter for Input Sensing***

In the family of differential voltage-to-current converters of Fig. 9.3.2, a high input CMRR was achieved by the current-source character of the output, while maintaining

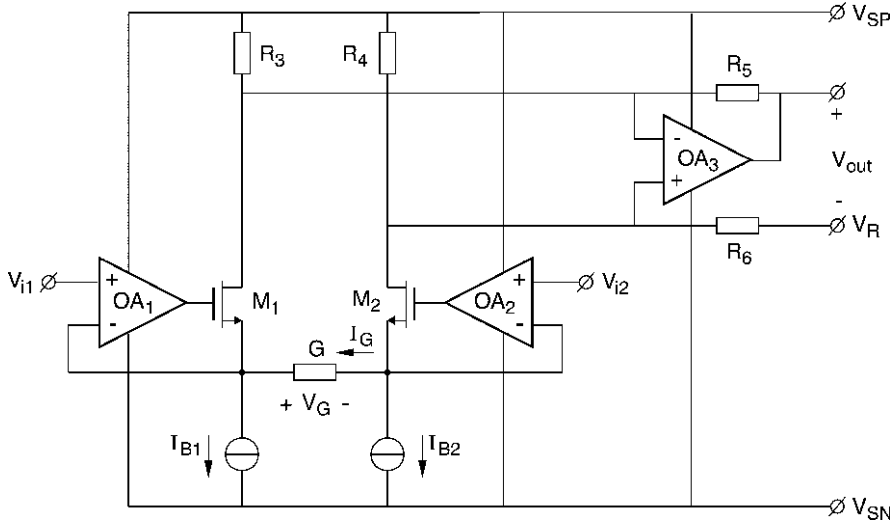


**Fig. 9.4.2** Instrumentation amplifier with a differential voltage-to-current converter at the input and a bridge-type amplifier for output-voltage level shifting

an accurate signal transfer without the use of accurate matching. Hence, it is obvious to use the differential V-I converter of Fig. 9.3.2 as an input stage for an instrumentation amplifier design. The final problem to be solved is to shift the output common-mode level down to an arbitrary reference voltage  $V_R$  somewhere in between the positive and negative rail voltages.

As a first solution, we may again use the bridge OpAmp for an output level shift stage. This gives rise to an overall structure for an instrumentation amplifier as depicted in Fig. 9.4.2.

The overall voltage gain is:

$$A_V = V_{od}/V_{id} = G(R_5 + R_6) \tag{9.4.3}$$

The power supply rejection ratio (PSRR) still depends on the balancing of the resistive bridge  $R_3, R_4, R_5,$  and  $R_6$  in the same way as calculated in formula (9.3.4). Calculated back to the input we find:

$$1/PSRR = -\Delta R_B/R_B(A_{VPS} + 1)A_V \tag{9.4.4}$$

with:  $\Delta R_B/R_B = 1 - R_5R_4/R_6R_3,$  and  $A_{VPS} = R_5R_3.$

A clear disadvantage of this first solution is that the PSRR depends on the matching of resistors.

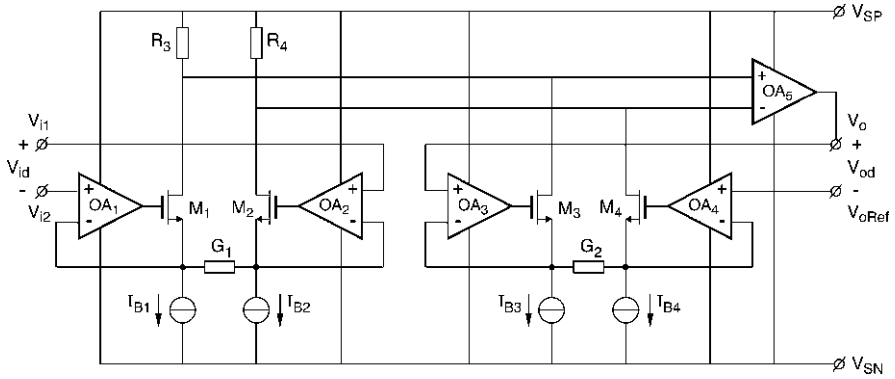


**Fig. 9.4.3** Instrumentation Amplifier with accurate differential V-I converters for input and output sensing

***Instrumentation Amplifier with Differential V-I Converters for Input and Output Sensing***

In a second solution we largely avoid the dependency of PSRR on resistor matching, but instead use the current-source isolation principle with two differential V-I converters to sense the input voltage as well as the feedback output voltage, and amplify the current difference to drive the output.

The current difference can be obtained by connecting the two differential V-I converters in cascode on top of each other [9.6], or in parallel of each other. An advantage of the cascode connection is that we use the same bias current for both V-I converters, which results in a lower noise than if we would have connected the V-I converters in parallel. On the other hand, the cascode connection needs more supply-voltage room. The latter is more important today with even lower supply voltages than it was in earlier days. Therefore, we have chosen for the parallel connection: an instrumentation amplifier based on the parallel connection of two V-I converters, one for input sensing and one feedback output sensing is shown in Fig. 9.4.3.

The instrumentation amplifier of Fig. 9.4.3 uses the absolute minimum number of passive elements to determine the gain, viz. the ratio of two conductances  $g_1$  and  $g_2$ .

The overall voltage gain is:

$$A_V = G_1/G_2 \tag{9.4.5}$$

The common-mode crosstalk ratio CMCR has been described by (9.3.6). This formula is equally valid to describe the CMCR at the output. The instrumentation amplifier of Fig. 9.4.3 is the most precise one, but also the most complex instrumentation amplifier.

The instrumentation amplifier of Fig. 9.4.3 has an interesting virtue, viz. that residual gain and non-linearity errors in the input V-I converter largely cancel equal errors in the output V-I converter.

**Instrumentation Amplifier with Simple Differential V-I Converters for Input and Output Sensing**

It is a special attribute of the above instrumentation amplifier namely that gain and non-linearity errors of one V-I-C cancel those of the other V-I-C. We may exploit this special attribute to simplify the instrumentation amplifier design by using simple degenerated differential transistor pairs as V-I converters and set the gain by an overall feedback resistor ratio.

This principle is shown in Fig. 9.4.4. We use P-channel CMOS transistors to eliminate back-gate modulation of their channels by bootstrapping the back-gates. A residual gain modulation by a  $g_m$  modulation of the CMOS transistors, due to differences in common-mode voltage levels between the input and output, has to be eliminated by using bootstrapped cascodes for the input transistors. The voltage gain  $A_V$  is:

$$A_V = \frac{R_5 + R_6}{R_6} \times \frac{R_2}{R_1} \tag{9.4.6}$$

with:  $R_1 = R_{11} + R_{12}$ ,  $R_2 = R_{21} + R_{22}$ .

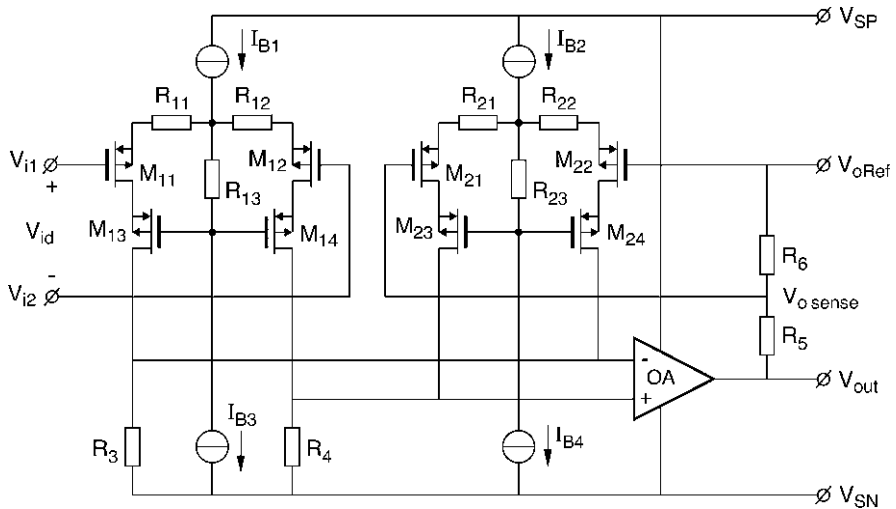


**Fig. 9.4.4** Instrumentation amplifier with simple differential V-I converters for input and output sensing

The voltage gain of the simple instrumentation amplifier of Fig. 9.4.4 is:

$$A_V = \frac{R_5 + R_6}{R_6}, \text{ at } R_1 = R_2 \quad (9.4.7)$$

This principle has been elaborated in the two following instrumentation amplifier realizations with a common-mode range that includes the negative rail voltage.

### ***Instrumentation Amplifier Bipolar with Common-Mode Voltage Range Including Negative Rail Voltage***

When we have to amplify differential voltage signals from sensors which have one terminal connected to the negative rail, we can no longer use the three-OpAmp semi-instrumentation amplifier design shown in Fig. 9.4.1, even though the input OpAmps might have an input CM range including the negative rail voltage. The feedback around the preamplifier stages prevents the common-mode range from including the negative rail voltage.

A possible way out would be to use PNP, or P-channel emitter follower, or source follower level-shift stages at the input. But these stages add additional noise and offset. Besides, the three-OpAmp semi-instrumentation amplifier has other drawbacks, as we have seen with Fig. 9.4.1.

Therefore, it is better to use PNPs or P-channel transistors directly as the input transistors of simple degenerated V-I converters followed by a folded cascode to realize a topology similar to that of Fig. 9.4.4. A bipolar design [9.7] is shown in Fig. 9.4.5.

The bipolar input transistors have a high output impedance and do not show much  $g_m$  modulation as a function of their common mode level. Hence, cascoding of these transistors is not needed. Moreover, there is not much voltage headroom for cascodes. If we set the voltage at  $R_{31}$  and  $R_{32}$  at about 200 mV, the bases of the input transistors may reach about  $-200$  mV below the negative rail voltage. When we specify a maximum differential input voltage  $V_{id}$  of  $\pm 100$  mV we have to degenerate the input transistors by a factor 4, which means that  $\frac{1}{2}R_1$  and  $\frac{1}{2}R_2$  have a four times larger resistance value than the emitter resistance  $r_e$  of the transistors  $Q_{11}$ ,  $Q_{12}$ ,  $Q_{21}$ ,  $Q_{22}$ .

The intermediate stage has Darlington transistors for a high current gain and a high voltage gain because the output impedance at the collector of  $Q_{44}$  is compensated for by the negative output impedance at the collector of  $Q_{43}$  through the action of a bootstrapped current mirror by  $Q_{47}$ . The circuit has been described in [9.7].

The output stage has Darlington transistors as an emitter follower. The output can reach the negative rail voltage because the gain setting resistor chain  $R_5$ ,  $R_6$  is

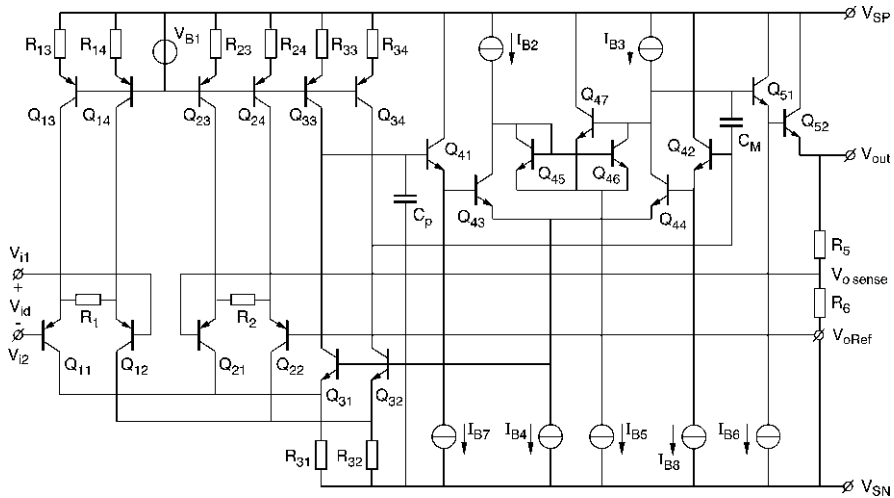


**Fig. 9.4.5** Bipolar instrumentation amplifier with input common-mode range which includes the negative rail voltage [9.7]

connected to the negative rail. The output is also referenced to ground by the connection to ground of the output-sensing differential pair  $Q_{21}$  and  $Q_{22}$ .

The result is an instrumentation amplifier with an input bias current of  $0.2 \mu\text{A}$ , an input offset voltage of  $0.3 \text{ mV}$ , an input noise voltage of  $30 \text{ nV}/\sqrt{\text{Hz}}$ , a CMRR of  $90 \text{ dB}$ , a common-mode voltage range up from  $-200 \text{ mV}$  below the negative rail voltage, and an input voltage range of  $\pm 100 \text{ mV}$ . The gain can be set between 1 and 1,000 by  $R_5$  and  $R_6$ . The gain error is typically  $0.1\%$  and non-linearity of typical  $0.1\%$ . The bandwidth is  $1 \text{ MHz}$ . The minimum supply voltage is  $2.5 \text{ V}$  [9.7].

### ***Instrumentation Amplifier CMOS with Common-Mode Voltage Range Including Negative Rail Voltage***

A basic circuit is shown in Fig. 9.4.6.

The differential V-I converters in CMOS will have a lower accuracy than in the bipolar circuit. There are two reasons: first, their maximum voltage gain  $\mu$  is so low that the CMRR will be too low, in the order of  $70 \text{ dB}$

$$1/H = \frac{1}{\mu} \times \frac{\Delta\mu}{\mu}, \tag{9.4.8}$$

see (4.3.4); second, their  $g_m$  is modulated by the common-mode drain-source voltage which prevents the gain error and non-linearities of the input sensing pair being more accurately compensated for by the output sensing pair than  $1\%$ . Therefore, we have to



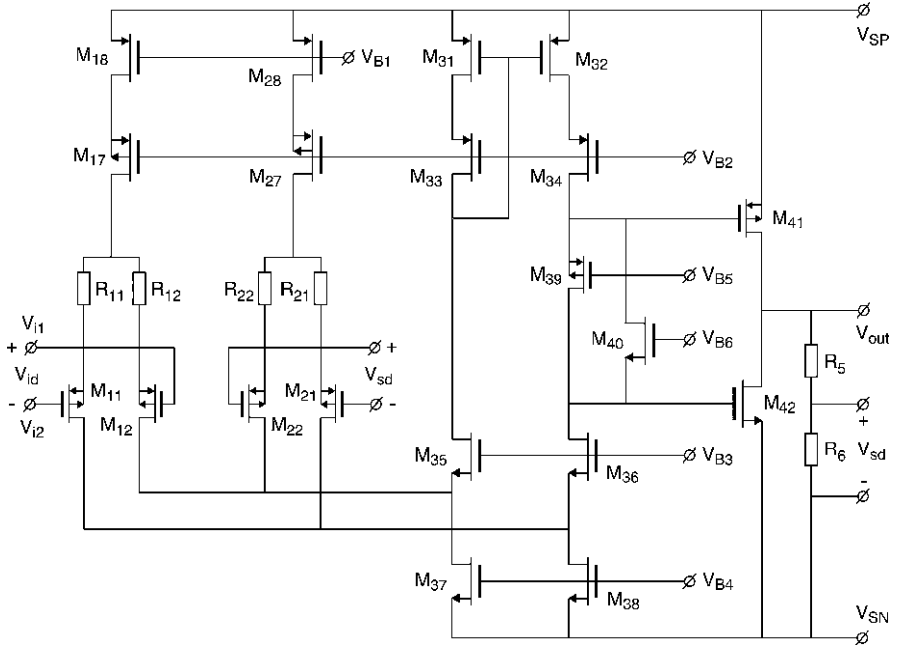


**Fig. 9.4.6** Basic CMOS instrumentation amplifier with input common-mode range including the negative rail voltage

cascode the CMOS transistors of the differential V-I converters. We have done this in Fig. 9.4.4. But in that case, we lost the negative-rail sensing capability because the cascode transistors took too much of the negative headroom. To solve this problem is too complicated to describe in this overview.

The output stage and class-AB biasing circuit have been explained with Fig. 5.3.21 and applied in the OpAmp circuit of Fig. 7.7.2.

The differential input voltage range has been chosen  $\pm 100$  mV. This means, in the CMOS case, that the resistors  $R_{11}$  and  $R_{12}$  need to have about the same  $g_m$  as the  $g_m$  of  $M_{11}$  and  $M_{12}$ .

The basic circuit of Fig. 9.4.6 has an expected accuracy of 1% and non-linearity of 0.1%, a CMRR of 70 dB, a noise of 30 nV/ $\sqrt{\text{Hz}}$ , and a bandwidth of 1–10 MHz.

### ***Instrumentation Amplifier Simplified Diagram and General Symbol***

There is a need to come up with a simplified schematic diagram and a general symbol for an instrumentation amplifier. The first is given in Fig. 9.4.7, the latter in Fig. 9.4.8.

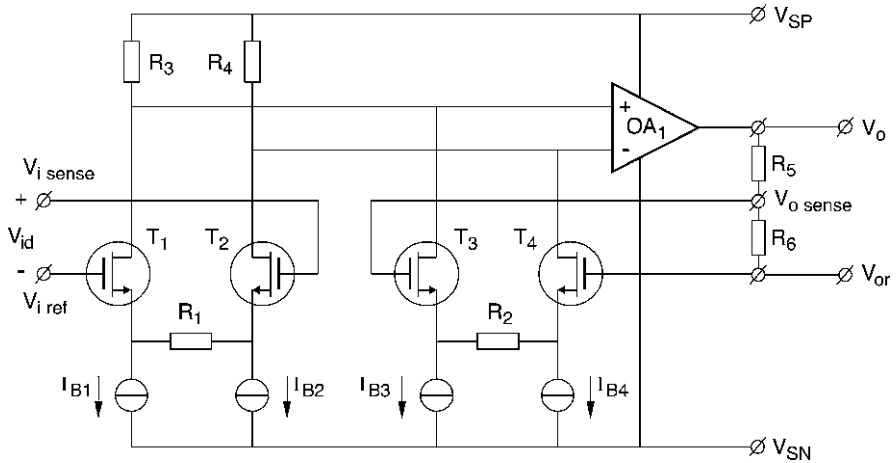
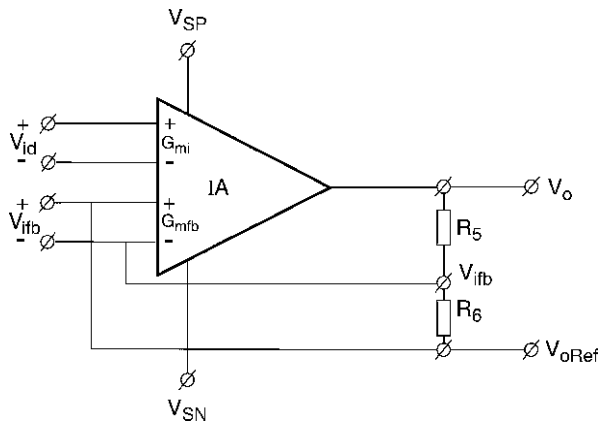


**Fig. 9.4.7** Simplified diagram of an instrumentation amplifier with differential current-to-voltage converters and ideal transistors

**Fig. 9.4.8** General symbol for an instrumentation amplifier (IA) showing gain setting resistors



### Conclusion

In this section we have seen how we can realize highly accurate instrumentation amplifiers. A semi-instrumentation amplifier can be realized with three OpAmps and a trimmed bridge circuit for obtaining a high CMRR. If we do not want to use trimming for obtaining a high CMRR, we must rely on current-source isolation. To that purpose, differential voltage-to-current converters can be used to realize instrumentation amplifiers with a high CMRR at the input as well as at the output. The instrumentation amplifier circuit can further be simplified by using matching of the input and output differential V-I converters. In this way, a bipolar and CMOS

instrumentation amplifier have been presented having input negative-rail sensing capability. Finally, a simplified circuit diagram and a symbol of an instrumentation amplifier with V-I converters is given.

### 9.5 Universal Class-AB Voltage-to-Current Converter Design Using an Instrumentation Amplifier

We have seen that a high-quality instrumentation amplifier can be realized by differential voltage-to-current converters. Now we can use an instrumentation amplifier (IA) to realize a high quality universal voltage-to-current converter. Universal means that signals with a physical positive and negative polarity can be processed. Particularly if we want a class-AB solution, a universal voltage-to-current-converter implementation with an instrumentation amplifier is preferable over that with an OFA. This will later be shown in Sect. 9.7.

Before using the real instrumentation amplifier, we will firstly use the semi-instrumentation amplifier and see its limitations.

#### *Universal V-I Converter Design with Semi-instrumentation Amplifier*

A universal voltage-to-current converter can be implemented using a semi-instrumentation amplifier, see Fig. 9.5.1. A measuring resistor  $R_M$  is connected in series with the output of the instrumentation amplifier and the load. The differential output sense terminals  $V_3$  and  $V_4$  are connected across  $R_M$ . A buffer amplifier  $OA_2$  is used to isolate output currents from bridge currents. The differential input sense terminals  $V_1$  and  $V_2$  are driven with the input voltage  $V_{id}$ .

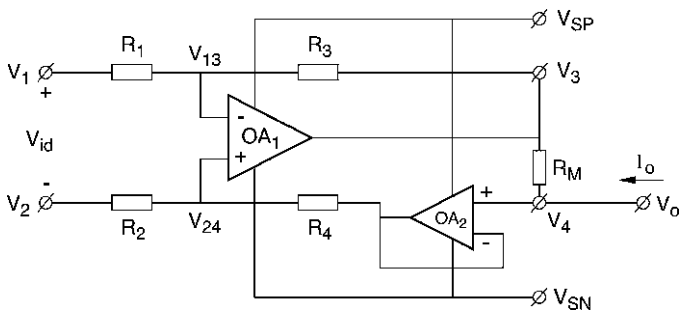


**Fig. 9.5.1** Universal voltage-to-current converter implemented with a bridge-type semi-instrumentation amplifier

The voltage-to-current transfer is:

$$G_M = I_o/V_{id} = -A_v/R_M \quad (9.5.1)$$

with:  $A_v = -R_3/R_1$ .

The common-mode output conductance is:

$$G_{OCM} = \frac{1}{R_{OCM}} = \frac{I_o}{V_o} = -\frac{V_3 - V_4}{V_4} \frac{1}{R_5} = -\frac{1}{H_R} \frac{1}{R_M} \quad (9.5.2)$$

with:  $1/H_R = -\Delta R_B/R_B(-A_{VR} + 1)$

$\Delta R_B/R_B = 1 - R_3R_2/R_4R_1$

$A_{VR} = -R_1/R_3$ .

$$1/H_R = -\Delta R_B/R_B(-A_{VR} + 1) \quad (9.5.3)$$

When we want to use the output to function in a large part of the supply-voltage range, the voltage across the resistor  $R_5$  should be relatively low, say 0.5 V at a supply voltage of 5 V. If the input voltage  $V_{id}$  is chosen 1 V, the voltage gain  $A_v$  should be set at  $-1/2$ , and hence the reverse voltage gain  $A_{VR}$  is  $-2$ . At a nominal output current of 1 mA, the current-measuring resistor  $R_5$  must be 500  $\Omega$ , and the voltage-to-current transfer  $I_o/V_{id}$  is 1 mS. At a bridge imbalance  $\Delta R_B/R_B$  of 1%, the reverse crosstalk ratio  $1/H_R$  is 0.3%. This results in a common-mode output conductance of  $G_{OCM}$  of 3  $\mu$ S. If we want a lower output conductance, the bridge has to be trimmed. Therefore, it is better to use a real instrumentation amplifier whose common-mode crosstalk does not depend on matching. This is done in the following paragraph.

### ***Universal V-I Converter Design with Real Instrumentation Amplifier***

A high quality voltage-to-current converter can be realized with a real instrumentation amplifier. This is shown in Fig. 9.5.2 with a simplified circuit diagram for an instrumentation amplifier with differential V-I converters, and shown in Fig. 9.5.3 with a general model. To this purpose, we connect a measuring resistor  $R_M$  in series with the output of the instrumentation amplifier and the load. The differential output sense and reference terminals are connected across  $R_M$ . The input voltage is connected to the differential input terminals.

The transconductance of the voltage-to-current converters of Figs. 9.5.2 and 9.5.3 is:

$$G_M = A_v/R_M \quad (9.5.4)$$

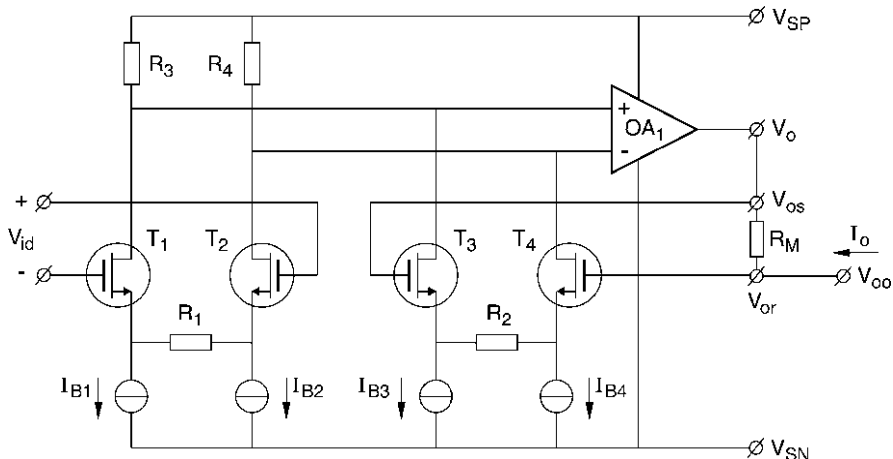


**Fig. 9.5.2** Universal voltage-to-current converter with a simplified schematic diagram for an instrumentation amplifier (IA)

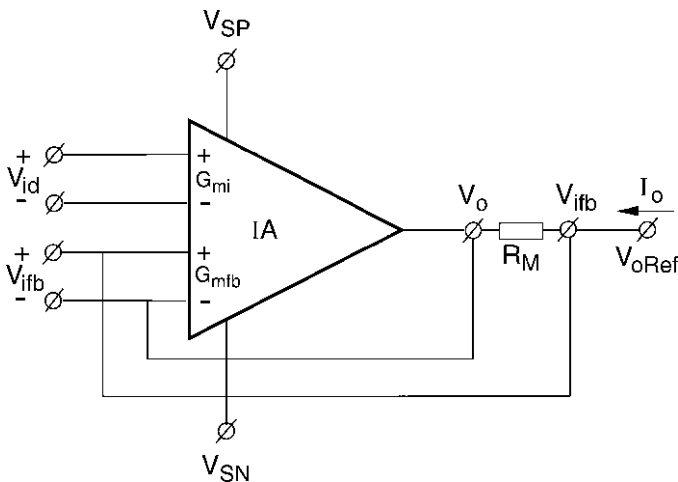


**Fig. 9.5.3** Universal voltage-to-current converter with a general model for an instrumentation amplifier (IA)

In the case of  $R_2/R_1 = 1$ , as was used with the differential input amplifiers of Figs. 9.4.4–9.4.6, the  $G_M$  equals  $1/R_M$ .

The common-mode output conductance is:

$$G_{OCM} = 1/H R_M \tag{9.5.5}$$

The common-mode rejection ratio  $H$  for the output differential sense amplifier has been calculated with (9.3.6). The common-mode output resistance

$R_{OCM} = 1/G_{OCM}$  can easily be a factor  $H = 10^4$  larger than that of the measuring resistor. This is a much better result than with the semi-instrumentation amplifier of Fig. 9.5.1 without trimming.

For the realization all designs of real instrumentation amplifiers can be used of Figs. 9.4.3–9.4.6.

**Conclusion**

We have shown in this section that the instrumentation amplifier with differential V-I converter can be used to realize high-quality universal voltage-to-current converters which function for physically positive as well as for negative input and output signals.

**9.6 Universal Class-A OFA Design**

In this chapter the design of universal class-A OFAs will be treated. The main goal is to design an OFA with output currents obeying the relation  $I_{O1} + I_{O2} = 2I_{Obias} + 2I_{O1}/H_0 = 0$ , or  $I_{O2} = -I_{O1}$ . This can be achieved by a floating, i.e., isolated, output stage. On a chip it is realistic to obtain the above by current-source isolation.

**Universal Class-A OFA Design with Floating Zener-Diode Supply**

A first approach could use current sources and zener diodes to create a kind of an internal floating battery [9.8]. This can be seen as a rough realization of the idea of a floating power supply presented in Fig. 9.1.1. This approach is shown in Fig. 9.6.1.

If we take the upper supply current source  $I_{OP}$  equal to the lower one  $I_{ON}$ , a floating supply voltage  $V_S = V_{SP} - V_{SN}$  will result across the zener diodes  $Z_{D1}$

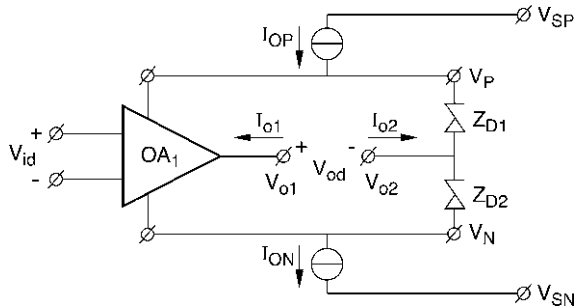


**Fig. 9.6.1** Universal class-A OFA realization with an OpAmp and floating zener-diode supply

and  $Z_{D2}$ . The diodes will take the excess current which is not needed by the OpAmp. The result is that the output bias current  $I_{ob}$  is nearly zero.

$$I_{o1} + I_{o2} = I_{ON} - I_{OP} = 2I_{ob} + 2I_{o1}/H_o \approx 0 \tag{9.6.1}$$

$$I_{o2} = -I_{o1} + 2I_{ob} + 2I_{o1}/H_o \approx -I_{o1} \tag{9.6.2}$$

The zener diodes divide the total supply-voltage range into one across the OpAmp for  $V_{o1}$  and one what remains in between the supply rails and the zeners. For this reason we lose at least a factor 2 in the total output voltage range [9.8].

### Universal Class-A OFA Design with Supply Current Followers

When we want to avoid the voltage loss of the fixed voltages across the zener diodes, we may exchange the zener diodes for current followers as depicted in Fig. 9.6.2.

These current followers catch and send the supply current of the OpAmp into the second output terminal. The output supply-voltage range can now be extended close into the rails. Moreover, the voltage swings across the total supply current sources  $I_{OP}$  and  $I_{ON}$  are now regulated constant by the cascodes  $M_1$  and  $M_2$ , which helps to make these currents signal independent and which enlarges the common-mode output impedance.

Not all OpAmp supply currents need to be provided by the total upper and lower supply current sources, only the current for the output transistors. A first approach with a voltage follower output stage is shown in Fig. 9.6.2b.

The formulas become very clean now:

$$I_{o1} + I_{o2} = I_{OP} - I_{ON} = 2I_{ob} + 2I_{o1}/H_o \approx 0 \tag{9.6.3}$$

$$I_{o2} = -I_{o1} + 2I_{ob} + 2I_{o1}/H_o \approx -I_{o1} \tag{9.6.4}$$

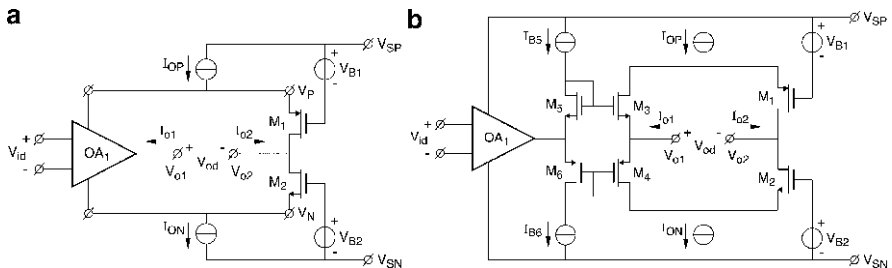


**Fig. 9.6.2** (a) Universal class-A OFA realized with an OpAmp and supply current followers (CF). (b) Universal class-A OFA realized with a VF output stage of an OpAmp and current followers (CF)

Not only the supply-voltage range has been used efficiently now, but also the bias currents  $I_{OP}$  and  $I_{ON}$  are used as efficiently as can be in class-A. If the total positive bias current  $I_{OP}$  is used for  $-I_{o1}$ , the total negative bias current  $I_{ON}$  will automatically be used for  $I_{o2}$ . This supposes that  $M_3$  and  $M_4$  are properly biased in class-AB by  $V_{B3}$  and  $V_{B4}$ , see Fig. 5.3.2a, b.

### Universal Class-A OFA Design with Long-Tailed-Pairs

An alternative output stage to the one with the current follower arises when we use a long-tailed-pair as output stage [9.9]. This is shown in Fig. 9.6.3.

The long-tailed pair functions as a pair of communicating vessels for currents between the two output terminals. The output bias current  $I_{ob}$  and the output current rejection ratio  $H_o$  determine the equality of the output currents  $I_{o1}$  and  $-I_{o2}$ :

$$I_{o1} + I_{o2} = I_{OP1} + I_{OP2} - I_{OP3} - I_{OP4} = 2I_{ob} + 2I_{o1}/H_o \approx 0 \tag{9.6.5}$$

$$I_{o2} = -I_{o1} + 2I_{ob} + 2I_{o1}/H_o \approx -I_{o1} \tag{9.6.6}$$

The way one output current is guided towards the other can clearly be seen. If we follow the output signal current  $I_{o1}$ , we see that it is blocked by the current source  $I_{OP1}$  from flowing into the positive supply.  $I_{o1}$  is forced to flow into  $M_1$  and  $M_2$  to the other output terminal as  $-I_{o2}$ . On its way there is no escape, because  $I_{OP3}$ ,  $I_{OP4}$  and  $I_{OP2}$  block its way toward the supply rails. The result is a very high output common-mode current rejection ratio  $H_o$ . The feedback through external connections, like the current follower of Fig. 1.3.2b, take the OFA into its functional working mode.

It is interesting that the accuracy of the output stage is even maintained when we use bipolar transistors. We can see this when we go through the long-tailed pair. Going from the left to the right output, we add the base current  $1/\beta$ , at emitter of  $Q_1$  and lose  $1/\beta_2$  at the base of  $Q_2$  [9.9].

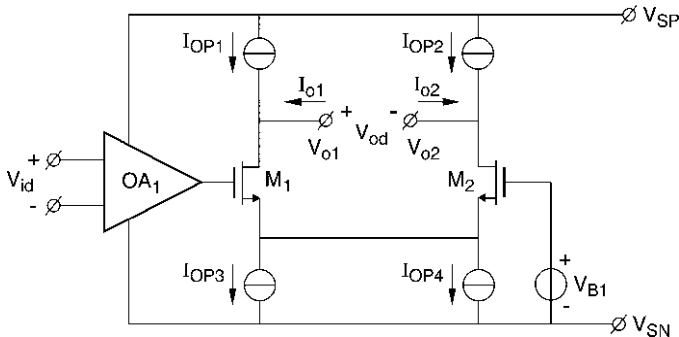
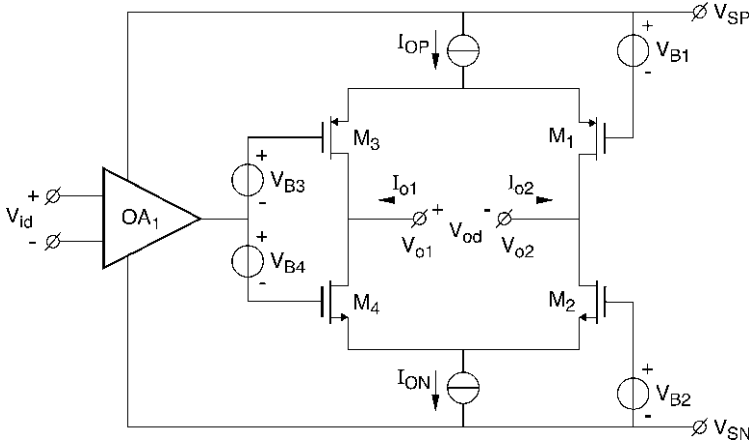


Fig. 9.6.3 Universal Class-A OFA realized with a long-tailed-pair output stage





**Fig. 9.6.4** Universal class-A OFA realized with two push-pull complementary long-tail pairs

A disadvantage of the single long-tailed pair is still that we can only use a half of the total output bias current  $I_{OP1} + I_{OP2}$  and  $I_{ON1} + I_{ON2}$  for one output current  $I_{o1}$  and  $I_{o2}$ . A more efficient use of the bias currents can be made if we use a P pair and an N pair together as depicted in Fig. 9.6.4.

The main design problem is the realization of the floating voltage sources  $V_{B3}$  and  $V_{B4}$ . These have to follow the supply voltages. We will present two approaches to this problem. In the first one we will drive the lower output transistors directly, and then cross the supply voltage and drive the upper output transistors indirectly. In the second approach we will use a similar mesh-drive circuit as we did for the R-R output stage of Fig. 5.3.21a, b.

A first complete CMOS class-A OFA design is presented in Fig. 9.6.5. The lower output transistors  $M_{31}$  and  $M_{32}$  are fed by a lower current source transistor  $M_{35}$ . The upper output transistors  $M_{33}$  and  $M_{34}$  are fed by an upper current source transistor  $M_{36}$ . The output transistors function as cascodes for these upper and lower current-source transistors for a high CM output impedance. A model bias stage accurately equates the currents through the upper and lower current source transistors. It is scaled down in current by a factor  $1/N$  in regard to the output stage, with transistors  $M_{41}$  through  $M_{46}$ . The model bias circuit also has the task of differentially driving the upper output transistors in opposite direction in regard to the lower output transistors. In this way the total output bias current is optimally used as maximum positive and negative output currents. Miller capacitors  $C_{M1}$  and  $C_{M2}$  take care of frequency compensation. The input stage is followed by a folded cascode stage. This cascode stage with transistors  $M_{21}$  through  $M_{28}$  provides a high internal voltage gain  $A_{vi}$ . In the order of  $10^4$  this is equal to the  $g_m$  of the input pair multiplied by the differential output resistance  $r_{d2}$  of the folded cascode stage.

This provides the OFA with an overall transconductance  $G_m$  which is equal to the internal voltage gain  $A_{vi}$  multiplied by the transconductance  $g_{m4}$  of the lower

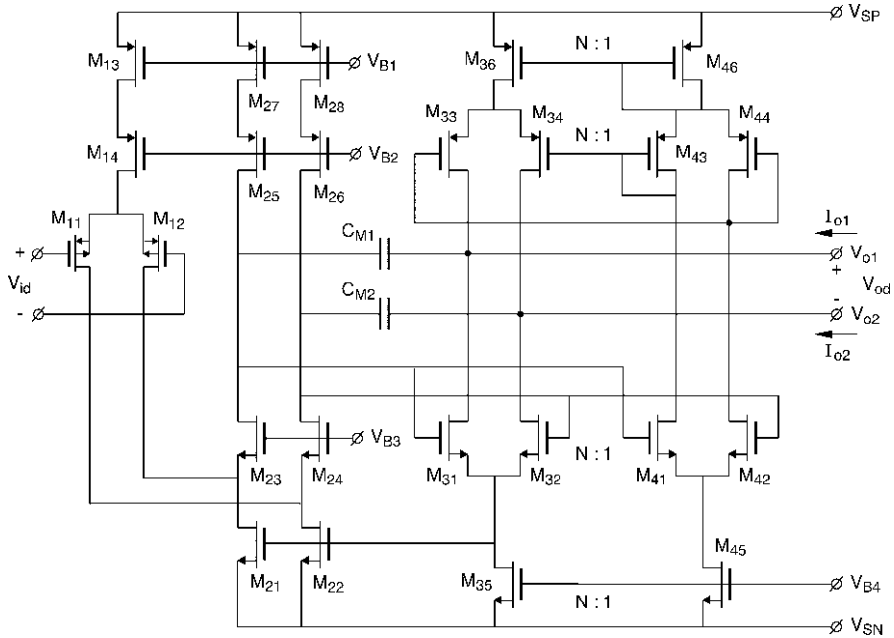


**Fig. 9.6.5** Universal Class-A OFA design with a push-pull complementary pair of long-tailed pair output stages and a model bias stage

output long-tailed pair transistors and doubled by the upper output long-tailed pair transistors as they are driven by the model bias stage.

The results are:

$$G_m = 2A_{vi}g_{m4'} \tag{9.6.7}$$

with

$$A_{vi} = g_{m1}r_{d2} \tag{9.6.8}$$

A feedback loop through the lower output transistors and the gates of  $M_{21}$  and  $M_{22}$  equates the upper and lower common-mode currents in the folded cascode-stage. The differential output impedance may not be that high due to the common-source connections of the long-tailed output pairs. But the series connection of the feedback around the output takes the output impedance to high levels, see Sects. 1.3 and 1.4. A completely alternative design is presented in Fig. 9.6.6. The output transistors are driven in opposite phases by the meshes  $M_{51}$ ,  $M_{52}$  and  $M_{53}$ ,  $M_{54}$  as explained with Fig. 5.3.21a, b. However, the output transistors do not have their sources connected to the supply rails but to the current sources  $M_{35}$  and  $M_{36}$ . Resistors  $R_{64}$ ,  $R_{69}$ , and  $R_{68}$  in the diode bias chains  $M_{63}$ - $M_{68}$  provide for the extra head room for the current sources. The current sources give the output transistors

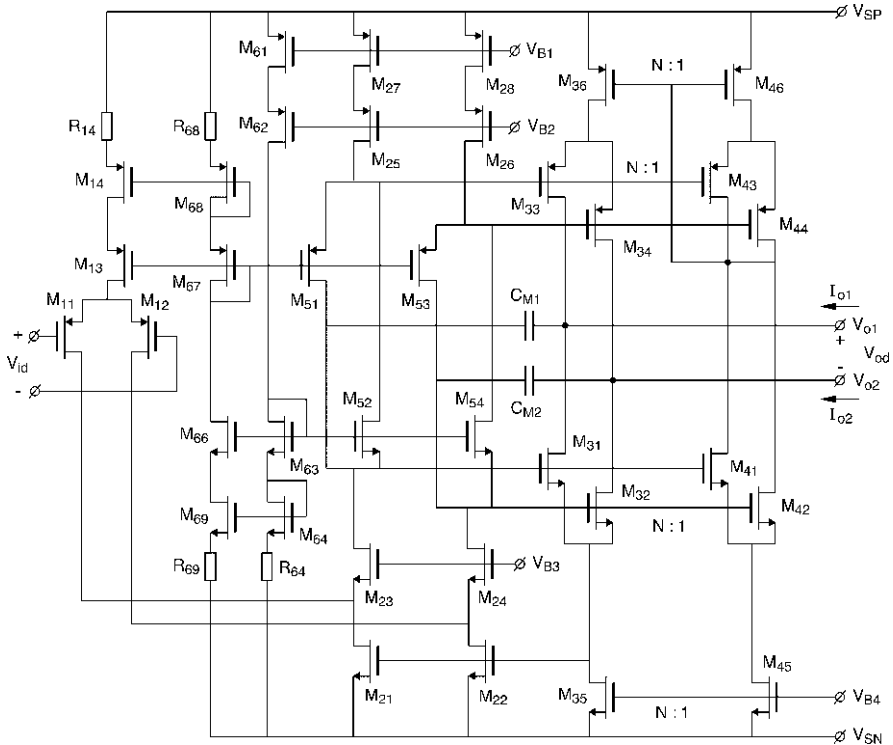


**Fig. 9.6.6** Universal Class-A OFA design with a push-pull complementary pair of long-tailed pair output stages and a model bias stage

a class-A bias instead of class-AB bias. The positive and negative current sources through  $M_{36}$  and  $M_{35}$  are equalized by the model bias circuit  $M_{41}$  through  $M_{56}$ . The rest of the explanation is similar to that of Fig. 9.6.5. The advantage of this alternative design over the previous one is a slightly better HF behavior because the upper output transistors are in parallel driven with the lower output transistors by the meshes. Whereas in the previous design, the upper output transistors are indirectly driven through the model bias stage.

The output voltages can approach the rail voltages except for one diode and one saturation voltage. The common-mode current rejection ratio at the output  $H_o$  is easily higher than  $10^4$ . That determines the dynamic equality of the output currents. The output bias current  $I_{ob}$  is of the order of 0.5% of the bias current sources  $I_{BP}$  and  $I_{BN}$ . This determines the offset between the two output currents. The bandwidth can easily be several tens of megahertz.

The OFA of Fig. 9.6.6 has some similarities with the differential OpAmp of Fig. 8.2.1. In that case the two output voltages were regulated equally but opposite to each other in regard to a reference voltage. There we needed two equal resistors to regulate the output voltages equally and the equality depends on the matching of the two resistors. With the OFA the output currents are regulated equally but

opposite to each other. This does not require matching of elements, apart from offset, because of the nature of the OFA.

**Conclusion**

In this section the designs of high-quality class-A OFAs have been described. These OFAs can be used in precision instrumentation applications where a free output signal current is desired at a high output impedance, with a signal-to-noise ratio of 120 dB in the audio frequency range, while a bandwidth can be obtained of several tens of megahertz. When used for the composition of gyrator filters, a quality factor  $Q$  higher than 1,000 can be obtained [9.9].

**9.7 Universal Class-AB OFA Realization with Power-Supply Isolation**

A first approach to solve the problem of designing a class-AB output stage, that is isolated from the supply-power ground, is the use of a power supply that is isolated from ground, i.e., floating [9.1]. This solution is depicted in Fig. 9.7.1.

If the input current can be disregarded, no output current can leak out of the mesh through the output stage and power supply, so the output currents must obey:

$$\begin{aligned}
 I_{o2} &= I_{SP} - I_{SN} = -I_{o1} \\
 I_{o2} &= -I_{o1} \\
 I_{o1} + I_{o2} &= 2I_{obias} + 2I_{o1}/H_o = 0
 \end{aligned}
 \tag{9.7.1}$$

This means that the output current  $I_{o1}$ , which sources out of one mode, must be accurately equal to the output current  $-I_{o2}$ , which sinks into the other mode, without depending on accurately matched components. If the output stage of the OpAmp is biased in class-AB, the whole OFA is biased in class-AB. A shortcoming of the circuit of Fig. 9.7.1 is that the maximum differential output voltage  $V_{od}$  is limited to half the total supply voltage  $V_S = V_{SP} + V_{SN}$ . This can be avoided by using a fully differential amplifier as presented in Chap. 8.

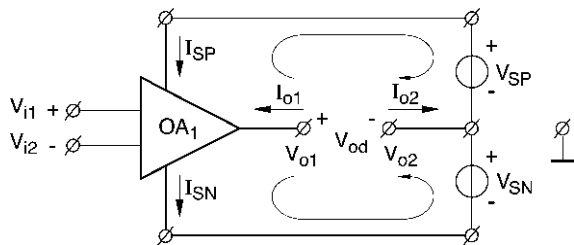
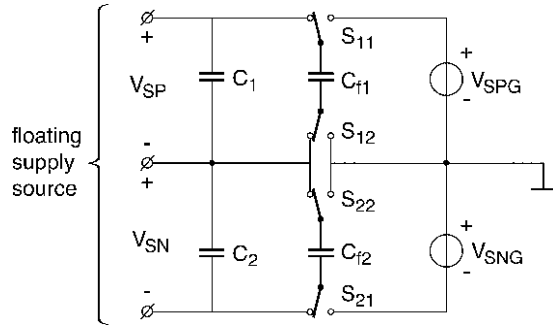


**Fig. 9.7.1** Universal Class-AB OFA realization with one OpAmp and a power-supply source that is isolated from ground, i.e., floating

**Fig. 9.7.2** Realizing a floating power supply source by the method of “flying” capacitors



### ***Universal Floating Power Supply Design***

In this section, the problem of realizing an isolated or floating output port has been shifted into the problem of realizing a power-supply source which is isolated from ground, or floating with regard to ground. This is a problem in itself. But it is realizable. Even on a chip, one can for example use the method of “flying” capacitors, see Fig. 9.7.2.

When no external capacitors may be used, relatively small on-chip capacitors allow for a small supply current. In some extraordinary cases an external battery or solar cell could be used.

### ***Conclusion***

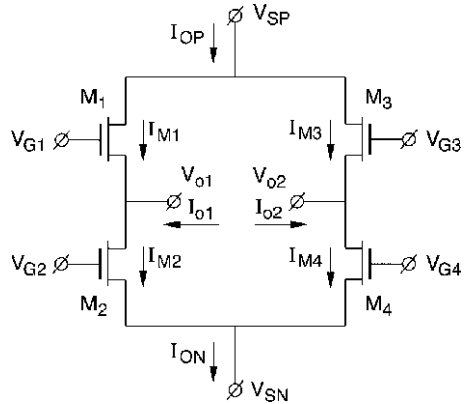
Power-supply isolation is an escape to shift the problem of a floating output stage into the supply of an OpAmp circuit. Realizing a floating supply source is often not easy and may be expensive. For low output currents the method with flying capacitors can be used on chip.

## **9.8 Universal Class-AB OFA Design**

The final task in designing universal OFAs is to provide the output stage with class-AB biasing without using a floating power supply. We will see in this section that class-AB biasing is not easy for OFAs. We will approach the problem systematically. In Fig. 9.8.1 the situation is depicted by the currents in four output transistors of an OFA.

Class-AB biasing means that the total positive and negative output currents  $I_{OP}$  and  $I_{ON}$  are strongly changing between their quiescent value  $I_{OQ}$  and their maximum

**Fig. 9.8.1** General push-pull configuration of an OFAs output stage



value  $I_{OM}$ . This changing must be allowed while the OFA requires that  $I_{o1}$  remains equal to  $I_{o2}$ . This can be written-out into three equations:

$$I_{ON} - I_{OP} = 2I_{ob} + 2I_{o1}/H_o \approx 0 \tag{9.8.1}$$

$$I_{M2} - I_{M1} + I_{M4} - I_{M3} = 2I_{ob} + 2I_{o1}/H_o \approx 0 \tag{9.8.2}$$

$$I_{o1} + I_{o2} = 2I_{ob} + 2I_{o1}/H_o \approx 0 \tag{9.8.3}$$

(see for  $I_{ob}$  and  $H_o$  Sect. 2.4).

Each of these three equations gives rise to a class-AB OFA realization. In the following designs we start from the first formula, then the second one, and finally the third one.

### ***Universal Class-AB OFA Design with Total-Output-Supply-Current Equalization***

In the first realization we use, for example, a mesh of two Operational Amplifiers, measure the total positive and negative supply currents and equalize them. That situation is drawn in Fig. 9.8.2.

The diodes  $M_1$  and  $M_2$  measure the positive and the negative total supply current  $I_{OP}$  and  $I_{ON}$ , respectively. These currents are reproduced in  $M_3$  and  $M_4$ , respectively, at a reduced level by a ratio of  $1/N$ . The second OpAmp  $OA_2$  senses the differences in  $I_{M3}$  and  $I_{M4}$  at its positive input terminal and drives the output in such a way that  $I_{M3}$  and  $I_{M4}$  are equalized, and so are  $I_{OP}$  and  $I_{ON}$ , as we hope.

An advantage of the use of this class-AB OFA is that the output bias current  $2I_{ob} = I_{o1} + I_{o2}$  is low, when the output currents themselves are low. Also the output bias noise current is low in that case. So the dynamic range of a voltage-to-current converter with such a universal class-AB OFA may be high, i.e., more than 140 dB.

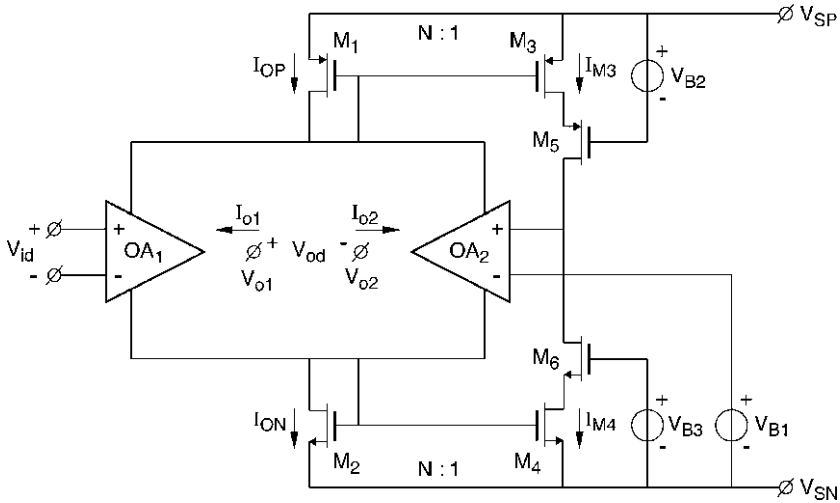


Fig. 9.8.2 Universal class-AB OFA realization with total-output-supply-current equalization

However, a problem arises by the fact that the transistors  $M_1$  through  $M_4$  are not perfectly scaled, or have different drain-source voltages, or different threshold voltages. This results in a non-linear current transfer as shown in Fig. 9.8.3. Say that the current  $I_{OP}$  through  $M_1$  is  $\delta = 1\%$  smaller than  $I_{ON}$  through  $M_2$ , and that we disregard the bias currents of the OpAmps, then the output current  $-I_{o2}$  is 1% smaller than  $I_{o1}$  at a positive value of  $I_{o1}$ , but  $-I_{o2}$  is 1% larger than  $I_{o1}$  at a negative value of  $I_{o1}$ . This means a kink in the transfer of  $-I_{o2} = f(I_{o1})$  at zero current.

We can explain this also in a different way:

$$I_{o2} = -I_{o1} + \delta |I_{o1}|, \text{ and } 1/|H_o| = \delta/2 \tag{9.8.4}$$

When  $I_{o1}$  is physically positive, it is measured and processed by  $I_{ON}$ . At the same moment  $I_{o2}$  is physically negative and is processed by  $I_{OP}$ . If the polarity is reversed the elements that process each of these currents change position. For this reason positive  $I_{o2}$  currents are processed in another relation with  $I_{o1}$  than negative  $I_{o2}$  currents are.

The result is a strongly non-linear signal transfer at zero current. If such an OFA is used for audio signals, a noticeable distortion will be heard. If such an OFA is used for filter applications, such as gyrator filters, see Fig. 3.11, then an instability of the filter characteristic will be found at quality factors  $Q$  larger than  $1/\delta$ . This effect is depicted in Fig. 9.8.3a, b.

The non-linearity will be partly masked for small signal currents within the class-A-biased range of the OpAmp in which the total supply current does not change much.

We may, of course, trim the transistor matching of the class-AB OFA of Fig. 9.8.1. If we do this, we can combine the advantage of a high dynamic range with a high linearity. But trimming is costly. We can first try to find a better way.

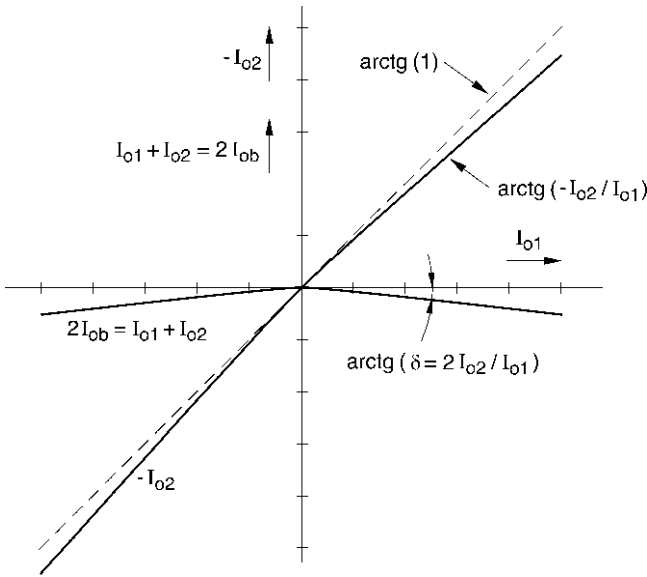


**Fig. 9.8.3 (a)** The non-linear relation between the two output-currents  $I_{o1}$  and  $I_{o2}$  because of a mismatch of  $\delta$  between the current-determining transistors

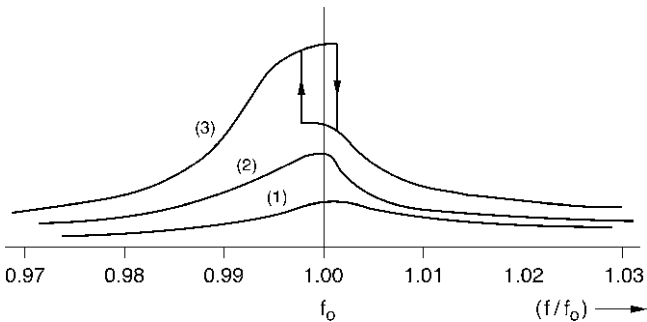


**Fig. 9.8.3 (b)** Amplitude characteristics may become instable, while using frequency filters of higher quality factors (1), (2), and (3) while using class-AB OFAs based on the topology of Fig. 9.8.1 with total-output-supply-current equalization

### ***Universal Class-AB OFA Design with Current Mirrors***

The second approach is to find a circuit realization functioning according to the Eq. 9.8.2 in which the currents in  $I_{M2}$  and  $I_{M4}$  are equalized with the currents in  $I_{M1}$  and  $I_{M3}$  [9.10]. We are able to do so by diagonally connecting current mirrors, as shown in Fig. 9.8.4. We may expect errors in the signal transfer of the order of 0.5% due to inaccurate matching of the inaccurate mirror transistor characteristics and



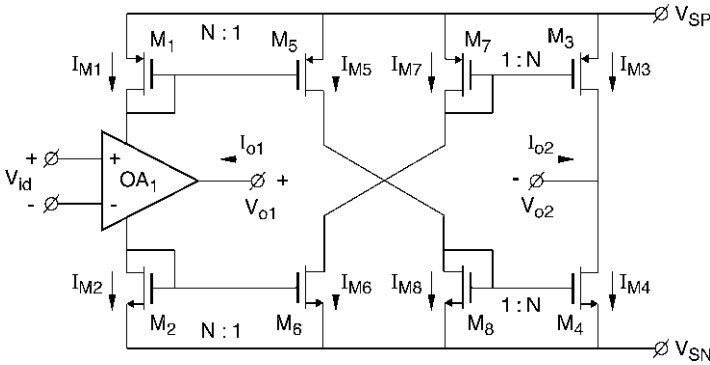
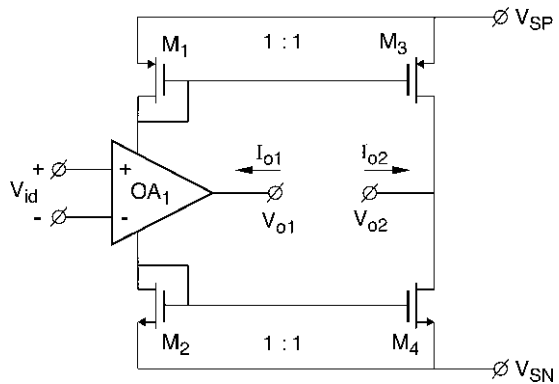


Fig. 9.8.4 Universal class-AB OFA realization with diagonally connected current mirrors

Fig. 9.8.5 Universal operational mirrored amplifier (OMA) realization



due to voltage dependent early effects. This also gives rise to non-linear distortion of the order of 0.5%.

Looking to the OFA circuit of Fig. 9.8.4 we might ask ourselves if we could not avoid mirroring the current signals twice. When we only mirror once, another functional block arises: the operational mirrored amplifier, or OMA [9.11–9.14]. The circuit is shown in Fig. 9.8.5.

The OMA can, as well as the OFA, be used for universal voltage-to-current converters. The output currents are now equal

$$I_{o2} + I_{o1} = \delta |I_{o1}|, \quad \text{and} \quad 1/|H_o| = \delta/2 \tag{9.8.5}$$

The mismatch  $\delta$  between the two currents is again caused by transistor mismatch, which gives errors and non-linearities in the order of 0.5%.

Though the polarity of the two currents are equal in the OMA, while the OFA has currents with opposite polarity, the OMA can nearly be used in all OFA applications. The advantages and disadvantages of the current-mirror-matching methods are equal

to the supply-current-matching methods. This means that a high signal-to-noise ratio for the output current signals can be obtained, but that a strong non-linearity kink occurs in the zero current point, and that filters may become unstable at high quality factors. Only trimming can alleviate these problems for class-AB biasing.

The non-linearity will be partially masked within the class-A region of the class-AB biasing for small current signals.

Notice that we still have to carefully cascode the current mirrors to avoid significant voltage modulation errors in the current transfer.

### Universal Class-AB OFA Design with Output-Current Equalization

The third approach uses the first equation (9.8.1) by which the output currents are directly measured and equated. The way we can approach this is to insert current-measuring resistors  $R_{M1}$  and  $R_{M2}$  in the output terminals and measure the difference between the voltages  $V_{M1}$  and  $V_{M2}$  across these resistances, and finally equate these voltages. The differential voltages across these resistors can only be measured with an instrumentation amplifier, having a high CMRR for the differential input voltages, while being able to accurately process the difference, see Figs. 9.4.3–9.4.8. A practical way to depict the situation is given in Fig. 9.8.6.

The instrumentation amplifier with  $T_1$  through  $T_4$  and  $OA_2$ , see Fig. 9.5.2, measures the voltage difference across a measuring resistor  $R_{M1}$  in series with the output of an OpAmp  $OA_1$ . The instrumentation amplifier is connected as a voltage-to-current converter with a measuring resistor  $R_{M2}$  in series with its output amplifier  $OA_2$ . The two end terminals of  $R_{M1}$  and  $R_{M2}$  give shape to the two output terminals of the universal class-AB OFA with  $V_{o1}$  and  $V_{o2}$ . The output currents  $I_{o1}$  and  $I_{o2}$  obey the third OFA equation (9.8.3).

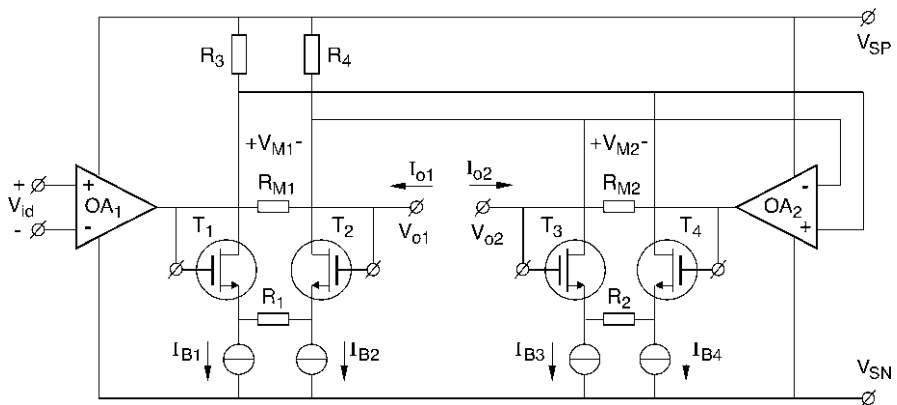


**Fig. 9.8.6** Universal class-AB OFA realization with output-current equalization by means of an instrumentation amplifier

Very essential now is that the same physical elements  $R_1, R_{M1}$ , and  $R_2, R_{M2}$  that measure the output currents in one polarity also measure the output current if their polarity reverses. This means that the current relation between  $I_{o1}$  and  $I_{o2}$  is basically linear. Only a linear scaling factor  $\alpha$  occurs.

For this we may write:

$$I_{o1} = -\alpha I_{o1} = -I_{o1} - (\alpha - 1)I_{o1} = -I_{o1} + \delta I_{o1} \tag{9.8.6}$$

$$I_{o1} + I_{o2} = \delta I_{o1} = 2I_o = 2I_{ob} + 2I_{o1}/H_o, \text{ and } 1/H_o \approx \delta/2 \tag{9.8.7}$$

We have a linear output current relation. There is no kink in the current transfer, nor an instability in filter characteristics at high quality factors. With these OFAs we can have a signal-to-noise ratio of the output currents in the order of 100 dB. The output current rejection ratio  $H_o$  is half the mismatch of the resistors.

### ***Universal Class-AB Voltage-to-Current Converter with Instrumentation Amplifier***

One simplification is obvious, though. If we need the OFA for realizing the function of a voltage-to-current conversion, we do not need the full OFA construction of Fig. 9.8.6, but the connection of an instrumentation amplifier with a current-measuring resistor  $R_M$  in series with the output, as shown in Fig. 9.5.2, satisfies our need. It is shown again in Fig. 9.8.7.

With an instrumentation amplifier, a high-quality universal class-AB voltage-to-current converter of Fig. 9.8.7 can be obtained. Without trimming, an output impedance

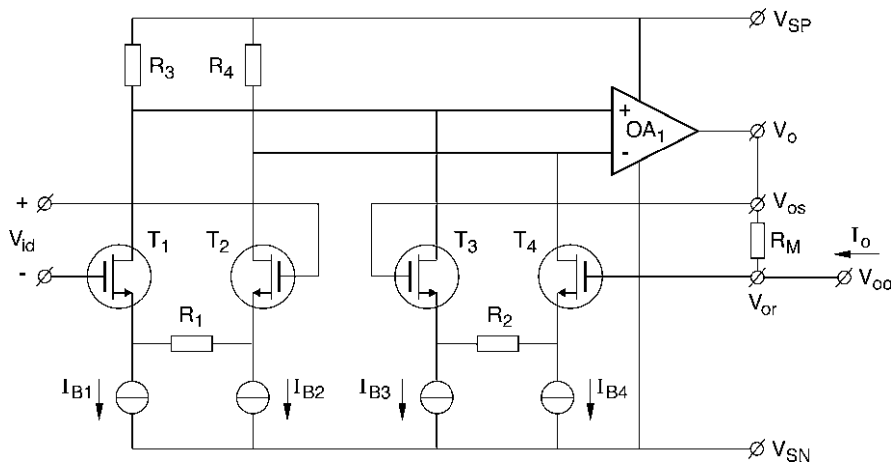


**Fig. 9.8.7** Universal class-AB voltage-to-current converter with instrumentation amplifier

of more than  $10^4 R_M$  can easily be obtained, at a non-linearity error of better than  $10^{-4}$ , a bandwidth of several tens of megahertz and a signal-to-noise ratio of 120 dB.

### Conclusion

We have seen in this section on universal class-AB OFAs that the combination of class-AB biasing and non-linearity cannot easily be met. Based on the way the output currents can be equalized, three possibilities are open.

Supply-current equalization and current-mirror equalization both show a non-linear kink in the current transfer at zero current. This gives rise to audible distortion when these circuits are used to process audio signals. Instability may occur when used in filters with a high quality factor. By trimming the non-linearity can be reduced. For small current signals the non-linearity is masked in the class-A region of the class-AB biasing. The signal-to-noise ratio of the relation between the output currents can be high. Current-mirror equalization leads to simple circuits.

Output-current equalization using an instrumentation amplifier achieves a high quality and highly linear result. A simplification can be made here. If we only need the function of a voltage-to-current conversion, we do not need the full OFA architecture, but an instrumentation amplifier connected as a voltage-to-current converter can do a high-quality job.

## 9.9 Problems

### Problem 9.1

For the instrumentation amplifier in Figure 9.4.6, calculate the common-mode rejection ratio CMRR if the input transistors  $M_{11}$  and  $M_{12}$  can have a processing-induced threshold voltage difference  $\Delta V_{th} = 3$  mV. The circuit is biased at  $I_{D31} = I_{D32} = I_{D18} = I_{D28} = 50 \mu\text{A}$ ,  $I_{quies41} = 100 \mu\text{A}$ , and the devices in the signal path are sized with  $W/L_{11} = W/L_{12} = W/L_{21} = W/L_{22} = 100\mu/2\mu$ ,  $W/L_{37} = W/L_{38} = 40\mu/2\mu$ ,  $W/L_{35} = W/L_{36} = 30\mu/1\mu$ ,  $W/L_{41} = 3.5W/L_{42} = 70\mu/1\mu$ . Source degeneration resistors are all equal to  $R_{11} = R_{12} = R_{21} = R_{22} = 5$  k $\Omega$ . Transistor parameters are  $V_{THN} = 0.5$  V,  $V_{THP} = -0.6$  V,  $K_N = 56 \mu\text{A}/\text{V}^2$ ,  $K_P = 16 \mu\text{A}/\text{V}^2$ ,  $\lambda_N = \lambda_P = 0.1 \text{ V}^{-1}$ .

### Solution

According to Eq. 4.3.4, the CMRR limit due to disbalancing of an input stage is

$$CMRR = \frac{\mu^2}{\Delta\mu} \tag{9.9.1}$$

Because the mirror  $M_{37}M_{38}$  repeats  $I_{D11}$  effects in  $I_{D38}$  as well as in  $I_{D37}$  there is no common-mode to differential crosstalk in the folded cascode stage, so the input stage voltage gain  $\mu$  is the only gain factor which degrades CMRR. The variation of  $\mu$  for the input stage due to the given  $\Delta V_{th}$  under the assumption of a small threshold voltage change from  $M_{11}$  to  $M_{12}$  is

$$\Delta\mu = \frac{d\mu}{dV_{th}} \Delta V_{th} \quad (9.9.2)$$

In the equation above, an expression for the voltage gain  $\mu$  as a function of  $V_{th}$  is needed to calculate the finite differences. The voltage gain of the input stage is given by its equivalent  $G_m$  and its equivalent  $G_{ds}$

$$\mu = \frac{G_m}{G_{ds}} \quad (9.9.3)$$

where the conductances are given by

$$G_m = \frac{1}{R_{11} + \frac{1}{\sqrt{2K_P \frac{W}{L_{11}} I_{D11}}}} \quad (9.9.4)$$

$$\frac{1}{G_{ds}} = R_{ds} = \mu_{11} R_{11} + \frac{1}{\lambda I_{D11}}$$

The variation of  $\mu$  for a small change in  $V_{th}$  is given by

$$\frac{d\mu}{dV_{th}} = \frac{dG_m}{dV_{th}} R_{ds} + \frac{dR_{ds}}{dV_{th}} G_m \quad (9.9.5)$$

The derivative of  $G_m$  related to  $V_{th}$  will be

$$\frac{dG_m}{dV_{th}} = \frac{dG_m}{dI_{D11}} \frac{dI_{D11}}{dV_{th}} \quad (9.9.6)$$

Combining  $G_m(I_{D11})$  and  $I_{D11}(V_{th})$  for transistors working in saturation region, Eq. 9.10.6 becomes

$$\begin{aligned} \frac{dR_{ds}}{dV_{th}} &= \frac{1}{2} K_P \frac{W}{L_{11}} (V_{SG11} + V_{THP}) \\ &\times \frac{1}{\left( R_{11} + \frac{1}{\sqrt{2K_P \frac{W}{L_{11}} I_{D11}}} \right)^2} \frac{1}{\sqrt{2K_P \frac{W}{L_{11}} \sqrt{I_{D11}^3}}} \end{aligned} \quad (9.9.7)$$

The derivative of  $R_{ds}$  related to  $V_{th}$  will be

$$\frac{dR_{ds}}{dV_{th}} = \frac{dR_{ds}}{dI_{D11}} \frac{dI_{D11}}{dV_{th}} \tag{9.9.8}$$

The expression of  $R_{ds}$  as a function of  $I_{D11}$  gives a derivative

$$\begin{aligned} \frac{dR_{ds}}{dV_{th}} &= -K_P(V_{SG11} + V_{THP}) \\ &\times \left( \frac{1}{2} \frac{\sqrt{2K_P \frac{W}{L_{11}} I_{D11}}}{\lambda} \frac{1}{\sqrt{I_{D11}^3}} \right) \end{aligned} \tag{9.9.9}$$

Numerically, the parameters involved in calculating CMRR are

$$\begin{aligned} G_m &= \frac{1}{R_{11} + \frac{1}{\sqrt{2K_P \frac{W}{L_{11}} I_{D11}}}} = 100 \text{ } \mu\text{A/V} \\ R_{ds} &= \mu_{11} R_{11} + \frac{1}{\lambda I_{D11}} = 800 \text{ k}\Omega \\ \frac{dG_m}{dV_{th}} &= 200 \text{ } \mu\text{A/V}^2 \\ \frac{dR_{ds}}{dV_{th}} &= 3.2 \text{ M}\Omega/\text{V} \\ \mu &= 80 \\ \Delta\mu &= \frac{d\mu}{dV_{th}} \Delta V_{th} = 1.44 \end{aligned} \tag{9.9.10}$$

Replacing these numbers in CMRR expression gives

$$CMRR = \frac{\mu^2}{\Delta\mu} = 73 \text{ dB} \tag{9.9.11}$$

It is worth noting the strong degradation of common-mode rejection due to an apparently small variation in threshold voltage. In a real implementation this number will be further degraded by additional geometrical mismatches and by the finite impedance of the biasing current source.

### Problem 9.2

For the voltage-to-current converter in Figure 9.5.1, calculate the typical, maximal and minimal transconductance  $G_M$  and the highest common-mode output

conductance for resistors sized as  $R_1 = R_2 = 10 \text{ k}\Omega$ ,  $R_3 = R_4 = 30 \text{ k}\Omega$  and  $R_M = 10 \text{ k}\Omega$ . The resistors are matched within  $M = 2\%$  and their absolute tolerance is  $\Delta R = 10\%$ .

### Solution

The Eq. 9.5.1 gives the expression of this circuit transconductance

$$G_M = A_v \frac{1}{R_M} = \frac{R_3}{R_1} \frac{1}{R_M} \quad (9.9.12)$$

The matching of resistors  $R_3$  and  $R_1$  affects the voltage gain  $A_v$  while the tolerance affects the value of  $R_M$ . Thus the limits of  $G_M$  become

$$\begin{aligned} G_{Mmax} &= \frac{R_3}{R_1} (1 + M) \frac{1}{R_M(1 - \Delta R)} = 340 \text{ }\mu\text{A/V} \\ G_{Mtyp} &= \frac{R_3}{R_1} \frac{1}{R_M} = 300 \text{ }\mu\text{A/V} \\ G_{Mmin} &= \frac{R_3}{R_1} (1 - M) \frac{1}{R_M(1 + \Delta R)} = 267 \text{ }\mu\text{A/V} \end{aligned} \quad (9.9.13)$$

It is easy to note that most of this error is induced by the high tolerance of  $R_M$ .

For the worst-case common-mode conductance, i.e., the highest possible, Equation set (9.5.2) shows

$$\begin{aligned} G_{OCMmax} &= -\frac{1}{H_{Rmax}} \frac{1}{R_M(1 - \Delta R)} - \frac{1}{H_{Rmax}} \\ &= \left(1 - \frac{R_3}{R_1} \frac{R_2}{R_1} (1 - M)^2\right) \left(1 + \frac{R_1}{R_3} (1 + M)\right) = 0.0134 \end{aligned} \quad (9.9.14)$$

The equations above give a maximal common-mode output impedance of

$$G_{OCMmax} = 1.5 \text{ }\mu\text{A/V} \quad (9.9.15)$$

### Problem 9.3

The universal voltage-to-current converter shown in Figure 9.5.3 uses the instrumentation amplifier depicted in Figure 9.4.3, built using a conductance  $G_1 = 2G_2 = 100 \text{ }\mu\text{A/V}$  and current sources have conductances  $G_{IB} = 0.5 \text{ }\mu\text{A/V}$  matched within  $\Delta G_{IB}/G_{IB} = 3\%$ . All operational amplifiers are considered to have  $CMRR = 80 \text{ dB}$ , and the conversion resistor is  $R_M = 10 \text{ k}\Omega$ . Calculate the differential transconductance and the common-mode output conductance,  $G_M$  and  $G_{OCM}$ .

### Solution

Combining Eqs. 9.5.3 and 9.4.5, the differential voltage gain and transconductance can be calculated.

$$A_v = \frac{G_1}{G_2} = 2$$

$$G_M = \frac{A_v}{R_M} = 200 \text{ } \mu\text{A/V}$$
(9.9.16)

The common-mode rejection ratio of the instrumentation amplifier's input stage limits the value of the common-mode output conductance, according to Eq. 9.5.4.

$$G_{OCM} = \frac{1}{H} \frac{1}{R_M}$$
(9.9.17)

The CMCR factor  $1/H$  can be calculated based on Eq. 9.3.6

$$\frac{1}{H} = \frac{G_{1B}}{G_1} - \frac{\Delta G_{1B}}{G_{1B}} + \frac{1}{H_{OA1}} + \frac{1}{H_{OA2}} = -69 \text{ dB}$$
(9.9.18)

and  $G_{OCM}$  becomes

$$G_{OCM} = \frac{1}{H} \frac{1}{R_M} = 35 \text{ nA/V}$$
(9.9.19)

## 9.10 References

- [9.1]. J.H. Huijsing, Design and application of the Operational Floating Amplifier (OFA): The most universal operational amplifier. *Analog Integr. Circ. Signal Process* 4(2), 115–129 (1993)
- [9.2]. D.D.H. Tellegen, On nullators and norators. *IEEE Trans. Circ. Theory* CT-13, 466–468 (1966)
- [9.3]. J.J. Ebers, J.J. Moll, Large-signal behavior of junction transistors. *Proc. IRE* 42, 1761–1772 (1954)
- [9.4]. Philips Semiconductors Application Note NE 5230
- [9.5]. G.J.A. van Dijk, A. Bakker, J.H. Huijsing, Low-power CMOS transadmittance amplifier with extended common-mode input range for a smart thermocouple interface, in *Proceedings of ProRisc Workshop*, Mierlo, Netherlands, 27–28 Nov 1997, pp. 143–147
- [9.6]. A.P. Brokaw, P.M. Timko, An improved monolithic instrumentation amplifier. *IEEE J. Solid State Circ.* SC 10(6), 417–423 (1975)
- [9.7]. B.J. van den Dool, J.H. Huijsing, Indirect current feedback instrumentation amplifier with a common-mode input range that includes the negative rail. *IEEE J. Solid State Circ.* 38(7), 743–749 (1993)



- [9.8]. E.H. Nordholt, Extending op amp capabilities by using a current-source power supply. IEEE Trans. Circ. Syst. **CAS-29**, 411–414 (1982)
- [9.9]. J.H. Huijsing, J. de Korte, Monolithic nullor – a universal active network element. IEEE J. Solid State Circ. **SC-12**(1), 59–64 (1977)
- [9.10]. A.S. Sedra, The current conveyer: history and progress. Proc. Int. Symp. Circ. Syst. **3**, 1567–1570 (1989)
- [9.11]. J.H. Huijsing, C.J. Veelenturf, Monolithic operational mirrored amplifier (OMA). Elect. Lett. **17**(3), 119–120 (1981)
- [9.12]. J.W. Haslett, M.K.N. Rao, A high quality controlled current source. IEEE Trans. Instrum. Meas. **IM-28**(2), 132–140 (1979)
- [9.13]. B.L. Hart, R.W.J. Barker, Universal operational-amplifier converter technique using supply-current sensing. Electron. Lett. **15**(16), 496–497 (1979)
- [9.14]. F.J. Lidgley, C. Toumazon, Accurate current follower. Electron. Wireless World **91**(1590), 17–19 (1985)

# 10. Low Noise and Low Offset Operational and Instrumentation Amplifiers

**Abstract** Chapter 10 gives an overview of techniques that achieve low-offset, low-noise, and high accuracy in CMOS operational amplifiers (OA or OpAmp) and instrumentation amplifiers (IA or InstAmp). Auto-zero and chopper techniques are used apart and in combination with each other. Frequency-compensation techniques are described that obtain straight roll-off amplitude characteristics in the multi-path architectures of chopper stabilized amplifiers. Therefore, these amplifiers can be used in standard feedback networks. Offset voltages lower than 1  $\mu\text{V}$  can be achieved.

## 10.1 Introduction

The simplest type of amplifier that can be made with a low offset voltage  $V_{os}$  and high common-mode rejection ratio (CMRR) is the operational amplifier (OA). But, this amplifier does not have a well-determined gain. The gain of an OA is normally so high, that feedback around the OA must be applied to produce an accurate result [10.1]. This situation is depicted in Fig. 10.1.1.

However, feedback destroys the CMRR because the feedback network may have unbalance and is connected to a ground reference. Therefore, other types of amplifiers have to be found to combine an accurate voltage gain, a low offset, and a high CMRR.

Instrumentation amplifiers (IA), on the other hand, can have the combination of accurate gain, low offset voltage  $V_{os}$ , and high common-mode rejection ratio. But, they are more difficult to implement than operational amplifiers. A general symbol for an instrumentation amplifier is given in Fig. 10.1.2.

This chapter discusses the design of low noise and low offset Operational Amplifiers and Instrumentation Amplifiers:

1. Introduction
2. Application of IA
3. Three-OpAmp IA
4. Current-Feedback IA
5. Auto-Zeroing

**Fig. 10.1.1** Operational amplifier (OA) in feedback network,  $V_{id} = 0$ ,  $I_{id} = 0$ ,  $I_{ic}(CM) = 0$ , input CMRR = Low

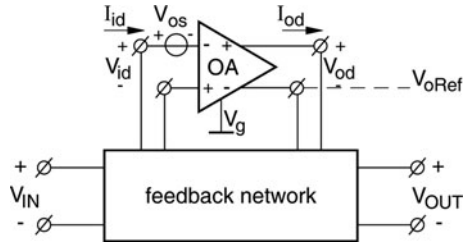
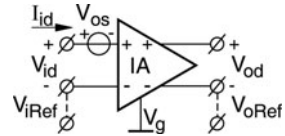


**Fig. 10.1.2** Instrumentation amplifier (IA),  $V_{id} \neq 0$ ,  $I_{id} = 0$ ,  $I_{ic}(CM) = 0$ ,  $V_{od} = A_v V_{id}$ , input CMRR = High



6. Chopping
7. Chopper-Stabilization
8. Chopping + AZ or Chopper-Stabilized
9. Ripple-Reduction Loop RRL
10. Capacitive Coupled Input
11. Gain Accuracy of IA
12. Summary Low Offset

## 10.2 Applications of Instrumentation Amplifiers

All applications of an IA use the combination of accurate gain and high CMRR. The first application example is a general one: to overcome a ground loop. This occurs when we want to transfer a voltage signal referred to a different ground potential  $V_{sRef}$  than that of the destination potential  $V_{oRef}$ . The situation is depicted in Fig. 10.2.1.

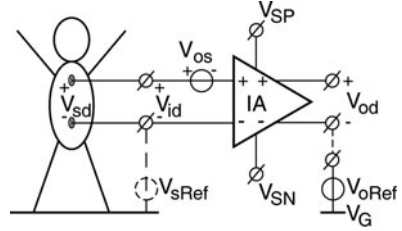
This is the case, for instance, when an instrument has to interface a sensor, like a thermocouple, that is connected to a remote ground. The small output voltage of the thermocouple requires a low offset voltage of the amplifier, while the remote ground can have a large potential difference in regard with the ground of the sensing instrument. This requires a high CMRR.

A second common application is the interfacing of the differential output voltage  $V_{Bd}$  of a sensor bridge that has a large common-mode voltage  $V_{BCM}$ , as shown in Fig. 10.2.2. Accuracy and low offset of the measurement in this application is of high priority.

A third application example is monitoring the voltage  $V_{Rsd}$  across a current-sense resistor  $R_s$  in supply lines of battery powered systems like cell phones and



**Fig. 10.2.4** Instrumentation amplifier for interfacing medical electrodes



### 10.3 Three-OpAmp Instrumentation Amplifiers

The most common approach to an IA is the three-OpAmp topology as shown in Fig. 10.3.1 (see Fig. 3.2.2. in Sect. 3.2).

The actual IA consists of an OA that is feedback by a resistor bridge network  $R_{11}$ ,  $R_{12}$ ,  $R_{13}$  and  $R_{14}$ . If the bridge is in balance, the gain for differential signals is:

$$A_d = -R_{12}/R_{11} \approx R_{14}/R_{13} \tag{10.3.1}$$

To achieve a high input impedance, buffer amplifiers  $OA_2$  and  $OA_3$  have been placed in front of the bridge resistors. These amplifiers are connected in a non-inverting gain configuration with  $R_{21}$ ,  $R_{22}$ , and  $R_{23}$ . Their extra gain is:

$$A_{d2} = (R_{21} + R_{22} + R_{23})/R_{21} \tag{10.3.2}$$

The total voltage gain is:

$$A_V = (R_{21} + R_{22} + R_{23})R_{12}/(R_{11}R_{21}) \tag{10.3.3}$$

The main problem of the three OpAmp approach is the CMRR. In this topology the CMRR is dependant on the matching of the feedback bridge resistors, as explained in Sect. 3.2:

$$CMRR = (R/\Delta R)A_V \tag{10.3.4}$$

in which  $\Delta R/R$  is the relative error in one of the bridge resistors in regard to its ideal value if the bridge were balanced. For instance:

$$\Delta R_{11}/R_{11} = 1 - R_{12}R_{13}/(R_{11}R_{14}) \tag{10.3.5}$$

Another shortcoming of the three-OpAmp approach is that the input CM range can not include the negative nor positive supply rail voltage. This is the consequence of the feedback connection from the output of the input buffer amplifiers  $OA_2$  and  $OA_3$  to their inputs. Only when a level shift is built-in in the positive input modes of these amplifiers one of the rail voltages can be reached.

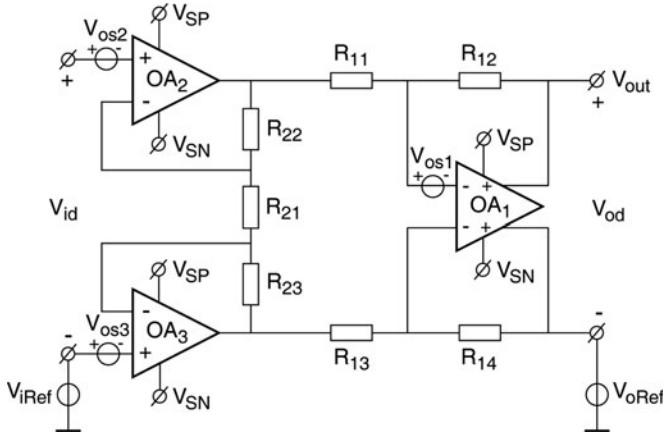


**Fig. 10.3.1** Three-OpAmp instrumentation amplifier with resistor-bridge feedback and input buffer amplifier

### 10.4 Current-Feedback Instrumentation Amplifiers

The fundamentally best way to achieve a high CMRR is to convert the differential input signal  $V_{id}$  into a type of signal that is insensitive to the CM voltage  $V_{iCM}$ . Such a signal could be a magnetic signal in a transformer, or a light signal between a light-emitting and light-sensing diode. But when we stay closer to the electrical domain, also an electrical current signal could be used, if we can make it sufficiently insensitive for the CM voltage. For a circuit on a chip the last method is preferable. Therefore the differential input voltage  $V_{id}$  is converted into a current and compared with the current from the conversion of the feedback part  $V_{fb}$  of the output voltage  $V_o$ . The architecture is called current-feedback amplifier [10.3], and is shown in Fig. 10.4.1.

The first voltage-to-current converter  $G_{m21}$  converts the differential input voltage  $V_{id}$  into a first current. The second converter  $G_{m22}$  converts the feedback output signal  $V_{fb}$  into a second current. Both currents are subtracted and compared by a control amplifier  $G_{m1}$  that drives the output voltage. A resistor divider  $R_2, R_1$  determines the part  $V_{fb}$  of the output voltage  $V_o$  that is fed back. The gain of the whole amplifier will be:

$$A_V = (G_{m21}/G_{m22})(R_2 + R_1)/R_1 \tag{10.4.1}$$

Often we can not easily make the transfer of  $G_{m21}$  and  $G_{m22}$  accurately different. But we can make  $G_{m21}$  and  $G_{m22}$  accurately equal. In that case the gain of the amplifier simplifies to:

$$A_V = (R_2 + R_1)/R_1, \quad \text{while: } G_{m21} = G_{m22} \tag{10.4.2}$$

**Fig. 10.4.1** Current-feedback instrumentation amplifier

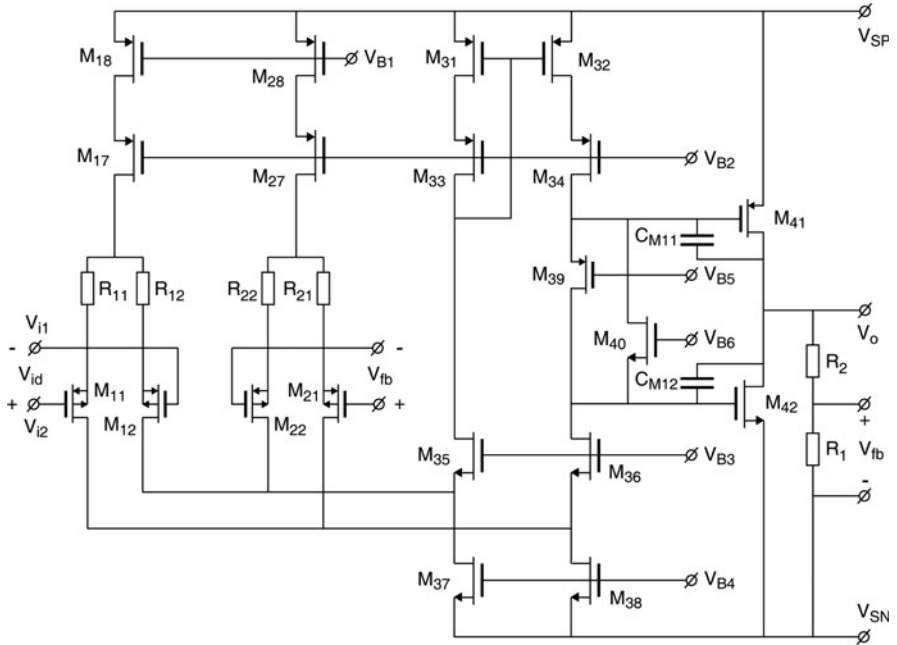
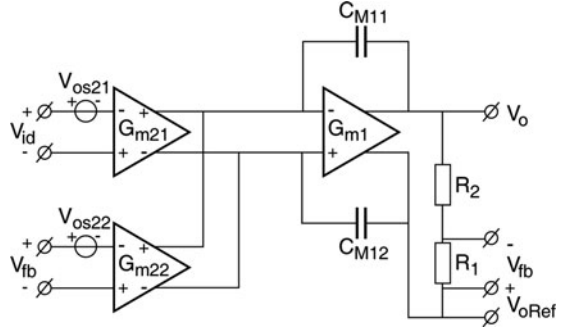


**Fig. 10.4.2** Simple circuit-diagram of an current-feedback instrumentation amplifier

The CMRR is now not determined by matching of main elements but just by the ratio of the  $G_m$  and small parasitic conductances, which keep the CMRR large.

The InstAmp is Miller compensated by the capacitors  $C_{M11}$  and  $C_{M12}$ .

A simple example of an current-feedback InstAmp is given in Fig. 10.4.2.

The input and feedback VI converters are as simple as possible. They can be degenerated to increase the differential input voltage range if needed. Their linearity is not good in itself, but they match quite well for gain accuracy. The input CM voltage range may include the negative supply-rail voltage  $V_{SN}$ . This allows the output voltage  $V_o$  being referenced to  $V_{SN}$ . The input stages are followed

by folded cascodes with a current mirror at their upper end. The push-pull output transistors are biased in class-AB by a class-AB mesh composed from  $M_{39}$  and  $M_{40}$  and proper bias voltages  $V_{B5}$  and  $V_{B6}$  (see Fig. 5.3.21 in Sect. 5.3).

A general symbol for an current-feedback IA is given in Fig. 10.4.3. It shows that inside the IA there are two  $G_m$  stages: one for the input  $G_{mi}$  and one for the feedback  $G_{mfb}$ .

It is interesting that the output as well as the input has a high CMRR. This means that we can connect the output reference voltage  $V_{oRef}$  terminal to any voltage as shown in Fig. 10.4.4. The voltage across the measuring resistor  $R_M$  and the current through  $R_M$  are not influenced by the voltage on  $V_{oRef}$ . Hence, we obtain a voltage controlled current source at the  $V_{oRef}$  terminal. The whole topology of Fig. 10.4.4 act as an accurate general-purpose V-I converter with a transconductance of  $1/R_M$ . Hence  $I_o = -V_{id}/R_M$ .

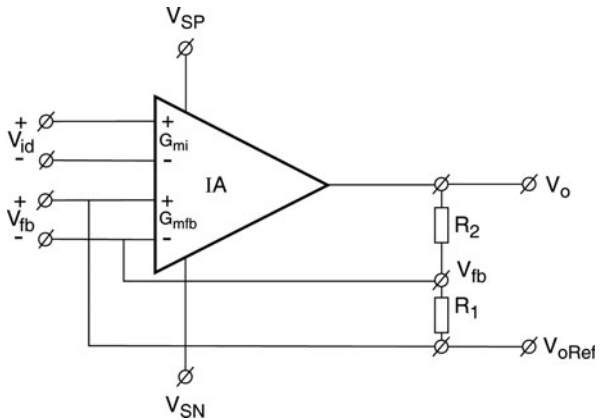


**Fig. 10.4.3** Symbol for an current-feedback instrumentation amplifier

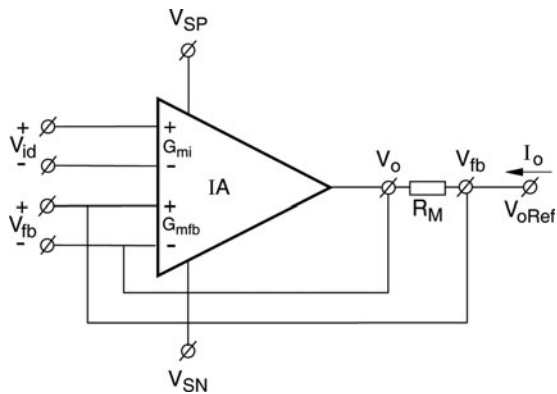


**Fig. 10.4.4** Universal voltage-to-current converter with an current-feedback instrumentation amplifier





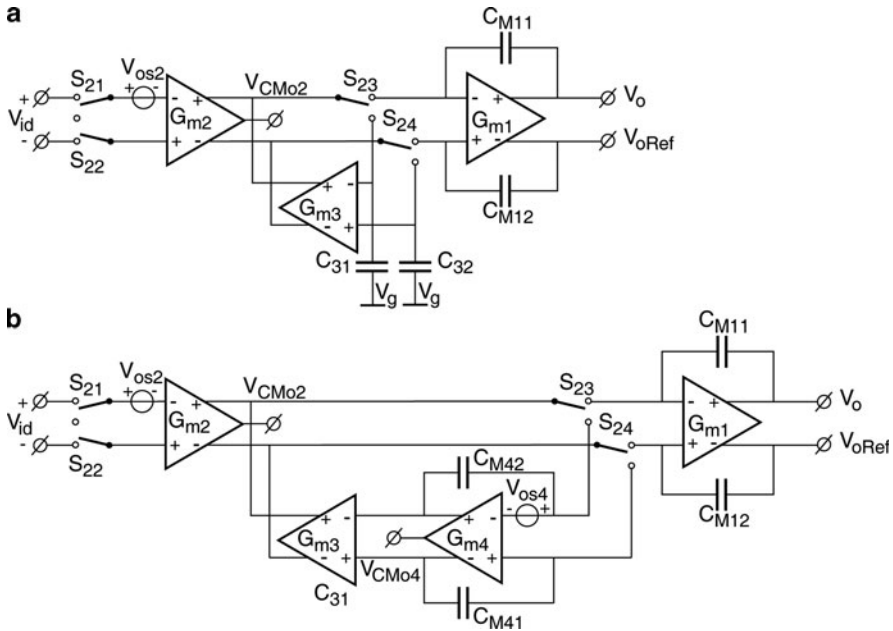
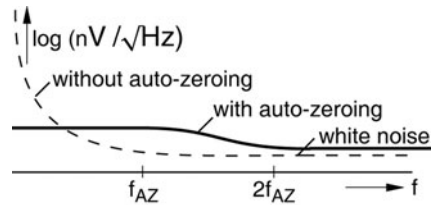


**Fig. 10.5.2** (a) Auto-zero OpAmp with storage capacitors  $C_{31}$  and  $C_{32}$  at the output and correction amplifier  $G_{m3}$ .  $V_{os} \approx 20 \mu V$ . (b) Auto-zero OpAmp with further improved auto-zero storage by an active integrator.  $V_{os} \approx 10 \mu V$

**Fig. 10.5.3** Noise densities with and without auto-zeroing



Very important is that the auto-zero action removes offset and  $1/f$  noise. But, extra noise  $V_{naz}$  is added in the frequency range below  $2f_{AZ}$  due to noise folding back from the bandwidth  $BW$  of the local auto-zero feedback loop. This is depicted in Fig. 10.5.3. Hence it is of importance to keep this  $BW$  not too much above  $2f_{AZ}$ . If the duty-cycle of the auto-zero loop is  $1/2$ , the noise level is at least raised by a factor  $2^{1/2}$ .

$$V_{naz} = V_n(\text{white}) BW^{1/2} / f_{az}^{1/2} + 2^{1/2} V_n(\text{white}) \tag{10.5.1}$$

A problem is that the auto-zero OA has no continuous-time transfer. This means that when the output has to follow a ramp, a staircase with steps at the clock

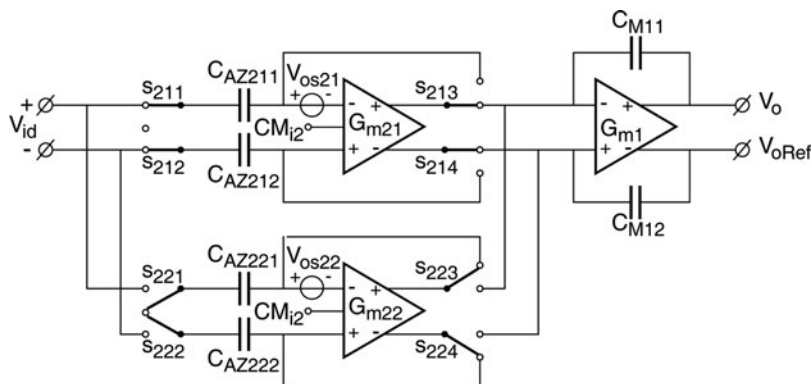


Fig. 10.5.4 Ping-Pong auto-zero OpAmp.  $V_{os} = \sim 100 \mu\text{V}$

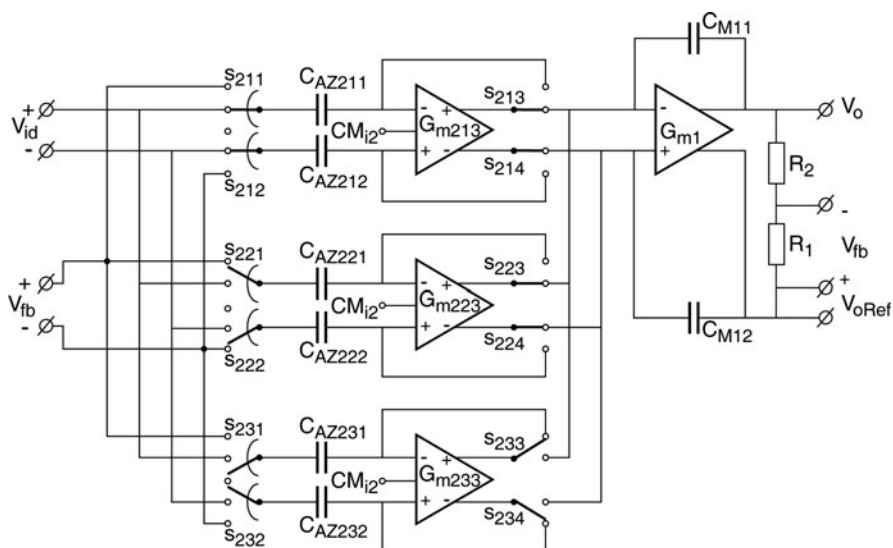


Fig. 10.5.5 Ping-Pong-Pang auto-zero InstAmp.  $V_{os} = 100 \mu\text{V}$

frequency is the result. Moreover, a factor  $2^{1/2}$  must be added to the noise as the amplifier is only used half of the time effectively. To overcome these problems the Ping-Pong auto-zero [10.5] concept of Fig. 10.5.4 has been invented.

In Fig. 10.5.4 two auto-zero input stages  $G_{m21}$  and  $G_{m22}$  alternately are connected between the input and the output stage in order to obtain a continuous-time solution. The stage that is not connected gets time to auto-zero itself. This allows the OA to be generally used in continuous-time feedback configurations.

We can extend the principle of ping-pong to ping-pong-pang in order to obtain a suitable InstAmp topology, as shown in Fig. 10.5.5.

In Fig. 10.5.5 three auto-zero input stages  $G_{21}$ ,  $G_{22}$  and  $G_{23}$  are used. Sequentially, two stages are connected to the output stage  $G_{m1}$ , while one stage is in auto-zero mode. In this way a continuous-time IA is shaped while its offset and  $1/f$  noise is strongly reduced by auto-zeroing.

The limitation of offset reduction is due to parasitic capacitors of capacitors and switches. When the input switches change from auto-zero mode to transfer mode and vice versa, parasitic capacitors to ground are charged and discharged. Any unbalance in this charge will change the offset voltage stored on the AZ capacitors. Offline auto-zero as in Fig. 10.5.2a or Fig. 10.5.2b would therefore be preferable.

In practice the offset can maximally be reduced by a factor on the order of 100 or 1,000 with auto-zeroing, reducing the offset from 10 mV to 100  $\mu$ V or 10  $\mu$ V.

It is very interesting to see that not only the offset voltage is reduced by the AZ function, but any differential input voltage at frequencies lower than the AZ frequency, if the gain is sufficiently large. This means that also the CMRR is drastically increased.

### 10.6 Chopper OpAmps and InstAmps

Before we discuss the chopper IA we will look at the chopper OA [10.6]. This OA one is depicted in Fig. 10.6.1. We suppose a  $6\sigma$  input offset of 10 mV for  $G_{m2}$ .

The choppers  $Ch_2$  and  $Ch_1$  alternatively turn the signals through the input stage  $G_{m2}$  straight and reverse. This means that the input voltage  $V_{id}$  will appear as a continuous-time current at the output. But the input offset voltage  $V_{os2}$  appears as a square wave current, superimposed in the output, as shown in Fig. 10.6.2.

If the OA is placed in a feedback application, the input voltage will show the residual offset voltage with a low-pass filtered square wave ripple on top of it.

In the noise spectra of the offset and  $1/f$  noise are now shifted to the clock frequency  $f_{cl}$  as noise and ripple, as shown in Fig. 10.6.3.

The resulting offset has mainly two origins: Firstly, clock skew in the chopper clocks. If the offset is 10 mV and the clock skew is  $10^{-4}$ , the resulting offset is 1  $\mu$ V. Secondly, the resulting offset is a result of imbalance of parasitic capacitors in the choppers. The parasitic capacitors are shown in Fig. 10.6.4.

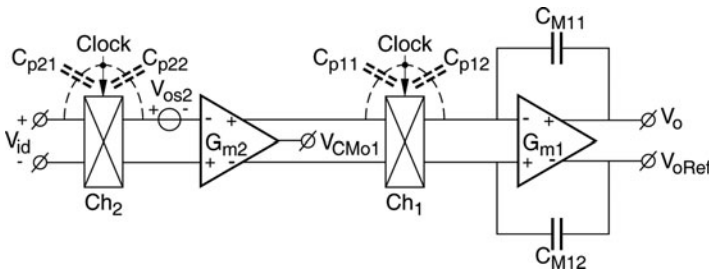
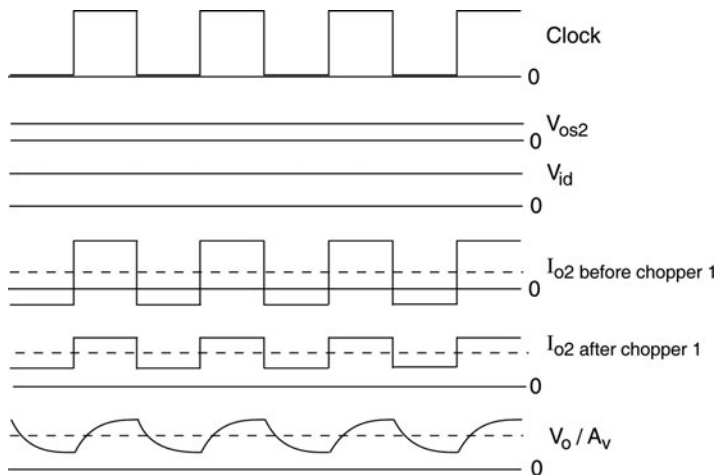
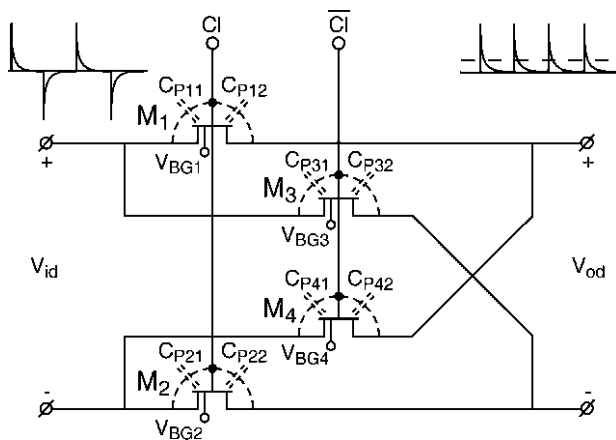
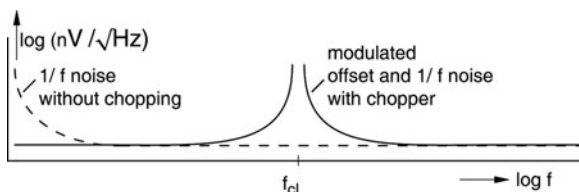


Fig. 10.6.1 Chopper OpAmp with cont-time transfer. Vos =  $\sim 10 \mu$ V, Vrip =  $\sim 10$  mV



**Fig. 10.6.2** Voltage and current signals as function of time in a chopper amplifier

**Fig. 10.6.3** Noise densities in an amplifier with and without chopping



**Fig. 10.6.4** Charge injection current in  $C_{p11}$  of Chopper  $Ch_1$  gets rectified at output

Suppose that chopper  $Ch_1$  (in between the input- and output stage) has only the capacitors  $C_{p11}$  and  $C_{p12}$  around transistor  $M_1$ . The capacitor  $C_{p12}$  produces alternative positive and negative current spikes at the output of the chopper  $Ch_1$ .

This does not contribute to the offset. However, capacitor  $C_{p11}$  also produces alternative spike currents at the input of chopper  $Ch_1$ . When going to the output, these alternative spike currents are being rectified by the function of the chopper  $Ch_1$ .

The rectified spikes represent an average DC current, which is an offset. Fortunately, the chopper is fully balanced. Hence, charge injection from the clock in one transistor cancels that of the other. But every imbalance in layout will cause a net offset. For chopper  $Ch_2$  at the input, the capacitor  $C_{p22}$  injects alternating current spikes on the clock edges. These spikes are translated in rectified input voltage spikes across the series impedances of the chopper and the input signal source. Also these rectified spikes go to the output as a net offset. Practical offset voltage to below  $1 \mu\text{V}$  can be obtained if the choppers, their clock lines, and the signal lines are carefully balanced in the layout. A common practice is to layout the clock lines as coaxial cables on the chip.

In our quest for low offset, noise and ripple we see two contradictory effects. On one hand, the higher the clock frequency, the smaller the ripple at the output and the lower the  $1/f$  noise residue. On the other hand we see a higher residual offset caused by clock skew and charge injection at higher clock frequencies. This contradiction can be relieved by using two choppers in series for each original chopper in a nested chopper configuration [10.7] according to Fig. 10.6.5.

The inner choppers  $Ch_{211}$  and  $Ch_{11}$  can be clocked at a 100 times higher frequency  $Cl_H$  to overcome  $1/f$  noise and ripple, while the outer choppers  $C_{221}$  and  $C_{12}$  are clocked at a 10 times lower frequency  $Cl_L$  to take away the residual offset by the charge injection of the inner choppers. This architecture can lead to offset voltages as low as on the order of  $0.1 \mu\text{V}$ . But a small  $\sim 100 \text{ V}\mu$  filtered input-referred ripple at  $Cl_H$  still remains due to the original offset, and an even smaller ripple at  $Cl_L$  due to charge injection of  $Ch_{11}$ .

An other way to reduce the ripple is to combine an auto-zeroed amplifier in a ping-pong fashion with a chopper amplifier in order to obtain a low-ripple continuous-time signal transfer [10.8]. The block diagram is shown in Fig. 10.6.6a.

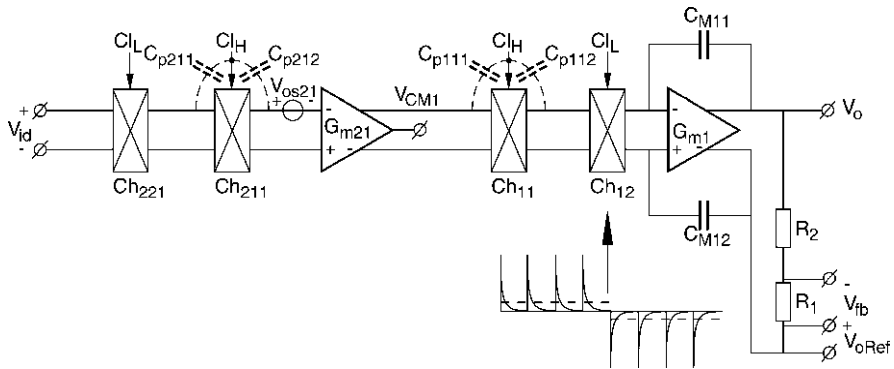
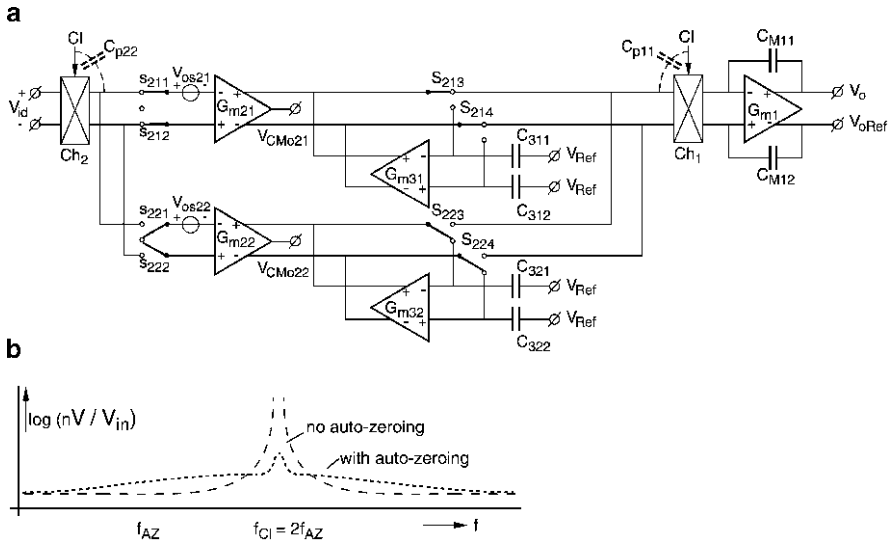


Fig. 10.6.5 Nested-chopper operational amplifier with better compromise between  $1/f$  noise, ripple, and offset.  $V_{os} = \sim 0.1 \mu\text{V}$ ,  $V_{rip} = \sim 100 \mu\text{V}$



**Fig. 10.6.6** (a) Operational chopper amplifier with Ping-Pong auto-zero input stages.  $V_{os} \approx 2\mu V$ ,  $V_{rip} \approx 10\mu V$ . (b) Noise in an operational chopper amplifier with Ping-Pong auto-zero input stages

The choppers Ch<sub>1</sub> and Ch<sub>2</sub> chop the signal alternately positive and negative through the whole set of two ping-pong auto-zeroing amplifiers G<sub>m21</sub> and G<sub>m22</sub>. The switches S<sub>211</sub> through S<sub>222</sub> and S<sub>213</sub> through S<sub>224</sub> sequentially switch the amplifiers G<sub>m21</sub> and G<sub>m22</sub> in a transfer or auto-zero mode in a full clock cycle.

The capacitors C<sub>311</sub> through C<sub>322</sub> differentially store the auto-zero correction voltages. The transconductances G<sub>m31</sub> and G<sub>m32</sub> correct the amplifiers G<sub>m21</sub> and G<sub>m22</sub> for their offsets, respectively. The auto-zero switches S<sub>213</sub> through S<sub>224</sub> switch the outputs of G<sub>m21</sub> and G<sub>m22</sub> between the stored voltages on the auto-zero capacitors and the input offset voltage of the output stage. This causes some extra charge injection. The amplifier achieves an offset of 2 μV and an input referred ripple on the order of 10 μV. The noise of the auto-zero amplifier is now transposed by the choppers to the clock frequency, which keeps the low frequencies cleaner, as shown in Fig. 10.6.6b.

An advantage of the ping-pong continuous-time topology is the simplicity of the frequency compensation. It is restricted to one set of Miller-compensation capacitors.

A chopper instrumentation amplifier can be constructed if we use two input stages G<sub>m21</sub> and G<sub>m22</sub>, each preceded by a chopper, Ch<sub>21</sub> and Ch<sub>22</sub>, respectively. This situation is shown in Fig. 10.6.7.

The gain is:

$$A_v = ((R_1 + R_2)/R_1)(G_{m21}/G_{m22}) \tag{10.6.1}$$

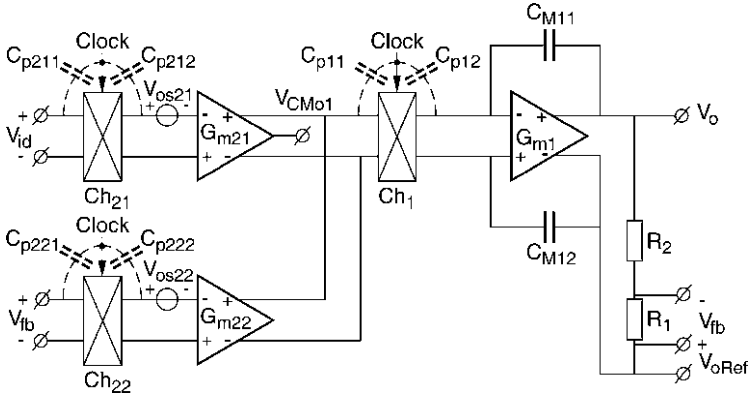


Fig. 10.6.7 Chopper instrumentation amplifier.  $V_{os} = \sim 20\mu\text{V}$ ,  $V_{rip} = \sim 20\text{mV}$

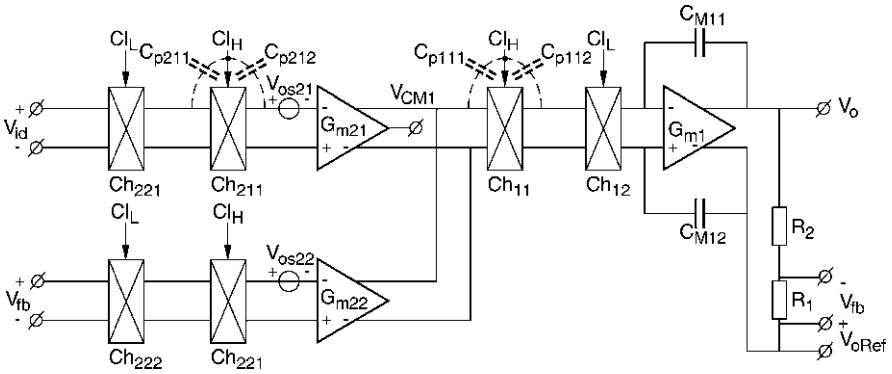


Fig. 10.6.8 Nested chopper instrumentation amplifier with better compromise between  $1/f$  noise, ripple, and offset.  $V_{os} = \sim 0.2\mu\text{V}$ ,  $V_{rip} = \sim 200\mu\text{V}$

The accuracy of the instrumentation amplifier fully depends on the equality of  $G_{21}$  and  $G_{22}$ . In Sect. 10.9 we will discuss ways to increase the accuracy of  $G_m$  stages. Even with an ordinary differential pair in weak inversion, and well matched tail currents, an accuracy better than 1% can easily be achieved without trimming.

The CMRR is also strongly increased by the chopper function for frequencies below the clock frequency. Easily 60 dB can be added to the CMRR by chopping. The improvement is limited, firstly, by the clock skew in the chopper clocks, and secondly, by unequal modulation of the charge injection spikes in the choppers as a function of the CM voltage. The resulting offset can be as low as  $20\mu\text{V}$ , which is twice that of the chopper OpAmp, and an input-referred ripple of  $20\text{mV}$ , which is twice of that of the OpAmp's. The factor 2 is an estimation, and results from the fact that there are two parallel input stages, while each has more offset due to degeneration.

To improve the offset and ripple, we may also apply the nested-chopper [10.7] principle to the chopper instrumentation amplifier, as shown in Fig. 10.6.8. By this



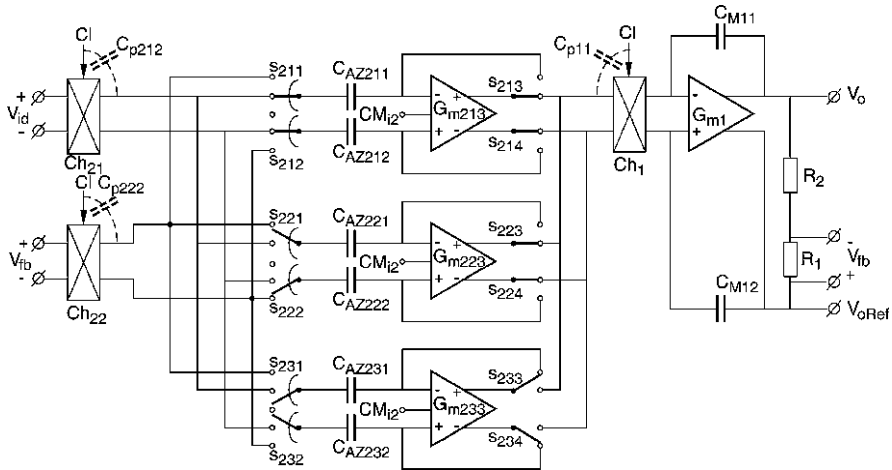


**Fig. 10.6.9** Chopper instrumentation amplifier with Ping-Pong-Pang auto-zero input stages.  $V_{os} = \sim 4\mu\text{V}$ ,  $V_{rip} = \sim 20\mu\text{V}$

a better compromise of chopper ripple and  $1/f$  noise on one hand and residual offset on the other hand can be achieved as explained with Fig. 10.6.5. An offset on the order of  $0.2\ \mu\text{V}$  can be achieved and a residual ripple on the order of  $200\ \mu\text{V}$ .

Finally, just like the chopper OA with ping-pong input stages, the chopper IA can be devised with ping pong-pang input stages, as explained with Fig. 10.5.5. This results in the circuit of Fig. 10.6.9. It roughly can obtain an offset  $V_{os}$  of  $4\ \mu\text{V}$ , and a ripple  $V_{rip}$  of  $20\ \mu\text{V}$ .

## 10.7 Chopper-Stabilized OpAmps and InstAmps

The output ripple from a chopper amplifier invites us to search for ways to reduce it. The chopper-stabilized amplifier is one of the best approaches [10.9]. A basic multipath nested Miller compensated OA topology is suited to incorporate chopper stabilization, as shown in Fig. 10.7.1a.

The basic OA is composed of two stages  $G_{m1}$  and  $G_{m2}$ . The output stage  $G_{m1}$  is differentially Miller compensated by  $C_{m11}$  and  $C_{m12}$ . The input stage  $G_{m2}$  forms the ‘high-frequency’ path. The input stage  $G_{m2}$  has an offset  $V_{os2}$ . When the OA is placed in a feedback loop, the offset  $V_{os2}$  appears at the input.

This input error voltage  $V_{id}$  is now measured and corrected by the chopper amplifier’s ‘gain’ path. This path starts with an input chopper  $Ch_2$  that translates the input error voltage  $V_{id}$  into a square wave. The sense amplifier  $G_{m5}$  produces a square-wave output error current proportional to  $V_{id}$  together with a DC output current due to its own DC offset  $V_{os5}$ . The chopper  $Ch_1$  chops the square-wave error current back to a DC error current, while the DC offset current is changed into

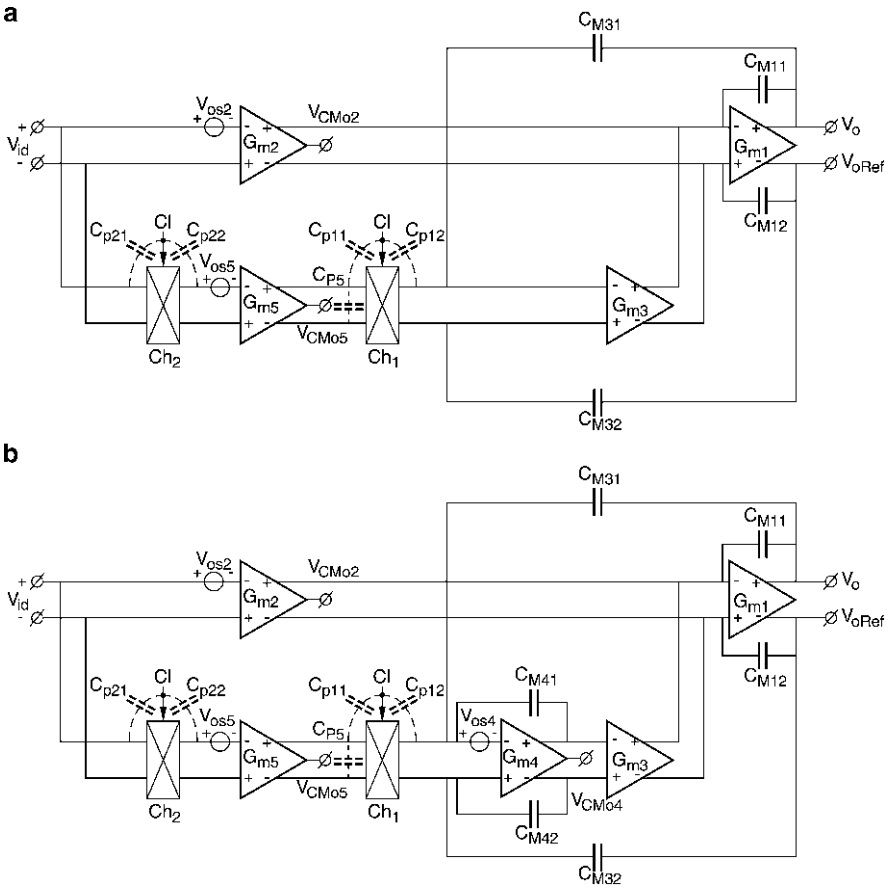


**Fig. 10.7.1** (a) Chopper-stabilized operational amplifier with multipath nested Miller compensation.  $V_{os} = \sim 10\mu V$ ,  $V_{rip} = \sim 10mV$ . (b) Chopper-stabilized operational amplifier with multipath hybrid-nested Miller compensation.  $V_{os} = \sim 10\mu V$ ,  $V_{rip} = \sim 100\mu V$

a square-wave current. The square-wave current due to offset of  $G_{m5}$  is filtered and reduced by the Miller integrator capacitors  $C_{M11}$  and  $C_{M12}$ . While the DC error current as a function of the input error voltage  $V_{id}$  is amplified by the DC gain of the intermediate amplifier  $G_{m3}$ . Finally the output current of  $G_{m3}$  is being added to the output current of the input amplifier  $G_{m2}$  in order to compensate its offset. It should be noted that the output CM levels of  $G_{m2}$  and  $G_{m5}$  have to be controlled to a CM level.

We have now obtained a two path amplifier: a high frequency low gain path through  $G_{m2}$ , and a low-offset low-frequency high gain path through  $G_{m5}$  and  $G_{m3}$ . The offset can only be reduced to the extent that the high-gain path has a higher gain than the low-gain path.

The above circuit has two shortcomings: Firstly, the gain of  $G_{m3}$  is only roughly 20% of that of  $G_{m2}$ , as this amplifier should be able to correct the offset of  $G_{m5}$  while not adding too much noise. This means that the offset is not reduced so much. Secondly, the integration function of the outer Miller capacitances  $C_{M31}$  and  $C_{M12}$  is not strong, particularly not at low overall closed loop gains where the overall closed bandwidth through the low-frequency path of  $G_{m5}$  is larger than the clock frequency. In that case the square-wave ripple at the input has nearly the full size of the initial offset of the offset sense amplifier  $G_{m5}$ .

For the above reasons it is much better to step on to the multipath hybrid nested Miller compensated OA of Fig. 6.2.22a which has an extra integrator in the ‘gain path’. This circuit with chopper stabilization is given in Fig. 10.7.1b. The extra integrator, firstly, is able to strongly reduce the ripple, and secondly, provides much more gain. The square-wave current due to offset of  $G_{m5}$  is strongly filtered out by the integrator  $G_{m4}$ . The integrator time constant can be chosen freely by the value of the integrator capacitors  $C_{M41}$  and  $C_{M42}$ . The residual ripple at the output of integrator  $G_{m4}$  is further reduced by the relative weak  $G_{m3}$ . The DC error current as a function of the input error voltage  $V_{id}$  is integrated and strongly amplified by the DC gain of the integrator  $G_{m4}$ . The integrated error voltage at the output of  $G_{m4}$  is added to the output current of the input amplifier  $G_{m2}$  through  $G_{m3}$  in order to compensate the offset of  $G_{m2}$ .

One of the old struggles with chopper-stabilization is that the two poles in the gain path lead to a non-straight 6 dB per octave roll-off, as shown in Fig. 10.7.2.

This problem can be solved in practice by applying the principle of hybrid nesting as described in Sect. 6.2 [10.10]. To that end we connect two differential hybrid-nested Miller capacitors  $C_{M31}$  and  $C_{M32}$  from the final output to the input of the integrator  $G_{M4}$ .

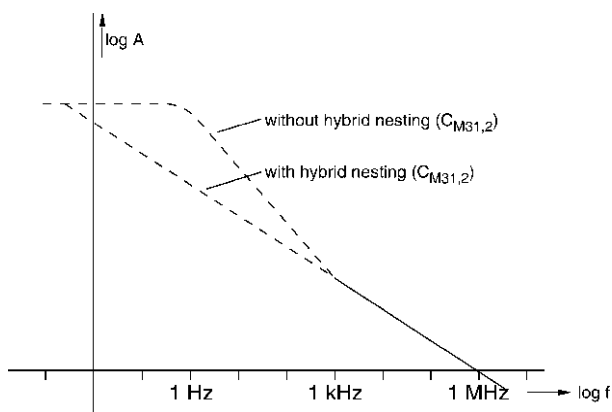


**Fig. 10.7.2** Amplitude characteristic of a chopper-stabilized amplifier with and without hybrid-nested Miller capacitors  $C_{M31}$  and  $C_{M32}$

If we choose the bandwidth of the two-stage Miller-compensated HF amplifier path equal to the bandwidth of the four-stage hybrid-nested Miller loop, the overall frequency characteristic becomes straight form very low frequencies to the bandwidth of the OA. Therefore we choose  $G_{m2}/(C_{M11} \text{ in series with } C_{M12}) = G_{m5}/(C_{M31} \text{ in series with } C_{M32})$ . The result is a straight frequency characteristic, as shown in Fig. 10.7.2.

The low-frequency behavior, and thus the offset of the whole amplifier is determined by that of the chopper loop. That means that we have to carefully balance the parasitic capacitors  $C_{p11}$  and  $C_{p22}$  of the choppers  $Ch_1$  and  $Ch_2$ , respectively, and their lay-out. Also the clock skew of the chopper clocks determine the offset. If the clock skew is  $10^{-4}$ , and the  $6\sigma$  offset of the chopper amplifier is 10 mV, an offset of 1  $\mu$ V is resulting.

There is one more source of offset we have to watch for. That is caused by a combination of the parasitic capacitor  $C_{p5}$  between the outputs of  $G_{m5}$  and the offset  $V_{os4}$  of the integrator amplifier. The chopper  $Ch_1$  chops this offset voltage up and down each chopper period on  $C_{p5}$ , while it rectifies its charge current into a DC value  $I_{p5}$  at the input of the integrator equal to:

$$I_{p5} = 4 V_{os4} C_{p5} f_{cl} \quad (10.7.1)$$

This current cannot be distinguished anymore from the DC output current of the chopper sense amplifier that is also presented at the input of the integrator. The resulting input offset  $V_{osi}$  is:

$$V_{osi} = I_{p5}/G_{m5} = 4 V_{os4} C_{p5} f_{cl}/G_{m5} \quad (10.7.2)$$

The resulting offset is smaller than 1  $\mu$ V referred to at the input, only if we take measures to make  $C_{p5}$  small, i.e., in the order of 0.1 pF. We can always chopper-stabilize or auto-zero-stabilize the integrator amplifier to further reduce this offset term.

The input referred ripple has now been reduced by a factor 100 from a square wave of about 10 mV in the chopper amplifier into a triangle wave of about 50  $\mu$ V in the chopper-stabilized amplifier. If we want to decrease the ripple further, we can auto-zero the chopper amplifier [10.11], as shown in Fig. 10.7.3.

We have now a combination of a chopper-stabilized amplifier in which the chopper amplifier is auto-zeroed. In this way the ripple can further be reduced to the 1  $\mu$ V level. The noise spectrum of such an amplifier is shown in Fig. 10.7.4. It still suffers from noise folding and a factor 22 from a duty-cycle of 50%. But at higher frequencies the HF path through  $G_{m2}$  takes over and the noise reaches its thermal floor.

An interesting alternative way to reduce the ripple is using a sample-and-hold after the integration [10.12], as shown in Fig. 10.7.5.  $V_{os} = \sim 3\mu$ V,  $V_{rip} = \sim 20\mu$ V.

In this design two passive integrators have been connected as a ping-pong sample and hold with  $C_{41}$ ,  $C_{42}$ , and  $C_H$ . The design is simple and elegant and has an offset of 3  $\mu$ V, while the ripple is on the order of 10  $\mu$ V.

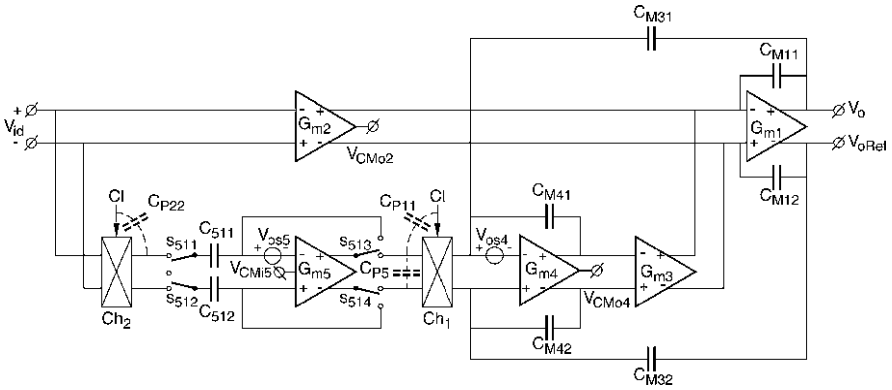


**Fig. 10.7.3** Ch-stab. OpAmp with auto-zero  $G_{m5}$ .  $V_{os} = \sim 1\mu V$ ,  $V_{rip} = \sim 10\mu V$

**Fig. 10.7.4** Noise densities of a chopper-stabilized multi-path instrumentation amplifier with and without auto-zeroing

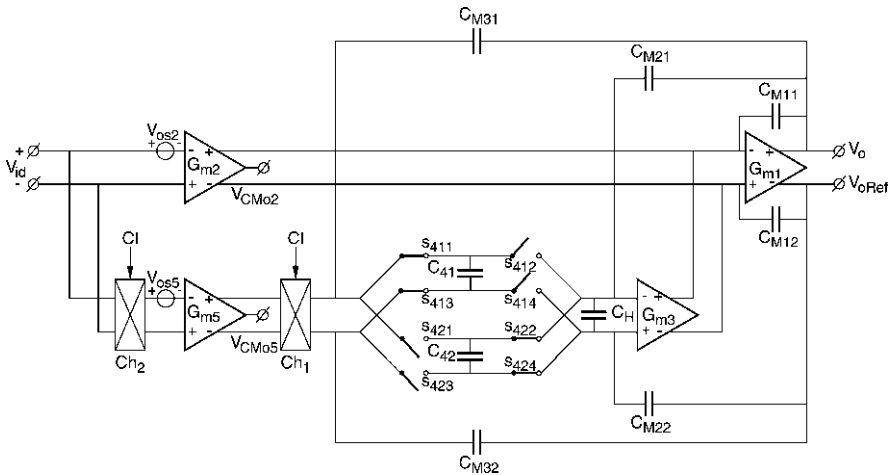
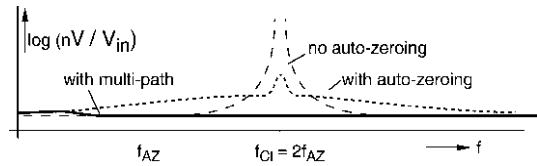


**Fig. 10.7.5** Chopper-stabilized OpAmp with passive integrator and sample & hold. (Rod Burt),  $V_{os} = \sim 3\mu V$ ,  $V_{rip} = \sim 20\mu V$

Now, the step has to be made to an instrumentation amplifier. Therefore the chopper-stabilized OA must be transformed into the current-feedback IA architecture [10.13]. The circuit is shown in Fig. 10.7.6.

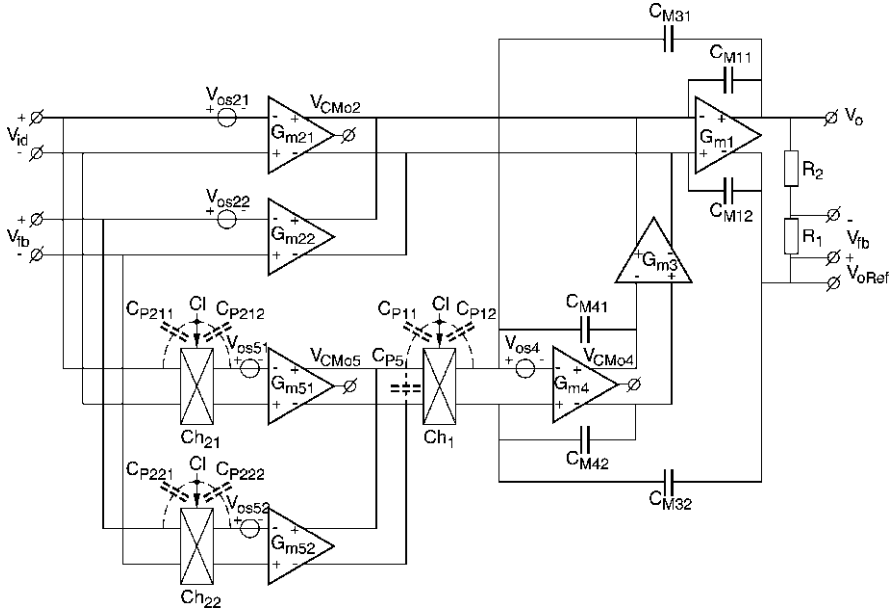


**Fig. 10.7.6** Chopper-stabilized InstAmp with multipath hybrid-nested Miller comp.  $V_{os} = \sim 20\mu V$ ,  $V_{rip} = \sim 200\mu V$

The IA has a HF path through  $G_{m21}$  and  $G_{m22}$  and a LF gain path through  $G_{m51}$  and  $G_{m52}$ . The LF gain path not only determines the offset and CMRR, but also sets the gain accuracy at low frequencies.

The gain at low frequencies is:

$$A_{VL} = (G_{m51}/G_{m52})(R_1 + R_2)/R_1, \tag{10.7.3}$$

and at high frequencies:

$$A_{VH} = (G_{m21}/G_{m22})(R_1 + R_2)/R_1 \tag{10.7.4}$$

An offset in the order of  $20\ \mu V$  and a ripple of out  $200\ \mu V$  can be obtained. The offset and ripple is a factor  $2^{1/2}$  larger than in the OA case because we have two input stages in parallel in both the HF and LF gain path. Also, also the noise is  $2^{1/2}$  times larger than in the OA case.

If we want to further reduce offset and ripple the chopper amplifiers can be auto-zeroed as in the OA case [10.13]. The resulting block diagram is shown in Fig. 10.7.7.

This topology may result in an input referred offset voltage lower than  $2\ \mu V$  and a ripple lower than  $20\ \mu V$ .

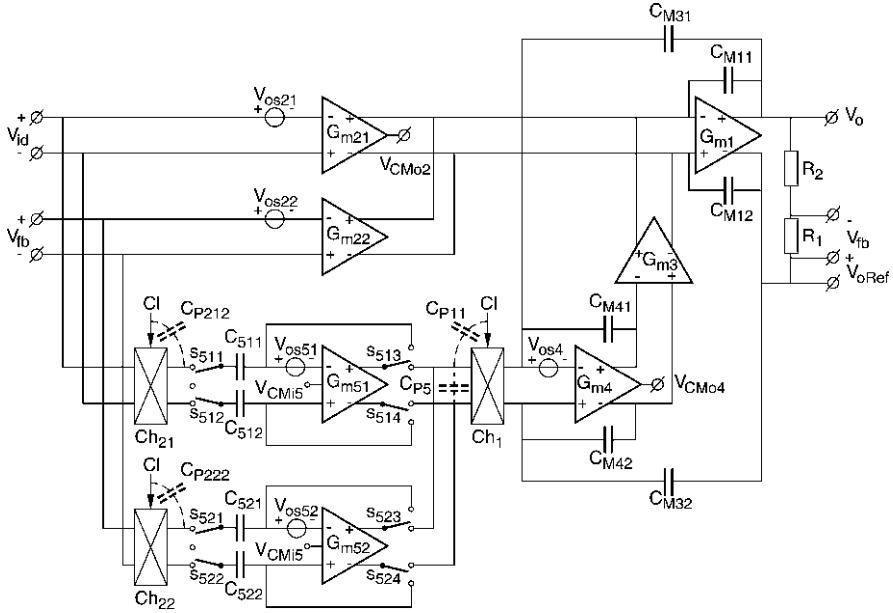


**Fig. 10.7.7** Chopper-stabilized InstAmp with auto-zero sense amplifiers.  $V_{os} = \sim 2\mu V$ ,  $V_{rip} = \sim 20\mu V$

### 10.8 Chopper-Stabilized and AZ Chopper OpAmps and InstAmps

The smooth continuous-time chopper amplifier is the best approach to low offset. However, a 0.01% clock skew multiplied by an initial  $6\sigma$  offset voltage of 10 mV of the first stage of a CMOS amplifier presents a lower limit to the residual offset on the order of 1  $\mu V$ . Moreover, the initial offset voltage on the order of 10 mV at  $6\sigma$  results in an input-referred chopper square wave ripple of 10 mV. Hence, the ripple and offset of the input amplifier must be further reduced.

The next step of improvement is to chopper-stabilize the chopper amplifier [10.14]. The topology is shown in Fig. 10.8.1.

If an amplifier has a high loop gain the differential input voltage becomes zero, except for the input offset voltage. This means in the case of the chopper-stabilized chopper amplifier of Fig. 10.8.1 that the right-hand side of chopper  $Ch_2$  sees  $V_{os2}$ . Hence, the left-hand input side carries a square wave voltage equal to  $V_{os2}$ . This allows us to directly connect the correction amplifier  $G_{m5}$  to the input without extra chopper. We do not need to discuss the chopper-stabilizer loop anymore, because we already discussed this at Fig. 10.7.1. However, there are major differences.

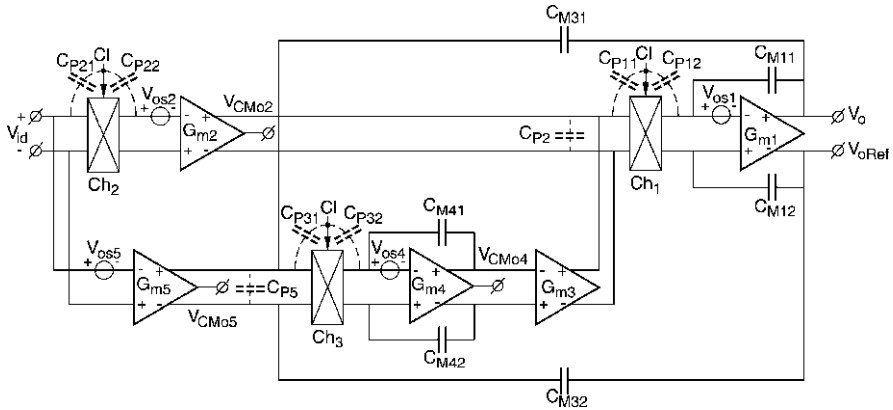


**Fig. 10.8.1** Chopper-stabilized chopper OpAmp with multipath hybrid-nested Miller compensation.  $V_{os} = \sim 1\mu V$ ,  $V_{rip} = \sim 50\mu V$

Firstly, the first stage of the main amplifier now determines the noise at low and high frequencies, while the correction loop determines the noise and ripple at the clock frequency.

Secondly, the hybrid nested capacitors  $C_{M31}$  and  $C_{M32}$  are not anymore connected to the input of the integrator, but to the input of chopper  $Ch_3$ , in order to maintain continuous negative feedback in the loop including  $Ch_1$  [10.10]. This means that the parasitic capacitor  $C_{p5}$ , at the output of the sense amplifier, is now in parallel increased by the series connection of  $C_{M31}$  and  $C_{M32}$ . This parallel combination of capacitors is now charged and discharged by the offset voltage  $V_{os4}$  of the integrator  $G_{m4}$ . To avoid the extra offset of this parallel combination of capacitors in combination with  $V_{os4}$ , either the offset  $V_{os4}$  has to be reduced, or  $C_{M31}$  and  $C_{M32}$  in parallel with  $C_{p5}$  can be reduced by connecting them through a (folded) cascode at the output of  $G_{m5}$  to chopper  $Ch_3$ .

Thirdly, the parasitic capacitor  $C_{p2}$  before chopper  $Ch_1$  is now charged and discharged to the offset voltage  $V_{os1}$  of the output stage  $G_{m1}$ . This causes spikes at the output through the first set of Miller capacitors  $C_{M11}$  and  $C_{M12}$  at the size of  $V_{os1} C_{p2} / C_{M1S}$ , with  $C_{M1S} = C_{M11} C_{M12} / (C_{M11} + C_{M12})$ . Therefore, the parasitic capacitor  $C_{p2}$  at the output of  $G_{m2}$  and  $G_{m3}$  has to be kept small.

The offset of  $G_{m5}$  causes a triangle ripple at the output of the integrator and a saw-tooth like ripple through  $Ch_1$  at the output. This can be eliminated if the offset of the sense amplifier  $G_{m5}$  is auto-zeroed similar to the chopper-stabilized amplifier if Fig. 10.7.3. To further reduce the offset caused by the parasitic capacitor  $C_{p5}$  in combination with the offset of the integrator amplifier  $G_{m4}$  this amplifier can also be auto-zero stabilized by an extra loop around it [10.14]. These features are shown in Fig. 10.8.2. In this way an offset of  $0.1 \mu V$  can be achieved with a ripple lower than  $10 \mu V$ . Nanosecond chopper spikes of several millivolts can still be observed at the output.



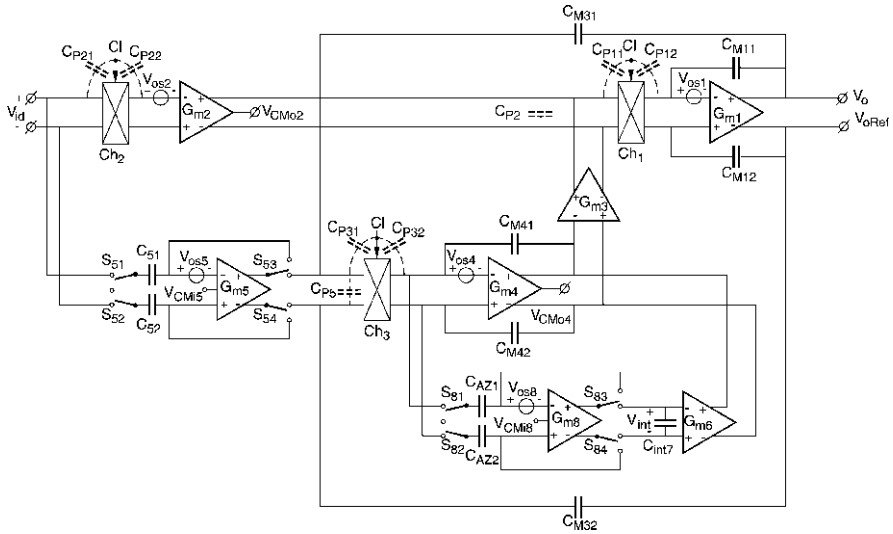


**Fig. 10.8.2** Chopper-stabilized chopper OpAmp with multipath hybrid-nested Miller compensation, auto-zero  $G_{m5}$  and  $G_{m4}$ .  $V_{os} = \sim 0.1\mu V$ ,  $V_{rip} = \sim 10\mu V$

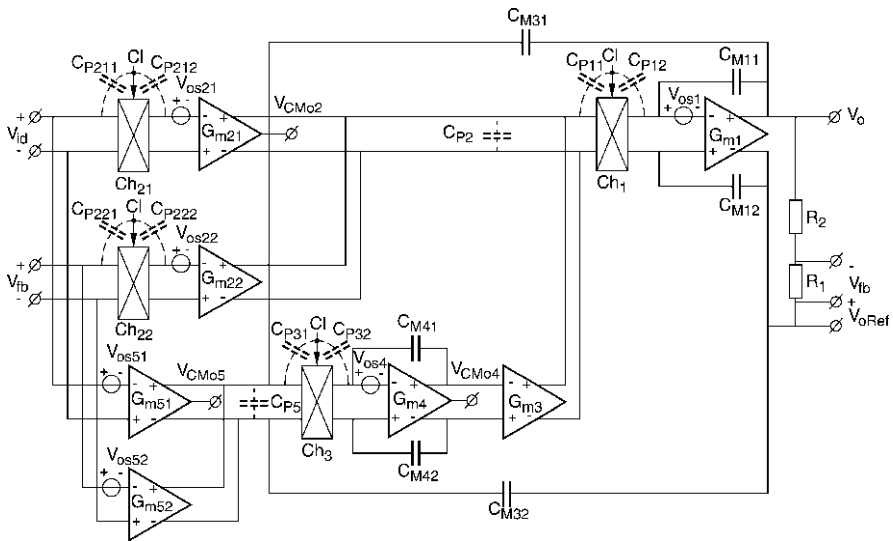


**Fig. 10.8.3** Chopper-stabilized chopper InstAmp with multipath hybrid-nested Miller compensation.  $V_{os} = 2\mu V$ ,  $V_{rip} = \sim 200\mu V$

A chopper-stabilized chopper instrumentation amplifier appears when the HF and LF amplifier paths are doubled [10.15] according to Fig. 10.8.3. In contrast to the chopper-stabilized IA of Sect. 10.7, the gain in a chopper IA is not set by the

ratio of  $G_{m51}$  and  $G_{m52}$  of the correction loop, but by the ratio of  $G_{m21}$  and  $G_{m22}$  of the main amplifier in cooperation with the feedback network.

$$A_v = G_{m21}(R_1 + R_2)/G_{m22}R_1 \tag{10.8.1}$$

The reason that the sense amplifiers  $G_{m51}$  and  $G_{m52}$  do not determine the gain by their ratio is because their influence is shifted to the clock frequency by the choppers around the main amplifiers  $G_{m21}$  and  $G_{m22}$ .  $G_{m52}$  is sensing the feedback ripple as a result of the offset of  $G_{m21}$  and  $G_{m22}$ . The output current of  $G_{m52}$  is rectified by chopper  $Ch_3$  and amplified by the integrator  $G_{m4}$  and coupled by  $G_{m3}$  to the output of  $G_{m21}$  and  $G_{m22}$  in order to compensate the offset of  $G_{m21}$  and  $G_{m22}$  in the main chopper path. The feedback signal-dependant part at the input of  $G_{m52}$  is compensated for by the signal-dependant part at the input of  $G_{m51}$ . Therefore the signal does not interfere with the offset cancellation.

The offset of the correction amplifiers  $G_{m51}$  and  $G_{m52}$  is chopped into a square wave by chopper  $Ch_3$ . The integrator does not amplify this square wave, but reduces it into a small triangular wave. Referred to the input it is translated by an attenuation of  $G_{m3}/G_{m21}$  and a chopper  $Ch_{21}$ . This means that the shape at the input results in a small saw-tooth at the double clock frequency.

The next step to reduce the saw-tooth ripple is to auto-zero the sense stages  $G_{m51}$  and  $G_{m52}$  [10.15]. This is shown in Fig. 10.8.4.

The most important offset contribution of the chopper-stabilized chopper instrumentation amplifier that is left, comes from the combination of the parasitic

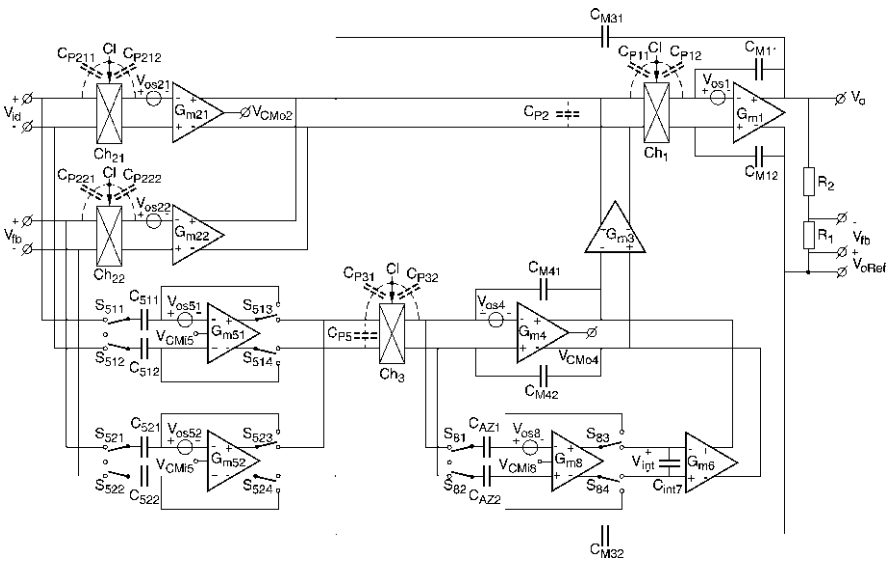


**Fig. 10.8.4** Chopper-stabilized chopper InstAmp with multipath hybrid-nested Miller comp. and auto-zero  $G_{m5}$  and  $G_{m4}$ .  $V_{os} = 0.2\mu V$ ,  $V_{rip} = \sim 20\mu V$

capacitance  $C_{p5}$  at the output of  $G_{m5}$  in combination of the offset voltage  $V_{os4}$  at the input of  $G_{m4}$ , see (10.7.2) This is particularly important as the hybrid nested Miller capacitors  $C_{M31}$  and  $C_{M32}$  are connected in parallel to the parasitic capacitor  $C_{p5}$  at the output of  $G_5$ . To further reduce this offset component also  $G_{m4}$  is auto-zeroed too, as shown in Fig. 10.8.4. In this way the final offset can be reduced to values well below 0.2  $\mu\text{V}$  with a ripple lower than 20  $\mu\text{V}$ .

It has to be kept in mind that the voltage gain of the correction loop  $G_{m5}$ ,  $G_{m4}$ ,  $G_{m3}$  must be taken  $10^5$  times larger than the voltage gain of  $G_{m2}$  in order to reduce its offset from 20 mV to 0.2  $\mu\text{V}$ .

## 10.9 Chopper Amplifiers with Ripple-Reduction Loop

The chopper-stabilized chopper amplifiers of Sect. 10.8 combine low offset, low ripple, and a straight 6 dB/octave frequency characteristic. The latter was obtained by hybrid nested Miller compensation with capacitors  $C_{M31}$  and  $C_{M32}$ , as explained before. An interesting simplification can be made if we do not make use of this basic frequency compensation technique, but if we select a ripple-reduction notch filter to reduce the chopped offset. The notch filter will also take away signals in a small band around the clock frequency. But if we do not care about the notch for signals, for instance because we are only interested in a frequency band below the clock frequency, we can allow ripple reduction by a notch filter.

A chopper amplifier with a feedback ripple-reduction loop (RRL) [10.17] as a notch filter is sketched in Fig. 10.9.1a. The circuit senses the ripple at the output by the sense capacitors  $C_{M31}$  and  $C_{M32}$ . The ripple currents through these capacitors are rectified by synchronous detection to DC by chopper  $\text{Ch}_3$ . The DC current is integrated by integrator  $G_{m4}$  on  $C_{M41}$  and  $C_{M42}$ , and fed back to the output current of  $G_{m2}$  through an amplifier  $G_{m3}$ .

Waveforms of unsettled chopper ripple and sense current in the circuit of Fig. 10.9.1a are shown in Fig. 10.9.1b. The ripple at the output approaches a square wave if the bandwidth of the closed loop gain of the OpAmp is larger than the clock frequency  $f_c$ . But, if the bandwidth of the closed loop gain is smaller than  $f_c$ , the output ripple looks more similar to a triangle wave.

Assuming that the polarity in the feedback RRL is correct and that the loop gain of the RRL is large enough, then the offset voltage  $V_{os2}$  of  $G_{m2}$  will be compensated and the ripple at the output will be reduced to nearly zero. The ripple reduction factor is equal to the DC loop gain of the ripple-reduction loop. The part of the loop through the integrator  $G_{m4}$ , and through  $G_{m3}$  amplifies DC offset correction signals. The part of the loop between the chopper  $\text{Ch}_1$  and chopper  $\text{Ch}_3$  through the output amplifier  $G_{m1}$  carries AC ripple signals at the clock frequency. Chopper  $\text{Ch}_1$  together with the output amplifier  $G_{m1}$  and Miller capacitors  $C_{M11}$  and  $C_{M12}$  can be regarded as a modulating switched-capacitor transimpedance amplifier. This converts the DC current at the input of chopper  $\text{Ch}_1$  into a ripple voltage at the clock frequency at the output with a transimpedance of  $Y_{M1} = 2f_c C_{M1}$ , with

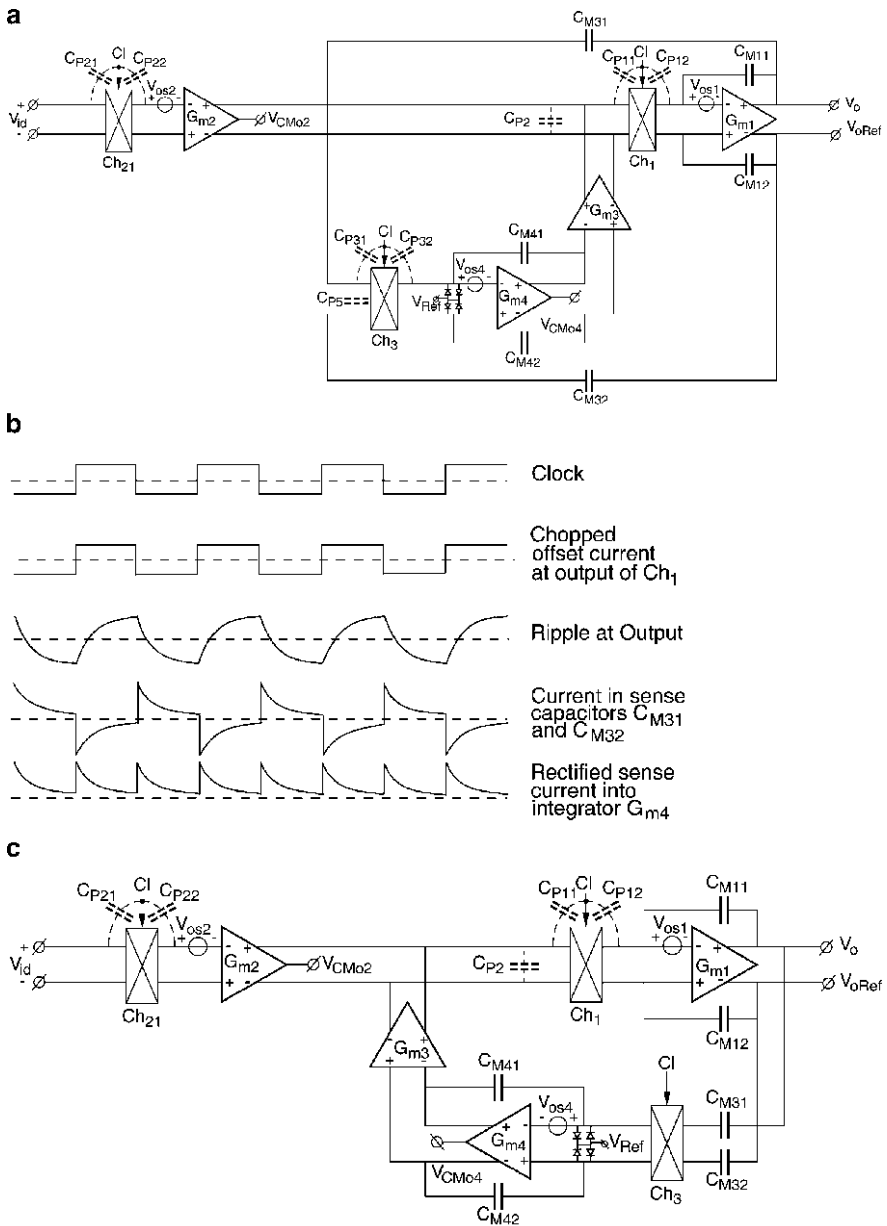


**Fig. 10.9.1** (a) Chopper Opamp with a ripple reduction loop as a notch filter.  $V_{os} = 10\mu V$  (at input),  $V_{orip} = \sim 10mV$  (at output). (b) Waveforms in Fig. 10.9.1. (c) Chopper Opamp with reverse drawn ripple reduction loop as a notch filter.  $V_{os} = 10\mu V$  (at input),  $V_{orip} = \sim 10mV$  (at output)

$C_{M1} = C_{M11} = C_{M12}$ . Sense capacitors  $C_{M31}$  and  $C_{M32}$  in combination with chopper  $Ch_3$  can be regarded as demodulating switched-capacitor impedances  $Z_{M3} = 1/(2f_c C_{M3})$ , with  $C_{M3} = C_{M31} = C_{M32}$ . They convert the output voltage ripple into a DC current that is being integrated on  $C_{M4}$ . The resulting voltage at the output of integrator  $G_{m4}$  thus represents the average rectified output ripple. The gain from the average output ripple voltage to the integrated DC voltage at the output of  $G_{m4}$  is limited to the finite DC gain  $A_{o4}$  of  $G_{m4}$ . The output voltage of  $G_{m4}$  is converted into an offset-compensating current by  $G_{m3}$ . Hence, the DC loop gain  $A_{L0}$  of the ripple-reduction loop and reduction factor  $R_r$  is:

$$R_r = A_{L0} = A_{o4} G_{m3} / 2f_c C_{M1} \quad (10.9.1)$$

If the factor part  $G_{m3}/2f_c C_{M1}$  is estimated at 1, the integrator  $G_{m4}$  needs a DC gain  $A_{o4} = 10^4$ , to obtain a ripple reduction factor  $R_r$  of  $10^4$ .

The bandwidth  $B_L$  of the notch filter at the clock frequency equals twice the frequency  $f_L$  where the AC loop gain  $A_L$  of the ripple-reduction loop is 1. The AC loop gain is:

$$A_L = (C_{M3}/C_{M4})(G_{m3}/2\pi f_c C_{M1}) \quad (10.9.2)$$

Hence, the bandwidth  $B_L$  is:

$$B_L = 2A_L = (C_{M3}/C_{M4})(G_{m3}/\pi C_{M1}) \quad (10.9.3)$$

In practice the bandwidth of the ripple-reduction notch filter is several kilohertz.

When we compare Fig. 10.9.1a with Fig. 10.8.1 we see that the only difference is that in Fig. 10.9.1a the input sense amplifier  $G_{m5}$  has been eliminated. And hence the capacitors  $C_{M31}$  and  $C_{M32}$  do not need to obey the rule for hybrid nesting anymore. They can be optimized for ripple sensing.

The functioning of the ripple-reduction loop (RRL) can be depicted in a simpler way if it is drawn reversed as shown in Fig. 10.9.1c. It clearly shows that the RRL measures the output ripple and feeds the correction signal back to correct the offset of the input transconductance  $G_{m2}$ .

The ripple-reduction loop cancels the ripple originating from the offset  $V_{os2}$  of  $G_{m2}$ . There is another ripple source, which originates from the offset of  $V_{os4}$  of the integrator amplifier  $G_{m4}$ . This is limiting the ripple reduction. The ripple originating from  $V_{os4}$  can be analyzed as follows. The chopper  $Ch_3$  switches the offset voltage  $V_{os4}$  each clock cycle back and forth on the sense capacitors  $C_{M31}$  and  $C_{M32}$ . The resulting alternating charge spikes through these capacitors are rectified by chopper  $Ch_3$  and fed back into integrator  $G_{m4}$ . At the output a ripple will occur with an average square-wave or triangle-wave AC voltage  $V_{orip}$  equal to the offset voltage  $V_{os4}$  of  $G_{m4}$ :

$$V_{orip} = V_{os4} \quad (10.9.4)$$

Referred to the input this roughly results in an equivalent input ripple  $V_{rip}$  of:

$$V_{rip} = V_{os4}2f_c C_{M1}/G_{m2} = V_{os4}f_c/\pi f_0, \tag{10.9.5}$$

in which  $f_0$  is the bandwidth of the amplifier.

One good solution to reduce this ripple is to auto-zero the integrator. One of the many circuits that can auto-zero the integrator is shown in Fig. 10.9.2. For simplicity, the same auto-zero circuit is used as was used in the chopper-stabilized chopper opamp of Fig. 10.8.2. In fact, the only difference with the whole circuit of Fig. 10.8.2 is that the auto-zeroed sense amplifier  $G_{m5}$  has been omitted including its sampling capacitors.

From the above chopper OpAmps with ripple-reduction loop a chopper instrumentation amplifier with RRL can easily be derived. When both sense amplifiers  $G_{m51}$  and  $G_{m52}$  of Fig. 10.8.3 are omitted the InstAmp of Fig. 10.9.3a and b appears.

A disadvantage of the current feedback instrumentation amplifier (CFIA) of Fig. 10.9.3a is that the gain is determined by the ratio of  $G_{m21}$  and  $G_{m22}$ . As these  $G_m$ 's are normally realized by simple differential pairs the accuracy may not be better than 1% without trimming. How to improve the gain accuracy automatically is described in Sect. 10.11.

A simple way to improve the accuracy is to go back to an OpAmp with a resistor bridge around it like described with Fig. 3.2.2. Without chopping, the CMRR would be not better than the inverse of the inaccuracy of the bridge multiplied by the gain setting of the bridge. But, if we chop the bridge as shown in Fig. 10.9.3b the average

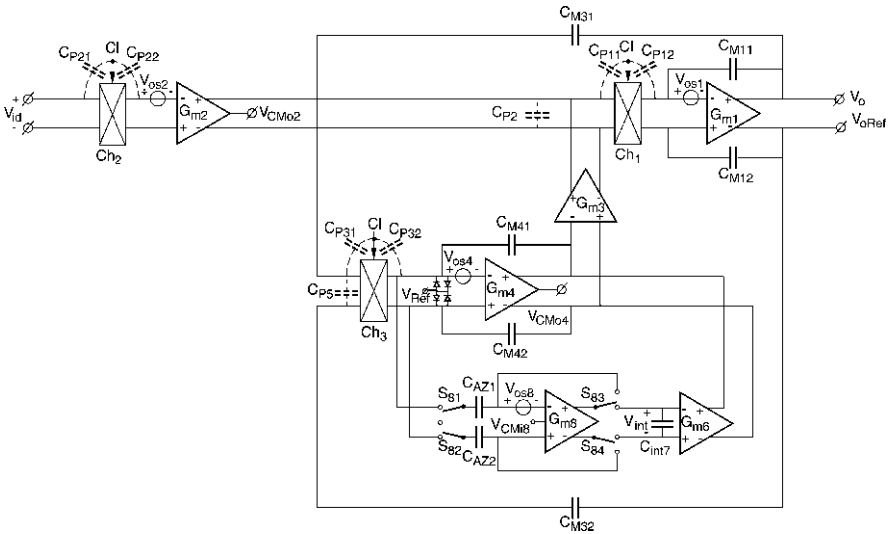


**Fig. 10.9.2** Chopper Opamp with ripple-reduction loop of which the integrator is auto zeroed.  $V_{os} = 1\mu V$ ,  $V_{orip} = \sim 10\mu V$  (at output)

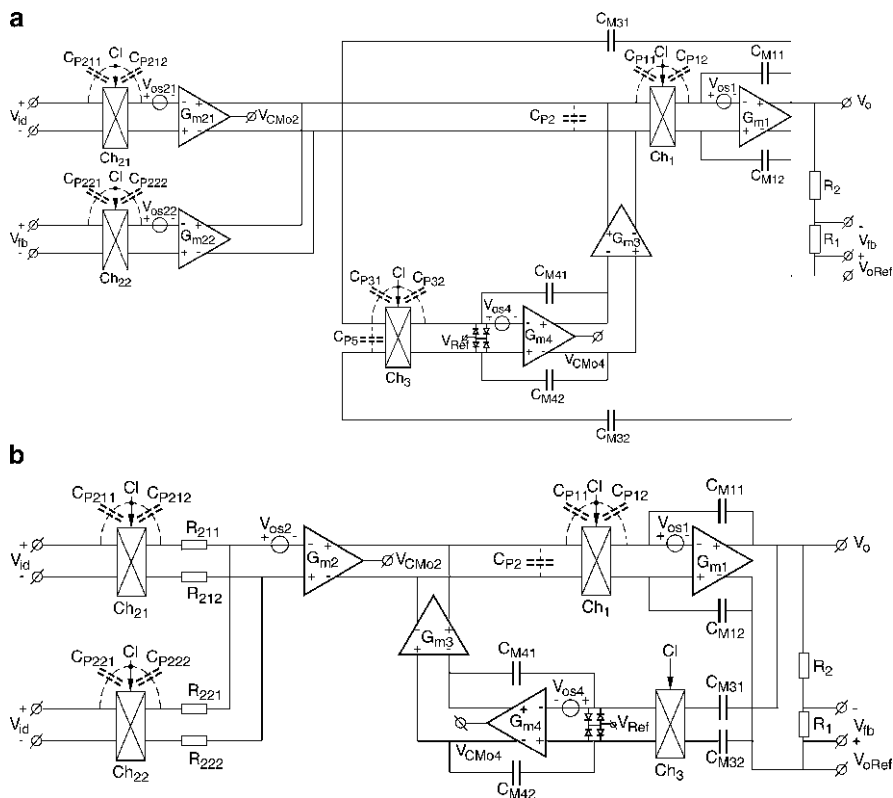


**Fig. 10.9.3** (a) Chopper InstAmp with ripple-reduction loop.  $V_{os} = 20\mu\text{V}$ ,  $V_{orip} = \sim 10\text{mV}$  (at output). (b) Chopper InstAmp with reverse drawn ripple-reduction loop.  $V_{os} = 20\mu\text{V}$ ,  $V_{orip} = \sim 10\text{mV}$  (at output)

CMRR is high, while the ripple is taken away by the RRL. The limitation on the CMRR is in differences of the series resistances of the choppers. These differences are not chopped away. These differences can be seen as differences in signal source resistances which are loaded by the bridge.

Applying auto-zeroing of the integrator the simplification in Fig. 10.9.4 over Fig. 10.8.4 is even clearer, as two auto-zeroed sense amplifiers  $G_{m51}$  and  $G_{m52}$  are omitted.

As an alternative to the auto-zero loop around the integrator  $G_{m4}$  a differential cascode buffer can be inserted between the sense capacitors  $C_{M31}$  and  $C_{M32}$  and chopper  $Ch_3$  [10.17]. The cascode buffer needs to have a low capacitance at the chopper-side output; otherwise the ripple is not reduced so much. Also, the output offset current of the cascode needs to be made low; otherwise  $Ch_3$  will modulate the offset current to the second harmonic of the chopping frequency, and an other type of ripple will appear at the output.

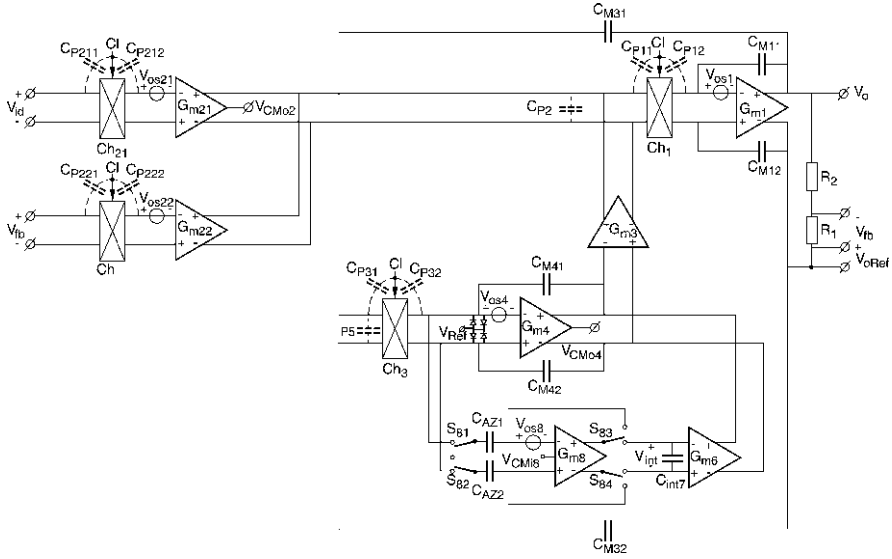


Fig. 10.9.4 Chopper InstAmp with ripple-reduction loop.  $V_{os} = 2\mu\text{V}$ ,  $V_{orip} = \sim 20\mu\text{V}$  (at output)

It is essential that the choppers  $Ch_1$ ,  $Ch_2$  and  $Ch_3$  are precisely synchronized, so that there is not much delay in the amplifier stages. Otherwise the compensation does not work precise and the ripple and resulting offset is larger.

When a signal step occurs the sense capacitors  $C_{m31,32}$  will punch the RRL slightly out of balance. The RRL will work to return to balance. But during this time a reducing ripple is seen at the output. When we want to get rid of this effect, one can built-in a step-sense circuit at the output, and if the step size is larger than a prescribed value, momentarily block the current through the sense capacitors by short-circuit and open-circuit switches.

When we want to eliminate the notch in the frequency characteristic further, and further reduce the chopper spikes of the chopper amplifier with RRL, one can embed it one level down in a chopper stabilized OpAmp topology, as shown in Fig. 10.9.5a. The feed-forward amplifier stage  $G_{m2}$  now bypasses the notch and the ripple at the higher frequencies.

The RRL can be reversely drawn for clarity, as shown in Fig. 10.9.5b.

In order to lower the offset and ripple of the OpAmp to the level of  $V_{os} = 1\mu\text{V}$  and  $V_{orip} = \sim 10\mu\text{V}$  (at output), respectively, the integrator  $G_{m7}$  has to be auto-zeroed likewise shown in Fig. 10.2 [10.20].

Finely, a low-offset, low-ripple InstAmp without notch in the frequency characteristic can be devised from the above OpAmps. This is drawn in Fig. 10.9.6. To lower the offset and ripple to the level of  $V_{os} = 2\mu\text{V}$ ,  $V_{orip} = \sim 20\mu\text{V}$  (at output) the integrator  $G_{m7}$  has to be auto-zeroed. This is a better InstAmp compared with Fig. 10.7.7 in terms of offset, ripple, and noise [10.20].



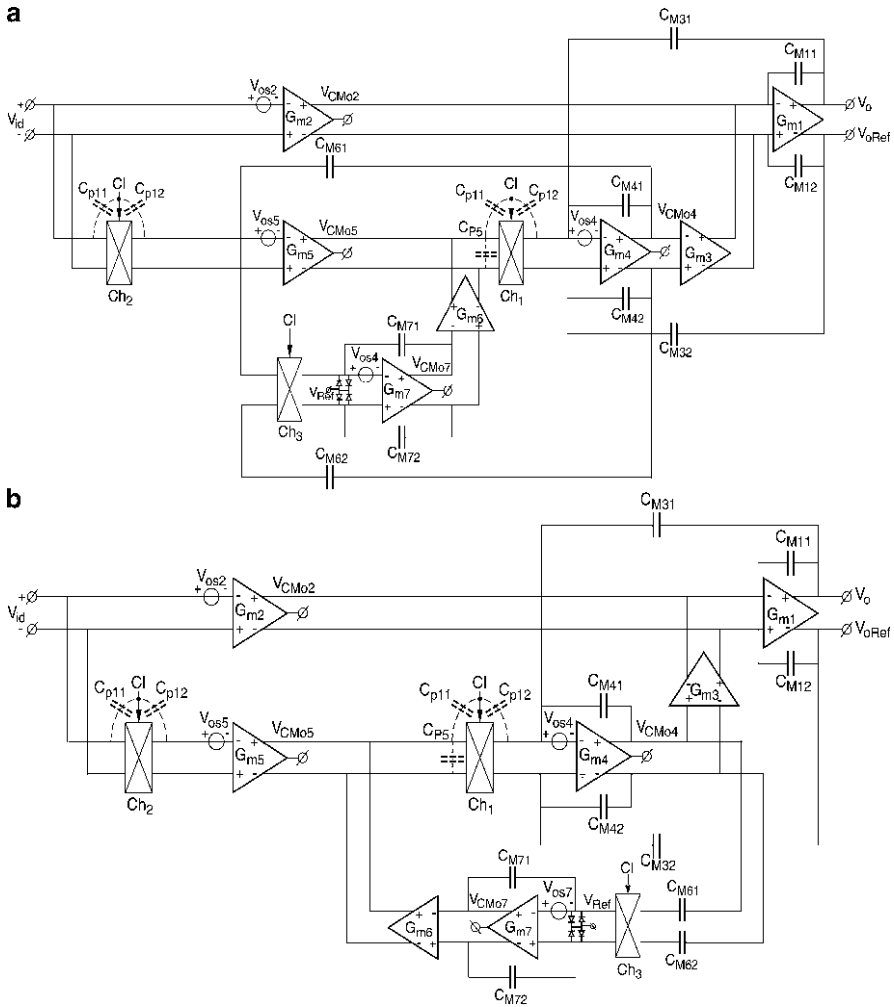


**Fig. 10.9.5** (a) Chopper-stabilized OpAmp with RRL.  $V_{os} = 10\mu V$ ,  $V_{orip} = \sim 100\mu V$  (at output).  $V_{os} = 1\mu V$ ,  $V_{orip} = \sim 10\mu V$  (at output) when  $G_{m7}$  is auto-zeroed. (b) Chopper-Stabilized OpAmp with reversed drawn RRL.  $V_{os} = 10\mu V$ ,  $V_{orip} = \sim 100\mu V$  (at output).  $V_{os} = 2\mu V$ ,  $V_{orip} = \sim 20\mu V$  when  $G_{m7}$  is auto-zeroed

### 10.10 Chopper Amplifiers with Capacitive-Coupled Input

There is an increasing request for interfacing high input CM voltages: Firstly, in high-voltage current-sense applications, such as power management in laptops; secondly, in solenoids of smart electro motors, for instance in electric or hybrid cars; thirdly, in biomedical sensors that make direct electrical contact to the body,

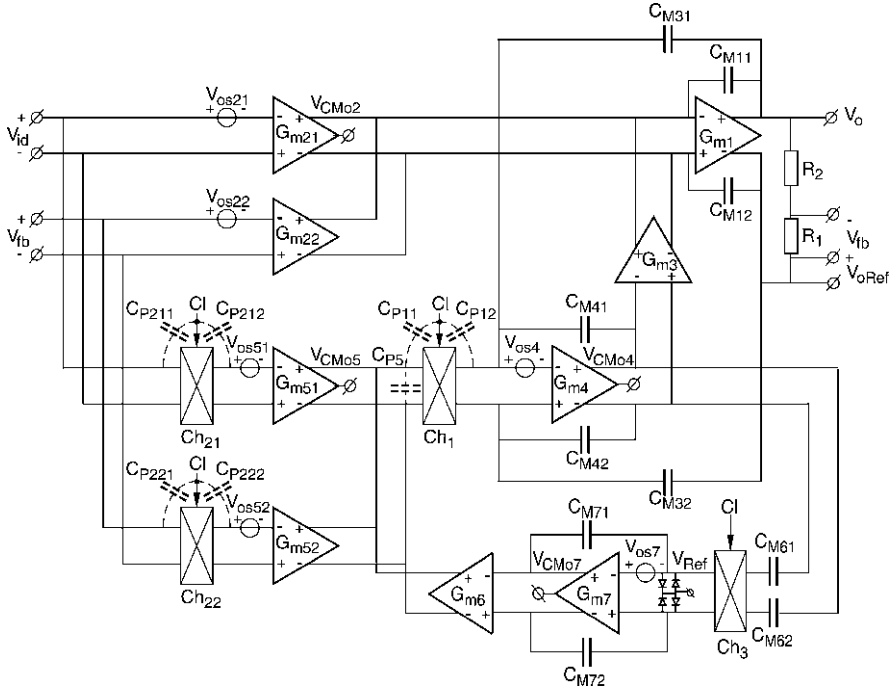


**Fig. 10.9.6** Chopper-Stabilized Instrumentation Amplifier with reversed drawn RRL.  $V_{os} = 2 \mu\text{V}$ ,  $V_{orip} = \sim 20 \mu\text{V}$  (at output) when  $G_{m7}$  is auto-zeroed (not drawn)

as in skin electrodes or implanted devices. Of course, high-voltage transistors can be used. But often the voltage requirements are higher than the values the transistors allow. And in the case of biomedical electrodes it might be the patient safety that forbids direct contact with a transistor’s gate. Therefore it is useful to see how we can transfer signals through on-chip metal-oxide-metal capacitors.

Figure 10.10.1a shows a chopper-stabilized OpAmp like that described at Fig. 10.7.1 with an additional chopper-capacitor-chopper combination as a chopped-capacitor coupled input. At the input the signal voltage is firstly chopped by  $Ch_2$ , next coupled through the capacitors  $C_{21}$  and  $C_{22}$  and finally chopped back by  $Ch_1$  and  $Ch_3$ . The input chopper  $Ch_2$  can be built from low-voltage CMOS transistors in an isolated N-well. Its clock can be differentially driven by two small capacitors from a grounded clock. The CM level of the clock at the chopper side has to be established by diodes coupled to the inputs. Hence, the input chopper  $Ch_2$  can be fully capacitive isolated from ground. To avoid unbalanced signal attenuation in the capacitors  $C_{21}$  and  $C_{22}$  by parasitic capacitances to ground on their bottom plates, these plate sides should be connected to the input chopper  $Ch_2$ . Unbalance in combination with offset will produce an extra ripple.

At the right-hand side of the couple capacitors the CM voltage level must be established at a certain internal level  $V_{Ref}$ . Transistors connected as head-to-tail

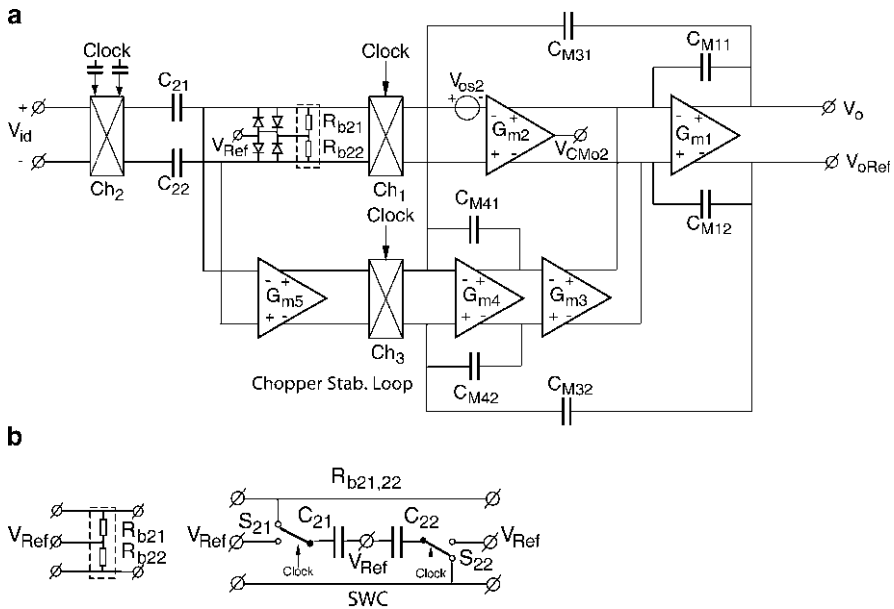


**Fig. 10.10.1** (a) Chopper-stabilized OpAmp with chopped-capacitor input. (b) Bias Resistors  $R_{b21}$  and  $R_{b22}$ , on the left hand side as normal resistors, and on the right-hand side as switched capacitors connected to  $V_{Ref}$

diodes serve to limit the CM swing at the input of the input amplifier  $G_{m2}$ . The high resistances of these diodes at zero  $V_{DS}$  softly serve to establish the level  $V_{Ref}$ . A firm reference level, which can cope with leakage currents and does not allow large offset, can be established either by regular resistors or by switched-capacitor resistors  $R_{b21}$  and  $R_{b22}$ . The switched-capacitor resistors are depicted in Fig. 10.10.1b. On the left hand we see the resistors, and at the right hand side the switched capacitors. For a capacitor value of 5 pF, and a clock frequency of 10 kHz, we find a CM resistance of  $R_{b21} = R_{b22} = 1/(5\text{pF} \cdot 2.10\text{kHz}) = 10\text{M}\Omega$ .

The head-to-tail connected diodes serve to limit the CM swing at the input of the input amplifier  $G_{m2}$ . The chopper-stabilization loop with sense amplifier  $G_{m5}$ ,  $Ch_3$ , integrator  $G_{m4}$ , and correction amplifier  $G_{m3}$  has been described with Fig. 10.7.1.

For lowering the 1/f noise and offset it is better to include the input amplifier  $G_{m2}$  in between the two choppers  $Ch_2$  and  $Ch_1$ . In this way a Chopper OpAmp arises, as shown in Fig. 10.10.2a with chopped-capacitor input. The ripple of the chopper amplifier could have been reduced by a stabilization loop like the chopper amplifier of Fig. 10.8.2. But then we need to also capacitive couple the sense amplifier  $G_{m5}$  to the input, for instance as it was done in Fig. 10.8.3. To avoid this extensive circuitry we rather completely eliminate the sense amplifier and keep only a ripple-reduction loop as explained with Fig. 10.9.1a. We have to keep in mind, though, that elimination of the sense amplifier produces a notch in the frequency response at the clock frequency.

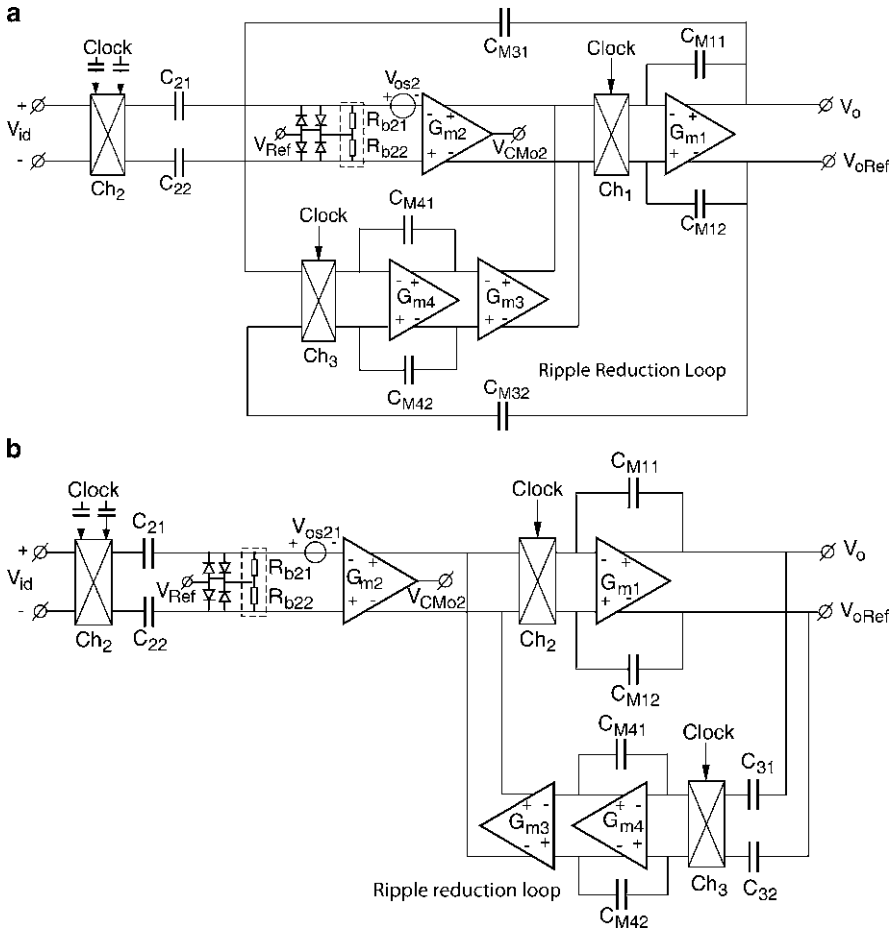


**Fig. 10.10.2** (a) Chopper OpAmp with chopped-capacitor input and ripple-reduction loop. (b) Chopper OpAmp with chopped-capacitor input and ripple-reduction loop drawn reverse

The signal through the coupling capacitors  $C_{21}$  and  $C_{22}$  will be attenuated by their load with parasitic capacitors like in the circuit of Fig. 10.10.1a. To keep the attenuation minimal and balanced, we should connect the bottom plates of the oxide isolated coupling capacitors to the input side, and take care that the parasitic capacitors of the diodes and are small and balanced enough. To further reduce the ripple we can take all measures as explained in Sect. 10.9.

It is just interesting to draw Fig. 10.10.2b little different with the ripple-reduction loop from the output side back to the input of chopper  $Ch_1$ . This is shown in Fig. 10.10.2b. It looks simpler to understand.

After the discussion of OpAmps with chopped-capacitor input coupling, it is easy now to make the step to instrumentation amplifiers. Figure 10.10.3 shows

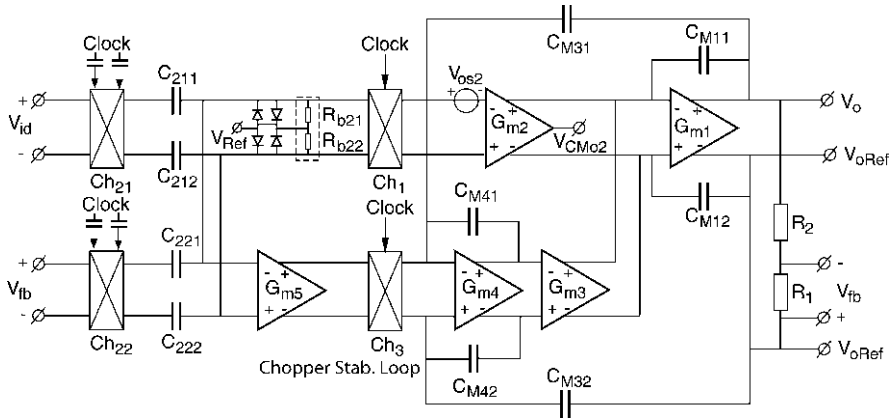
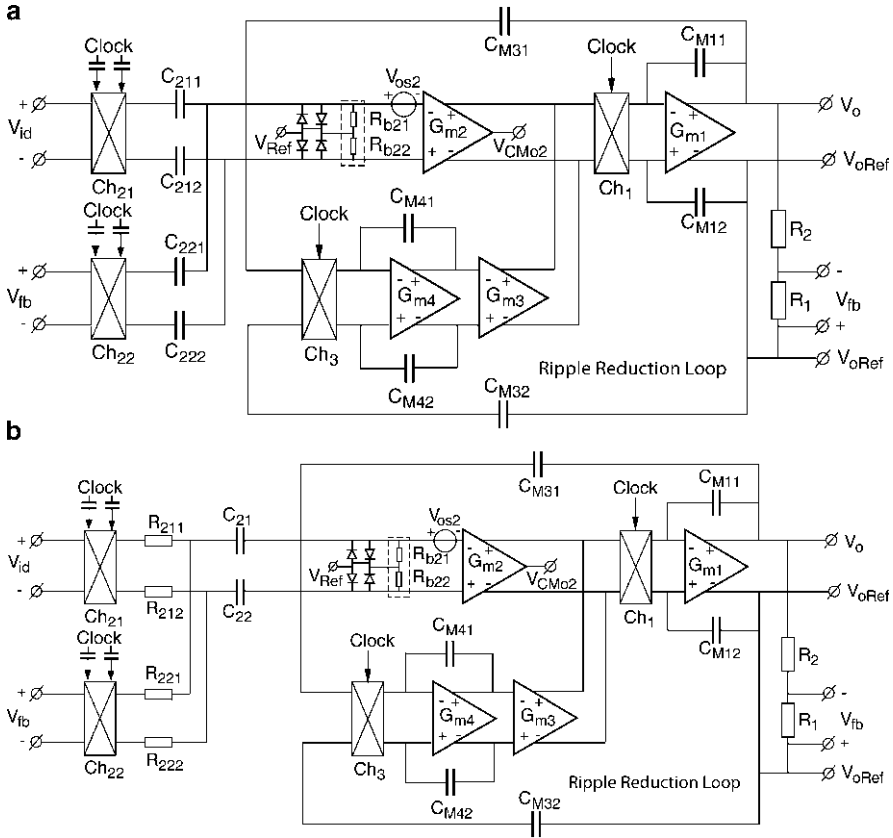


Fig. 10.10.3 Chopper-stabilized InstAmp with chopped-capacitor bridge input

a chopper-stabilized InstAmp with chopped-capacitor input coupling. The input capacitors  $C_{211}$ ,  $C_{212}$ ,  $C_{221}$ , and  $C_{222}$  together with the input choppers  $CH_{21}$  and  $CH_{22}$  make up a chopped-capacitor bridge InstAmp like the resistor-bridge InstAmp of Fig. 3.2.2. The closed-loop gain can be set either by the ratio of  $(C_{211}, C_{212}) / (C_{221}, C_{222})$  or by the feedback attenuator  $R_1 / (R_1 + R_2)$ . Unbalance in the input capacitors will not so much deteriorate the CMRR, as it did in the bridge InstAmp of Fig. 3.2.2, because the whole capacitor bridge is being chopped. The input impedance of this InstAmp will not be very high as a result of the chopped-capacitor bridge at the input. For  $C_{211}$  and  $C_{212}$  of 10 pF, and a clock frequency of 10 kHz, the input impedance  $R$  is  $1 / (10\text{pF} \cdot 10\text{kHz}) = 5\text{M}\Omega$ . As this value is not so high an unbalance of the impedances in the input signal source attenuated by the input impedance of the amplifier may cause a slightly lower CMRR.

In line with the OpAmp of Fig. 10.10.2a it is better to include the input amplifier  $G_{m2}$  in-between the two choppers  $Ch_2$  and  $Ch_1$  for lowering its  $1/f$  noise and offset. In this way a chopper InstAmp arises, as shown in Fig. 10.10.4a with chopped-capacitor input. Like in Fig. 10.10.2b ripple-reduction loop has been used to lower the chopper ripple. The CMRR will remain high by the chopping of the whole capacitor bridge, and only restricted by the loading of possible unbalanced source resistances as in the circuit of Fig. 10.10.3.

It is interesting to see that we can replace the chopped-capacitor bridge by a chopped-resistive bridge followed by capacitive coupling, as shown in Fig. 10.10.4b to obtain the same goal. The coupling capacitors  $C_{21}$  and  $C_{22}$  isolate the CM voltage of the bridge mid points from ground. Now the transfer function of the bridge between input and output is determined by resistors. This topology can be used to our advantage if the resistors can be made more accurate or more linear than capacitors. A further advantage is that the capacitive peak charge currents with



**Fig. 10.10.4** (a) Chopper InstAmp with chopped-capacitor bridge input coupling and ripple-reduction loop. (b) Chopper InstAmp with capacitive coupled chopped-resistor bridge input and ripple-reduction loop

full capacitive coupling are absent. A disadvantage is that the choppers now are loaded by a resistive bridge. The chopper series resistances may deteriorate the bridge accuracy. Moreover, the resistive bridge creates more noise. The CMRR remains high due to the chopping of the whole bridge.

To increase the input impedance it is better to step away from the bridge-type InstAmp and go to the current-feedback InstAmp. This topology is presented in Fig. 10.10.5 in combination with chopped-capacitor input coupling. The input impedance of in the InstAmp of Fig. 10.10.5 will now be made up by the chopped parasitic ground-plate capacitances at the chopper side of the input capacitances  $C_{211}$ ,  $C_{212}$ ,  $C_{221}$ , and  $C_{222}$ , and the parasitic ground capacitors of the elements following. If we suppose that the input capacitances have a value of 10pF, and the parasitic ground capacitances 1pF, we can expect an input chopped-capacitor resistance of  $1/(1\text{pF}\cdot 2.10\text{kHz}) = 50\text{M}\Omega$ .

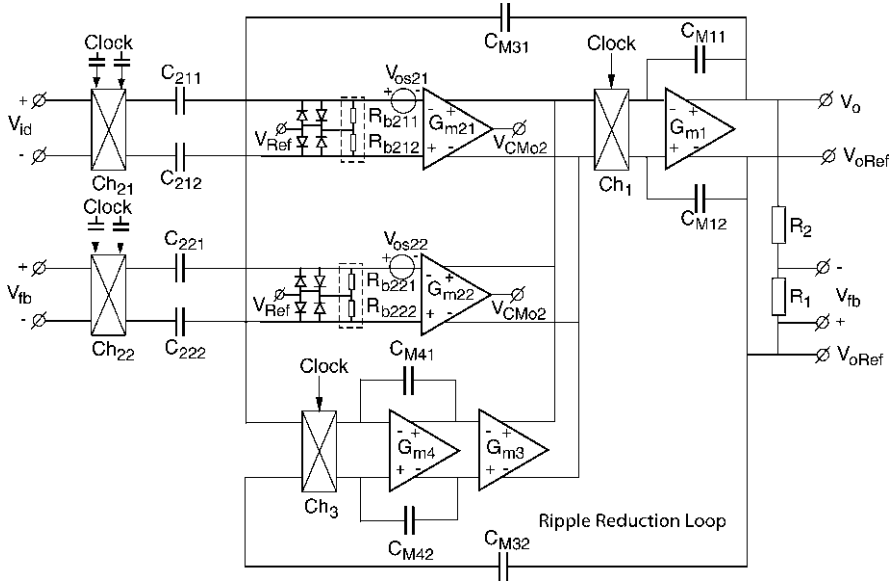


**Fig. 10.10.5** Current-feedback chopper InstAmp with chopped-capacitor coupling and ripple-reduction loop with high-impedance input

A disadvantage of the circuit of Fig. 10.10.5 is that the accuracy can be deteriorated, firstly, by inequality of  $G_{m21}$  and  $G_{m22}$  (cures for this inaccuracy are presented in the next paragraph), secondly, if the parasitic ground capacitances that load the coupling capacitances are not well matched.

The last circuit that will be discussed here is the Chopper InstAmp with Chopped-Capacitor input and Ripple-Reduction Loop and with Biomedical Electrode offset voltage compensation of Fig. 10.10.6. A basic problem of biomedical electrodes is that they may generate a DC offset of several 100 mV, while AC voltages of the order of  $\mu\text{V}$  have to be measured. A natural solution would be to couple these electrodes by capacitors. However, if we want to measure signals from a well determined frequency of 1 Hz and higher, and the input resistance of the amplifier can be reliably made 100 M $\Omega$ , then we still need 10 nF input coupling capacitors. And those can not be easily integrated on chip. Therefore an additional integrator loop following the output is made with a large time-constant. It uses a special chopped-capacitor integrator [10.19] depicted as  $G_{m7}$  and  $G_{m6}$ . At the output of that integrator a compensation voltage  $V_{DCcomp}$  will appear that will increase proportionally to the offset. This compensation voltage will be fed through a third input chopper  $Ch_{23}$  into  $C_{231}$  and  $C_{232}$  to compensate the DC offset at the input. As a basis the InstAmps of Fig. 10.10.4a or Fig. 10.10.5 can be used. For simplicity we have chosen Fig. 10.10.4a. The offset that can be cancelled is limited by the supply voltage.

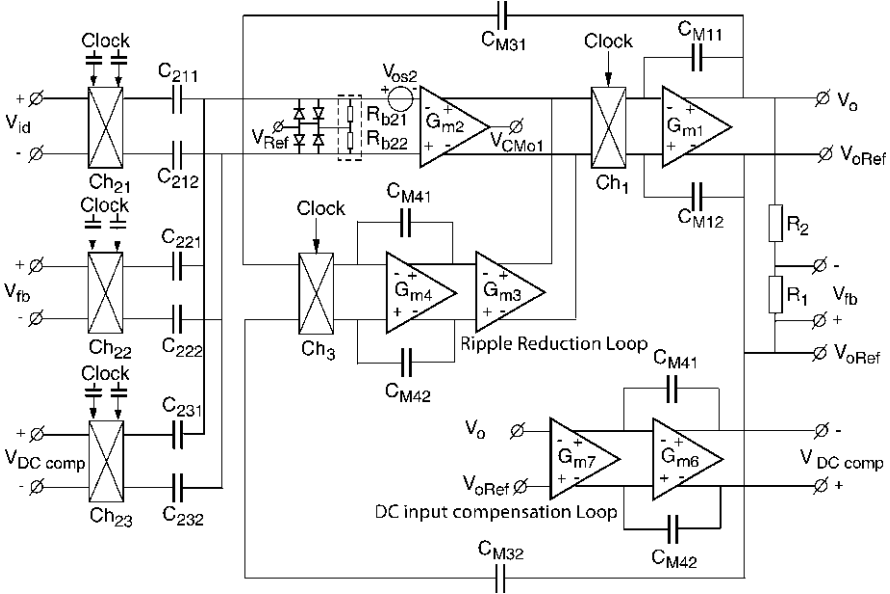


Fig. 10.10.6 Chopper InstAmp with chopped-capacitor input and ripple-reduction loop with biomedical electrode offset voltage compensation

### 10.11 Gain Accuracy of Instrumentation Amplifiers

The inaccuracy of current-feedback instrumentation amplifiers is proportional to the relative difference in  $G_m$  of the input stage and feedback stage. The input stages are drawn in Fig. 10.11.1. For accurate matching the transistors need to be large. For high CMRR and for a high signal-to-noise ratio the input transistors need to have the highest possible  $G_m$ . This means they have to be biased in weak inversion with a relative large width/length ratio. Also the current sources  $I_{T1}$  and  $I_{T2}$  need to be matched well, as the  $G_m$  of the differential input transistor pairs is dependent on their tail current. Therefore the current-source transistors need to be made less sensitive to differences in their gate-source threshold voltages by biasing them in strong inversion using long transistors, or in weak inversion in combination with degeneration resistors.

The most used input stage is of the P-Channel type for two reasons: Firstly, P-Channel transistors always have an isolated back gate. This makes it possible to bootstrap the back gates with the source voltages. By this measure the input  $G_m$  is much less dependent on the input CM voltage. This raises the CMRR from about 50–80 dB. Secondly, P-Channel transistors have less 1/f noise than N-Channel transistors. Folded cascodes behind the input stage allow the input CM voltage to include the negative rail, and increase the voltage gain of the input stage.



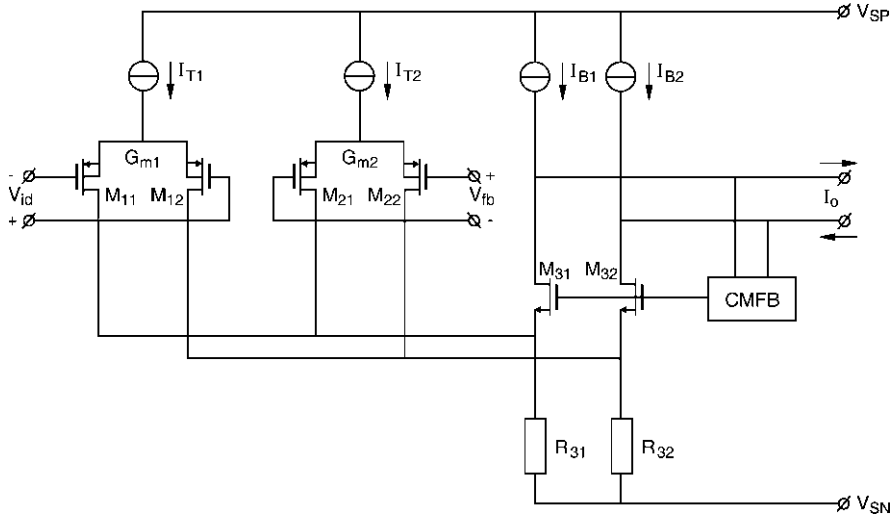


Fig. 10.11.1 Basic input stages for an current-feedback InstAmp

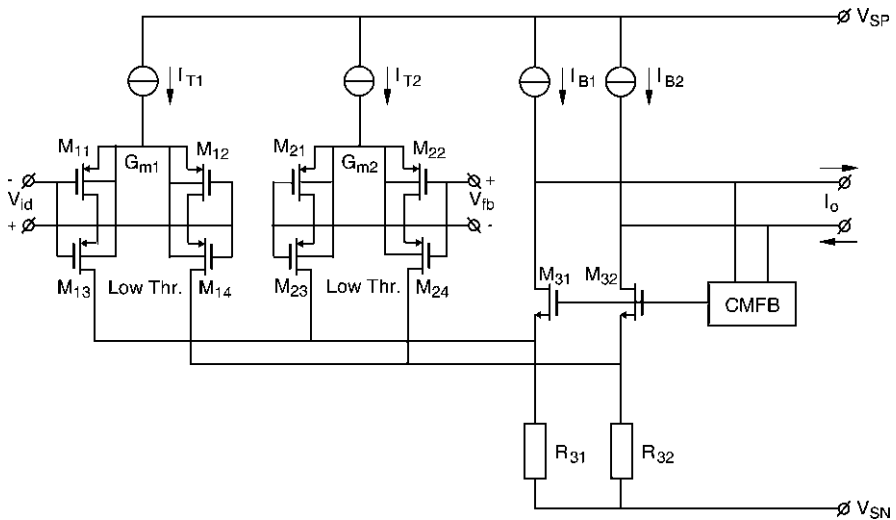


Fig. 10.11.2 Cascoded input stages for an current-feedback InstAmp

To further increase the CMRR of the input stages the input transistors have been cascoded in Fig. 10.11.2. This can be easily done if transistors are available with two different threshold voltages. For the input transistors we use the higher threshold transistors, and for the cascode transistors the lower threshold transistors. In that way both transistors function in saturation at high voltage gain. Cascoding of the

input transistors also helps to decrease the gain dependency of  $G_m$  to the CM voltage.

For the same reason the tail-current source transistors should be cascoded. We can even improve further if we built up the tail-current source with the same transistor combination as that of the differential pair and keep the elements at the same current density, the impedances of tail current and input transistors will compensate each other. This results in a higher CMRR and lower CM dependency of  $G_m$ .

In the next examples the input transistors are degenerated in order to improve the accuracy. This ultimately increases the supply current over square noise voltage ratio of the input stages. But sometimes this is the easiest.

In Fig. 10.11.3 the input transistors are degenerated to improve the accuracy and linearity. This was already described in Sect. 9.3 with Fig. 9.3.1. The resistors also give a standard way to calibrate the source resistors, and thereby the gain.

If we need to improve the accuracy and linearity more, the transistor parameters like  $G_m$  and voltage gain have to be increased by using a combination of transistors. In this way the transfer is accurately determined by the degeneration resistors and the transistor parameters fall out of the equations. Figure 10.11.4 shows how we can design an input stage that has compound P transistors and of which the input CM range includes the negative supply rail voltage  $V_{SN}$ .  $M_{11}$  and  $M_{12}$  are the input transistors. Their drain current is kept constant by  $M_{13}$  and  $M_{14}$ . These transistors take on the current needed to drive the degeneration resistors  $R_{11}$  and  $R_{12}$  and feed that current to the output load resistors  $R_{31}$  and  $R_{32}$ .  $M_{15}$  and  $M_{16}$  are folded cascodes to allow the input voltage include the negative rail voltage  $V_{SN}$  [10.18]. A disadvantage of this circuit is that the current over square noise ratio is roughly 8–16 times worse than that of a simple differential input pair.

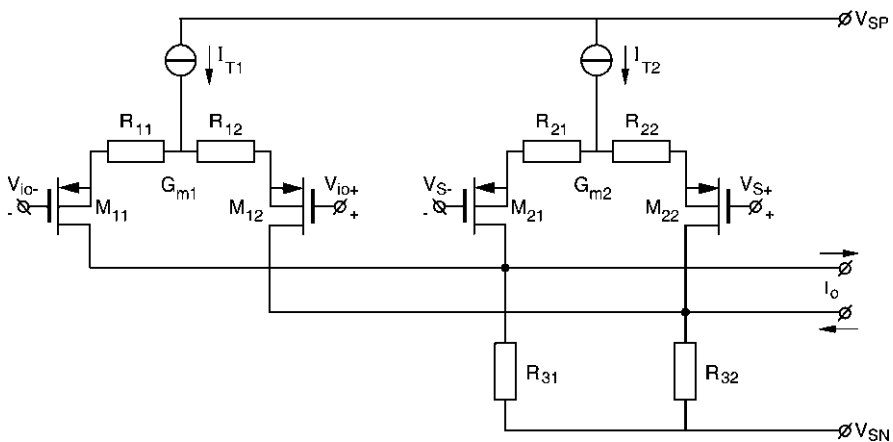


Fig. 10.11.3 Input stages of current-feedback InstAmp with degenerated input stages

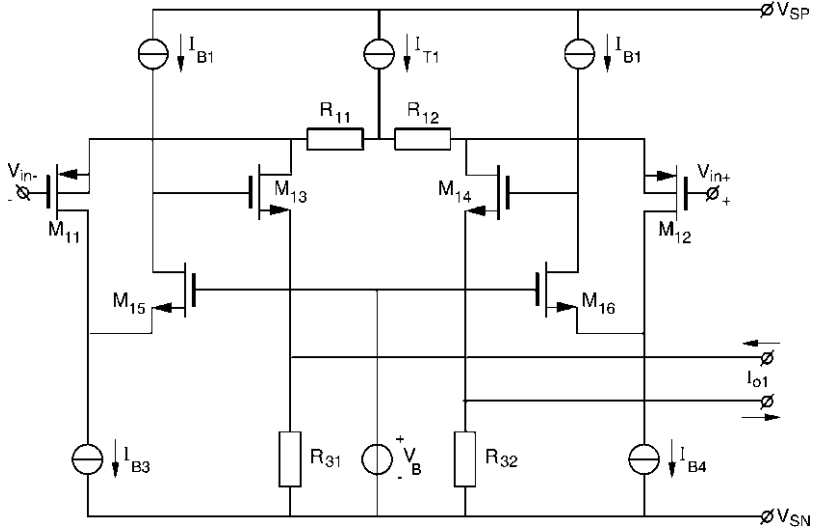


Fig. 10.11.4 Input stage with degenerated compound P transistors

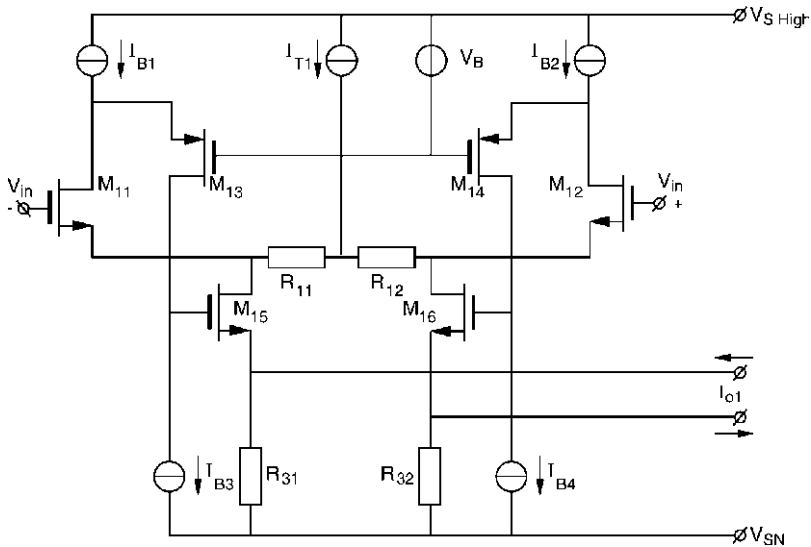
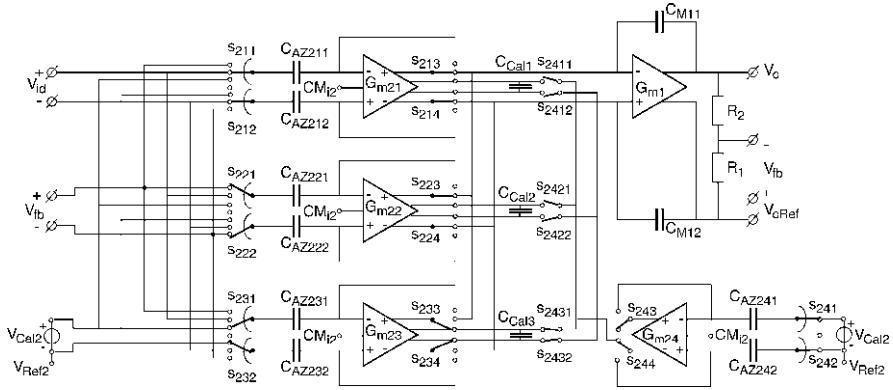


Fig. 10.11.5 Input stage with degenerated compound N transistors

Figure 10.11.5 shows an accurate input N transconductance which input CM range includes the positive supply voltage  $V_{SP}$ . It has the same functionality as the circuit of Fig. 10.11.4 [10.16].

We must keep in mind that these degenerated input transconductances result in a roughly 8–16 times higher supply current over square voltage-noise ratio than the



**Fig. 10.11.6** Chopper InstAmp with auto-zeroed Ping-Pong-Pang input stages and auto-gain calibration

basic differential pair of Fig. 10.11.1 with transistors biased in weak inversion. The reason is that the current has to be split into several sources and transistors, each of which contribute to noise, and that the  $G_m$  is lowered by degeneration.

In the following three examples of dynamic element matching (DEM) will be presented in which the accuracy and linearity of instrumentation amplifiers is improved with only a small penalty on higher supply power over square noise voltage.

The Ping-Pong-Pang auto-zero InstAmp of Fig. 10.5.5 can be provided with an auto-gain calibration, as shown in Fig. 10.11.6. The circuit has three input stages of which at any moment sequentially two stages are used to compose the feedback InstAmp topology, while the ‘third’ stage is being, firstly, auto-zero trimmed and, secondly, auto-gain trimmed. The auto-zero offset trim has been explained at Fig. 10.5.5. The auto-gain trim can be done in many ways. In Fig. 10.11.6 the ‘third’ stage in its calibration phase is connected at its input to a calibration voltage  $V_{Cal2}$ , while its output current is compared to a current from a calibration stage  $G_{m24}$ . That stage is also connected at its input to the calibration voltage  $V_{Cal2}$ . The current difference between the outputs of  $G_{m23}$  and  $G_{m24}$  is integrated and stored on  $C_{Cal3}$ . The voltage on  $C_{Cal3}$  is used to calibrate the transconductance of  $G_{m23}$  by controlling its tail bias current. In a next phase one of the other amplifiers is being calibrated and  $G_{m23}$  is being used as one of the input amplifiers of the InstAmp. Each input stage has its own storage capacitor for its gain trim.

An important advantage of the combination of auto-zero and auto-gain is that the non-linear transconductances of the input stages are more accurately equalized than if these stages were only auto-zeroed. This leads to low inaccuracies, in the order of  $10^{-4}$ , and also to low non-linearity’s, in the order of  $10^{-4}$ .

In the same way the chopper instrumentation amplifier with Ping-Pong-Pang auto-zero input stages of Fig. 10.6.8 can be auto-gain calibrated. This leads to an

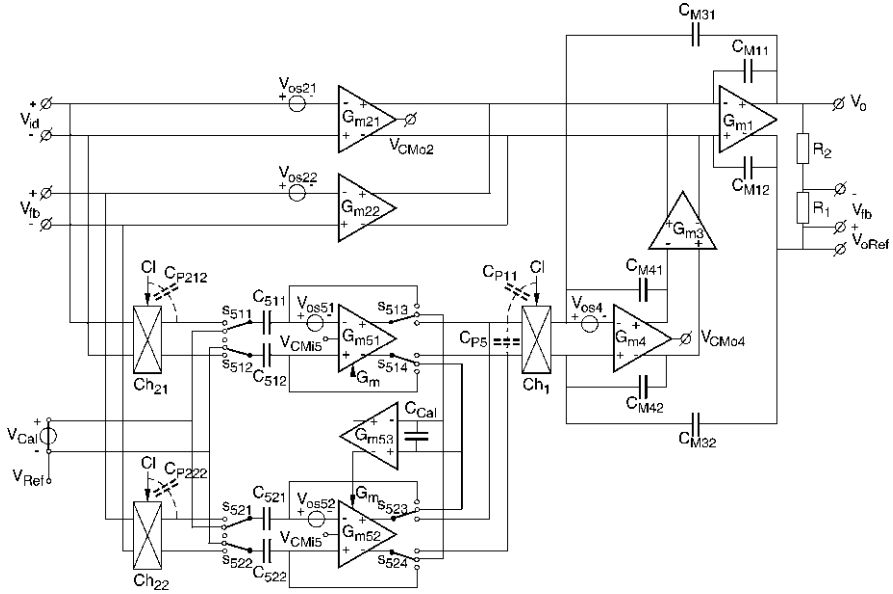


**Fig. 10.11.7** Chopper stabilized InstAmp with auto-zero sense amplifiers and auto-gain calibration

accurate and low-ripple auto-zero chopper instrumentation amplifier. This has not been shown separately.

The chopper-Stabilized InstAmp with auto-zeroed sense amplifiers of Fig. 10.7.7 can also be provided with auto-gain calibration [10.22]. This circuit is sketched in Fig. 10.11.7.

Calibration of the two offset sense amplifiers  $G_{m51}$  and  $G_{m52}$  needs only to result in the equality of these two amplifiers. This means that in the auto-calibration phase both inputs can simply be connected to a calibration voltage  $V_{Cal}$  and that the output currents can be compared. The difference of the output currents is being integrated and stored on a capacitor  $C_{Cal}$ . The voltage on the store capacitor controls through  $G_{m53}$  the difference of the tail bias currents and thus the difference of the transconductances. At a large control loop gain the transconductances of  $G_{m51}$  and  $G_{m52}$  become equal. The auto-zero and auto-calibration can be placed in one main auto-correction phase.

We have to keep in mind that with chopper-stabilized instrumentation amplifiers the stabilization loop accurately controls the gain at low frequencies. At high frequencies the gain is set by differences in the main amplifier input stages, which are not auto-calibrated. Normally, this is not a problem because at high frequencies the gain is not accurate anyway because of lack in overall loop gain.

In the above example the auto-gain calibration was done in a time-discrete way. A time-continuous way to achieve a high accuracy and remove differences in the two input  $G_m$ 's of a chopper instrumentation amplifier can be obtained by applying

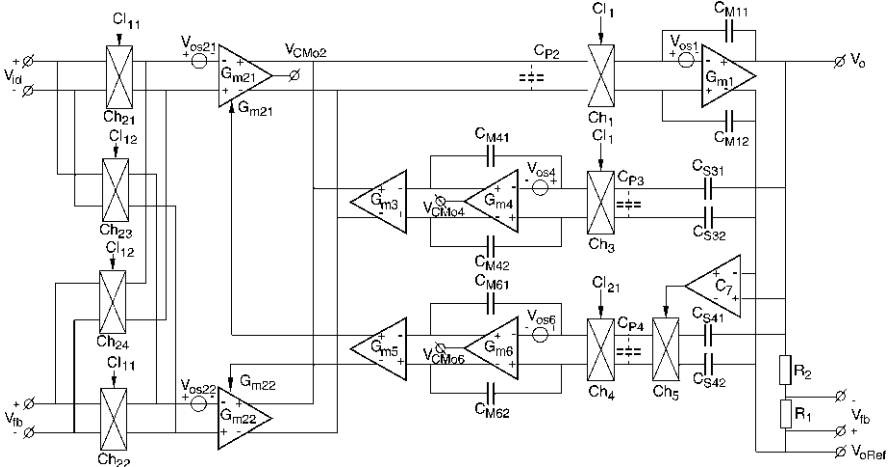


**Fig. 10.11.8** Current-feedback InstAmp with ripple-reduction loop and gain-error-reduction loop (order of gain error is 0.01%)

dynamic-element matching (DEM) of the two input stages. To that purpose the two input stages are chopped back and forth between input and feedback. As a result of non-equal gains of the input stages an output ripple will arise at the frequency by which we interchange the input stages. If we DEM the input stages, for instance, at half the chopper frequency, a ripple will occur at the output at half the chopper frequency. This gain-error ripple can be reduced by a gain-error reduction loop (GERL) [10.21] independently of the offset RRL, which runs at the full clock frequency, as in the chopper InstAmp of Fig. 10.9.3a of the previous paragraph. The resulting circuit is shown in Fig. 10.11.8.

The gain-error reduction loop is made up from the capacitors  $C_{S41}$  and  $C_{S42}$ , which sense the output ripple, chopper  $Ch_4$ , integrator  $G_{m6}$ , and correction amplifier  $G_{m5}$ . The last one differentially corrects a small part (for instance 2%) of the bias currents of the input  $G_m$ 's. The result is a multiplicative correction on the input signals. If the gain is too large because  $g_{m21}$  is larger than  $g_{m22}$ , the output ripple is positive in regard to the clock for a positive input signal. But the output ripple will be negative in regard to the clock for a negative input signal. Both situations need a correction in the same direction. Therefore a comparator  $C_7$  is used to measure the output polarity. A chopper  $Ch_5$  is inserted to multiply the sense signal by the output polarity.

This analog GERL can also be made up in a digital way by using an ADC after  $Ch_4$ , a digital integrator, followed by a DAC. In that way the digital loop can be provided with long-term memory for the best gain setting in times that the signal is small, and measured when the signal is not so small.

If the CM voltage levels of the input and feedback output are different the CM voltage levels of the input transistor pairs are alternatively chopped high and low.

This has two side effects: Firstly, if the input stages have a  $G_m$  that depends on the CM voltage. This dependency is not taken away by the DEM action. Therefore the overall gain is slightly depending on the difference of the input and feedback CM voltage level. Hence, it is very important to choose input stages with a highly CM-independent  $G_m$ , as described in the beginning of this paragraph. Secondly, parasitic capacitors between the back gates and ground will cause large CM current spikes in the input stages. When these CM current spikes are larger than the bias currents the signal transfer is hampered. To lower the CM current spikes, the back gates of the input transistors and the cascodes can be actively bootstrapped to their CM input levels by class-AB source followers [10.21].

Conclusion: The combination of automated offset and gain calibration leads to an accurate equalization of the non-linear characteristics of the input stages. This results not only in a low offset, of the order of microvolts, but also in a low inaccuracy, of the order of  $10^{-4}$ , and moreover in a low non-linearity, of the order of  $10^{-4}$ , as the curved  $G_m$  characteristics of input and feedback are accurately matched. The continuous-time chopping and calibration method of simple differential transistor pairs in weak inversion leads to the lowest ratio between supply current and the square input voltage noise.

## 10.12 Summary Low Offset

Table 10.12.1 gives an overview of the roughly estimated offset and ripple of the Operational Amplifiers in the Sects. 10.5–10.9.

Chopping generally can reduce offset by a factor of 10,000. But the ripple stays equal to the offset without other measures. Auto-zeroing reduces the offset by a factor of 100–500, depending whether the AZ store capacitors are placed at the input or at the output. Further improvement can be obtained when we combine chopping and auto-zeroing. Abbreviations used in Table 10.12.1 are: AZ = Auto-Zeroing, N = Nested, ChSt = Chopper-Stabilized, Ch = Chopping.

**Table 10.12.1** Summary of offset and ripple that can be obtained

OpAmps	$V_{os}$	$V_{rip}$	InstAmps	$V_{os}$	$V_{rip}$
A Z	20–100 $\mu$ V		AZ	20–100 $\mu$ V	
Chopper	10 $\mu$ V	10 mV	Chopper	20 $\mu$ V	20 mV
N Chopper	0.1 $\mu$ V	100 $\mu$ V	N Chopper	0.2 $\mu$ V	200 $\mu$ V
ChSt	10 $\mu$ V	100 $\mu$ V	ChSt	20 $\mu$ V	200 $\mu$ V
ChSt + AZ	1 $\mu$ V	10 $\mu$ V	ChSt + AZ	2 $\mu$ V	20 $\mu$ V
Ch + ChSt	1 $\mu$ V	100 $\mu$ V	Ch + ChSt	2 $\mu$ V	200 $\mu$ V
Ch + ChSt + AZ	0.1 $\mu$ V	10 $\mu$ V	Ch + ChSt + AZ	0.2 $\mu$ V	20 $\mu$ V
Ch + RRL	1 $\mu$ V	100 $\mu$ V	Ch + RRL	2 $\mu$ V	200 $\mu$ V
Ch + RRL + AZ	0.1 $\mu$ V	10 $\mu$ V	Ch + RRL + AZ	0.2 $\mu$ V	20 $\mu$ V

## 10.13 References

- [10.1]. J. Huijsing, *Operational Amplifiers, Theory and Design* (Kluwer Academic Publishers, Dordrecht, 2001), pp. 456, Chapter 1
- [10.2]. J. Huijsing, *Operational Amplifiers, Theory and Design* (Kluwer Academic Publishers, Dordrecht, 2001), pp. 456, Chapter 3
- [10.3]. B. van den Dool, J. Huijsing, Indirect current feedback instrumentation amplifier with a common-mode input range that includes the negative rail, *IEEE J. Solid-St. Circ.* **28**(7), 743–749 (1993)
- [10.4]. J. Huijsing, *Operational Amplifiers, Theory and Design* (Kluwer Academic Publishers, Dordrecht, 2001), pp. 456, Chapter 9
- [10.5]. I.E. Opris, G.T.A. Kovacs, A rail-to-rail ping-pong OpAmp, *IEEE J. Solid-St. Circ.* **31**(9), 1320–1324 (1996)
- [10.6]. C. Enz, E. Vittoz, F. Kruppenacher, A CMOS chopper amplifier, *IEEE J. Solid-St. Circ.* **22**(3), 708–715 (1987)
- [10.7]. A. Bakker, K. Thiele, J. Huijsing, A CMOS nested chopper instrumentation amplifier with 100 nV offset, *IEEE J. Solid-St. Circ.* **35**(12), 1877–1883 (2000)
- [10.8]. A. Tang, Ping-pong amplifier with auto-zeroing and chopping, U.S. Patent 6,476,671, 11 May 2002. Analog Devices
- [10.9]. C. Enz, G. Temes, Circuit techniques for reducing the effect of OpAmp imperfections: Autozeroing, correlated double sampling and Chopper Stabilization, *P. IEEE*, **84**(11), 1584–1614 (1996)
- [10.10]. J. Huijsing, J. Fonderie, B. Shahi, Frequency stabilization of chopper-stabilized amplifiers, U.S. Patent 7,209,000, 24 April 2007
- [10.11]. J.F. Witte, K. Makinwa, J. Huijsing, A CMOS chopper offset-stabilized OpAmp, 2006 *European Solid-State Circuits Conference, Proceedings*, pp. 360–363
- [10.12]. R. Burt, J. Zhang, A micropower chopper-stabilized operational amplifier using a SC notch filter with synchronous integration inside the continuous-time signal path, *IEEE J. Solid-St. Circ.* **41**(12), 2729–2736 (2006)
- [10.13]. J.F. Witte, J. Huijsing, K. Makinwa, A current feedback instrumentation amplifier with 5 $\mu$ V offset for bidirectional high – side current sensing, *IEEE Solid-State Circuits Conference 2008, San Francisco, Session 3.5, 4–6 Feb 2008*
- [10.14]. J. Huijsing, J. Fonderie, Chopper Chopper-Stabilized operational amplifiers and methods, U.S. Patent 6,734,723, 11 May 2004
- [10.15]. J. Huijsing, B. Shahi, Chopper Chopper-Stabilized instrumentation and operational amplifiers, U.S. Patent 7,132,883, 7 Nov 2006
- [10.16]. J.F. Witte, K.K.A. Makinwa, J.H. Huijsing, *Dynamic Offset Compensated CMOS Amplifiers* (Springer, Dordrecht, Heidelberg, London, New York, 2009)
- [10.17]. R. Wu, K.A.A. Makinwa, J.H. Huijsing, A chopper current-feedback instrumentation amplifier with a 1 mHz 1/f noise corner and an AC-coupled ripple-reduction loop, *IEEE Solid-State Circuits Conference 2009 8–12 Feb 2009*, pp. 322–323, 323a
- [10.18]. J.H. Huijsing, B. Shahi, Accurate voltage to current converters for rail-sensing current-feedback instrumentation amplifiers, U.S. Patent 7,202,738, 10 April 2007
- [10.19]. T. Denisson et al., A 2  $\mu$ W 100 nV/rtHz chopper-stabilized instrumentation amplifier for chronic measurement of neural field potentials, *IEEE J. Solid-St. Circ.* **42**(12), 2934–2945 (2007)
- [10.20]. Q. Fan et al., A 21 nV/ $\sqrt{\text{Hz}}$  (10.5 nV/ $\sqrt{\text{Hz}}$ ) chopper-stabilized multi-path current-feedback instrumentation (Operational) amplifier with 2  $\mu$ V Offset, *IEEE Solid-State Circuits Conference 2010, San Francisco, 8–11 Feb 2010*
- [10.21]. R. Wu, J.H. Huijsing, K.A.A. Makinwa, A current-feedback instrumentation amplifier with a Gain-Error Reduction Loop (GERL) achieving 0.05% gain accuracy and



1ppm/degreeC gain drift, IEEE Solid-State Circuits Conference 2011, San Francisco, Feb 20–23, 13.5

- [10.22]. R.E. Boucher, J.H. Huijsing, Auto-gain correction and common mode voltage cancellation in a precision amplifier, U.S. Patent 7,696,817B1, 7 April 2010

# Biography

**Johan H. Huijsing** was born on May 21, 1938.

He received the M.Sc. degree in Electrical Engineering from the Delft University of Technology, Delft, the Netherlands in 1969, and the Ph.D. degree for this University in 1981 for his thesis on operational amplifiers.

He has been an assistant and associate professor in Electronic Instrumentation in the Faculty of Electrical Engineering of the Delft University of Technology since 1969, where he was a full professor in the chair of Electronic Instrumentation from 1990 until 2003. From 1982 through 1983 he was a senior scientist at Philips Research Labs in Sunnyvale, California, USA. From 1983 until 2005 he was a consultant for Philips, Sunnyvale, and since 1998 he is a consultant for Maxim, Sunnyvale, CA.

The research work of Johan Huijsing is focussed on the systematic analysis and design of operational amplifiers, analog-to-digital converters and integrated smart sensors. He is author or co-author of some 250 scientific papers, 30 US-patents and 15 books, and co-editor of 13 books. He is fellow of IEEE for contributions to the design and analysis of analog integrated circuits. He received the title of Simon Stevin Meester for applied Research by the Dutch Technology Foundation.

He was initiator and co-chairman until 2005 of the international Workshop on Advances in Analog Circuit Design, which has been held annually since 1992. He was a member of the programme committee of the European Solid-State Circuits Conference from 1992 until 2002. He has been chairman of the biennial national Workshop on Sensor Technology, from 1991 until 2002, and chairman of the Dutch STW Platform on Sensor Technology from 1991 until 2002.

October 1, 2010.



# Index

## A

- All-NPN
  - 1GHz, all-NPN class-AB OpAmp with MNMC, 249, 250
  - high-frequency all-NPN OpAmp with mixed PC and MC, 239–241
  - LM101 class-AB all-NPN OpAmp with MC, 242–243
  - NE5534 class-AB OpAmp with bypassed NMC, 244–245
  - precision all-NPN class-AB OpAmp with NMC, 245–246
  - precision HF all-NPN class-AB OpAmp with MNMC, 246–249
  - 2 volt power-efficient all-NPN class-AB OpAmp with MDNMC, 249–251
- Applications, 3, 5, 7, 12, 18, 31–56, 73, 82, 112, 117, 118, 131, 139, 155, 165, 170, 173, 189, 213, 225, 239, 242–243, 292, 294, 296, 302, 309, 315, 337, 340, 351–354, 358, 361, 382–383
- Auto-Gain calibration for Instamps, 392–394
- Auto-Zero (AZ), 351, 358–361, 372–376, 379–383, 392–394, 396–397
- Auto-Zero chopper-stabilized OpAmps and InstAmps, 372–376
- Auto-Zero instrumentation amplifier, 351, 366, 370, 383, 394
- Auto-Zero Opamp, 358–361, 370
- AZ. *See* Auto-Zero

## B

- Back-gate influence, 79–80
- Balancing techniques, 60–65, 72–74
- Basic bipolar R-R-out class-A OpAmp, 226–228

## Bias

- FBB, 128–140, 152, 155, 249, 259–261
- FFB, 112–128
- generator for constant  $G_m$ , 67, 68
- offset, bias and drift, 59–73, 155
- Biasing for constant transconductance  $G_m$ , 67–70, 214
- Boosting
  - input class-AB boosting, 223–224
  - voltage-gain boosting, 224–226
- Bridge instrumentation amplifier, 35–36

## C

- Capacitive input chopper amplifiers, 352, 382–389
- Cascade
  - folded-cascode OpAmp, 215–221, 281, 287
  - telescopic-cascode OpAmp, 219–220, 294
- Cascoded input stages, 176, 204, 205, 323, 334, 357, 389, 390
- Charge injection in chopper amplifier, 362–365
- Chopper
  - instrumentation amplifier (IA), 364–366, 374–376, 379, 383, 385, 394, 395
  - operational amplifier (OA/OpAmp), 361–377, 379, 381–386
- Chopper amplifiers
  - with capacitive input, 382–389
  - with Ping-Pong auto-zero, 364
- Chopper-stabilized chopper InstAmps, 372–376, 386
- Chopper-stabilized chopper OpAmps, 372–376, 379
- Chopper-stabilized OpAmps, 366–376, 382–384
- Chopper techniques, 376, 386
- Classification

- Classification (*cont.*)
  - based on number of floating ports, 1–2
  - of output stages, 110–112
  - of overall topologies, 155–161
- CM-out control
  - fully differential CMOS OpAmp
    - with linear-mode, 292–294
    - with LTP, 294–295
    - with R-R buffered resistive, 297–299
    - with R-R resistive, 299–301
    - with switched-capacitor, 302–303
  - fully differential GA-CF CMOS OpAmp
    - with input-CM feedback, 296–297
  - fully differential telescopic CMOS OpAmp with linear-mode, 294
- CMRR. *See* Common-mode rejection ratio
- CM voltage. *See* Common-mode voltage
- Common-mode
  - CMRR, 13–15, 22–24, 26, 28, 36, 41, 63, 73–81, 85, 86, 96, 156, 252, 258, 318, 320–321, 325–327, 330–331, 343, 345–349, 351–357, 361, 365, 371, 379–380, 386–387, 389–391
  - common-mode cross-talk ratios (CMCR), 13–15, 36, 41, 42, 73–81, 85, 90, 318, 322, 349
  - extension of the common-mode input range, 95–96
  - voltage range
    - instrumentation amplifier bipolar including negative rail voltage, 324–325
    - instrumentation amplifier CMOS including negative rail voltage, 325–326
- Common-mode rejection ratio (CMRR)
  - with auto-zero(AZ), 361
  - with chopper techniques, 365, 386
- Common-mode (CM) voltage, 4, 12–14, 18, 22–24, 35, 36, 41, 55, 65–66, 73–76, 78, 82–85, 87–91, 94, 95, 97, 98, 156, 202, 219, 220, 252, 256–258, 291, 293–295, 297, 298, 300, 303–305, 318, 319, 323–326, 352, 353, 389
- Compact
  - compact 2 volt R-R-in/out CMOS class-AB OpAmp with MC, 256–259
  - compact 1.2 volt R-R-out BiCMOS class-AB OpAmp with MNMC, 265–267
  - compact 1.2 volt R-R-out CMOS class-AB OpAmp with MC, 259–261
  - compact 2 volt R-R-out CMOS class-AB OpAmp with MC, 254–256
  - compact 1.2 volt R-R-out CMOS class-A OpAmp with MC, 252–254
- Compensation
  - frequency, 67, 83, 140–141, 160–197, 242, 256, 262, 267, 272, 277, 315, 334, 364, 376
  - input voltage and current, 160–161, 221–223
- Compound output stages
  - FBB, 130–134
  - FFB, 117–119
- Configuration
  - fully differential
    - GA-CF, 291–299
    - GA-CF-GA, 299–301
    - GA-GA-GA-GA, 302–303
  - GA-CF, 213–226, 231, 235, 239, 261, 291, 293, 295–299
  - GA-CF-GA, 251–262, 265, 299, 300
  - GA-CF-VF, 226, 231–237, 239, 313–314
  - GA-CF-VF/GA, 239–242, 245–247
  - GA-GA, 226–231, 253
  - GA-GA-GA, 244, 261–271
  - GA-GA-GA-GA, 271–281, 291, 301, 302
  - GA-GA-VF, 231, 235–239
  - GA-GA-VF/GA, 242–251
- Constant  $G_m$  by model bias generator, 68
- Constant  $g_m$  input stages
  - in CMOS by constant sum of  $V_{GS}$ , 92–95
  - in CMOS by multiple input stages, 86–87
  - in CMOS by saturation control, 91–92
  - by constant sum of roots of tail currents, 86–87
  - by constant sum of tail-currents, 83–86
  - by spill-over control, 87–91
- Constant transconductance  $G_m$ , 67–70
- Current
  - amplifier, 5–6, 37–38
  - current followers (CF), 6–9, 110, 157–159, 213–214, 218, 281, 301, 314, 315, 322–323
  - current-to-voltage converter, 3, 7, 9, 32–33, 38–42, 46, 51, 52, 54, 307, 310–321, 327–331, 339, 342–345, 347–348, 355, 357
  - input voltage and current compensation, 160–161, 221–223
  - mirror, 6, 39–40, 49, 50, 52, 82–88, 91, 119, 120, 138, 150, 157–159, 163,

- 213–218, 223, 230, 238, 242, 249, 257, 276, 281, 282, 302, 304, 324, 341–343, 345, 355–356, 453
  - output current limitation circuits, 141, 143–145
  - saturation protection and current limitation, 141–145
  - Current-sense amplifier, 353
- D**
- Damping Network for HF Stability Control, 192–193
  - Definition of OpAmps, 1–10
  - Degenerated input stages, 391
    - with compound transistors, 392, 393
  - Design examples, 213–288
  - Differential V-I converter
    - differential accurate V-I converter, 317–318, 322
    - differential CMOS accurate V-I converter, 318–319
    - differential simple V-I converter, 316–317, 323–324
    - differential voltage-to-current converters, 40–42, 310, 316–321, 327, 328
  - Drift
    - offset, bias and drift, 59–70
  - Dynamic range, 31, 44–52, 55, 56, 339, 340, 353
  - Dynamic range over supply-power ratio, 45–46, 52
- E**
- Electrodes, 353, 354, 382–383, 388, 389
  - ESD protection, 267
  - Extension of the common-mode input range, 95–96
- F**
- FBB. *See* Feedback class-AB biasing
  - Feedback class-AB biasing (FBB), 112, 128–140, 152, 239, 245, 249
    - compound output stages, 130–134
    - rail-to-rail general amplifier output stages, 135–140
    - voltage-follower output stages, 129–130
  - Feedforward class-AB biasing (FFB), 112–128, 140, 151, 239
    - compound output stages, 117–119
    - feedforward HF compensation, 220–221
    - rail-to-rail general-amplifier output stages, 119–128
    - voltage follower output stages, 112–117
  - FFB. *See* Feedforward class-AB biasing
  - Floating ports
    - classification based on number, 1–2
  - Folded-cascode OpAmp, 215–221, 281, 287
  - Four-GA-stage
    - conditionally stable multipath hybrid nested Miller compensation (MHNMC), 187–189
    - frequency compensation, 184
    - hybrid nested Miller compensation (HNMC), 184–186
  - Frequency compensation, 67, 83, 142, 160–197, 242, 256, 262, 267, 272, 277, 315, 334, 364, 376
    - four-GA-stage, 184
    - one-GA-stage, 163–165
    - three-GA-stage, 177–178
    - two-GA-stage, 166–167
  - Fully differential OpAmps, 291–307, 337
    - fully differential CMOS OpAmp
      - with linear-mode CM-out control, 292–294
      - with LTP CM-out control, 294–295
      - with R-R buffered resistive CM-out control, 297–299
      - with R-R resistive CM-out control, 299–301
      - with switched-capacitor CM-out control, 302–303
    - fully differential GA-CF CMOS OpAmp
      - with input-CM feedback CM-out, 296–297
    - fully differential GA-CF configuration, 291–299
    - fully differential GA-CF-GA configuration, 299–301
    - fully differential GA-GA-GA-GA configuration, 302–303
    - fully differential telescopic CMOS OpAmp with linear-mode CM-out control, 294
- G**
- Gain
    - accuracy, 352, 356, 371, 379, 389–396
    - definition of: offset voltage and current, input and output impedance, gain, 11–12

Gain boosting  
 voltage and current, 160  
 voltage-gain boosting, 224–226

Gain-error reduction loop (GERL) for InstAmps, 395

General bipolar class-AB OpAmp with Miller compensation, 235–237

1GHz, all-NPN class-AB OpAmp with MNMC, 249, 250

Gyrator floating, 43–44

**H**

HF stability for high-capacitive load, 191

HF stability with damping network, 192–193

HF stability with quench capacitor, 193–195

HF stability with RNMC, 195–196

High capacitive load, 189–193, 195–197

High frequency (HF) compensation  
 feedforward, 220–221  
 high-frequency all-NPN OpAmp with mixed PC and MC, 239–242

High-slew-rate bipolar class-AB voltage-follower buffer, 234–235

High-speed bipolar class-AB OpAmp, 231–234

Hybrid nested Miller compensation (HNMC)  
 four-GA-stage, 184–186

**I**

IA or InstAmp. *See* Instrumentation amplifiers

Improved basic  
 bipolar R-R-out class-A OpAmp, 228–229  
 CMOS R-R-out class-A OpAmp, 229–231

Current-feedback instrumentation amplifier, 351, 355–357, 379, 387–391, 395

Input and output impedance  
 definition, offset voltage and current, input and output impedance, gain, 11–12

Input bias current  
 definition, input bias current, input common-mode rejection ratio, 13–14

Input class-AB boosting, 223–224

Input common-mode rejection ratio  
 definition, input bias current, input common-mode rejection ratio, 13–14

Input stages, 2, 16, 45, 59, 106, 155, 213, 296, 310, 357

Input voltage and current compensation, 160–161

Input voltage compensation, 221–223

Instrumentation amplifiers (IA/InstAmp), 35–36, 40, 42, 55, 309–349, 351–357, 364–366, 370, 371, 374–376, 379, 381, 383, 385–396

bipolar with common-mode voltage range including negative rail voltage, 324–325

with capacitive bridge input, 35–36, 320, 321, 386, 387

with capacitive input, 322, 385–386

CMOS with common-mode voltage range including negative rail voltage, 325–326

with differential V-I converter for input sensing, 320–323

with differential V-I converters for input and output sensing, 322–323

(semi) with three OpAmps, 319–320

simplified diagram and general symbol, 326–328

universal class-AB voltage-to-current converter, 344–345

universal class-AB voltage-to-current converter design, 328–331

universal V-I converter design  
 with real IA, 329–331  
 with semi-instrumentation amplifier, 328–329

Instrumentation current amplifier, 42–43

Instrumentation voltage amplifier, 41, 42

Inverting  
 current amplifier, 39–40  
 voltage amplifier, 33, 35–36, 47, 49  
 voltage integrator, 48, 49

Isolation techniques, 60, 70–74

**L**

LM101 class-AB all-NPN OpAmp with MC, 242–243

Low-drop-out regulator HF stability, 192

Low noise, 70–73, 217, 247, 351–397

Low offset, 1, 21, 66, 217, 351–397

Low power, 45, 189–190, 195–197

Low-voltage bias circuit for constant Gm, 70

**M**

Macromodels, 11, 53, 54  
 mathematical, 16–17

- Miller-compensated, 17–18
  - nested-Miller-compensated, 18
  - SPICE, 16–19
  - $\mu$ A741 OpAmp with Miller compensation (MC), 237–239
  - Measurement techniques for OpAmps, 19–24
    - gain and offset measurements, 22
    - gain measurement of OpAmp, 21–22
    - gain measurement of OTA, 20–21
    - general measurement setup for, 22–24
  - Miller compensation (MC)
    - compact 2 volt R-R-in/out CMOS class-AB OpAmp, 256–259
    - compact 1.2 volt R-R-out CMOS class-AB OpAmp, 259–261
    - compact 2 volt R-R-out CMOS class-AB OpAmp, 254–256
    - compact 1.2 volt R-R-out CMOS class-A OpAmp, 252–254
    - general bipolar class-AB OpAmp, 235–237
    - LM101 class-AB all-NPN OpAmp, 242–243
    - $\mu$ A741 OpAmp, 237–239
    - two-GA-stage, 170–172
  - Multi-GA-stage compensations, 189
  - Multipath hybrid nested Miller compensation (MHNMC)
    - four-GA-stage, 187–189
    - four-GA-stage conditionally MHNMC, 189
    - 1.2 volt R-R-out CMOS class-AB OpAmp, 276–281
  - Multipath nested Miller compensation (MNNMC)
    - compact 1.2 volt R-R-out BiCMOS class-AB OpAmp, 265–267
    - 1GHz, all-NPN class-AB OpAmp, 249
    - precision HF all-NPN class-AB OpAmp, 246–249
    - three-GA-stage, 181–184
    - 1 volt R-R-in/out bipolar class-AB OpAmp, 271–276
    - 1 volt R-R-out CMOS class-AB OpAmp, 261–265
- N**
- NE5534 class-AB OpAmp with bypassed NMC, 244–245
  - Nested chopper operational amplifier, 363
  - Nested Miller compensation (NMC), 18, 177–181, 184, 208, 237, 244–246, 251, 265, 267–271
  - NE5534 class-AB OpAmp with bypassed NMC, 244–245
  - precision all-NPN class-AB OpAmp, 245–246
  - RNMC, 195–197
  - three-GA-stage, 178–181
  - 1.8 volt R-R-in/out bipolar class-AB OpAmp (NE5234), 267–271
  - No internal poles, 165–166
  - Noise, 1, 9, 12, 17–20, 22–24, 33, 35, 38, 39, 45–52, 55, 56, 60, 62, 63, 70–73, 88, 95, 157, 199, 217–219, 229, 230, 238, 241, 242, 246, 247, 253, 255, 257, 305, 322, 324–326, 337, 339, 343–345, 351–397
  - Non-ideal OpAmps, 50–52, 55
  - Non-inverting voltage amplifier, 3–4, 33–35, 47–48, 52
  - Non-linear distortion, 200–205, 342
  - Notch filter, 376–378
  - Nullor concept, 1
- O**
- OCA. *See* Operational current amplifier
  - OFA. *See* Operational floating amplifier
  - Offset, bias and drift, 59–70
  - Offset voltage and current
    - definition, offset voltage and current, input and output impedance, gain, 11–12
  - One-GA-stage frequency compensation, 163–165
  - OpAmp. *See* Operational amplifiers
  - Operational amplifiers (OpAmp), 1–10, 16–24, 27, 28, 45, 50–53, 55, 56, 100, 106–107, 114, 133, 134, 136, 155, 157, 159, 160, 162–164, 166, 167, 170, 177–180, 182–189, 198–200, 203, 205, 210–211, 213–220, 224–231, 235–251, 269, 271, 281, 291–307, 319, 339, 348, 351, 352
  - Operational current amplifier (OCA), 2, 5–6, 8–9, 14–16, 37–38
    - definition, output bias current, output common-mode current rejection ratio, 14–15
  - Operational floating amplifier (OFA), 2, 7–9, 15–16, 36, 38–44, 54, 291, 309–349
    - using all definitions, 16
  - Operational inverting amplifier (OIA), 2–3, 8, 9, 11–16, 31–33, 35, 38



Operational inverting amplifier (OIA) (*cont.*)  
 definition, offset voltage and current, input  
 and output impedance, gain, 11–12

Operational transconductance amplifier  
 (OTA), 20–21, 213–215, 220, 224

Operational voltage amplifier (OVA), 2–5,  
 8–9, 12–16, 33–36, 45, 67, 81  
 definition, input bias current, input  
 common-mode rejection ratio,  
 13–14

OTA. *See* Operational transconductance  
 amplifier

Output bias current  
 definition, output bias current, output  
 common-mode current rejection  
 ratio, 14–15

Output common-mode current rejection ratio  
 definition, output bias current, output  
 common-mode current rejection  
 ratio, 14–15

Output stages, 105–152

FBB  
 compound, 130–134  
 rail-to-rail general amplifier, 119–128  
 voltage-follower, 112–117, 129–130

FFB  
 compound, 117–119  
 rail-to-rail general-amplifier, 119–128  
 voltage follower, 112–117

OVA. *See* Operational voltage amplifier

Overall design, 155–211

Overall topologies  
 classification, 155–161

## P

Parallel compensation (PC)  
 two-GA-stage, 167–170

Phase margin at high capacitive load, 190,  
 194–196

Ping-Pong auto-zero, 360, 364

Ping-Pong-Pang auto-zero instrumentation  
 amplifier, 364

Power efficiency of output stages, 105–110

Precision all-NPN class-AB OpAmp with  
 NMC, 245–246

Precision HF all-NPN class-AB OpAmp with  
 MNMC, 246–249

## Q

Quench capacitor for HF stability control,  
 193–195

## R

Rail-to-rail-in/out (R-R-in/out)  
 compact 2 volt R-R-in/out CMOS class-AB  
 OpAmp with MC, 256–259  
 1 volt R-R-in/out bipolar class-AB  
 OpAmp with MNMC, 271–276  
 1.8 volt R-R-in/out bipolar class-AB  
 OpAmp (NE5234) with NMC,  
 267–271

Rail-to-rail (R-R) input stages, 82–96  
 CMOS by back-gate driving, 95

Rail-to-rail-out (R-R-out)  
 basic bipolar R-R-out class-A OpAmp,  
 226–228  
 compact 1.2 volt R-R-out BiCMOS  
 class-AB OpAmp with MNMC,  
 265–267  
 compact 1.2 volt R-R-out CMOS class-AB  
 OpAmp with MC, 259–261  
 compact 2 volt R-R-out CMOS class-AB  
 OpAmp with MC, 254–256  
 compact 1.2 volt R-R-out CMOS class-A  
 OpAmp with MC, 252–254  
 improved basic bipolar R-R-out class-A  
 OpAmp, 228–229  
 improved basic CMOS R-R-out class-A  
 OpAmp, 229–231  
 1.2 volt R-R-out CMOS class-AB OpAmp  
 with MHNMC, 276–280  
 1 volt R-R-out CMOS class-AB OpAmp  
 with MNMC, 261–265

Reverse nested Miller compensation (RNMC),  
 195–197

Ripple-reduction loop (RRL), 352, 376–389,  
 395, 396

Ripple-reduction loop for chopper amplifiers,  
 376–382, 385, 387–389, 395

RNMC. *See* Reverse nested Miller  
 compensation

RRL. *See* Ripple-reduction loop

## S

Sample & hold, 225, 369, 370

Saturation  
 output current limitation circuits,  
 143–145  
 output saturation protection circuits,  
 141–143  
 protection and current limitation, 141–145

Sensor bridge, 320, 352, 353

Skin-electrode offset compensation, 353,  
 382–383

Slew rate, 16–18, 24, 109, 133, 196, 198–202, 223, 224, 226, 234, 235, 237–239, 253, 281, 288  
 high-slew-rate bipolar class-AB voltage-follower buffer, 234  
 Stability for high-capacitive load, 191  
 Summary low offset, 396–397

## T

Telescopic-cascode OpAmp, 268  
 Three-GA-stage  
 frequency compensation, 177–178  
 multipath nested Miller compensation (MNMC), 181–184  
 nested Miller compensation (NMC), 178–181, 197, 244–246, 267–271  
 Three-OpAmp instrumentation amplifier, 319–320, 324, 351, 354–355  
 Total CMCR, 80–81  
 Two-GA-stage  
 frequency compensation, 166–167  
 Miller compensation (MC), 170–172  
 parallel compensation (PC), 167–170

## U

Unipolar  
 bipolar accurate V-I converter, 314–315  
 CMOS accurate V-I converter, 313–314  
 OpAmp accurate V-I converter, 315–316  
 OpAmp-gain-boosted accurate V-I converter, 312–313  
 single-transistor V-I converter, 312  
 voltage-to-current converter, 311–316  
 Universal  
 class-AB OFA design, 338–345  
 current mirrors, 341–343  
 output-current equalization, 343–344  
 total-output-supply-current equalization, 339–341  
 class-AB OFA realization with power-supply isolation, 337–338  
 class-AB voltage-to-current converter design using an instrumentation amplifier, 328–331  
 class-AB voltage-to-current converter with instrumentation amplifier, 344–345  
 class-A OFA design, 331–337  
 floating zener-diode supply, 331–332  
 long-tail-pairs, 333–337  
 supply current followers, 332–333  
 floating power supply design, 338

V-I converter design  
 real instrumentation amplifier, 329–331  
 semi-instrumentation amplifier, 328–329

## V

VCF. *See* Voltage and current follower  
 VF. *See* Voltage follower  
 Voltage and current follower (VCF), 7–9, 133  
 Voltage and current gain boosting, 160  
 Voltage compensation  
 input, 221–223  
 Voltage follower (VF), 4–6, 8, 9, 18, 21, 35–36, 82, 107, 109–119, 128–133, 140, 145, 234, 242, 297, 298, 314, 315, 332  
 FBB voltage-follower output stages, 129–130  
 FFB voltage follower output stages, 112–119  
 Voltage follower (VF) buffer  
 high-slew-rate bipolar class-AB voltage-follower buffer, 234  
 Voltage-gain boosting, 224–225  
 Voltage-to-current converter, 7, 9, 38–42, 46, 54, 307, 310–321, 327–331, 339, 342–345, 347, 348, 355, 357  
 differential  
 accurate V-I converter, 317–318  
 CMOS accurate V-I converter, 318–319  
 simple V-I converter, 316–317  
 voltage-to-current converters, 310, 316–320, 328  
 unipolar  
 bipolar accurate V-I converter, 314–315  
 CMOS accurate V-I converter, 313–314  
 OpAmp accurate V-I converter, 315–316  
 OpAmp-gain-boosted accurate V-I converter, 312–313  
 single-transistor V-I converter, 312  
 voltage-to-current converter, 311–316  
 universal  
 class-AB voltage-to-current converter with instrumentation amplifier, 344–345  
 voltage-to-current converter design using an instrumentation amplifier, 328–331  
 2 Volt power-efficient all-NPN class-AB OpAmp with MDNMC, 249–251

- 1 Volt R-R-in/out bipolar class-AB OpAmp with MNMC, 271–276
- 1.2 Volt R-R-out CMOS class-AB OpAmp with MHNMC, 276–280
- 1.8 Volt R-R-in/out bipolar class-AB OpAmp (NE5234) with NMC, 267–271
- 1 Volt R-R-out CMOS class-AB OpAmp with MNMC, 261–265